

BEYOND THE
STANDARD MODEL



XVIIIth Rencontre de Moriond - Leptonic Session
La Plagne, Savoie, France, March 13-19, 1983

BEYOND THE STANDARD MODEL

ISBN 2-86332-023-8

Editions Frontières
B.P. 44
91190 GIF SUR YVETTE - France

Printed in Singapore by Kim Hup Lee
Printing Co. Pte. Ltd.

Proceedings of the Leptonic session of the
EIGHTEENTH RENCONTRE DE MORIOND .
La Plagne-Savoie-France, March 13-19, 1983 18.1983

Vol. 2

BEYOND THE STANDARD MODEL

edited by
J. TRAN THANH VAN

The Leptonic Session of the Eighteenth Rencontre de Moriond on
BEYOND THE STANDARD MODEL
was organized by

J. TRAN THANH VAN

with the active collaboration of

A. BOUQUET
J.F. GRIVAZ
F. JACQUET
G. KANE
A. MOREL
L. OLIVER
and J. RANDER

C 83/074
GERMAN
BIBLIOTHEQUE
M
39
1983

Associated Editor: Mrs. O. Lebey

AVANT-PROPOS

La XVIIIème Rencontre de Moriond a eu lieu à la Plagne - Savoie (France).

Le but principal des Rencontres de Moriond est de faire le point sur les récents développements de la physique contemporaine et aussi de promouvoir une collaboration effective entre expérimentateurs et théoriciens dans le domaine de la physique des particules élémentaires. Bien qu'il soit de plus en plus difficile - étant donné les dimensions des équipes - de maintenir un effectif relativement réduit afin de permettre de nombreux échanges informels, tous les participants ont contribué à créer une atmosphère de dialogue et d'échange si propice à une meilleure communication humaine et scientifique. Ce succès, nous le devons à tous les participants que nous remercions vivement.

Ce souci de recherche de nouvelles formes de communication, de nouveaux terrains d'échange et de dialogue qui depuis l'origine, anime les Rencontres de Moriond, nous a amenés à susciter la création des Rencontres de Méribel pour les biologistes et les Rencontres de Moriond-Astrophysique.

Des séminaires interdisciplinaires ont été organisés afin de susciter des réflexions communes sur les récents développements dans certains domaines et sur leurs répercussions sur les autres disciplines.

Nous tenons à adresser nos remerciements à tous ceux qui ont contribué à la réussite de ces Rencontres, ainsi qu'au Centre National de la Recherche Scientifique, au Commissariat à l'Energie Atomique, et à l'OTAN qui nous ont apporté leur aide efficace.

J. TRAN THANH VAN

FOREWORD

The XVIIth Rencontre de Moriond was held at La Plagne, Savoie (France).

The first such meeting was at Moriond in the French Alps in 1966. There experimental as well as theoretical physicists, not only shared their scientific preoccupations but also the household chores. The participants at the first meeting were mainly French physicists interested in electromagnetic interactions. In subsequent years, a session on high energy strong interactions was also added.

The main purpose of these meetings is to discuss recent developments in contemporary physics and also to promote effective collaboration between experimentalists and theorists in the field of elementary particle physics. By bringing together a relatively small number of participants, the meeting helps to develop better human relations as well as a more thorough and detailed discussion of the contributions.

This concern for research and experimentation of new channels of communication and dialogue which from the start animated the Moriond Meetings, inspired us to organize a simultaneous meeting of biologists on Cell Differentiation and to create the Moriond Astrophysics meeting. Common meetings between biologists, astrophysicists and high energy physicists are organized to study the implications of the advances in one field into the others. I hope that these conferences and lively discussions may give birth in the future to new analytical methods or new mathematical languages.

At the XVIIIth Rencontre de Moriond, four physics sessions and two biology sessions were organized :

- * January 23-29 . Gluons and Heavy Flavours
- * March 13-19 . Beyond the Standard Model
- . Galaxy and the Early Universe
- . Cell Recognition
- * March 19-25 . Antiproton-Proton Physics
- . Cell Differentiation

This book contains the invited lectures given at the "Beyond the Standard Model" session of the XVIIIth Rencontre de Moriond.

I thank the organizers of the XVIIIth Rencontre de Moriond :

- J. TAVLITZKI for the Biology meetings,
- J. AUDOUZE, Ph. CRANE, Th. GAISSER and D. HEGYI for the Astrophysics meeting,
- A. CAPELLA, L. MONTANET, J. PEOPLE and F. RICHARD for the "Gluons and Heavy Flavours" session,
- A. BOUQUET, J. F. GRIVAZ, F. JACQUET, G. KANE, A. MOREL, L. OLIVER and J. RANDER for the "Beyond the Standard Model" session,
- F. VANNUCCI for the antiproton-proton physics session,

and the conference secretaries M.BAILLY, J. BORATAV, A. DOS SANTOS, O. GEIST, C. JOUANEN, O. LEBEY, B. LELOUP, L. NORRY who have devoted much of their time and energy to the success of this Rencontre.

I am also grateful to Mr MEIGNEN, Mr PELICAN, Mr BUSURIS and Ms CABAUD, who contributed through their hospitality and cooperation to the well-being of the participants enabling them to work in a relaxed atmosphere.

This Rencontre is sponsored by the "Centre National de la Recherche Scientifique" and by the "Commissariat à l'Energie Atomique". The Astrophysics meeting is also sponsored by NATO. I would like to express my thanks for their encouraging support.

I wish sincerely that a fruitful exchange and an efficient collaboration between the physicists, the astrophysicists and the biologists will arise from this Rencontre as in the previous Rencontres.

J. TRAN THANH VAN

CONTENTS

I. PROTON LIFETIME AND OSCILLATION EXPERIMENTS

J. VAN DER VELDE	"Results on proton decay from the IBM detector".	13
E. BELLOTTI	"Recent results from the Mont Blanc experiment".	27
T.N. PHAM	"Two-body proton decays in SU(5)".	43
H. WEERTS	"Limits on neutrino-oscillations using a fine grained calorimeter at FNAL".	53
F. VANNUCCI	"Decays of massive neutrinos".	63
F. NIEBERGALL	"Search for decay of heavy neutrinos in neutrino beams".	71
A. BODEK	"Status of the CCFR neutrino oscillation experiment at FNAL".	77
Y. EISENBERG	"Neutrino oscillation experiments at CERN".	85

II. ELECTRON POSITRON PHYSICS

K. WACKER	"Recent results from SPEAR".	91
E.H. THORNDIKE	"A review of e+e- annihilation results from CLEO".	105
P.M. TUTS	"Topics in upsilon spectroscopy and B physics with CUSB".	123
G. GOLDHABER	"Review of PEP experiments".	137
S. YAMADA	"Recent results from PETRA on QED, electroweak interactions and new particle searches".	177

III. MUON AND NEUTRINO PHYSICS

K. RITH	"What can the EMC-effect tell us about quarks and gluons in nuclei?	207
A. BODEK	"A comparison of the deep inelastic structure functions of deuterium, aluminum and steel nuclei".	223

M.J. LONGO	"Prompt neutrino results from FERMILAB".	231
D. CUTTS	"Elastic neutrino electron scattering".	241
J. PANMAN	"Study of a new detector for neutrino-electron scattering".	253
P.H.A. VAN DAM	"Measurement of the neutral current coupling constants in (anti-)neutrino interactions with deuterium".	259
W. VAN DONINCK	"Application of a multivariate discriminant analysis to high energy physics in bubble chambers".	265
B. GOBBI	"Search for right-handed currents in muon decay".	279
C. SANTONI	"Bounds on supersymmetric particles from a proton beam-dump experiment".	293

IV. THEORETICAL LECTURES

C.A. SAVOY	"Supersymmetric particle physics : a panorama".	299
G. ALTARELLI	"Virtual effects of SUSY particles".	329
A. SONI	"Left-right symmetry and CP violation".	339
G. VENEZIANO	"CP and U(1) problems, and their relationship in QCD".	355
K. LANE	"New tests for quark and lepton substructure".	369
H. FRITZSCH	"Electromagnetism as the origin of the lepton and quark masses".	379
L. BAULIEU	"Squarks contributions to p-p collisions".	391
M. CAPDEQUI-PEYRANERE	"Weak corrections to the $e^+e^- \rightarrow \gamma\gamma, \gamma Z$ reactions".	397

V. MONOPOLES AND DARK MATTER.

C. CALLAN		401
-----------	--	-----

B. C. BARISH	"The search for magnetic monopoles"	417
S. ERREDE	"A search for magnetic monopole catalysis of nucleon decay".	
J.R. PRIMACK	"What is the dark matter ? Implications for galaxy formation and particle physics."	433
P. LANGACKER	"Cosmological neutrinos and their detection".	445
		465
VI. CONCLUSIONS		
G.J. FELDMAN	"Conference summary"	481

Results on Proton Decay from the IMB Detector*

THE IRVINE-MICHIGAN-BROOKHAVEN COLLABORATION

R. M. Bionta², G. Blewitt⁴, C. B. Bratton⁵, B. G. Cortez^{2,a},
S. Errede², G. W. Foster^{2,a}, W. Gajewski¹, M. Goldhaber³,
J. Greenberg², T. J. Haines¹, T. W. Jones^{2,7}, D. Kielczewska^{1,b},
W. R. Kropp¹, J. G. Learned⁶, E. Lehmann⁴, J. M. LoSecco⁴,
P. V. Ramana Murthy^{1,2,c}, H. S. Park², F. Reines¹, J. Schultz¹,
E. Shumard², D. Sinclair², D. W. Smith^{1,d}, H. W. Sobell¹,
J. L. Stone², L. R. Sulak², R. Svoboda⁶, J. C. van der Velde²,
and C. Wuest¹.

- (1) The University of California at Irvine
Irvine, California 92717
- (2) The University of Michigan
Ann Arbor, Michigan 48109
- (3) Brookhaven National Laboratory
Upton, New York 11973
- (4) California Institute of Technology
Pasadena, California 91125
- (5) Cleveland State University
Cleveland, Ohio 44115
- (6) The University of Hawaii
Honolulu, Hawaii 96822
- (7) University College
London, United Kingdom

ABSTRACT

Results are presented from the first 80 days live-time in the Irvine-Michigan-Brookhaven proton decay detector. No candidates for proton decay into $e^+\pi^0$ are found in the 3300 metric-ton fiducial volume during this exposure of 720 ton-years, setting a 90% C.L. limit of 6.5×10^{31} year for proton lifetime/branching ratio for this mode.

*Presented by J. van der Velde

The IMB proton decay detector consists of a large rectangular volume of water located at a depth of 1670 mwe in a salt mine east of Cleveland, Ohio. The six surfaces of the volume are covered by 2048 (5 inch diameter) photomultiplier tubes (PMT) which detect Cherenkov light emitted by relativistic charged particles in the water. The distances between the tube planes in the E-W, N-S, and vertical directions are 22.8 m, 16.8 m, and 18.0 m, respectively. The fiducial volume begins 2.0 m in from the tube planes and contains 2.0×10^{33} nucleus, 1/9 of which are free protons.

Filling the detector was completed on July 30, 1982 and useful data taking commenced in September. I will report on 80 days of live time taken prior to January 1, 1983.

OPERATION AND CALIBRATION OF THE DETECTOR

The detector is divided into 32 "patches" each consisting of 64 PMT. An event trigger consists of the time coincidence (within 120 ns) of any two patches which themselves had a coincidence of > 3 PMT in 60 ns. This "two patch" trigger is "OR-ed" with another trigger which consists of > 12 PMT from the full detector in 60 ns. The trigger rate is 2.7/sec, virtually all due to atmospheric muons. The average dark noise in the tubes is 2.5 KHz with occasional tubes as high as 50 KHz. The number of noise triggers is negligible once the detector becomes dark adapted (a few hours after being exposed to light).

For each PMT which fires within ± 250 ns of the trigger time we record the time (T_1), the pulse height (Q), and whether or not the tube had a pulse (T_2) in a longer time scale running to 7.5 μ sec after the trigger. The detector is calibrated using two different known sources of light: a "laser ball" situated in the center of the detector is driven by a 337 nm Nitrogen laser and emits isotropic bursts of light at various known times and known (relative) light levels. The absolute light-level, which is directly related to the energy of showering particles, is calibrated using single cosmic rays. These cosmic rays also tell us the absolute PMT efficiencies and give us measurements of light scattering and absorption in the water. Light absorption is also measured using the laser ball and in external test stands.

Figure 1 shows a schematic cross section of a single straight track passing through the detector. For $\beta = 1$ the Cherenkov cone of light is

emitted at an angle of 41° with respect to the track. Successive isochronous wave fronts are shown emanating from the track as it traverses the detector. The arrival times and pulse heights allow us to reconstruct the track position and angle. From each hit PMT we can project back to the track and determine the flight path (D) and distance along the track (L) at which the photon was emitted, assuming that it was not scattered. Figure 2a shows the integrated pulse height (proportional to total photoelectron count) recorded as a function of L (in % of track length) for 150 computer simulated muons generated to enter and exit within 4 m radius circles centered at the top and bottom of the detector. The true entry points were chosen and then the track angles were reconstructed using the photoelectron (PE) weighted directions of the hit tubes. (This is our normal procedure for reconstructing track angles from a given vertex. It gives the correct direction to within 1° for these muons whose correct vertex has been assigned.) Note the sharp response function of the phototubes as the Cherenkov cone hits the side walls of the detector. The fact that the step-function of the Cherenkov cone is not flat is due to absorption in the water. Note especially the low ($\sim 1\%$) light intensity outside the Cherenkov cone. This shows the effect of knock-on electrons generated in the material preceding the detector and in the early part of the track's path through the water. There is no Rayleigh scattering included in the simulated events shown in Figure 2a. The effect of Rayleigh scattering can be seen in Figure 2b where we make a similar plot for a selected sample of real muons chosen to have entry and exit points similar to those of Figure 2a. This gives us a measure of the amount of Rayleigh scattering we must put into the simulated ("Monte Carlo") events. The response function of the real events does not have quite as sharp a rise as the simulated events. We can reproduce this effect in the simulated events if we smear the entry points by about 2 m, consistent with our error in their determination.

Correction for water absorption of photons is a strong function of wave length (λ) and can only be done in an approximate way for each PMT hit since we don't measure λ . The light from near the beginning of the track ($L = 0$) has typically traveled through 20 m of water whereas that near the end of the exiting track has traveled only ~ 1 m. Our correction for water absorption over this difference in distance can be seen in Figure 2c where the response function now is approximately flat.

Another important piece of information we need in order to properly generate Monte Carlo events is the absolute efficiency of the PM tubes to respond to Cherenkov light generated by a single relativistic track and passed through a distance D of water. Starting with the known Cherenkov spectrum we must modulate it by water absorption and scattering, PMT glass transmission and photocathode response, and PMT single PE capture efficiency. We use our test-stand measurements of water absorption, our previously described value for Rayleigh scattering, the PMT manufacturer's (EMI) values for glass transmission and photocathode response, and 50% capture efficiency. This reproduces the efficiency vs D curve to within a few percent over the entire range $D = 0$ to 24 m, as can be seen in Figure 3.

The time jitter in the PM tubes can be measured "in situ" by analyzing pulses from the laser ball. If we calibrate the tubes with the ball in one position, and then move it to various other positions and reconstruct its location, the error in that reconstruction is a direct measure of our spatial resolution for a point source of light. It is important to understand this spatial resolution since this type of vertex reconstruction by time-of-flight is used extensively in rejecting background and calculating efficiencies for events which originate in the fiducial volume. Figure 4 shows that the spatial resolution for reconstructing a point source is ~ 50 cm. This is directly related to the time jitter in the tubes of ~ 11 ns (FWHM) at the single PE level. If we put the measured average time jitter (including pulse height slewing) into the Monte Carlo simulations we find that typical vertex error for back-to-back (or multibody) nucleon decays are ~ 60 cm. Events which give light mostly in one direction (e.g., the majority of atmospheric neutrino interactions and neutrino modes of nucleon decay) have spatial resolution of ~ 50 cm perpendicular to the track and ~ 150 cm along the track.

In summary, we now have all of the ingredients necessary in order to accurately simulate events:

-Track generation

This is straight forward in a homogeneous medium like water.

-Light generation

The simple β -dependent Cherenkov effect is used.

-Light scattering and absorption

These have been measured as discussed above.

-PMT efficiency

Measured in situ using cosmic rays.

-PMT time response

Measured using the laser ball.

-PMT pulse height to energy conversion

We are in the process of refining our conversion of pulse height to ionization energy. This is done initially in a relative way using neutral density filters in the laser system to linearize the Q response of each PMT. The absolute scale is then determined by cosmic rays. We estimate our present systematic uncertainty as $\pm 15\%$. This uncertainty has no significant effect on the conclusions presented in this paper.

DATA ANALYSIS

Currently we are processing data with three independent systems in order to develop the most efficient methods for saving all events with vertex inside the fiducial volume. A brief account of the processing of one day's data by one of these systems goes as follows:

Raw Triggers = 240,000/24 hrs = 2.75 Hz

	<u>Remainder</u>
On-line geometrical cuts	88,000
Preliminary point fitting, nearest neighbor algorithms, etc.	15,000
Point fit required to be inside fiducial volume	1,200
Moment-of-inertia angle cut	200
Angle cut vs. center-of-mass of PMT hits.	30

The above cuts are made entirely in software. At this point this group does a "fast scan" of the 30 events/day using interactive geometrical handling and reconstruction. The scan is performed after adding a random 10% sample of "signal" Monte Carlo events of various types into the data stream. This serves the dual purpose of determining the scanning efficiency and also keeping the scanners' attention since they almost never find any real events that look like proton decay.

After scanning we find about one real event per day with vertex in the fiducial volume. The efficiency for simulated events in the fiducial volume to pass all of the same criteria as the real events ranges from $\sim 60\%$ for single neutrino produced muons up to $\sim 85\%$ for $p \rightarrow e^+\pi^0$ events. Cross correlation between the three independent analysis groups in finding the same real events is good, especially for wide angle events with > 2 tracks. Disagreements between the groups almost always involve events which are close to the edge of the fiducial volume or else can be explained in terms of the different selection criteria used.

RESULTS

In the first 80 days of live-time 69 events were found with vertices originating inside the fiducial volume. About 80% of these are single track events and multitrack events in which separate Cherenkov cones cannot be clearly recognized. The events are uniformly distributed throughout the fiducial volume and, within our statistics, isotropic in direction. (Our present statistics do not allow us to see the small anisotropies expected for atmospheric neutrino interactions.) This can be seen in Figures 5a and 5b which show top and side views of unit vectors representing the position and direction of the highest energy track in each event. Note particularly in Figure 5b that there is no evidence for contamination from the 2×10^7 pre-dominantly downward-going cosmic ray muons which were in the original data.

To measure energy we use the variable E_C which is proportional to the total Cherenkov light emitted in the event. This is proportional to total charged track length above Cherenkov threshold and for showering tracks gives a measurement of total energy in MeV which is limited mostly by statistics ($\sigma \approx 10\% / E(\text{GeV})$). At present, as mentioned earlier, there is an additional $\pm 15\%$ systematic uncertainty in E_C . For each non-showering charged π or μ in the event one must add ~ 250 MeV to E_C to account for rest mass and energy loss below threshold.

The distribution in E_C of the 69 events is shown in Figure 6. The curve is our estimate of the shape of the distribution expected for atmospheric neutrino events modulated by our event selection procedures. The overall rate of neutrino events we calculate as 1.0 ± 0.5 per day, where the uncertainty is due primarily to lack of knowledge about the atmospheric neutrino flux below 1 GeV. Clearly most, if not all, of the events we see are consistent with being due to atmospheric neutrinos.

SEARCH FOR $p \rightarrow e^+\pi^0$

In order to look for $p \rightarrow e^+\pi^0$ we select a subset of the 69 events which have two reasonably well defined Cherenkov cones with included angle of at least 100° and in which the number of PMT for each track is at least 40. The three events which satisfy these criteria are listed in Table I. The criteria we can apply to search for $p \rightarrow e^+\pi^0$ are as follows:

$$(1) \quad 650 < E_C < 1250 \text{ MeV}$$

$$(2) \quad \theta_{12} > 140^\circ$$

$$(3) \quad E_2/E_C > .35 \quad (E_2 \text{ is for the track of lesser energy})$$

$$(4) \quad \text{No observed } \mu \rightarrow e \text{ decay.}$$

None of the events in the table satisfies all of the above criteria so we conclude that we have no possible candidates for $p \rightarrow e^+\pi^0$. The lifetime limit based on this result can be calculated as follows:

$$\tau/B(e^+\pi^0) > (2.0 \times 10^{33}) \cdot (10/18) \cdot (.68) \cdot (1/2.3) \cdot (0.9) \cdot (80/365).$$

Where:

τ = proton lifetime

$B(e^+\pi^0)$ = branching ratio into $e^+\pi^0$

and the various factors are, in order:

2.0×10^{33} = nucleons in the fiducial volume

$10/18$ = proton fraction in water

$.68$ = ave. nuclear escape probability for the π^0
(.60 for oxygen, 1.0 for free hydrogen)

2.3 = 90% C.L. factor of 2.3 events
0.9 = detection efficiency
80/365 = live-time in yrs.

So that we obtain the following 90% C.L. limit for $p + e^+\pi^0$:

$$\tau/B (e^+\pi^0) > 6.5 \times 10^{31} \text{ yr.}$$

The significance of this result in terms of prior expectations is as follows. An assessment of grand unified theories based on minimal SU (5) symmetry predicts $4.5 \times 10^{29} \pm 1.7$ yr for the quantity $\tau/B (e^+\pi^0)$ (1). The upper value for the exponent predicts that we should have seen seven $p + e^+\pi^0$ events in the present sample. Hence our result would appear to rule out this version of grand unified theories. On the experimental side, the KGF experiment has reported(2) three contained candidates for proton decay, one of which is interpreted as $p + e^+\pi^0$. If we naively calculate the number of $e^+\pi^0$ events we expect based on this single event we predict 10 events (in fact more than 10 if we account for the smaller π^0 escape probability in iron as opposed to water). This would appear to cast doubt on that particular KGF event as being due to $p + e^+\pi^0$.

In summary, the IMB detector is working nicely and continues to take data with a live-time efficiency of about 75%. Our first results indicate that the background for $p + e^+\pi^0$ and other two body nucleon decay modes is quite low so that a sensitivity of at least 5 times the present result would appear possible.

Data on other decay modes of the proton and neutron as well as information about possible NN oscillations in oxygen should be forthcoming soon.

Our first results on a search for strongly interacting monopoles have also been reported at this conference by S. Errede.

I would like to thank the organizers of this XVIIIth Recontre de Moriond, and especially Tran Than Van and his wife Kim, for their efficient organization and warm hospitality.

TABLE I. WIDE ANGLE TWO-TRACK EVENTS

Event No.	No. of PMT	E_C CHERENKOV ENERGY (MeV) ^a	E_1 (MeV) ^a	E_2 (MeV) ^a	θ_{12} (Deg)	OBS. MUON DECAYS
151-35037	188	1000 \pm 100	600 \pm 90	400 \pm 60	135 \pm 7	1
225-07794	166	950 \pm 100	700 \pm 130	250 \pm 80	125 \pm 25	1
388-19376	340	1700 \pm 170	1050 \pm 170	650 \pm 100	115 \pm 15	0

^aDoes not contain additional possible systematic errors of 15%.
 E_C is calculated assuming the particles are showering. If one particle is a charged pion or muon, as must be the case in the first two events in the table, 250 MeV must be added to the energy of one track and to the total energy listed.

REFERENCES AND FOOTNOTES

- (a) Also at Harvard University.
- (b) Permanent addresses: Warsaw University, Poland.
- (c) Tata Institute of Fundamental Research, Bombay, India.
- (d) Now at University of California at Riverside.
- 1. Summaries of rate calculations and references to original literature can be found in the following reviews: Proceedings of the 1982 Workshop on Proton Decay, NAL-HEP-82-24 (D. S. Ayres, ed.), p. 64; W. J. Marciano, BNL 31036, presented at Orbis Scientiae (1982).
- 2. M. R. Krishnaswamy, et al., Phys. Lett. 115B, 4, p. 349 (1982).

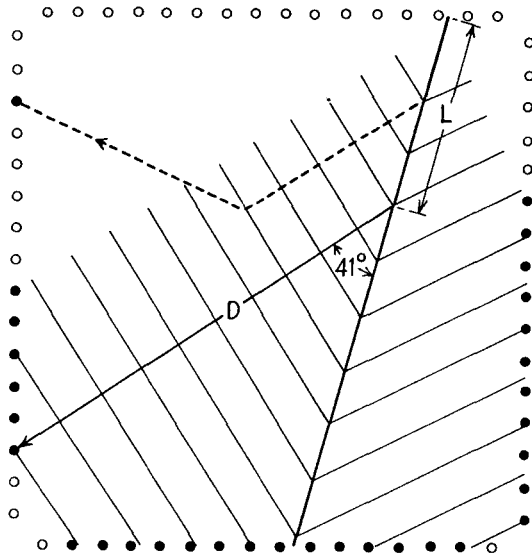


Figure 1. Schematic of successive isochronous wavefronts from single track emitting Cherenkov light. Dotted line represents scattered photon.

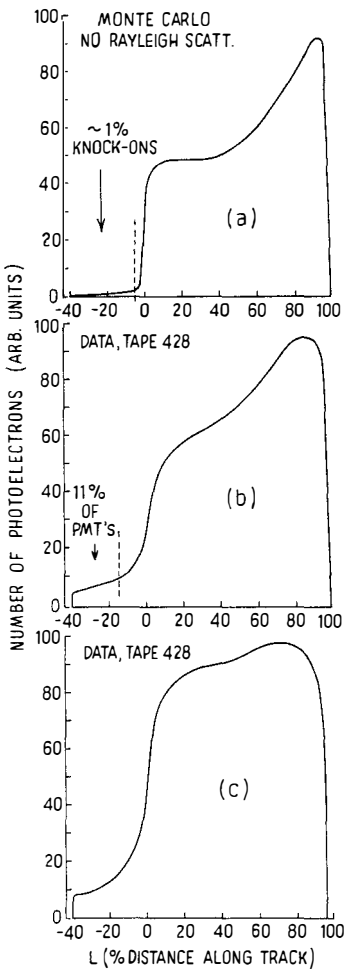


Figure 2. a. Monte Carlo calculation of light yield from straight-through muons. Note that pulse is not flat on top due to absorption of light in water. (At $L = 0$, $D \approx 22\text{m}$; $L = 80\%$, $D \approx 4\text{m}$.)

b. Light yield (uncorrected for absorption) for a selected sample of real muons going through the center of the detector. Note level of scattering for $L < 0$.

c. Light yield from data after correcting for absorption in the water.

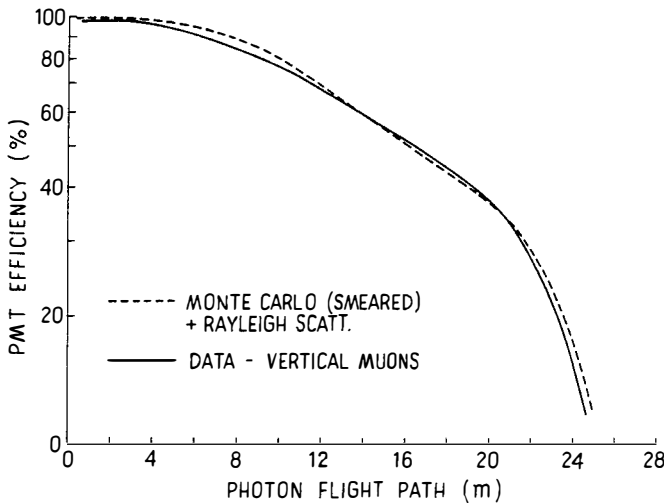


Figure 3. PMT efficiency (occupancy) as a function of photon flight path D in the water. Monte Carlo includes effects of PMT efficiency and absorption and scattering in the water.

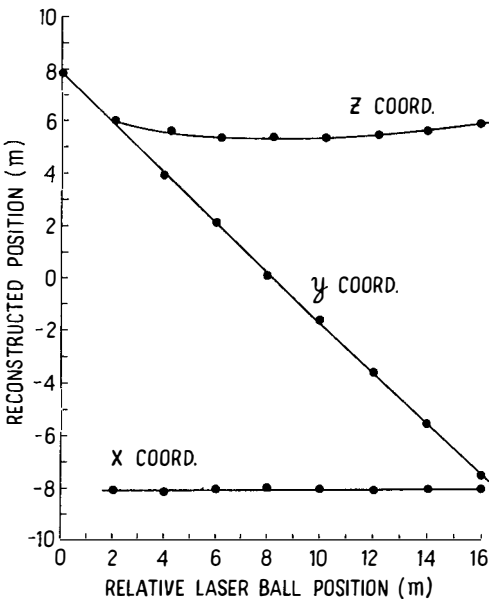


Figure 4. Reconstructed position of the laser ball as it is moved along a beam oriented in the y direction. (The beam was slightly bowed in the z direction.) The results indicate a point source reconstruction error of $\sigma \sim 50$ cm in each coordinate.

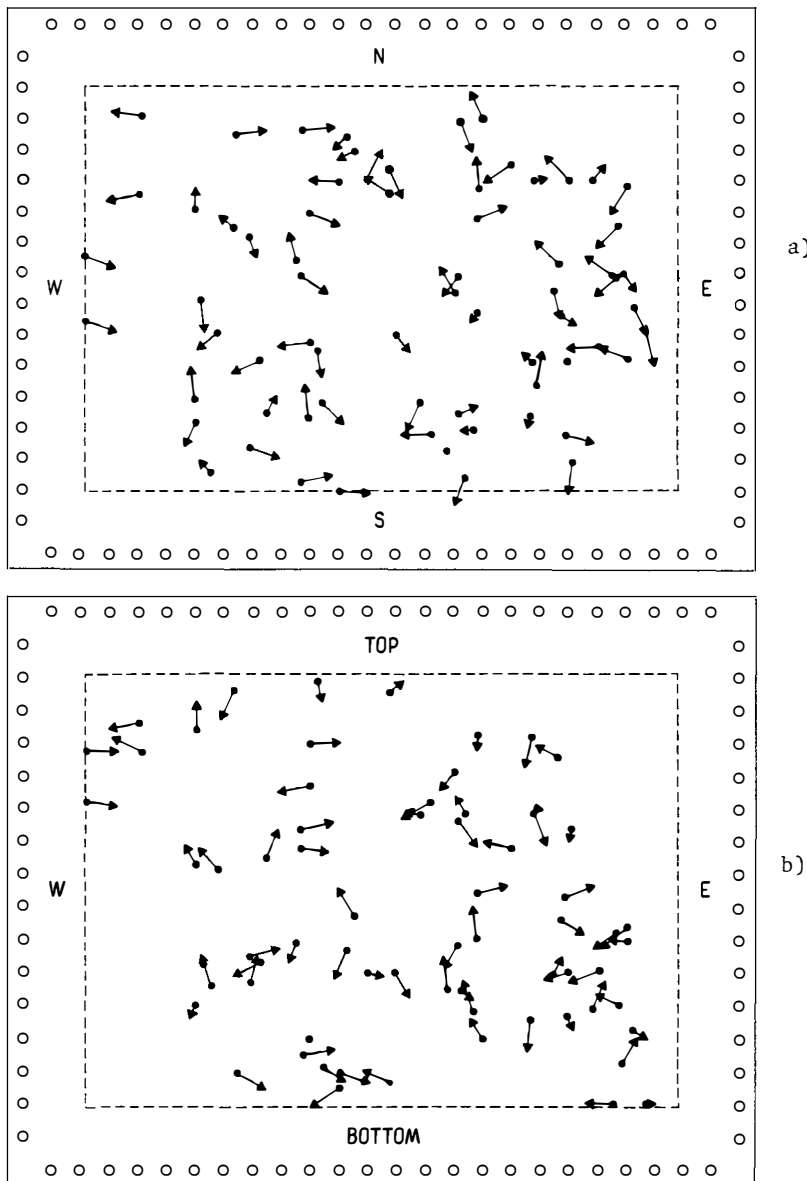


Figure 5. a. Unit vector projections of 69 data events as seen from the top.

b. Same as a., as seen from side.

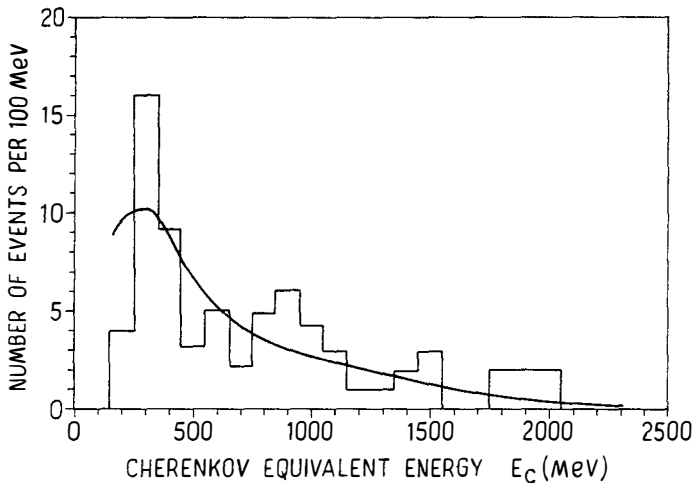


Figure 6. Distribution of E_C (see text) for 69 events. The curve was calculated using Gargamelle Bubble Chamber data for neutrino event topologies modulated by calculated atmospheric fluxes and our data cuts. The curve is normalized to the data, as the expected neutrino rate is uncertain by as much as a factor of two.

RECENT RESULTS FROM THE MONT BLANC EXPERIMENT

NUSEX Collaboration: LNF-Milan-Turin-CERN⁽⁺⁾

Presented by E. Bellotti

Dipartimento di Fisica dell'Università and Sezione INFN Milano



ABSTRACT

Data collected in more than 5000 hours of operation of a 150 tons tracking calorimeter installed in the Mont Blanc Laboratory are presented. Besides ~ 5800 single muons and ~ 84 μ -bundles, 7 confined events have been observed. One of them cannot easily be explained as a ν induced interaction and it is compatible with the hypothesis that it is due to a proton decay; features of the 6 other events are also briefly discussed.

(+) G. Battistoni, E. Bellotti, G. Bologna, P. Campana, C. Castagnoli, V. Chiarel la, D.C. Cundy, B. D'Ettorre Piazzoli, E. Fiorini, P. Galeotti, E. Iarocci, C. Liguori, G. Mannocchi, G.P. Murtas, P. Negri, G. Nicoletti, P. Picchi, M. Price, A. Pullia, S. Ragazzi, M. Rollier, O. Saavedra, . Satta, L. Trasatti and L. Zanotti.

I - INTRODUCTION

The detector installed in the Mont Blanc tunnel has been operated from the end of May '82 for more than 5300 hours of live time. Preliminary results have been published elsewhere¹⁾. Hereafter, the site, the laboratory and the detector will be shortly described, while more details will be given on tests done at CERN with e , π and ν beams and on data collected up to now at Mont Blanc.

II - THE SITE

The detector is installed in a so called "garage" beside the road tunnel under the Mont Blanc. The overburden of the laboratory has a complicated shape (Fig.1), but it is in every direction larger than $4.5 \cdot 10^3$ m of water equivalent. The dimension and the layout of the laboratory are sketched in Fig.2, from which it appears that the detector size is the largest compatible with the room available.

III - THE DETECTOR

The detector (Fig.3) is a tracking digital calorimeter; it is essentially a sandwich of iron layers, 1 cm thick (0.6 rad. length), interleaved with limited streamer tubes, the active elements of the detector. These tubes, developed in Frascati²⁾, $.9 \times .9$ cm² in cross section and 3.5 m long, are always active and show many suitable properties for such an experiment. These properties can be summarized as follow:

gas mixture: these tubes can be operated with non expensive gas mixtures (presently CO₂, Ar and n-pentane) and they need a very low flow rate (1 volume/3-6 days)

plateau: they show a large voltage plateau (~ 500 V)

read-out: they can be read by external pick-up strips in our case, allowing a bidimensional read-out (Fig.4) which is essential in pattern reconstruction.

The detector size is $\sim 3.5 \times 3.5 \times 3.5$ m³ and its total mass is ~ 150 tons ($\langle \delta \rangle \approx 3.5$ g/cm³); the number of limited streamer tubes is ~ 43.000 and that of read-out channels is ~ 82000 .

Signals from strips are amplified, discriminated and stored for 7 μ s in a shift-register; moreover a prompt OR among the basic unit of 32 strips is generated and it is used for triggering purposes.

Triggers are generated as follows:

- A general OR among all the signals from the y strips of an entire layer of 320 tubes (one plane) is generated. If two contiguous planes give an OR signal within 2 μ s, the complete pattern of OR signals from all the planes is analyzed. At present we define "good trigger" a configuration of OR signals from:

- four contiguous planes
- three contiguous planes plus two other contiguous planes
- three couples of contiguous planes

or more complicated patterns.

The OR rate from a single plane is ~ 320 Hz, while the trigger rate is $\sim 6/\text{hour}$ and it is mainly due to ^{60}Co contamination in iron, natural radioactivity and atmospheric muons.

It must be remarked that the minimum trigger can be generated by quite a small energy deposition; for instance a μ of ~ 100 MeV can trigger the read-out.

Starting from the beginning of August a new piece of data has been added to the previous ones. Whenever a "good trigger" is recorded, a clock for each plane is started, and it stops only either when the first hit is recorded from that plane or when it is reset by the computer. This procedure allows to store the relative time delay of hits and eventually the one that comes from the decay of a muon stopping inside the detector. Efficiency for μ^- is almost 0 (due to the μ^- being absorbed in Fe nuclei before decay), while it is $\sim 35\%$ for μ^+ ; time resolution is ≈ 100 nsec. In this way we can say in 17% of the cases which way the track goes, and its charge.

IV - TESTS

During '81 a test module with the same features (1 cm iron plates, 3.5 m long tubes, same electronic ...) as the Mont Blanc detector, but smaller dimensions (30 plates, ~ 3000 read-out channels) was exposed to e , π and ν beams (details are reported in ³).

Electron and pion data are used for calibration purposes, while the neutrino data are essential to study the unavoidable background due to atmospheric ν interactions. Atmospheric and accelerator ν 's have similar spectra, but accelerator beams contain ν_μ only and have a single direction, while both ν_μ 's and ν_e 's are present in cosmic radiation and enter isotropically the detector.

Our test detector was exposed to an unfocused ν beam from 10 GeV protons, in two geometrical conditions: at 0° (i.e. with beam orthogonal to the iron plates) and 45° . In total ~ 400 events (50% at 0° and 50% at 45°) were collected. They have been classified according to Table I³.

TABLE I

Topology	0°	45°
1 prong	99	110
2 prongs	49	49
> 2 prongs	16	16
one or two prongs with e.m. shower	14	11
neutral current candidates	17	13

A typical 2 prongs and a 3 prongs event are shown in Fig.5.

V - RESULTS

Useful data have been collected in June and July (~ 1050 hours) with 84% of the resistive tubes in operation and from August up to now (~ 4250 h) with the detector fully active.

The collected data are synthetically reported in Table II.

TABLE II

single muons	5825
muons stopping in the detector	58
parallel muons	73
fully contained events	7

This statistics correspond to ~ 90 tons \times year (total mass \times live time)

Examples of these events are shown in Fig.6. Atmospheric muons not only provide an useful and continuous monitoring of the detector, but they also are interesting by themselves. However discussion will be restricted to fully confined events which are directly connected with the problem of nucleon stability.

Some features of the confined events are listed in Table III and they are shown in Fig. 7.

Events from n°1 to n°4 are discussed in ¹⁾ and here we report only the conclusion of that discussion. Events 524-40, 526-122 and 532-9 can easily be interpreted as due to ν interactions and, at present, we assume this interpretation as the most probable. Event 503-19 cannot easily be interpreted as due to a ν interaction because of its pattern and energy-momentum mismatch. Note that only 6% of the ν induced events in the test run are three prongs event.

In conclusion less than 0.05 event like this one is expected. On the other

TABLE III

ev. number	date	n° of tracks	total energy (GeV)	total momentum (GeV)	possible interpretation
1 503-19	July 23 th '82	3	~ .90	~ 0.4	p-decay
2 524-40	Aug. 1 st	3	1.300 ± .200		ν_μ or ν_e anelastic int.
3 526-122	Aug. 4 th	1 (?)	.370 ± .020	.350 ± .020	elastic ν_μ interaction
4 532-9	Aug. 6 th	1	.330 ± .015	.330 ± .015	"
5 1062-133	Jan. 9 th '83	1	1.500 ± .150	1.500 ± .150	elastic ν_μ interaction
6 1091-338	Feb. 2 nd	1+2	≥ .800	-	?
7 1095-10	Feb. 25 th	2	.720 (if $\mu\pi$)	.420	two prongs ν interaction

hand, this event is kinematically compatible with the hypothesis $p \rightarrow \mu^+ K^0$ or $p \rightarrow 3\mu$ decay, if one take into account Fermi motion on nucleons.

Interpretation of this event as due to $n \leftrightarrow \bar{n}$ oscillation and subsequent \bar{n} annihilation is under investigation, but it seems quite unlikely.

Ev. 1062-133 is probably a single μ and can be interpreted as an elastic ν interaction. Ev. 1091-338 shows a complicated pattern and cannot be easily interpreted; it fits badly the ν hypothesis as the n decay hypothesis; in any case (at least at this stage of the analysis) it cannot be used to prove the existence of the nucleon decay process.

Ev. 1095-10. It is a 2 prongs event and can be interpreted as an inelastic ν interaction. The decay $n \rightarrow \nu K^0$ does not fit well because the $\pi^+ \pi^-$ energy and invariant mass, as measured from the two prongs, are larger than expected in the hypothesis of n decay at rest.

VI - CONCLUSIONS

The detector is working with a pretty good efficiency since June 1982.

Analysis of muon (single and multiple) events is in progress; we expect to extract from these data information on the energy distribution and composition of the primary cosmic rays.

Seven confined events (with visible energy greater than 150 MeV) have been observed; six of them can be interpreted as ν_μ or ν_e interactions; their number is in agreement with expectation based on atmospheric ν energy spectrum and flux. One event can be hardly explained as ν interaction, while it fits well the p decay hypothesis, but prior to state firmly the existence of nucleon decay process, other candidates must be observed. If one assumes the Ev. 503-19 is a

genuine p-decay, the nucleon mean life comes out to be $\sim 2 \cdot 10^{31}$ years; if it is assumed to be a ν induced event, the lower limit for τ/B , where B is the branching ratio for decay channels where most of the nucleon mass appears in "visible" particle (μ, π, K^+, K^0 etc...) is $\sim 10^{31}$ years.

REFERENCES

- (1) G. Battistoni et al., Phys. Lett. 118B, 461 (1982).
- (2) G. Battistoni et al., Nucl. Instr. and Methods 152, 423 (1978)
ib. 164, 57 (1979) "Resistive cathod transparencies" in press.
- (3) G. Battistoni et al., "An experimental study of the neutrino background in underground experiments on nucleon decay" preprint.

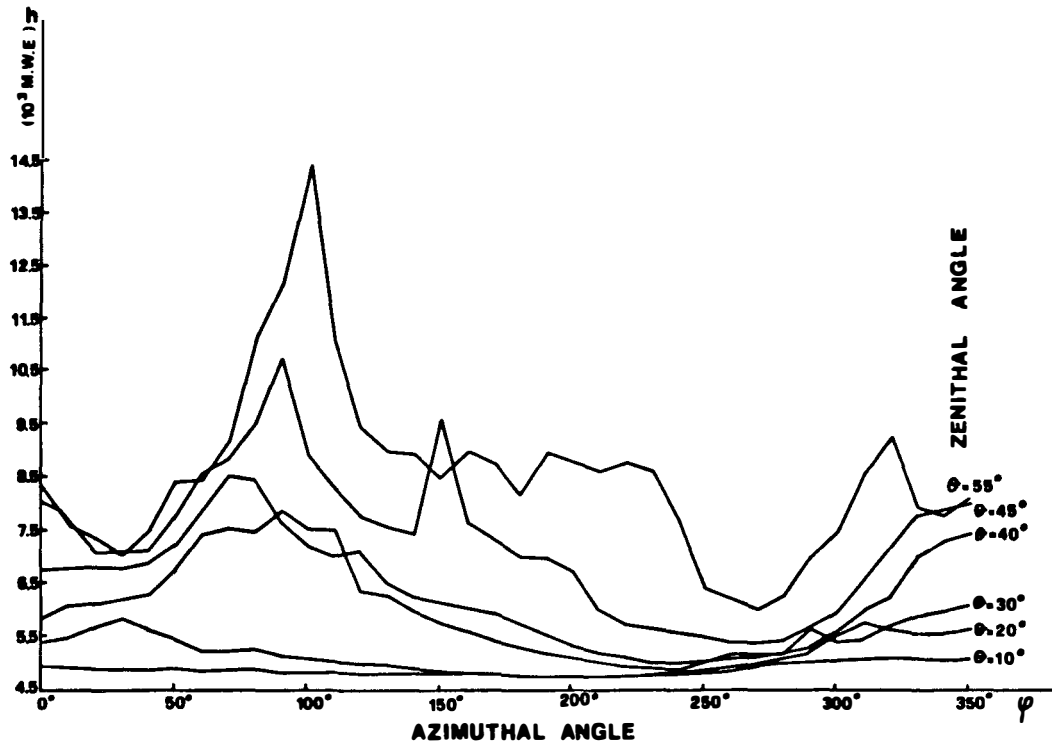


Fig. 1. Overburden as a function of zenithal and azimuthal angles.

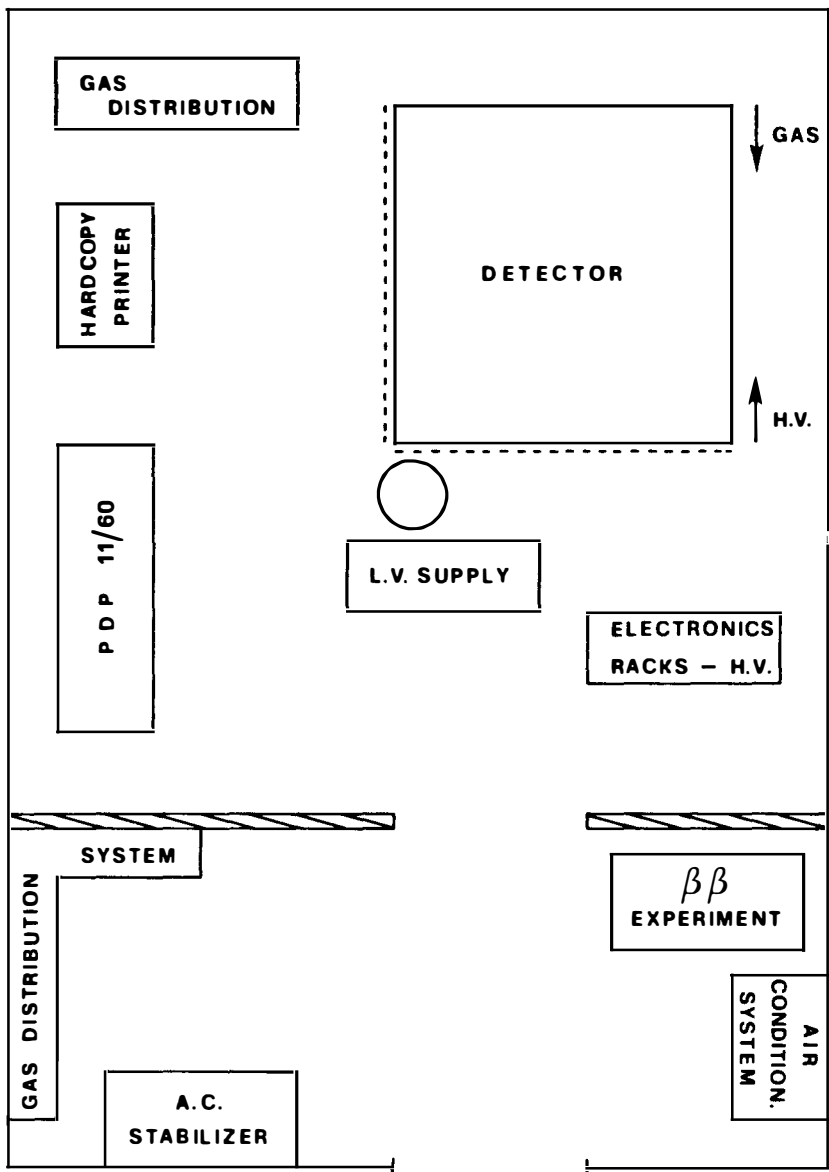


Fig. 2. Layout of the "garage".

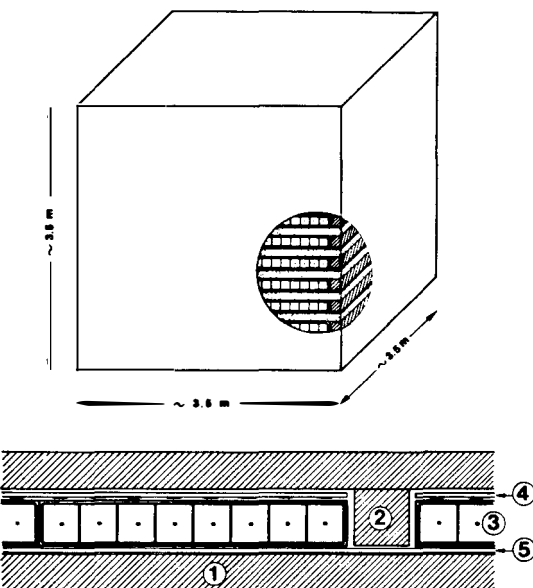


Fig. 3. a) Sketch of the detector.
 b) Details of the detector: 1) iron slab, 2) iron spacer, 3) limited streamer tubes, 4) longitudinal strips, 5) transversal strips.

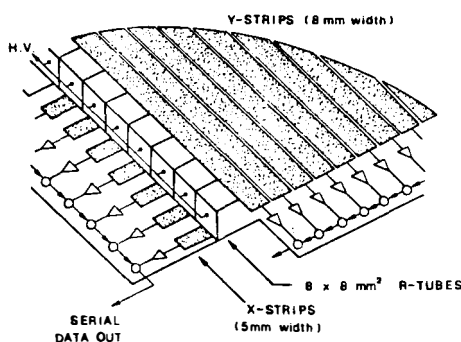
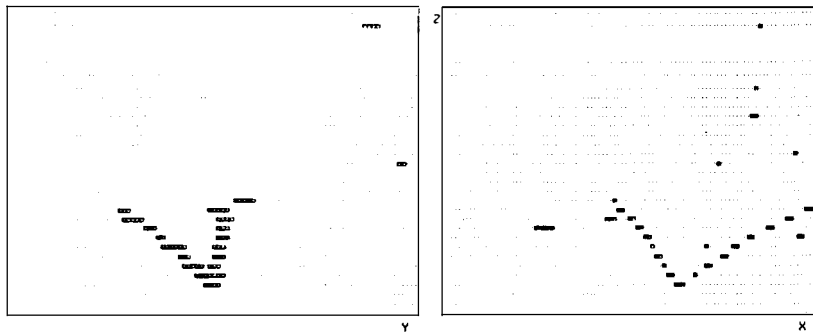


Fig. 4. Read-out strips.

NEUTRINO BEAM

RUN # 307 EVENT # 16822



NEUTRINO BEAM

RUN # 304 EVENT # 24168

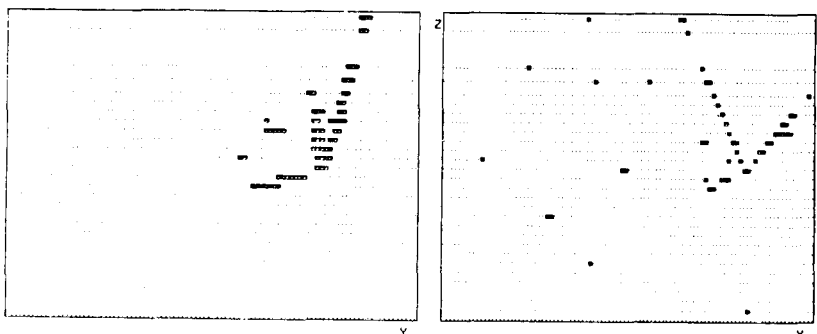


Fig. 5. Examples of a) 2 prongs event; b) 3 prongs event in the test module.

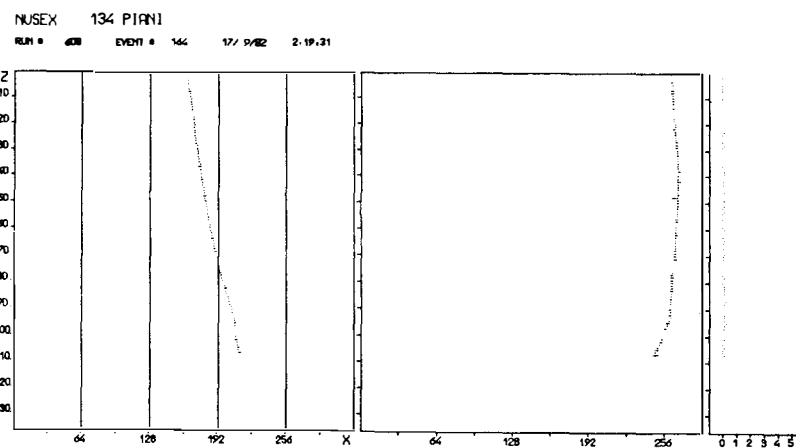
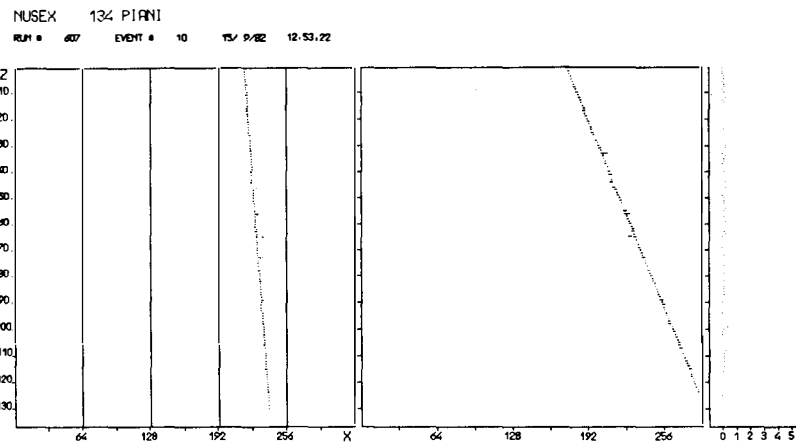


Fig. 6. Examples of a) single muon, b) stopping muon; two views and time are shown.

NUSEX 134 PIANI
 RUN # 596 EVENT # 20 10/9/82 13:58:15

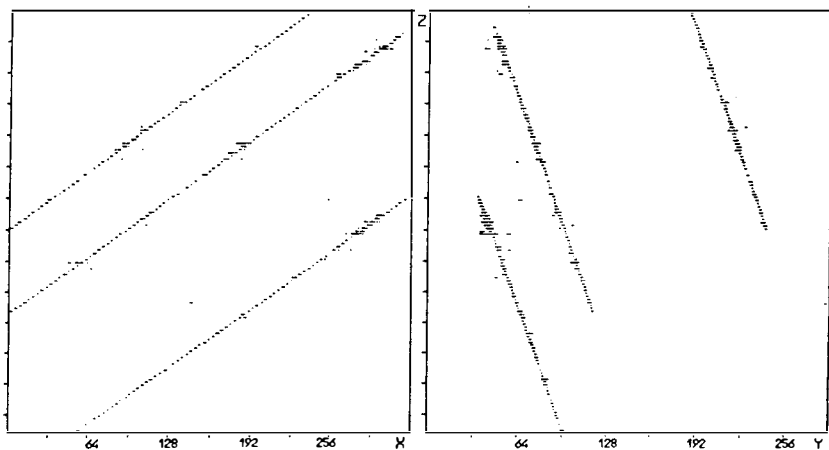


Fig. 6 c). Parallel muons.

NUSEX 112 PIANI
 RUN # 503 EVENT # 19 23/7/82 12:24:34

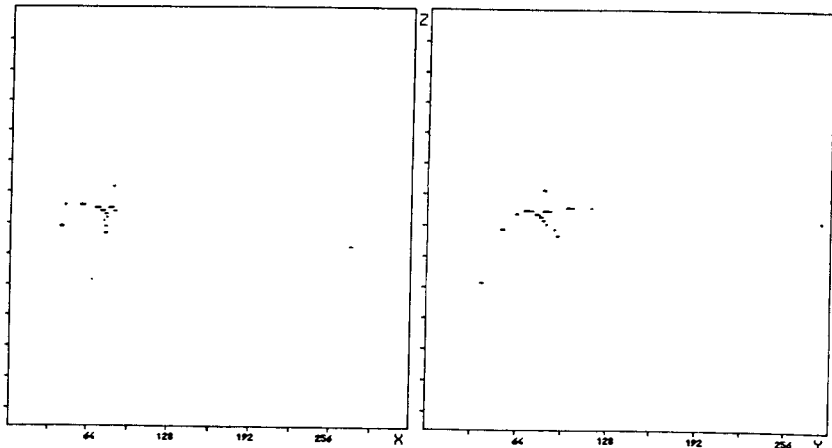
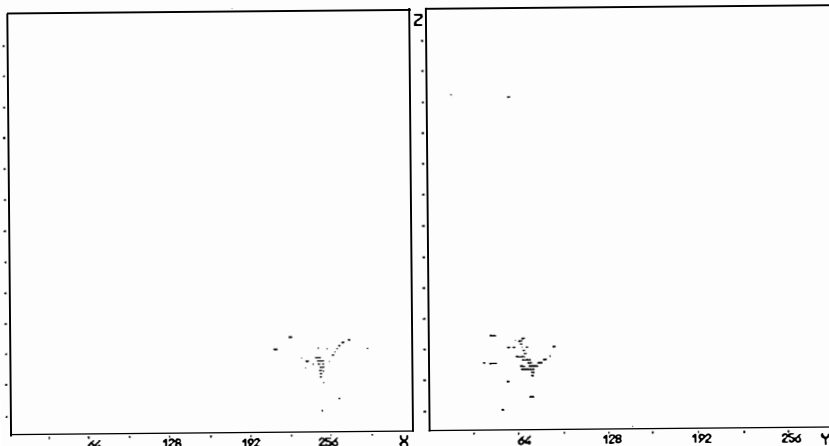


Fig. 7 a). Confined events (see text).

NUSEX 134 PIANI
RUN # 526 EVENT # 40 1/8/82 17:9:0



NUSEX 134 PIANI
RUN # 526 EVENT # 122 4/8/82 7:41:34

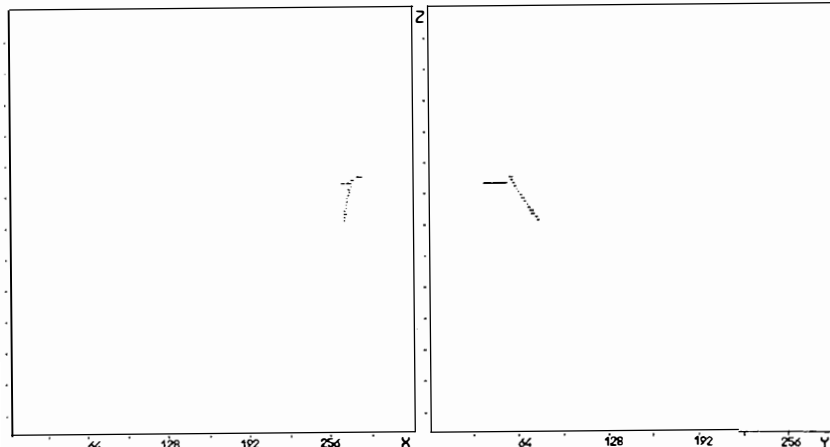
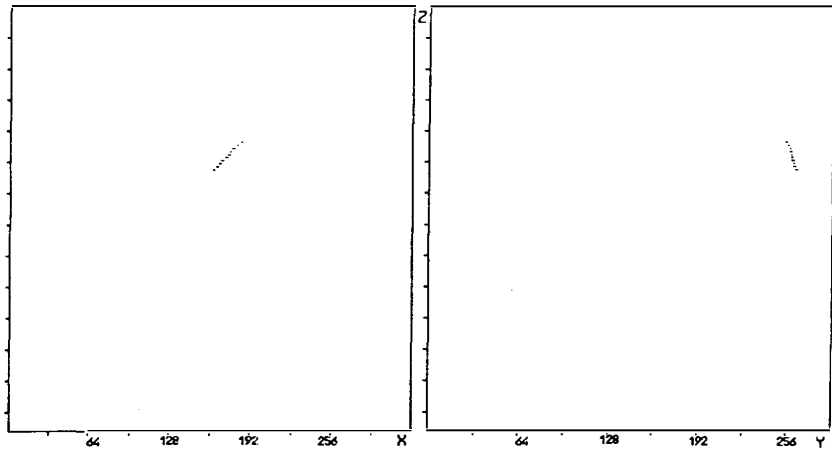


Fig. 7 b) c). Confined events (see text).

NUSEX 134 PIANI
RUN # 532 EVENT # 9 6/8/82 20:31:42



NUSEX 134 PIANI
RUN # 1062 EVENT # 133 9/1/83 7:41:45

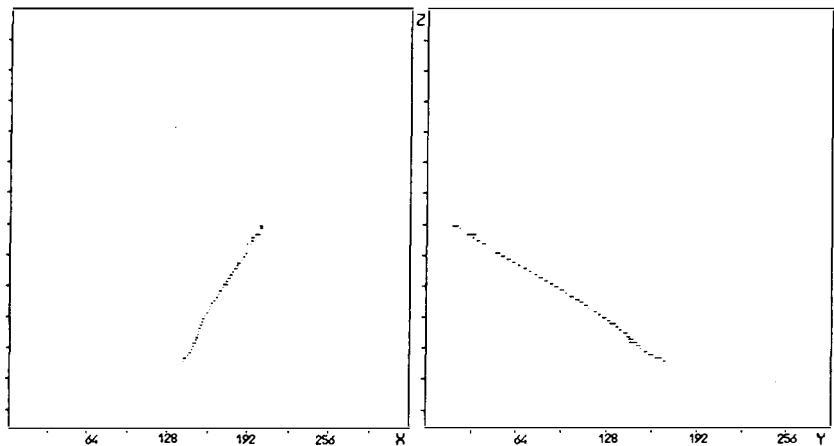
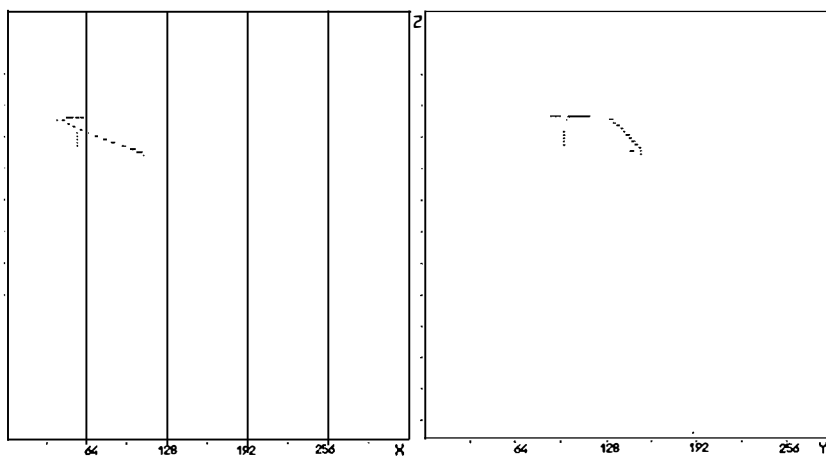


Fig. 7 d) e). Confined events (see text).

NUSEX 134 PIANI

RUN # 1091 EVENT # 338 15/2/83 14:50, 5



NUSEX 134 PIANI

RUN # 1095 EVENT # 10 25/2/83 1:54, 5

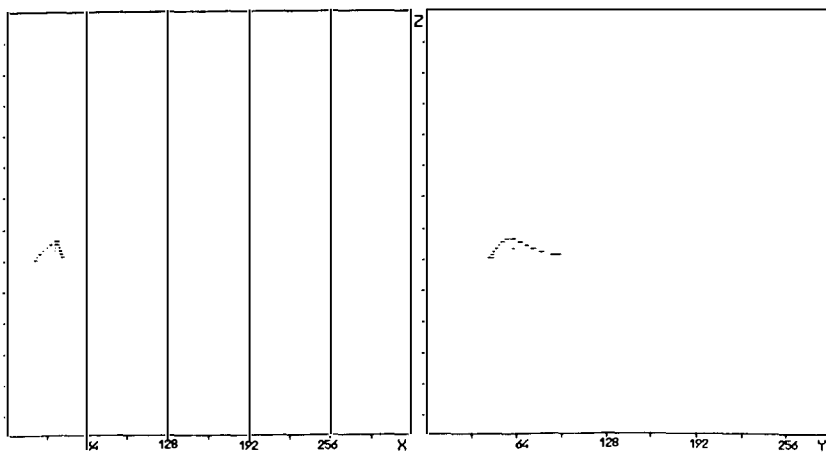


Fig. 7 f) g). Confined events (see text).

TWO-BODY PROTON DECAYS IN SU(5)

T. N. PHAM

Centre de Physique Théorique
Ecole Polytechnique, 91128 - Palaiseau Cedex FranceABSTRACT

Assuming a resonance parametrisation to extrapolate the soft pion amplitude to the physical region, we find that meson-nucleon resonance effects suppress most of the Current Algebra $p \rightarrow \eta e^+$ decay amplitude but only slightly modify other decay amplitudes. The decays $p \rightarrow \omega e^+$ and $p \rightarrow \rho^0 e^+$ are also computed using the divergence of the vector currents (or Born term). In the standard SU(5) model, the decay $p \rightarrow \pi^0 e^+$, $p \rightarrow \omega e^+$, and $p \rightarrow K^0 \mu^+$ are the most important modes with branching ratios 40%, 10% and 6% respectively. From the nonrelativistic harmonic oscillator wave function, the proton lifetime is found to be $\tau(p) = 1.02 \times 10^{29}$ yrs for $M_X = 4 \times 10^{14}$ GeV.

In view of the recent results¹ on proton decays it is important to have a reliable theoretical prediction of the proton lifetime less subjected to uncertainties associated with our incomplete knowledge of hadron matrix elements. In this talk, I would like to report on a new calculation of the two-body decay rates of the proton within the standard theory² SU(5) done in collaboration with Y. Dupont and T.N. Truong at the Centre de Physique Théorique de l'Ecole Polytechnique³. Previous calculations of the proton decays are based on the quark fusion model useful in obtaining the inclusive decay rates⁴ (i.e. $p \rightarrow e^+ X$) which are insensitive to the detailed dynamics of the outgoing quarks but questions could be raised on its reliability because of the low value of proton mass. In this way the current estimate for the proton lifetime is in the range $10^{30} - 10^{31}$ yrs which are on the boundary of experimental limits. More information can also be learned from the exclusive two-body decay modes, especially their branching ratios which are independent of the grand unification mass M_X and serve to distinguish between various versions of Grand Unified Theories (GUT). The quark fusion model has also been used to obtain the exclusive two-body decay rates⁵ and the results indicate that relativistic effects are important and a better treatment less dependent on the quark dynamics is required. For two-body decays with a pseudoscalar meson (π, K, η) in the final state, Current Algebra combined with Dispersion Relation seem to be most appropriate for this purpose. Unlike the case of Hyperon S-wave nonleptonic decays where corrections to soft pion amplitude are less important, the two-body decays of proton with an anti-lepton (e^+, μ^+) and a pseudoscalar meson in the final state requires a large extrapolation from the soft pion limit ($p_e^2 = m_p^2$) to the physical region ($p_e^2 = m_e^2 \approx 0$). Since the decay amplitudes involve only one hadron in the final state, the extrapolation can be done in a simple manner by multiplying the soft pion amplitude by the usual Omnès function $D^{-1}(t)$ evaluated at $t = p_e^2 \approx 0$ which could produce important corrections to the soft pion amplitude because of resonance effects in the meson-nucleon systems (The so-called hard pion correction). With this correction factor taken into account, the two-body decay amplitudes can be calculated in terms of the $e^+ - p$ transition matrix element from which SU(6) - like algebraic relations between different decay amplitudes are derived. This is the only model-dependent quantity which can be obtained from the 3-quark proton wave function and for convenience we shall use the standard 3-quark non-relativistic harmonic oscillator wave function. Although the absolute decay rates depend on the detailed form of the wave function, the ratio between different decay amplitudes are determined mainly by its spin-isospin part and are therefore model independent to a good approximation. I shall now describe the calculations and present the results we obtained.

Consider for example the decay mode $p \rightarrow \pi^0 e^+$ which is one of the most important mode and the easiest to observe in current experiments. As with the case of non-leptonic decays of hyperons, Current Algebra and soft pion technique must be used to reduce the decay amplitude to the $e^+ - p$ transition matrix element $\langle e^+ | \mathcal{L}_X(0) | p \rangle$ which is simpler to handle than the decay amplitude itself.

The decay amplitude for $p \rightarrow \pi^0 e^+$ is given by

$$\mathcal{M}_L(p, k, q) = \langle e^+ \pi^0 | \mathcal{L}_X(0) | p \rangle \quad (1)$$

with p, k, q are respectively the momenta of the proton, the outgoing positron and pion. $\mathcal{L}_X(0)$ is the effective Lagrangian for the baryon number-violating interactions which are mediated by the exchange of a superheavy gauge boson X in Grand Unified Theories (GUT). In SU(5) it is given by²

$$\begin{aligned} \mathcal{L}_X = & \frac{4G\lambda}{\sqrt{2}} \epsilon_{ijk} [\bar{u}_{kL}^c \gamma_\mu u_{jL} (2\bar{e}_L^+ \gamma_\mu d_{iL} + \bar{e}_R^+ \gamma_\mu d_{iL} \\ & + \bar{\mu}_L^+ \gamma_\mu s_{iL} + \bar{\mu}_R^+ \gamma_\mu s_{iR}) \\ & + \bar{u}_{kL}^c \gamma_\mu d_{jL} (\bar{v}_{eR} \gamma_\mu d_{iR} + \bar{v}_R^c \gamma_\mu s_{iR})] \end{aligned} \quad (2)$$

G is the effective coupling constant defined by

$$G = g_{\text{GUT}}^2 / 4\sqrt{2} M_X^2$$

and λ is the short-distance QCD enhancement factor ($\lambda = 3.7$). Defining

$$\mathcal{M}_L(p, k, q) = \bar{u}_{e+}(k) \Gamma(k, q) u(p) \quad (3)$$

In the soft pion limit ($q \rightarrow 0, k \rightarrow p$) with the positron momentum taken off the mass shell ($k^2 + p^2 = m_p^2$), using PCAC and standard Current Algebra technique, we have :

$$\Gamma(p, q) u(p) = \frac{-i\sqrt{2}}{f} \frac{1}{\pi} [\langle 0 | [Q_3^5, \eta(0)] | p \rangle + q_\mu \mathcal{M}_\mu(p, q)] \quad (4)$$

where

$$-M_\mu(p, q) = -i \int d^4x \exp(iq \cdot x) \langle 0 | T\{\eta(0) A_{3\mu}(x)\} | p \rangle$$

$\eta(x)$ is a "current" associated with the positron (in analogy with the e.m. currents) given by

$$\eta(x) = \frac{\delta \mathcal{L}_X}{\delta e^+} \quad (5)$$

The M_μ - term receives a contribution from the proton-pole which is singular as $q_\mu \rightarrow 0$. It can be shown that $q_\mu M_\mu$ satisfies the dispersion relation with the absorptive part given by unitarity which we shall need in extrapolating the soft-pion amplitude to the physical region (i.e. hard pion corrections).

The regular part of $\Gamma(k, q)$ can be found by subtracting the Born term from the l.h.s. and the r.h.s. of Eq. (4). (This is the standard prescription used in similar cases when the Born term is present as in hyperon non-leptonic decays⁷). Thus in the limit $q_\mu \rightarrow 0$, the amplitude is well defined in the neighbourhood of $t = m_p^2$ and is given by :

$$\Gamma(k, q) = \Gamma(k, q)_{\text{regular}} + \Gamma(k, q)_{\text{pole}} \quad (6)$$

with $(f_\pi = M_\pi$ the pion decay constant).

$$\begin{aligned} \Gamma(k, q)_{\text{regular}} u(p) &= \frac{-i\sqrt{2}}{f_\pi} [\langle 0 | [Q_3^5, \eta(0)] | p \rangle \\ &+ (q_\mu M_\mu + \frac{f_\pi}{i\sqrt{2}} \Gamma(k, q)_{\text{pole}} u(p))] + O(t - m_p^2) \end{aligned} \quad (7)$$

Using the Goldberger-Treiman relation for G_A/G_V , we obtain in the neighbourhood of $t = m_p^2$:

$$\Gamma(k, q) u(p) = [F(t) + iG(t)] u(p) \quad (8)$$

with

$$F(t) = \frac{-i\sqrt{2}}{f_\pi} [(a' + b' \gamma_5) + g_{App} (a \gamma_5 + b) (1 + \frac{2m_p^2}{t - m_p^2})] \quad (9 \text{ a})$$

$$G(t) = \frac{i\sqrt{2}}{f_\pi} (a \gamma_5 + b) \frac{2m_p^2 g_{App}}{t - m_p^2} \quad (9 \text{ b})$$

$G(t)$ contributes to the decay amplitude terms proportional to the lepton mass and thus can be neglected. The virtual $e^+ - p$ transition matrix elements are defined as :

$$\langle 0 | \eta(0) | p \rangle = (a + b\gamma_5) u(p) \quad (10 \text{ a})$$

$$\langle 0 | [Q_3^5, \eta(0)] | p \rangle = (a' + b'\gamma_5) u(p) \quad (10 \text{ b})$$

g_{App} is the axial vector current matrix element between proton states.

By letting $t = \frac{m_e^2}{p^2} \approx 0$ in Eqs.(9) we obtain the physical decay amplitude. This is the standard Current Algebra result⁸⁻¹⁰. Because of the S and P wave resonances of the meson-nucleon system in the $1.4 \sim 1.7$ GeV region, the extrapolation of (9) to $t = 0$ may be strongly affected by these resonances which must now be taken into account. Let us define ($t = k^2$)

$$\Gamma(k, q) u(p) = (A(t) + B(t)\gamma_5 + \frac{1}{2} G(t)) u(p)$$

where $A(t)$ and $B(t)$ satisfy dispersion relation in t with a cut starts from $t_0 = (m_\pi + m_p)^2$ to ∞ and satisfy low energy theorem given by (9). The final state theorem requires that, on the cut and below the inelastic threshold, $A(t)$ and $B(t)$ have, respectively the phases of S - and P - wave πN phase shifts (S_{11} and P_{11}). These phase shifts are small near t_0 but become large at higher energy. There are two S_{11} resonances at 1.55 and 1.65 GeV. The P_{11} resonances is at 1.7 GeV. They are all fairly inelastic and couple to both the πN and ηN channels. The general treatment of the integral equations for $A(t)$ and $B(t)$ is complicated⁶. It is simpler to assume the dominance of these resonances in the form factors $A(t)$ and $B(t)$. We shall simulate the effect of the two S_{11} resonances as a simple pole at $\frac{m_a^2}{m_p^2}$ and the P_{11} resonance at $\frac{m_b^2}{m_p^2}$. We have

$$A(t) = -\frac{i/2}{f_\pi} \left[(a' + g_{App} b) \left(1 + \frac{2m_p^2}{t-m_p^2} - \frac{2m_p^2}{m_a^2 - m_p^2} \right) \left(\frac{\frac{m_a^2 - m_p^2}{2}}{\frac{m_a^2}{2} - t} \right) \right]$$

$$B(t) = -\frac{i/2}{f_\pi} (b' + g_{App} a) \left(1 + \frac{2m_p^2}{t-m_p^2} - \frac{2m_p^2}{m_b^2 - m_p^2} \right) \left(\frac{\frac{m_b^2 - m_p^2}{2}}{\frac{m_b^2}{2} - t} \right) \quad (11)$$

Note that the above expressions satisfy current algebra constraint at $t = \frac{m_p^2}{m_p^2}$

and also generate terms of the order $O(t - \frac{m^2}{p})$ as corrections to soft pion amplitudes. The physical decay amplitudes are obtained by setting $t = 0$. Eq. (11) can be easily applied to other decay modes. Using the non relativistic quark model with harmonic oscillator wave function, we obtain :

$p \rightarrow \pi^0 e^+$:

$$\begin{aligned} A(0) &= \frac{3}{2} g [1 + D + F - (1 - D - F) \frac{\frac{m^2}{p}}{\frac{m^2}{a}}] \\ B(0) &= \frac{1}{2} g [1 + D + F - (1 - D - F) \frac{\frac{m^2}{p}}{\frac{m^2}{b}}] \end{aligned} \quad (12)$$

$p \rightarrow \pi^+ \bar{\nu}_e$:

$$\begin{aligned} A(0) &= -\frac{g}{\sqrt{2}} [1 + D + F - (1 - F) \frac{\frac{m^2}{p}}{\frac{m^2}{a}}] \\ B(0) &= -\frac{g}{\sqrt{2}} [1 + D + F - (1 - D - F) \frac{\frac{m^2}{p}}{\frac{m^2}{b}}] \end{aligned} \quad (13)$$

$p \rightarrow K^0 \mu^+$

$$A(0) = -\sqrt{2}g [(1 + D - F) - (1 + F - D) \frac{\frac{m^2}{p}}{\frac{m^2}{a}}]; B(0) = 0 \quad (14)$$

$p \rightarrow K^+ \bar{\nu}_\mu$

$$A(0) = -\frac{g}{3\sqrt{2}} D (1 + \frac{\frac{m^2}{p}}{\frac{m^2}{a}}); B = A \quad (15)$$

$p \rightarrow \eta e^+$

$$\begin{aligned} A(0) &= -\frac{\sqrt{3}}{2} g [(1 + D - 3F) - (1 + 3F - D) \frac{\frac{m^2}{p}}{\frac{m^2}{a}}] \\ B(0) &= -\frac{1}{2\sqrt{3}} g [(1 + D - 3F) - (1 + 3F - D) \frac{\frac{m^2}{p}}{\frac{m^2}{b}}] \end{aligned}$$

The Current Algebra results given by the 1st terms agree with previous calculations.

$$g = \frac{\sqrt{2} \kappa}{f_\pi}, \quad \kappa = 12\lambda \left(\frac{Gm_p^2}{\sqrt{2}} \right) \left(\frac{\omega}{3\sqrt{3} \pi m_p} \right)^{3/2} m_p$$

and D, F are the current value of G_A/G_V :

$$D + F = |G_A/G_V| = 1.25 \pm 0.01$$

$$D = 0.44, \quad F = 0.81$$

(ω is the oscillator level spacing and has a value about 520 MeV). As can be seen from (16), there is an important correction to soft pion result for $p \rightarrow n e^+$ because of the 2nd term. This produces a very large suppression of the amplitude relative to the soft pion value by a factor of 10. For other decay modes, corrections to soft pion amplitudes are less important. These corrections increase the amplitudes for $\pi^0 e^+$, $K^+ \bar{\nu}_\mu$ modes by 5% and 40% respectively but suppresses the $K^0 \mu^+$ mode by 15% and thus have no appreciable effects on the total two-body decay rates which are dominated by the $\pi^0 e^+$ and $\pi^+ \bar{\nu}_e$ modes. Below are their relative rates which are independent of the spatial part of the non relativistic 3-quark wave function at the origin as well as the super heavy gauge boson mass M_X :

$$\begin{aligned} \Gamma(p \rightarrow \pi^+ \bar{\nu}_e) &= 0.40 \Gamma(p \rightarrow \pi^0 e^+) \\ \Gamma(p \rightarrow n e^+) &= 2.4 \times 10^{-4} \Gamma(p \rightarrow \pi^0 e^+) \\ \Gamma(p \rightarrow K^0 \mu^+) &= 0.14 \Gamma(p \rightarrow \pi^0 e^+) \\ \Gamma(p \rightarrow K^+ \bar{\nu}_\mu) &= 0.56 \times 10^{-2} \Gamma(p \rightarrow \pi^0 e^+) \end{aligned} \quad (17)$$

Our relative rates seem to agree qualitatively with the values given by Kane and Karl⁵ using the relativistic quark fusion model. Thus using the standard resonance parametrisation, we have been able to extrapolate the soft pion amplitude to the physical region in a simple manner. This is a large improvement over the Current Algebra Result⁸⁻¹⁰. To the extent that this resonance parametrisation is valid, our relative decay rates (Eq. (17)) are essentially model independent.

In the same spirit we can compute the decay rates $p \rightarrow \omega e^+$ and $p \rightarrow \rho^0 e^+$. The basic idea is to consider the $e^+ - p$ matrix elements of the isoscalar and iso-vector vector currents associated with ω and ρ^0 defined as :

$$\begin{aligned}
 \langle e^+ | v_\mu(0) | p \rangle &= \bar{u}_{e^+}(k) [\gamma_\mu (g_V(q^2) + \gamma_5 g_A(q^2)) \\
 &\quad + i \frac{\sigma_{\mu\nu} q_\nu}{m_p} (f_V(q^2) + \gamma_5 f_A(q^2)) u(p)]
 \end{aligned} \quad (18)$$

The matrix element for $p \rightarrow ve^+$ ($v = \rho^0, \omega$) are defined similarly by :

$$m(p \rightarrow ve^+) = \varepsilon_\mu \bar{u}_{e^+}(k) [\gamma_\mu (g_V + \gamma_5 g_A) + i \frac{\sigma_{\mu\nu} q_\nu}{m_p} (f_V + \gamma_5 f_A)] u(p) \quad (19)$$

The charge form factor at $q^2 = 0$ can be easily found using the divergence condition

$$\begin{aligned}
 \partial_\mu v_\mu^\omega &= [Q^\omega, \mathcal{L}_X] = -\frac{3}{2} \mathcal{L}_X \\
 \partial_\mu v_\mu^0 &= [Q_3, \mathcal{L}_X] = -\frac{1}{2} \mathcal{L}_X
 \end{aligned}$$

from which we obtain the charge coupling using vector meson dominance (VMD) approximation :

$$\begin{aligned}
 g_V^\omega + \gamma_5 g_A^\omega &= -\frac{3}{2} \frac{(a+b\gamma_5)}{m_p} \frac{m_\rho^2}{f_\rho} \\
 g_V^0 + \gamma_5 g_A^0 &= -\frac{1}{2} \frac{(a+b\gamma_5)}{m_p} \frac{m_\rho^2}{f_\rho}
 \end{aligned} \quad (20)$$

This gives

$$\Gamma(p \rightarrow \omega e^+) = 9 \Gamma(p \rightarrow \rho^0 e^+) \quad (21)$$

which is the non relativistic quark model result⁵. Since the outgoing positron is energetic, the magnetic terms (f_V, f_A) may be important. These terms cannot be obtained from the above divergence condition but a nucleon pole approximation (Born term) shows that they are negligible for $p \rightarrow ve^+$ decay but important in $p \rightarrow \rho^0 e^+$ decay because of the large value of the anomalous isovector nucleon magnetic moments.

$$\begin{aligned}
 f_V^0 + \gamma_5 f_A^0 &= -\frac{1}{2} \frac{(a+b\gamma_5)}{m_p} \left(\frac{m_\rho^2}{f_\rho} \right) \left(\frac{\mu_p - \mu_n - 1}{2} \right) \\
 f_V^\omega + \gamma_5 f_A^\omega &= -\frac{3}{2} \frac{(a+b\gamma_5)}{m_p} \left(\frac{m_\rho^2}{f_\rho} \right) \left(\frac{\mu_p + \mu_n - 1}{2} \right)
 \end{aligned}$$

This increases the $p \rightarrow \rho^0 e^+$ decay rate by a large factor. We find

$$\Gamma(p \rightarrow \rho^0 e^+) = 0.9 \Gamma(p \rightarrow \omega e^+) \quad (23)$$

which agrees more or less with the relativistic quark model calculation⁵. For the $p \rightarrow \omega e^+$ decay, using $g_{\rho\pi\pi}^2/4\pi = 2.86$, we find

$$\Gamma(p \rightarrow \omega e^+) = 0.23 \Gamma(p \rightarrow \pi^0 e^+) \quad (24)$$

The 3-body decay mode with the two-pion in the continuum may be a sizeable fraction of the total decay rates. Current Algebra Calculation with $\pi\pi$ final state interactions effects (which increase the rate by 50%) show that^{9,11}

$$\Gamma(p \rightarrow \pi\pi e^+) \approx 0.25 \Gamma(p \rightarrow \pi^0 e^+) \quad (25)$$

Together with other less important decay modes, this leads to :

$$\begin{aligned} \text{B R } (p \rightarrow \pi^0 e^+) &\approx 0.4 \\ \text{B R } (p \rightarrow K^0 \mu^+) &\approx 0.06 \\ \text{B R } (p \rightarrow \omega e^+) &\approx 0.1 \end{aligned} \quad (26)$$

which tell us that the $p \rightarrow \pi^0 e^+$ decay is the most important mode. Using standard quark model parameter and for a typical $M_X = 4 \times 10^{14}$ GeV, this partial rate is

$$\Gamma(p \rightarrow \pi^0 e^+) = 3.92 \times 10^{-30} (\text{yrs})^{-1} \quad (27)$$

giving a proton lifetime

$$\tau(p) = 1.02 \times 10^{29} \text{ yrs} \quad (28)$$

which is two orders of magnitude shorter than the present lower experimental limit.

The main source of uncertainties in the calculation of the decay rates are the values of M_X which depends on the QCD scale parameter $\Lambda_{\overline{\text{MS}}}$ and the quark model parameter for the proton wave function at the origin. The branching ratio given in (26) is however independent of these parameters and may be used to distinguish between various Grand Unified Theories.

I would like to thank Tran Thanh Van and the Organisers of the Conference for the warm hospitality extended to me at Moriond.

REFERENCES AND FOOTNOTES

- [1] J. van der Velde, Report on the IMB experiments, and E. Bellotti, Report on the Mont Blanc experiment, Talks given at this meeting.
- [2] H. Georgi and S. Glashow, Phys. Rev. Lett. 32, 438 (1974); A. Buras et al., Nucl. Phys. B135, 66 (1978).
For a recent review, see P. Langacker, Phys. Rep. 72, 187 (1981).
- [3] Y. Dupont, T.N. Pham and Tran N. Truong, Ecole Polytechnique, preprint CPT A538.0183. Full details of the calculation is given in this paper.
- [4] A. Buras et al., quoted in Ref. 2.
- [5] M.B. Gavela et al., Phys. Rev. D23, 1580 (1981).
G. Kane and G. Karl, Phys. Rev. D22, 2808 (1980).
Refernices to previous works can be found in P. Langacker, Ref. 2.
- [6] G.R. Farrar, Phys. Rev. D4, 212 (1971); T. N. Pham and Tran N. Truong, Phys. Rev. D16, 896 (1977).
- [7] This prescription is given in R.E. Marshak, Riazuddin and C.P. Ryan, Theory of Weak Interactions in Particle Physics, Wiley and sons, New York NY (1969), p. 580.
- [8] Y. Tomozawa, Phys. Rev. Lett. 46, 463 (1981).
- [9] M. Claudson, M.B. Wise and L.J. Hall, Nucl. Phys. B195, 297 (1981).
- [10] Similar result is given by V. Bererinsky, I. Ioffe and Ya. Kogan, Phys. Lett. 105B, 33 (1981). I would like to thank P. Langacker for informing me of this work.
- [11] M.B. Wise, R. Blankenbecler and L. Abbott, Phys. Rev. D23, 1591 (1981).

LIMITS ON NEUTRINO-OSCILLATIONS USING
A FINE GRAINED CALORIMETER AT FNAL

D. Bogert, R. Burnstein*, R. Fisk, S. Fuess, J. Morfi.
T. Ohska, M. Peters^X, L. Stutte, J.K. Walker, H. Weerts
Fermi National Accelerator Laboratory
Batavia, Illinois

J. Bofill, W. Busza, T. Eldridge, J.I. Friedman, M. Goodman,
H.W. Kendall, I.G. Kostoulas^O, T. Lyons, R. Magahiz, T. Mattison,
A. Mukherjee, L. Osborne, R. Pitt, L. Rosenson, A. Sandacz,
M. Tartaglia, R. Verdier, S. Whitaker, G.P. Yeh
Massachusetts Institute of Technology
Cambridge, Massachusetts

M. Abolins, R. Brock, A. Cohen, J. Ernwein⁺,
D. Owen, J. Slate
Michigan State University
East Lansing, Michigan

F.E. Taylor
Northern Illinois University
DeKalb, Illinois

Presented by H. Weerts

* Permanent address: Illinois Institute of Technology,
Chicago, Illinois

^X Permanent address: University of Hawaii, Honolulu, Hawaii

^O Permanent address: Hughes Aircraft Co., Los Angeles, California

⁺ Permanent address: CEN-Saclay, Sif-sur-Yvette, France



Abstract

A limit on $\nu_\mu \rightarrow \nu_\tau$ oscillations has been determined in a fine grained calorimeter exposed to the dichromatic neutrino beam at Fermilab. Candidate ν_τ events were selected to fit the hypothesis of ν_τ quasi-elastic scattering followed by a decay of the final state τ -lepton into $e\nu_e\nu_\tau$ or $\mu\nu_\mu\nu_\tau$. Such events typically have missing energy, due to two undetected neutrinos, and consist of a muon track or an electron shower and at most one additional track from the primary vertex. The upper limits on Δm^2 for $\nu_\mu \rightarrow \nu_\tau$ oscillations at maximum mixing are: $\Delta m^2 < 12 \text{ eV}^2$ for the neutrino and $\Delta m^2 < 14.4 \text{ eV}^2$ for the antineutrino case.

I. Introduction

To set a limit on $\nu_\mu + \nu_\tau$ oscillations a search for neutrino interactions with a possible τ -lepton in the final state was performed. Only the purely leptonic decay modes: $\tau \rightarrow \mu \nu_\mu \nu_\tau$ and $\tau \rightarrow e \nu_e \nu_\tau$ were considered. Because of the two neutrinos in the final state there will be energy missing in these events. To ensure the optimal sensitivity to missing energy and to enable a clean electron identification, only events with very low hadronic energy (quasi-elastic type) were accepted. For this class of interactions the neutrino energy can be well approximated by the energy of the final state lepton. In case of a ν_τ interaction however measuring the muon from the τ -decay leads to an underestimation of the neutrino energy. This is illustrated by Fig. 1, which shows the spectrum of muons from a τ -decay with $P_\tau = 30$ GeV/c.

To detect possible missing energy in the final state, the correlation between neutrino energy and radius, provided by the dichromatic beam²⁾ was exploited. Figure 2 shows a Monte Carlo prediction for this correlation for quasi-elastic ν_μ events. Events with missing energy will populate the region below the dense band (π -band) which was therefore the signal region.

The cross-sections for quasi-elastic type ν_μ and ν_τ processes are equal according to theoretical expectation in the energy regime considered. Thus the number of ν_τ candidates and the number of quasi-elastic ν_μ events within the π -band directly determine R , the ratio of ν_τ to ν_μ at the detector position.

II. Detector

The experiment was performed using the fine grained neutrino detector at Fermilab (E594), which has a total mass of 340 tons and consists of 608 flash-chambers and 37 proportional tubes. Here only the detector characteristics relevant to this analysis will be described. Further details can be found in Refs. 3 and 4. The proportional tubes generate a variety of triggers and measure the muon trajectory through the toroidal magnets. The muon momentum resolution for momenta between 20 and 100 GeV/c is 10% and varies slowly with momentum. The flash-chambers which consist of 5x5 mm tubes sample every 22% of a radiation and 3.1% of an absorption length. This fine sampling ensures good angular resolution for muons and showers, good electron

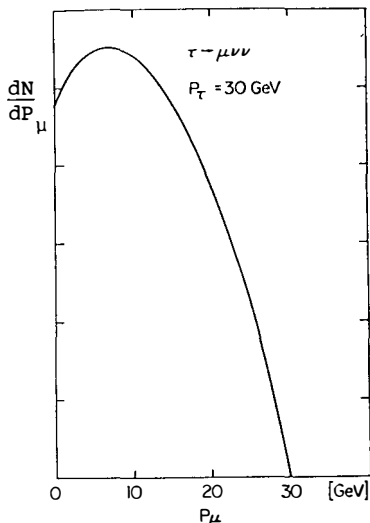


Fig. 1 Muon spectrum from τ -decay.

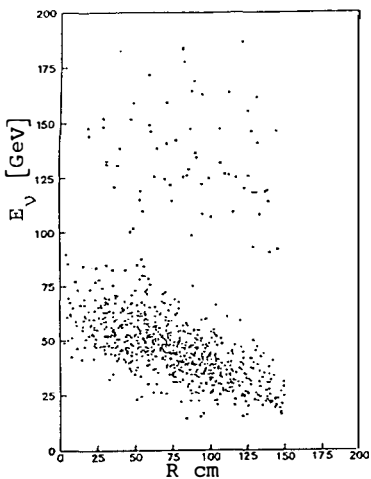


Fig. 2 Monte Carlo E_ν -Radius scatter plot

identification and a clear separation of deep-inelastic type events from quasi-elastic type events (Refs. 3, 4).

III. Data Analysis

The data sample considered here was taken during the 1982 dichromatic run and consists of neutrinos at π and K momenta of 165, 200 and 250 GeV/c and antineutrinos at 165 GeV/c. In the following the selection criteria and results for the muon and electron channels will be described separately.

Muon channel. Only events that satisfied a special trigger were considered for this analysis. The trigger consisted of 2 components: 1) a muon traversing all the toroidal magnets ($P_\mu > 10$ GeV/c) and 2) a maximum pulse height from the proportional tubes, which corresponds to an energy of roughly 10 GeV (a muon traversing the entire calorimeter deposits 5 GeV). The measured average electronic efficiency of this trigger is 86%. An additional cut was made on the number of flash tubes that fired within a 50 cm radius from the vertex. At most 30 hits were allowed in this region, excluding the muon. This selected events with very low hadron energy, whose properties are consistent with quasi-elastic final states.

On an energy versus event radius scatter plot, the above mentioned signal region and π -band were defined as follows: At a given radius a neutrino energy distribution predicted by a beam simulation is described by a mean value and a standard deviation. The π -band was defined as the mean value plus or minus 2.5 standard deviations. The signal region was the area below the π -band. Figure 3 shows the neutrino energy versus radius scatter plot for the data, which should be compared to the Monte Carlo prediction in Figure 2. Figure 4 illustrates the distribution in $Y = (E_b - E_\mu)/E_b$ for data and Monte Carlo, where E_b is the average beam energy at a given radius and E_μ the measured energy of the muon. There is good agreement between data and Monte Carlo.

The following sources were considered as contributing to the background in the signal region:

- i) True quasi-elastic ν_μ events with energies below the π -band, due to the intrinsic spread of the neutrino energy and due to muon momentum resolution. The fraction of true ν_μ quasi-elastic events in the signal region is defined as ϵ_q^s , which is calculated by Monte Carlo to be .012 for all the ν_μ and .013 for the $\bar{\nu}_\mu$ data (see Table I).

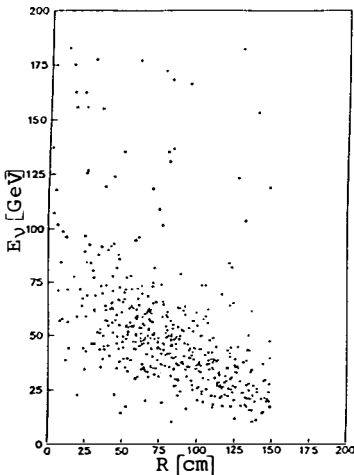


Fig. 3 Data, E_ν -Radius scatter plot.

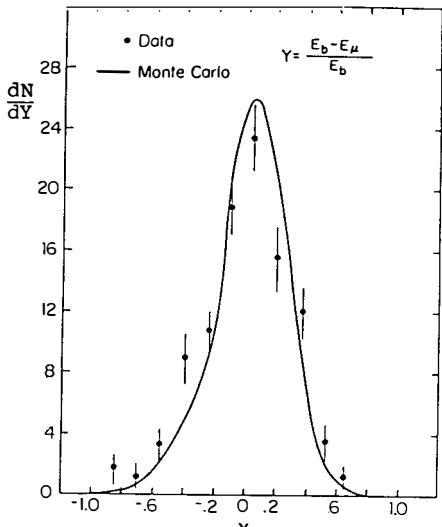


Fig. 4 Y -distribution for data and Monte Carlo.

ii) Wide band background, from π^- and K -decays before the momentum selection. This background was estimated by a Monte Carlo beam simulation and the ratio of wide band flux in the signal region to the total flux in the π -band was found to be 0.3% for neutrinos and 0.6% for antineutrinos.

iii) The inverse muon decay $(\nu_\mu e^- \rightarrow \mu^- \nu_e)$. This process contributes only in the neutrino exposure and was eliminated by requiring $E_\mu \theta_\mu^2 > 3$ Mev (see Ref. 5).

Table I shows the number of events in the π -band and the signal region calculated by subtracting background iii) only. Also shown are the efficiencies to detect an event of a given type in one of the two regions. These efficiencies include acceptances and software efficiencies, while electronic efficiencies cancel in the calculation of R .

Table I

Candidates and detection efficiencies for ν_τ and ν_μ quasi-elastic interactions.

Beam		π -band	Signal region
	Events	640	10
ν_μ	$\epsilon_q(\nu_\mu N \rightarrow \mu^- N')$	$\epsilon_q^b = .82$	$\epsilon_q^s = .012$
	$\epsilon_\tau(\nu_\tau N \rightarrow \tau^- N')$	$\epsilon_\tau^b = .24$	$\epsilon_\tau^s = .12$
		$\downarrow \mu^- \bar{\nu}_\mu \nu_\tau$	
	Events	406	3
$\bar{\nu}_\mu$	$\epsilon_q(\bar{\nu}_\mu N \rightarrow \mu^+ N')$	$\epsilon_q^b = .82$	$\epsilon_q^s = .011$
	$\epsilon_\tau(\nu_\tau N \rightarrow \tau^+ N')$	$\epsilon_\tau^b = .20$	$\epsilon_\tau^s = .13$
		$\downarrow \mu^+ \nu_\mu \bar{\nu}_\tau$	

Electron channel. The electron signal $\tau \rightarrow e \nu_\tau \nu_e$ was searched for using all of the deep-inelastic data without a muon in the final state. All the events were passed through similar software filters as those used for the extraction of the $\nu_\mu e \rightarrow \nu_\mu e$ signal. Details of this procedure have been described in Refs. 3 and 4. The filtered events were then scanned to have an electron shower and at most one additional track in the final state. It should be noted that for the electron channel no missing energy

requirement is made, since the ν_e background is small (<1%), and all events after background subtraction are used to set an upper limit for R. The normalization of this channel is again with respect to the ν_μ quasi-elastic events in the π -band and therefore a 10 GeV minimum energy cut was imposed on the electrons. The efficiency of the detection of the electron-channel relative to the ν_μ normalization sample is $\epsilon_e = 71\%$. This was determined by replacing the hit cell pattern of the muon in the ν_μ quasi-elastic events by that of electron showers from a calibration beam and then scanning these events. In total 34 candidates were found in the ν_μ and 13 in the $\bar{\nu}_\mu$ sample.

The backgrounds contributing to this channel are:

- i) Neutral current events with electromagnetic showers, which simulate electron showers. Applying the analysis to charged current events, ignoring the muon, it was found that this background contributed 22 events in the ν_μ and 3.3 events in the $\bar{\nu}_\mu$ beam.
- ii) ν_e 's from K_{e3} -decays. These neutrinos contribute about 1% to the total flux over the entire dichromatic energy region. The number of such events was estimated from the number of electron events with energy above the π -band. This eliminates 7(ν_μ) and 1($\bar{\nu}_\mu$) events respectively.
- iii) $\nu_\mu e + \nu_\mu e$ - scattering which produces a background sharply peaked at low $E_{e\theta e}^2$. This background was removed by requiring $E_{e\theta e}^2 > 8$ MeV, thus eliminating 5(ν_μ) and 3($\bar{\nu}_\mu$) events respectively.

After all the above backgrounds were subtracted there remained 0 candidates in the ν_μ and 5.7 candidates in the $\bar{\nu}_\mu$ sample. Table II summarizes the electron channel results.

Table II

Summary of the electron channel.		
	ν_μ	$\bar{\nu}_\mu$
Sample after scanning	34	13
Backgrounds:		
i) dense hadron showers	22	3.3
ii) K_{e_3}	7	1
iii) $\nu_\mu e^- + \nu_\mu e^-$	5	3
Signal	0	5.7

IV. Results

Defining R as the ratio of ν_τ to ν_μ in the beam, R^μ and R^e as R multiplied by the branching ratios for $\tau \rightarrow \mu \nu_\mu \nu_\tau$ (18%) and $\tau \rightarrow e \nu_e \nu_\tau$ (16%), the observed number of events for the muon channel in the signal region (N_s) and in the π -band (N_b) can be expressed as:

$$N_s = N_q (R^\mu \epsilon_\tau^s + \epsilon_q^s) \quad (1a)$$

$$N_b = N_q (R^\mu \epsilon_\tau^b + \epsilon_q^b) \quad (1b)$$

The efficiencies ϵ_q^b , etc. are defined in Table I. N_q , the true number of quasi-elastic ν_μ interactions and R can be calculated from equation (1). The contribution of wide band background was neglected in equation (1), but is taken into account in the calculation of R . Similarly, in the electron channel, the number of events in the signal is:

$$N_e = N_q R^e \epsilon_e \quad (2)$$

Table III summarizes the upper limits for R^μ and R^e independently. R^μ is calculated from eqs. 1a and 1b and R^e from eqs. 2 and 1b.

Table III

Upper limits for R^μ and R^e (90% confidence).

Beam	R^μ	R^e
ν_μ	.054	.015
$\bar{\nu}_\mu$.004	.029

Combining the muon and the electron channels by a maximum likelihood method, the upper limits to 90% confidence for R are:

$$R \leq .09 \ (\nu_\mu) \quad R \leq .13 \ (\bar{\nu}_\mu)$$

If this result is interpreted in terms of $\nu_\mu \rightarrow \nu_\tau$ oscillations, the upper limit for R can be expressed in terms of the square of the mass difference of the neutrino mass eigen states (Δm^2) and the mixing angle θ . The probability for $\nu_\mu \rightarrow \nu_\tau$ is:

$$P(\nu_\mu \rightarrow \nu_\tau) = \sin^2(2\theta) \sin^2(1.27 \Delta m^2 L/E) \quad (3)$$

where L is the distance between origin and observation of the neutrino in kilometers and E is the energy in GeV. For maximum mixing the upper limits for Δm^2 are:

$$\nu_\mu: \Delta m^2 \leq 12 \text{ ev}^2 \quad \bar{\nu}_\mu: \Delta m^2 \leq 14.4 \text{ ev}^2 \quad (90\% \text{ C.L.})$$

Table IV shows the present limits by other experiments, the detector used and the decay modes to which they were sensitive. (For a complete review see Ref. 6)

Table IV

Results on $\nu_\mu \rightarrow \nu_\tau$ oscillations

Beam	Δm^2 [ev 2]	Detector/Ref.	Decay modes
ν_μ	<3	emulsion/7	all
	<5	bubble chamber/8	$e\nu_e \nu_\tau$
	<12	E594	$e\nu_e \nu_\tau; \mu\nu_\mu \nu_\tau$
$\bar{\nu}_\mu$	<2.4	bubble chamber/6	$e\nu_e \nu_\tau$
	<6.7	bubble chamber/6	$e\nu_e \nu_\tau$
	<14.4	E594	$e\nu_e \nu_\tau; \mu\nu_\mu \nu_\tau$

The emulsion experiment clearly sets the best limit since it is sensitive to all decay modes whereas all other experiments are limited in that respect. This experiment was sensitive to two decay modes ($\tau \rightarrow \mu\nu_\mu \nu_\tau$ and $\tau \rightarrow e\nu_e \nu_\tau$) and for the first time exploited the technique of missing energy in quasi-elastic interactions to identify possible ν_τ interactions.

Acknowledgement

We would like to thank the staff of the Neutrino Department and the Physics Department at FNAL for their support. This work was supported in part by grants from the National Science Foundation and the Department of Energy.

References.

1. Yung-Su Tsai, Phys. Rev. D4 (1971) 2821.
2. D. Edwards, S. Mori, S. Pruss, Fermilab TM-661, 1976.
3. L. Stutte, Proceedings of the 1981 International Conference on Neutrino Physics and Astrophysics, Vol. 1, P. 377, 1981.
4. F.E. Taylor, Proceedings of the XVIIth Rencontre de Moriond 1982, Vol. 1, P. 267, edited by J. Tran Thanh Van, Editions Frontieres, Gif Sur Yvette, France.
5. M. Jonker et al, Phys. Lett. 93B (1980) 203
6. C. Baltay, Proceedings of Neutrino '82, Supplement, P. 2, 1982.
7. N. Ushida et al., Phys. Rev. Lett. 47 (1980) 1694.
8. N. Armenise et al, CERN-preprint, CERN/EP 80-226 (1980).

DECAYS OF MASSIVE NEUTRINOS

F. Vannucci*)

LPNHE, Univ. Paris, France

ABSTRACT

There are no reasons to assume that neutrinos are massless. If they are heavy, they may decay into different channels. Existing data and future experiments are used to set limits on the instability of neutrinos in a large range of masses.

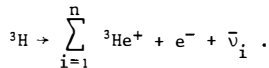
*) Visitor at CERN, Geneva, Switzerland.

1. MASSIVE NEUTRINOS

If neutrinos are massive, the weak eigenstates ν_e , ν_μ , ν_τ , etc., do not have definite mass but are linear combinations of the mass eigenstates ν_1 , ν_2 , ν_3 , etc.

The possible effects of neutrino masses vary with their scale:

- in the range of small masses [$0(\text{eV})$], neutrinos may undergo measurable oscillations;
- in the range of higher masses [$0(\text{MeV})$], neutrinos may decay with lifetimes accessible to experimental study. The possibility of such large masses, not ruled out by astrophysical constraints, forces us to re-examine the present limits, since leptonic decays will consist of an incoherent sum of separate channels. For instance the tritium experiment¹⁾ should be analysed in terms of:



This point of view leads to unusual consequences: because of different kinematical constraints in different processes, the " ν_e " produced in tritium decay is not necessarily the same as the " ν_e " produced in π or K decays.

The current mass limits leave open the possibility of substantial masses: for instance, the limit on $m(\nu_\mu)$ only applies to the dominantly coupled mass eigenstate (ν_2 ?) and does not forbid a much heavier component (ν_3 , ...).

2. PRODUCTION OF HEAVY NEUTRINOS

Heavy neutrinos may be produced either via oscillations or by direct production.

- i) The main component of a neutrino beam (ν_μ) may oscillate to a heavy neutrino ν_H . The mass difference being large, the oscillation length is tiny and the overall effect is to produce an admixture of ν_H in the predominantly ν_μ beam. If $U_{H\mu}$ is the mixing matrix element between ν_H and ν_μ , the fluxes will be in the ratio $|U_{H\mu}|^2:1$. Actually, an extra helicity factor²⁾ favours the production of ν_H over ν_μ . The matrix elements are the same as the one appearing in the analysis of oscillation experiments.
- ii) There are several processes which may generate heavy neutrinos. The ν_τ is a candidate for a heavy neutrino; it is directly produced in the decay $F \rightarrow T\nu_\tau$. Another source is given by π^0 . Whilst $\pi^0 \rightarrow \nu\bar{\nu}$ is forbidden for massless neutrinos, it is possible for heavy neutrinos. In fact the branching ratio of $\pi^0 \rightarrow \nu_H\bar{\nu}_H$ is of the order of 10^{-9} . The same decay mode exists for K^0 , η , η' , Finally, the Z^0 is a powerful source of ν_H , since it gives equal contributions in the various channels $Z^0 \rightarrow \nu_H\bar{\nu}_H$ up to masses of ~ 40 GeV.

3. DECAYS OF HEAVY NEUTRINOS3.1 Leptonic decays

If neutrinos exist with a mass above 1 MeV they will decay into e^+e^- according to the diagram of Fig. 1a. The same type of diagram is responsible for μ decay. The evaluation of the lifetime is similar, except for a coupling strength U_{He} which measures the overlap between ν_H and ν_e . The partial lifetime is:

$$\tau = 2.8 \times 10^4 \frac{1}{m_\nu^5} \frac{1}{|U_{He}|^2} \text{ (s)} .$$

If neutrinos with even heavier masses exist, then other channels, in particular hadronic ones, will open up. With increasing mass, we find the modes: $\mu^-e^+\nu_e$, $e^-\pi^+$, $\mu^-\mu^+\nu_\mu$, $\mu^-\pi^+$, ...

In fact the hadronic channels become predominant as soon as they are kinematically allowed.

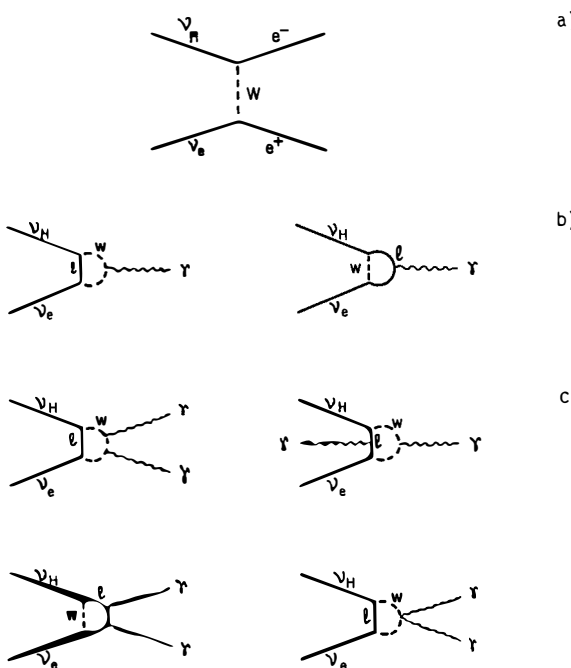


Fig. 1 Graphs of the various ν_H decays

3.2 Radiative decays

The decay mode $\nu_H \rightarrow \nu\gamma$ is possible even for very small masses of ν_H . But the decay probability corresponds to the GIM-suppressed diagrams of Fig. 1b, and the lifetime is rather long³⁾:

$$\tau = 2.9 \times 10^{12} \frac{1}{m_\nu^5} \frac{1}{|U_{H\ell}|^2} \text{ (s)}$$

in the case of three generations of charged leptons. Adding a new heavy lepton, the minimum possible lifetime in the standard model³⁾ is

$$\tau = 3.8 \times 10^7 \frac{1}{m_\nu^5} \frac{1}{|U_{H\ell}|^2} \text{ (s)} .$$

Now a miracle happens if, instead of radiating one photon, the charged loop radiates two photons (Fig. 1c). The mechanism is no longer GIM-suppressed, and the lifetime for $\nu_H \rightarrow \nu_e \gamma\gamma$ is now⁴⁾

$$\tau = 7.1 \times 10^{10} \frac{1}{m_\nu^9} \frac{1}{|U_{He}|^2} \text{ (s)} .$$

There is very interesting competition between the different decay modes: below a mass of 100 keV the channel $\nu\gamma$ predominates, then comes $\nu\gamma\gamma$, until e^+e^- opens up at 1 MeV; but because of the mass dependence, the mode $\nu\gamma\gamma$ takes over again for masses above 20 MeV and seems to remain the dominant decay for very heavy neutrinos.

4. MASSLESS DETECTOR FOR MASSIVE NEUTRINOS

How to search for such effects? Because of the Lorentz boost and to avoid neutrino interactions which will generate background, a decay experiment is best done at low energy.

A proposal exists to look for $\nu_H \rightarrow \nu_e e^+ e^-$ and $\nu_H \rightarrow \nu_e \gamma\gamma$ in the CERN Proton Synchrotron (PS) beam⁵⁾. The detector has a massless (helium bag) decay volume, terminating in a calorimeter where e^+ , e^- , and γ can convert.

Here we rely on the ν_H production by oscillations from ν_μ . The limit is expressed in terms of m_ν versus $|U_{H\ell}| \times |U_{He}|$, where $U_{H\ell}$ and U_{He} denote the mixing elements at production and at decay. Figure 2 shows the limits obtained with the various production sources of ν_H and their two decay modes. These limits can be compared with the ones obtained when looking for secondary peaks in the spectra of charged leptons produced in the leptonic decays of pseudoscalar mesons⁶⁾. The experiment discussed here is much simpler, and is more powerful by several orders of magnitude.

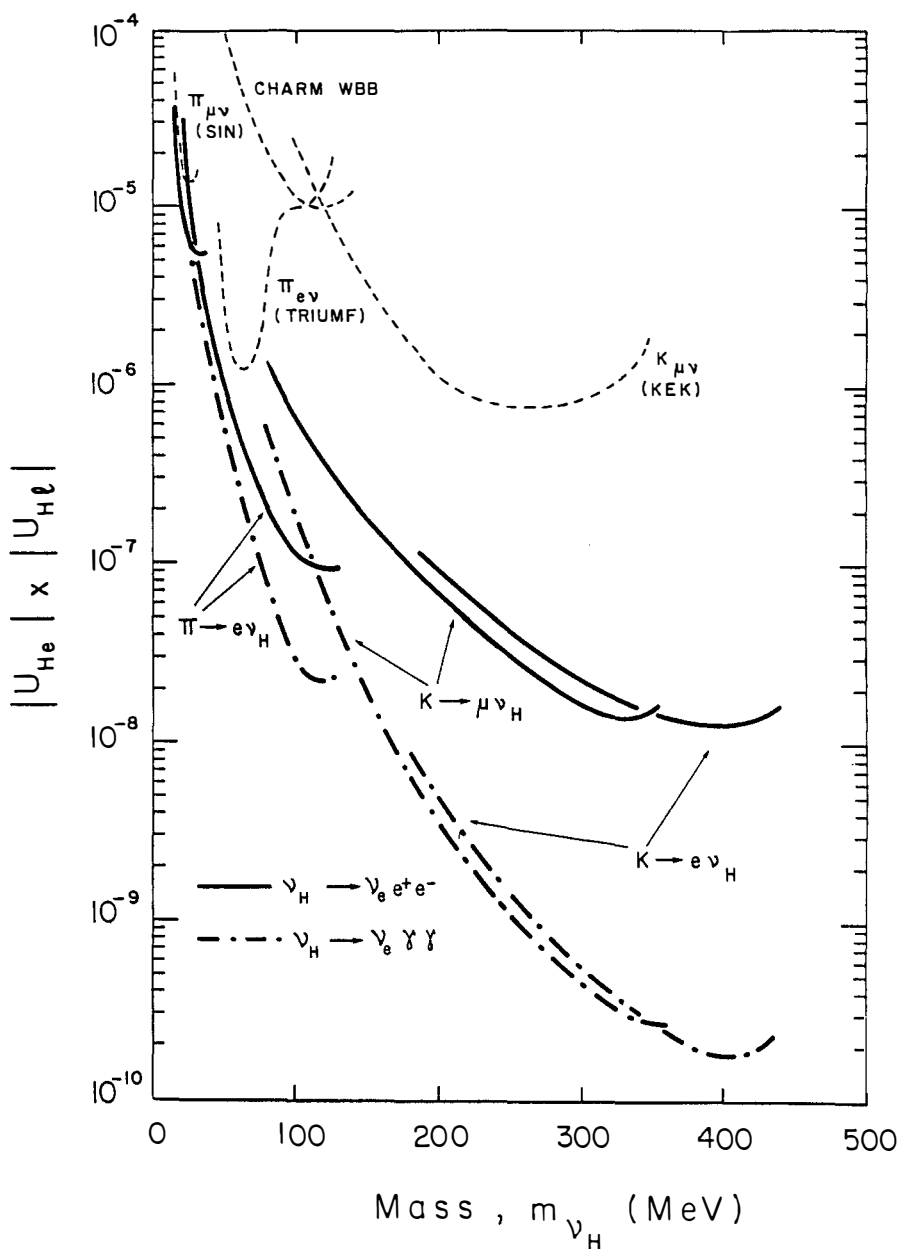


Fig. 2 Limits from the PS experiment compared to existing results

When ν_H is produced in the decays $\pi, K \rightarrow e\nu_H$, the same matrix element $U_{H\ell}$ appears at production and at decay. In that case the limits on coupling strength can be expressed directly as a limit on the lifetime of ν_H . For instance, the PS experiment gives a lower limit of 30 s for a ν_H of mass 100 MeV. This is to be compared with the μ lifetime of 2×10^{-6} s for a similar mass.

5. SOLAR MASSIVE NEUTRINOS

To investigate the region of smaller masses, laboratory experiments are inadequate. Here the Sun proves to be an interesting source of neutrinos, with the great advantage of giving 10^{11} m of decay path, before the observation above the Earth's atmosphere. If one believes in the standard model, one knows the initial flux of neutrinos emitted by the Sun. In particular there exist several monoenergetic neutrino rays. Such rays would give quasi-monoenergetic photon rays in the case of the decay $\nu_H \rightarrow \gamma\gamma$. More generally, decays of solar neutrinos would create a background of photons due to the decays $\nu_H \rightarrow \gamma\gamma$ and $\nu_H \rightarrow \gamma\gamma\gamma$, or a background of e^+e^- due to the decay $\nu_H \rightarrow \nu e^+e^-$. Limits on the corresponding fluxes give useful constraints on neutrino masses down to 100 keV. It is not easy to find the relevant astrophysical measurements. The flux of e^+ in interplanetary space seems to be $10^{-4} \text{ cm}^{-2} \text{ s}^{-1} \text{ MeV}^{-1}$ ⁷⁾. Also, $10^{-3} \text{ cm}^{-2} \text{ s}^{-1} \text{ MeV}^{-1}$ seems a conservative limit on photon flux in the range 0(100 keV). With these numbers one can extract the limit, plotted in Fig. 3, for neutrino masses between 100 keV and 10 MeV, assuming the optimistic lifetime for $\nu_H \rightarrow \gamma\gamma$.

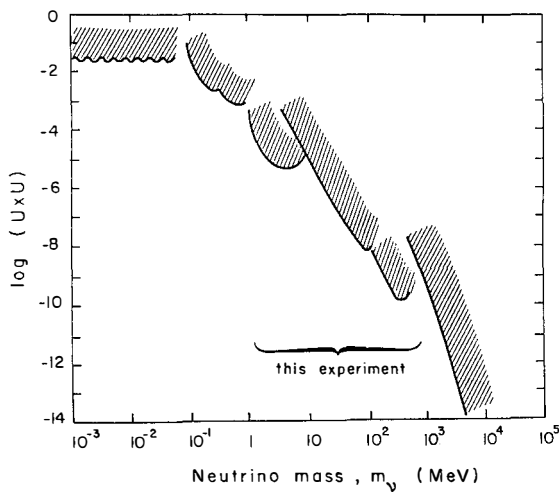


Fig. 3 Limits on couplings of heavy neutrinos from various sources

6. HEAVY NEUTRINOS AT LEP

What has been discussed up to now is limited to neutrino masses smaller than the K mass. A practical source of heavier neutrinos happens to be the Z^0 , which democratically populates all channels $\nu_H \bar{\nu}_H$ for neutrinos of mass up to ~ 40 GeV. Because of the mass dependence of the lifetime, it could happen that such neutrinos decay almost immediately! For the decay $\nu_H \rightarrow \nu \gamma \gamma$ one finds, with the mass expressed in GeV, the possibly very short lifetime

$$\tau = 7.1 \times 10^{-17} \frac{1}{m_\nu^9} \frac{1}{U^2} \quad (\text{s}) .$$

At LEP one expects of the order of 1000 decays $Z^0 \rightarrow \nu \bar{\nu}$ per day. If the detectors are not full of decaying neutrinos, one can set a very stringent limit, corresponding to 2 m of decay path, i.e. the radius of a canonical LEP detector, on the coupling of heavy neutrinos:

$$U_{\text{He}}^2 < \frac{10^{-9}}{m_\nu^{10}} .$$

7. CONCLUSIONS

Figure 3 summarizes near-future expectations in the search for massive neutrinos. Low masses correspond to the domain of neutrino oscillations. Here the mixings cannot be pushed very much and the limits are in the few percent range. Between 100 keV and 1 MeV limits come from photon fluxes above the atmosphere. It seems that such limits could be improved easily with a dedicated experiment. Between 1 MeV and 10 MeV the limit comes from the ^8B contribution to the solar spectrum. The range 10 MeV-400 MeV is covered by the searches in neutrino decays with the limits to be set by the PS proposal. Finally comes the region of LEP, with possibilities of probing couplings down to 10^{-25} !

Neutrino decays appear to give a complementary approach to oscillations. While oscillations test the domain of small masses but relatively large couplings, neutrino decays allow to probe the region of higher masses but very small couplings. For this reason, and because the theoretical guidance is rather weak in this field, neutrino decays, just like oscillations, are worth the effort of systematic searches.

REFERENCES

- 1) V.A. Lyubimov et al., *Phys. Lett.* 94B (1980) 266.
- 2) R.E. Schrock, *Phys. Rev. D* 24 (1981) 1232.
- 3) A. De Rújula and S.L. Glashow, MIT preprint CTP 852 (1980).
A. De Rújula, MIT preprint CTP 848 (1980).
- 4) J. Nieves, Puerto Rico preprint PRE 26311 (1982).
R. Ghosh, Stony Brook preprint ITP-SB 82-42 (1982).
- 5) D. Perret-Gallix et al., CERN/PSCC 83-12 (1983).
- 6) R.S. Hayano et al., *Phys. Rev. Lett.* 49 (1982) 1305.
D.A. Bryman et al., TRIUMF preprint TRI-PP 82-43 (1982).
- 7) D. Toussaint and F. Wilczek, *Nature* 289 (1981) 777.

SEARCH FOR DECAY OF HEAVY NEUTRINOS IN NEUTRINO BEAMS

CHARM Collaboration

F.Bergsma, J.Dorenbosch, M.Jonker and C.Nieuwenhuis
NIKHEF, Amsterdam, The Netherlands

J.V.Allaby, U.Amaldi, G.Barbiellini, L.Barone, C.Berger, A.Capone, W.Flegel,
M.Metcalf, L.Lanceri, J.Panman and K.Winter
CERN, Geneva, Switzerland

I.Abt, J.Aspiazu, F.W.Büsser, H.Daumann, P.D.Gall, F.Niebergall, K.H.Ranitzsch,
P.Schütt and P.Stähelin
II. Institut für Experimentalphysik, Universität Hamburg, Hamburg, Fed. Rep.
Germany

P.Gorbunov, E.Grigoiev, V.Kaftanov, V.Khovansky and A.Rosanov
Institute for Theoretical and Experimental Physics, Moscow, USSR

A.Baroncelli, B.Borgia, C.Bosio, M.Diemoz, U.Dore, F.Ferroni, E.Longo, L.Luminari,
P.Monacelli, F.de Notaristefani, P.Pistilli, C.Santoni, L.Tortora and V.Valente
Istituto Nazionale di Fisica Nucleare, Rome, Italy

Presented by F.Niebergall



ABSTRACT

A search for heavy neutrinos was conducted in the 400 GeV proton beam dump neutrino beam and in the 400 GeV wide band neutrino beam at CERN. Neutrinos decaying into two electrons and a light neutrino were searched for. Upper limits on the mixing angle are derived for neutrino masses in the range 10-140 MeV.

In the conventional theory of weak interactions neutrinos are assumed to be massless, but experimentally a finite neutrino mass cannot be excluded. The present limit on the τ neutrino mass is 250 MeV. Assuming production of τ neutrinos by leptonic decays of the F-meson and by the subsequent τ decay, the neutrino beam produced by high energy protons interacting in a Cu beam dump would contain a large fraction of such heavy neutrinos.

If neutrinos are massive their weak eigenstates are linear combinations of the mass eigenstates:

$$\nu_1 = \sum U_{1i} \nu_i \quad (1 = e, \mu, \tau, \dots, i = 1, 2, 3, \dots) \quad (1)$$

Neutrino beams can therefore contain a fraction of heavy neutrinos produced in π and K decay [1], [2]. Neutrinos with a mass larger than a few MeV can decay into a light neutrino and two electrons. For neutrinos with a mass larger than 110 MeV other decay channels are opened ($\nu_i \rightarrow e\mu\nu$, $\nu_i \rightarrow e\pi$, etc.) [1]. The decay probability for heavy neutrinos is proportional to the square of the mixing angles defined in (1). A search was made for neutrinos decaying into a pair of electrons:

$$\nu_i \rightarrow e^+ e^- \nu_e \quad (2)$$

In the beam dump experiment decays of heavy neutrinos were searched for in an empty decay region of 35 m length and $3 \times 3 \text{ m}^2$ cross section parallel to the CDHS [3] and the CHARM [4] neutrino detectors. A search for heavy neutrinos produced in π and K decays was performed in the horn focussed wide band neutrino beam by making use of the fine-grain CHARM calorimeter [5].

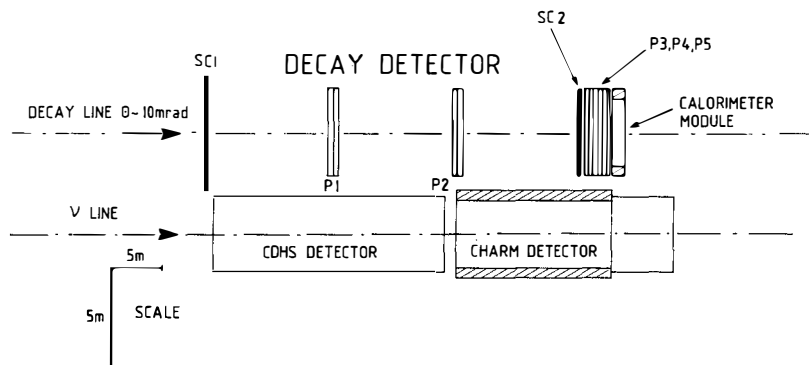


Fig. 1 Layout of the decay beam dump experiment. SC1 and SC2 are scintillator planes. SC1 is used as veto counter. P1 to P5 are packs of 4 planes of proportional drift tubes each.

The layout of the beam dump experiment is shown in Fig. 1. A scintillation counter plane of $6 \times 4.8 \text{ m}^2$ active area (SC1) defines the beginning of the decay volume. The decay region is parallel to the neutrino beam line at a mean distance of 5 m, corresponding to an angle with respect to the incident proton beam of 10 mrad. One module of the CHARM calorimeter was displaced to the end of the decay region. It has an active area of $3 \times 3 \text{ m}^2$ and is used to measure the energy of electromagnetic cascades with a resolution of $\Delta E/E < 0.30$ for shower energies $E > 5 \text{ GeV}$. The decay volume is subdivided into three regions using two packs of proportional tubes (P1 and P2) [5]. Each pack consists of four planes of proportional drift tubes, covering a surface of $4 \times 4 \text{ m}^2$, preceded by a lead plate of 1/2 radiation length thickness. In order to improve the angular resolution of the shower and to better reconstruct the decay point, a low density detector was added in front of the CHARM calorimeter module. This comprised three packs of proportional tubes (P3, P4 and P5) preceded by a plane of scintillation counters (SC2). The estimated angular resolution for an electromagnetic shower is a few mrad.

The detector was exposed to a neutrino flux produced by 1.7×10^{18} protons on a solid copper target and 0.7×10^{18} protons on a laminated copper target with an effective density of 1/3 of solid copper. In the combined exposures, 21000 events were collected satisfying the trigger requirements: no hits in the scintillator plane SC1 and a hit in at least 4 scintillator planes of the calorimeter module. These events include: cosmic ray events (a track not pointing to the scintillator plane SC1), parasitic events (tracks from neutrino interactions in the CDHS and CHARM detectors or in the floor), beam associated muons and neutrino interactions. The events recognized as neutrino interactions having the shower vertex after the scintillator plane SC2 were used to check the performance of the detector. We observe 340 ± 45 neutrino interactions. Based on the number of neutrino interactions found in the CHARM calorimeter 440 ± 50 neutrino interactions were expected.

The decay candidates were required to have at least one hit in the scintillator plane SC2 and a shower energy larger than 3 GeV. The sample was scanned to search for candidates which are consistent with having two electrons. The scanning criteria were: a) in the case of single hit in the scintillator plane SC2 the pulse height was required to be larger than that corresponding to the energy released by the passage of 1.5 minimum ionizing particles, b) not more than 2 tracks in the proportional-tube packs P3, P4 and P5 or in the calorimeter module and c) shower angle and energy compatible with the decay of a heavy neutrino with mass below 140 MeV. No event satisfies these criteria.

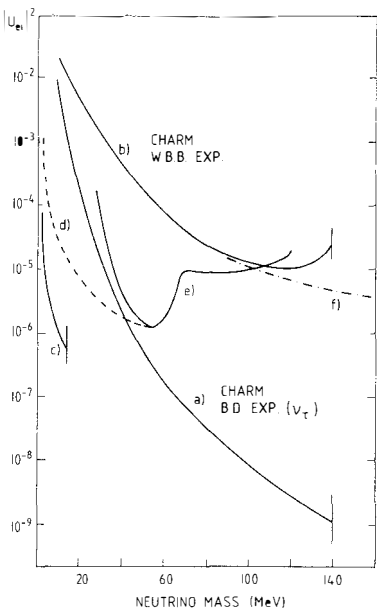
Assuming that the ν_τ couples mainly to a single mass eigenstate, an upper limit can be set on the mixing angle $U_{e\tau}$. The expected number of neutrino decay events in the decay region was computed according to the expression:

$$N = N_F P[F \rightarrow \nu_\tau \tau] A P[\nu_\tau \rightarrow e^+ e^-] . \quad (3)$$

N_F is the number of F mesons produced by protons in the dump. It was computed from the number of prompt charged current muon neutrino events observed in the CHARM calorimeter [7]. During the exposure 1830 ± 250 prompt neutrino events with a muon in the final state were collected. These events are produced essentially by muon neutrinos coming from the semileptonic decay of D mesons ($BR = 0.1$). A ratio $\sigma(p\text{Cu} \rightarrow FFX)/\sigma(p\text{Cu} \rightarrow DDX) = 0.2$ was assumed. $P[F \rightarrow \nu_\tau \tau]$ is the probability

of the F meson to decay into a heavy neutrino ($BR = 0.03$). The factor A gives the fraction of neutrinos that cross the decay region. The production of F mesons was simulated by a Monte Carlo program assuming a distribution for the Feynman variable x corresponding to $(1-x)^4$ and a transverse momentum distribution proportional to $\exp(-2P_t)$. The flux of τ neutrinos computed using this model agrees with the limit put in an earlier beam dump experiment [6] on the number of events induced by ν_τ . $P[\nu + e^+ e^- \bar{\nu}_e]$ is the probability for the heavy neutrinos to decay in the fiducial decay region, scaled from the decay matrix element in the neutrino mass range 10-140 GeV is shown in Fig. 2 as a function of the neutrino mass, together with previous results on $(U_{e1})^2$ [8], [9], [10].

Fig. 2 Limits at 90% c.l. on $(U_{e1})^2$ as a function of the neutrino mass:
 a) limits obtained in the proton beam dump experiment; b) limits obtained in the wide band neutrino beam experiment; c) limits from solar neutrino measurements [8]; d) limits from the measurement of the branching ratio $\pi \rightarrow \nu e$ [9]; e) limits obtained from the search for monoenergetic peaks in the region below the value predicted for zero mass neutrino in $\pi \rightarrow \nu e$ decay [9]; f) limits from the measurement of the branching ratio $K \rightarrow \nu_e e^- 10$.



In the case of the wide-band neutrino beam experiment, no assumption was made on the nature of the heavy neutrino. The search for "two electron events" was performed in a sample of 1.3×10^6 neutrino and 1.4×10^6 antineutrino interactions collected in the CHARM calorimeter [5]. The neutrinos and antineutrinos were produced by 1.4×10^{18} and 5.7×10^{18} protons on target respectively.

Candidate events were selected from those muonless events appearing as showers of narrow width, characteristic of showers initiated by electrons and photons in the CHARM calorimeter [11]. The selected events were required to have a shower energy E deposited in the calorimeter between 7.5 GeV and 50 GeV and a value of the variable $E^2\theta^2$ below 0.54 GeV 2 (θ is the angle between the shower axis and the direction of the incoming neutrino). 331 neutrino and 769 antineutrino events were selected.

The events surviving the selection criteria are due to the following known sources:

- a) elastic and quasi-elastic charged current events induced by the electron-neutrino contamination of the beam;
- b) events induced by the scattering of neutrinos on electrons;
- c) neutral-current events with a γ or a π^0 in the final state produced by coherent scattering of muon neutrinos on nuclei;
- d) decay of heavy neutrinos into $e^+ e^- \nu$.

The different distributions in the four types of reactions in $E^2\theta^2$, (a) and (c) are flat], and in the energy deposited in the first scintillator after the vertex, [a) and b) start with one charged particle], can be used to disentangle the sample of events.

We find that the number of events attributed to heavy neutrino decay is compatible with zero (1±41 events in the case of a muon partner and 1±49 events in the case of an electron partner).

From this result a limit on the product of the mixing angles defined in (1) can be obtained. The expected number of neutrino decay events in the CHARM apparatus is computed according to the equation:

$$N = \{N_\pi P[\pi \rightarrow \nu_i + \dots] A_\pi + N_K P[K \rightarrow \nu_i + \dots] A_K\} P[\nu_i \rightarrow e^+ e^- \nu_e] \varepsilon \quad (4)$$

N_π and N_K are the numbers of π and K decays. $P[\pi(K) \rightarrow \nu_i + \dots]$ is the probability for $\pi(K)$ to decay into a heavy neutrino. It is proportional to the square of U_{ei} or to the square of U_{ui} depending on whether the heavy neutrino is produced with an electron or a muon. This probability is obtained from the probability for π or K to decay into a zero mass neutrino times a factor ρ depending on the neutrino mass m . In the case of two body decay ρ takes care of the fact that for finite neutrino mass there is less suppression due to helicity conservation than in the case of a zero mass neutrino [1]. The geometrical factors A_π and A_K give the fraction of the heavy neutrinos from π and K decay crossing the CHARM detector.

$P[\nu_i \rightarrow e^+ e^- \nu_e]$ is the probability for the heavy neutrinos to decay in the fiducial volume of the detector. The decay length is 12 m. The global efficiency of the cuts applied in the analysis (ε) includes the efficiency to select electromagnetic showers induced by two electrons and the efficiency of the shower energy cuts.

The limits at 90% c.l. on $(U_{ei})^2$ and on $(U_{ei}U_{\mu i})$ in the neutrino mass range 10-140 MeV are shown in Figs. 2 and 3. The limits on $(U_{ei}U_{\mu i})$ cannot be directly compared with published limits because they refer only to $(U_{ei})^2$ and $(U_{\mu i})^2$ [8], [9], [10], [11], [12], [13].

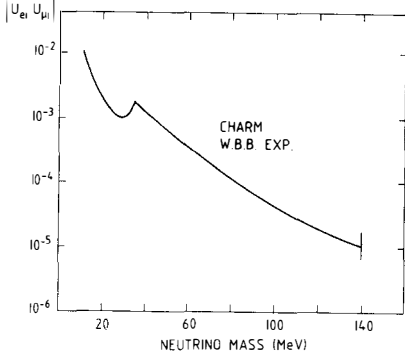


Fig. 3 Limits at 90% c.l. on $(U_{ei}U_{\mu i})$ as a function of the neutrino mass from the WBB experiment.

In conclusion, there is no evidence for the decay into two electrons of heavy neutrinos with masses in the range 10-140 MeV.

REFERENCES

- 1.) R.E.Shrock, Phys. Rev. D24 (1981) 1232
- 2.) M.Gronau, SLAC-PUB-2967 August 1982
- 3.) M.Holder et al., Nucl. Instrum. Methods 148 (1978) 235
- 4.) A.N.Diddens et al., Nucl. Instrum. Methods 178 (1980) 27
- 5.) M.Jonker et al., Nucl. Instrum. Methods 200 (1982) 183
- 6.) P.Fritze et al., Phys. Lett. 96B (1980) 427
- 7.) Preliminary results from the CHARM Collaboration
- 8.) D.Toussaint and F.Wilczek, Nature Vol. 289 (1981) 777. The limits are obtained from: K.Beurmann et al., Acta Phys. Hung. 29, Suppl.1 (1970) 173, T.Cline and G.Porreca Acta Phys. Hung. 29, Suppl.1 (1970) 145 and R.Mewaldt et al., 14th Int. Cosmic Ray Conf. 1 (1975) 349
- 9.) D.A.Bryman et al. TRI-PP-82-43 November 1982
- 10.) D.Berghofer et al., Proc. Int. Conf. on Neutrino Physics and Astrophysics, Maui, Hawaii, 1981 (eds. R.J.Cence, E.Ma and A.Roberts) (Univ. of Hawaii, Honolulu, 1981), vol. 2, p 67. The limits are derived from: K.Heard et al., Phys. Lett. 55B (1975) 327 and J.Heintze et al., Phys. Lett. 60B (1976) 302
- 11.) M.Jonker et al., Phys. Lett. 117B (1982) 272
- 12.) R.Abela et al., Phys. Lett. 105B, (1981) 263
- 13.) N.J.Baker et al., Phys. Rev. Lett. 47 (1981) 1576
- 14.) R.S.Hayano et al., Phys. Rev. Lett. 49 (1982) 1305

STATUS OF THE CCFR NEUTRINO OSCILLATION EXPERIMENT AT FNAL

D. Garfinkle, F. Merritt, M. Oreglia, P. Reutens,
University of Chicago; P. Auchincloss, R. Blair,
C. Haber, M. Ruiz, F. Sciulli, M. Shaevitz, W.
Smith, R. Zhu, Columbia University; R. Coleman,
H.E. Fisk, B. Jin, D. Levinthal, W. Marsh, P.
Rapidis, D. Jovanovic, H. White, Fermi National
Accelerator Laboratory; A. Bodek, F. Borcherding,
N. Giokaris, K. Lang, I.E. Stockdale, University
of Rochester.

Talk presented by A. Bodek, University of
Rochester, Rochester, New York, 14627, U.S.A.



ABSTRACT: An existing neutrino detector (CCFR) and a specially constructed second detector are used to search for a disappearance of flux from the narrow band muon neutrino beam at FNAL. The detectors are located 715m and 1116m from the source of 40-230 GeV neutrinos, thus making the experiment sensitive to the oscillation parameters $10 < \delta m^2 < 1000 \text{ eV}^2$ for $\sin^2 2\theta \geq 0.05$. A report on the status of the data analysis is presented.

THEORY AND INSIGHTS

The consequences of a neutrino mass and a unitary mixing matrix have been frequently discussed in recent years¹⁾. For three lepton generations the neutrino mass eigenstates are $\nu_\alpha = \sum_j U_{\alpha j} \nu_j$, $\alpha = e, \mu, \tau$, $j = 1, 2, 3$, where U contains three mixing angles and one CP violating phase defined in the same manner as that for the Kobayashi-Maskawa mixing of quarks. The CP violation would be evidenced by a difference in the oscillation rates for $\nu_\mu \rightarrow \nu_e$, $\bar{\nu}_\mu \rightarrow \bar{\nu}_e$.

Evolution of a pure mass eigenstate proceeds as e^{-iEt} . If the neutrinos possess energies much larger than their masses, the probability amplitude for observing muon neutrinos at a distance L from a pure ν_μ source is $A(\nu_\mu \rightarrow \nu_\mu) = 1 - A_{12} [1 - \cos(\frac{2\pi L}{L_{12}})] - A_{13} [1 - \cos(\frac{2\pi L}{L_{13}})] - A_{23} [1 - \cos(\frac{2\pi L}{L_{23}})]$. (1)

In the preceding equation the $A(IJ)$ are functions of the four mixing parameters, and the oscillation lengths are defined as

$$L_{ij} \equiv \frac{4\pi E_\nu}{m_{ij}^2 - m_j^2} \equiv \frac{4\pi E_\nu}{\delta m_{ij}^2}. \quad (2)$$

If one of the oscillation channels C dominates, the $A(IJ)$ ($I, J \neq C$) are small, so the intensity corresponding to Equation 1 reduces to the single harmonic form

$$P(\nu_\mu \rightarrow \nu_\mu) \approx 1 - \sin^2 2\theta \sin^2 \left(\frac{1.27 \delta m^2 L}{E_\nu} \right), \quad (3)$$

where δm^2 is in eV^2 , L in km and E in GeV . The effect of an oscillation is maximal when $1.27 \delta m^2 L / E$ is near $\pi/2$; therefore, a figure of merit for the measurement of δm^2 is realized in E/L . The FNAL neutrino beam area ($E/L = 50$) is sensitive to δm^2 in the $10 - 1000 eV^2$ range. The CERN PS ($E/L = 3$) to $1 - 10 eV^2$, reactors ($E/L = 1$) to $0.1 - 5 eV^2$, and so forth.

Oscillations can be detected from an initially pure beam of ν_μ either by exclusively searching for ν_e and ν_τ downstream of the source, or by measuring a disappearance of the ν_μ flux as a function of distance from the source. Upper limits on the channels $\nu_\mu \rightarrow \nu_\tau$ ²⁾ and $\nu_\mu \rightarrow \nu_e$ ³⁾ have been set by exclusive experiments for δm^2 roughly between 10 and 1000 eV² and θ larger than 7 to 10°. However, recent results from a β decay experiment⁴⁾ indicate an electron neutrino mass of 14 to 46 eV. Further evidence for neutrino masses in this range is suggested by astrophysical measurements of an abundance of dark matter in the universe.⁵⁾

The exclusive measurements, however, are not sensitive to the oscillation channels $\nu_\mu \rightarrow \nu_x$, where x refers to any new generation having a charged lepton too massive to be produced in present neutrino beams. Similarly, the exclusive searches are insensitive to the oscillations $\nu_\mu \rightarrow (\bar{\nu}_\mu)_L$ in which the left handed antineutrino is sterile by virtue of its small V-A coupling. Disappearance experiments are sensitive to both of these oscillation channels.

In general, we do not expect the mixing angles to be large. If the Cabibbo angle is to be considered as indicative of possible mixing in the neutrino sector, then an experiment should be sensitive to θ on the order of 13°($\sin^2(2\theta)=0.2$) or smaller. We have, therefore, performed a disappearance experiment sensitive to $\theta \geq 6^\circ$ in the range $1000 > \delta m^2 > 10$ eV².

THE NEUTRINO LINE AND DETECTORS

An overview of the FNAL neutrino line and the two detectors relevant to this experiment is given in Fig. 1. The narrow band dichromatic train⁶⁾ selects monoenergetic pions and kaons within an 11% momentum bite in the range of 100 GeV/c to 250 GeV/c, which decay in a 352m evacuated decay pipe. The hadrons and muons are absorbed in an aluminum and iron beam dump followed by iron impregnated earth berm. Two monitoring stations were located 137m and 292m into the decay pipe. The downstream station housed a segmented-wire-ionization-chamber (SWIC) for measurement of the beam profile, an ion chamber for counting the charged particle flux, and x- and y- (transverse) split plate ion chambers to track and enable steering of the beam within 2cm of the nominal center line at the

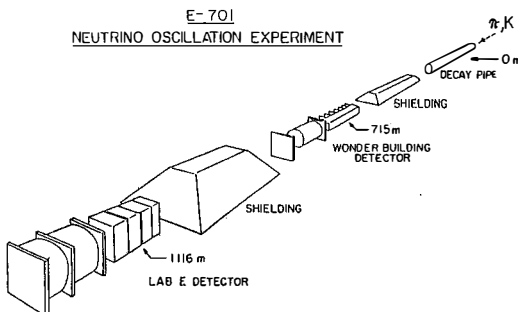


Fig. 1. General location of the Wonder Building and Lab E detectors in the Fermilab neutrino beam.

downstream detector. The upstream station contained similar SWIC, ion and split plate chambers, as well as a fourth space which accommodated either an RF-cavity flux monitor (normally in), a scanning x-y scintillator, or a Cherenkov vessel for measuring the particle composition of the beam.

The target centers of the two detectors were located 891m (the Wonder Building) and 1292m (Lab E) from the upstream end of the decay pipe. Both detectors consisted of a target calorimeter instrumented with spark chambers, followed by a toroid muon spectrometer. Figure 2 shows the apparatus in Lab E and the Wonder Building. The Lab E target consists of 56 scintillation counters measuring 3m x 3m x 2.5cm and viewed by four photomultiplier tubes through wavelength-shifter bars. The 56 Wonder Building target counters are constructed of doped acrylic measuring 1.5m x 1.5m x 2.5cm, viewed by two phototubes through waveshifter bars. Counters were positioned after every 10cm of steel plates having the same transverse dimensions as the counters; each target had 112 iron plates for a total target mass of 444 metric tons in Lab E and 108 tons in the Wonder Building. Minimum ionizing muons from the beam were used to calibrate the counters; in addition, the Lab E detector had been calibrated with a hadron beam in an earlier experiment. A hadron energy resolution $\Delta E = 0.9 \sqrt{E}$ GeV was realized in both calorimeters for hadron showers having a vertex at least 12cm from the edge of the counters. The detectors are described in greater detail in References 7, 8, and 9.

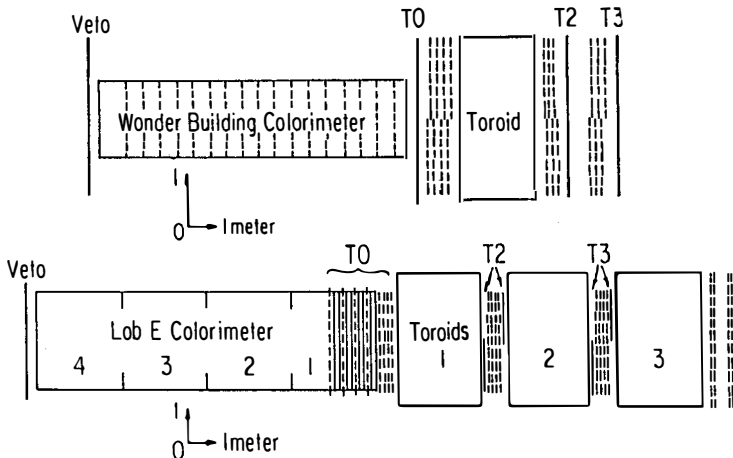


Fig. 2. Side views of the two detectors. The transverse scales are in the ratio 1.56 (L.E./W.B.). Broken lines indicate spark chambers.

A $3\text{m} \times 3\text{m}$ spark chamber was located after every 20cm of steel in the Lab E target, while the Wonder Building had $3\text{m} \times 1.5\text{m}$ chambers for every 30cm of steel. These chambers were read out magnetostriictively with a resolution of 0.5 mm. The muon spectrometer in Lab E consisted of three segmented steel toroids measuring 2m radius by 1.6m long, with a 7.5cm radius center bore for the coils. Each toroid was interleaved with doped acrylic scintillators every 20cm of steel, and was followed by five spark chambers. A total transverse momentum kick of 2.4 GeV/c was realized by the three toroid system, giving an 11% muon momentum resolution in the 7 to 400 GeV/c range. A single toroid magnet measuring 1.5m radius by 2.4m and having a 1.2 GeV/c transverse momentum kick was used in the Wonder Building. This magnet was followed by six planes of spark chambers and provided a resolution of 15%.

Two trigger conditions were used to obtain the charged current events to be used in the first round neutrino oscillation analysis. A "muon trigger" required a signal in counters T0 and T2 (indicated in Fig. 2), no signal in a charged particle veto counter preceding the target, and at least one minimum ionizing signal in the target calorimeter. The T2

condition assured that the muon could be momentum analyzed. The "penetration trigger" required that 5 GeV be measured in the calorimeter in association with at least one muon penetrating 2m or more of steel. Other triggers were also in operation for the longer range goal of cross section and structure function measurements.

DATA ANALYSIS

Our initial oscillation analysis minimizes the systematic errors by working with ratios of events at the two detectors. Consequently, a knowledge of the neutrino flux is needed only in order to correct for detector livetimes. The analysis is restricted only to events from appropriately scaled fiducial volumes in the two detectors; the scaling is done as if all the neutrinos originated from the center of the decay pipe. This naive assumption about the neutrino origin introduces a parallax error of 1-3% in the event ratios, which can be corrected using a more sophisticated calculation. Each event is projected to a corresponding point in the target of the other detector; events are accepted only if they satisfy the trigger and software requirements in both detectors.

The beam center was determined to better than 1cm from the vertex distribution of small-angle pion neutrino events. We then required that the x-y vertex of an acceptable event be within 57cm of the beam center line in the Wonder Building, and within 89cm at Lab E. These radius cuts on the 37 counters and steel plates that define the fiducial volumes lead to fiducial target masses of 33 and 83 metric tons for the Wonder Building and Lab E, respectively; roughly equal event rates were measured in the two detectors with these volumes.

The data for this experiment were recorded between January and July of 1982. Positive secondary particles were produced with train settings of 100, 140, 165, 200 and 250 GeV/c, for a total of 3.4×10^{18} protons on target. The strict cuts listed in the previous section, elimination of data from problematic run periods, and the condition that both detectors be "live" simultaneously (this excluded 20% of the data) reduced the usable data to 8×10^3 kaon and 23×10^3 pion events at Lab E, and 8×10^3 kaon and 21×10^3 pion events at the Wonder Building. These numbers permit a statistical

accuracy of about 4% on the two-laboratory ratio of charged current neutrino events when they are divided into 10 neutrino energy bins.

Systematic errors affecting the ratios arise from the length of the decay pipe, any possible offset in the two detector center lines, and possible variations in the reconstruction efficiencies for the two detectors. Estimates of these effects introduce errors on the data of about 1%. In addition, there are small uncertainties totalling about 1% from the relative target density between the labs (4% larger in Lab E), the detector livetimes (97% or larger) and veto deadtimes (typically 0.5% in Lab E and 1.5% at the Wonder Building).

A study of the integrity of our fully processed data has not yet been completed; however, one can get an impression of the statistical power of the experiment by examining a Monte-Carlo generated oscillation signal using the statistics obtained in the real data. Figure 3 depicts the ratio of Lab E neutrinos to Wonder Building neutrinos as a function

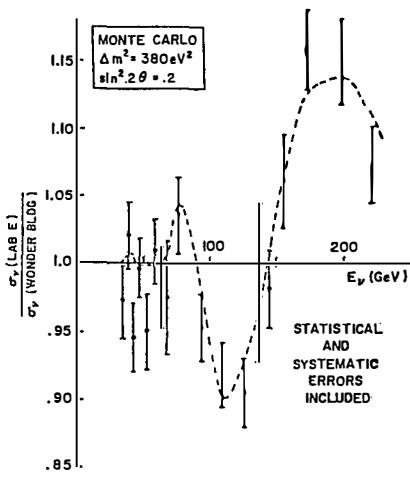


Fig. 3. Monte Carlo 'fake' data for the hypothesis $\Delta m^2 = 380 \text{ eV}^2$ and $\sin^2(2\theta) = 0.2$ for a data sample equal to E-701 statistics.

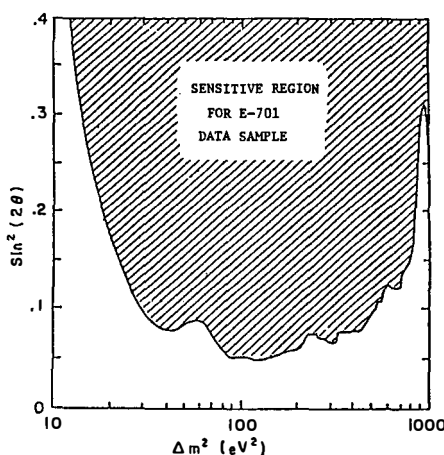


Fig. 4. Sensitivity versus Δm^2 and $\sin^2(2\theta)$ for the E-701 data sample.

of neutrino energy for the hypothetical values $\delta m^2 = 380$ eV² and $\theta = 13^\circ$. Figure 4 shows the limits (90% C.L.) that this experiment can place on δm^2 and θ in the absence of any observed signal given the statistics of Fig. 3.

REFERENCES

- 1) See, for example, the review by P.H. Frampton and P. Vogel, Phys. Rep. 82, 339 (1982).
- 2) N. Ushida et al., Phys. Rev. Lett. 47, 1694 (1981).
- 3) C. Baltay, Proc. of ν-82 International Conference on Neutrino Physics and Astrophysics, Balatonföred, Hungary, 14-19 June 1982; J. Blietschau et al., Nucl. Phys. B133, 205 (1978).
- 4) V. A. Lubimov et al., Phys. Lett. 94B, 266 (1980).
- 5) R. Cowzik and J. McClelland, Phys. Rev. Lett. 29, 669 (1972).
- 6) H. E. Fisk and F. Sciulli, Ann. Rev. Nucl. Part. Sci. 32, 499 (1982).
- 7) W. H. Smith, Proc. Summer Institute on Particle Physics, Stanford Linear Accelerator Center, Menlo Park, California, 16-27 August, 1982.
- 8) R. E. Blair, Ph.D. thesis, California Institute of Technology, Pasadena, California (1982, unpublished).
- 9) J. R. Lee, Ph.D. thesis, California Institute of Technology, Pasadena, California (1981, unpublished).

NEUTRINO-OSCILLATION EXPERIMENTS AT CERN

Yehuda Eisenberg^{*)}
CERN, Geneva, Switzerland



ABSTRACT

A progress report of the CDHS and CHARM experiments measuring ν -oscillations at the CERN PS is presented. Expected rates and upper limits for the ν -mass differences and mixing angles are also given.

^{*)} On leave from the Weizmann Institute, Rehovoth, Israel

Recently the interest in neutrino oscillations¹⁾ has prompted several new experiments, aimed at obtaining new upper limits on the ν mass differences and mixing angles. I wish to report here the present status of two such experiments, the CDHS and CHARM, performed at the CERN PS generated neutrino beam and searching for ν_μ oscillations.

Very briefly, neutrino oscillations are a quantum interference effect where a neutrino of a given flavour will acquire with time components of different flavour neutrinos, as a consequence of having a non-zero mass²⁾. Thus since in the standard model neutrinos are supposed to be mass-less, one does not expect in this model any oscillations. Restricting ourselves to the simple case of 2 neutrino flavours only, say ν_μ and ν_e , and neglecting also the theoretically less probable¹⁾ case of oscillations into anti-neutrinos, one obtains a simple formula for the appearance probability of one flavour neutrinos in a beam of the other flavour, as a function of time (distance) and mixing angle θ :

$$p(\nu_\mu \rightarrow \nu_e) = \sin^2 2\theta \times \sin^2(1.27 \times L \delta m^2 / E_\nu) \quad (1).$$

The units in eq.(1) are as follows: the difference of the squares of the 2 neutrinos, $\delta m^2 = m^2_1 - m^2_2$, is in eV²; the neutrino energy E_ν is in MeV and the distance from the neutrino source, L , is expressed in metres. It is clear from eq. (1) that the first minimum in the ν_μ flux occurs at a distance L such that $L/E_\nu \sim 1/\delta m^2$, and its value at the minimum is $(1 - \sin^2 2\theta)$. Thus, from simultaneous measurements at two distances and several neutrino energies E_ν , one can determine both δm^2 and $\sin^2 2\theta$.

The set up of the present experiments is shown in figure 1. The PS proton beam strikes a 60 cm long Be target followed by a 50 m long decay tunnel, which is terminated by Fe absorbers, concrete and earth. About 140 m downstream are placed the so-called near detectors (3 modules out of 13 for CHARM and 4 out of 19 for the CDHS detectors; for details see ref. 3). About 880 metres further downstream are placed the so-called FAR detectors, which are the rest of the CDHS and CHARM detectors, left in their original position. Since the runs are bare target runs (no horn or other focusing), the simple $\sim 1/R^2$ law for the intensity decrease with distance from target serves as a good approximation. For the present set-up this means an intensity drop at the far detector by a factor of ~ 30 , which is reduced to about 13 (for both experiments) since the FAR detector is more massive than the Near (by \sim factor 3). Since the ν -beam in the present experiments³⁾ will yield reasonable rates for $E_\nu \sim 0.4\text{-}4$ GeV, from eq.(1) the δm^2 region covered will be ~ 0.4 to 4 eV².

Neutrino oscillation experiments are usually limited¹⁾ by systematic errors since they involve basically a comparison between two or more experiments

performed under different conditions. The present set-up reduces most of the systematic errors, which, we hope, would be no more than $\sim 3\%$.

1. The exposure of both detectors is simultaneous, and thus beam intensity uncertainties will cancel out to a large extent.
2. The neutrino beam is simple and thus errors in the $1/R^2$ factor as well as those arising from the fact that the two detectors subtend different solid angles, are minimal.
3. The modules in the Far and Near detectors are quite identical and to make the detectors more similar the Near detector was placed with its axis at 22° to the ν beam, which is the angle at which the Far detector axis (facing the SPS ν -beam) is away from the PS ν beam (see fig.1).

We can estimate now the new limits that the present experiments can put on δm^2 and $\sin^2 2\theta$. The exposure took place from 15 February to 30 March 1983. We obtained a total of about $1 \cdot 10^{19}$ protons on target ($\sim 1.2 \cdot 10^{13}$ p/pulse) and the total number of ν interactions inside the fiducial volume for the two experiments is roughly as follows (the tonnage of the fiducial volume is also given):

	Near detector	Far detector
CDHS	150 tons 80,000 events	500 tons 7,000 events
CHARM	30 tons 25,000 events	100 tons 2,000 events

clearly²⁾ CDHS will have more events, but CHARM will be able to measure lower E_ν events.

The present existing (90% c.l.) limits¹⁾ are shown in fig. 2, where δm^2 is plotted vs. $\sin^2 2\theta^{4-7})$. The channel which so far has not been so well explored is the oscillation $\nu_\mu \leftrightarrow \nu_\tau$, to which the new experiments will contribute most (CERN '83, dashed line, in fig. 2). However, even in the relatively well-covered sector $\nu_e \leftrightarrow \nu_\mu$, the CHARM experiment (and more so the forthcoming BEBC experiment at the same beam) could improve the limits in the δm^2 region of 1-2 eV 2 and small $\sin^2 2\theta$ (.1-.2), by searching for appearance of ν_e events in the far detector. It should be noted that since neutral current (NC) interactions in the CHARM detector are easily recognizable, CHARM can also measure the NC/CC ratio in both detectors, which is sensitive to ν -oscillations, and is almost free of any systematic errors.

I am grateful to CERN for its kind hospitality and I wish to thank many of my colleagues for interesting discussions. I wish also to thank the Minna-James-Heineman Stiftung of Hannover for their kind support.

REFERENCES

1. For a summary of recent results see R.J.N. Phillips, lecture notes for the Kupari-Dubrovnik School, September 1982 (Rutherford Laboratory report RL-82-100), and
F. Vannucci, CERN Fixed Target Workshop, Dec. 1982 (Proc. to appear soon).
2. S.M. Bilenky and B. Pontecorvo, Phys. Rep. 41 (1978) 215;
A. de Rujula et al., Nucl. Phys. B168 (1980) 64.
3. The CDHS proposal, CERN/OSCC/80-106 (1980), and the
CHARM proposal, CERN/PSCC/81-8 (1981).
4. H. Kwon et al., Phys. Rev. D24 (1981) 1097.
5. J.L. Vuilleumier et al., Phys. Lett. 114B (1982) 298.
6. N.J. Baker et al., Phys. Rev. Lett. 47 (1981) 1576.
7. O. Erriquez et al., Phys. Lett. 102B (1981) 73.

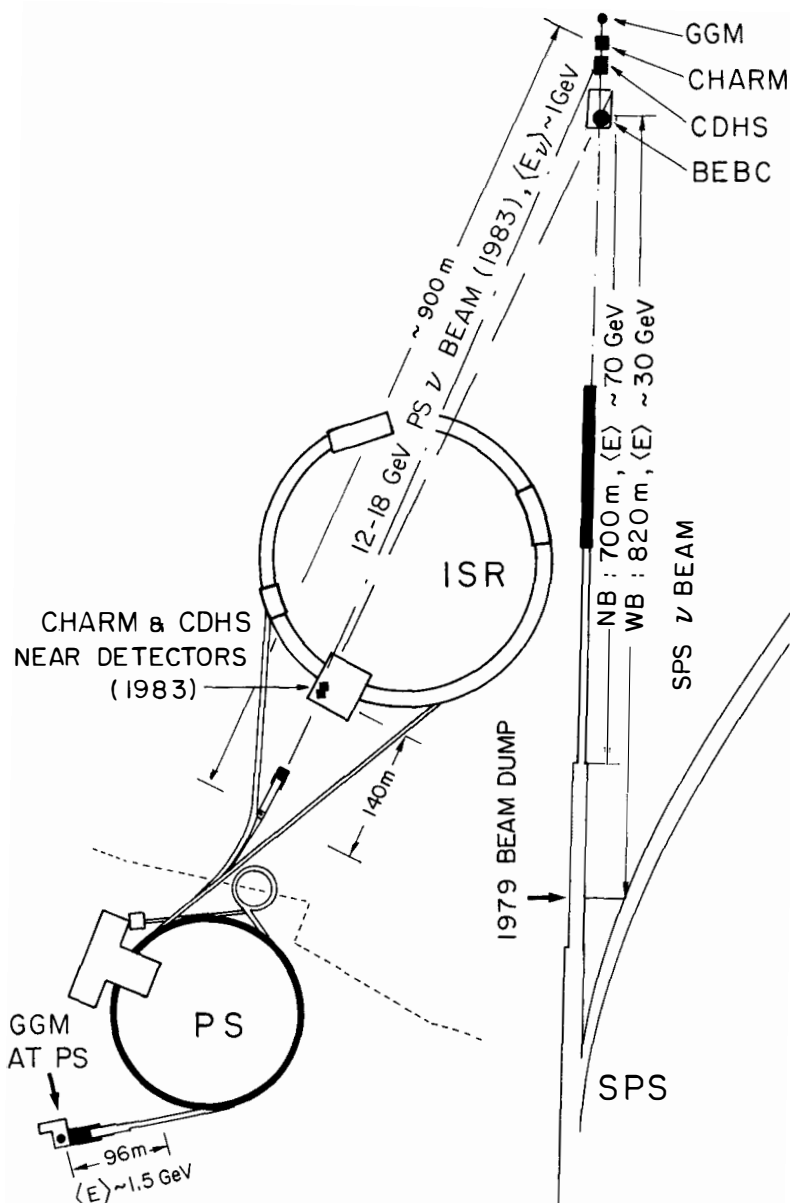


Fig. 1 Set-up of the PS ν -beam for the present ν -oscillation experiments at CERN

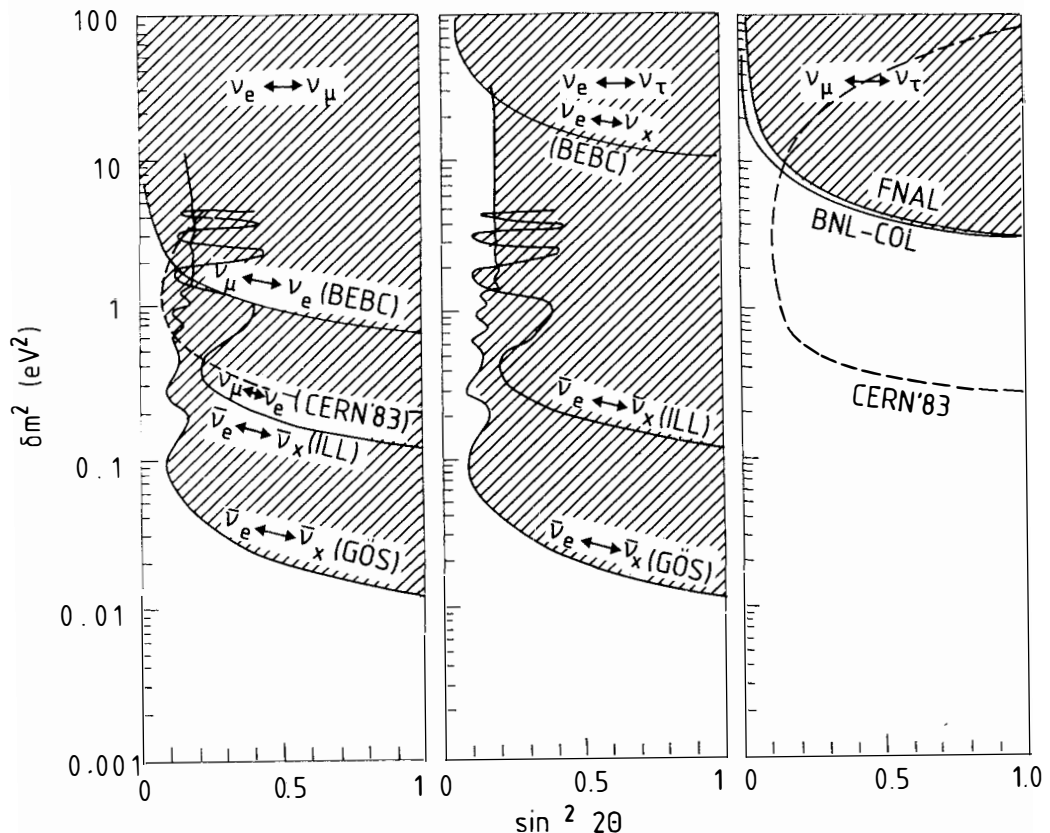


Fig. 2 Existing 90% C.L. on δm^2 and mixing angle θ for ν -oscillations (shaded areas are excluded): ILL⁴) and Gösgen⁵) are from reactors. BNL-COL⁶) and BEBC⁷) are high energies. Dashed lines: expected, present experiments

RECENT RESULTS FROM SPEAR

Klaus Wacker
(representing the Crystal Ball collaboration ^{*})
Stanford Linear Accelerator Center
Stanford University, Stanford, California 94305

Abstract

The first part of this talk is an experimental review of the properties of the Θ meson. Results or upper limits come from radiative J/ψ decays and $\gamma\gamma$ scattering for the final states $\eta\eta$, $\pi\pi$, KK and $\rho\rho$. In the second part, an upper limit is given for the production of low-mass particles in radiative J/ψ decays. Constraints for the existence of low-mass gluonic and Higgs mesons are derived.

1. Introduction

The investigation of radiative J/ψ - decays has in recent years led to a number of interesting results in old-fashioned, non-charm physics. The highlights were the discovery of two new mesons, the Θ^1 and the τ^2 . Although these mesons have perfectly normal quantum numbers, they are unusual in two ways: Firstly, they are unexpected, i.e. they do not fit into existing multiplets in the naive quark model; secondly, they are produced in a channel in which no constituent quarks are transferred from the initial to the final state, whereas they do not seem to be produced copiously in "normal" hadronic reactions³. There have been many speculations that their main constituents are gluons⁵.

Recent results from SPEAR come from two experiments, which are both running at other storage rings now: Crystal Ball and Mark II. (Crystal Ball is now running at DORIS, Mark II at PEP. A new experiment, Mark III, is now running at SPEAR, but there are no results at the time of this conference). In the on-going analysis of SPEAR data, radiative J/ψ - decays play a major role in both groups. I will present here a necessarily biased selection of recent results. In the first part, I will give an overview of the present experimental knowledge of the Θ meson. In the second part, I will present an upper limit on the production of low-mass π pairs in radiative J/ψ - decays and discuss limits on low-mass gluonia or low-mass Higgs mesons.

2. Brief Characterization of the Experiments

The Crystal Ball⁶ is a nonmagnetic detector specialized in the detection of electromagnetically showering particles. Its main part is a segmented array of NaI (Tl) shower counters arranged spherically around the interaction point. It covers 93% of 4π solid angle. The energy resolution is $\sigma_E/E = 2.6\%/\sqrt{E}$. NaI (Tl) endcaps cover an additional 5% of 4π . Inside the main sphere there are two cylindrical spark chambers and one multiwire proportional chamber for the detection of charged particles and for measurement of their angles. The Crystal Ball has taken a data sample corresponding to 2.2×10^6 produced J/ψ 's.

Mark II⁷ is a magnetic detector which uses 16 cylindrical layers of drift chambers as its main device to track charged particles. The momentum resolution is $\sigma_p^2/p^2 = (1.5\%)^2 + (0.5\%p)^2$. Outside of this there is a layer of scintillation counters used to measure the time-of-flight (ToF) of charged particles. It can distinguish pions from kaons below 1.3 GeV/c at the one-stan-

standard-deviation level. Outside of the magnet coil there are lead-liquid-Argon shower counters with an energy resolution of $\sigma_E/E = 14\%/E^{1/2}$. The efficiency for low-energy photons is low, it reaches 50% of the maximum efficiency at about 200 MeV. Mark II has 1.3×10^6 J/ψ 's. Only half of these data, however, were taken with operational shower counters.

It is clear that the strengths of the two detectors are complementary: The Crystal Ball is good at detecting photons and neutral hadrons decaying into photons, whereas Mark II is good at detecting charged hadrons.

3. What Do We Know about the Θ Meson?

3.1. $J/\psi \rightarrow \gamma nn$

The Θ meson was discovered by the Crystal Ball in radiative J/ψ - decays through its decay mode into nn^1 . Fig. 1 shows the $\eta\eta$ mass distribution. The

curves show fits to the histogram which included a Breit-Wigner function to describe the Θ and a constant term for the background. The broken curve included also a Breit-Wigner function for the $f'(1515)$ meson with mass and width as given by ref. 4. There was no statistically significant evidence for f' production, and the Θ parameters found by the two fits agreed within errors. The fitted Θ parameters (from the fit including f') were:

$$M_\Theta = (1670 \pm 50) \text{ MeV}$$

$$\Gamma_\Theta = (160 \pm 80) \text{ MeV}.$$

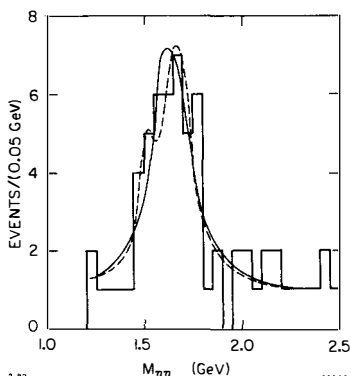


Fig. 1.

nn mass distribution in the reaction $J/\psi \rightarrow \gamma nn$ (Crystal Ball). The curves are explained in the text.

The rate of Θ production was measured to be:

$$BR(J/\psi \rightarrow \gamma\Theta) \times BR(\Theta \rightarrow nn) = (3.8 \pm 1.6) \times 10^{-4}.$$

We know from its production and decay mechanism that the Θ must have positive G and C parity and zero isospin. The spin and parity J^P are restricted to the series $0^+, 2^+, 4^+, \dots$. The Crystal Ball analyzed the angular distribution and found that spin 2 was favoured over spin 0 with a likelihood ratio of 1:0.045. Higher spins were not considered. It has to be noted that the likelihood ratio does not take systematic errors into account.

Both the Crystal Ball and Mark II have looked for other decay modes of the Θ . No signal was found for the decay into $\pi\pi$. The Crystal Ball found an upper limit of $\text{BR}(\text{J}/\psi \rightarrow \gamma\Theta) \times \text{BR}(\Theta \rightarrow \pi\pi) < 6.0 \times 10^{-4}$ (90% C.L.) using the reaction $\text{J}/\psi \rightarrow \gamma\pi^0\pi^0$ (see Fig. 8). Mark II⁸ found this number to be $< 3.2 \times 10^{-4}$ (90% C.L.) using charged pions. Mark II did find signals consistent with Θ in the KK and $\rho\rho$ decay modes.

3.2. $\text{J}/\psi \rightarrow \gamma\text{K}^+\text{K}^-$

To investigate the reaction $\text{J}/\psi \rightarrow \gamma\text{K}^+\text{K}^-$ ⁸, events were selected with two oppositely charged particles which had a ToF consistent with that expected for kaons. A major background comes from the reaction $\text{J}/\psi \rightarrow \text{K}^+\text{K}^-\pi^0$, which was shown to be mostly due to $\text{J}/\psi \rightarrow \text{K}^\pm\text{K}^\mp$. Most of these events could be removed by requiring that the kaons be acollinear by at least 30° . The missing mass was required to be consistent with Θ . From here on, two different methods were used. In method I, it was required that one photon shower was observed in the liquid-Argon shower counters. The missing vector was computed from the two charged tracks. Its component transverse to the direction of the observed shower, p_{Ty} , is expected to peak at zero for $\text{K}^+\text{K}^-\gamma$ events, whereas it has a broad, flat distribution for $\text{K}^+\text{K}^-\pi^0$ events in which one of the decay photons of the π^0 has escaped detection. p_{Ty} was required to be less than 40 MeV. Finally, a kinematic fit with 4 constraints was done and events with $\chi^2 < 15$ were kept. The resulting K^+K^- mass spectrum is shown in Fig. 2. It shows a peak with position and width compatible with the Θ . The two curves represent fits analogous to those shown in Fig. 1. The background term turned out to be compatible with Θ .

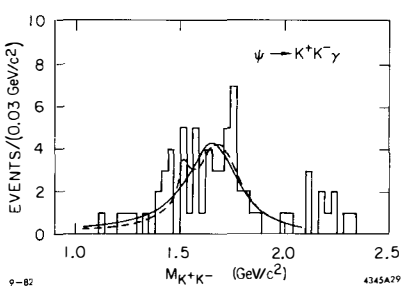


Fig. 2.

K^+K^- mass distribution in the reaction $\text{J}/\psi \rightarrow \gamma\text{K}^+\text{K}^-$ (Mark II, method I). The curves are explained in the text.

Method I yielded a very clean, but small data sample. It was investigated whether one could increase the data sample without increasing the background to unacceptable levels by loosening some of the cuts. In particular, if Mark II can do without detecting the photon, they gain not only by the increase in geometric acceptance by a factor of 1.5, but also because they can use the data taken without operational shower counter. With the other cuts essentially the same, this was called method II. There are several known and unknown sources of background

which enter the event sample of method II. Radiative Bhabha events, which are harder to identify without the shower counter, constitute 10% of the event sample. These events tend to be peaked both at the highest and the lowest masses, only 1% is expected to be in the Θ mass region. Another background comes from $J/\psi \rightarrow K^{\pm*} K^{\mp} \rightarrow K^{\pm} K^{\mp} \pi^0$ is a background at high $K^{\pm} K^{\mp}$ masses. The

reaction $\psi \rightarrow K^0 K^0$, where the K^0 decays into neutrals and the K^0 decays into $K^{\pm} \pi^{\mp}$, enters the data sample, when the pion is misidentified as a kaon. This fake $-K^{\pm} K^{\mp}$ mass peaks at around 1050 MeV. More background may come from multiparticle final states and other unknown sources.

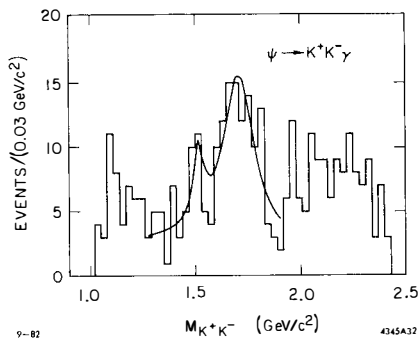


Fig. 3.

$K^{\pm} K^{\mp}$ mass distribution in the reaction $J/\psi \rightarrow \gamma K^{\pm} K^{\mp}$ (Mark II, method II). The curve is from a fit analogous to the broken curves in Figs. 1 and 2.

Fig. 3 shows the resulting $K^{\pm} K^{\mp}$ mass plot. As expected, there is more background than in Fig. 2, but also a bigger Θ signal. There is also some evidence for f' production. A fit analogous to the one represented by the broken curve in Fig. 1 yielded the following results:

$$M_{\Theta} = 1700 \pm 30 \text{ MeV} \quad \Gamma_{\Theta} = 156 \pm 20 \text{ MeV} \\ \text{BR}(J/\psi \rightarrow \gamma \Theta) \times \text{BR}(\Theta \rightarrow K^{\pm} K^{\mp}) = (6.0 \pm 0.9 \pm 2.5) \times 10^{-4}.$$

The first error is statistical, the second systematic. The background in the Θ region was about 25% of the events.

Whereas the larger sample was used to determine resonance parameters, the cleaner sample of method I was used to do a spin determination with the same method as used by the Crystal Ball. The result is that spin 2 is favoured over spin 0 by 1:0.22. If systematic errors could be neglected, one could multiply this likelihood ratio with the one from the Crystal Ball to obtain an overall confidence level. However, systematic errors are not easily expressed in terms of likelihood ratios, and it has not been done here. Furthermore, there is at least one possible common error: Both data samples may contain f' events, which are known to have spin 2 and which would shift the likelihood ratio in favour of spin 2.

3.3. $J/\psi \rightarrow \gamma \rho^0 \rho^0$

To investigate the reaction $J/\psi \rightarrow \gamma \rho^0 \rho^0$, Mark II has looked into the final

state $\gamma \pi^+ \pi^- \pi^-$. The method used to select these events was similar to method I described in the previous paragraph: Events were selected with one observed photon and four charged tracks consistent with pions according to ToF. The missing mass recoil against the charged particles was required to be consistent with zero. The remaining background after these cuts is the channel $\pi^0 \pi^+ \pi^+ \pi^-$, which has the highest branching ratio of all hadronic J/ψ - decays. It is reduced by a cut in $p_{t\gamma}$. The remaining background of about 40% of the sample is subtracted using events with higher $p_{t\gamma}$ as background sample and using the known shape of the $p_{t\gamma}$ distribution for normalization.

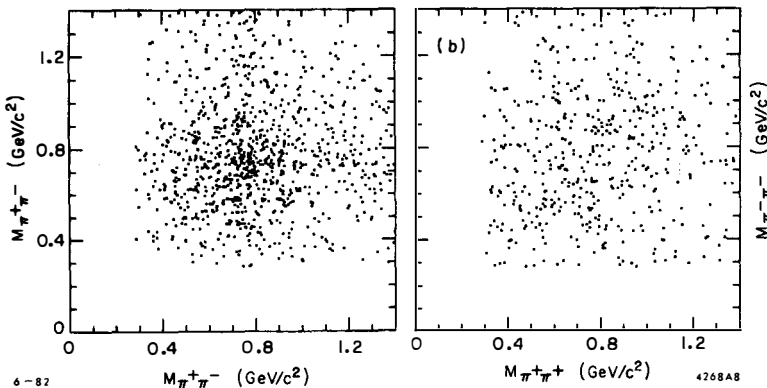


Fig.4. Scatterplot of a) $\pi^+ \pi^-$ vs. $\pi^+ \pi^-$ mass and b) $\pi^+ \pi^+$ vs. $\pi^- \pi^-$ mass in the reaction $J/\psi \rightarrow \gamma \pi^+ \pi^+ \pi^- \pi^-$ (Mark II).

Fig. 4a shows a scatterplot of $\pi^+ \pi^-$ versus $\pi^+ \pi^-$ mass (2 combinations per event). For comparison, Fig. 4b shows a scatterplot of the like-sign mass combinations. There is a clear enhancement in the unlike-sign combinations at the mass of $\rho(770)$. The fraction of $\gamma \rho^0 \rho^0$ events, as opposed to uncorrelated $\gamma \pi^+ \pi^+ \pi^- \pi^-$, was determined by a maximum-likelihood fit. The $\rho^0 \rho^0$ distribution used in the fit was a product of two Breit-Wigner functions, symmetrized to take the presence of identical Bosons in the final state into account. A similar fit was done to the π^0 background events and the results were subtracted binwise. The resulting $\rho^0 \rho^0$ mass distribution is shown as solid line in Fig. 5. In another fit the channel $\gamma \rho^0 \pi^+ \pi^-$ was also allowed to contribute. The results are shown as dots in Fig. 5. This resulted in a lower $\rho^0 \rho^0$ contribution at some points, but did not change the overall shape. Instead of uncorrelated $\gamma \rho^0 \pi^+ \pi^-$, it was also tried to fit $\gamma A_1^{\pm} \pi^{\mp}$ $\rightarrow \gamma \rho^0 \pi^+ \pi^-$, without significant change in the result.

There is a clear enhancement at around 1600 MeV and no significant signal elsewhere. When the $\rho^0 \rho^0$ mass spectrum was fitted with a Breit-Wigner function, a

mass of 1650 ± 50 MeV with a width of 200 ± 100 MeV was obtained. These parameters are compatible with the Θ , however,

the Mark II authors did not claim that this signal was the Θ . The reasons for this reserve were firstly that the enhancement was right above the $\rho\rho$ threshold and secondly that a spin determination was not possible. For these reasons a nonresonant threshold effect could not be excluded. A branching ratio was given for the reaction $J/\psi \rightarrow \gamma\rho^0\rho^0$ with $m_{\rho^0\rho^0} < 2$ GeV, independent of any resonance interpretation. It was measured to be $(1.25 \pm 0.35 \pm 0.40) \times 10^{-3}$.

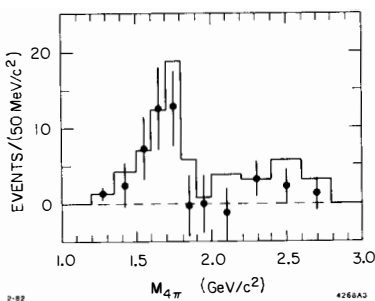


Fig. 5.

$\rho^0\rho^0$ mass distribution in the reaction $J/\psi \rightarrow \gamma\rho^0\rho^0$ (Mark II). The solid line and the dots represent two different fits (see text).

3.4. $\gamma\gamma \rightarrow nn$

The radiative J/ψ - decays mentioned so far are the only reactions in which the Θ has been seen. This reaction is, according to perturbative QCD in lowest order, mediated by 2 gluons. Since QCD also predicts that gluons can form bound states, it has been conjectured that the Θ is such a gluonic meson. In order to check this hypothesis, it is useful to look for other channels to which the Θ may couple. The two-photon channel lends itself as it has the same quantum numbers as two gluons, but different couplings. A pure gluonium state, which has no electrically charged constituents, has a very small coupling to $\gamma\gamma$. It is expected that gluonic mesons mix with ordinary mesons of the same quantum numbers (f and f' in case of the Θ). Measurement of the partial width $\Gamma(\Theta \rightarrow \gamma\gamma)$ helps determine the mixing parameters.

The Crystal Ball has looked for Θ production in $\gamma\gamma$ scattering in the nn decay mode. The data were taken at center-of-mass energies between 4 and 7 GeV and represent an integrated luminosity of 21 pb^{-1} . We are looking for the reaction $e^+e^- \rightarrow e^+e^-nn \rightarrow e^+e^-\gamma\gamma\gamma\gamma$, where the outgoing electrons are scattered under very small or 0 angle and are not observed. According to QED, the final state hadrons are produced by the collision of two virtual, but very nearly on-shell photons. Candidate events were selected¹⁰ by requiring that there were 4 clean photon showers and nothing else in the detector. The two-photon origin of these events was established by observing that a) the energy seen is less than the center-of-mass energy and b) the transverse momentum distribution of the 4-photon system peaks at 0.

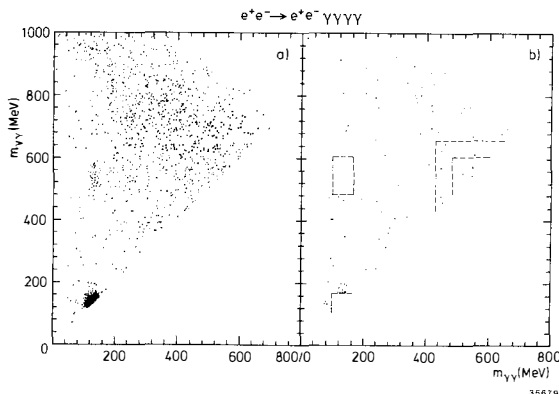
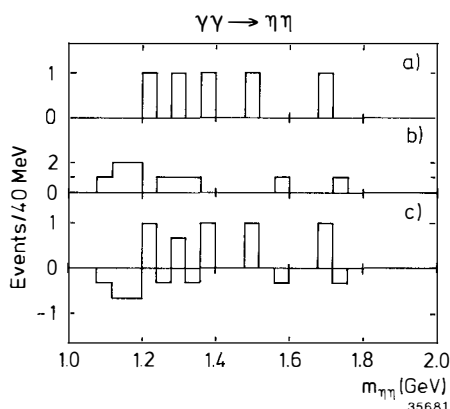


Fig. 6.

a) Scatterplot of high vs. low $\gamma\gamma$ mass for 4-photon events with $1040 < m(4\gamma) < 1480$ MeV, 3 combinations per event (Crystal Ball).
 b) same as a), but $\pi^0\pi^0$ and $\pi^0\eta$ events removed. The broken lines indicate the $\pi^0\pi^0$, $\pi^0\eta$, and $\eta\eta$ regions and the $\eta\eta$ control region.

We first turn our attention to a 4-photon mass (W) region where we know¹⁰ that there are signals from $f \rightarrow \pi^0\pi^0$ and $A_2 \rightarrow \pi^0\eta$. Fig. 6a shows a scatterplot of high vs. low $\gamma\gamma$ mass with 3 combinations per event, which clearly shows $\pi^0\pi^0$ and $\pi^0\eta$ signals. There is also a continuum background which is mostly due to wrong combinations of events in the peaks. When these events were removed (Fig. 6b), very few events remained which did not show any clustering in the $\eta\eta$ region. Events in the $\eta\eta$ region indicated in the figure were considered possible signal events, whereas the larger, surrounding $\eta\eta$ control region was used to estimate background. Fig. 7 shows the distribution of events in the signal and the control region and the normalized difference as function of W .



There is no signal. To obtain an upper limit for the Θ , events in the W range 1400-1800 MeV were used. The 2-photon flux was calculated according to ref. 11. It was assumed that the

Fig. 7.

a) Distribution of events in the $\eta\eta$ region as function of W (Crystal Ball)
 b) The same for events in the $\eta\eta$ control region
 c) Normalized difference of distributions a) and b).

Θ has spin 2 and is in a helicity state $\pm 2^*$. The resulting upper limit was

$$\Gamma(\Theta \rightarrow \gamma\gamma) \times \text{BR}(\Theta \rightarrow \eta\eta) < 0.3 \text{ keV (95% C.L.)}.$$

Systematic errors were included. If, instead of helicity ± 2 , an isotropic angular distribution was assumed, the upper limit increased by a factor of 1.9 due to decreased acceptance. If the spin were zero, the upper limit would increase by another factor of $2L + 1 = 5$.

The TASSO collaboration^{12,13} at PETRA found two more upper limits on $\Theta \rightarrow \gamma\gamma$.

They are

$$\Gamma(\Theta \rightarrow \gamma\gamma) \times \text{BR}(\Theta \rightarrow K\bar{K}) < 0.3 \text{ keV (95% C.L.)}$$

$$\Gamma(\Theta \rightarrow \gamma\gamma) \times \text{BR}(\Theta \rightarrow \rho^0\rho^0) < 1.2 \text{ keV (95% C.L.)}.$$

These numbers cannot be compared directly, since the branching ratios are not known. One can form ratios with the corresponding partial widths in ψ decays such that the branching ratios cancel. The results are summarized in Table 1. The $\rho^0\rho^0$ signal of section 3.3 was assumed to be due to Θ . The best upper limit for $\Gamma(\Theta \rightarrow \gamma\gamma)/\Gamma(J/\psi + \gamma\Theta)$ comes from the $K\bar{K}$ channel.

tensor meson T	decay channel X	$\frac{\Gamma(J/\psi \rightarrow \gamma T) \times \text{BR}(T \rightarrow X)}{\text{eV}}$	ref.	$\frac{\Gamma(T \rightarrow \gamma\gamma) \times \text{BR}(T \rightarrow X)}{\text{eV}}$	ref.	$\frac{\Gamma(T \rightarrow \gamma\gamma)}{\Gamma(J/\psi + \gamma T)}$
Θ	$\eta\eta$	24 ± 10	1	< 300		< 13
	$K\bar{K}$	$76 \pm 11 \pm 32$	8	< 300	13	< 4
	$\rho^0\rho^0$	$79 \pm 22 \pm 25$	9	< 1200	12	< 15
f	all	95 ± 25	4	2900 ± 500	4	31 ± 10
f'	$K\bar{K}$	$11 \pm 4 \pm 6$	8	$110 \pm 20 \pm 40$	13	10 ± 10

Table 1

Comparison of the production of tensor mesons by $\gamma\gamma$ scattering and by radiative ψ -decays. Where two errors are given, the first is statistical and the second systematic.

This ratio does not mean much by itself, but it can be compared to other tensor mesons. Measurements exist for f and f' , although they have large errors in case of the f' . We find that $\Gamma(f \rightarrow \gamma\gamma)/\Gamma(\psi \rightarrow \gamma f)$ is considerably bigger than the corresponding Θ upper limit. If we interpret $\Gamma(T \rightarrow \gamma\gamma)/\Gamma(J/\psi + \gamma T)$ as a qualitative measure of the charge as opposed to gluon content of a meson, we find the

*The reason for this assumption is that it is true for the f^{10} .

numbers consistent with the naive picture that the f consists mostly of u and d quarks, the f' mostly of s quarks and the Θ mostly of gluons. However, one should not overinterpret this ratio - it is just the only way to compare the experimental results in the absence of absolute branching ratio measurements.

3.5. Θ Summary

Since its discovery in the reaction $J/\psi \rightarrow \gamma \eta \eta$, considerable progress has been made in the experimental knowledge about the Θ . Another decay channel, $KK\bar{K}$, has been identified. If the signal seen in $\rho^0 \rho^0$ also comes from the Θ , then the known branching ratio for $J/\psi \rightarrow \gamma \Theta$ is $(5.3 \pm 1.7) \times 10^{-3}$, which is as large as the largest known branching ratio in radiative J/ψ - decays, that of the ψ . Meaningful upper limits have been obtained for $\Gamma(\Theta \rightarrow \gamma \gamma)$. Of course, much more information is needed. Most notably, a high-statistics spin determination with good confidence level is lacking.

quantity	value		ref.
Θ mass, width (MeV)	1670 ± 50	160 ± 80	1
	1700 ± 30	156 ± 20	8
	$[1650 \pm 50]$	200 ± 100	9
$BR(J/\psi \rightarrow \gamma \Theta)BR(\Theta \rightarrow nn)$	$(3.8 \pm 1.6) \cdot 10^{-4}$		1
$BR(J/\psi \rightarrow \gamma \Theta)BR(\Theta \rightarrow KK)$	$(12.0 \pm 1.8 \pm 5.0) \cdot 10^{-4}$		8
$BR(J/\psi \rightarrow \gamma \Theta)BR(\Theta \rightarrow \pi\pi)$	$< 6 \times 10^{-4}$ (90% C.L.)		1
	$< 3.2 \times 10^{-4}$ (90% C.L.)		8
$BR(J/\psi \rightarrow \gamma \rho \rho, m_{\rho \rho} < 2 \text{ GeV})$	$[(3.75 \pm 1.05 \pm 1.20) \cdot 10^{-3}]$		9
$\Gamma(\Theta \rightarrow \gamma \gamma)BR(\Theta \rightarrow nn)$	$< .3 \text{ keV}$ (95% C.L.)		
$\Gamma(\Theta \rightarrow \gamma \gamma)BR(\Theta \rightarrow KK)$	$< .3 \text{ keV}$ (95% C.L.)		13
$\Gamma(\Theta \rightarrow \gamma \gamma)BR(\Theta \rightarrow \rho \rho)$	$< 3.6 \text{ keV}$ (95% C.L.)		12
spin 2 vs. spin 0	95%		1
Confidence Level	78%		8

Table 2

Experimental results about the Θ meson. Where two errors are given, the first is statistical, the second systematic. Branching ratios were corrected for unseen charge states assuming isospin 0. The numbers from ref. 9 are not necessarily related to Θ .

The most interesting question, whether Θ is a gluonic meson, is not easy to answer. There is no quantum number "gluoniumness" - the gluon content of a meson has to be inferred using all available information and allowing for mixing with quarkonia. With our present knowledge the result is model-dependent at best.

Table 2 shows a compilation of experimental results about the Θ .

4. An Upper Limit for Low-Mass Particles Produced in Radiative J/ψ - Decays

The motivation for a search for low-mass particles produced in radiative J/ψ - decays comes from a number of predictions for the existence of a low-mass gluonic meson. The result will also be used to place a constraint on a possible low-mass Higgs meson.

4.1. The Experimental Upper Limit

The Crystal Ball has investigated the reaction $J/\psi \rightarrow \gamma\pi^0\pi^0$. To do this, events were selected which have 3, 4, or 5 clusters of neutral energy and no charged tracks. A π^0 can appear as 1 or 2 clusters, depending mainly on its energy. The energy distribution in every cluster was fitted with either one or the sum of two electromagnetic shower patterns in order to determine whether it is due to a single photon or to two merged photons from a π^0 . The events where then kinematically fitted to the hypothesis $\gamma\pi^0\pi^0$, where the π^0 mass was put in as a constraint when the χ^2 probability was better than 10%.

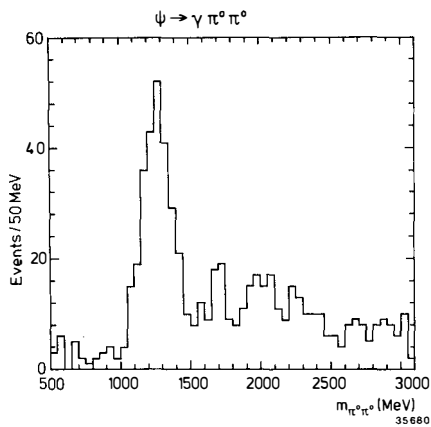


Fig. 8.

$\pi^0\pi^0$ mass distribution for the reaction $J/\psi \rightarrow \gamma\pi^0\pi^0$ (Crystal Ball).

Fig. 8 shows the $\pi^0\pi^0$ mass distribution. The most prominent feature is a peak due to the $f(1270)$ meson, the analysis of which has been published¹⁸. We further note that there are very few events below 1 GeV. Fig. 9 shows the detection efficiency as function of $\pi^0\pi^0$ mass. The efficiency does not vary rapidly over the mass range 500-3100 MeV. (It does drop sharply below 500 MeV due to the overlap of photons from two different pions). We observe 28 events in the mass range 500-1000 MeV with an average efficiency of 32%. This corresponds to a branching ratio of about 4×10^{-5} . To obtain upper limits for any narrow object with a width not bigger than 100 MeV, we use sideband subtraction to estimate background. The result is

$$BR(J/\psi \rightarrow \gamma X \rightarrow \gamma\pi^0\pi^0) < 1.3 \times 10^{-5} \text{ (95% C.L.)}$$

for any X with $500 < m_X < 1000$ MeV and $\Gamma_X < 100$ MeV.

4.2. Is there a Scalar Gluonium?

One of the bound states of gluons predicted by QCD is expected to have the quantum numbers of the vacuum, $J^{PC} = 0^{++}$. The possible mixing of this state with the vacuum leads in some models to predictions of very low masses. Note that for masses below about 1 GeV, $\pi\pi$ is the only open two-body decay channel and 1/3 of $\pi\pi$ has to be $\pi^0\pi^0$ due to isospin invariance. As the upper limit is far below typical branching ratios for radiative J/ψ - decays into gluonia, any narrow

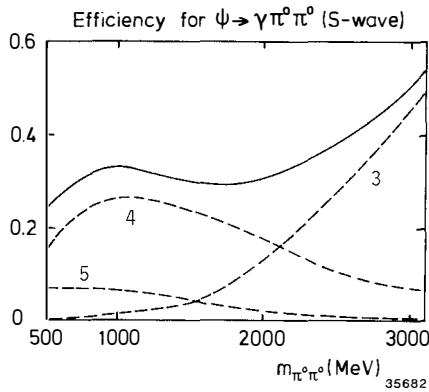


Fig. 9.

Detection efficiency for $J/\psi \rightarrow \gamma\pi^0\pi^0$ as function of $\pi^0\pi^0$ mass. The broken curves show the efficiencies for events with 3, 4, and 5 clusters, the solid curve is the sum. The $\pi\pi$ system is assumed to be in an S-wave.

4.3. Is there a Light Higgs Meson?

Gauge theories of electroweak interactions predict the existence of at least one Higgs meson¹⁹. Little is known about its mass. Theoretical considerations suggest a mass on the order of 10 GeV or more, however, this is not a stringent limit. The best experimental lower limit comes from the Crystal Ball²⁰: $m_H > 50$ MeV.

Higgs mesons lighter than J/ψ are produced in radiative J/ψ - decays with the following branching ratio²¹:

$$\begin{aligned} BR(J/\psi \rightarrow \gamma H) &= BR(J/\psi \rightarrow \mu^+ \mu^-) \frac{G_F m_\psi^2}{4\sqrt{2} \pi \alpha} \left(1 - \frac{m_H^2}{m_\psi^2}\right) \\ &\sim 6 \cdot 10^{-5} \left(1 - \frac{m_H^2}{m_\psi^2}\right). \end{aligned}$$

Higgs particles are expected to decay into pairs of the heaviest particles al-

luonium state with a mass between 500 and 1000 MeV can be ruled out. This contradicts the prediction¹⁴ of $m(0^{++}) \sim 700$ MeV which was obtained using QCD sum rules. However, later sum rule calculations^{15,16} resulted in higher 0^{++} masses of between 1 and 1.6 GeV which cannot be ruled out by this result. More recently, lattice calculations¹⁷ resulted in scalar gluon masses between 700 and 900 MeV. This can be ruled out unless this object is very wide.

lowed by kinematics. A Higgs particle in the mass range of 500 to 1000 MeV would decay mostly into $\pi\pi$ pairs, a third of which would be neutral pions. Combining the upper limit on $\pi^0\pi^0$ production with the predicted branching ratio for $J/\psi \rightarrow \gamma H$, we obtain an upper limit on the branching ratio for $H \rightarrow \pi\pi$:

$$BR(H \rightarrow \pi\pi) < 72\% \text{ (95\% C.L.) for } 500 < m_H < 1000 \text{ MeV.}$$

Theoretical estimates¹⁹ predict that the $\pi\pi$ - decay mode strongly dominates $\mu\mu$, the only other sizable decay mode in this mass range. $\pi\pi$ branching ratios are expected to be close to 100%, although there is some uncertainty and branching ratios less than 72% are conceivable at the higher end of the mass range. With this exception, Higgs mesons in the mass range 500 to 1000 MeV are ruled out.

To summarize this section, a stringent upper limit was obtained for low-mass (500-1000 MeV) particles produced in radiative J/ψ - decays. A narrow gluonic meson is ruled out and the existence of a Higgs meson is very unlikely in this mass range.

References:

- * The Crystal Ball Collaboration at SPEAR: C. Edwards, R. Partridge, C. Peck, F.C. Porter (Caltech); D. Antreasyan, Y.F. Gu, J. Irion, W. Kollmann, M. Richardson, K. Strauch, K. Wacker, A. Weinstein (Harvard); D. Aschman, T. Burnett, M. Cavalli-Sforza, D. Coyne, C. Newman, H.F.W. Sadrozinski (Princeton); D. Gelphman, R. Hofstadter, R. Horisberger, I. Kirkbride, H. Kolanoski, K. Königsmann, R. Lee, A. Liberman, J. O'Reilly, A. Osterheld, B. Pollock, J. Tompkins (Stanford); E.D. Bloom, F. Bulos, R. Chestnut, J. Gaiser, G. Godfrey, C. Kiesling, W. Lockman, M. Oreglia, D.L. Scharre (SLAC)
- 1. C. Edwards et al., Phys. Rev. Lett. 48 (1982), 458
- 2. C. Edwards et al., Phys. Rev. Lett. 49 (1982), 259
- 3. The π may have been observed in $\bar{p}p$ annihilations: P. Baillon et al., Nuovo Cimento A50 (1967), 393. A clear preference for the assignment $J^P = 0^-$ was indicated in this publication. However, as the $E(1420)$ designation has since been accepted as the $J^P = 1^+$ state seen in $\pi^- p$ interactions⁴, a new name was given to the pseudoscalar state.
- 4. Particle Data Group, Physics Lett. 111B (1982)
- 5. For a review of gluonic mesons see e.g. E.D. Bloom, 21st Int. Conf. on High Energy Physics, Paris 1982.
- 6. M. Oreglia, Ph.D. thesis, Stanford University, SLAC-236 (1980)
M. Oreglia et al., Phys. Rev. D25 (1982), 2259
J. Gaiser, Ph.D. thesis, Stanford University, SLAC-255 (1982)
- 7. R. Schindler, Ph.D. thesis, Stanford University, SLAC-219 (1979)
- 8. M.E.B. Franklin, Ph.D. thesis, Stanford University, SLAC-254 (1982)
- 9. D.L. Burke et al., SLAC-PUB-2941 (1982)
- 10. C. Edwards et al., Phys. Lett. B110 (1982), 82

11. G. Bonneau, M. Gourdin, F. Martin, Nucl.Phys. B54 (1973), 573
12. TASSO Collaboration, M. Althoff et al., Z.Phys. C16 (1982), 13
13. TASSO Collaboration, M. Althoff et al., Phys.Lett. 121B (1983), 216
14. V.A. Novikov et al., Nucl.Phys. B165 (1980), 67
15. M.A. Shifman, Z.Phys. C9 (1981), 347
16. P. Pascual and R. Tarrach, Phys.Lett. 113B (1982), 495
17. K. Ishikawa, M. Teper and G. Schierholz, Phys.Lett. 116B (1982), 429
18. C. Edwards et al., Phys.Rev. D25 (1982), 3065
19. J. Ellis, M.K. Gaillard and D.V. Nanopoulos, Nucl.Phys. B106 (1976), 292
J. Ellis, XIVth Rencontre de Moriond, Les Arcs 1979
20. K. Königsmann, XVIIth Rencontre de Moriond, Les Arcs 1982
21. F. Wilczek, Phys.Rev.Letters 39 (1977), 1304

A REVIEW OF e^+e^- ANNIHILATION RESULTS FROM CLEO*

H. Kagan
Ohio State University, Columbus, Ohio 43210

and

W. W. Mackay
Harvard University, Cambridge, Massachusetts 02138

and

E. H. Thorndike
University of Rochester, Rochester, New York 14627

(For the CLEO Collaboration - Cornell, Harvard,
Ohio State, Rochester, Rutgers, Syracuse,
Vanderbilt)

ABSTRACT

CLEO results on T spectroscopy and b quark decay are reviewed. New results include a measurement of the branching ratio for $B \rightarrow \psi X$, and improved upper limit on $(b \rightarrow u)/(b \rightarrow c)$, a first look for CP violation in b decay, and an improved upper limit on flavor changing neutral currents in b decay.

*Supported by the National Science Foundation and the U.S. Department of Energy.

I. INTRODUCTION

The CLEO detector began taking data at the Cornell Electron Storage Ring (CESR) in the fall of 1979. We review the results obtained with that detector through March 1983. In the interests of brevity, we concentrate on recent results, and omit most experimental details. We also mention results that may be expected in the near future.

Figure 1 shows the hadronic cross section from e^+e^- annihilation into one photon, as a function of center of mass energy, from 9.4 to 10.6 GeV.¹⁾ The conspicuous features are three narrow resonances, the $\Upsilon(1S)$, $\Upsilon(2S)$ and $\Upsilon(3S)$, and one broad resonance, the $\Upsilon(4S)$. The widths of the first three resonances are consistent with the energy resolution of CESR, $4.1 \text{ MeV} \times (S/100 \text{ GeV}^2)$. The natural width of these resonances is tens of kilovolts. In contrast the $\Upsilon(4S)$ is noticeably broad.

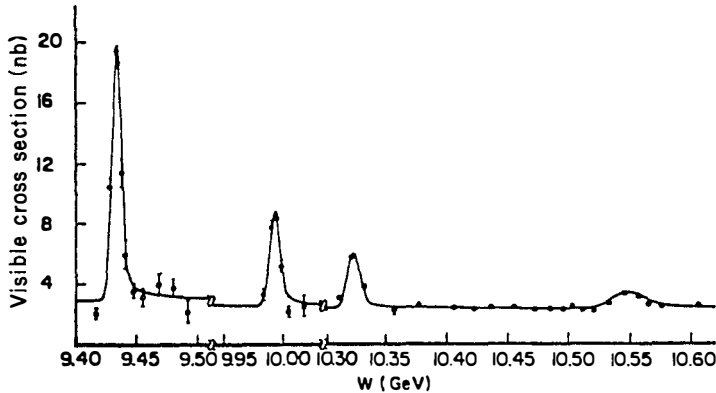


Figure 1. Cross section for $e^+e^- \rightarrow \text{hadrons}$, as a function of center-of-mass energy, in the Υ energy region.

These resonances are generally interpreted as the first four radial excitations of 3S_1 states of $b\bar{b}$ quark pairs. Within this interpretation the first three resonances are narrow because their strong decay is suppressed by the OZI rule. The broad width of the fourth resonance indicates that it is above the threshold for production of $B\bar{B}$ meson pairs. Thus the $\Upsilon(4S)$ decays strongly into $B\bar{B}$ with no suppression and hence has a much greater width.

The general features of the annihilation process in the energy range 9.4 GeV to 10.6 GeV define three distinct areas of physics. (1) The narrow resonances and continuum allow an investigation of the process by which the underlying quarks and gluons materialize into hadrons. (2) A rich spectroscopy of bound $b\bar{b}$ systems can be studied, starting with the narrow Υ systems.

resonances. (3) The $T(4S)$ is a "factory" producing bare b , and can be used to study B mesons and the weak decay of b quarks. The following discussion will limit itself to results on $b\bar{b}$ spectroscopy and $T(4S)$ physics.

II. UPSILON SPECTROSCOPY

The rich level structure of $b\bar{b}$ bound states expected from potential model calculations²⁾ is shown in Fig. 2. The 3S_1 states are easily studied since they are directly produced in the one photon annihilation process in e^+e^- collisions. Data on the widths of the 3S_1 states are given in Section A. The 3P_J states can be reached from the 3S_1 states by E1 photon transitions. The 1P_1 and 1S_0 states are more difficult to access, requiring either a weak $\pi\pi$ transition (e.g., from 3S_1 to 2P_1) or a combination of $\pi\pi$ and photon transitions (e.g., from 3S_1 to 1S_0). In Section B we discuss $\pi\pi$ and photon transitions.

A. Widths of $T(1S)$, $T(2S)$ and $T(3S)$

In Figure 1 we show the hadronic cross section for e^+e^- annihilation. The area under each resonance seen in the hadronic cross section is proportional to the width of that resonance into e^+e^- (Γ_{ee}) times the branching ratio of the resonance into hadrons ($\Gamma_{had}/\Gamma_{tot}$). Our measurements³⁾ for $\Gamma_{ee}\Gamma_{had}/\Gamma_{tot}$ for the three narrow upsilon resonances are given in Table I. These measurements, together with a measurement of the branching ratio of each resonance into lepton pairs, yields the total width of that resonance.

The branching ratio for $T(1S) \rightarrow \mu^+\mu^-$ was measured some time ago by CLEO⁴⁾ and by others.⁵⁾ More recently CLEO has made an improved measurement⁶⁾ of the

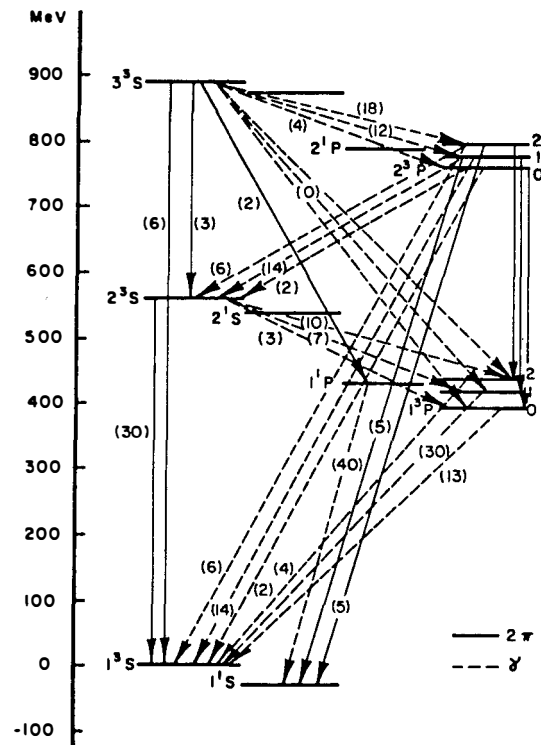


Figure 2. Level structure of $b\bar{b}$ bound states expected from potential model calculations (Ref. 2).

branching ratio for $T(1S) \rightarrow \mu^+ \mu^-$, and also measured the decays⁶⁾ of $T(2S)$ and $T(3S)$ to $\mu^+ \mu^-$, and the decay⁷⁾ $T(1S) \rightarrow \tau^+ \tau^-$. One expects the branching ratios to $\mu^+ \mu^-$, $\tau^+ \tau^-$ and $e^+ e^-$ to be equal, assuming e , μ and τ are all point-like leptons. The new results, along with the old world average and a new world average for $T(1S)$, are given in Table I.

Noting that $\Gamma_{ee} \Gamma_{had} / \Gamma_{tot}$ equals $\Gamma_{tot} B_{\mu\mu} (1 - 3B_{\mu\mu})$, we obtain Γ_{tot} from the information given in Table I and list it there also.

Table I. Γ_{ee} , $B_{\mu\mu}$ and Γ_{tot} for Narrow Upsilon Resonances

	$T(1S)$	$T(2S)$	$T(3S)$
$\Gamma_{ee} \left[\frac{\Gamma_{had}}{\Gamma_{tot}} \right] (\text{KeV})$	1.17 ± 0.09	0.49 ± 0.05	0.38 ± 0.04
$B_{\ell\ell} (\%)$			
old world average	3.3 ± 0.6		
CLEO, $\mu^+ \mu^-$	2.7 ± 0.4	1.9 ± 1.4	3.3 ± 1.5
CLEO, $\tau^+ \tau^-$	3.4 ± 0.6		
new world average	3.0 ± 0.3		
$\Gamma_{tot} (\text{KeV})$	42 ± 6	27 ± 18	13 ± 5

B. Transitions among the T Resonances

Yan⁸⁾ has developed a model for $\pi\pi$ transitions among $b\bar{b}$ bound states. It involves emission of two gluons, which hadronize into a pion pair. Gluon emission is treated by multipole expansion of the gluon field. Current algebra and PCAC place constraints on the $\pi\pi$ system.

Some time ago CLEO observed the transitions $T(2S) \rightarrow \pi^+ \pi^- T(1S)$ ⁴⁾ and $T(3S) \rightarrow \pi^+ \pi^- T(1S)$,⁹⁾ as did CUSB.¹⁰⁾ The branching ratios observed can be accommodated by Yan's model. The $\pi\pi$ mass distribution for $T(2S) \rightarrow \pi^+ \pi^- T(1S)$ is similar to that for $\psi' \rightarrow \pi^+ \pi^- \psi$, peaking toward the high end of the mass range. In contrast, the $\pi\pi$ mass distribution in the decay $T(3S) \rightarrow \pi^+ \pi^- T(1S)$ is rather flat.

The value of Γ_{tot} for the $T(2S)$ allows us to determine the ratio $\Gamma(T(2S) \rightarrow \pi\pi T(1S)) / \Gamma(\psi' \rightarrow \pi\pi\psi)$. This ratio is sensitive to the spin of the gluon mediating the decay and is expected to be 0.11 for vector gluons and 1.0 for scalar gluons.⁸⁾ Using the data for $\psi' \rightarrow \pi\pi\psi$ from Ref. 11 and our data (Table I) we obtain 0.071 ± 0.04 for this ratio. This result is in agreement with the vector hypothesis and incompatible with the scalar hypothesis.

CLEO has just completed a 20 pb^{-1} run at $T(2S)$. We expect to have improved statistics on the $T(2S) \rightarrow \pi\pi T(1S)$ reaction. We are also analyzing the recent

2S data for structure in the photon spectrum, and for the cascade decays $T(2S) \rightarrow \gamma\gamma T(1S)$, $T(1S) \rightarrow \mu^+\mu^-$ or e^+e^- . Results are not available on these reactions at this time.

III. BARE b

In Section I we asserted that the $T(4S)$ was a bare-b factory. Further, the b-flavored hadrons produced in $T(4S)$ decays are expected to be stable against strong and electromagnetic decays. They must decay weakly, if at all. The weak decay of the b-flavored hadrons was observed soon after the $T(4S)$ was discovered.¹²⁾ However it was only recently that B mesons have actually been reconstructed.¹³⁾

In Section A we discuss the recent reconstruction of B mesons. Inclusive features of B decay--kaon yields, charged particle multiplicities, branching ratios to ψ --are presented in Section B. In Section C non-standard models of b-decay are discussed, and it is shown that CLEO data rule out most of them. The standard model of b-decay is outlined in Section D, and the observables of b-decay related to this model.

Semileptonic decays of B mesons are treated in Section E, which gives new results on the $(b \rightarrow u)/(b \rightarrow c)$ ratio, the semileptonic decay branching ratio and the lepton charge asymmetry. Section F deals with events containing two leptons. These provide limits on flavor changing neutral currents, the B^\pm/B^0 lifetime ratio, and (in principle) $B^0-\bar{B}^0$ mixing.

Most results are based on a data sample of 40 pb^{-1} on $T(4S)$ and 17 pb^{-1} on the continuum below the $T(4S)$, taken from February to November 1982.

A. B Meson Reconstruction

From the mean charged multiplicity at $T(4S)$, we anticipate that a B meson will decay, on average, into 9 particles (charged plus neutral). Further we expect the relative momentum of B and \bar{B} from $T(4S)$ decay to be small. Hence it follows that the B and \bar{B} decay products will be completely intermixed. One readily concludes that it is not possible to reconstruct an "average" B meson decay. The combinatorial backgrounds (mixing particles from B and \bar{B}) are fierce, and the likelihood of missing a particle (e.g., a π^0) is very high. The only hope is to concentrate on low multiplicity decay modes, preferably ones with some characteristic features.

As will be shown in Section E, the dominant decay of b is to c. One thus expects that the dominant decay of B is to a charmed meson plus pions. We therefore looked for decays of B to $D^{*\pm}$ or D^0 , and one or two charged pions. The $D^{*\pm}$ was identified via the decay chain $D^{*+} \rightarrow D^0\pi^+$, $D^0 \rightarrow K^-\pi^+$. In this decay, the K^\pm need not be identified explicitly since we have excellent

resolution in the $D^* - D^0$ mass difference due to the low Q value of the reaction. The direct D^0 from B decay was identified by its $K^-\pi^+$ decay mode, using kaons identified by dE/dx or TOF. Thus our final states consisted of 3 to 5 charged particles and no neutrals, and had as a characteristic feature the $D^{*\pm}$ or D^0 , allowing background suppressing cuts to be made. Further background suppression was achieved by requiring that the particles assumed to form a B added up to the beam energy.

The mass distribution for the four decay modes under consideration is shown in Fig. 3. A peak of 18 events is seen. We estimate the background in several different ways, and find it to be 4-7 events.

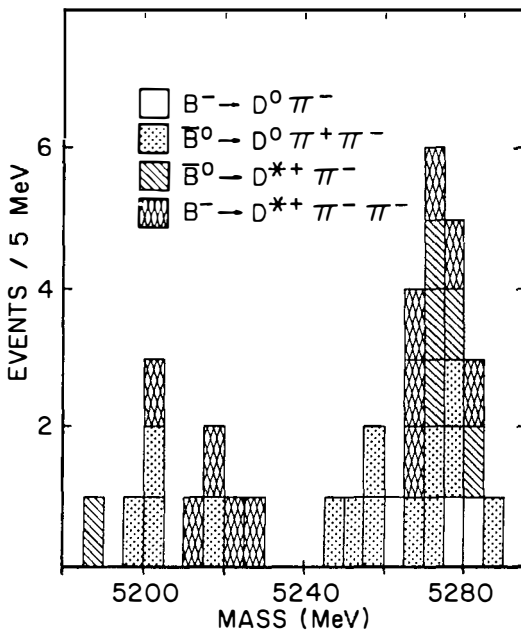


Figure 3. Mass distribution for B meson candidates. The $B \rightarrow$ final-state decay labels should be interpreted as including the charge conjugate reaction also.

We find a mass of $5274.2 \pm 1.9 \pm 2.0$ MeV for the neutral B , and $5270.8 \pm 2.3 \pm 2.0$ MeV for the charged B . The $\bar{B}^0 - B^-$ mass difference is $3.4 \pm 3.0 \pm 2.0$ MeV, consistent with the theoretical prediction¹⁴⁾ of 4.4 MeV (but also with zero). The average of the charged and neutral B masses is $5272.3 \pm 1.5 \pm 2.0$ MeV. This corresponds to a mass difference of 32.4 ± 5.0 MeV between the mass of $T(4S)$ and twice the B meson mass. Using this mass difference and the theoretical value of 4.4 MeV for the $\bar{B}^0 - B^-$ mass difference, we

obtain the branching fractions $B(T(4S) \rightarrow B^+ B^-) = 0.60 \pm 0.02$ and $B(T(4S) \rightarrow B^0 \bar{B}^0) = 0.40 \pm 0.02$. The branching ratios for the four B decay modes used here for reconstructing B's are in the few percent range. A more complete description of this B reconstruction work appears in Ref. 13.

The decay chain $B \rightarrow D^{*+} \pi^-$, $D^{*+} \rightarrow D^0 \pi^+$ can be used to provide information on the B spin. The decay angle distribution of D^0 in the D^{*+} rest frame, using the D^{*+} boost axis as z axis, can be used to determine elements of the D^* spin density matrix. In particular, ρ_{00} must be 1 for spin 0 B, but can have any value between 0 and 1 for spin 1 B. From the D^0 decay angle distribution we find $\rho_{00} = 0.93 \pm 0.30$, agreeing nicely with the expected spin 0.

B. Inclusive Features of B Meson Decay

1. Charged particles multiplicities

By studying the charged particle multiplicities in T(4S) events, and in T(4S) events containing leptons, we can determine the mean charged multiplicity for nonleptonic and semileptonic B decays. We find

$$\begin{aligned} N_B &= 5.75 \pm 0.1 \pm 0.2, \\ N_S &= 4.1 \pm 0.35 \pm 0.2, \text{ and} \\ N_h &= 6.3 \pm 0.2 \pm 0.2. \end{aligned}$$

N_B , N_S and N_h are, in order, the average, semileptonic, and nonleptonic B mean charged multiplicities.¹⁵⁾

We can apply the preceding results to study the degree of hadronization present in B-meson decay under the assumption that b quarks always decay into final states containing a c quark. If, for example, the c quark fragments into an equal mixture of D and D^* mesons, then we can subtract the measured charged multiplicity of such a mixture¹⁶⁾ (2.5 ± 0.1) to obtain $0.55 \pm 0.35 \pm 0.2$ and $3.8 \pm 0.2 \pm 0.2$ as the number of charged hadrons produced in addition to charmed mesons in semileptonic and nonleptonic b decay respectively.

2. Charged and Neutral Kaon Yields

Some time ago,¹⁷⁾ we reported charged and neutral kaon yields from T(4S) and from the continuum, and used the ratio of the kaon yields to determine the fraction of b decays to c to be $1.09 \pm 0.33 \pm 0.13$.

A preliminary analysis of the new data sample gives the kaon yields shown in Table II. From the ratio of $K^\pm + K^0$ on the T(4S) and the continuum, we determine the relative amounts of $b \rightarrow c$ and $b \rightarrow u$ in b decay. For pure $b \rightarrow c$, this ratio is expected to be 1.80 ± 0.10 , while for pure $b \rightarrow u$, it is 0.95 ± 0.10 . The errors reflect uncertainties in the Monte Carlo calculation. Our new data yield $(b \rightarrow c)/(b \rightarrow \text{all}) = 0.72 \pm 0.15$. This result is consistent with, but

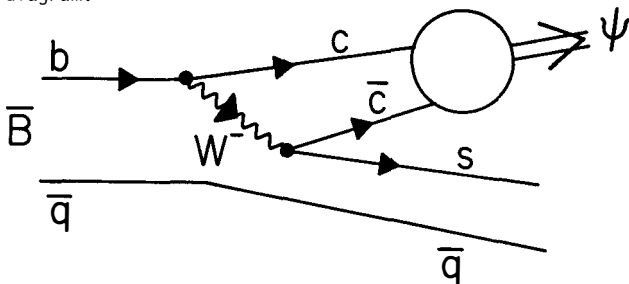
less accurate than, the result obtained from the lepton momentum spectrum described in Section E.

Table II. The average number of charged and neutral kaons per event for the continuum and for $T(4S)$.

	continuum	$T(4S)$
K^\pm	$0.90 \pm 0.03 \pm 0.15$	$1.53 \pm 0.12 \pm 0.22$
K^0	$0.86 \pm 0.02 \pm 0.10$	$1.31 \pm 0.08 \pm 0.10$

3. Branching Ratio for $B \rightarrow \psi + \text{Anything}$

Fritzsch¹⁸⁾ has estimated a 3-5% branching ratio for $B \rightarrow \psi + \text{anything}$, from the following diagram.



We have measured that branching ratio and find Fritzsch's estimate to be high.

We detect ψ 's by the $\mu^+ \mu^-$ and $e^+ e^-$ decay modes. For $\mu^+ \mu^-$, we require that both particles be identified as muons. There are 41 dimuon events in our 40 pb^{-1} $4S$ sample. The $\mu^+ \mu^-$ invariant mass distribution is shown in Fig. 4a. The shape of the background distribution is determined by combining μ^+ and μ^- from different dimuon events. The dashed curve is this background, normalized to the events in the 2.5-4.0 GeV mass interval. There are 6 events within $\pm 1.5 \sigma$ of the ψ mass, while the background computation gives 2.3 ± 0.5 . From these numbers we conclude that the branching ratio to ψ is greater than zero at 97% confidence level, less than 2% at 98% confidence level, and can be written as $[0.7^{+0.7}_{-0.4}] \%$.

For $\psi \rightarrow e^+ e^-$, we require that one particle be positively identified as an electron, and the other particle be not inconsistent with being an electron. The set of events is thus those with at least one identified electron. The shape of the background is determined by combining an electron from one event with a charged particle from another event, the particle having charge opposite to the electron in its own event. The $e^+ e^-$ invariant mass distribution is shown in Fig. 4b. The dashed curve is the background, normalized between 2.5 and 4.0 GeV.

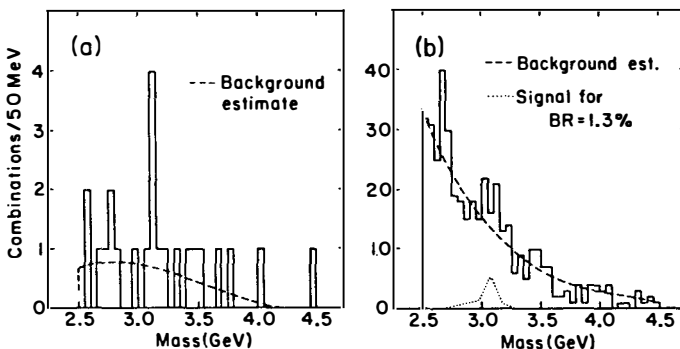


Figure 4. Mass distributions for (a) $\mu^+ \mu^-$ and for (b) $e^+ e^-$.

There are 59 events in the ψ mass region, where the background calculation gives 40 ± 6 events. From these numbers we conclude that the branching ratio to ψ is greater than zero at 99% confidence level, less than 2% at 88% confidence level, and can be written as $(1.3 \pm 0.7)\%$.

We combine the branching ratios obtained from $\mu^+ \mu^-$ and $e^+ e^-$ decay modes to obtain a branching ratio for $B \rightarrow \psi + X$ of $\begin{pmatrix} 1.0 & +0.5 \\ & -0.4 \end{pmatrix}\%$.

We have not demonstrated that ψ comes from $T(4S)$ rather than from the continuum under it. While there is no theoretical reason to expect ψ from the continuum, the best experimental upper limit we can obtain (from 17 pb^{-1} of continuum data) for the contribution to an apparent $B \rightarrow \psi X$ decay is 0.8%, at 90% confidence level. Thus we cannot rule out the possibility that the ψ signal comes entirely from the continuum.

C. Non-Standard Models of b Decay

We have explored, in a systematic way, the consistency of data on b decays with possible models of the decay. We find two classes of models consistent with all the data--one of which is the standard model.

Figure 5 divides models of b decay into seven classes. Within the current broad theoretical framework, we believe this classification is all-inclusive, i.e., any possible model will fall into one of the seven classes. We now show that CLEO data excludes 5 of the 7 classes.

The possibility that b is stable is excluded by the observation of $T(4S)$, with its decay into many particles.

The exotic decays of b are ruled out by considering five inclusive variables measured for $T(4S)$: mean charged energy, muon yield, electron yield, proton yield and lambda yield. Depending upon whether the leptons in the decay $b \rightarrow llq$ are predominantly muons and electrons, or predominantly taus and neutrinos, the event

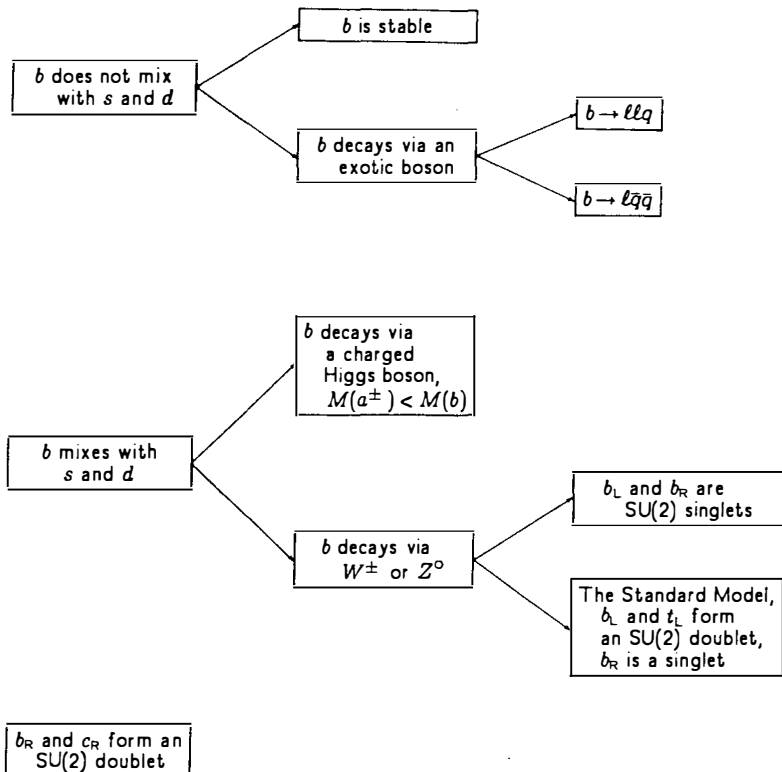


Figure 5. A classification of models of b quark decay.

would have too many μ 's and/or e 's, or too little charged energy. No compromise can simultaneously satisfy muon yield, electron yield, and mean charged energy. The decay $b \rightarrow l \bar{q} q$ always makes a baryon. If the baryon is a neutron, charged energy is lowered; if a proton, proton yield is raised. The arguments for leptons are the same as for $b \rightarrow l l q$. Thus, there is no compromise that can have high enough charged energy, and simultaneously few enough μ , e , p , and Λ . We exclude the possibility that either $b \rightarrow l l q$ or $b \rightarrow l \bar{q} q$ are the sole decay modes of the b at a very high confidence level (see Ref. 19 for further details).

If there is a charged Higgs boson a^\pm lighter than the b quark, then the b quark will decay $b \rightarrow q a^\pm$ essentially 100% of the time, because the decay is semi-weak, while the standard-model decay is weak. The Higgs boson will in turn decay $\tau \nu$ and/or $c \bar{s}$. This possibility for b decay is ruled out by data on charged energy and muon and electron yields. If the Higgs decays dominantly to $\tau \nu$ the muon and electron yields will be reasonable, but the charged energy will be too low. If Higgs decays dominantly to $c \bar{s}$, the muon and electron yields will be too

low, while the charged energy will be reasonable. There is no mix of $\tau\nu/c\bar{s}$ that can simultaneously have a high energy μ and e yield and a high energy value for charged energy. (See Ref. 19 for further details.)

If b mixes with s and/or d , but is itself a singlet, then the GIM mechanism will not operate, and flavor changing neutral currents will be present. In particular, the decays $B \rightarrow Xe^+e^-$ and $B \rightarrow X\mu^+\mu^-$ must occur. Kane and Peskin²⁰⁾ have shown that, for these models, $\frac{Br(B \rightarrow X\ell^+\ell^-)}{Br(B \rightarrow X\ell^\pm\nu)} > 0.12$. In Section F we show that this ratio is in fact < 0.05 , ruling out this class of models.

Having ruled out 5 classes of models of b quark decay, we are left with the standard model, and with one non-standard, topless model, originally noted by Tye and Peskin.²¹⁾ Here b forms a right-handed doublet with c . This model in many ways mimics the standard model, as far as b decay is concerned, and at present cannot be excluded.

It is worth noting that the reconstruction of B mesons (see Section A) also rules out the five classes of non-standard models just ruled out by inclusive data. Further, the observed decay modes ($B \rightarrow D$ or D^* plus 1 or 2 pions) are consistent both with the standard model and with Tye and Peskin's b , c right-handed doublet model.

D. The Standard Model of b Decay

In the standard model of b decay, b is in a left-handed doublet with t , mixes with s and d , and decays via W^- , the neutral current decay being suppressed by the GIM mechanism. The mixing is described by the K.M. matrix, which is parametrized by the angles θ_1 , θ_2 , θ_3 and one phase δ . A frequently used representation is

$$\begin{bmatrix} d' \\ s' \\ b' \end{bmatrix} = \begin{bmatrix} c_1 & s_1 c_3 & s_1 s_3 \\ -s_1 c_2 & c_1 c_2 c_3 + s_2 s_3 e^{i\delta} & c_1 c_2 s_3 - s_2 c_3 e^{i\delta} \\ -s_1 s_2 & c_1 s_2 c_3 - c_2 s_3 e^{i\delta} & c_1 s_2 s_3 + c_2 c_3 e^{i\delta} \end{bmatrix} \begin{bmatrix} d \\ s \\ b \end{bmatrix}$$

$$c_i(s_i) \equiv \cos(\theta_i)(\sin(\theta_i)).$$

The angles and phase are not specified by the standard model, but rather are parameters to be determined by data. Nuclear β decay determines the $d \rightarrow d'$ element c_1 , i.e., the Cabibbo angle θ_1 . Strange particle decays determine the $s \rightarrow d'$ element $s_1 c_3$, and in conjunction with the determination θ_1 allow one to place the limit $c_3 > .87$, $|s_3| < 0.5$. The phase δ allows the possibility of CP violation. The small size of CP violation in neutral kaon decays determines that δ is close to (but slightly different from) either 0 or π . For purposes other than CP violation, it is sufficiently accurate to set $\delta = 0$ or π . Neutral kaon

phenomena, in particular the $K_L^0 - K_S^0$ mass difference, determines a relation between s_2 and s_3 , namely, $s_2 = 0.2 + \frac{1}{2}(\cos \delta + \frac{1}{2}) s_3 \pm 0.1$. (Some theorists question the validity of this relation.)

b decay can determine two elements of the K.M. matrix. The $b \rightarrow u$ transition depends upon the $b \rightarrow d'$ elements $s_1 s_3$, while the $b \rightarrow c$ transition depends upon the $b \rightarrow s'$ element $c_1 c_2 s_3 - s_2 c_3 e^{i\delta}$. The most directly accessible observables are the B lifetime τ_B and the ratio of branching ratios

$\text{Br}(b \rightarrow u \ell \nu) / \text{Br}(b \rightarrow c \ell \nu) \equiv \begin{bmatrix} b \rightarrow u \\ b \rightarrow c \end{bmatrix}$. Contours of constant τ_B and $(b \rightarrow u) / (b \rightarrow c)$ are shown in the s_2 - s_3 plane in Fig. 6. Thus these observables are not predicted by the standard model.

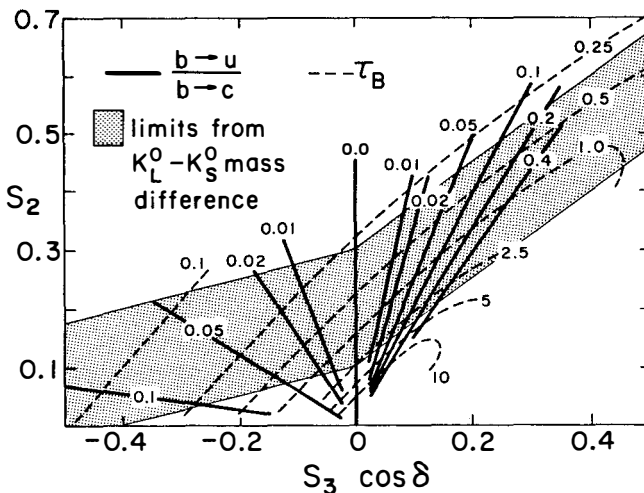


Figure 6. Contours of constant $(b \rightarrow u) / (b \rightarrow c)$ and B lifetime in the s_2 - s_3 plane, for $\delta=0$ and for $\delta=\pi$. The unshaded region is excluded by neutral kaon information.

Two observables that are predicted by the standard model are the semi-leptonic decay branching ratio and the decay $B \rightarrow X \ell^+ \ell^-$. The latter, a flavor-changing-neutral-current-mediated decay, is predicted to vanish. The former is subject to strong interaction corrections, as noted in Section E.

In the phenomena mentioned so far in this section, the light antiquark bound to the b quark in the B meson is a spectator. We now mention some phenomena in which the light antiquark plays an essential role. Exchange and annihilation diagrams contribute differently to B^\pm and B^0 decay, causing the non-leptonic decay rates and consequently the semileptonic decay branching ratios to differ. Box diagrams allow B^0 and \bar{B}^0 to mix. With mixing comes the possibility of CP violation. These phenomena will be considered in Sects. E, F.

E. Semileptonic Decays of B Mesons

The dominant sources of high momentum muons and electrons from T(4S) decays are $B \rightarrow X\ell\nu$ and $B \rightarrow X\bar{e}v$. (Semileptonic decays of charm and the decay $B \rightarrow X\tau\nu$ make small contributions above 1 GeV, and can be treated as a correction.) Since the B mesons are not at rest, the lepton spectrum receives a small, calculable Doppler smearing.

The muon and electron momentum spectra from T(4S) decays are shown in Fig. 7. They have been normalized to the same area. The agreement between the two spectra is excellent. The solid curve is a calculation assuming a V-A interaction and a 50%-50% mix of $B \rightarrow D\ell\nu$, $B \rightarrow D^*\ell\nu$. If the b quark decays to a u quark, then the hadronic system X in the decay $B \rightarrow X\ell\nu$ can have a mass M_X lighter than the D meson mass. M_X can be as light as m_π , and is expected²²⁾ to average around 500 MeV. Curves for two values of M_X in the range appropriate for $b \rightarrow u\ell\nu$ are also shown on Fig. 7.

A small component of $b \rightarrow u$ decays among a dominant $b \rightarrow c$ decay would reveal itself as an excess of events beyond the end point of the $B \rightarrow (D \text{ or } D^*)\ell\nu$ curve. The solid curve is a good representation of the data, and no excess at high momentum is apparent. We therefore interpret the measured spectra to obtain an upper limit on the $(b \rightarrow u)/(b \rightarrow c)$ ratio. We do this as a function of M_{X_u} , the mean mass of the hadronic system in the decay $b \rightarrow u\ell\nu$. Results are shown in Fig. 8. Since the effective value of M_{X_u} is assuredly less than 1 GeV,²²⁾ we can conclude that $(b \rightarrow u)/(b \rightarrow c)$ is less than 0.05. This restricts the allowed values of s_2 and s_3 , as can be seen from Fig. 6.

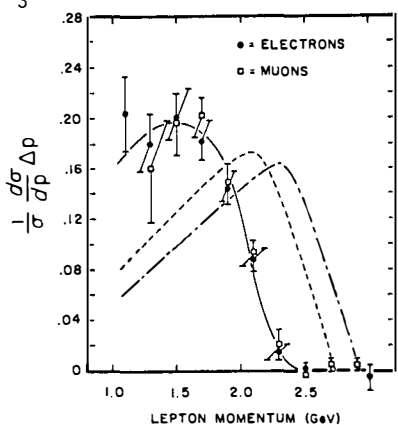


Figure 7. Muon and electron momentum spectra from T(4S) decays. The curves are theoretical calculations for $B \rightarrow X\ell\nu$ assuming a V-A interaction. Assumptions about X are: solid curve, 50% D, 50% D^* ; broken curve, $X = \pi$, dashed curve, $M_X = 1.0$ GeV.

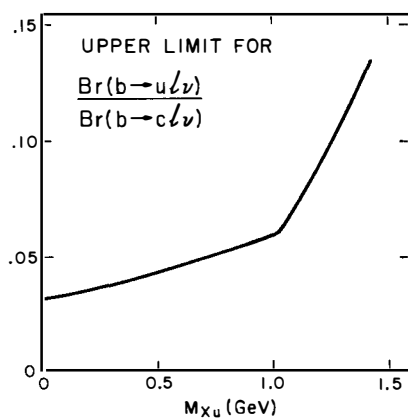


Figure 8. Upper limits (90% c.l.) on the $(b \rightarrow u)/(b \rightarrow c)$ ratio as a function of the mean mass of the hadronic system in the decay $b \rightarrow u\ell\nu$.

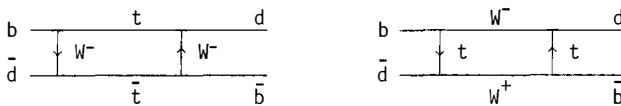
CLEO has published measurement of the B semileptonic decay branching ratio²³⁾ based on a 5.5 pb^{-1} data sample. Those measurements had substantial systematic errors due to the uncertainty in the shape of the lepton spectrum. Analysis of the 40 pb^{-1} data sample has not progressed to the point that we can quote a branching ratio from the new data. We can, however, use the shape of the lepton spectrum from the new data to correct the old data, thereby reducing the systematic errors. The corrected numbers are:

$$\text{Br}(B \rightarrow X\bar{e}v) = 0.120 \pm 0.017 \pm 0.013$$

$$\text{Br}(B \pm X\bar{\mu}v) = 0.102 \pm 0.014 \pm 0.015$$

If one treats the light quark in the B as a spectator, and also ignores QCD effects (i.e., considers only quark counting plus phase space), then the b semi-leptonic decay branching ratio is expected to be 16.9%.²⁴⁾ Hadronic enhancements lower this number to 14.6%.²⁴⁾ Including non-spectator effects (a W exchange diagram) lowers the neutral B branching ratio further, such that the average becomes 12.4%.²⁴⁾ CLEO results suggest that hadronic enhancements and non-spectator effects are about as expected.

B^0 and \bar{B}^0 are expected to mix $B^0 \rightleftharpoons \bar{B}^0$, e.g., via the diagrams



If CP is violated, the transition rates need not be equal, and one can have unequal numbers of B^0 and \bar{B}^0 's decaying. This would reveal itself as a lepton charge asymmetry, since B^0 and \bar{B}^0 decay to oppositely charged leptons.

Using the 40 pb^{-1} 4S data sample, we have taken a first look for CP violating effects in B decay, measuring muon and electron charge asymmetries. We find:

$$\frac{N_{\mu^+} - N_{\mu^-}}{N_{\mu^+} + N_{\mu^-}} = +0.02 \pm 0.04$$

$$\frac{N_{e^+} - N_{e^-}}{N_{e^+} + N_{e^-}} = -0.02 \pm 0.05$$

Thus there is no evidence for CP violation. The size of the effect expected if the source of CP violation is the phase δ in the KM matrix is less than 1%,²⁵⁾ and so would not have been seen with the present accuracy.

F. Dilepton Events

The dominant source of T(4S) decays containing two high momentum charged leptons is the semileptonic decay of both B mesons. We refer to this source as "parallel decays," as distinguished from "cascade decays," when one lepton comes

from B decay and the other lepton comes from semileptonic decay of charm, which in turn came from B decay. Usually one of the leptons from cascade decays is low momentum. For our purposes, cascade decays will be considered background.

If the charged and neutral B had the same semileptonic decay branching ratio, then the number of parallel decay events could be predicted from the number of single lepton events. However, if charged and neutral B branching ratios differ, this is no longer the case. The parallel decay rate is proportional to the mean square branching ratio \bar{b}^2 , while the single lepton event rate is proportional to the mean branching \bar{b} . The averages are taken over the B charge states: $\bar{b} = f_{\pm}b_{\pm} + f_0b_0$; $\bar{b}^2 = f_{\pm}b_{\pm}^2 + f_0b_0^2$; where b^{\pm} , b_0 , \bar{b} and \bar{b}^2 are the charged B, neutral B, mean and mean squared semileptonic decay branching ratios, and f_{\pm} and f_0 are the fractions of B^+B^- and $B^0\bar{B}^0$ decays from $\Upsilon(4S)$. Defining $\alpha \equiv \bar{b}^2/(b)^2$, one easily shows that $N_{\mu\mu} = \alpha N_{\mu}^2/(4N_{B\bar{B}})$, where $N_{\mu\mu}$, N_{μ} , and $N_{B\bar{B}}$ are the numbers of dimuon, single muon, and $B\bar{B}$ events, respectively. Similar formulae apply to dielectron and μ -e event. (There is a small correction factor depending on ratios of efficiencies.)

The quantity α is a measure of the difference between charged and neutral B branching ratios. For equal branching ratios, $\alpha = 1$, while for different branching ratios, α exceeds 1, approaching 2 for very different branching ratios. The number of dileptons provides a measurement of α , which in turn gives information on the ratio of charged B to neutral B semileptonic decay branching ratios.

As noted in Section E, B^0 and \bar{B}^0 are expected to mix. As a consequence, the neutral $B\bar{B}$ decays will occasionally be from $B^0\bar{B}^0$ or \bar{B}^0B^0 rather than from B^0B^0 . Defining the mixing parameter $y \equiv (N_{B^0\bar{B}^0} + N_{\bar{B}^0B^0})/N_{B^0\bar{B}^0}$, we have $y = 0$ corresponding to no mixing, and $y = 1$ corresponding to complete mixing. Parallel decays of $B^0\bar{B}^0$ or \bar{B}^0B^0 give like-sign dileptons, which thus provide a measurement of the mixing parameter.

In addition to parallel and cascade decays, a potential additional source of dileptons is the flavor-changing-neutral-current decay $B \rightarrow X\ell^+\ell^-$. This decay would result in $\mu^+\mu^-$ or e^+e^- events, but not μe events. From our dilepton sample, we can place an upper limit on flavor changing neutral currents.

The number of dilepton events of various sorts obtained from the 40 pb^{-1} $4S$ data sample are given in Table III. The background dileptons, due to one or both of the apparent leptons actually being a hadron, have been calculated from the sample of single lepton events using probabilities of hadrons faking leptons determined from a $\Upsilon(1S)$ data sample. From Table III one notes that the number of like-sign dileptons is consistent with background (no evidence for $B^0-\bar{B}^0$ mixing), and the total number of dileptons, after background subtraction, is close to the number expected from parallel decays with $\alpha = 1$ (no evidence for difference in

charged and neutral B semileptonic decay branching ratios, no evidence for flavor changing neutral currents). We make these three conclusions quantitative below.

Table III. Numbers of Dilepton Events.

	Events	Background	$\frac{N_{\ell\ell}^2}{\ell\ell} / 4N_{B\bar{B}}$
$\mu^+ \mu^-$	36.6	13.6	
$\mu^+ \mu^+ + \mu^- \mu^-$	10	8.8	
sum	46.6	22.4	24.2
$e^+ e^-$	34	9.0	
$e^+ e^+ + e^- e^-$	6	6.6	
sum	40	15.6	22.2
μe opposite	54	17.9	
μe same	17	11.4	
sum	71	29.3	46.3

1. Mixing. The expected number of dileptons is 93. Of these, 40%, or 37 should be from neutral B decay. With complete mixing, half of this number, or $18\frac{1}{2}$, would be like sign. The background-corrected number of like-sign dileptons is 6 ± 8 , consistent with no mixing, but not ruling out substantial mixing at a very high confidence level.

2. α . After correction for background, there are 90 ± 18 dileptons; the number predicted from the number of single lepton events, assuming $\alpha = 1$, is 93. This yields $\alpha = 1.0 \pm 0.2$. At 90% confidence level, α is less than 1.3. Using the branching fractions f_{\pm} , f_0 for $T(4S)$ into $B^+ B^-$, $B_0 \bar{B}_0$ as determined from the B mass in Section A, i.e., 60%/40%, this limit on α translates into

$$0.3 < \frac{\text{Br}(B^{\pm} \rightarrow X\ell\nu)}{\text{Br}(B_0 \rightarrow X\ell\nu)} < 4.6 .$$

3. F.C.N.C. After correction for background, there are 49 ± 12 $\mu\mu$ and ee events. Of these at least 46 are expected from parallel decays ($\alpha \geq 1$). At 95% confidence level, there are fewer than 26 events from $B \rightarrow X\mu^+\mu^-$ or $B \rightarrow Xe^+e^-$. This translates into a limit on the branching ratio of

$$\text{Br}(B \rightarrow X\ell^+\ell^-) < 0.4\% \quad (95\% \text{ c.l.}).$$

This limit should be contrasted with a branching ratio expected in a topless model with GIM not operating of $> 1\%$.

REFERENCES

- 1) D. Andrews et al., Phys. Rev. Lett. 44, 1108 (1980); Phys. Rev. Lett. 45, 219 (1980).
- 2) S.-H. H. Tye, CLEO internal report CBX 82-25 (unpublished).
- 3) R. K. Plunkett, Ph.D. thesis, Cornell University, 1982 (unpublished).
- 4) J. J. Mueller et al., Phys. Rev. Lett. 46, 1181 (1981).
- 5) C. Berger et al., Z.Phys. C1, 343 (1979); C. Berger et al., Phys. Lett. 93B, 497 (1980); H. Albrecht et al., Phys. Lett. 93B, 500 (1980); B. Niczyporuk et al., Phys. Rev. Lett. 46, 92 (1981).
- 6) D. Andrews et al., Phys. Rev. Lett. 50, 807 (1983).
- 7) R. Giles et al., Phys. Rev. Lett. 50, 877 (1983).
- 8) T. M. Yan, Phys. Rev. D22, 1652 (1980); Y. P. Kuang and T. M. Yan, Phys. Rev. D24, 2874 (1981).
- 9) J. Green et al., Phys. Rev. Lett. 49, 617 (1982).
- 10) G. Mageras et al., Phys. Rev. Lett. 46, 1115 (1981); Phys. Lett. 118B, 453 (1982).
- 11) R. L. Kelley et al., (Particle Data Group), Rev. Mod. Phys. 52, No. 2, Pt.2, S1 (1980).
- 12) C. Bebek et al., Phys. Rev. Lett. 46, 84 (1981); K. Chadwick et al., Phys. Rev. Lett. 46, 88 (1981).
- 13) S. Behrends et al., Phys. Rev. Lett. 50, 881 (1983).
- 14) E. Eichten, Phys. Rev. D22, 1819 (1980).
- 15) M. S. Alam et al., Phys. Rev. Lett. 49, 357 (1982).
- 16) R. Schindler et al., Phys. Rev. D24, 78 (1981).
- 17) A. Brody et al., Phys. Rev. Lett. 48, 1070 (1982).
- 18) H. Fritzsch, Phys. Lett. 86B, 164 (1970); Phys. Lett. 86B, 343 (1979).
- 19) A. Chen et al., Phys. Lett. 122B, 317 (1983).
- 20) G. L. Kane and M. E. Peskin, Nucl. Phys. B195, 29 (1982).
- 21) M. E. Peskin and S.-H. H. Tye (private communication).
- 22) G. Altarelli, N. Cabibbo, G. Corbo, L. Maiani and G. Martinelli, Nucl. Phys. B208, 365 (1982).
- 23) K. Chadwick et al., Phys. Rev. D27, 475 (1983).
- 24) Jacques P. Leveille, Proceedings of a CLEO Collaboration Workshop, CLEO Preprint CLEO 81/05, July 1981 (unpublished).
- 25) John S. Hagelin, Proceedings of a CLEO Collaboration Workshop, CLEO Preprint CLEO 81/05, July 1981 (unpublished).

TOPICS IN UPSILON SPECTROSCOPY AND B PHYSICS WITH CUSB

P. M. Tuts
S.U.N.Y. at Stony Brook
Stony Brook, NY
U.S.A.

ABSTRACT

We discuss some recent results in Υ spectroscopy and B meson physics from the CUSB collaboration at CESR. In particular, the recent observation of the $\chi_b(1^3P_J)$ state at (9901 ± 3) MeV in both the inclusive, $(\Upsilon(2S) \rightarrow \gamma \chi_b)$, and exclusive, $(\Upsilon(2S) \rightarrow \gamma \chi_b \rightarrow \gamma \gamma \Upsilon(1S))$, photon spectra. Splittings and branching ratios are given. Results on the search for $\Upsilon''' \rightarrow B^* B$, limits on the B meson mass, and the relative couplings strengths for b quark decay are also given.

1.0 INTRODUCTION

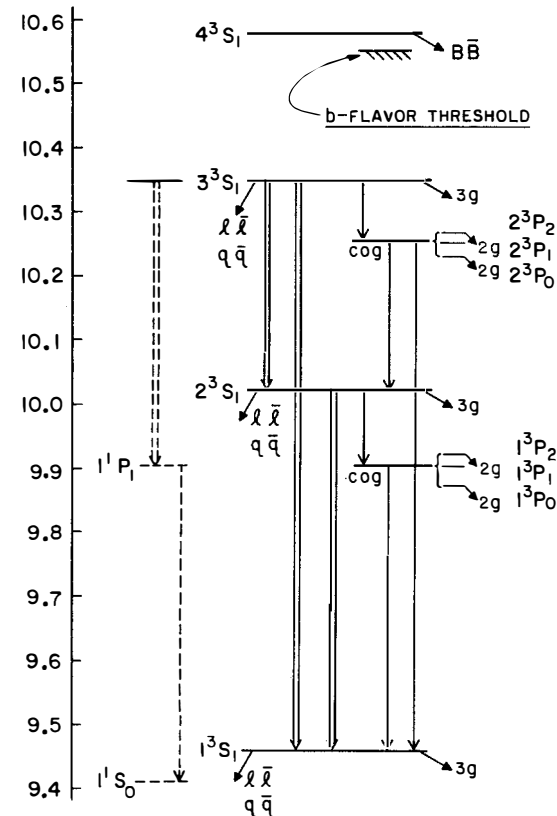
The Υ system, which consists of a bound b quark and its antiquark, has proved to be a very rich testing ground for the study of b quarks, in terms of both their decay properties, and the forces that bind them (for a review of Υ physics see Ref. 1). The experimental study^{2]} of the Υ system at CESR has progressed extremely rapidly, from the observation^{3]} of the Υ , Υ' , Υ'' , and Υ''' states in 1980, to the observation by CUSB^{4]} of the χ_b in 1982, and the χ_b in^{5]} 1983. In this paper we will discuss the CUSB results on the observation of the χ_b states from Υ' decays together with a summary of some of our results on B physics from recent running on the Υ''' as well as some other selected results from M(GeV)

CUSB^{6]}. The Υ system spectrum is a very rich one, see Figure 1, with three bound triplet S states and one quasi-bound state just above the b flavor threshold; the P wave states are experimentally accessible through electric dipole (E1) transitions from the $\Upsilon'(2^3S_1)$ and $\Upsilon''(3^3S_1)$ states.

Figure 1. The bound $\Upsilon(b\bar{b})$ spectrum. The single and double lines indicate experimentally observed γ and $\pi\pi$ transitions respectively. The dashed lines indicate transitions that have not yet been observed.

2.0 THE CUSB DETECTOR

The CUSB detector, which is shown in perspective in Figure 2, is a high resolution segmented NaI and lead glass calorimeter. The innermost portion consists of four planes of tracking chambers, which are followed by ~ 9 radiation lengths of NaI crystals (324), ~ 7 radiation lengths of lead glass blocks (256), and NaI end caps (168). Interspersed between the five NaI layers



CUSB

COLUMBIA
STONY BROOK
LOUISIANA STATE
MPI MUNICH

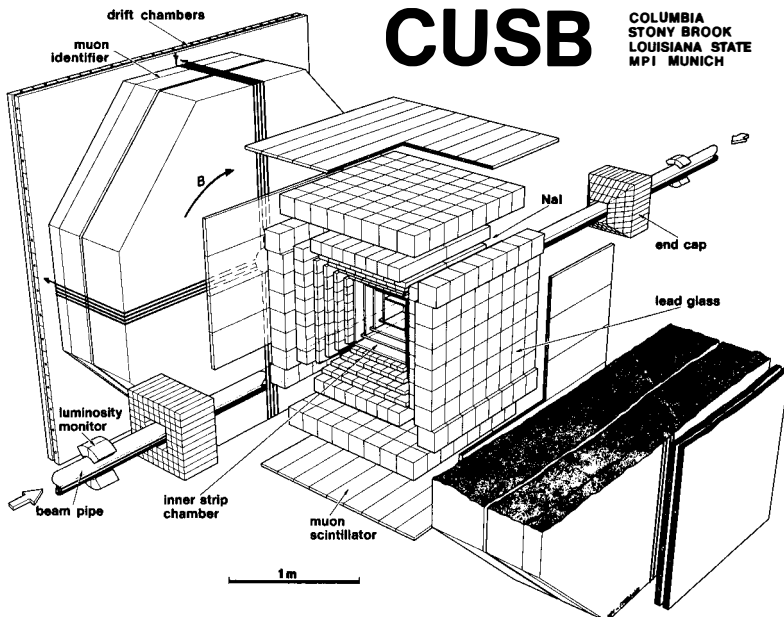


Figure 2. Perspective view of the CUSB detector, with the main detection elements listed. The end caps are shown pulled out for ease of display. The chambers between the NaI layers are not shown.

were additional tracking chambers; these chambers were removed for the most recent γ' running in an effort to improve the resolution of the central detector from $\sigma E/E \sim 4\% / E^{1/4}$ (E in GeV). Outside the lead glass array there is a scintillator hodoscope which provides us with a two muon trigger (in addition, horizontally moving muons pass through an iron muon identifier system). The solid angles are $\sim 80\%$, and $\sim 36\%$ of 4π for back to back electrons, and muon pairs respectively. The relative energy calibration of all the NaI crystals is maintained by continuously monitoring the positions of the photon lines from ^{137}Cs (.66 MeV) and ^{60}Co (1.17, 1.33 MeV) sources which are mounted on the NaI crystals. This monitoring takes place simultaneously with data taking, allowing for continuous gain monitoring of the entire system. The lead glass calibration is maintained through daily monitoring of LED light sources placed on the blocks. The energy calibration obtained in this manner is then corrected for Monte Carlo calculated losses in the inactive material between crystals. The final energy calibration is then checked against summed photon energies from exclusive photon events and Bhabha scattering events; it differs by only a few percent.

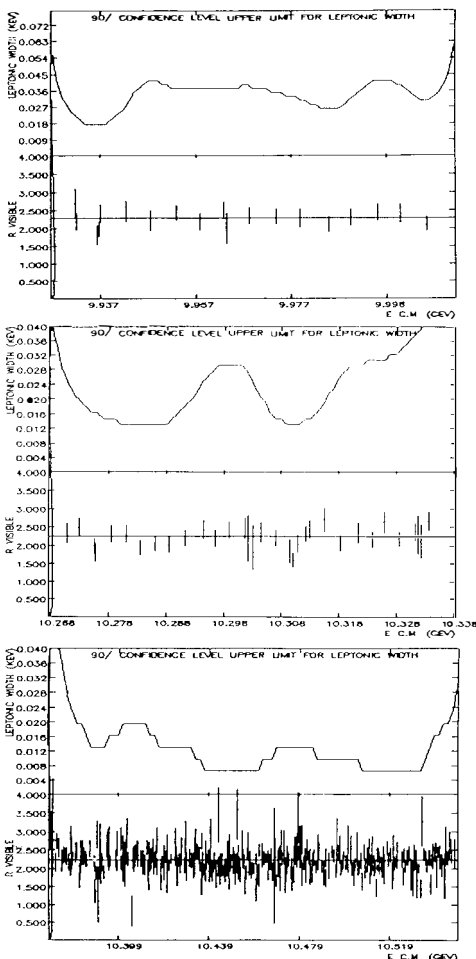
3.0 χ SPECTROSCOPY3.1 The N^3S_1 States

The agreement of the measured leptonic widths and masses of the four χ states observed in R (shown in Figure 1 of Ref. 7) with potential models²¹ has lead to the association of these states with the first four triplet S states of the $b\bar{b}$ system. The values are summarised in Table I where masses are scaled to $M(\chi)=9460$ MeV as measured^{8]} at VEPP-4. Note that the $\chi(4^3S_1)$ state lies above the b flavor threshold since the observed^{3]} width is significantly wider than the measured machine resolution, providing us with a B factory with which to study B decay.

3.2 Search For Other States

Besides the four prominent resonances that have been observed in the e^+e^- cross section, we have searched for others in the continuum regions between the various resonances. The scans and the results are shown in Figures 3a,b,c for the regions below the χ' , below the χ'' and between the χ'' and the χ''' respectively. The most thorough scanning was carried out in the latter region, where there is a prediction^{9]} for the lowest lying vibrational state, having a leptonic width of 70-270 eV.

Figure 3. The 90% CL upper limit leptonic width in KeV for narrow resonances (top), and the scan data points in R for the energy regions: (a) $9.93 < M < 10.01$ GeV/c^2 , (b) $10.27 < M < 10.335$ GeV/c^2 , (c) $10.37 < M < 10.55$ GeV/c^2 .



There is no evidence for any narrow states (i.e. of machine resolution) in any of the regions. In particular, a vibrational state with leptonic width greater than 20 eV is excluded, in conflict with vibrational state predictions.

Table I. The masses and leptonic widths for the 3S states of the Υ system. The Υ mass is from Ref. 8. The theoretical predictions are from Ref. 2, with the leptonic widths calculated using the Υ experimental value.

Resonance	-- Mass (MeV/c ²) --		Leptonic width (keV)	
	Experiment	Theory	Experiment	Theory
$\Upsilon(1^3S_1)$	9459.7	9459.7	1.14 ± 0.05	$1.05-1.07$
$\Upsilon(2^3S_1)$	10020.5 ± 0.7	10025	0.50 ± 0.03	.44-.50
$\Upsilon(3^3S_1)$	10350.0 ± 0.7	10322-10360	0.35 ± 0.03	.31-.40
$\Upsilon(4^3S_1)$	10578.0 ± 3.0	10568-10640	0.21 ± 0.05	.25-.31

3.3 Decays Of The $\Upsilon''(3^3S_1)$

Since the CUSB results on the decays of the $\Upsilon(3S)$ have been discussed elsewhere^{4]} and in the Moriond Workshop proceedings^{7]}, we will limit ourselves here to a brief summary of those results. The most significant discovery made was the observation of the χ_b' (or $2^3P_{J=0,1,2}$) state in both the inclusive photon spectrum, $\Upsilon(3S) \rightarrow \gamma + X$, and the exclusive decay chain $\Upsilon(3S) \rightarrow \gamma + \chi_b'$, $\chi_b' \rightarrow \gamma + (\Upsilon(2S) \text{ or } \Upsilon(1S))$ with the final S state decaying to e^+e^- or $\mu^+\mu^-$. The results were obtained from a sample of $\sim 65\,000$ hadronic events on the $\Upsilon(3S)$ peak, and are summarised (together with the results from $\Upsilon(2S)$ decays) in Table III. In addition, the $\pi^+\pi^-$ hadronic transitions from the $\Upsilon(3S)$ to the $\Upsilon(2S)$ and $\Upsilon(1S)$ have been measured^{10]} and are summarised in Table II.

Table II. The hadronic $\pi\pi$ transition branching ratios measured by CUSB (see Ref. 10). The theoretical predictions are from Ref. 11.

Transition	Branching Ratio (%)	
	Experiment	Theory
$\Upsilon' \rightarrow \Upsilon \pi^+ \pi^-$	18 ± 6	17-18
$\Upsilon'' \rightarrow \Upsilon' \pi^+ \pi^-$	3.1 ± 2.0	1.5-2.3
$\Upsilon'' \rightarrow \Upsilon \pi^+ \pi^-$	3.9 ± 1.3	1.4-3.4

3.4 Decays Of The $\chi'(2^3S_1)$

3.4.1 Inclusive Photons -

Encouraged by the success of having discovered the χ_b states in the decays of the $\chi(3S)$, the CUSB group has spent the last running period at CESR (Dec 1982 - March 1983) studying the decays of the $\chi(2S)$ with the hope of observing the χ_b state in E1 photon transitions. Such transitions have been observed in both the inclusive and exclusive photon spectra^{5]}, and can be associated with the χ_b states ($1^3P_J=0,1,2$). During this run CESR delivered $\sim 30 \text{ pb}^{-1}$ of integrated luminosity, corresponding to $\sim 230\,000$ hadronic events in CUSB, of which $\sim 153\,000$ are observed $\chi(2S)$ decays (or $\sim 180\,000$ produced $\chi(2S)$ events). The principal philosophy behind the photon algorithm for shower recognition from the transverse and longitudinal shower shape has not changed from the $\chi(3S)$ analysis⁴. However, we have since increased the efficiency for hadronic event recognition by $\sim 30\%$, and tightened the photon criteria so as to maintain a constant photon finding efficiency of 13% over the energy range from 80 to 500 MeV. In addition the resolution for showers was improved to $\sigma_E/E \sim 3.6\% / E^{1/4}$ (E in GeV), due in part to the removal of the chambers between the NaI layers. The inclusive photon spectrum from the $\chi(2S)$ is shown in Figure 4a. There is evident structure at ~ 125 MeV which is not visible in the $\chi(1S)$ or continuum spectra. The background curve is obtained from the spectrum by fitting the region from 65 to 280 MeV with a cubic plus 3 gaussians of arbitrary position and normalization (the width of

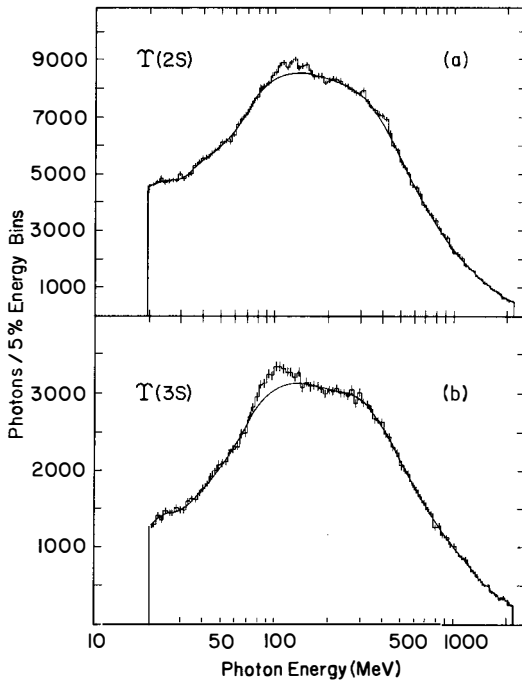


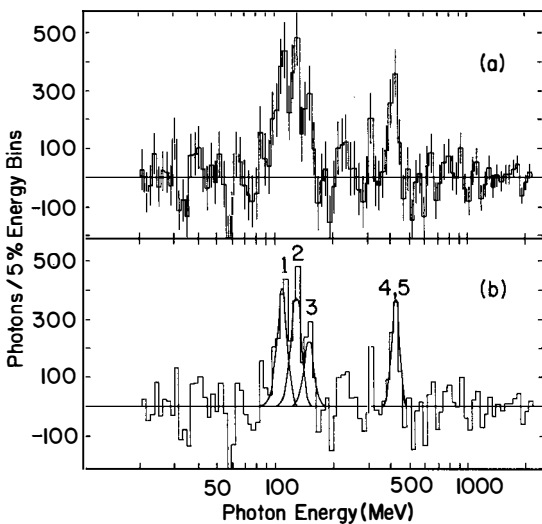
Figure 4. The inclusive photon spectra, $\chi(nS) \rightarrow \gamma X$, for decays of (a) the $\chi(2S)$, and (b) the $\chi(3S)$. The solid line is the background, for details see text.

each was held fixed at $\sigma_E/E \sim 6\%$), and the remainder of the spectrum with polynomials (excluding two bins around 430 MeV, where we expect to see a signal). The cubic fit is also required to match the polynomial fits at the

boundaries. The solid line shown in Figure 4a represents the cubic and polynomial terms alone. The contribution from the decay $\chi(2S) \rightarrow \pi^0\pi^0\chi(1S)$ (which has a BR~ 10%) is automatically taken into account because it contributes a smooth distribution from 20 to 420 MeV, peaking at 175 MeV on the plot. In addition, we show, in Figure 4b, the inclusive photon spectrum for decays of the $\chi(3S)$ using both the new hadronic event and photon finding algorithm. We still see a distinct excess of photons in the 100 MeV region, leading to the the same^{4]} BR($\chi(3S) \rightarrow \gamma + 2^3P_J$) ~34%.

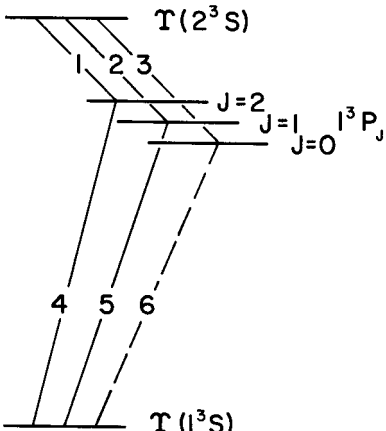
Returning to the $\chi(2S)$ spectrum, we find a prominent excess in the region from 90 to 160 MeV (3110 ± 323 counts) and another smaller excess in the region around ~427 MeV of 833 ± 166 counts, as shown in

Figure 5. The background subtracted photon spectrum for $\chi(2S) \rightarrow \gamma\chi$. The error bars are shown in (a), and (b) shows the fits to the excess. The numbers in (b) refer to Figure 6.



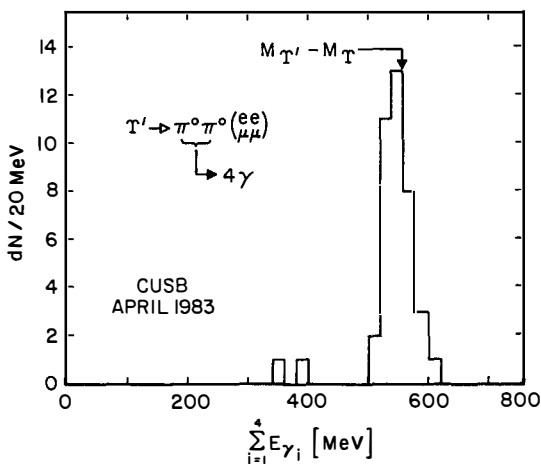
the subtracted spectrum of Figure 5a. The three gaussian fit to the excess at ~125 MeV yields photon line energies of 108, 128, and 149 MeV respectively. The individual gaussians are shown in Figure 5b superimposed on the subtracted spectrum, where the numbers refer to the photon lines indicated on Figure 6. Since the lines are more widely separated than in the 2^3P_J case and since our resolution is slightly improved, we are able to partially resolve the three photon lines as evidenced by figures 4a, and 5b. The final energy scale, after Monte Carlo correction for

Figure 6. The E1 transitions for $\chi(2S) \rightarrow \gamma\chi_b$ and $\chi_b \rightarrow \gamma\chi(1S)$ decays. The dashed line indicates that this transition is suppressed.



energy loss in the inactive material, is determined by a sample of $\gamma(2S) \rightarrow \gamma(1S)\pi^0\pi^0 \rightarrow \gamma(1S) + 4\gamma$ events, where the summed 4γ energy (including $\gamma(1S)$ recoil) must add to $M(\gamma') - M(\gamma) \sim 561$ MeV (as shown in Figure 7). This amounts to a 2% upward correction to the energy scale. If indeed these photons correspond to the E1 transitions to a P wave state, then one expects to see the 'mirror' transition from the P wave back down to the

Figure 7. The total energy distribution for the four γ 's from the hadronic decay $\gamma(2S) \rightarrow \pi^0\pi^0\gamma(1S)$, where $\gamma(1S) \rightarrow e^+e^-$ or $\mu^+\mu^-$.



ground state, $\gamma(1S)$. The energy of the two photons (plus recoil energy of ~ 10.5 MeV) must therefore equal $M(\gamma(2S)) - M(\gamma(1S))$. The product branching ratios for the three transitions via the P wave state are in the ratio of 2:5: ~ 0 for the $J=2,1,0$ spin states respectively (as is shown in the following section on exclusive $\gamma(2S)$ decays). Thus from the measured inclusive photon lines we find that $(108 \times 2 + 128 \times 5) / 7 + 427 + 10.5 \sim 560$ MeV (including recoil) is precisely the $M(2S) - M(1S)$ mass difference, from which we conclude that we have indeed seen the decay chain from the $\gamma(2S)$ to the $\gamma(1S)$ via an intermediate state that we associate with the χ_b . The photon excess observed in the 125 MeV region leads to a $BR(\gamma(2S) \rightarrow \gamma\chi_b) = (15.5 \pm 2.5)\%$ with an additional systematic uncertainty of $+5\%$ and -2.5% ; if the excess at $(427 \pm 1 \pm 8)$ MeV is from the above decay chain, then we find the $BR(\gamma(2S) \rightarrow \gamma\chi_b) \times BR(\chi_b \rightarrow \gamma\gamma(1S)) = (4 \pm 1)\%$. Using the above ratio of product BR's we find $BR(1^3P_2 \rightarrow \gamma\gamma(1S)) = (20 \pm 5)\%$, and $BR(1^3P_1 \rightarrow \gamma\gamma(1S)) = (47 \pm 18)\%$.

The individual intensities of the three lines are consistent with those expected for E1 transitions (i.e. proportional to $k^3(2J+1)$, where k is the photon energy). After correction for that factor we find them to be 1.04 ± 0.3 , 1, and 1.13 ± 0.5 for the $J=2,1$, and 0 states respectively, normalizing to the middle line. This evidence, together with the good agreement of the cog position with potential models, leads us to associate the observed lines with the lowest three triplet P wave states, $1^3P_{J=0,1,2}$. We summarise the inclusive photon results for the 1^3P_J and 2^3P_J states in Table III.

Table III. Summary of inclusive photon transitions. For potential model predictions, see Ref. 2.

Line	E _γ Energy (MeV)	-- Mass (MeV/c ²) --		BR(γ(nS)→γ(n-1)P _J)			E1 width (keV)	
		Experiment	Theory	n	J	BR(%)	Expt.	Theory
2 ³ P ₂	84.5 _{±2.0} _{±4}	10265		3	2			
2 ³ P ₁	99.5 _{±3.2} _{±4}	10250		3	1			
2 ³ P ₀	117.2 _{±5.0} _{±4}	10232		3	0			
2Pcog	93.1 _{±5}	10256 _{±5}	10242-10271	a	11	34 _{±3}	8.4 _{±1.4}	4.8-7.6
1 ³ P ₂	108.2 _{±0.3} _{±2}	9912		2	2	6.1 _{±1.4}		
1 ³ P ₁	128.1 _{±0.4} _{±3}	9892		2	1	5.9 _{±1.4}		
1 ³ P ₀	149.4 _{±0.7} _{±5}	9870		2	0	3.5 _{±1.4}		
1Pcog	119.4 _{±3}	9900 _{±3}	9888-9924	a	11	15 _{±2.5}	4.9 _{±1.0}	3.1-4.4

3.4.2 Exclusive Photons -

In addition to the observation of the χ_b s in the inclusive spectrum, we have observed them in the exclusive events $\chi(2S) \rightarrow \gamma \chi_b \rightarrow \gamma \gamma \chi(1S) \rightarrow \gamma \gamma (e^+e^-)$ or

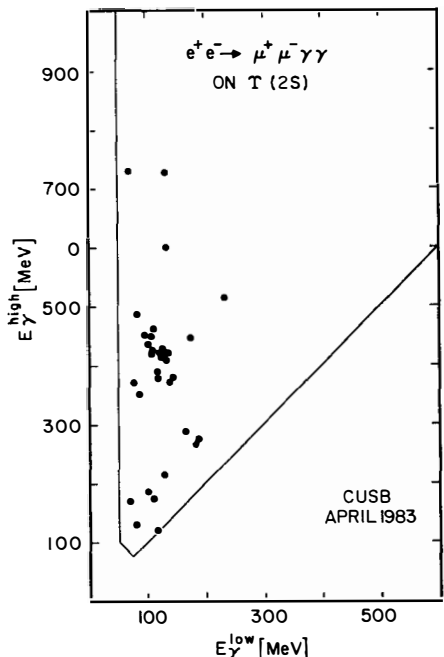


Figure 8. Scatter plot of γ energies for $\mu^+\mu^-$ final state cascade decays of the $\chi(2S)$.

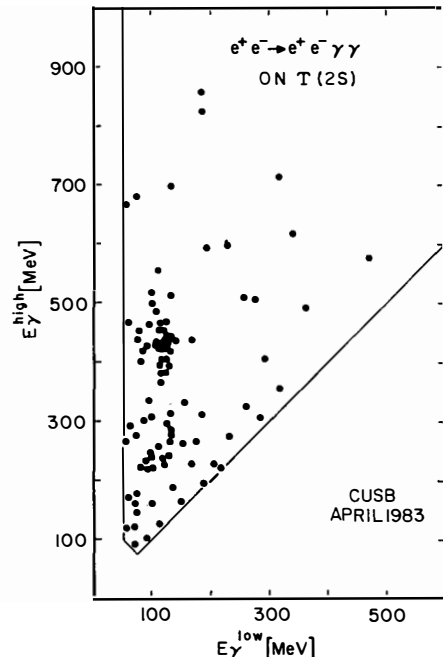


Figure 9. Scatter plot of γ energies e^+e^- final state cascade of the $\chi(2S)$.

$\mu^+\mu^-$). Again, the procedure is the same as that for the $\chi(3S)$ exclusive events described elsewhere^{4,7}, except that the muon solid angle was increased to 36% of 4π . The acceptances for these exclusive events are 17% for events with e^+e^- final states and 12% for those with $\mu^+\mu^-$. The data are plotted in scatter plots of the two photon energies, E_γ^{low} vs E_γ^{high} , for electron and muon final state events separately in figures 8,9 respectively. Both plots show a distinct clustering at $(E_\gamma^{\text{low}}, E_\gamma^{\text{high}}) \sim (120, 430)$ MeV which we interpret as radiative cascade events via the χ_b . The fact that we are indeed observing cascade events to the $\chi(1S)$ is well demonstrated in figure 10 which shows the sum of the two photon energies with a clear peak at the $\chi(2S)-\chi(1S)$ mass difference (after recoil correction).

The backgrounds are of interest only in the region of the clustering; hadronic cascade backgrounds via $\pi^0\pi^0$ are negligible above a summed energy of ~ 500 MeV. Other backgrounds for the $\mu^+\mu^-$ events are negligible (1 ± 1 events), whereas for e^+e^- events there is a background from double radiative Bhabha events which is calculated to be 4 ± 3 events in the region of

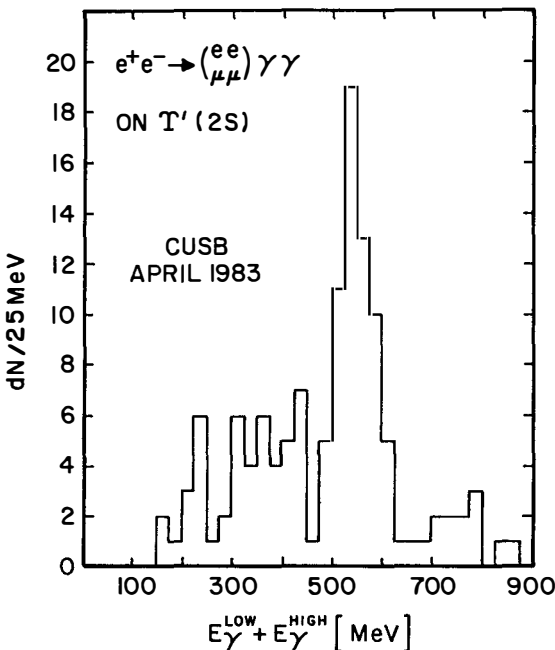


Figure 10. The summed photon energy for all the cascade events in Figures 8 and 9.

clustering of $80 < E_\gamma^{\text{low}} < 150$ MeV. The total observed number of events in that region is 51. Correcting for acceptance and background (together with a $B_{\mu\mu} = 0.028 \pm 0.003$) we derive the product branching ratio $\text{BR}(\chi(2S) \rightarrow \gamma\chi_b) \times \text{BR}(\chi_b \rightarrow \gamma\chi(1S)) = (3.9 \pm 0.9)\%$. We have compared the splitting observed in these exclusive events with that obtained from the inclusive analysis, by combining both the e^+e^- and $\mu^+\mu^-$ data, constraining the $\gamma\gamma$ energy sum to 560 MeV (corrected for recoil and weighted by resolution) and fitting the low energy photon spectrum. The spectrum is shown in figure 11, where two clear peaks are visible; a two Gaussian fit (of equal widths) leads to fitted peak values of (106 ± 3) MeV and (127 ± 2) MeV with a resolution of $\sigma_E/E = (4.5 \pm 0.7)\%$. The

fitted intensities are in the ratio of $(.45 \pm .19):1$. The total product branching ratio, and intensity ratios, are in agreement with theoretical predictions (see Table IV), which leads us to make the association of these two lines with the 1^3P_2 and 1^3P_1 states. These results are summarised in Table IV.

Figure 11. The projection of the low energy photon for $\gamma(2S)$ decays, showing peaks at 106 and 127 MeV.

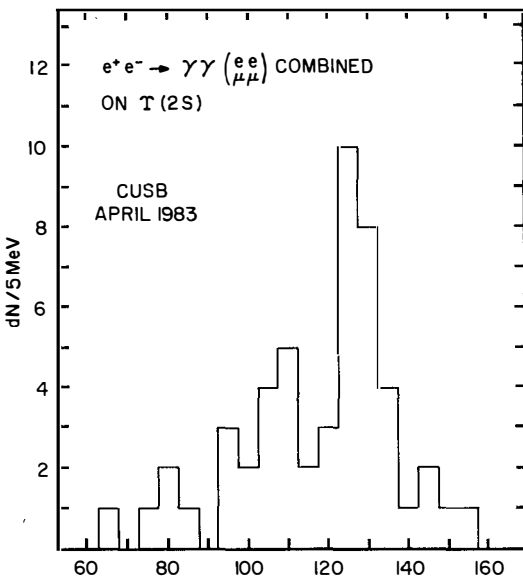


Table IV. Summary of $\gamma(2S)$ and $\gamma(3S)$ exclusive events. E_{γ}^{LOW} (MeV)

Reaction	Branching Ratio (%)	
	Experiment	Theory
$\sum_j = \frac{1}{2} \text{BR}(\gamma'' \rightarrow \gamma_j \chi_{bj}) \times \text{BR}(\chi_{bj} \rightarrow \gamma \gamma')$	5.9 \pm 2.1	3.3
$\sum_j = \frac{1}{2} \text{BR}(\gamma'' \rightarrow \gamma_j \chi_{bj}) \times \text{BR}(\chi_{bj} \rightarrow \gamma \gamma)$	3.6 \pm 1.2	2.8
$\sum_j = \frac{1}{2} \text{BR}(\gamma'' \rightarrow \gamma_j \chi_{bj}) \times \text{BR}(\chi_{bj} \rightarrow \gamma \gamma')$	< 3.0	1.1
$\text{BR}(\gamma' \rightarrow \gamma_j \chi_{b2}) \times \text{BR}(\chi_{b2} \rightarrow \gamma \gamma)$	1.3 \pm .7	3.3 \pm .3
$\text{BR}(\gamma' \rightarrow \gamma_j \chi_{b1}) \times \text{BR}(\chi_{b1} \rightarrow \gamma \gamma)$	2.6 \pm .8	
$\text{BR}(\gamma' \rightarrow \gamma_j \chi_{b0}) \times \text{BR}(\chi_{b0} \rightarrow \gamma \gamma)$	< .4	

4.0 B PHYSICS

In this section we present a brief summary of some of the recent results obtained by CUSB in the area of B physics. For more details on the CUSB B physics see Ref. 7.

4.1 Search For B^* 's

In a sample of 39 000 $\gamma(4S)$ events, we have searched for the decay $\gamma(4S) \rightarrow B^* B$, where the $B^* \rightarrow \gamma B$. The energy of the γ is expected to be ~ 50 MeV from scaling arguments. We do not observe any events in the inclusive photon spectrum of $\gamma(4S)$ decays [21], as shown in Figure 12. The shaded region in the figure indicates the expected signal if there were one photon per event. A

Figure 12. The continuum subtracted inclusive photon spectrum, $\gamma(4S) \rightarrow \gamma X$. The shaded curve represents the expected photon signal if there were one 50 MeV γ per event.

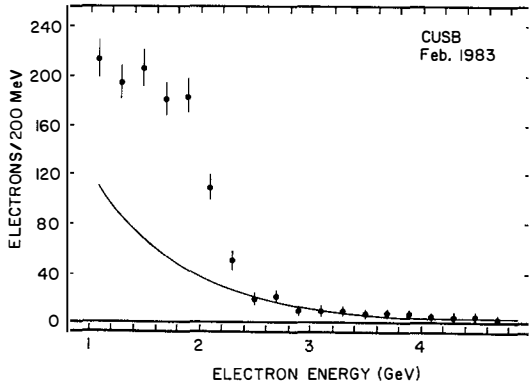
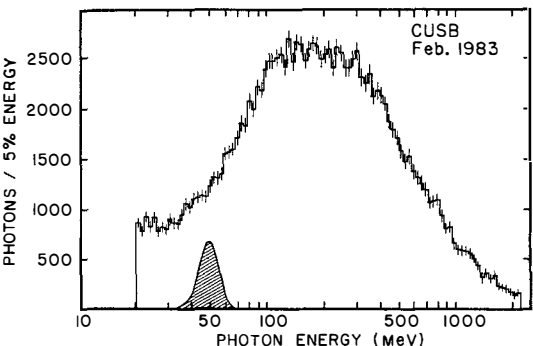
maximum likelihood analysis yields an upper limit on $\text{BR}(\gamma(4S) \rightarrow B^* B) < 7\% \text{ (90\% CL)}$

for $40 < E_\gamma < 60 \text{ MeV}$. From these results and the measured width of the $\gamma(4S)$, we calculate^{12]} that $5263 < M_B < 5278 \text{ MeV}$, in good agreement with the recently obtained CLEO value^{13]}.

4.2 Electron Spectrum From B Decay

We have measured the electron spectrum ($> 1 \text{ GeV}$ electrons) for B decays on the $\gamma(4S)$. The experimental spectrum is shown in Figure

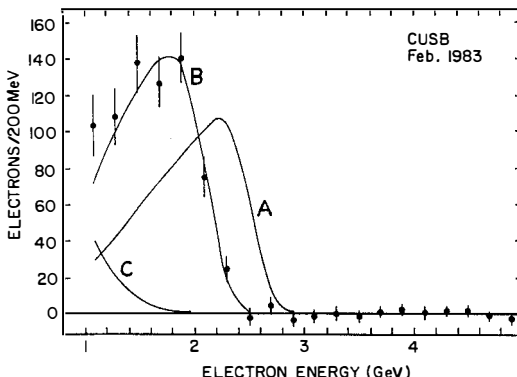
Figure 13. The measured electron spectrum ($E_e > 1 \text{ GeV}$) for $\gamma(4S)$ decays. The solid line is the measured background off resonance.



13, where the solid line is a fit to the measured continuum spectrum taken off the $\gamma(4S)$ peak. The continuum spectrum comes from electrons from D decay (recall that only $\sim 30\%$ of the events at the γ''' energy are resonance events). The efficiency for $> 1 \text{ GeV}$ electrons is $\sim 7\%$ (due to 20% electron identification and 34% solid angle). We observe 711 ± 47 events (after subtraction of 114 events from γ conversions and hadronic interactions) which leads to a $\text{BR}(B \rightarrow e \bar{v} X) = (13.7 \pm 0.9 \pm 2)\%$. The above branching ratio was obtained assuming that 88% of electrons from $B \rightarrow e \bar{v} X$ decay are above 1 GeV, and a 12% background contribution from $B \rightarrow D X$ decays.

The shape of the electron spectrum has been used to determine the ratio of contributions from $b \rightarrow u$ vs $b \rightarrow c$, by comparison with the calculations of Altarelli et al [4]. The three curves in Figure 14 represent the expected spectra for the cases that $m_q = 1.8$ GeV/c 2 (curve B), or that $m_q = 150$ MeV/c 2 (curve A), and the contribution from $B \rightarrow D$ decay (curve C). A maximum likelihood calculation results in a spectrum consistent with no $b \rightarrow u$ contribution, the 90% CL limit leads to $\text{BR}(B \rightarrow e \bar{X}_u)/\text{BR}(B \rightarrow e \bar{X}_c) < 7\%$ or in terms of the coupling parameters of the mixing matrix $|V_{bu}/V_{bc}|^2 < .03$ (for details see Ref. 7).

Figure 14. The subtracted electron spectrum on the $\Upsilon(4S)$. The curves are: (A) complete $b \rightarrow u$, (B) complete $b \rightarrow c$, and (C) electrons from D decay.



5.0 CONCLUSIONS

The Υ system has provided an amazing laboratory for the study of both weak and strong interactions. The Υ spectrum²¹ has filled out experimentally in the last year with the addition of the χ_b and χ_b' members^{4,5} to the Υ family, in support of the flavor independent potential model predictions for the bound $b\bar{b}$ system. The E1 rates are in agreement with theoretical expectations⁵¹, and the hadronic transitions between triplet S states have been measured¹⁰ and agree with those predicted by the QCD multipole expansion¹¹, although some of the spectra for these transitions are unexpected theoretically. In B physics, the B meson mass has been measured¹² and tight bounds have been placed on the quark mixing matrix parameters from the shape of the B decay electron spectrum⁷. Although much has been accomplished these past few years, there still remains the challenge of explicitly resolving the P wave lines, and observing the singlet S state, the η_b (see Figure 1). We hope to accomplish these tasks with the addition of a BGO upgrade¹⁵ of the CUSB detector. The first quadrant of BGO should be installed and running by the end of 1983 (the η_b must await a full cylinder of BGO), and perhaps by the next Moriond meeting we will be able to report on yet more exciting results.

6.0 ACKNOWLEDGEMENTS

The author wishes to acknowledge the US National Science Foundation for his research support. Thanks must go to Juliet Lee-Franzini, Paolo Franzini, and Dean Schamberger for valuable discussions, and also to the CUSB collaboration. J. Tran Thanh Van and the organizers are to be congratulated for arranging a very stimulating conference.

7.0 REFERENCES

1. P. Franzini and J. Lee-Franzini, Phys. Rep. 81, 239(1982); P. Franzini and J. Lee-Franzini, Ann. Rev. Nucl. Part. Sci. 33, 1(1983).
2. For a detailed list of references see Ref. 1.
3. D. Andrews et al., Phys. Rev. Lett. 44, 1108(1980); *ibid.* 45, 219(1980); T. Böhringer et al., Phys. Rev. Lett. 44, 1111(1980); G. Finocchiaro et al., Phys. Rev. Lett. 45, 222(1980).
4. K. Han et al., Phys. Rev. Lett. 49, 1612(1982); G. Eigen et al., Phys. Rev. Lett. 49, 1616(1982).
5. C. Klopfenstein et al., submitted to Phys. Rev. Lett. (1983); F. Pauss et al., submitted to Phys. Rev. Lett. (1983).
6. The recent members of the CUSB collaboration include: P. Franzini, K. Han, D. Peterson, E. Rice, D. Son, J.K. Yoh, S. Youssef, T. Zhao (Columbia U.); J. Horstkotte, C. Klopfenstein, J. Lee-Franzini, R. D. Schamberger, M. Sivertz, L. J. Spencer, P. M. Tuts (SUNY, Stony Brook); H. Dietl, G. Eigen, E. Lorenz, G. Mageras, F. Pauss, H. Vogel (MPI, Munich); R. Imlay, G. Levman, W. Metcalf, V. Sreedhar (LSU); S. W. Herb (Cornell U.).
7. P. Franzini, in these proceedings.
8. A. S. Artamonov et al., Inst. of Nucl. Phys. Preprint 82-94 (1982).
9. W. Buchmuller and S.-H. H. Tye, Phys. Rev. Lett. D22, 594 (1980).
10. G. Mageras et al., Phys. Rev. Lett. 46, 1115 (1981); G. Mageras et al., Phys. Lett. 118B, 453 (1982).
11. Y.-P. Kuang and T.-M. Yan, Phys. Rev. D24, 2874 (1981).
12. R. D. Schamberger et al., Phys. Rev. Lett. D26, 720(1982).
13. E. Thorndike, in these proceedings.
14. G. Altarelli et al., Univ. of Rome Preprint 302 (1982).
15. P. M. Tuts and P. Franzini, Proceedings of the International Conference on Bismuth Germanate, edited by C. Newman-Holmes (Princeton University, Princeton, NJ, 1983) p596.

REVIEW OF PEP EXPERIMENTS

Gerson Goldhaber*

Department of Physics, and Lawrence Berkeley Laboratory,
University of California, Berkeley, California USAABSTRACT

Recent physics results from four PEP experiments: Mark II, MAC, DELCO, and TPC are presented herewith. The topics discussed deal with flavor tagging of charmed and bottom quarks, τ and D^0 lifetimes, Electroweak interference effects, searches for new particles and dE/dx measurements.

*Work supported in part by the U.S. Department of Energy under contract DE-AC03-76SF00098.

I will present the following data from PEP in my talk:

1. A brief description of the 4 PEP detectors from which data is presented here.
2. Results on flavor tagging:
 - Charm tagging via D^{*+} identification. Results from Mark II and DELCO.
 - Charm and bottom quark tagging via semileptonic decays. Results from Mark II and MAC.
3. τ and D^0 lifetime measurements with a Vertex Detector (Mark II).
4. Electroweak interference effects. Results from Mark II and MAC.
5. Search for new and peculiar particles and specific decay modes;
 - Search for a μ^* (MAC).
 - Search for $e^+e^- \rightarrow \psi + x$ and $e^+e^- \rightarrow T + x$ (Mark II).
6. Particle identification in the TPC.

1. The PEP Detectors

I present herewith summaries of 4 PEP Detectors as compiled by G. Gidal et al.^[1] for the Particle Data Group at LBL.

A. Luminosity at PEP

There has been a considerable improvement in Luminosity at PEP. In particular peak Luminosity of $3.3 \times 10^{31} \text{ cm}^{-2} \text{ sec}^{-1}$ have been reached. Average running days have produced over 1000 nb^{-1} .

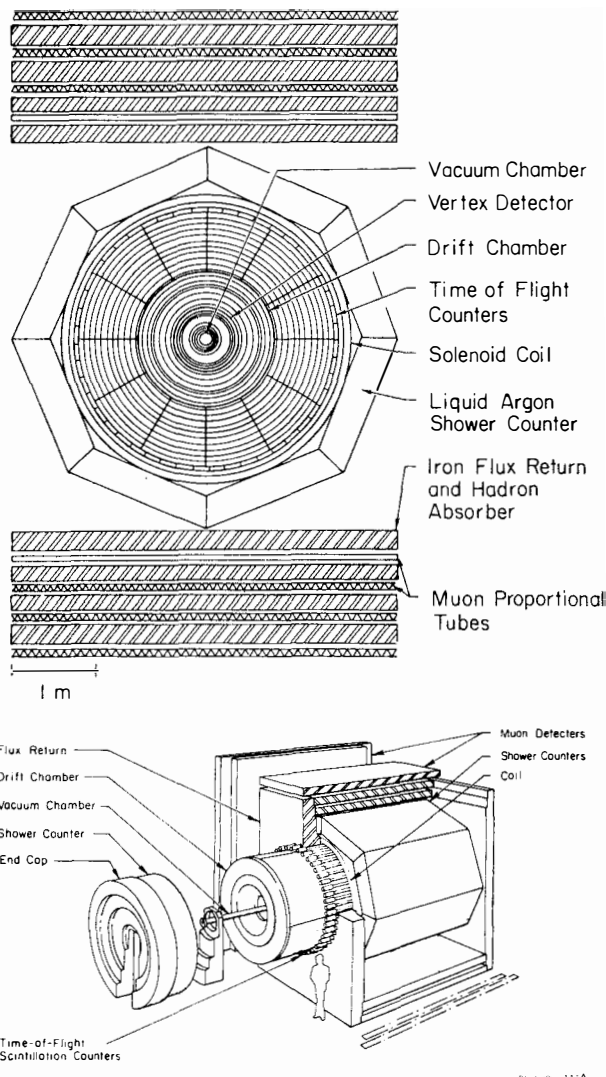
MARK II

LOCATION	PEP e^+e^- storage ring SLAC, Stanford, CA, USA
MAGNET	4.6 kG Al coil solenoid, 1.5 m radius (currently running at 2.3 kG)
TRACKING	<p>Central drift chamber: Active length = 2.64 m, inner radius = 0.41 m, outer radius = 1.45 m 6 axial layers, 10 stereo layers ($\pm 3^\circ$) 50% ethane, 50% argon $\sigma \simeq 200 \mu$</p> <p>Vertex drift chamber: Cylindrical drift chamber, 1.2 m long, inner radius = 10 cm, outer radius = 35 cm Only axial wire layers (4 near $r = 12$ cm, 3 near $r = 30$ cm) $\sigma \simeq 100 \mu$ Be beam pipe ($0.006X_0$) Combined $(\Delta p/p)^2 = (0.015)^2 + (0.01p)^2$ Tracks extrapolated to interaction point within 100μ</p>
SHOWER COUNTERS	<p>8 modules of Pb-liquid argon ($15X_0$ each), arranged in octagon outside coil Covers 64% of 4π 2 mm Pb sheets separated by 3 mm liquid argon gaps 37 layers ($0.4X_0$ sampling) are ganged to provide 6 samples in depth Readout in 3.8 cm wide strips in ϕ, θ, u directions $\Delta E/E \simeq 13\%/\sqrt{E}$</p>
TIME OF FLIGHT	<p>48 scintillation counters read out at both ends Cover 75% of 4π 1.50 m flight path at $\theta = 90^\circ$; $\sigma = 340$ ps K, π separation up to $1.35 \text{ GeV}/c$ at 1σ level</p>
END CAPS	2 layers Pb-proportional chamber ($5X_0$) with 4 successive cathode strip readouts $(\theta, \phi, R\text{-spiral}, L\text{-spiral})$ 50% argon, 50% ethane
MUON DETECTION	Proportional tubes interleaved with steel absorber (4 layers each for total thickness of 1 m) covering 55% of 4π
SMALL ANGLE TAGGING	6 planar drift chambers followed by shower counters
LUMINOSITY MONITOR	Octagonal shower counters cover $22 \text{ mrad} < \theta < 80 \text{ mrad}$ contain 18 layers $1/4''$ Pb and $1/2''$ scintillator, read out with BBQ wave shifter, front 5 layers separately from back 13 $\Delta E/E = 15.5\%/\sqrt{E}$ 3 sets of scintillation counters

REFERENCES

1. G.S. Abrams et al., Phys Rev. Lett. **43** (1979) 477, and *ibid* 481.
2. W. Davies White et al., Nucl. Instr. & Meth. **160** (1979) 227.
3. G.S. Abrams et al., IEEE Trans. Nucl. Sci. **NS 25** (1978) 1, *ibid* 309, and **NS 27** (1980) 59.
4. J.A. Jaros, Proc. Int. Conf. on Instrumentation for Colliding Beam Physics, SLAC-250 (1982).

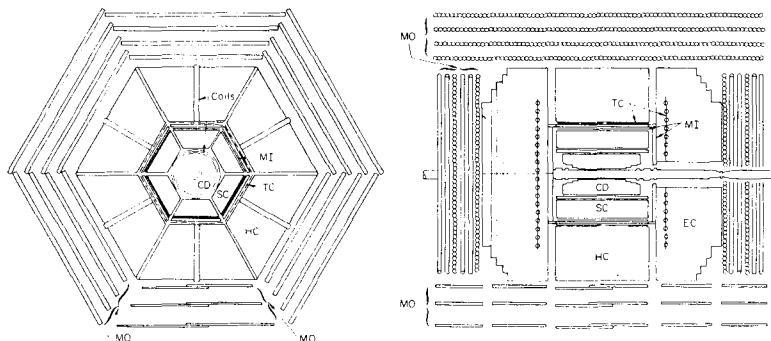
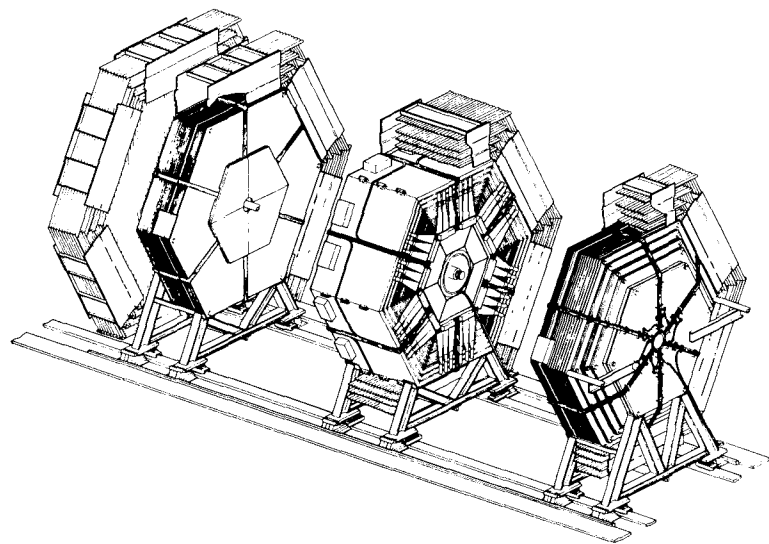
MARK II



MAC (MAgnetic Calorimeter)

LOCATION	PEP e^+e^- storage ring SLAC, Stanford, CA, USA
MAGNETS	5.7 kG solenoid, 7.5 cm thick Al coil Diameter = 1 m, length = 2.3 m 17 kG iron toroids, 1 m thick
TRACKING	Cylindrical drift chamber 2.2 m long, 12-45 cm tracking radius Argon - 10% methane at 1 atm. 10 layers, double sense wires ≥ 5 points on tracks over $\Delta\Omega = 95\%$ of 4π 3° stereo gives $\Delta z = 4$ mm dE/dx to $\pm 15\%$ $\sigma_p/p = 6.5\% p$
MUON DETECTION	Muon tracking chambers 4 planes of 10 cm diameter drift tubes surrounding magnetized iron toroids $\sigma_p/p = 30\%$ $\Delta\Omega = 97\%$ of 4π
SHOWER DETECTORS	Barrel: 14 X_0 of Pb - proportional chamber sandwich $\sigma_E/E = 20\%/\sqrt{E}$ z-coordinate from charge division $\sigma_\phi = 0.8^\circ$, $\sigma_\theta = 1.3^\circ$ Endcaps: 14 X_0 of Fe - proportional chamber sandwich $\sigma_E/E = 45\%/\sqrt{E}$ ϕ -coordinate from cathode strips $\sigma_\phi = 2^\circ$, $\sigma_\theta = 1.5^\circ$ Total: $\Delta\Omega = 97\%$ of 4π
HADRON CALORIMETER	5.5 λ_{abs} of Fe - proportional chamber sandwich $\sigma_E/E = 75\%/\sqrt{E}$ $\sigma_\theta = 2^\circ$; $\sigma_\phi = 1^\circ$ (barrel), 4° (endcaps) $\Delta\Omega = 97\%$ of 4π
TIME OF FLIGHT	144 scintillation counters (72 barrel, 72 endcaps) $r = 1.3$ m $\Delta t = 1$ ns $\Delta\Omega = 97\%$ of 4π
LUMINOSITY MONITOR	4 scintillator/shower counter telescopes at 32 mrad horizontally
REFERENCES	<ol style="list-style-type: none"> 1. R.L. Anderson et al., IEEE Trans. NS 25, (1978) 340. 2. W.T. Ford, SLAC-PUB-2894, March 1982 (Proceedings SLAC International Conference on Instrumentation for Colliding Beams).

MAC (MAgnetic Calorimeter)



MAC Detector Components:

CD - Central Drift Chamber
 SC - Shower Chamber (Central)
 TC - Trigger/TOF Scintillators
 HC - Hadron Calorimeter (Central)

EC - End-cap Shower and
 Hadron Calorimeters
 MO, MI - Muon Drift Chambers
 Coils - Solenoid and Toroid

XBL 831-7898

Fig. 2

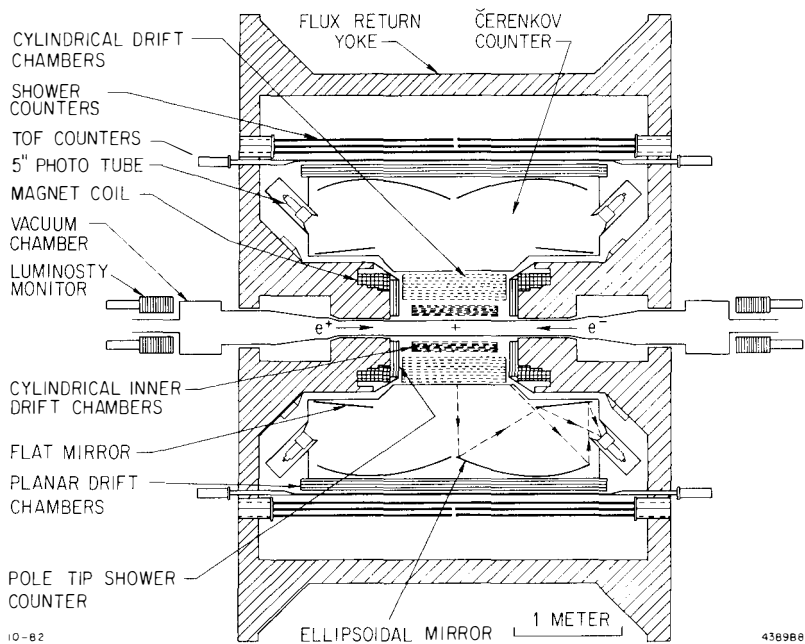
DELCO

LOCATION	PEP e^+e^- ring SLAC, Stanford, CA, USA
MAGNET	Open-geometry (aperture $ \cos\theta < 0.78$) Pole-tip diameter 101 cm, separation 125 cm $B_0 = 3.3 \text{ kG}$, $\int B dl = 1.8 \text{ kG-m}$
TRACKING	Central (cylindrical) drift chambers: 94 cm maximum wire length, 12-49 cm radius Low mass (2.3% X_0) Depth (z) measurement by narrow angle stereo 16 points on tracks with $ \cos\theta < 0.69$ Outer (planar) drift chambers: 285 cm wire length, 160 cm $\langle \text{radius} \rangle$ Depth measurement by wide angle stereo 6 points on tracks with $ \cos\theta < 0.65$ Multiple hit digital electronics (4 ns bin width) $\sigma_p/p = \sqrt{(2\% p)^2 + (6\%)^2}$
CERENKOV COUNTER	1 atm. isobutane threshold counter ($\gamma_t = 19.1$) 36 cells each with (pTP-coated) 5" RCA 8854 quantacon Radiator length 55-110 cm, $\langle p.e. \rangle = 18$, $\langle N_0 \rangle = 80 \text{ cm}^{-1}$ $\sigma_t = 300 \text{ ps}$ Acceptance $ \cos\theta < 0.62$
SHOWER COUNTERS	Barrel ($ \cos\theta < 0.62$) : 48 Pb-scintillator counters, $6X_0$ Pole-tip ($0.79 < \cos\theta < 0.98$) : 36 Pb-scintillator BBQ counters, $5X_0$
TIME OF FLIGHT	52 counters 324 cm length, 180 cm $\langle \text{radius} \rangle$ $\sigma_t = 350 \text{ ps}$ Acceptance $ \cos\theta < 0.67$
LUMINOSITY MONITOR	12 Pb-scintillator BBQ counters, $16X_0$ Acceptance 25-68 mrad relative to beam axis

REFERENCES

1. W. Bacino et al., Phys. Rev. Lett. **40** (1978) 671.
2. W.E. Slater et al., Nucl. Instr. & Meth. **154** (1978) 223.
3. D. Ouimette et al., IEEE Trans. NS **29**, No. 1 (1982) 290.

DELCO



XBL 831-7897

Fig. 3

TPC

LOCATION	PEP e^+e^- ring, Interaction Region (IR) 2 SLAC, Stanford, CA, USA
MAGNET	1982-83: 4 kG Al coil solenoid (1.32 X_0 coil package) 1984: 14.5 kG superconducting coil (0.86 X_0 package) Diameter = 2.15 m, length = 3.0 m
TRACKING	<p>Time Projection Chamber (TPC) 2.0 m long (in z) at 20 to 100 cm radius (r) Argon-methane (80%-20%) at 8.5 atm. Max. drift 1.0 m in 20 μsec, 75 kV/m drift electric field 183 proportional wire hits on tracks with $\cos \theta < 0.71$, each wire gives r, z and amplitude for six 60° sectors at each end and provides dE/dx meas. by multiple ionization sampling 15 3-dim. space points from induced cathode signals on several of 13,824 channels to give r, ϕ, and z (from the drift time), for $\cos \theta < 0.71$ ≥ 2 3-d points and ≥ 15 wire hits over 97% of 4π sterad Track pair resolution of 1-2 cm $dE/dx \pm 3.5\%$ for Bhabhas $\pm 4.0\%$ for tracks in jet events with ≥ 120 samples $\sigma_p/p^2 = \pm 3.6\%$ for $p \geq 2$ GeV/c position resolution in bending plane is 190 microns and in axial (z) direction 340 microns; presently low magnet field and drift distortions increase σ_p/p^2</p> <p>Inner drift chamber at 13 to 19 cm radius 8.5 atm Ar-CH₄ (80%-20%), 150 microns in bend plane 1.2 m long covering 95% of 4π, with 4 axial layers</p> <p>Outer drift chamber at 1.19 to 1.24 m radius 1 atm Ar-CH₄ (80%-20%), 200 microns in bend plane 3 m long covering 77% of 4π, with 3 axial layers</p>
POLE-TIP CALORIMETER	<p>Gas, proportional mode, sampling Pb-laminate calorimeter 2 modules, 13.5X₀ deep, at z = 1.1 m, covering 18% of 4π Argon-methane (80%-20%) at 8.5 atm; total of 51 samples Three 60° stereo views, each with 13 and 4 samples in depth Projective strip geometry with 8 mrad angular segment $\sigma_E/E = \pm 11\%/\sqrt{E}$, below 10 GeV $\pm 6.0\%$ for Bhabhas at 14.5 GeV</p>
HEXAGONAL CALORIMETER	<p>Gas, limited Geiger mode, sampling Pb-laminate calorimeter 6 modules, 10X₀ deep, 4.2 m long at 1.2 m radius Argon-ethyl bromide (96%-4%) at 1 atm. Solid angle coverage of 75% (90% including PTC) 3 correlated 60° stereo views using wire and cathode signals in 40 samples (27 and 13 samples in depth) Projective strip geometry with 9 mrad angular segment $\sigma_E/E = \pm 14\%/\sqrt{E}$, below 1 GeV $\pm 12\%$ for Bhabhas at 14.5 GeV</p>
MUON DETECTOR	<p>Magnet flux return + 2 layers iron, total 810 g/cm Triangular, double layer, extruded Al proportional tubes Argon-methane (80%-20%) at 1 atm. 3 layers with axial wires and 4th layer at 90 deg. Endcap with 3 layers provides 98% of 4π sterad coverage Resolution = 1 cm, expect 3 mm when operated as drift tube</p>
TRIGGER	≥ 2 charged over 85% of 4π sterad; neutral energy of ≥ 4 GeV, or energy in two or more calorimeter modules of ≥ 1.5 GeV; ≥ 1 charged and neutral energy of ≥ 750 MeV or energy in two or more calorimeter modules of ≥ 1.5 GeV
REFERENCES	<ol style="list-style-type: none"> 1. TPC: H. Aihara et al., IEEE Trans. NS 30 (1983). 2. IDC: W. Gorn et al., IEEE Trans. NS 26 (1979) 67. 3. HEX: H. Aihara et al., IEEE Trans. NS 30 (1983). 4. MUON: J. Bakken et al., IEEE Trans. NS 30 (1983). 5. TRIG: M. Ronan et al., IEEE Trans. NS 29 (1982) 427

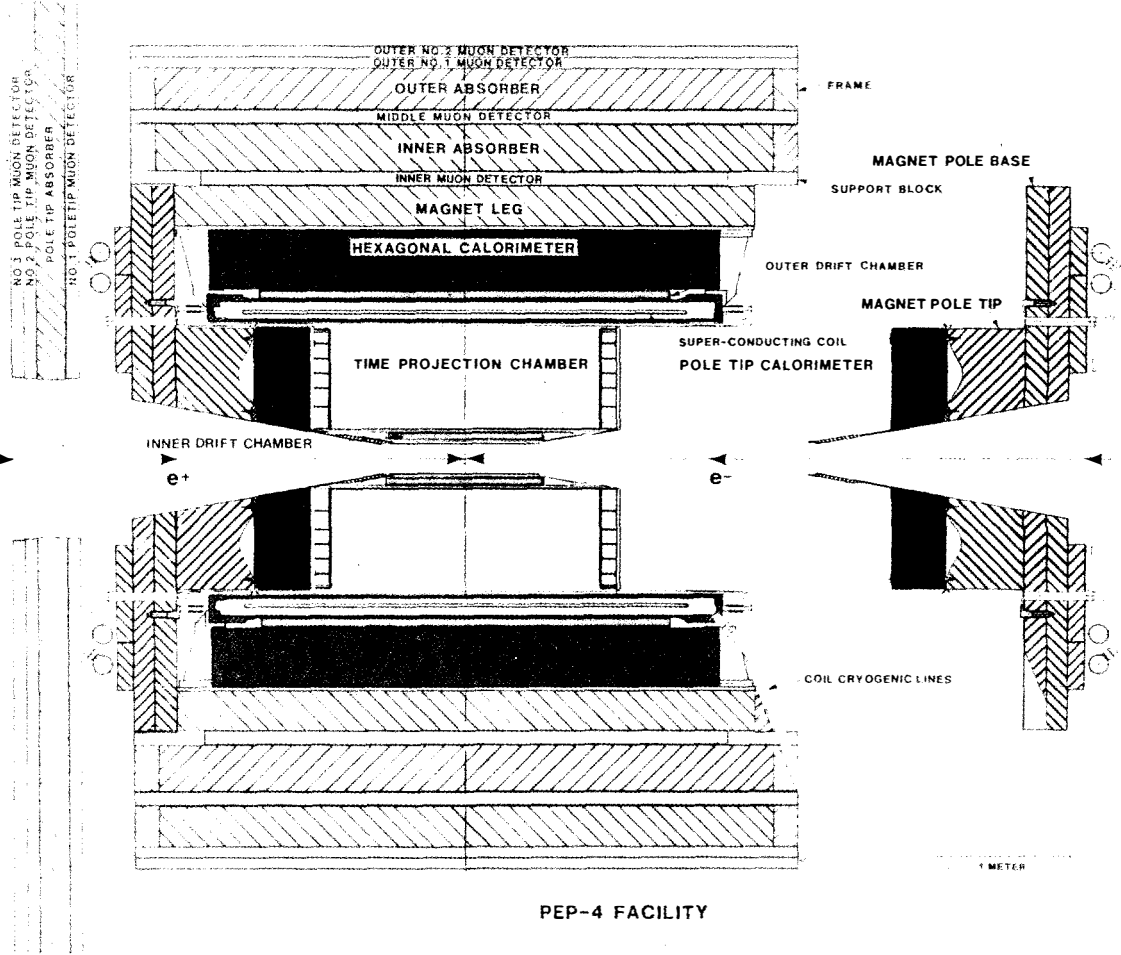


Fig. 4

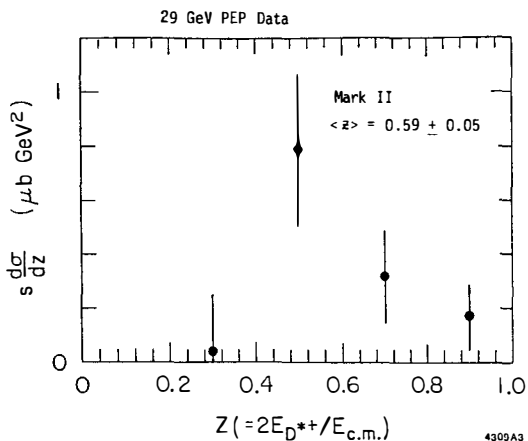


Fig. 15

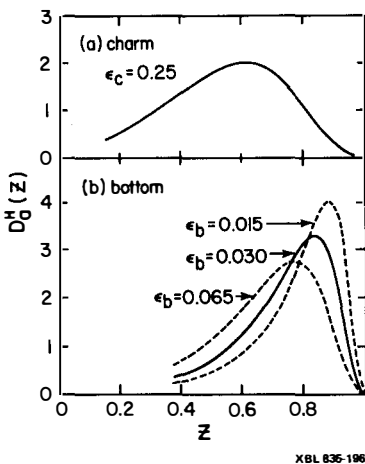


Fig. 17

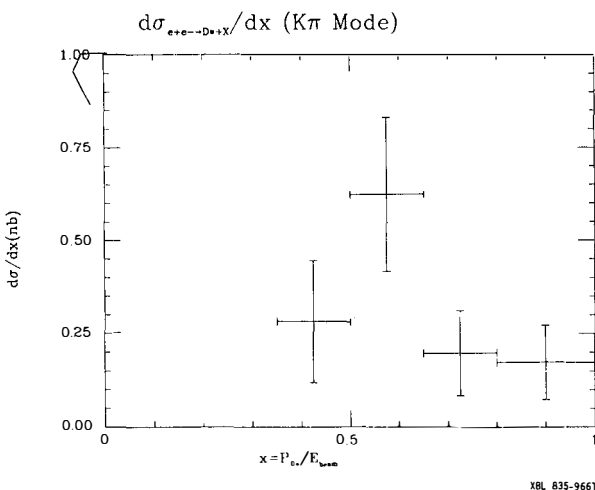


Fig. 16

Fig. 15 - Charmed quark to D^{*+} fragmentation function. $\langle z \rangle = 0.59 \pm 0.05$. (MARK II)

Fig. 16 - Charmed quark to D^{*+} fragmentation function. $\langle z \rangle = 0.6 \pm 0.1$. (DELCO)

Fig. 17 - (a) Charmed quark fragmentation function. Functional form of Peterson et al. for $\epsilon_c = 0.25$.

(b) Bottom quark fragmentation function for the ϵ_b values shown. These correspond to the fitted values obtained from the study of semielectronic decays in the Mark II.

2. Flavor Tagging

There are two fortunate circumstances which allow flavor tagging even though complete particle identification is not always available. These are charm tagging via D^{*+} identification and charm and bottom tagging via lepton identification from semileptonic decays.

◦ Charm Flavor Tagging via $D^{\star+}$ Identification

D^{*+} identification is possible even without K-identification due to the very tight kinematical constraint in the decay $D^{*+} \rightarrow \pi^+ D^0$ where the bachelor π_B^{+} has a kinetic energy of 5.7 MeV in the D^{*+} c.m. system. This feature is exploited by plotting the mass difference $\Delta = M(D^{*+}) - M(D^0)$ which gives a peak centered at $\Delta = 145.4 \pm 0.2$ MeV. Here the D^0 is primarily observed through its $D^0 \rightarrow K^- \pi^+$ ($Br = 3.0 \pm 0.6\%$) decay mode, and if K-identification is available (DELCO) through the $D^0 \rightarrow K^- \pi^+ \pi^+ \pi^-$ ($Br = 8.5 \pm 2.1\%$) decay mode. Furthermore a charm associated "satellite enhancement" S^0 , discussed below, can also serve in D^{*+} tagging.

◦ A Charm Associated Enhancement

As illustrated by the Mark II data from SPEAR in a $K^-\pi^+$ mass plot aside from the D^0 peak at $M(K^-\pi^+) = 1.863$ GeV there is a second broader charm associated "satellite" peak S^0 with $M \approx 1.61$ GeV and $\Gamma \approx 0.12$ GeV (see Figure 5).

These values are approximate since the S° enhancement is skewed towards low mass values. The mass interval 1.48 - 1.68 GeV contains about 90% of the enhancement.

Figure 6 shows that the S° enhancement persists at the various SPEAR energy regions: 3.77 GeV the ψ'' , 3.9 - 4.5 GeV and 4.5 - 5.5 GeV. Furthermore it is absent at the ψ and ψ' energies. This indicates that the S° satellite enhancement is charm associated and we interpret it as primarily due to the more copious decay mode $D^0 \rightarrow K^-\pi^+\pi^0$, $B_r = 9.3 \pm 2.8\%$ with perhaps a small contribution from the $D^+ \rightarrow K^-\pi^+\pi^+$ decay mode. The way this comparatively sharp S° enhancement arises is illustrated in Figure 7 which gives the features of the Dalitz plot for the decay $D^0 \rightarrow K^-\pi^+\pi^0$. We note that this decay mode proceeds via the two intermediate state (pseudo scalar meson + vector meson) channels:

$D^0 \rightarrow K^- \rho^+$ and $D^0 \rightarrow K^* \pi^+$ as well as a third channel $D^0 \rightarrow K^* \pi^0$ (1)

which is of no relevance here and is not shown on the Dalitz plot. In view of the fact that we have the decay of $J^P = 0^-$ (the D^0) to a $J^P = 0^-$ and $J^P = 1^-$ state it must proceed via $L^P = 1^-$ in relative orbital angular momentum between the pseudo scalar and vector meson. As a consequence of the angular momentum addition $\vec{L} + \vec{J} (V) = 0$ the vector meson is produced fully aligned and hence with a $\cos^2\theta$ distribution in the vector meson c.m. This expresses itself as a mass-squared distribution along the p^+ and K^{*-} bands which peak at the ends of these

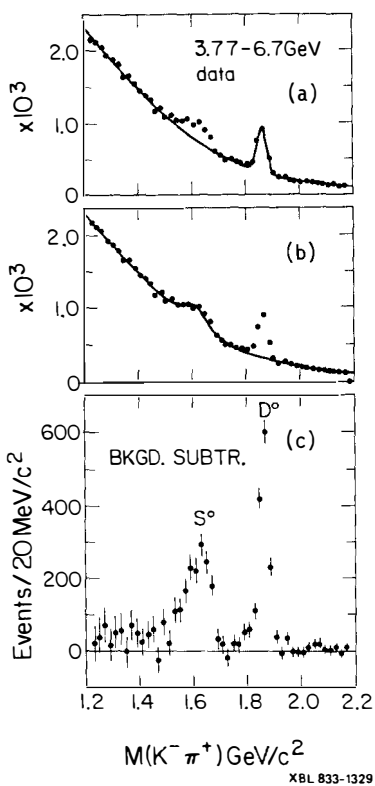


Fig. 5

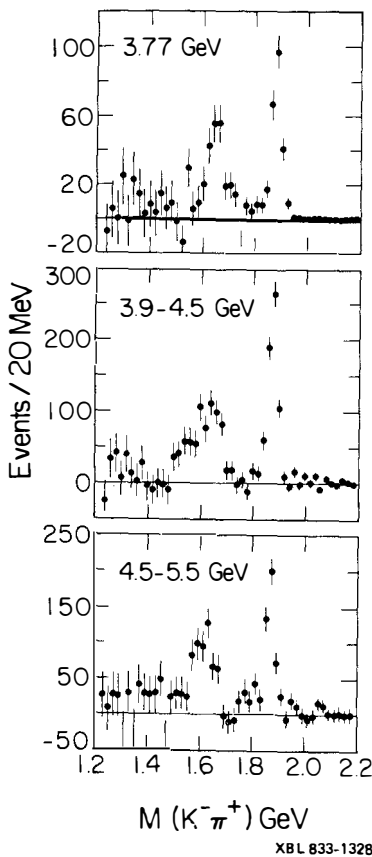


Fig. 6

Fig. 5 - The D^0 resonance and S^0 enhancement. The signals correspond to 1340 D^0 events and 1470 S^0 events. The S^0 signal thus more than doubles the number of charm tags for the $K^- \pi^+$ decay mode. (a) The curve is a fit to background and the D^0 signal. (b) The curve is a fit to background and the S^0 signal. (c) The data with background (as determined from the above fits) subtracted. Mark II at SPEAR.

Fig. 6 - The D^0 and S^0 signals for 3 energy regions as noted with background subtracted. Mark II at SPEAR.

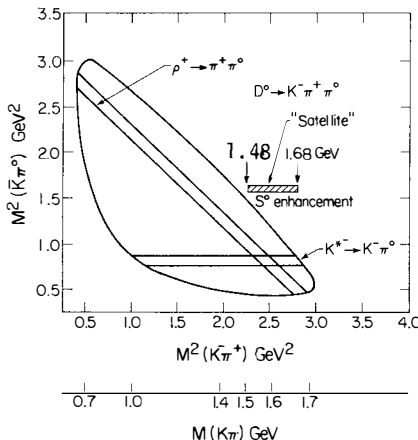


Fig. 7 - The Dalitz plot boundary for the reaction $D^0 \rightarrow K^- \pi^+ \pi^0$ showing the ρ^+ and K^{*+} bands. The S^o enhancement corresponds to the high $K^- \pi^+$ end of these resonance bands. Both M^2 and M scales are shown.

XBL 833-1325

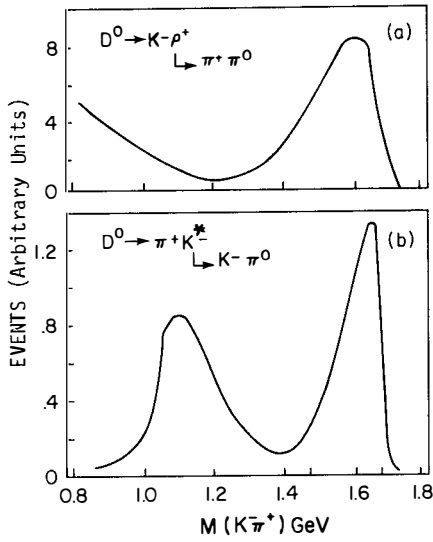


Fig. 8

XBL 835-195

Fig. 8 - The calculated shapes of the $K^- \pi^+$ mass projections of the ρ^+ and K^{*+} bands. The observed enhancements are the result of the vector meson alignment from D^0 decay.

Fig. 9 - The S^o signal fitted by a combination of the ρ^+ and K^{*+} distributions. Mark II at SPEAR.

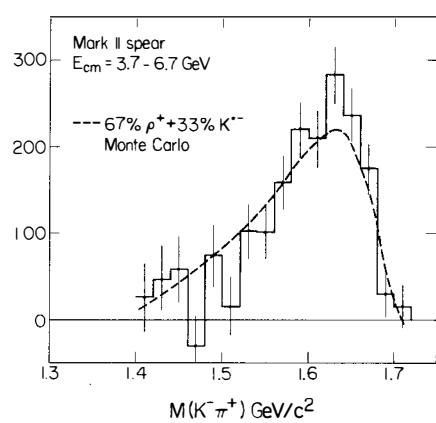


Fig. 9

XBL 833-1327

bands. Figure 8 shows these as reflected into $M(K^-\pi^+)$ evaluated by a Monte Carlo calculation. Figure 9 shows a possible fit to the S° peak with 2/3 of the intensity ascribed to the ρ^+ band and 1/3 to the κ^{*-} band with no account taken of possible interference between the two bands. Thus the S° peak is explained as an enhancement in $M(K^-\pi^+)$, primarily due to the $D^\circ \rightarrow K^-\pi^+\pi^0$ decay mode.^{2,3]}

The associated π^0 in the relevant portion of the Dalitz plot is of rather low momentum in the D° c.m. system. This implies a rather low π^0 detection efficiency and precluded the direct observation of the S° enhancement in the Mark II study of the $D^\circ \rightarrow K^-\pi^+\pi^0$ Dalitz plot.^{3]}

What is important in what follows is that since the S° peak corresponds to a low momentum π^0 (in the D° c.m.), mass difference $\Delta_D = M(\pi^+D^\circ) - M(D^\circ)$ which has an experimental full width of ~ 2 MeV in the Mark II at PEP, is still applicable as $\Delta_S = M(\pi^+S^\circ) - M(S^\circ)$ although the full width now broadens to ~ 10 MeV. Figure 10 shows a Monte Carlo calculation at 5.2 GeV including the detector resolution. The calculation at 29 GeV is very similar and is in good agreement with the observed experimental distributions.

- D^{*+} Studies at PEP

Figure 11 shows the Δ distribution for the Mark II data at 29 GeV, here a cut on $M(K^-\pi^+)$ of 1.76 - 1.96 GeV was applied to select the D° band. The Δ distributions are shown for the z values $z > 0.4$ and the more restrictive $z > 0.6$. Here $z = E(D^*)/E_{beam}$. Figure 12 shows the $M(K^-\pi^+)$ distributions for a Δ interval of 143 - 147 MeV.

- Physics Results from D^{*+} Studies

There are four physics results which are obtained from the identified D^* mesons.

- (i) The charmed quark fragmentation function. One finds that the charmed quark fragmentation into D^* 's occurs at considerably higher z values than for the light quarks. $\langle z \rangle \approx 0.6$. (Mark II and DELCO.)
- (ii) The cross section for D^{*+} production. This inclusive cross section $\sigma(D^{*+}) \approx 0.2 - 0.25$ nb is rather large and corresponds to an R value of $R \approx 2.0 - 2.5$. Thus D^* production (if we allow a similar cross section for D^{*0}) essentially saturates the expected charm quark production, namely:

$$R_c = 3 \left(\frac{4}{9} + \frac{1}{9} \right) \quad (2)$$

for charmed and bottom quark pairs (assuming the latter primarily proceed via charm decay). Here, $2 R_c = 2 \times \frac{5}{3} = 3.33$ is expected for the inclusive charm production R value (both charges and all charmed mesons and Baryons). (Mark II and DELCO.)

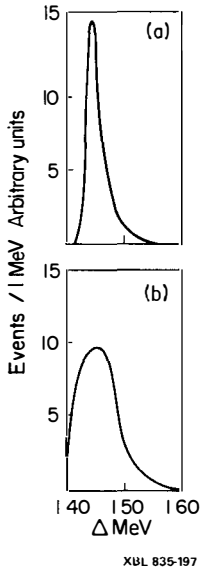


Fig. 10

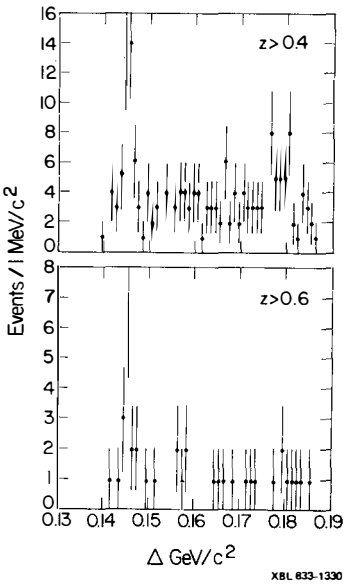


Fig. 11

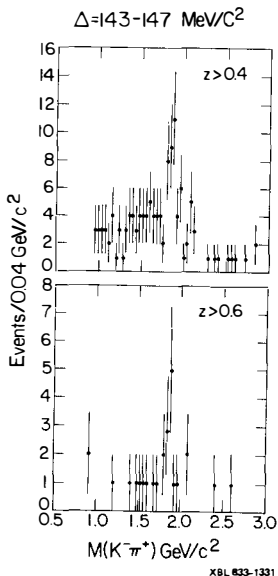


Fig. 12

Fig. 10 - (a) The Δ signal from D^{*+} decays with $M(K^-\pi^+)$ in the D° region.
 (b) The Δ signal from D^{*+} decays with $M(K^-\pi^+)$ in the S° region.
 Monte Carlo calculations at $E_{cm} = 5.2$ GeV. Results at 29 GeV are essentially the same.

Fig. 11 - Experimental Δ distributions at $E_{cm} = 29$ GeV, for $M(K^-\pi^+) = M_{D^\circ} \pm 0.1$ GeV/c^2 and 2 cuts on z . Mark II at PEP.

Fig. 12 - Experimental $M(K^-\pi^+)$ distribution $E_{cm} = 29$ GeV for 2 cuts on z . The D° signal is clear while the S° is small since a narrow Δ region, 143-147 MeV, is shown here. Mark II at PEP.

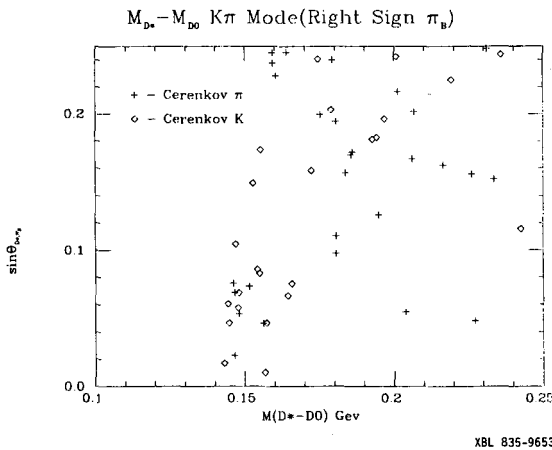


Fig. 13 (a)

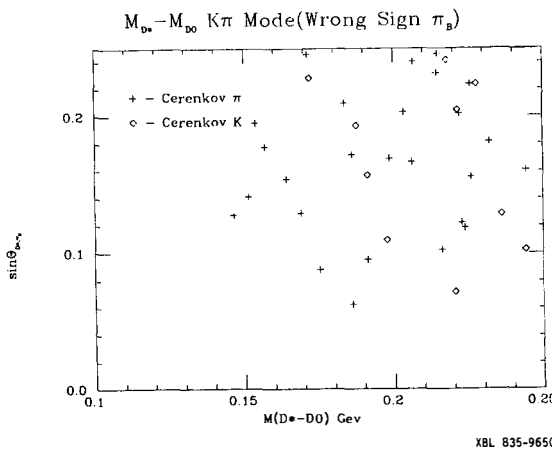
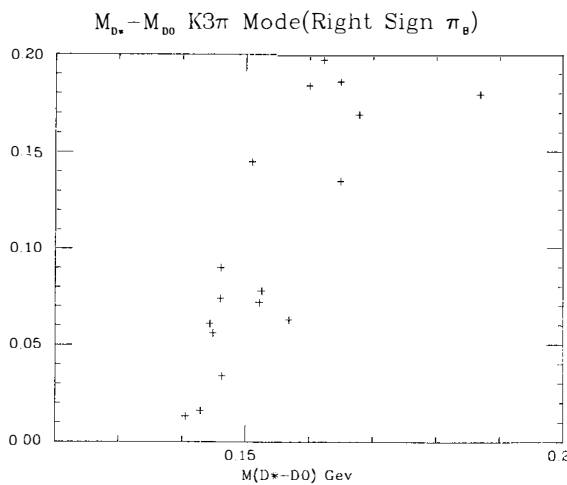
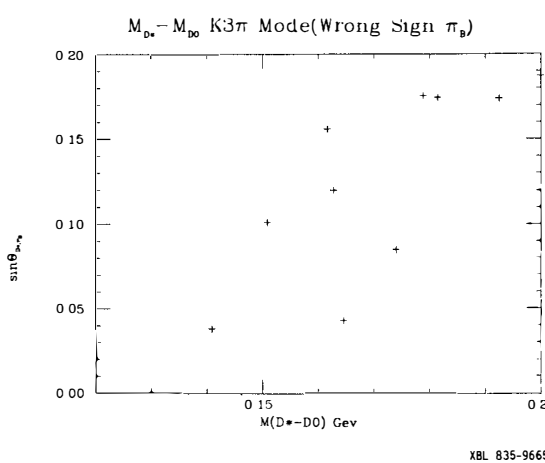


Fig. 13 (b)

Fig. 13 - Scatter plot of $\sin \theta_{D^*}, \pi_B$ vs. Δ for $M(K-\pi^+) = M_{D^0} + 0.3$ GeV/c^2 . This data thus contains both D^0 and S^0 signals. K and/or π by Cerenkov identification: (a) "right sign" π_B ; (b) "wrong sign" π_B ; i.e., background. (DELCO). $\sigma(D^{*+}) = 0.18 \pm 0.04 \pm 0.06$ nb from these data.



(a)



(b)

Fig. 14 - Scatter plot of $\sin \theta_{D^* \pi_B}$ vs. Δ for $D^0 \rightarrow K^-\pi^+\pi^-\pi^+$ decay mode.
(DELCO)
 $\sigma(D^{*+}) = 0.16 \pm 0.06 \pm 0.09$ nb from these data.

- (iii) The D^{*+} gives tagged D^0 events which are used for a D^0 lifetime measurement in the Mark II Vertex detector.
- (iv) The angular distribution and asymmetry of the charged quark distribution relative to the e^+ direction (so far only results from TASSO are available, see talk by Yamada at this conference).

The mass constraint Δ which characterizes D^* events, can be expressed differently as well. The kinetic energy of the bachelor pion π_B^+ in the decay $D^{*+} \rightarrow \pi_B^+ D^0$ has a kinetic energy of $T_{\pi_B^+}^* = 5.7$ MeV in the D^* rest system (or a momentum of $p_{\pi_B^+}^* \sim 40$ MeV/c). This implies that $p_{\pi_B^+}^*$ is the maximum transverse momentum π_B^+ can have in the laboratory system. i.e., $p_{\pi_B^+} \sin \theta \leq p_{\pi_B^+}^*$ where θ is the laboratory angle between the D^* direction and the π_B^+ direction.

This feature was emphasized by the DELCO experiment. In Figures 14 and 15 I show a scatter plot from DELCO of $\sin \theta$ vs. Δ . Typical $p_{\pi_B^+}$ values are ~ 400 MeV/c hence all D^* events should occur for $\sin \theta \lesssim 0.1$. As can be noted from Figures 14a and b this is indeed the case. In the DELCO experiment the Cerenkov counters were used for K and/or π identification and thus they were able to separate "right sign π_B^+ " candidates, i.e., $\pi_B^+ D^0$ from "wrong sign π_B^+ " events i.e., $\pi_B^- D^0$. The latter can be considered as a measure of the background.

Furthermore in view of the Cerenkov identifications the DELCO experiment was also able to study D^{*+} candidates with the D^0 decay mode $D^0 \rightarrow K^- \pi^- \pi^+ \pi^+$, see Figures 15a and b.

The Charmed Quark Fragmentation Function

The results that emerged from the Mark II experiment ^{4]} are that the heavy quark fragmentation function D_Q^H peaks at considerably higher z values then those for light quarks. The qualitative features are, that just like in the case of Λ^0 decay for example, the heavy particle (proton) carries a large fraction of the Λ^0 momentum. In our case the charmed meson carries off a large fraction of the charmed quark momentum. This idea has been cast into a quantitative form by Peterson et al. ^{5]} who suggest the expression:

$$D_Q^H = \frac{A}{z [1 - 1/z - \epsilon_Q/(1 - z)]^2} \quad (3)$$

where A is a normalization constant and ϵ_Q is a constant characteristic of the individual quark mass. $\epsilon_Q \approx 0.25$ gives a reasonable fit to the data for charmed quarks. The results from the DELCO experiment are very similar. See Figures 15, 16 and 17.

Semileptonic Charm and Bottom Decays

Prompt lepton production in hadronic events from high energy e^+e^- annihilation provides a tag for the presence of hadrons containing charm (c) or bottom (b) quarks. The production rates and momentum spectra of such leptons depend on the semileptonic branching ratios and the momentum spectra of the parent hadrons. Furthermore the momentum spectra of these hadrons provide information on the fragmentation properties of c and b quarks. As in the case of charmed quark fragmentation the b quarks fragment predominantly into high momentum hadrons.

A. Studies in the Mark II Detector

In the Mark II analysis the total momentum and transverse momentum spectra of prompt electrons in hadronic events are measured. The transverse momentum p_\perp is measured with respect to the thrust axis defined by all the charged particles in the event. The hard p_\perp distribution of electrons from bottom decays relative to charm decays allows one to separate the contributions of b and c quarks to the prompt electron signal.

The Mark II data, corresponds to an integrated luminosity of 35 pb^{-1} . The electron-hadron separation algorithm is based on measurements of the ratio $r_i \equiv E_i/p$, where E_i is the energy deposition in one of three groupings, $i = 1 - 3$, of layers in the Mark II Liquid Argon-Lead calorimeter. Each of these groupings combines all layers in the first 8 radiation lengths which have the same strip orientation. To minimize the effects of neighboring particles, particularly photons, the energy deposition E_i is taken from a narrow lateral region, comparable in size to one strip width ($\approx 4 \text{ cm}$), centered about the extrapolated particle trajectory. The algorithm demands that each value of r_i and that $\sum r_i$ be greater than an appropriate minimum value. The electron identification efficiency was determined with electrons from Bhabha events and photon conversions. This efficiency varies from 78% at $1 \text{ GeV}/c$ to 93% at the highest momenta.

The probability, as a function of p and p_\perp , that a hadron will be misidentified as an electron was determined from: Hadron interactions in the calorimeter exposed in a pion test beam as well as with pions from the decay $\psi \rightarrow 2(\pi^+\pi^-)\pi^0$ in data from SPEAR. Accidental overlap with nearby photons was estimated from jet studies. The misidentification probabilities are typically 0.5%, but can be as large as 3% for a track momentum $1 \text{ GeV}/c$ in the core of a jet.

A hadronic event sample was selected by requiring $N_{\text{ch}} \geq 5$ and total detected energy $E^+ + E^- > E_{\text{cm}}/4$. There were a total of 10691 such events. To eliminate real electrons which are not part of the prompt signal, a visual scan was performed to remove a small number of electron candidates arising from:

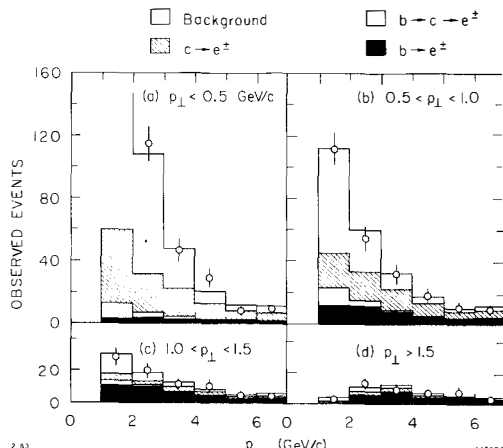


Fig. 18

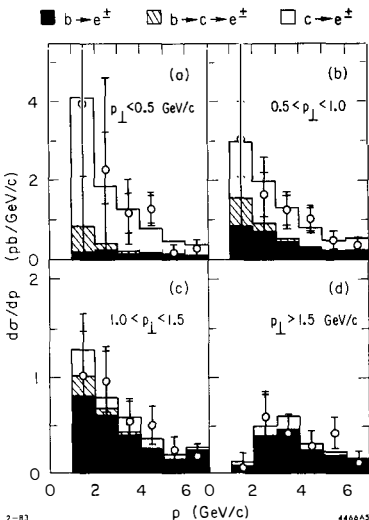


Fig. 19

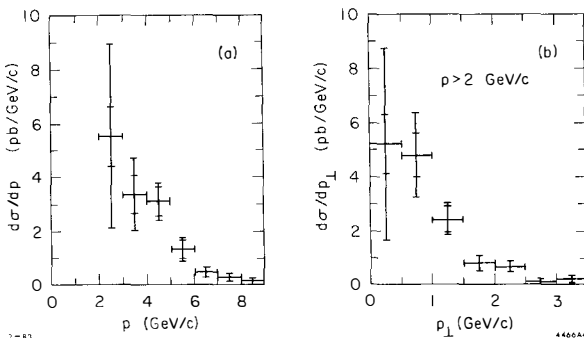


Fig. 20

Fig. 18 - Observed prompt electron momentum spectra in 4 regions of transverse momentum p_{\perp} . Background contributions unshaded. (Mark II)

Fig. 19 - Prompt electron momentum spectra in 4 regions of transverse momentum p_{\perp} . Two sets of error bars are shown for each data point. The smaller ones are statistical only. The larger ones are the statistical and systematic errors added in quadrature. The highest momentum bin includes all momenta ≥ 6 GeV/c. The histograms show the results of the fit. The three contributions shown are (i) b primary (solid), (ii) c secondary (diagonally hatched), and (iii) c primary (unshaded). (Mark II)

Fig. 20 - Differential cross sections for prompt electrons with $p > 2$ GeV/c: (a) total momentum and (b) transverse momentum. Two sets of error bars are shown for each data point as in figure. (Mark II)

- τ pair production;
- beam-gas interactions;
- the process $e^+e^- \rightarrow e^+e^- + \text{hadrons}$;
- background electrons from photon conversions and Dalitz decays were removed by a pair finding algorithm, which removes about 70% of the electrons.

After removal of these backgrounds on an event by event basis, 930 electron candidates with $p > 1$ GeV/c remained. These were partitioned into 24 p , p_\perp

Background contributions to each bin from misidentified hadrons, and electron pairs was calculated. In Figure 18 the observed electron spectra are shown. In three of the lowest momentum and transverse momentum bins [Figure 18a: $p < 3.0$ GeV/c and Figure 18b: $p < 2.0$ GeV/c] backgrounds account for almost 75% of the observed signal. In the remaining bins, however, the background levels are much less severe. Excluding these three bins, the background fractions for Figure 19 are 46%, 36%, 30%, and 23% respectively. Figure 20 shows the total momentum and transverse momentum differential cross sections for prompt electrons with $p > 2$ GeV/c. Two sets of errors are plotted for each point. The smaller error bars represent the statistical errors. The larger ones show the quadratic sum of the statistical and systematic errors. The systematic errors are dominated by the uncertainty in the hadron misidentification probabilities. The total inclusive cross section for this sample is $14.4 \pm 1.6 \pm 5.2$ pb.

A maximum likelihood fit to the observed populations in the various p , p_\perp bins was performed leaving out the 3 high background bins and accounting for the signal above background in terms of the following contributions:

- (i) Bottom decays in $b\bar{b}$ events (b primary)
- (ii) Charm decays in $b\bar{b}$ events (c secondary)
- (iii) Charm decays in $c\bar{c}$ events (c primary)

To represent contributions (i) - (iii) a Monte Carlo simulation with a Feynman-Field hadronization model and gluon radiation as incorporated by Ali et al. [6] was performed. The semileptonic electron spectra produced by the heavy meson decay models in the Monte Carlo agreed satisfactorily with measured spectra from the DELCO (charm) and CLEO (bottom) experiments.

In the fit ϵ_c was fixed at 0.25 in accordance with the D^+ results given above. The remaining parameters were:

- $B_e(b) = (11.6 \pm 2.1 \pm 1.7)\%$;
- $B_e(c) = (6.3 \pm 1.2 \pm 2.1)\%$; and
- $\epsilon_b = 0.030 \pm 0.032 \pm 0.023$

The histograms in Figures 18 and 19 show the results of the fit and the relative contributions of (i) - (iii) to the prompt electron signal in each p , p_\perp bin. The $\chi^2/D.F.$ of the fit is 14.0/18. Here we must note that the $B_e(c)$ and $B_e(b)$ values are averages over charged and neutral branching ratios weighted by the corresponding experimental production ratios. Thus in the case of charmed particles, since D^+ and D^0 are primarily produced via D^* 's and since only the D^{*+} feeds the D^+ mesons a D^+/D^0 production ratio of $\sim \frac{1}{3}$ to $\frac{1}{2}$ is expected. A different parameterization was also studied namely the form $z^\alpha(z-1)$, which gives qualitatively similar results. For either of these parameterizations, the average value of z_b is $\langle z \rangle_b = 0.75 \pm 0.05 \pm 0.04$.

B. Studies in the MAC Detector

A very similar analysis was recently performed for semileptonic muon decays in the MAC detector. Here again the data was divided into p and p_\perp bins (20 bins in all).

For the MAC analysis, chambers covering all of the central hadron calorimeter and much of the encaps are used, subtending a total solid angle of 77% of 4π .

The sample for their analysis consists of 25,000 multihadron events, each having more than 4 charged prongs and energy deposited in all calorimeters greater than the beam energy. The sample corresponds to an integrated luminosity of 54 pb^{-1} at about 29 GeV center-of-mass energy. Within these events, tracks reconstructed in the drift chambers surrounding the calorimeter constitute muon candidates. A momentum assignment was made for each of these tracks by extrapolating it back through the toroidal magnetic field of the calorimeter to the primary event vertex, taking into account the ionization loss of the particle in the calorimeter. The momentum resolution was about 30%, mostly due to multiple scattering.

Discrimination against punch-through was achieved for muon candidates with $p > 2 \text{ GeV}/c$ by rejecting tracks:

- whose path length through the iron in the calorimeters was less than about 80 cm (one-third of candidates removed by this cut);
- with evidence in the outer drift chamber of more than one particle having emerged from the calorimeter in the same vicinity (17% of candidates removed);
- with ionization in the outermost calorimeter layer in more than two adjacent segments (5% of candidates removed);
- a few non-hadronic events were removed from the remaining sample by scanning.

The final sample contained 476 events.

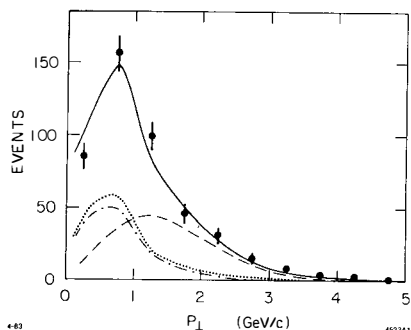


Fig. 21

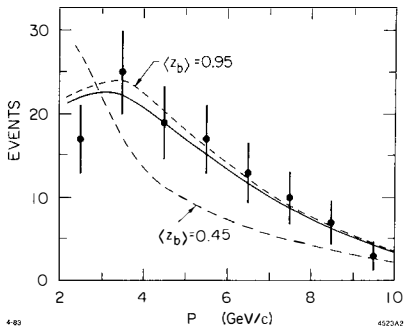


Fig. 22

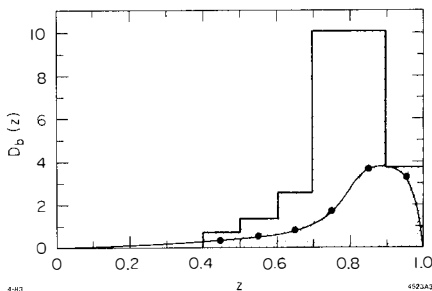


Fig. 23

Fig. 21 - P_{\perp} spectrum of muons with $b\bar{b}$ (dashed curve), $c\bar{c}$ (dot-dashed), background from decay and punch-through (dotted), and total (solid curve) predictions. (MAC)

Fig. 22 - Total momentum of muons with $p_{\perp} > 1.5$ GeV/c. Dashed curves are the best fits obtained with the b fragmentation fixed to a narrow range of z . The solid curve is the best overall fit. (MAC)

Fig. 23 - The shaded region is the envelope of acceptable b quark fragmentation functions. The curve represents the Peterson et al. function for $\epsilon_b = 0.008$. (MAC)

A Monte Carlo model was used to find the level of background remaining in the sample from π and K decays. This was found to be $(23 \pm 1)\%$.

The punch-through background was determined empirically from hadronic decays of tau leptons. From a sample of 1600 tau pair events, roughly 3 muon candidates in hadronic jets attributable to punch-through were found. Differences between the energy spectra of tau and multihadron jets were accounted for by taking the ratio of the energy deposited in the outermost calorimeter layer in the two samples. From these studies, the punch-through fraction in the inclusive muon sample was found to be $(9 \pm 7)\%$.

Figure 21 shows the p_{\perp} spectrum of the observed muons, along with Monte Carlo predictions for muons from b and c quarks, and the overall (decay plus punch-through) background prediction.

The background is concentrated at low values of p_{\perp} , and is well separated from the $b\bar{b}$ predicted spectrum.

Figure 22 shows the momentum spectrum for muons with $p_{\perp} > 1.5$ GeV/c, the regions containing the highest fraction of $b\bar{b}$ events. The dashed lines illustrate the effect of fixing the b fragmentation function at particular values of z , and allowing the c fragmentation function and the semileptonic branching fractions of both quarks to vary to obtain best fit to the p by p_{\perp} array. Low values of $\langle z_b \rangle$ are clearly ruled out. The solid curve is the predicted spectrum for the best fit, allowing all parameters to vary.

The semimuonic branching ratio for the b quark, averaged over the neutral and charged B mesons was found to be (15.5 ± 5.4) . The c fragmentation function was not determined by the data, with the one-sigma envelope allowing $0.17 < \langle z_c \rangle < 0.67$. The semimuonic c branching fraction was found to be (7.6 ± 9.7) %, the large uncertainty being due to the dependence of the branching fraction on the exact fragmentation function.

If the functional form for fragmentation, suggested by Peterson et al.,^{5]} was used, they found that $\epsilon_b = 0.008 \pm 0.037$ - 0.008, but with a somewhat worse chi-squared than for a more sharply peaked function. (See curve in Figure 23.)

3. τ and D^0 Lifetime Measurements in the Mark II Detector.

Recently a vertex detector^{7]} was installed in the Mark II. This is a high precision drift chamber which allows one to probe decay lengths in the submillimeter region. This device (see Figure 24) has achieved a resolution comparable to the decay lengths being measured.

It is a relatively short cylindrical drift chamber, 1.2 m long, with seven axial layers of drift cells. Four are about 11 cm from the beam line, and three

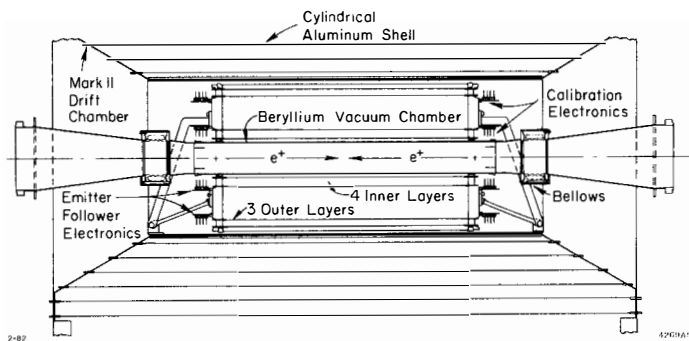


Fig. 24 - The Mark II Vertex detector.

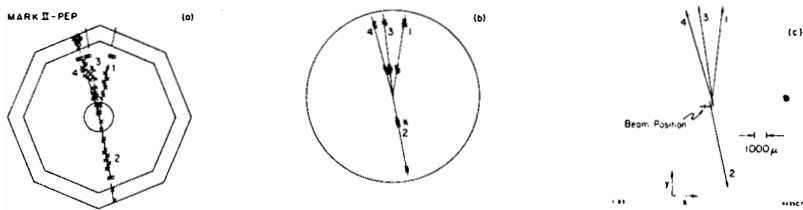


Fig. 25 - (a) $e^+e^- \rightarrow \tau^+\tau^-$ as seen in the Mark II detector at PEP; (b) close-up of the same event in the vertex detector; (c) extreme close-up of the same event showing particle trajectories extrapolated to the vicinity of the interaction point.

at about 30 cm. To keep multiple scattering to a minimum the chamber has been built directly around a beryllium beam pipe 0.6% of a radiation length thick. The beam pipe serves as the inner gas seal for the chamber. The average resolution per layer in hadronic events is about 100μ .

A study of the measured distance between the two tracks in Bhabha events after extrapolation to the origin give a distribution of the distance between them with $\sigma \approx 100 \mu$. An integrated luminosity of 20 pb^{-1} was accumulated at $E_{\text{cm}} = 29 \text{ GeV}$ with this chamber.

◦ τ Lifetime

The τ lifetime provides a sensitive check of the standard model of weak interactions. With the assumption that τ decay proceeds in direct analogy with muon decay, and that τ neutrino is massless. The tau lifetime can be related to the muon lifetime, namely:

$$\tau_{\tau} = \tau_{\mu} \cdot \left(\frac{m_{\mu}}{m_{\tau}} \right)^5 \cdot B(\tau \rightarrow e\nu\bar{\nu}) . \quad (4)$$

Experimentally $B(\tau \rightarrow e\nu\bar{\nu}) = 17.6 \pm 1.1\%$, (5)

so $\tau_{\tau} = 2.8 \pm 0.2 \times 10^{-13} \text{ s}$, (6)

where the error reflects the uncertainty in the electronic branching ratio.

A number of models have been considered under which this simple prediction could fail^{8,9,10]}.

Furthermore the tau lifetime would be extended if the tau neutrino were massive enough so as to significantly limit the phase space of the decay.

Tau leptons are pair-produced in e^+e^- annihilations, so that each tau has the beam energy. Thus the lifetime can be measured by determining the average decay length of the taus. At PEP with $E_{\text{cm}} = 29 \text{ GeV}$, it is expected to be about 700μ . The decay length can be measured when the tau decays in the three-charged-prong topology. It is the distance between the production point, i.e., the beam position, and the position of the decay vertex.

Events are selected in which at least one of the taus has decayed in the three-charged prongs topology and the total charged of the prongs is zero. The three particle invariant mass is required to be in the range $0.7 < m_{3\pi} < 1.5 \text{ GeV}/c^2$, and tau pairs produced by the two-photon process are rejected. Figure 25

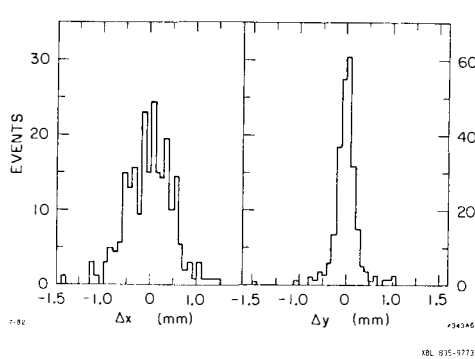


Fig. 26

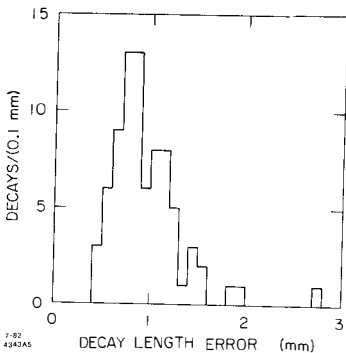


Fig. 27

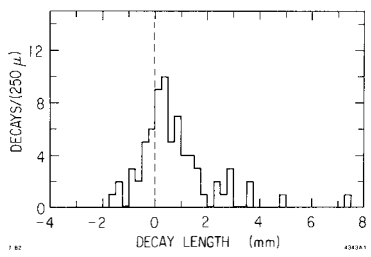


Fig. 28

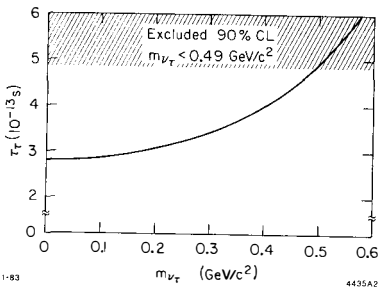


Fig. 29

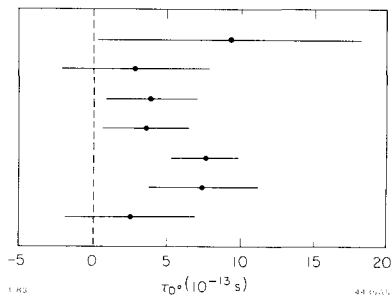


Fig. 30

Fig. 26 - Horizontal and vertical hadronic vertex positions relative to the beam position. (MARK II)

Fig. 27 - Calculated error in the decay length. (MARK II)

Fig. 28 - Measured decay lengths. (MARK II)

Fig. 29 - Variation of the τ lifetime with the mass of the τ neutrino. (MARK II)

Fig. 30 - Measured proper times for the seven D^0 events. (MARK II)

shows such an event in the Mark II detector.

The rms beam size at PEP is 500 μ horizontally and about 50 μ vertically. The average beam position is remarkably stable from one fill to the next. This was measured by finding the average intersection point for an ensemble of well-measured tracks. As a cross check, this determination of the beam position was compared to the vertex position measured in hadronic events. Figure 26 shows that these methods agree. The width of the Δx distribution is consistent with the known beam size, and the width of the Δy distribution is consistent with the vertex resolution, indicating that the beams are stable.

The decay vertex position and its error ellipse are determined from the three pion trajectories and their associated errors with a chi-square minimization procedure. Events with a vertex chi-squared per degree of freedom greater than 6 were excluded. The best estimate for the projected decaylength is then given in terms of the decay vertex position relative to the beam position (x_v, y_v) , the sum of the beam and vertex error matrices (σ_{ij}) , and the τ direction cosines (t_x, t_y) by the following expression:

$$l_p = \frac{x_v \sigma_{yy} t_x + y_v \sigma_{xx} t_y - \sigma_{xy} (x_v t_y - y_v t_x)}{\sigma_{yy} t_x^2 + \sigma_{xx} t_y^2 - 2\sigma_{xy} t_x t_y} \quad (7)$$

The tau direction is well approximated by the direction of the 3π system. Then the decay length is:

$$l = \frac{\bar{p}_{3\pi}}{p_{3\pi}^z} l_p \quad , \quad (8)$$

where $\bar{p}_{3\pi}$ is the total momentum of the three pion system.

Figure 27 shows the calculated error in the decaylength, which depends on the opening angles and orientation of the decay, the tracking errors, and the beam size.

The measured decay lengths are shown in Figure 28, where only those events with decaylength errors less than 1.5 mm are included. The mean of the distribution is obviously positive and its shape is asymmetric. The distribution is fitted with a maximum likelihood technique which takes the decaylength error into account event-by-event. The fitting function is the convolution of the Gaussian decay length error with an exponential decay distribution. The average decay

length is $710 \pm 120 \mu$.

After correction for hadron contamination and initial state radiation, this yields: $\tau_\tau = 3.31 \pm 0.57 \pm 0.60 \times 10^{-13}$ s, where the first error is the statistical error and the second is the systematic. The measurement is compared to the other measurements which have appeared in the literature in Table I. The number of decays studied and the average decay length error are also shown for comparison.

Table I
 τ Lepton Lifetime Measurements.

Experiments	Number of Decays	Average Decay Length Error (mm)	τ_τ (10^{-13} s)
TASSO	599	10	0.8 ± 2.2
MARK II	126	4	4.6 ± 1.9
MAC	280	4	$4.1 \pm 1.2 \pm 1.1$
CELLO	78	6	$4.7 \pm 3.9 \pm 2.9$

MARK II			
Vertex Detector	71	0.9	$3.31 \pm .57 \pm .60$

Theory			
(Universal coupling strength)			2.8 ± 0.2

All of the measurements are consistent with the expected lifetime. The present experiment confirms that the tau couples to the charged weak current with universal strength within the errors,

$$g_\tau/g_e = 0.92 \pm 0.086 \pm 0.090 \quad . \quad (9)$$

If one assumes that the coupling has the universal strength, one can set a limit on the mass of the tau neutrino. Figure 29 shows how the lifetime varies as a function of the tau neutrino mass^[11] along with the 90% confidence level upper limit set by this measurement. One finds $m_\nu < 0.49$ GeV/c², which is compatible with the 0.25 GeV/c² limit deduced earlier from the shape of the decay lepton spectrum^[12].

◦ D° Lifetime

As Kalmus^[13] reported at the Paris conference, charmed meson lifetimes seem to be stabilizing as follows: The D° lifetime is about 4×10^{-13} s, about half the D⁺ lifetime of 9×10^{-13} s.

The D° lifetime was measured with the Mark II vertex detector using a sample of D°'s which had been cleanly identified by the main tracking chamber. At the moment the main virtue of this measurement is that it is subject to very different systematic errors from the earlier measurements. Like the other, measurements however it also suffers from low statistics. An integrated luminosity of 17 pb^{-1} gave seven well-measured D° decays.

The clean event sample comes about by selecting D°'s from D* decays. For the lifetime analysis below, events with $z > 0.6$ were selected. They seem to be essentially free of background. The high momentum cut also makes it unlikely that these D°'s have originated from B decays.

The decay vertex is determined by vertexing the K and π from the D°. The decay length is then determined with the same technique used in the tau analysis above. The average decay length is about 500μ , and the average vertex error about 700μ . Figure 30 shows each of the 7 measurements with its error. A similar maximum likelihood fit as for the τ above gives a D° lifetime of

$$\tau_{D^\circ} = 3.7 \pm \frac{2.5}{1.5} \pm 1.0 \times 10^{-13} \text{ s} \quad . \quad (10)$$

This result is in agreement with the current world average.

◦ Limits on the B Meson Lifetime

If their decays were not suppressed, the hadrons containing the b quark would be expected to decay with a lifetime

$$\tau_B^\circ \sim \tau_\mu \cdot \left(\frac{m_\mu}{m_b} \right)^5 \cdot \frac{1}{9} = 10^{-15} \text{ s} \quad . \quad (11)$$

The (qualitative) factor 9 comes from the number of available final states. The B meson lifetime is expected to be longer, however, since the decay is suppressed by the presumably small mixing between the second and third quark generations. The B meson lifetime thus gives a measure of the quark mixing, at least if one assumes universal weak coupling strength^[14].

Two experiments have obtained upper limits for the B lifetime by measuring the average impact parameter of energetic muons. Events are selected which have high mass jets and an identified high-momentum muon as discussed above. Using the thrust axis as an estimate of the B meson direction, a signed impact parameter can be determined from the lepton trajectory and the known beam position.

The upper limits obtained are as follows: The JADE experiment finds $\tau_B < 1.4 \times 10^{-12}$ s and the MAC experiment finds $\tau_B < 3.7 \times 10^{-12}$ s, both limits at the 95% confidence level. Thus there is as yet no evidence for a B lifetime accessible to current measurements. A Mark II measurement is in progress on the electron tagged events discussed above. When completed, this should have a sensitivity of 3×10^{-13} sec.

4. Electro Weak Interference Effects.

As shown in Yamada's talk at this conference the results from the five PETRA Groups: TASSO, JADE, MARK J, CELLO, and PLUTO make a very convincing case for Electro-Weak interference. In this respect the higher energy available at PETRA, mainly 34 GeV, compared to the energy at PEP, 29 GeV, helps. Tables II and III show the corresponding results. Here we must note that Mark II uses a more limited interval in $\cos\theta$ viz. $|\cos\theta| < 0.7$ while MAC uses nearly full $\cos\theta$ range. Figures 31 to 34 show the relevant angular distributions.

The above experiments compared their data to the QED calculation with α^3 corrections according to Behrend and Kleiss^{15]}.

TABLE II
The Data Sets
Electro-Weak Interference Effects

Detector	Particles	Luminosity pb^{-1}	Number of Events	Bkgrnd. %
Mark II $ \cos\theta < 0.7$	$\mu\mu$	50.0	2703	2.4
	$\tau\tau$	46.6	1607	14.8
	ee	50.0	40,989	0.06
MAC $ \cos\theta < 0.94$	$\mu\mu$	40.0	3067	4.2
	ee	40.0		

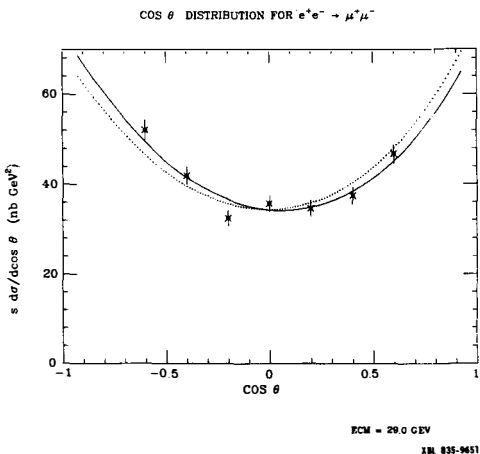


Fig. 31 - Angular distribution for μ pairs. Solid curve is fit to data. Asym = $(-4.4 \pm 1.9)\%$. Dotted curve is QED with α^3 corrections. (MARK II)

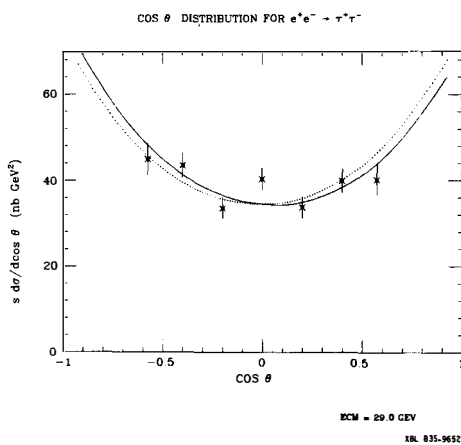


Fig. 32 - Angular distribution for τ pairs. Solid curve is fit to data. Asym = $(-4.1 \pm 2.7)\%$. Dotted curve is QED with α^3 correction. (MARK II)

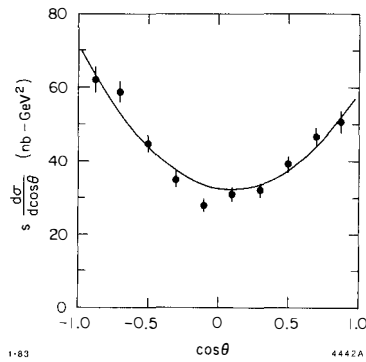


Fig. 33 - Angular distribution for μ pairs. Solid curve is fit to data.
 $\text{Asym} = (-7.6 \pm 1.8)\%.$ (MAC)

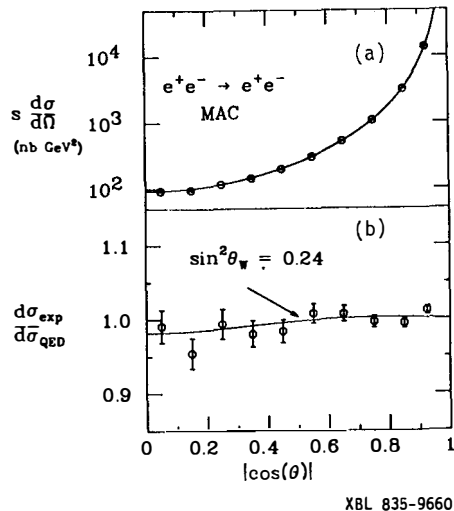


Fig. 34 - (a) Angular distribution for Bhabha scattering. (b) Ratio of experimental to QED distributions. Curve corresponds to fit with $\sin^2\theta_W$ as given.

TABLE III
Results From Electroweak Interference Effects.

Results	Mark II	MAC
$g_a^e g_a^\mu$	$0.25 \pm 0.11 \pm 0.02$	0.31 ± 0.08
$g_a^e g_a^\tau$	$0.23 \pm 0.15 \pm 0.02$	
g_v^2	$0.03 \pm 0.05 \pm 0.03$	
$\sin^2 \theta_w$	0.22 ± 0.06	0.24 ± 0.085
g_a^2 (all)	$0.22 \pm 0.07 \pm 0.02$	

5. Searches for New and "Peculiar Particles."

Many searches which have been made for new particles have been presented at the 1982 Paris conference or have been published earlier. Here I will only touch on a few new or augmented results.

◦ Study of $\mu\mu\gamma$ and $\mu\mu\gamma\gamma$ Events

In a search for $e^+e^- \rightarrow \mu^*\mu$ and $e^+e^- \rightarrow \mu^+\mu^-$ the MAC Group has presented $m(\mu\gamma)$ and $\cos\theta_\mu$ distributions, see Figures 35 to 37. The conclusion from these measurements is that the results are consistent with 3rd and 4th order QED (the curves in the figures). It is interesting to note that due to interference between initial and final state radiation effects purely QED processes give rise to very considerably asymmetries in the μ angular distributions. Figure 37 shows a plot of $M_{\mu^-\gamma}$ versus $M_{\mu^+\gamma}$ for the $\mu\mu\gamma\gamma$ events. There $\mu^*\mu^*$ production would show up as an enhancement along the 45° axis of this figure. The dotted lines show the experimental uncertainty in this region. This places a limit on $\sigma(\mu^*\mu^*)/\sigma(\mu\mu) < 2 \times 10^{-3}$ for $2 < M_{\mu^*} < 14$ GeV/c² at the 90% CL.

◦ Search for $e^+e^- \rightarrow \psi + x$ and $e^+e^- \rightarrow \tau + x$.

A search for ψ and τ production via decays into lepton pairs was made in the Mark II detector. This is based on a total luminosity of 35 pb^{-1} yielding 6276 hadron events which were restricted to have their thrust axis within $|\cos\theta| < 0.7$. Lepton pairs were selected as follows:

- At least one lepton had $p > 1$ GeV/c relative to the thrust axis;
- Both lepton have momenta ranging between 1.4 - 11 GeV/c;
- Only pairs of ee or $\mu\mu$ were accepted.

With these criteria the efficiency for ψ detection is estimated at 1.5%.

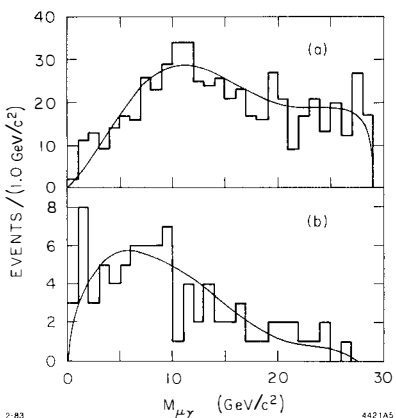


Fig. 35

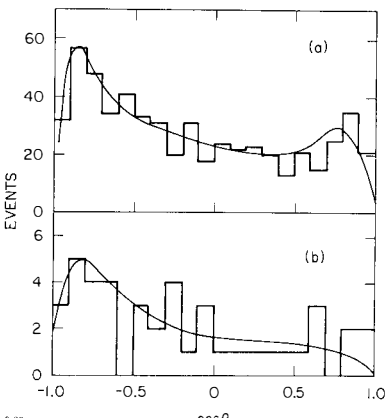


Fig. 36

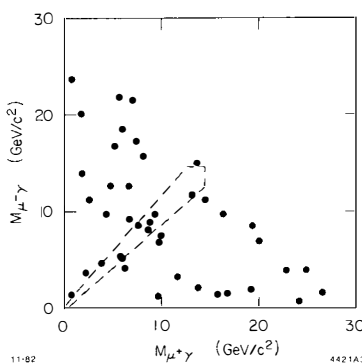


Fig. 37

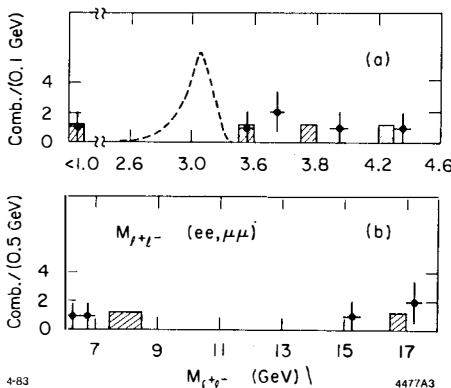


Fig. 38

Fig. 35 - (a) The $m_{\mu\gamma}$ distribution for the $\mu\mu\gamma$ final state (282 events). The solid curve is the α^3 order QED prediction. (b) Distribution of $m_{\mu\gamma}$ for the $\mu\mu\gamma\gamma$ final state (21 events). The curve is the α^4 QED calculation. (MAC)

Fig. 36 - (a) Polar angle distribution of muons for the $\mu\mu\gamma$ final state Asym = $(-21.6 \pm 4.1)\%$. The solid curve is the α^3 order QED prediction Asym(QED) = $(-21.1 \pm 1.3)\%$. (b) Muon angular distribution for the $\mu\mu\gamma\gamma$ final state Asym = $(-38 \pm 14)\%$. The curve is the α^4 order QED calculation Asym(QED) = $(-36.6 \pm 4.8)\%$. (MAC)

Fig. 37 - Scatter plot of the invariant masses of $\mu^+\gamma$ and $\mu^-\gamma$ combinations for the $\mu\mu\gamma\gamma$ final state. Dashed lines indicate a range of two standard deviations of the $\mu\gamma$ mass resolution about the 45° line. (MAC)

Fig. 38 - Search for $e^+e^- \rightarrow \psi + x$ and $e^+e^- \rightarrow T + x$ at $E_{cm} = 29$ GeV. (Mark II) The shaded events correspond to the expected invariant mass distribution from a Monte Carlo calculation with 5 quark flavors. The dotted curve is the ψ signal expected from the "non-perturbative model."

Perturbative QCD calculations give levels $\sim 10^{-3}$ to 10^{-4} of $\sigma(\mu\mu)$ for $\sigma(e^+e^- \rightarrow \psi + x)$ which are too small to observe with present statistics. However some non-perturbative models^[16] suggest

$$\sigma(ee \rightarrow \psi x) \approx 10^{-1} \sigma(\mu\mu) \approx 10 \text{ pb} \quad . \quad (12)$$

A study of $\mu\mu$ and ee pairs in hadronic events yielded the data in Figure 38 for both ψ and $\Upsilon(9.4)$ region. Also shown is the ψ signal expected on the above non-perturbative model. No candidates were found which places a 90% CL upper limit on $\sigma(ee \rightarrow \psi + x) < 4.4$ pb, and $\sigma(ee \rightarrow \Upsilon + x) < 4.7$ pb. This same search corresponds to a sample of 940 $b\bar{b}$ decays. The flavor changing neutral currents in b decay for $M(\ell^+\ell^-) > 1.6$ GeV gives the limit $Br(b \rightarrow \ell^+\ell^- x) < 0.8\%$. Furthermore a limit $Br(b \rightarrow \psi + x) < 4.9\%$ at the 90% CL is also obtained. However in the latter case we heard of the observation of such a decay mode by the CLEO Group presented by Thorndyke at this conference. They find $Br(b \rightarrow \psi + x) = (0.64 \pm 0.23)\%$.

6. Particle Identification with the TPC.

So far the TPC Group have analyzed 5 pb^{-1} of PEP data and some early results are shown herewith.

o The dE/dx Capability.

Figure 39a shows the dE/dx measurements on a single cosmic ray muon as seen in some 180 wires.

Note the high pulses due to the Landau fluctuations! Figure 39b gives the corresponding pulse height distribution and shows the location of the pulse height cutoff at the 65% level. This still leaves signals from 167 wires and yields the "truncated mean dE/dx " value.

Figure 40 gives this truncated dE/dx distribution vs. momentum for hadronic events and Figure 41 gives corresponding Monte Carlo results. Pions, kaons, protons, and electrons are clearly separated below the minimum ionizing region. As an example, Figure 42 gives the dE/dx ratio to that for pions for $0.45 < p < 0.74$ GeV/c. Figure 43 gives the corresponding results for $2.7 < p < 4.1$ GeV/c and shows partial K, p separation in the relativistic rise region.

Figure 44 gives the π , K , and p fractional distributions obtained from the above.

Finally the TPC Group presented a prompt μ rate in hadronic events. Figure 45 shows their results compared with results from several PETRA Groups. For

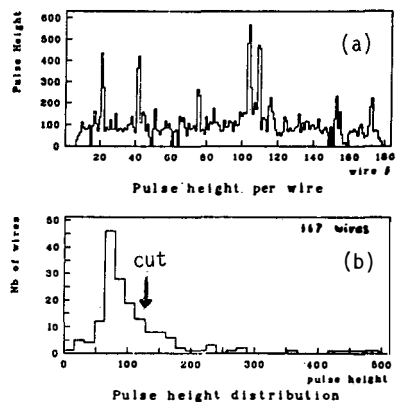


Fig. 39

XBL 835-9659

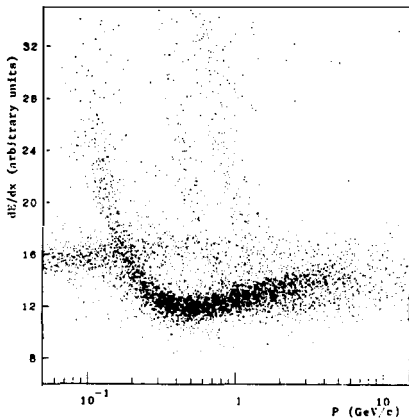


Fig. 40

XBL 835-9658

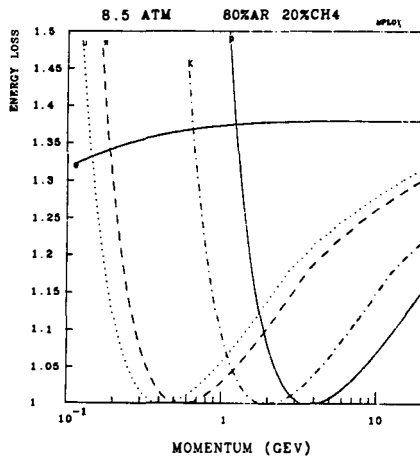


Fig. 41

XBL 835-9662

Fig. 39 - (a) dE/dx measurements on a single cosmic ray muon. Up to 180 individual dE/dx measurements are made on the track. (b) The corresponding pulse height distribution. The truncated mean value is determined by a cut selecting the lowest 65% of the signals. (TPC)

Fig. 40 - Truncated mean dE/dx distributions for particles from hadronic events at PEP. (TPC)

Fig. 41 - Monte Carlo calculations of truncated mean dE/dx distributions for the TPC running conditions at PEP.

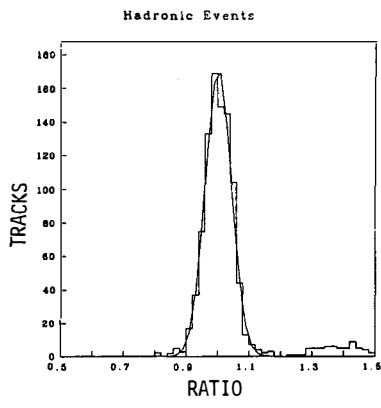
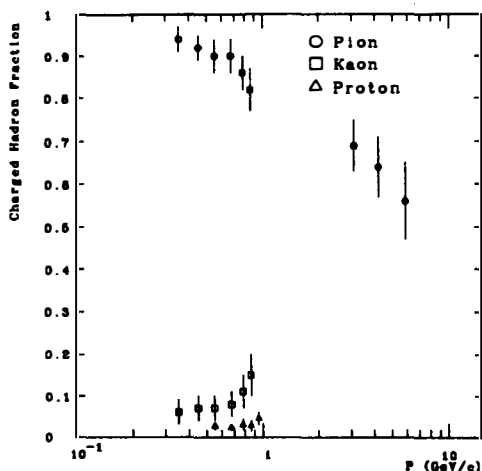


Fig. 42



XBL 835-9663

Fig. 44

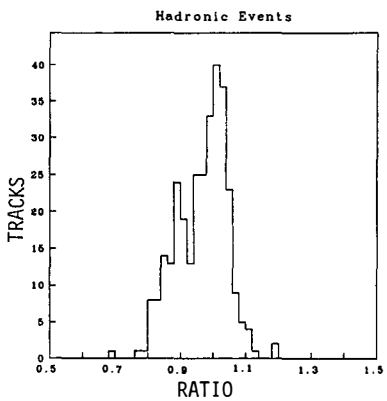
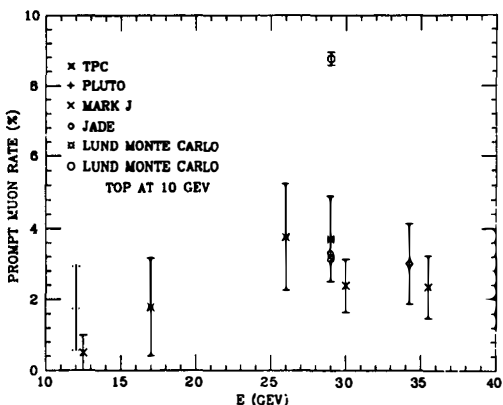


Fig. 43



XBL 835-9654

Fig. 45

Fig. 42 - Ratio of measured dE/dx to expected dE/dx for pions. Momentum range $0.45 < p < 0.740$ GeV/c. (TPC)

Fig. 43 - Ratio of measured dE/dx to expected dE/dx for pions. Momentum range $2.7 < p < 4.1$ GeV/c. (TPC)

Fig. 44 - Charged hadron fraction for π , K , and p . Hadronic events at PEP. (TPC)

Fig. 45 - Percentage of prompt muons in hadronic events at PEP. TPC results compared to PETRA results.

for $p_\mu > 2$ GeV/c. Also shown is the expected rate from Monte Carlo calculation with and without the presence of a top quark at the PEP energy (29 GeV).

REFERENCES

- 1] G. Gidal, B. Armstrong, and A. Rittenberg. LBL-91 Supplement UC-37, March 1983.
- 2] R.N. Cahn, M.S. Chanowitz, and J.D. Jackson. Private communication.
- 3] R.H. Schindler et al., Phys. Rev. D24, 78 (1981).
- 4] J.M. Yelton et al., Phys. Rev. Lett. 49, 430 (1982).
- 5] C. Peterson et al., Phys. Rev. D27, 105 (1983).
- 6] A. Ali et al., Phys. Lett 93B, 155 (1980).
- 7] J.A. Jaros, SLAC Report 250, SLAC-PUB-3044, Stanford, California (1982).
- 8] X. Li and E. Ma, Phys. Rev. Lett 47, 1788 (1981).
- 9] D. Miller, Phys. Rev. D23, 1158 (1981).
- 10] G.L. Kane, SLAC-PUB-2326 (1979).
- 11] S. Narison, CNRS 78/P.997 (1978).
- 12] W. Bacino et al., Phys. Rev. Lett 42, 749 (1979).
- 13] G. Kalmus, Rapporteur's talk at XXI International Conference on High Energy Physics, Paris, 1982.
- 14] H. Harari, SLAC-PUB-2234 (1978); M. Gaillard and L. Maiani, LAPP-TH-09 (1979). P.H. Ginsparg, S.L. Glashow and M.B. Wise. Phys. Rev. Lett. 50, 1415 (1983).
- 15] H.J. Behrend et al., DESY 92/056 (1982).
- 16] G.L. Kane et al., Phys. Lett B90, 164 (1980).

RECENT RESULTS FROM PETRA
ON
QED, ELECTRO-WEAK INTERACTIONS
AND
NEW PARTICLE SEARCH

Sakue Yamada*
LICEPP, Faculty of Science
University of Tokyo, Bunkyo-ku, Tokyo

Recent PETRA results on QED, electro-weak interactions and new particle searches are reviewed. Pure QED reactions are studied and the validity of QED is tested at $s \sim 1200$ GeV 2 . Effects of electro-weak interaction are observed. They are consistent with the standard model predictions. There is no evidence found for new particles including toponium, supersymmetric particles, heavy leptons, excited leptons and fundamental scalar particles.

* Mailing address: DESY, Notekstr. 85, D-2000 Hamburg 52

Introduction

PETRA was operated mostly around $\sqrt{s} = 34.5$ GeV in the past year. Since the beginning of PETRA, an integrated luminosity of approximately 80 pb^{-1} has been accumulated at each interaction region. The weighted average energy is about 34.5 GeV. After the energy increase in Summer 1982, a high energy scanning for topponium was performed above 38 GeV.

A large number of results have been published or reported at conferences from the five experiments: CELLO, JADE, MARK-J, PLUTO and TASSO. In this report, recent results of these experiments are reviewed on QED, electro-weak interactions and new particle searches. Although detailed description of analyses are not included in this summary, they can be found in the original references.

Topics covered here are the following.

1) QED and electro-weak interactions

$$\begin{aligned} e^+ e^- &\rightarrow \gamma\gamma \\ &\rightarrow e^+ e^- \\ &\rightarrow \mu^+ \mu^-, \tau^+ \tau^- \end{aligned}$$

R_{had}
charm quark tagging by D^* detection

2) Search for new particles

topponium
super-symmetric leptons
excited leptons
heavy leptons
charged Higg's or technipions

The Study of QED and Electro-Weak Interactions

$$\underline{e^+ e^- \rightarrow \gamma\gamma}$$

This reaction is a pure QED process. The validity of the theory can be evaluated by a cut off parameter, Λ , as follows¹⁾:

$$\frac{d\sigma}{d\Omega} = \frac{\alpha^2}{s} \frac{1+x^2}{1-x^2} \left[1 \pm \frac{s^2}{2\Lambda_\perp^4} (1-x^2) \right], \quad x \equiv \cos\theta \quad (1)$$

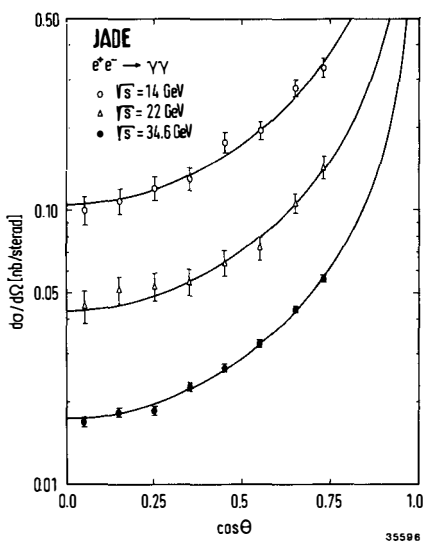


Fig.1: The differential cross section of the reaction $e^+e^- \rightarrow \gamma\gamma$ for c.m. energies 14.0, 22.0 and 34.6 GeV. The lines show the lowest order QED expectations.

Exact QED corresponds to $\Lambda = \infty$. The differential cross section from recent JADE results is shown in Fig.1.²⁾ The agreement between the data and the QED predictions is very good. For the value of Λ , the 95% C.L. lower limit is about 60 GeV. Limits on the cut off parameters from all the experiments are summarized in Table 1.

Table 1

95% C.L. lower limits on the cut off parameters, Λ_{\pm} , for $e^+e^- \rightarrow \gamma\gamma$ in GeV

	CELLO ³⁾	JADE ²⁾	MARK-J ⁴⁾	TASSO ⁵⁾	PLUTO ⁶⁾
Λ_+	59	61	58	42	46
Λ_-	47	57		34	36

The radiative correction is given by the formula

$$\left(\frac{d\sigma}{d\Omega} \right)_{\text{obs}} = \left(\frac{d\sigma}{d\Omega} \right)_0 (1 + \delta) \quad (2)$$

where δ is the correction which depends on the beam energy, scattering angle and event selection criteria such as the energy threshold for detection and the

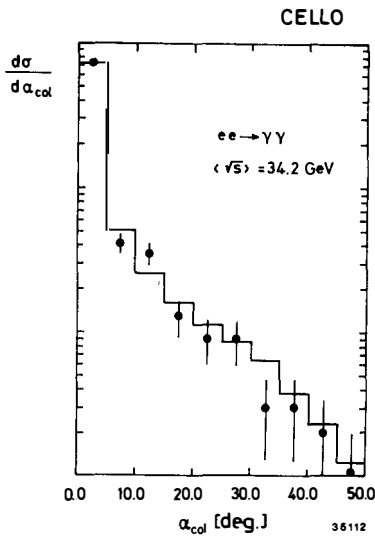


Fig.2: The acollinearity angle distribution of the photons. The histogram is the α^3 QED prediction.

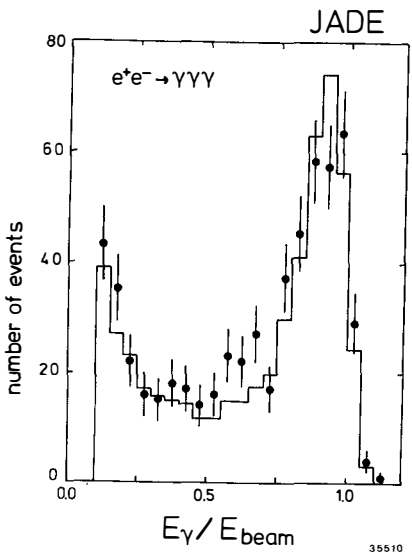


Fig.3: The photon energy distribution normalized by the beam energy for $e^+e^- \rightarrow \gamma\gamma\gamma$ events. The histogram is the α^3 QED expectation.

acollinearity angle. It is usually calculated by taking into account processes of the order α^3 ⁷⁾. A similar correction is applied to the small angle Bhabha scattering^{8,9)}, which is used to obtain luminosity. For the conditions of the PETRA experiments, the correction amounts to the order of $\pm 10\%$. In order to examine the validity of the radiative correction, it is necessary to study effects of higher order processes. They were tested by some groups. Fig.2 shows the acollinearity distribution of $\gamma\gamma$ measured by CELLO. JADE analysed $\gamma\gamma\gamma$ annihilation events and various features were studied. The energy distribution of the produced photons is shown in Fig.3. Both results demonstrate good agreement between data and α^3 predictions.

$e^+e^- \rightarrow e^+e^-$

Test of QED for the Bhabha scattering used to be done in terms of cut off parameters defined by the formula

$$\frac{d\sigma}{d\Omega} = \frac{\alpha^2}{4S} \left[\frac{10 + 4x + 2x^2}{(1-x)^2} F_t^2(t) - \frac{2(1+x^2)}{1-x} F_t(t) F_s(s) + (1+x^2) F_s^2(s) \right] \quad (3)$$

$$F_S(s) = 1 \mp \frac{s}{s - \Lambda_{\pm}^2} \quad , \quad F_t(t) = 1 \mp \frac{t}{t - \Lambda_{\pm}^2} \quad (4)$$

High statistics data is available now at high energies. The differential cross section measured by TASSO is shown in Fig.4¹⁰⁾. The data is consistent with $\Lambda_{\pm} = \infty$, and 95% C.L. limits are given to Λ_{\pm} as

$$\Lambda_{-} > 251 \text{ GeV}, \quad \Lambda_{+} > 150 \text{ GeV}.$$

The limit on Λ_{-} is larger than on Λ_{+} . This tendency is seen in the data of other experiments²⁾. It might be an effect of the weak interaction, which could cause a small deviation from the QED cross section at 34 GeV.

Bhabha scattering cross section is modified in the electro-weak theory as follows¹¹⁾:

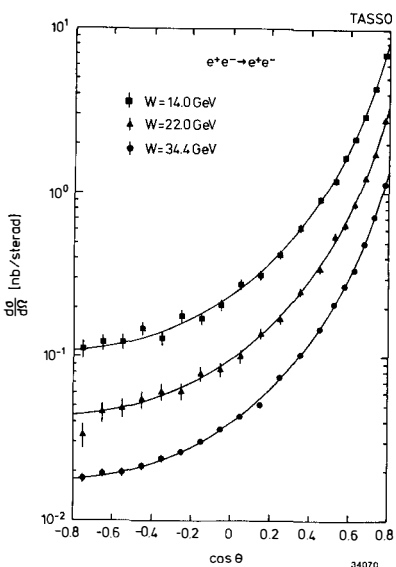


Fig.4: The differential cross section of Bhabha scattering at 12, 22 and 34 GeV. The curves are predictions of lowest order QED.

electron axial vector and vector weak charge. In the standard model, which is successful in many aspects¹²⁾, they are expressed to be

$$g_V = \frac{1}{2} (-1 + 4 \sin^2 \theta_W) \quad , \quad g_A = -\frac{1}{2} \quad (7)$$

$$\begin{aligned} \frac{d\sigma}{d\Omega} = \frac{\alpha^2}{8S} & \left[4 \frac{s^2}{t^2} \{1 + (g_V^2 - g_A^2)\xi\}^2 + \right. \\ & (1 - \cos\theta)^2 \{1 + (g_V^2 - g_A^2)\chi\}^2 + \\ & \frac{1}{2} (1 + \cos\theta)^2 \{(1 + \frac{s}{t} + (g_V^2 + g_A^2))^2 \cdot \right. \\ & (\frac{s}{t}\xi + \chi))^2 + (1 + \frac{s}{t} + (g_V^2 - g_A^2))^2 \cdot \\ & \left. \left. (\frac{s}{t}\xi + \chi)\right)^2 \} \right] \end{aligned} \quad (5)$$

$$\xi = \frac{G_F M_Z^2}{2\sqrt{2}\pi\alpha} \frac{t}{t - M_Z^2}, \quad \chi = \frac{G_F M_Z^2}{2\sqrt{2}\pi\alpha} \frac{s}{s - M_Z^2} \quad (6)$$

ξ and χ are the measures of the weak effect including the Fermi coupling constant and the Z^0 propagator. They are non-negligible at PETRA energies. For instance, at $S = 1200 \text{ GeV}^2$, $\chi = -0.25$ for $M_{Z0} = 90 \text{ GeV}$. g_A and g_V are the

electron axial vector and vector weak charge. In the standard model, which is successful in many aspects¹²⁾, they are expressed to be

For $\sin^2 \theta_W = 0.229^{13}$, g_V almost vanishes. Expected deviations from lowest order QED are shown in Fig.5 for various values of $\sin^2 \theta_W$. The cross section becomes smallest for $\sin^2 \theta_W = 0.25$, where $g_V = 0$. Data from each experiment is compared with the QED and electro-weak predictions in Fig.6^{2,10,14,15}). Although both predictions are consistent with data, a better fit is obtained for electro-weak predictions.

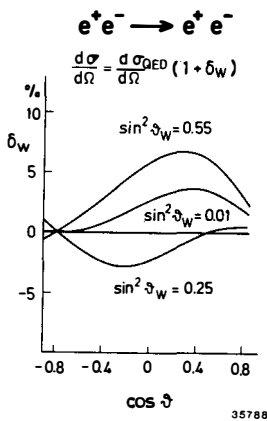
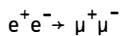


Fig.5: Expected deviation of the Bhabha scattering cross section from QED due to electro-weak interaction at $\sqrt{s} = 35$ GeV. The curves correspond to different values of $\sin^2 \theta_W$.

Higher order QED was also examined for Bhabha scattering. The acoplanarity angle distribution¹⁰⁾ and the photon spectrum of $e\gamma\gamma$ events²⁾ are shown in Fig.7 and 8, respectively. In both cases good agreement with α^3 QED is observed.



At the present PETRA energy this reaction shows the cleanest electro-weak effect among many reactions. The differential cross section is written as¹⁶⁾:

$$\frac{d\sigma}{d\Omega} = \frac{\alpha^2}{4s} \left[(1 + \cos^2 \theta) \{1 + 2g_V^e g_V^\mu \chi + (g_V^e g_V^\mu + g_A^e g_A^\mu)^2 \chi^2\} + \cos \theta (4g_A^e g_A^\mu \chi + 8g_V^e g_V^\mu e g_A^\mu \chi^2) \right] \quad (8)$$

In the standard model with $\sin^2 \theta_W = 0.229$, one expects only a small effect of z_0 in the total cross section, where the interference term vanishes and the pure weak contribution is not large enough at PETRA energies. The ratio, $R_{\mu\mu}$, of the total cross section to the QED expectation is shown in Fig.9¹⁷⁾. Only statistical errors are shown in the figure. Systematic errors of the absolute normalization are between 3 and 5%, depending on the experiment. The ratio is consistent with 1.0.

Clean deviation from QED is observed in the forward backward (F/B) asymmetry of the muon angular distribution:

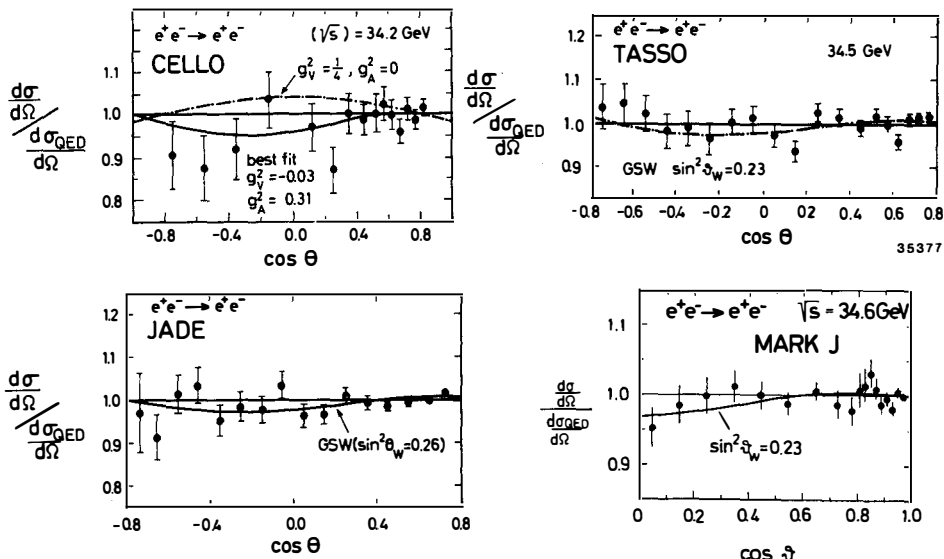


Fig.6: The ratio of the differential cross section to the QED prediction for the reaction $e^+e^- \rightarrow e^+e^-$. The curves are expectations of electro-weak interaction.

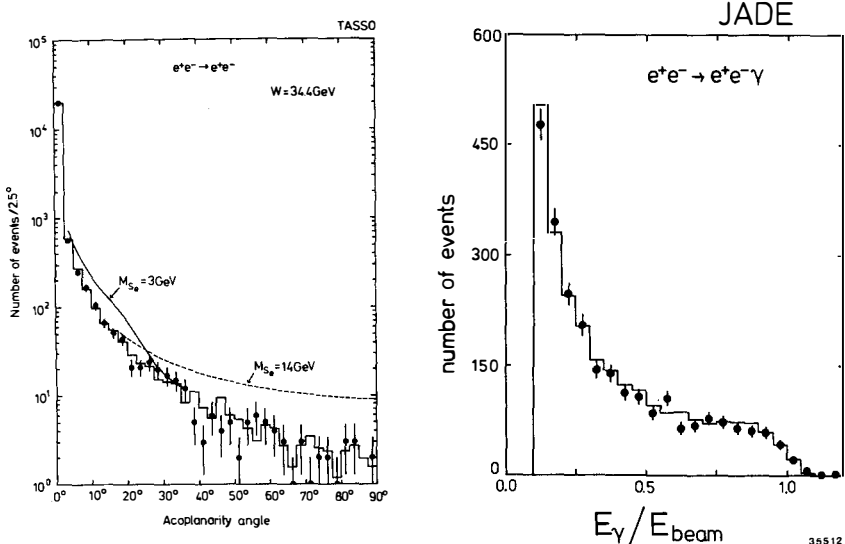


Fig.7: The acoplanarity angle distribution for the reaction $e^+e^- \rightarrow e^+e^-$. The histogram is the α^3 QED prediction. For the curves see the text for the scalar lepton search.

Fig.8: The photon spectrum normalized by the beam energy for the reaction $e^+e^- \rightarrow e^+e^-\gamma$. The histogram is the α^3 QED prediction⁸⁾.

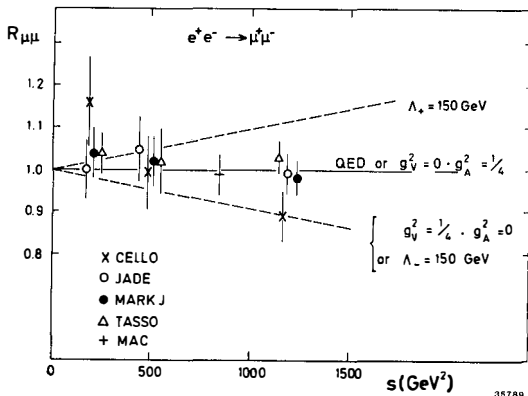


Fig.9: The ratio of the total cross section to the QED prediction for $e^+e^- \rightarrow \mu^+\mu^-$. The line at $R_{\mu\mu} = 1$ is the QED expectation and also the electro-weak interaction with $g_V = 0$, $g_A = 1/2$. The broken lines show the expected deviations for the given cut off parameters, which are defined similarly as (4) for $e^+e^- \rightarrow \nu^+\nu^-$.

$$\begin{aligned}
 A &= (F-B)/(F+B) \\
 &= \frac{3}{2} g_A^e g_A^\mu X
 \end{aligned} \tag{9}$$

For $g_A^e = g_A^\mu = -\frac{1}{2}$ and $M_{Z0} = 90$ GeV, the expected asymmetry is -9.4% at 34.5 GeV.

Recent results of the muon angle distribution are shown in Fig.10^{17,18)}. Nice agreement between the observation and the electro-weak interaction prediction is seen. Each group made a careful study of systematics of the detector and the analysis. Systematic errors on the charge asymmetry are less than 1%. Estimated asymmetry values for the full angle range $|\cos\theta| < 1.0$ are summarized in Table 2. The average of all observation is $(-11.3 \pm 1.3)\%$. The data has been corrected for the asymmetry due to the pure α^3 QED processes, which amounts to a few %. Higher order corrections which involve both QED and weak interaction have not been made.

The energy dependence of the muon asymmetry is shown in Fig.11. The data are compared with the expectations of different Z^0 masses. By fitting all the PETRA data to the formula

$$A_{\mu\mu} = 2.7 \cdot 10^{-4} g_A^e g_A^\mu \frac{s}{s/m_Z^2 - 1}, \quad g_A^e = g_A^\mu = -\frac{1}{2}, \tag{10}$$

TABLE 2

Summary of the muon forward backward asymmetry^{17,18,19,20,21)}

	\sqrt{s} (GeV)	Asymmetry \pm st. err. \pm (sys. err.) (%)
CELLO	34.2	- 6.4 \pm 6.4
JADE	34.5	-11.6 \pm 1.9 \pm (1)
MARK-J	34.6	-11.7 \pm 1.7 \pm (1)
PLUTO	34.7	-12.0 \pm 3.2 \pm (1)
TASSO	34.5	- 9.1 \pm 2.3 \pm (0.5)
average	34.5	-11.3 \pm 1.3

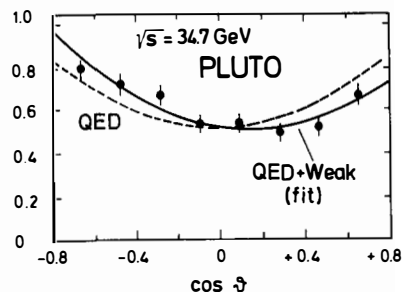
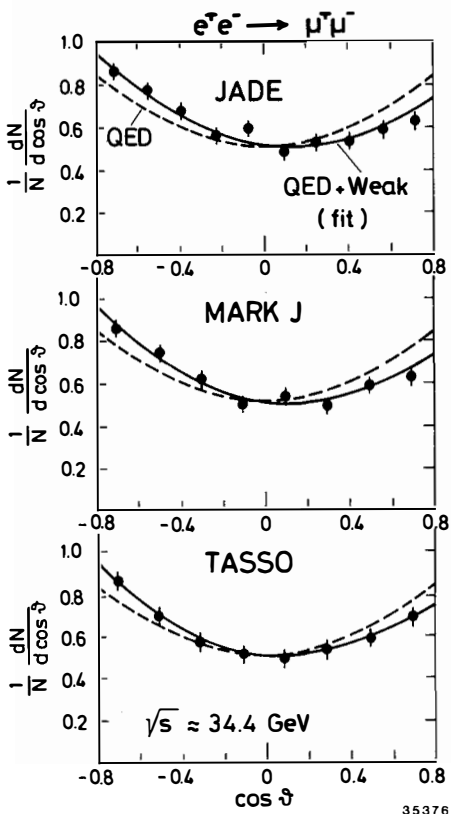


Fig.10: The muon angle distribution for the reaction $e^+e^- \rightarrow \mu^+\mu^-$. The solid lines are fits to $a(1+\cos^2\theta + b\cos\theta)$ and the broken lines to $a'(1+\cos^2\theta)$.

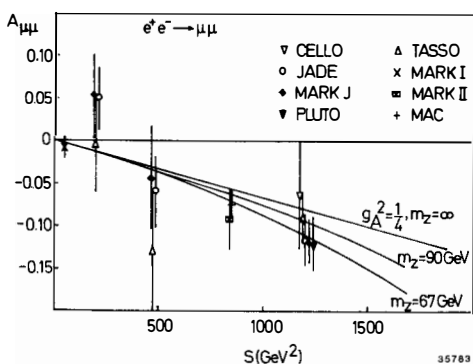


Fig.11: The s dependence of the muon F/B asymmetry. The curves show the expectations by the equation (10) for different Z^0 masses.

corrections to the F/B asymmetry has been tested by these groups. α^3 QED contributes to the F/B asymmetry in two different ways. One is an interference of the lowest order process and the box diagram in $e^+e^- \rightarrow \mu^+\mu^-$, and the other is an interference of the initial state radiation and the final state radiation in $e^+e^- \rightarrow \mu\mu\gamma$. They contribute oppositely to the asymmetry and both effects are mixed in the data with a certain ratio, depending on the selection criteria of the events²²⁾. The MARK-J group studied the F/B asymmetry as a function of the collinearity angle between the muons¹⁹⁾. The expected asymmetry is calculated by the program of Berends, Kleiss and Jadach with and without the weak effect²³⁾. They are

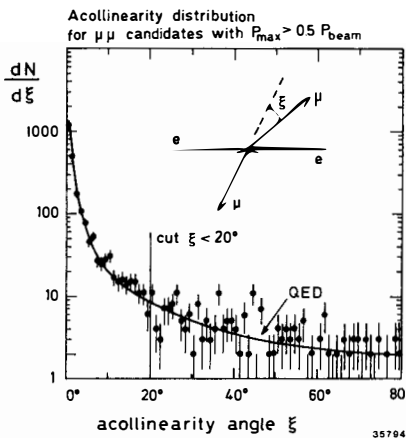


Fig.12: The acollinearity angle distribution of $e^+e^- \rightarrow \mu^+\mu^-$.

95% C.L. limits on the Z^0 mass is obtained as $55 < M_{Z^0} < 110$ GeV.

Detailed investigations are also done for radiative corrections on μ -pair annihilation. The acollinearity distribution and the photon energy distribution for $\mu\mu\gamma$ events are studied by MARK-J and JADE, respectively. They are compared with the QED predictions in Fig.12 and 13. They agree well. Higher order QED

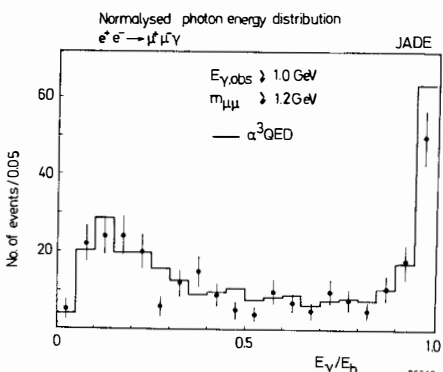


Fig.13: The normalized hard photon energy distribution for the reaction $e^+e^- \rightarrow \mu^+\mu^-\gamma$.

shown in Fig.14. Different contributions from pure QED in two regions ($\xi=0$, $\xi>0$) are clearly seen. When the weak effect is included, the asymmetry value decreases about 10% for the small ξ region, but less for the large ξ region. It is understood if one considers that the effective μ -pair energy is lower for the larger ξ , since initial radiation emits higher energy. Observed data are compared with the prediction including the experimental resolution in Fig.15. The agreement is good within statistics. When this higher order correction is made to the MARK-J data, the asymmetry is enhanced by (0.6~0.7)%¹⁹.

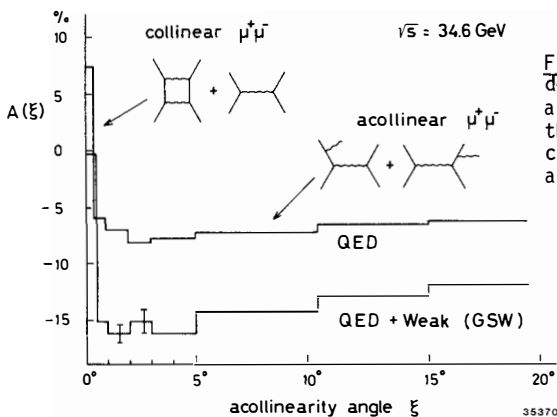


Fig.14: The acollinearity angle dependence of the muon F/B asymmetry which are expected when the higher order effects are included. The two cases are shown: a) pure QED and b) QED + Weak.

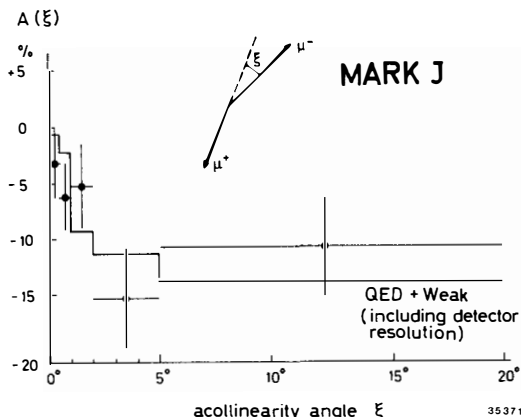


Fig.15: The acollinearity angle dependence of the muon F/B asymmetry. The histogram is the expectation of higher order effects including both α^3 QED and higher order electro-weak processes²³.

Similar examination of the QED asymmetry was done by the JADE group using $\mu\gamma$ events¹⁸. Since large angle photons above 1 GeV are required to be detected, the interference effect is more enhanced than in the case of the MARK-J study, where radiation goes mainly into the beam pipe. The muon angle distribution for these events with $E_\gamma > \frac{1}{2} E_b$ is shown in Fig.16. The F/B asymmetry is plotted as a function of the photon energy in Fig.17 together with

187
the MARK-J data. The agreement is good within statistics. When this higher order correction is made to the MARK-J data, the asymmetry is enhanced by (0.6~0.7)%¹⁹.

the QED and the higher order electroweak expectations²³⁾. The data agrees with the both expectations within statistics.

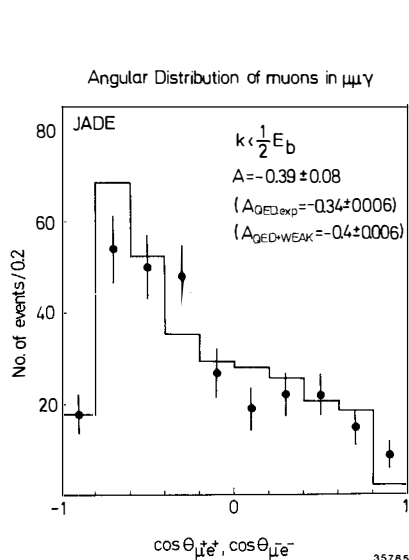


Fig.16: The muon angle distribution for the reaction $e^+e^- \rightarrow \mu\mu\gamma$. The histogram is the expectation of α^3 QED²²⁾.

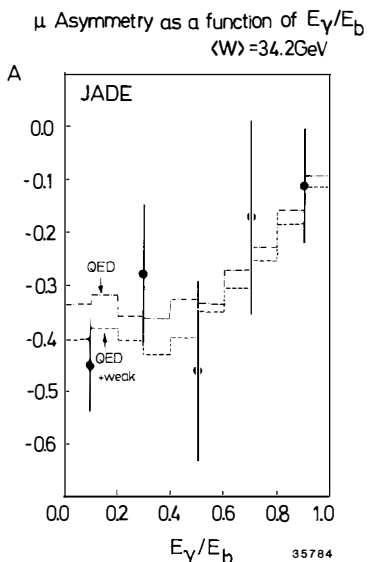
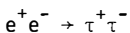


Fig.17: The muon F/B asymmetry plotted as a function of the photon energy normalized by the beam energy for $e^+e^- \rightarrow \mu\mu\gamma$. The histograms are the expectation of QED and higher order electro-weak calculation²³⁾.



Similar electro-weak effects appear in this reaction like the muon production. The results are summarized in Fig.18 and Table 3^{18,19,20,24)}. The averaged asymmetry of all the experiments is

$$\langle A_{\tau\tau} \rangle = (-7.6 \pm 2.3)\%$$

at the mean energy of 34.5 GeV. The data agrees with the standard model predictions.

Table 3

The forward backward asymmetry of $e^+e^- \rightarrow \tau^+\tau^-$
in %; only statistical errors are given.

	CELLO	JADE	MARK-J	TASSO
$A_{\tau\tau}$	-10.3 ± 5.2	-7.9 ± 4.0	-7.8 ± 4.0	-5.6 ± 4.5

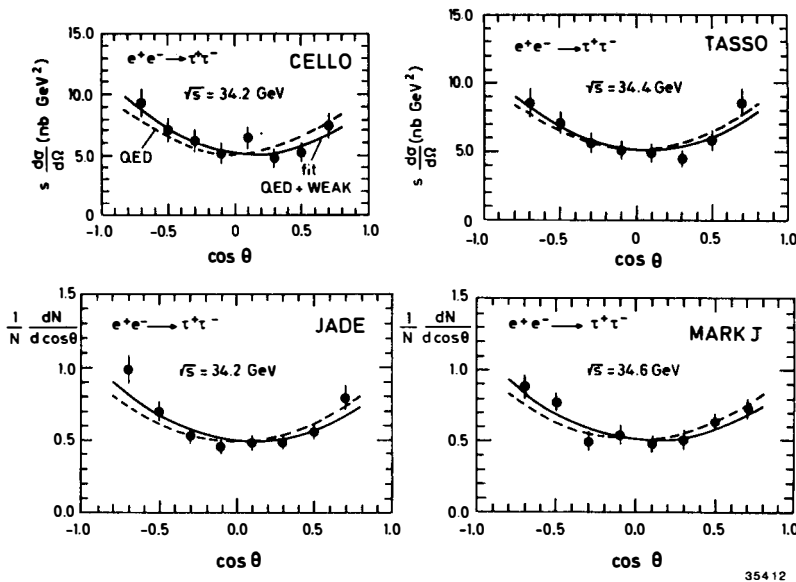


Fig.18: The angle distribution of τ for $e^+e^- \rightarrow \tau^+\tau^-$.

By comparing the muon asymmetry and the tau asymmetry, the universality of g_A can be tested.

$$\frac{g_A^\mu}{g_A^\tau} = \frac{A_{\mu\mu}}{A_{\tau\tau}} = 1.49 \pm 0.32$$

Using the value of g_A^e , which is obtained by the ve scattering data combined with the e^+e^- colliding experiments data²⁵⁾,

$$g_A^e = -0.52 \pm 0.02(\text{stat}) \pm 0.02(\text{syst}),$$

we obtain from (10) for $M_{Z0} = 90$ GeV,

$$g_A^\mu = -0.56 \pm 0.07$$

and $g_A^\tau = -0.38 \pm 0.12$.

These values are consistent with the universality and they are all consistent with -0.5, which is expected in the standard model.

A new feature which can be studied for $e^+e^- \rightarrow \tau^+\tau^-$ is the measurement of the τ polarization. It is possible because the momentum spectrum of the decay product depends on the τ polarization²⁶⁾. At the PETRA energies the τ polarization is approximately expressed as

$$P_\tau(\theta) = 2\chi (g_V^e g_A^\tau + g_V^\tau g_A^e) \frac{2\cos\theta}{1+\cos^2\theta}. \quad (11)$$

The formula contains new combinations of coupling constants. The CELLO group made the first attempt to measure the polarization by analysing the $\tau \rightarrow \rho\nu, \pi\nu, e\nu\nu, \mu\nu\nu$ decays²⁷⁾. Fig.19 shows the momentum distributions of ρ , π , e and μ after the background subtraction. The difference of the polarization in the forward hemisphere and the backward hemisphere gives the contribution from the second term of the equation (11). Their result is

$$\frac{1}{2} (P_f - P_b) = (1 \pm 22)\%.$$

Combined with the value of g_A^e , g_V^τ is -0.05 ± 1.4 . Although the error is still large, the value is consistent with the universality and the standard model.

Combined analysis of $e^+e^- \rightarrow e^+e^-$ and $e^+e^- \rightarrow \mu^+\mu^-$

Assuming the universality, the data of $e^+e^- \rightarrow e^+e^-$ and $e^+e^- \rightarrow \mu^+\mu^-$ are combined to estimate the values of g_A and g_V . The 95% C.L. contour for (g_V, g_A) which is obtained by each experiment, is presented in Fig.20^{2,14,19,20)} together

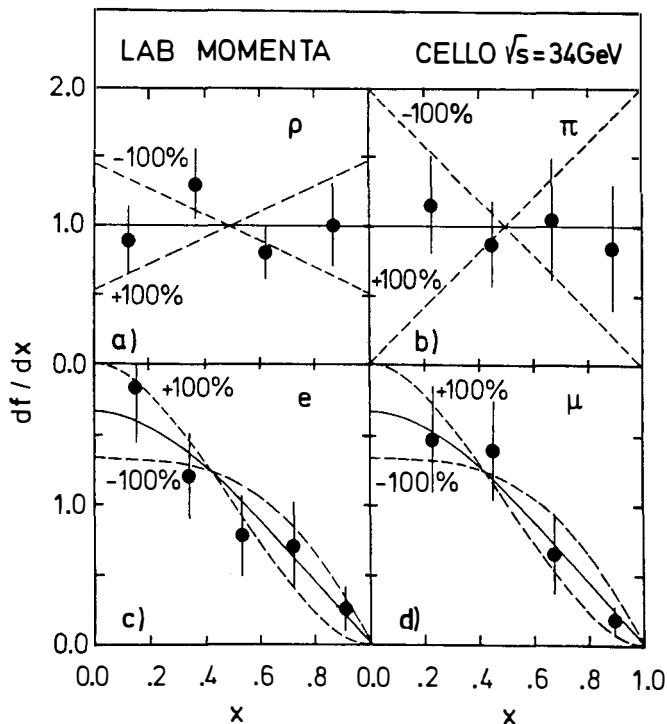


Fig.19: The laboratory momentum spectra of ρ , π , e and μ from τ decay after background subtraction. The solid lines show the expectation for no polarization. The dashed lines are for $\pm 100\%$ polarization.

with the ve scattering result. The simultaneously allowed region of all the experiments is consistent with the standard model prediction with $\sin^2 \theta_W = 0.23$.

Test of larger gauge groups

Since the data is well described by the GSW standard model, one can put a limit on the existence of the extra vector current which appears in the extended gauge group $SU(2)_L \times U(1) \times G^{28}$. For such groups the vector coupling

is modified as

$$g_V^2 = \frac{1}{4} (1 - 4 \sin^2 \theta_W)^2 + 4C \quad (12)$$

by assuming the universality. The effect of the additional term can be tested only in the e^+e^- interactions. Limits on the value of C (95% C.L.) are listed in Table 4^{2,14,19,20}.

Table 4

95% C.L. limits on the existence of an extra vector coupling, c .

CELLO	0.031
JADE	0.031
MARK-J	0.025
TASSO	0.012

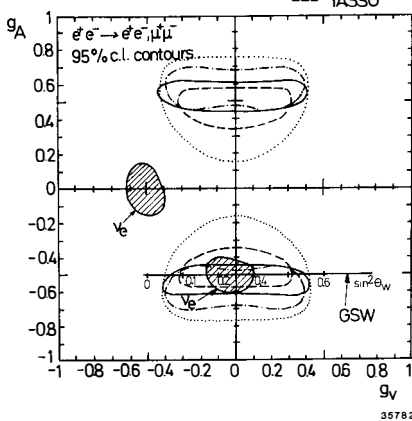


Fig.20: The contours of the 95% C.L. limit for (g_V, g_A) obtained by the combined fits to $e^+e^- \rightarrow e^+e^-$ and $e^+e^- \rightarrow \mu^+\mu^-$.

Electro-weak Effects in the Hadron Production

In the quark parton picture, the multihadron production is an analogue of the muon pair annihilation. When the differences of the electric charge, the weak charge, the colour factor and the QCD correction are taken into account, the total cross section can be written similar to the muon production²⁹. The expected weak effect in the standard model is shown in Fig.21 as a function of $\sin^2 \theta_W$. The deviation is minute at the PETRA energies. Precise measurements of the hadronic cross section were performed by JADE³⁰, MARK-J³¹ and TASSO³². Since dominant errors are systematic errors, they were extensively studied and reduced to the level of 3~6%. The results are shown in Fig.22. Fits are made

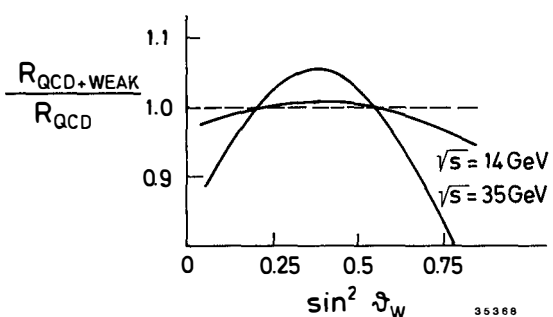


Fig.21: Expected deviation of the hadron total cross section from the one photon process cross section due to the electro-weak effect as a function of $\sin^2 \theta_W$.

Table 5

Quark and lepton weak coupling constants in the standard model

q, l	g_A	g_V
u, c	$\frac{1}{2}$	$\frac{1}{2} \left(1 - \frac{8}{3} \sin^2 \theta_W \right)$
d, s, b	$-\frac{1}{2}$	$\frac{1}{2} \left(-1 + \frac{4}{3} \sin^2 \theta_W \right)$
e, μ, τ	$-\frac{1}{2}$	$\frac{1}{2} \left(-1 + 4 \sin^2 \theta_W \right)$

asymmetry for $|\cos \theta| < 1.0$,

$$A_{D^*} = -0.28 \pm 0.13.$$

The equation (10) is modified for fractionally charged quarks in such a way that the r.h.s. is divided by the quark electric charge. The TASSO group performed the first measurement of g_A^C by combining the D^* asymmetry with the value of g_A^e , which is estimated from all the muon asymmetry data of the PETRA experiments assuming the universality, thus

to the data in the context of the standard model. The values of $\sin^2 \theta_W$, which give the best fit, are listed in Table 6. They are consistent with the values obtained by the measurements of the pure lepton interactions.

It is interesting to study the weak coupling constant of each quark flavour. Charm quark tagging was tried by TASSO by detecting the D^* mesons in the hadron final states³³⁾. The D^* identification was done by observing the small mass difference of the $K\pi\pi$ and $K\pi$ system³⁴⁾. The observed D^* angular distribution shows a forward backward asymmetry as shown in Fig.23. Since the D^* has a hard fragmentation function, it may well reflect the original C quark direction. A fit to the data is made with the formula $N(1 + \cos \theta + \cos^2 \theta)$. It gives the extrapolated

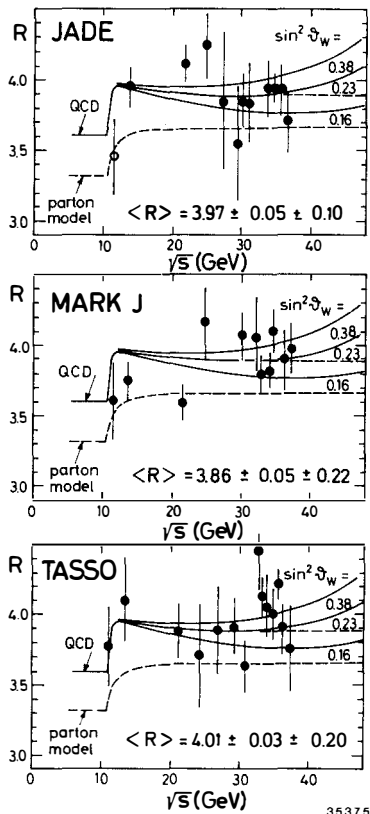


Fig.22: The ratio, R , of the hadron total cross section to the pointlike muon pair cross section is shown as a function of the total energy. The second error is the systematic normalization error. The solid curves present the expectations by the standard model for the indicated values of $\sin^2 \theta_W$ with the QCD correction. The broken line is the prediction of the simple quark parton model without the QCD correction and the weak contribution.

$$g_A^e \cdot g_A^C = -0.49 \pm 0.23,$$

$$g_A^{e2} \equiv g_A^{\mu 2} = 0.30 \pm 0.04,$$

$$g_A^C = 0.89 \pm 0.44.$$

The result agrees with the standard model prediction,

$$g_A^C = \frac{1}{2}.$$

Table 6

$\sin^2 \theta_W$ values obtained by fitting R

JADE:	0.23 ± 0.05	$\alpha_s = 0.20 \pm 0.08$ at $\sqrt{s} = 30$ GeV
MARK-J:	0.41 ± 0.12 0.15	$\alpha_s = 0.17$ fixed
TASSO:	$= 0.40 \pm 0.15 \pm 0.02$	$\alpha_s = 0.18$ fixed

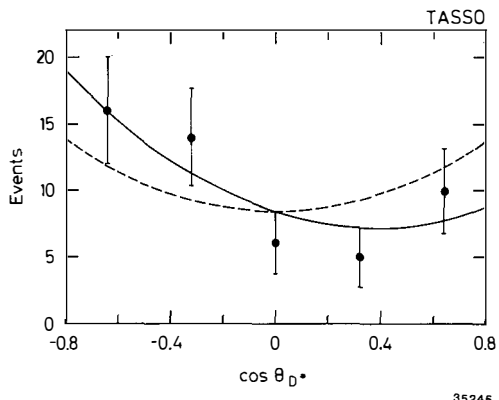


Fig. 23: The angular distribution of D^* in the reaction $e^+e^- \rightarrow D^{\star\pm} + X$.

The solid line shows the best fit, from which the extrapolated asymmetry of -0.28 ± 0.13 is obtained for $|\cos\theta| < 1.0$.

Search for New Particles

Topponium

Much effort has been made at PETRA to search for the top quark, which makes the third generation doublet with the b-quark³⁵⁾. Both the open top production and the topponium formation were searched for up to 36.72 GeV by 1981³⁶⁾. After the energy increase of PETRA in Summer 1982, energy scanning for the ground state topponium was performed between 37.94 and 38.63 GeV. The results from JADE, MARK-J and TASSO are shown in Fig. 24³⁷⁾. There is no evidence for a narrow resonance observed. The combined data gives the upper limit (90% C.L.) on the $\Gamma_{ee} B_{\text{had}}$ to be 0.8 keV, which is significantly smaller than ~ 4 keV which is expected for the $Q = 2/3$ topponium ground state.

There is no evidence for broad or spherical events, which are expected from the open top, up to the highest scanned energy.

The search will be continued by further increasing the PETRA energy in Spring 1983. There is a good reason to believe that the top quark exists. Some models assume that the bottom quark is a left- and right-handed singlet and the top quark does not exist. In such models the bottom quark may decay by the flavour changing neutral current. The branching ratio of the $b \rightarrow \mu^+\mu^-X$ decay is predicted to be larger than 1%. Dimuon inclusive events were searched for by the MARK-J group and no evidence was found. They got the 95% C.L. limit

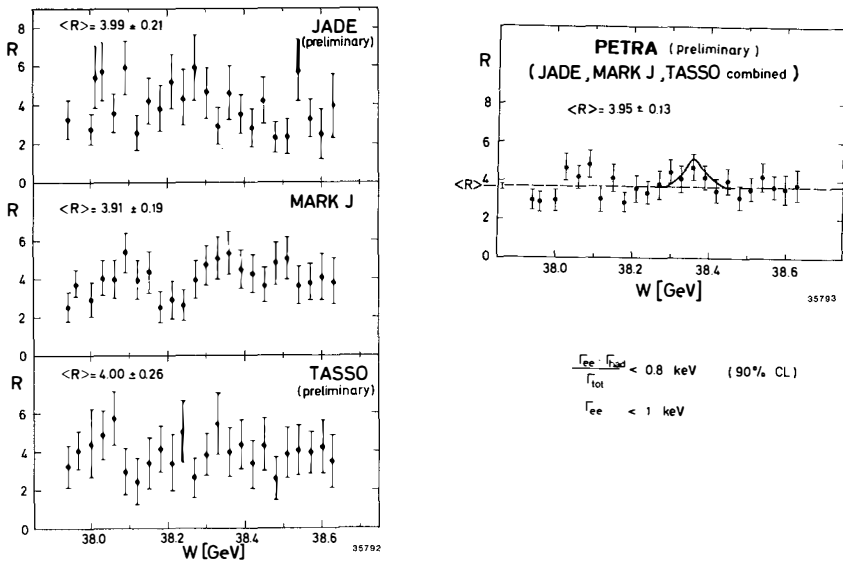


Fig.24: The results of the narrow resonance search by the energy scanning between 37.94 and 38.63 GeV. The combined data of the three experiments sets 90% C.L. upper limit on the $\Gamma_{ee} \cdot \Gamma_{had}$ to be 0.8 keV.

of 0.7% on the branching ratio, which excludes the five quark models with the weak singlet bottom quark.

Supersymmetric Particles

Supersymmetric models³⁹⁾ anticipate scalar partners to all the fermions and fermion partners to all the bosons. There are models which give different mass scales but there are not any definite predictions. Much work is left to experimental investigations. Scalar leptons and heavy photinos (spin 1/2 partner of the photon) were searched at PETRA.

The scalar lepton search was done under the assumptions that the two types of scalar lepton, s_e and t_e , which correspond to the left handed and the right handed lepton, have the same mass and that they are pair produced and decay into leptons of the same lepton number and unobservable massless photinos. The cross section is given for $(s_e + t_e)$ by

$$\frac{d\sigma}{d\Omega} = \frac{\alpha^2 \beta^3}{8S} \left[1 + \left\{ 1 - \frac{4K}{1-2\beta\cos\theta + \beta^2} \right\}^2 \right] \quad (13)$$

where $K = 1$ is assumed. The formula gives the cross section for $(S_\mu + t_\mu)$ and $(S_\tau + t_\tau)$, if $K = 0$ ⁴⁰.

The way the scalar leptons show up depends on their masses. When they are light and their decay products satisfy the lepton pair selection conditions, e.g. on the momenta and the acoplanarity angle, they increase the cross sections of the corresponding lepton reactions such as $e^+e^- \rightarrow e^+e^-$ and $e^+e^- \rightarrow \mu^+\mu^-$. If their masses are heavy, the decay products do not satisfy the cuts for the two body reactions because of the large missing momentum and energy. However, they can be detected by examining the acoplanarity angle or the acoplanarity angle of the final state leptons. As we have seen in the beginning of this report, the observed distribution of these angles are well explained by α^3 QED. Furthermore, the QED background with hard photons can be removed by requiring that there is nothing detected in the recoil direction of the acoplanar lepton pair. This last method should provide a clean signal for the scalar leptons if one is sure about the missing energy. Each group used its own method among these techniques. In some cases two methods are combined to cover a wide mass range.

In Fig.7 the acoplanarity distribution of Bhabha scattering measured by TASSO is shown together with the expected deviations from QED if scalar electrons of mass 3 GeV or 14 GeV are mixed¹⁰. They obtained the upper limits on the scalar e and/or μ production cross sections as shown in Fig.25. For the pointlike scalar $e(\mu)$, the mass limit is 16.6 GeV (16.4 GeV) (95% C.L.).

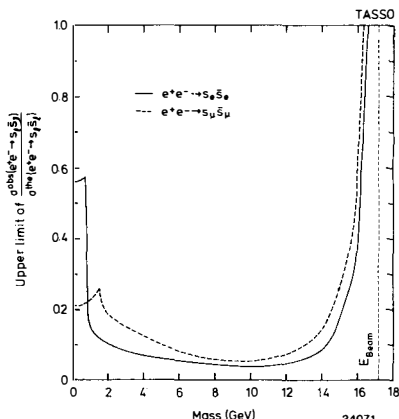


Fig.25: The upper limit on the ratio of the observed to the theoretical scalar lepton production cross sections. The low mass part is estimated from the absolute cross section of the QED reactions, $e^+e^- \rightarrow e^+e^-$, and $e^+e^- \rightarrow \mu^+\mu^-$ at $\cos\theta \sim 0$. The high mass part is obtained from the allowed deviation of the acoplanarity distribution of the QED predictions.

CELLO, JADE and MARK-J used the last method. They looked for acoplanar lepton pair events with missing transverse momenta. They found no events. The upper limit on the mass of each scalar lepton is summarized in Table 7^{10,41,42,43)}.

Table 7

The upper limits (95% C.L.) on the mass of scalar leptons in GeV

	s_e, t_e	s_μ, t_μ	s_τ, t_τ
CELLO	16.8	16	15.3
JADE	16	17	14
MARK-J		15	14
TASSO	16.6	16.4	

The CELLO group searched for the massive photino which may be produced in pair by scalar electron exchange and decay into a photon and a massless gravitino³⁾. The similar method as above was applied to the $\gamma\gamma$ final state. They required that both photons have low energies, which satisfy the relation

$(\frac{E_{\gamma 1}}{E_b}) \cdot (\frac{E_{\gamma 2}}{E_b}) < 0.5$, where E_b is the beam energy. The acoplanarity angle could be small for the light mass photinos. There was no event found, which satisfy the selection conditions. Since both photinos must decay in the detector to be detected, the limit on the photino mass is given as a function of a parameter, d , which determines the photino lifetime as⁴⁴⁾

$$\tau_{\tilde{\gamma}} = \frac{8\pi d^2}{\frac{5}{m_\lambda}}. \quad (14)$$

The result is shown in Fig.26 for $m_{s_e} = 40$ GeV.

Excited Leptons

If leptons are composite particles⁴⁵⁾, there may be an excited lepton, l^* , which couples to the ground state lepton by the following interaction¹⁾⁴⁶⁾:

CELLO

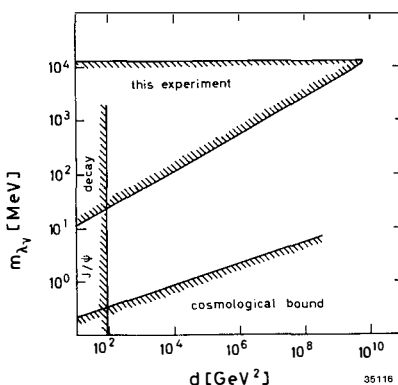


Fig.26: 95 C.L. limits on the mass of massive photino versus the scale parameter d . For details see ref. 3).

limits on M_{e^*} for $\lambda = 1$, i.e. $M_{e^*} > 61$ GeV.

A direct search of e^* was done by JADE by studying the $e\gamma$ mass combinations in the reaction $e^+e^- \rightarrow e^+e^-\gamma$ ²⁾. The result is shown in Fig.27, which is in good agreement with the α^3 QED expectation⁸⁾. Upper limits on the coupling constant, λ , are obtained using the cross section^{1,46)}

$$\frac{d\sigma}{dt} = - \frac{2\pi\alpha^2 \lambda^2}{M_{e^*}^2 s^2} \left[\frac{t^2 + (t - M_{e^*}^2)^2}{s} + \frac{s^2 + (s - M_{e^*}^2)^2}{t} \right]. \quad (17)$$

The limit is compared with what is obtained from the equation (16) in Fig.28. It is reduced substantially for $M_{e^*} < 34$ GeV.

Similar studies were done for the excited muons and no evidence was found⁴⁷⁾. Recent results from JADE¹⁸⁾ are shown for the reaction $e^+e^- \rightarrow \mu^+\mu^-\gamma$ in Fig.29 and 30. The invariant mass distribution of the $\mu\gamma$ system agrees well with the α^3 QED prediction. The 95% C.L. upper limit on the coupling constant is obtained from the cross section for the reaction $e^+e^- \rightarrow \mu^+\mu^- + \mu^*\mu^+$ ^{1,46)}

$$\frac{d\sigma}{d\Omega} = \frac{\alpha^2 \lambda^2}{2M} (1 - \frac{M^2}{s})^2 \left[\frac{2M^2}{s} + (1 - \frac{M^2}{s}) \sin^2 \theta \right], \quad (18)$$

where M is the mass of μ^* .

$$L_{int} = \frac{\lambda e}{2M_{1*}} \bar{\psi}_1 \sigma_{\mu\nu} \psi_1 F^{\mu\nu} + h.c., \quad (15)$$

where λ is the coupling constant of $11*\gamma$ relative to the electric charge and M_{1*} is the mass of the excited lepton. The interaction (15) modifies the cross section for the reaction $e^+e^- \rightarrow \gamma\gamma$ due to e^* exchanges. The reaction can be well described by QED as we have seen. The cut off parameter Λ_+ for the reaction is related to M_{e^*} and λ as follows¹⁾:

$$\Lambda_+^2 (e^+e^- \rightarrow \gamma\gamma) = \frac{M_{e^*}^2}{\lambda} \quad (16)$$

Hence, Table 1 gives the 95% C.L. lower

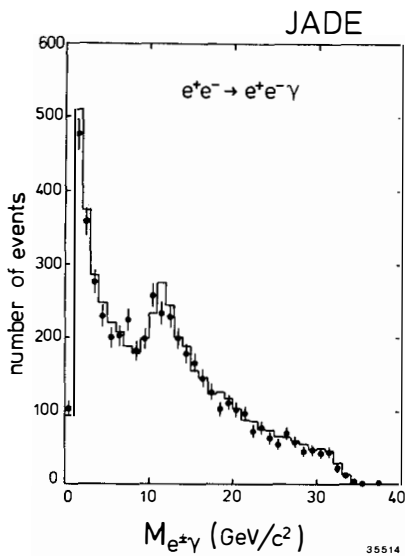


Fig.27: The mass distribution of $e^\pm\gamma$ for the reaction $e^+e^- \rightarrow e^+e^-\gamma$. The histogram shows the expectation of α^3 QED.

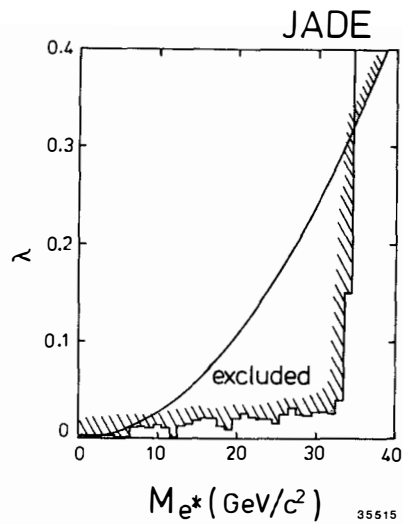


Fig.28: The upper limits on the ee^* coupling constant λ . The histogram is the result of the e^* search in the $e\gamma$ mass distribution. The curve shows the limit obtained from the cut off parameter Λ_+ for the reaction $e^+e^- \rightarrow \gamma\gamma$.

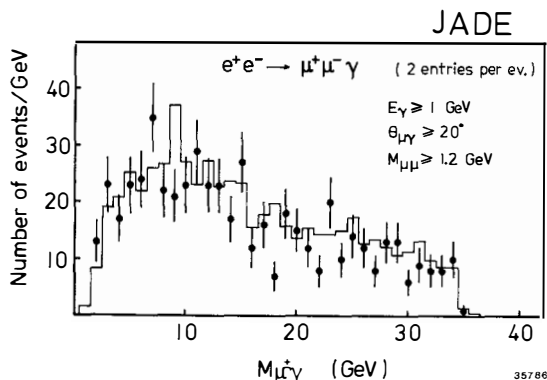


Fig.29: The mass distribution of the $\mu\gamma$ system for the reaction $e^+e^- \rightarrow \mu^+\mu^-\gamma$. The histogram is the prediction of α^3 QED.

Electron Type Neutral Heavy Lepton

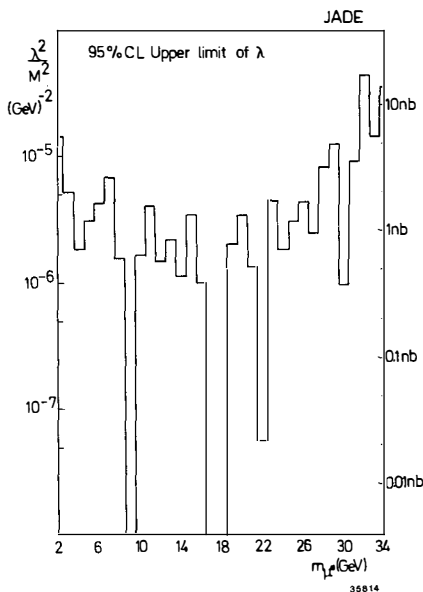


Fig.30: 95% C.L. upper limit of the coupling constant, λ^2/M^2 , for the reaction $e^+e^- \rightarrow \mu^*\mu$.

E^0 49). It is produced in the reaction $e^+e^- \rightarrow E^0 + \bar{\nu}_e$ or $E^0 + \nu_e$ by W^\pm exchange with V-A or V+A coupling. E^0 decays weakly via virtual W^\pm into $e^- + ((ud), (cs), ev, \mu\nu$ or $\tau\nu$). In their analysis the decay is treated like a decay of the heavy sequential lepton⁵⁰⁾. When the neutrino carries a high momentum, the total transverse momentum of the observed particles may be largely unbalanced. The acoplanarity angle of the two jet axes with respect to the beam is calculated and events with large acoplanarity were searched. The observed acoplanarity is shown in Fig.31. The data is consistent with the expectation from the normal multihadron events and there are two events left above the indicated cut. The 95% C.L. limits on the E^0 mass are obtained based on the left events, although they are consistent with the background from the reaction $e^+e^- \rightarrow \gamma + \text{hadrons}$, where the photon escapes through the small detector gap. The limits are

$$M_{E^0} \geq 24.5 \text{ GeV} \quad (\text{for V+A coupling})$$

$$M_{E^0} \geq 22.5 \text{ GeV} \quad (\text{for V-A coupling})$$

Acoplanar events with clear missing energy are a good signal for new particles as we have discussed in the scalar lepton search. The same recipe can be applied to hadronic events. Such analyses require more careful and elaborated event simulations because of the quark fragmentation. On the other hand, one gains in the number of expected events for certain new particles for which hadronic decay dominates. For instance, heavy leptons which decay weakly via virtual weak bosons are expected to have larger hadronic branching ratios than pure leptonic ones, when they are heavy.

A systematic search for new heavy leptons was done by JADE by such a method⁴⁸⁾, which included a search for the electron type neutral heavy lepton

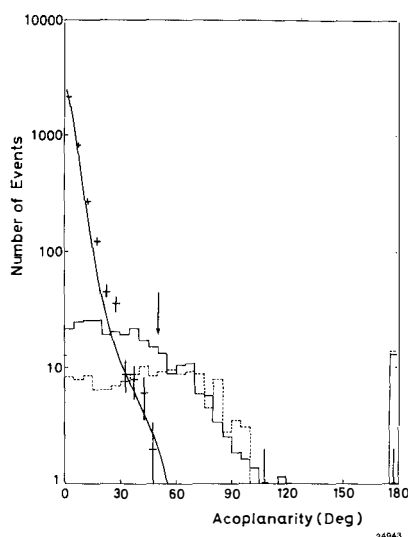


Fig.31: The acoplanarity angle distribution of the two jet axes. The data agrees with the Monte Carlo simulation of the normal multihadron events, which is shown by the curve. The dashed histogram is the expectation for E^0 . The solid histogram is the expectation for the sequential heavy leptons. See ref. 48.

A similar analysis was done to look for heavy sequential leptons, L^\pm , of which mass limit (95% C.L.) was obtained to be $M_L > 18$ GeV.

Charged Higg's or Techipions

Extensive searches for pointlike charged scalars, charged Higg's⁵¹⁾ or technipions⁵²⁾, were performed^{41,43,53)}. In the standard model only the neutral Higg's particle is expected as the fundamental scalar. Although it is an essential test of the standard model to look for it, there are not any adequate reactions at present energies without the toponium. On the other hand, one can do a reverse test by looking for what is not needed in the standard model. The charged Higg's appears if more than one Higg's multiplet is used for the purpose of the spontaneous symmetry breaking. The technipion appears if the symmetry is dynamically broken.

These particles are pair produced as $e^+e^- \rightarrow H^+H^-$ and decay preferably into heavy particles. The leptonic decay is expected to be dominated by the $\tau\nu$ mode and the hadronic decay is expected to go mainly into cb pairs. The CELLO, JADE and MARK-J group studied the case where one or both of H^\pm decay into $\tau\nu$. For such decays the missing energy is large, and the same methods, which are described in the scalar lepton search or heavy lepton search are used. The detection efficiency for the events changes as a function of the branching ratio into $\tau\nu$. Since no evidence for such particles is found, the mass limits are given as the contours in the $(B_{\tau\nu}, M_{H^\pm})$ plane as shown in Fig.32. The TASSO group investigated four jet events which are consistent with the pure hadronic decays of H^+H^- pairs. They studied the two cases: $H^+ \rightarrow cs$ (100%) and $(H \rightarrow cs):(H \rightarrow cb) = 1:1$. They excluded the area of the small $H \rightarrow \tau\nu$ branching ratio as shown in Fig.32.

Limits on mass and branching ratio into $\tau\nu_\tau$ for technipion or H^\pm from PETRA experiments

CELLO ..., JADE —, MARK J - - , TASSO --

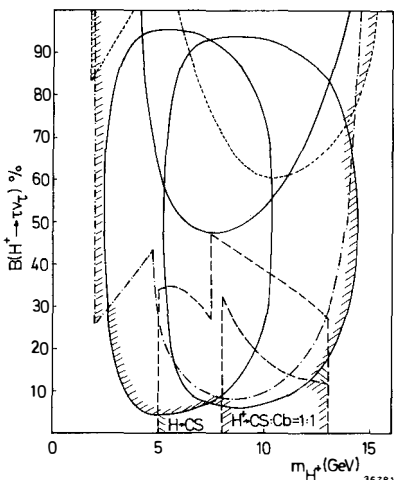


Fig.32: The combined limits from PETRA experiments on the mass and the branching ratio into $\tau\nu$ for the technipion or H^\pm .

From the combined data of all the experiments, one can conclude that the existence of the charged Higg's particles or the techninipions is excluded between 5 GeV and 13 GeV.

In conclusion, the validity of QED is tested at $s \sim 1200$ GeV. Clear electro-weak effects are observed in the asymmetry of μ , τ and possibly c quarks. The standard model predictions agree with the data. The top or toponium has not been seen yet. There are no evidences found for new particles such as super symmetric particles, excited leptons, heavy leptons or fundamental charged scalars.

The maximum energy of PETRA will be increased to 43 GeV in Spring and the investigations will be continued.

Acknowledgements

We acknowledge many people of the PETRA experiments for discussions and for providing unpublished new data, especially Drs. C. Kiesling, P. Grosse-Wiesmann, W. Bartel, R. Felst, B. Naroska, A. Sato, H. Takeda, A. Böhm, J. Salicio, U. Timm, H. Burkhardt, H.-U. Martyn, G. Mikenberg and G. Wolf. We wish to thank the DESY directorate for the kind hospitality while this report was prepared. We acknowledge Mrs. Platz for typing the manuscript. Finally, but not the least, we should be grateful to the organizers of the conference, especially to J. Tran Thanh Van for the splendid meeting and warm hospitality.

References

- 1) A.M. Litke, Ph.D. thesis, Harvard University, 1970
- 2) JADE-Collaboration, W. Bartel et al., DESY 83-35, to be published in Z. Physik
- 3) CELLO-Collaboration, H.-J. Behrend et al., Phys. Lett. 123B (1983) 127
- 4) MARK-J-Collaboration, B. Adeva et al., Phys. Rev. Lett. 48 (1982) 967
- 5) TASSO-Collaboration, R. Brandelik et al., Phys. Lett. 94B (1980) 259
- 6) PLUTO-Collaboration, Ch. Berger et al., Phys. Lett. 94B (1980) 87
- 7) F.A. Berends et R. Gastmans, Nucl. Phys. B61 (1973) 414
F.A. Berends and R. Kleiss, Nucl. Phys. B186 (1981) 22
- 8) F.A. Berends, K.J.F. Gaemers and R. Gastmans, Nucl. Phys. 68B (1974) 541
- 9) F.A. Berends and G.J. Komen, Phys. Lett. 63B (1976) 432
- 10) TASSO Collaboration, R. Brandelik et al., Phys. Lett. 117B (1982) 365
- 11) R. Budny, Phys. Lett. 55B (1975) 227
- 12) S.L. Glashow, Nucl. Phys. 22 (1961) 579, Rev. Mod. Phys. 52 (1980) 539
A. Salam, Phys. Rev. 127 (1962) 331, Rev. Mod. Phys. 52 (1980) 525
S. Weinberg, Phys. Rev. Lett. 19 (1967) 1264, Rev. Mod. Phys. 52 (1980) 514
For recent experimental tests see a review by M. Davier, Proceedings of the 21st Int. Conf. on High Energy Physics, Paris 1982, p. C3-471
- 13) Review of Particle Properties: Phys. Lett. 111B April (1982)
- 14) CELLO-Collaboration, H.-J. Behrend et al., Z. Phys. C16 (1983) 301
- 15) MARK-J-Collaboration, D.P. Barber et al., Phys. Rev. Lett. 46 (1981) 1663
private communication for recent data
- 16) R. Budny, Phys. Lett. B45 (1973) 340
G. Pöcsik, Ann. of Phys. 105 (1977) 259
- 17) CELLO-Collaboration, H.-J. Behrend et al., Z. Phys. C14 (1982) 283
JADE-Collaboration, W. Bartel et al., Phys. Lett. 108B (1982) 140
MARK-J-Collaboration, B. Adeva et al., Phys. Rev. Lett. 48 (1982) 1701
TASSO-Collaboration, R. Brandelik et al., Phys. Lett. 110B (1982) 173
- 18) JADE-Collaboration, B. Naroska, Invited talk at the Europhysics Conference
on Electroweak Effects at High Energies, Erice, 1983
- 19) MARK-J-Collaboration, J. Salicio, A. Böhm, " "
- 20) TASSO-Collaboration, G. Mikenberg, " "
- 21) PLUTO-Collaboration, private communication
- 22) F.A. Berends, K.J.F. Gaemers and R. Gastmans, Nucl. Phys. 63B (1973) 381

23) F.A. Berends, R. Kleiss and S. Jadach, Nucl. Phys. B202 (1982) 63

24) CELLO-Collaboration, H.-J. Behrend et al., Phys. Lett. 114B (1982) 282

25) G. Barbiellini, Proceedings of the Int. Symp. on Lepton and Photon Interactions, Bonn (1981) p.623

26) J.E. Augustin, Proceedings of the LEP Summer Study, CERN 79-01, p.499
 G. Goggi, ibid. p.483
 H.D. Dahmen, L. Schülke and G. Zech, Phys. Lett. 81B (1979) 361

27) CELLO-Collaboration, H.-J. Behrend et al., DESY 83-019

28) H. Georgi, S. Weinberg, Phys. Rev. D17 (1978) 275
 V. Barger, W.Y. Keung and E. Ma, Phys. Rev. Lett. 44 (1980) 1169
 E.H. Groot, D. Schildknecht and G.J. Gounaris, Phys. Lett. 90B (1980) 427
 Phys. Lett. 95B (1980) 149

29) C. Jarlskog and F.J. Yndráin, Phys. Lett. 63B (1976) 215
 J. Jersak, E. Laermann and P.M. Zerwas, Phys. Lett. 98B (1981) 363

30) JADE-Collaboration, W. Bartel et al., DESY 83-50

31) MARK-J-Collaboration, quoted by G. Heinzelmann, Proceedings of the 21st International Conference on High Energy Physics, Paris 1982, p. C3-59

32) TASSO-Collaboration, R. Brandelik et al., Phys. Lett. 113B (1982) 499

33) TASSO-Collaboration, M. Althoff et al., DESY 83-10

34) S. Nussinov, Phys. Rev. Lett. 35 (1976) 1672
 J.M. Yelton et al., Phys. Rev. Lett. 49 (1982) 430
 C. Bebek et al., Phys. Rev. Lett. 49 (1982) 610
 G. Goldhaber, Proceeding at this Conference

35) M. Kobayashi and T. Maskawa, Prog. Theor. Phys. 49 (1973) 652

36) Summary is found in the review
 J. Bürger, Proceedings of the Int. Symp. on Lepton and Photon Interactions, Bonn 1981, p. 115

37) JADE-Collaboration, private communication
 MARK-J-Collaboration, B. Adeva et al., Phys. Rev. Lett. 50 (1983) 799
 TASSO-Collaboration, private communication

38) H. Georgi and S. Glashow, Nucl. Phys. B167 (1980) 173
 V. Barger, W.Y. Keung and R.J.N. Phillips, Phys. Rev. D24 (1981) 1328
 G.L. Kane and M.E. Peskin, Nucl. Phys. B195 (1982) 29

39) For recent works see a review by
 P. Fayet, talk at the XVI-th Rencontre de Moriond (1981)
 also see: Quick Reports of the CERN Supersymmetry vs Experiment Workshop, TH. 3311/Ep. 82/63-CERN

40) G.R. Farrar and P. Fayet, Phys. Lett. 89B (1980) 191

41) CELLO-Collaboration, H.-J. Behrend et al., Phys. Lett. 114B (1982) 287

42) JADE-Collaboration, D. Cords, Proceedings of the 20th Int. Conf. on High Energy Physics, Wisconsin 1980, p. 590
 For s_μ , t_μ private communication and for s_τ , t_τ ref. 53)

- 43) MARK-J-Collaboration, B. Adeva et al., Phys. Lett. 115B (1982) 345
- 44) N. Cabibbo, G.F. Farrar and L. Maiani, Phys. Lett. 105B (1981) 155
- 45) For a review see
M.E. Peskin, Proceedings of the Int. Symp. on Lepton and Photon Interactions, Bonn 1981, p. 880
- 46) H. Terazawa, M. Yasue, K. Akama and M. Hayashi, Phys. Lett. 112B (1982) 387
A factor 1/2 is missing in the definition of λ in this paper.
- 47) MARK-J-Collaboration, B. Adeva et al., Phys. Rev. Lett. 48 (1982) 967
- 48) JADE-Collaboration, W. Bartel et al., Phys. Lett. 123B (1983) 353
- 49) J.D. Bjorken and C.H. Llewellyn Smith, Phys. Rev. D7 (1973) 887
F. Bletzacker and H.T. Nieh, Phys. Rev. D16 (1977) 2115
- 50) Y.S. Tsai, Phys. Rev. D4 (1971) 2821
- 51) E. Golowich and T.C. Yang, Phys. Lett. 80B (1979) 245
L.N. Chang and J.E. Kim, Phys. Lett. 81B (1979) 233
H.E. Haber, G.L. Kane and T. Sterling, Nucl. Phys. B161 (1979) 493
- 52) S. Weinberg, Phys. Rev. D13 (1976) 974, D19 (1979) 1277
L. Susskind, Phys. Rev. D20 (1979) 2619
K.D. Lane and M.E. Peskin, Proceedings of the 15th Rencontre de Moriond 1980, p. 469
for further ref. see references in the exp. papers 53)
- 53) JADE-Collaboration, W. Bartel et al., Phys. Lett. 114B (1982) 211
TASSO-Collaboration, M. Althoff et al., Phys. Lett. 122B (1983) 95

WHAT CAN THE EMC-EFFECT TELL US ABOUT
QUARKS AND GLUONS IN NUCLEI?

K. RITH
Fakultät für Physik
Freiburg University
Hermann-Herder-Strasse 3
D-7830 Freiburg i. Br.



Abstract: Results of the nucleon structure functions F_2^N for iron and deuterium, measured by the EMC, are presented. Their ratio differs significantly from unity. Consequences for quark- and gluon-distributions inside nuclei are discussed as well as several phenomenological models which could be used to describe the observed effect.

1. Introduction

The European Muon Collaboration (EMC) has performed extensive measurements of the nucleon structure function F_2 in high energy muon nucleon interactions¹⁾ using targets of liquid hydrogen²⁾, deuterium³⁾ and of iron⁴⁾. In this contribution results on the nucleon structure function F_2^N for iron and deuterium are compared. Their ratio shows a significant deviation from unity (EMC-effect). This leads to the conclusion that quark and gluon momentum distributions for nucleons embedded in nuclei are different from those in free nucleons. The results, possible implications and several phenomenological models which could be used to understand the observed effect will be discussed in detail.

2. The nucleon structure function F_2^N , quark and gluon distributions

In the quark parton model the nucleon structure function $F_2(x)$ represents the momentum distribution of the charged quarks inside the nucleon. For the deuteron it is given by

$$\begin{aligned} F_2^N(D) &= \frac{1}{2} (F_2^p + F_2^n) \\ &= \frac{5}{18} x (u + \bar{u} + d + \bar{d} + c + \bar{c} + s + \bar{s}) - \frac{1}{3} x (c-s) \\ &\approx \bar{Z}_q^2 x \sum_f (q_f(x) + \bar{q}_f(x)). \end{aligned} \quad (1)$$

F_2^p and F_2^n are the structure functions for a free proton and a free neutron. x is defined as $Q^2/2M_p v$, where Q^2 is the square of the four momentum transfer from the lepton to the nucleon, M_p is the proton mass and v is the energy transferred from the lepton to the nucleon. In an infinite momentum frame $q_f(x)$ is the probability that a quark of flavour f carries the fraction x of the nucleon momentum. $\bar{Z}_q^2 = \frac{5}{18}$ is the mean square of the quark charge numbers.

If nuclear effects are neglected the nucleon structure function F_2^N for iron is given by

$$F_2^N(Fe) = \frac{1}{56} (30 F_2^n + 26 F_2^p) = F_2^N(D) (1-k(x)), \quad (2)$$

with

$$k(x) = \frac{1}{14} \frac{F_2^p - F_2^n}{F_2^p + F_2^n}. \quad (3)$$

$k(x)$ is a correction factor which takes into account that iron is no perfect iso-

scalar target and that proton and neutron structure functions are different.

Approximating F_2^N by⁵⁾

$$F_2^N \approx (1 - 0.75 x) F_2^p, \quad (4)$$

one gets for $x = 0.65$, the highest x -value covered by the EMC data, a correction of $\sim 2.3\%$.

Gluons do not contribute directly to the cross section obtained in deep inelastic scattering. But the evaluation of the momentum sum rule $\int_0^1 F_2^N(x) dx$ shows that only 45% of the nucleon momentum is carried by charged quarks, 55% is carried by neutral constituents, the gluons, and the momentum sum rule has to be modified to

$$\int_0^1 (F_2^N + x \cdot g(x)) dx = \frac{5}{18}. \quad (5)$$

$g(x)$ is the momentum distribution of the gluons inside the nucleon. $g(x)$ and $q(x)$ are correlated by the elementary process of gluon emission by quarks and the creation of quark-antiquark-pairs out of gluons. Due to these processes and gluon-gluon interactions the momentum distributions become Q^2 -dependent. The coupling of $g(x)$ and $q(x)$ and their Q^2 -dependence is expressed by the Altarelli-Parisi-equations⁶⁾. Thus the analysis of the pattern of scalebreaking of the structure functions in terms of these equations allows a determination of the gluon distribution $g(x)$ and its Q^2 -dependence⁷⁾.

With these preliminaries it is obvious that if nuclear effects cause a change of the momentum distribution of quarks there also will be a corresponding change of the momentum distribution of gluons.

3. Models for nuclear effects

In the models which have been used so far to calculate the modifications of the nucleon structure function F_2^N due to nuclear effects it is common to view the nucleus as a dilute gas of slowly moving nucleons weakly bound to each other and having their internal properties like mass, radius or spin unchanged compared to the free nucleus case. The effective quark momentum distribution measured in deep inelastic lepton nucleus scattering is then a convolution of the quark momentum distribution inside a nucleon and the momentum distribution of the nucleons inside the nucleus. The methods used to calculate the corrections for deuterium⁸⁾ are simply transferred to the nucleus case. The results depend a lot on the assumptions made on the shape and tails of the nucleon momentum-distributions and the momentum balance in the scattering process. These assumptions are only poorly known. In fig. 1 the ratio of the structure function F_2^A for a nucleus,

with mass number A , to the sum of the free nucleon structure functions for proton and neutron, weighted with the corresponding nucleon numbers, is plotted as a function of x for an iron nucleus. The solid line in this figure shows the results of Bodek and Ritchie⁹⁾ who use a Fermi-gas-model¹⁰⁾ including high momentum tails¹¹⁾. The dot-dashed line indicates how the result would change if the high momentum tail would not be included in the calculations and the triple-dot-dashed line shows the result one would obtain when the kinematics is calculated with an $(A-1)$ nucleus as a spectator for all momenta.

In the Few-Nucleon-Correlation Model of Frankfurt and Strikman¹²⁾ the momentum

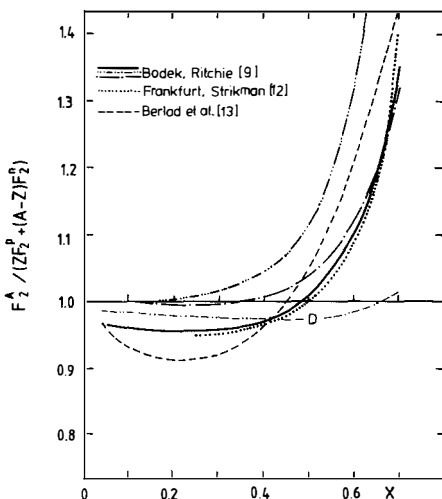


Fig. 1

distribution is produced by quark plus gluon exchange between pairs of neighbouring nucleons. Their result is represented by the dotted line in fig. 1.

As well Bodek and Ritchie as Frankfurt and Strikman use non-relativistic wave functions. Berlad, Dar and Eilam¹³⁾ argue that in highly relativistic interactions like deep inelastic scattering the momentum distribution of nucleons in a nucleus can not be deduced from its non-relativistic wave function. To calculate the effective momentum distribution of quarks in nuclei they instead present a quark-parton variety of the Collective-Tube-Model¹⁴⁾ where the nucleus is viewed in an infinite momentum frame and is Lorentz-contracted to several 'pancakes' of overlapping nucleons. The main result of their calculations (dashed line in fig. 1) is that there is a high probability for quarks and gluons to carry a larger momentum fraction than in a free nucleon. This causes the effective quark and gluon momentum distributions to be enhanced at high x and to extend for above $x = 1$, the kinematical limit being $x = A$.

The results of all these calculations show a similar behaviour. The ratio

$F_2^A/(Z F_2^P + (A-Z) F_2^N)$ is rising with x for $x > 0.2$. The value is about 1.2 - 1.3 at $x = 0.65$ and increases rapidly to higher values of x . Below $x \sim 0.45 - 0.5$ it is a few percent smaller than one with very little x dependence. (For the deuteron these corrections are much smaller than for iron as can be seen by a comparison with the curve labeled D which shows the deuterium corrections according to Bodek and Ritchie).

Apart from the similarities in the global behaviour there are significant differences in the details. This, and the fact that they in addition depend on poorly known assumptions, is the reason why several groups like BCDMS, CDHS or EMC do not correct their structure function values for these effects and present only effective distributions while most of the other groups apply a correction without telling explicitly how their assumptions and the corresponding corrections look like.

But in a nucleus the nucleons are packed much tighter together than in the deuteron which is a loosely bound system with a mean nucleon distance of about 4 fm compared to the mean nucleon charge radius of ~ 0.8 fm. Therefore apart from kinematical smearing their in addition might be a lot of other nuclear effects which can affect the quark momentum distribution and are not included in the corrections described so far.

4. The data

The EMC iron and deuterium data provide a good tool to look for these nuclear effects. Apart from the different targets these data have been taken with the identical apparatus and have been treated with the same analysis chain. Therefore a comparison can be made where the systematic errors are well understood. The nuclear corrections for deuterium are smaller than $\sim 3\%$ in the kinematic region covered by the experiment. Therefore the measured deuteron structure function can be interpreted as the representation of quark distributions inside free nucleons, while the iron-structure function (if corrected for a hypothetical target with the same number of protons and neutrons according to equation (3)) represent these distributions for nucleons inside a nucleus.

The iron data are the final data set for the four muon beam energies of 120, 200, 250 and 280 GeV. The values of the nucleon structure function $F_2^N(\text{Fe}) = \frac{1}{56} F_2^{\mu\text{Fe}}$ are shown in fig. 2a as a function of Q^2 for fixed values of x . The data are corrected for the non-isoscalarity of iron according to equation (3), no Fermi-motion correction has been applied. The errors shown are statistical only. Apart from statistical fluctuations there is perfect agreement between these four data sets and the x and Q^2 dependence is very well defined. It is worthwhile to mention that points, where different data sets overlap correspond to events taken in

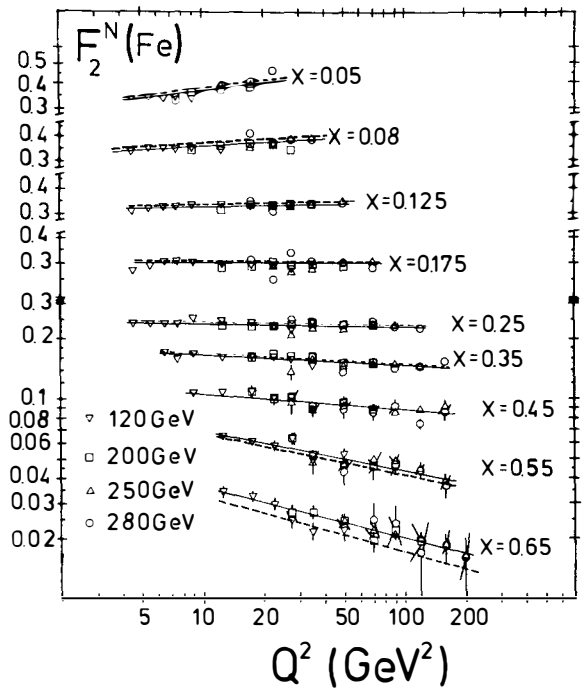


Fig. 2a

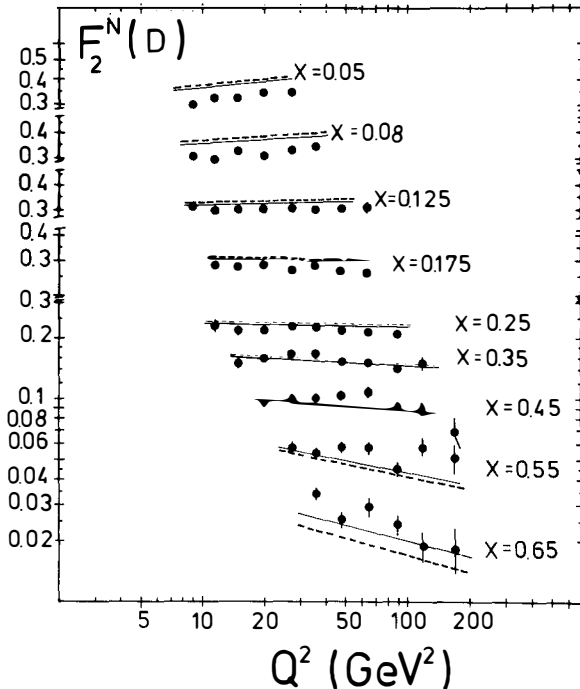


Fig. 2b

different parts of the apparatus and have completely different systematic errors for each energy. The solid lines represent a simple parametrization of the iron data, the dashed lines indicate where one would expect the deuterium data according to the Fermi-motion corrections a la Bodek and Ritchie.

The deuterium data have been obtained with a single muon beam energy of 280 GeV. The values of $F_2^N(D) = \frac{1}{2} F_2^{\mu D}$, not corrected for Fermi motion, are shown in fig. 2b. The curves are identical to those of fig. 2a, which means that the deuterium data should be well represented by the dashed line if the simple nuclear models were correct. Obviously this is not the case. At low x the structure function for deuterium should be 2-3% larger than for iron but it is smaller by about 15%, at high x the iron data should be larger than the deuterium data by about 20-25%, but they are smaller than the deuterium data by about 15%. This means that at $x = 0.65$ there is a discrepancy of 35-40% between models and experimental result. Within the limits of statistical and systematic errors there is no or little Q^2 dependence of this behaviour within the region of overlap as can be seen by a comparison of the lines and the data points. The ratio of the measured nucleon structure functions $F_2^N(\text{Fe})/F_2^N(D)$ has been calculated point by point using only data points with a total systematic error smaller than 15%. For each x -value the result has been averaged over Q^2 . The corresponding Q^2 -range is determined by the deuterium data and varies from $9 \leq Q^2 \leq 27 \text{ GeV}^2$ for $x = 0.05$ over $11.5 \leq Q^2 \leq 90 \text{ GeV}^2$ for $x = 0.25$ up to $36 \leq Q^2 \leq 170 \text{ GeV}^2$ for $x = 0.65$. The x dependence of the ratio is shown in fig. 3 where the error bars are statistical only. The ratio is falling from ≈ 1.15 at $x = 0.05$ to a value of ~ 0.89 at $x = 0.65$. In terms of quark distributions this means that at high x (valence region) where an enhancement of the effective quark momentum distribution in iron compared to the free nucleon case is predicted, it is depleted, while at low x (sea region) where only little difference is expected there is an increase.

Having no model for this behaviour available we have performed a straight line fit of the form

$$F_2^N(\text{Fe})/F_2^N(D) = a + bx$$

which for the slope b gives the result

$$b = -0.52 \pm 0.04 \text{ (statistical)} \pm 0.21 \text{ (systematic)}.$$

To calculate the systematic error of the slope we have assumed that even in the ratio none of the individual systematic errors cancels which clearly is the most conservative assumption. We have distorted the measured F_2^N values by the individual systematic errors of the data sets (increasing the iron data for all errors

and lowering the deuterium data and vice versa), calculated the slope for each error and added the differences quadratically. The possible effect of the systematic uncertainties on the slope is indicated by the shaded area in fig. 3. Uncertainties in the relative normalisation of the two data sets will not change the slope of the observed x -dependence but can only move it up and down by up to seven percent. The difference $F_2^N(\text{Fe}) - F_2^N(\text{D})$ however is very sensitive to the relative normalisation.

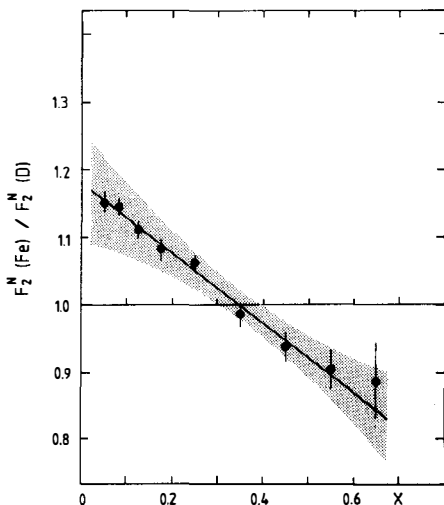


Fig. 3

5. Comparison to other data

In the high Q^2 region of our data there are no results of other experiments available which have measured the nucleon structure function for nuclear targets and deuterium with the identical apparatus. To get further informations one therefore has to combine data of different experiments. This is always very problematic because there might be different systematic uncertainties which can not be taken into account in the same way as for data of one experiment alone. Nevertheless we have compared our data to the deuterium data of the CHIO group¹⁵⁾ and the carbon data of the BCDMS group¹⁶⁾ which are in the same Q^2 range. The results are shown in fig. 4 where in addition to the EMC results the ratios of the EMC iron data to the CHIO deuterium data and of the BCDMS carbon data to the EMC deuterium data are plotted. Independently which EMC data set is used the ratios show a similar x dependence and one can conclude that a real physics effect is observed.

But there is still more information. After the EMC results have been presented the SLAC-MIT-Rochester group has reanalyzed their electron-deuterium⁶⁾ and empty

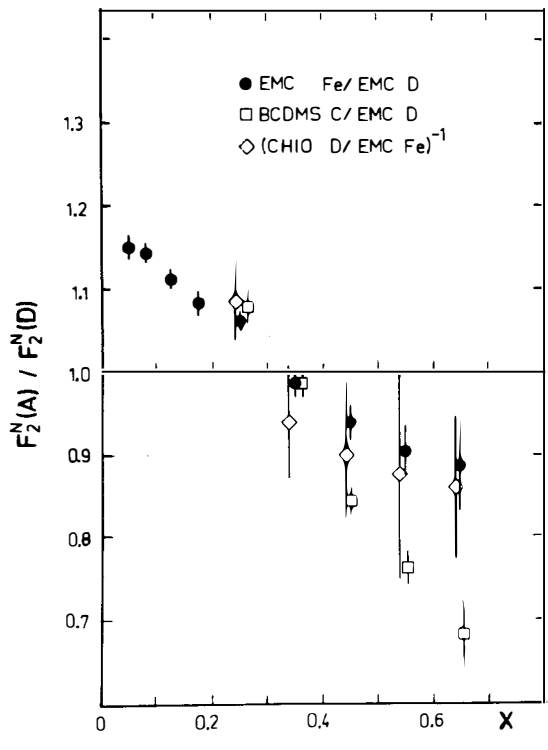


Fig. 4

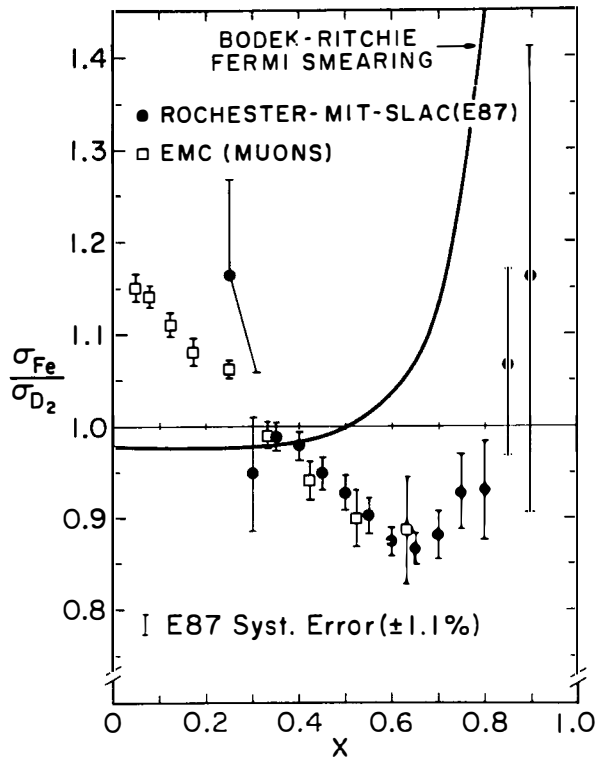


Fig. 5

target steel data¹⁷⁾. The steel data cover a kinematic range $4 < Q^2 < 21 \text{ GeV}^2$ and $0.25 < x < 0.90$. The result is shown in fig. 5. It confirms the effect seen in the EMC data. In the region $0.3 - 0.65$ the agreement is perfect. As well the x dependence as the magnitude of the ratio is nearly identical which gives us further confidence that our absolute normalisation is well determined and the systematic errors quoted are conservative limits. At $x > 0.7$ the ratio is rising again suggesting that for $x > 0.8$ the effects of Fermi motion become dominant.

An additional preliminary data set of this group obtained with an empty aluminium target¹⁸⁾ extends the low Q^2 data also to lower x . Also these data show a rise of the ratio with decreasing x , the slope being a little bit less steep than for the EMC iron data. Finally one should remember that photoproduction¹⁹⁾ and low energy low Q^2 -data²⁰⁾ show that at very low x (Q^2) the ratio falls again below one to a value around 0.8.

6. Consequences

Taking all these informations together the following picture emerges: quark distributions measured in deep inelastic scattering off nuclei are far from being identical with those in free nucleons. In the valence region ($x > 0.3$) a depletion of the quark momentum distribution in nuclei compared to the free nucleon case is observed while in the sea-region ($x < 0.3$) there is a significant increase. This behaviour depends only little on Q^2 and probably also on mass number A . In addition at very low x there are the effects of shadowing (Q^2 and A dependent) and at high x the kinematical smearing due to the nucleon motion inside the nucleus can cause the quark distribution to extend far above $x = 1$, the kinematical limit being $x = A$.

As a consequence also the gluon distribution will be different. Gluon- and Sea-distributions extracted so far from neutrino-iron²¹⁾ or neutrino-marble²²⁾ structure functions represent the distributions in these nuclei and not in free nucleons.

Probably there is little effect on the QCD analysis of data obtained with a nuclear target²³⁾. But one should keep in mind that the Altarelli-Parisi-equations⁶⁾ require an integration from x to 1. In the case of nuclear targets the integral has to be extended to $x=A$, the x -dependence of the structure functions, even if made QCD compatible, being unknown. Fortunately the contribution of this region to the integral is suppressed by the splitting functions, therefore it may not influence the final result very much. But obviously a QCD-analysis combining data sets of different nuclear targets should no longer be done.

Of course there is some impact on the interpretation of nucleon-nucleus scattering data, where in the analysis the same structure functions for incoming nucleon and

target nucleon are being used.

But there is also another important consequence. We observe a change of quark distribution due to nuclear effects. Therefore these results may help a lot for the understanding of nuclear physics in terms of quarks and gluons which has started to develop during the last years.

7. Further models for nuclear effects.

At the time when the EMC-data have been first presented the effect appeared quite surprising and many people argued that one could hardly think of any effect which could produce the observed behaviour. They obviously didn't realize that there have been many publications²⁵⁾ and a lot of conferences²⁶⁾ where 'quarks (mesons) in nuclei' have been the main topic and where several phenomena have been discussed which indeed can change the quark distributions in nuclear matter compared to the free nucleon case. But to my knowledge there didn't exist theoretical predictions how these effects could influence the nucleon structure functions obtained in deep inelastic lepton nucleus scattering.

In the mean time several calculations have been published. They are still in an early stage and do not reproduce all features of the data. For an experimentalist it is rather difficult to judge how serious one of these models is compared to the others. During many discussions I have learned that in this field for each argument there might exist a counter-argument which is as convincing. Therefore without a clear judgement I will just list the most popular phenomenological models to indicate which effects may contribute.

Change of nucleon radius. Nucleons which are embedded in nuclei might change their internal properties like mass or radius due to a distortion of the surrounding pion cloud by the attraction to other nucleons. There are two extreme models for the change of the nucleon radius R inside the nucleus. An increase of R by about 30% has been proposed²⁷⁾ to explain inelastic electron - Fe⁵⁶ data²⁸⁾, the other model²⁹⁾ demands that nucleons inside a nucleus should be compressed to bags of very small radii by a very significant pion cloud to get compatibility of the bag model of the nucleon with classical nuclear physics. There is some doubt on the accuracy of both calculations^{30,31)}. Nevertheless one should keep in mind that there is no evidence to suggest that the nucleon should not change its size when put inside a nucleus³²⁾. Furthermore a collective change of the structure of each individual nucleon is probably the most easiest way to produce the large effect seen in our data.

Isobar admixture. A fraction of the nucleons may transform by a spin-flip of a single quark caused by a quark plus gluon or pion exchange between nucleons into excited baryon states like Δ 's³³⁾. The contamination of Δ 's has been extensively

studied for the deuteron case and there found to be small ³⁴⁾. A larger fraction has been predicted for ^3He , ^3H ³⁵⁾. Some authors calculate that the Δ' admixture should also be small in large nuclei ³⁶⁾. Szwed ³⁷⁾ claims that there is evidence for a big contamination. His calculations (dashed-dotted line in fig. 6: 15% Δ -admixture, dashed-triple-dotted line: 9% Δ and 3.3% decrease of gluon momentum) show that the assumption of a 9-15% contamination of Δ -isobars in iron together with a small decrease of gluon momentum is sufficient to explain the observed difference of the structure functions for bound and free nucleons.

Multiquark states. In the MIT-bag model ³⁸⁾ the free nucleon is a three-valence-quark-($|3q\rangle$)-bag with a radius of ~ 1 fm. The average spacing between nucleons in heavy nuclei is about 1.8 fm. Therefore it has been assumed that a nucleus does not only consist of a collection of individual $|3q\rangle$ bags but that some of the nucleons overlap and form multiquark states like $|6q\rangle$, $|9q\rangle$, ... bags ³⁹⁾. It is very likely that these states will behave differently than individual nucleons

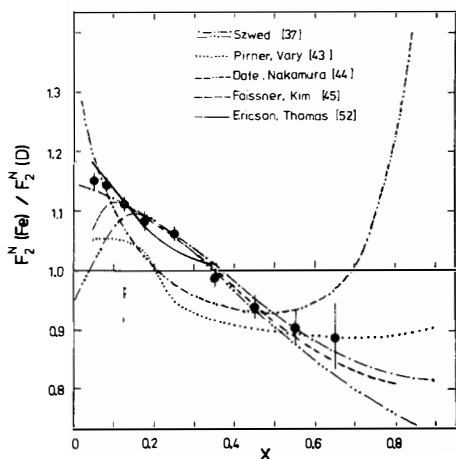


Fig. 6

and especially that the momentum distributions for quarks in a multiquark-bag will be different than in a free nucleon. This model has been applied to several examples ⁴⁰⁾, especially it has been used to describe the 'anomalous nuclear enhancement' in large p_t hadron production off nuclear targets ⁴¹⁾ and elastic and inelastic e^- - ^3He and e^- - ^4He scattering data ⁴²⁾. Using the concept of multiquark states several authors have tried to explain the observed Fe/D ratio. Pirner and Vary ⁴³⁾ have used in their calculations for iron the same cluster probabilities they have found for ^3He ($p_{|3q\rangle} = 0.84$, $p_{|6q\rangle} = 0.16$, $p_{|9q\rangle} = p_{|12q\rangle} = \dots = 0$) and a modified sea distribution for the $|6q\rangle$ states. The result (dotted line in fig. 6) shows some increase of the Fe/D ratio at low and high x but in total the agreement with the experimental data is rather poor. Date ⁴⁴⁾ has also included

multiquark clusters with more than six valence quarks. He found that to get fair agreement with the data (double-dashed-double dotted line in fig. 6) the sea quarks in multiquark clusters have to be enhanced while the gluons are rather suppressed compared to the free nucleon case. Faissner and Kim⁴⁵⁾ started from the observation that nucleons inside a nucleus tend to form clusters. They assumed that all these clusters are α -particles, each α being a $|12q\rangle$ bag with a radius which is $\sqrt[3]{4}$ times larger than the radius of a $|3q\rangle$ bag. This larger radius corresponds via the uncertainty relation to a shift of the quark momenta to lower x . This causes, similar to the arguments of Jaffe⁴⁶⁾ an increase of the momentum distribution at low x and an associated decrease at high x . The dashed line in fig. 6 shows the result of their calculations if a contamination of 3 α -clusters is assumed. It fits the data rather well. In my opinion their input is rather unlikely but it is interesting to note that a collective increase of the radii of all nucleons by 10-15% can produce similar results.

Percolation of quarks. Baym⁴⁷⁾ has pointed out that many nucleon bags may overlap when the baryon density inside a nucleus becomes high enough. Then not only multiquark bags can form but also single quarks will be able to flow in a chain of overlapping bags freely through the whole nucleus. This free flow of quarks (colour) which possibly may be observable in nuclei at normal density is known as "percolation". The long range of these percolating quarks will again cause an increase of the momentum distribution at low x and an associated depletion at high x ⁴⁶⁾. A similar picture is the model of Nikolaev and Zakharov⁴⁸⁾ where the low momentum quarks can spread out over the whole nucleus. There they can gain momentum due to interactions with quarks of other nucleons with higher momentum until their range is reduced to that of one nucleon. This causes a redistribution of quark momenta and produces shadowing at very low x and antishadowing at medium low x .

Additional Sea. Due to the mutual interactions (exchange of mesons or equivalently $q\bar{q}$ pairs) between the nucleons inside a nucleus there might exist an additional nuclear sea. Hence the quark sea in the nucleus is more than the intrinsic sea of individual nucleons. This additional sea per nucleon is concentrated at low x and could cause partly the observed enhancement of the iron data at low x . It is predicted to rise linearly with mass number A and should also be observable in Drell-Yan data⁴⁹⁾.

Quasi-real pions. A similar idea is to attribute the whole change in the nuclear sea to $q\bar{q}$ pairs in the form of quasi-real pions. The role of pions inside the nucleus has been discussed since a long time⁵⁰⁾ and they are a basic ingredient of recent theoretical developments like the 'cloudy bag model'^{25,51)}. It has been suggested by Llewellyn Smith²³⁾ that the whole enhancement of the Fe/D ratio at low x is due to the presence of a few (6-10) extra pions in the iron nucleus com-

pared to the free nucleon and Ericson and Thomas⁵²⁾ have shown that the magnitude and x-dependence of the effect are well reproduced (for $x < 0.3$) with this assumption (full curve in fig. 6). They also conclude that the enhancement should depend approximately linearly on A and that in nuclei with a large neutron-excess π^- are favoured over π^+ .

8. Summary

- The EMC-effect has been observed in data of different experiments and shows that quark and gluon momentum distributions for free nucleons are modified by nuclear effects if the nucleons are embedded in nuclei. This might be the link for the common understanding of nuclear and particle physics in terms of quarks and gluons.
- There are many phenomena known and discussed which can change the effective quark distribution and with each of the models it is possible to reproduce at least approximately the experimental result. But further and more detailed calculations are needed to sort out which effect is the most important one or which combination of effects is needed to describe all features of the data.
- Especially we need quantitative predictions about the A-dependence, sea configuration etc like in^{49,52)} which can be tested in future experiments.
- Of course we need more experimental data on more nuclear targets. The measurement of structure functions alone will not be sufficient, but we also will have to look into hadronic final states and to study for instance the π^+/π^- or π/K ratio or the J/ψ cross section etc for different targets, where indications of differences are already seen⁵³⁾. In conclusion: we have made an interesting discovery, but there is still a lot of work to be done until it will be completely understood.

REFERENCES

1. For a review of muon scattering see J. Drees, H.E. Montgomery, CERN-EP/83-41 (submitted to Ann. Rev. Nucl. Part. Sci.).
2. EMC, J.J. Aubert et al., Phys. Lett. 105B (1981) 315.
3. EMC, J.J. Aubert et al., Phys. Lett. 123B (1983) 123.
4. EMC, J.J. Aubert et al., Phys. Lett. 105B (1981) 322.
5. A. Bodek et al., Phys. Rev. D20 (1979) 1471.
6. G. Altarelli and G. Parisi, Nucl. Phys. B126 (1977) 298.
7. For a review see for instance: J. Drees, Proceedings of the 1981 Int. Symposium on Lepton and Photon Interactions at High Energies, ed. W. Pfeil, Bonn 1981, P. 474; F. Eisele, Proceedings of the 21st Int. Conference on High Energy Physics, ed. P. Petian and M. Porneuf, Paris 1982, P. C3-337.

8. W.B. Atwood and G.B. West, Phys. Rev. D7 (1973) 773; L.L. Frankfurt and M.I. Strikman, Nucl. Phys. B148 (1979) 107.
9. A. Bodek and J.L. Ritchie, Phys. Rev. D23 (1981) 1070; D24 (1981) 1400.
10. E.J. Moniz et al., Phys. Rev. Lett. 26 (1971) 445; R.A. Smith and E.J. Moniz, Nucl. Phys. B43 (1972) 605.
11. W. Czyz and K. Gottfried, Nucl. Phys. 21 (1961) 676; Ann. Phys. (N.Y.) 21 (1963) 47; K. Gottfried, Ann. Phys. (N.Y.) 21 (1963) 29.
12. L.L. Frankfurt and M.I. Strikman, Nucl. Phys. B181 (1981) 22.
13. G. Berlad et al., Phys. Rev. D22 (1980) 1547.
14. G. Berlad et al., Phys. Rev. D13 (1976) 161; S. Fredriksson, Nucl. Phys. B111 (1980) 167; L. Bergstrom and S. Fredriksson, Phys. Lett. 68B (1977) 177; 78B (1978) 337.
15. B.A. Gordon et al., Phys. Rev. D20 (1979) 2645.
16. D. Bollini et al., Phys. Lett. 104B (1981) 403; J. Feltesse, (contribution to this conference).
17. A. Bodek et al., SLAC-PUB 3041 (1983).
18. A. Bodek (contribution to this conference).
19. D.O. Caldwell et al., Phys. Rev. Lett. 42 (1979) 553; Phys. Rev. D7 (1973) 1362.
20. M. May et al., Phys. Rev. Lett. 35 (1971) 35; S. Stein et al.; Phys. Rev. D12 (1975) 1884; J. Eickmeyer et al., Phys. Rev. Lett. 36 (1976) 289; J. Bailey et al., Nucl. Phys. B151, (1979) 367; M. Miller et al., Phys. Rev. D24 (1981) 1; J. Franz et al., Z. Phys. C10 (1981) 105.
21. H. Abramowicz et al., Z. Phys. C12 (1982) 289.
22. F. Bergsma et al., CERN-EP/82-194 (1982).
23. C.H. Llewellyn-Smith (to be published in Phys. Lett.).
24. A. Edwards, talk given at the 21st Int. Conference on High Energy Physics, Paris 1982.
25. For references see for instance: A.W. Thomas, CERN-TH 3368 (1982) (to appear in Advances in Nuclear Physics, Vol. 13 (1983)).
26. See for instance: Nucl. Phys. A335 (1980); Nucl. Phys. A358 (1981); Nucl. Phys. A374 (1982); Progress in nuclear and particle physics, ed. D. Wilkinson, Vol 1 (1978), Vol 8 (1982); 'Mesons in nuclei', ed. M. Rho and D. Wilkinson, North Holl. 1979.
27. J.V. Noble, Phys. Rev. Lett. 46 (1981) 412.
28. R. Altemus et al., Phys. Rev. Lett. 44 (1980) 965.
29. G.E. Brown and M. Rho, Phys. Lett. 82B (1979) 177; G.E. Brown et al., Phys. Lett. 94B (1979) 383.
30. P.D. Zimmermann, Phys. Rev. C26 (1982) 265.
31. G.A. Miller, CERN TH-3516 (1983).
32. A. Watt, private communication.
33. A.M. Green, Reports on Progress in Physics 39 (1976) 1109; H.J. Weber and H. Arenhövel, Phys. Rep. 36C (1978) 277.
34. C. Horne et al., Phys. Rev. Lett. 33 (1974) 380; H. Benz and P. Söding, Phys. Lett. 52B (1974) 367; H. Brown et al., Phys. Rev. Lett. 33 (1974) 312; B.M. Abramov et al., JETP Lett. 21 (1975) 90; V. Bakken et al., Physica Scripta 19 (1979) 491; L.L. Frankfurt and M.I. Strikman, Phys. Rep.

76C (1981) 215.

35. A.M. Green and T.H. Schucan, Nucl. Phys. A188 (1972) 289; M. Ichimura et al., Nucl. Phys. A196 (1972) 17.
36. M. Harvey, Nucl. Phys. A352 (1981) 326; M.H. Storm and A. Watt, Nucl. Phys. A to be published.
37. J. Szwed, Cracow University Preprint TPJU-1/83 (1983).
38. A. Chodos et al., Phys. Rev. D9 (1974) 3471; Phys. Rev. D10 (1974) 2599; T.A. De Grand et al., Phys. Rev. D12 (1975) 2060.
39. E. Lehman, Phys. Lett. 62B (1976) 296; V.A. Matveev and P. Sorba, Nuovo Cim. Lett. 20 (1977) 435; H. Högaasen et al., Z. Phys. C4 (1980) 131; L. Bergström and S. Fredriksson, Rev. of Mod. Phys. 52 (1980) 675.
40. L.S. Kisslinger, Phys. Lett. 112B (1982) 307; A. Faessler et al., Phys. Lett. 112B (1982) 201; P.J. Mulders and A.W. Thomas, CERN TH-3443 (1982).
41. M. Wakamatsu, Phys. Rev. C23 (1981) 2203; S. Date and A. Nakamura, Progr. Theor. Phys. 69 (1983) 565.
42. H.J. Pirner and J.P. Vary, Phys. Rev. Lett. 46 (1981) 1376; M. Namiki et al., Phys. Rev. C25 (1982) 2157.
43. M.J. Pirner and J.P. Vary, University of Heidelberg preprint UNI-HD-83-02 (1983).
44. S. Date, Waseda University preprint WV-HEP-83-4 (1983) (submitted to Phys. Rev. Lett.).
45. H. Faissner and B.R. Kim, (private communication); B.R. Kim, talk given at the spring meeting of the German Physical Society, Wuppertal March 1983.
46. R.L. Jaffe, Phys. Rev. Lett. 50, (1983) 228.
47. G. Baym, Physica 96A (1979) 131.
48. N.N. Nikolaev and Z.I. Zakharov, Phys. Lett. 55B (1975) 397.
49. R.M. Godbole and K.V.L. Sarma, Phys. Rev. D25 (1982) 120.
50. M. Ericson and M. Rho, Phys. Rep. 5C (1972) 57.
51. A.W. Thomas, CERN TH-3552 (1983).
52. M. Ericson and A.W. Thomas, CERN TH-3553 (1983).
53. H. Wahlen, Wuppertal University preprint WUB 83-4 (1983).

A COMPARISON OF THE DEEP INELASTIC STRUCTURE FUNCTIONS
OF DEUTERIUM, ALUMINUM AND STEEL NUCLEI

A. Bodek, N. Giokaris, W. B. Atwood, D. H. Coward, D. L. Dubin,
M. Breidenbach, J. E. Elias, J. F. Friedman, H. W. Kendall,
J. S. Poucher and E. M. Riordan
Rochester - SLAC - MIT Collaboration

Presented by A. Bodek, University of Rochester, Rochester, NY 14627



Abstract

We have compared the deep inelastic electromagnetic structure functions of deuterium, aluminum and steel nuclei using data from two SLAC experiments. The kinematic dependence of the ratio of aluminum and deuterium structure functions is similar to the dependence of the ratio of steel and deuterium structure functions. The data cannot be understood simply by corrections due to Fermi motion effects, and indicate that the quark momentum distributions in the nucleon become distorted in the nucleus. Our results are consistent with recent measurements with high energy muon beams.

The structure functions of the neutron (F_2^{en}) and proton (F_2^{ep}) have been determined from deep-inelastic electron scattering experiments^{1,2)} using hydrogen and deuterium targets. Within the quark-parton model, these structure functions, at sufficiently large momentum transfers, determine the quark momentum distributions in the nucleon. Detailed studies of the atomic weight dependence of inelastic electron scattering cross sections^{2,3)} have concentrated primarily in the low x , and low Q^2 region where the application of the quark-parton model is not valid, and where other effects such as nuclear shadowing⁴⁾ may be important. The atomic weight dependence in the large x and large Q^2 region has not been studied until recently.

Recent results^{5,6)} from the European Muon Collaboration (EMC) indicate that there is a significant difference between the nucleon structure functions extracted from data obtained from muon-steel and muon-deuterium scattering experiments. This difference exhibits a trend which is opposite from that expected from Fermi motion effects.⁷⁾ Recent bag model calculations,⁸⁾ motivated by these recent results, suggest that the quark distributions in a nucleon become distorted in a nucleus via mechanisms such as six quark bag states.

In this communication we report an observation of a significant difference between the structure functions of steel and deuterium and also between the structure functions of aluminum and deuterium extracted from deep inelastic electron scattering data taken in two experiments at the Stanford Linear Accelerator Center (SLAC). Such a comparison is important not only as a search for changes in the quark structure of nucleons in nuclei as a basic physics question, but also because all present high statistics muon and neutrino high energy scattering experiments utilize heavy nuclear targets. The nuclear corrections^{7,8)} mentioned above can affect the interpretation of the structure function results when compared to the predictions of Quantum Chromodynamics (QCD), especially when data from different target nuclei have been combined in such a comparison.

The SLAC experiments^{9,10)} (experiments E87 and E49B) were designed to measure deep inelastic electron scattering from hydrogen and deuterium at large values of x and Q^2 in order to extract the proton and neutron structure functions. In SLAC experiment⁹⁾ E87 the structure functions were extracted using hydrogen and deuterium targets and a steel empty target replica. In SLAC experiment¹⁰⁾ E49B an aluminum empty target was used. Results on the ratio of neutron and proton structure functions were reported^{9,10)} in 1973 and 1974 and in a later comprehensive article which described both experiments in detail and examined the scaling of the neutron and proton structure functions in the SLAC energy range. We have recently analysed the empty target data in order to compare the steel and deuterium and aluminum and deuterium structure functions. We comment briefly on those points of the experiment related to these comparisons.

In experiment E87, the differential cross sections for the scattering of electrons from hydrogen, deuterium and steel were measured with the SLAC 8-GeV spectrometer at laboratory scattering angles (θ) of 15° , 19° , 26° and 34° . In experiment E49B similar measurements were made for hydrogen, deuterium and aluminum. At each angle, measurements were made over a range of scattered electron energy E' for several values of incident electron energy E between 4.5 and 20 GeV. In experiment E87 the electron beam passed through 14 cm long liquid hydrogen and liquid deuterium targets with walls made of 0.001" thick stainless steel.¹¹⁾ The empty target contributions were measured using a steel empty target replica with 0.007" thick walls, chosen so that the amount of radiator in the steel target replica was nearly the same as that for the full targets. Thus the radiative corrections for full and empty target data were essentially identical.^{12,13)} The rates measured with the empty target replica were divided by the ratio of the wall thicknesses (7.0) before subtraction from the full target rates. The measurements with hydrogen, deuterium and empty replica targets were interspersed to minimize systematic errors in the ratios. In the current analysis, we have used the data from the steel empty target replica to extract the structure functions for steel. For experiment E49B the liquid H_2 and D_2 target cells were cylinders 7 cm diameter with 0.003" thick aluminum walls.¹⁴⁾ Here the empty target contributions were measured using an aluminum empty replica with 0.018" thick walls again chosen so that the amount of radiator on the aluminum target replica was nearly the same as that for the full targets. The electron contribution from background processes such as π^0 decay and electron pair production was determined by reversing the spectrometer polarity and measuring the charge symmetric positron cross sections. This background, which was subtracted from the electron cross section, was significant (<30%) only at the lowest values of E'/E . The measurements with hydrogen, deuterium and aluminum targets were interspersed to minimize systematic errors.

The measured raw cross sections were corrected for the small acceptance differences between steel and deuterium and between aluminum and deuterium targets.¹⁵⁾ A small correction (0.3% to 1.7%) was applied for the neutron excess in steel and aluminum (using fits to neutron and proton data)⁹⁾ so that σ_{Fe} and σ_{Al} as reported here are the cross sections per nucleon for hypothetical steel and aluminum nuclei with equal number of neutrons and protons. The radiative corrections^{2,16)} changed the σ_{Al}/σ_D and σ_{Fe}/σ_D ratio by less than 1%. Values of σ_{Al}/σ_D and σ_{Fe}/σ_D as a function of the variable $x=Q^2/2Mv$ are shown in figures 1a and 1b respectively. The values were obtained by calculating the ratios at all kinematic points with $w>1.8$ GeV/c^2 and forming weighted averages¹⁷⁾ over small intervals in x . Here $W=(M^2+2Mv-Q^2)^{1/2}$ is the final state invariant mass, M is the mass of the proton, $v = E - E'$ is the energy transfer, and

$Q^2 = 4EE' \sin^2 \theta/2$ is the invariant square of the four momentum transfer.^{18,19)}

The random errors arising from counting statistics dominate the typically 1% error in the cross sections obtained by adding in quadrature the errors from random fluctuation (e.g. flux monitors, liquid target densities and rate dependent effects). Only random errors are shown in the errors of the points in Figures 1a and 1b. Most systematic errors in the cross sections (solid angle, incident and scattered electron energy calibration, monitor calibration) and most uncertainties in the radiative corrections cancel in the ratios σ_{Al}/σ_D and σ_{Fe}/σ_D .

The number of nucleons/cm² in the steel empty target replica was measured to an accuracy of $\pm 0.8\%$ by weighing sections cut out of the target in the region which was traversed by the beam and measuring the areas with a planimeter. The number of nucleons/cm² in the liquid deuterium target was determined to an accuracy¹⁰⁾ of $\pm 0.8\%$. We estimate an overall systematic error of $\pm 1.1\%$ in the σ_{Fe}/σ_{D_2} ratio. The systematic error in the σ_{Al}/σ_{D_2} ratio is $\pm 3\%$ at present and a more accurate determination of the target mass is being performed in order to further reduce this error. The electron data show a significant x dependence between the steel and deuterium cross sections. The observed effect is consistent with recent results obtained with muons by the EMC collaboration.^{5,6)}

In view of the small statistical and systematic errors we conclude that the difference between the steel and deuterium cross sections is due to nuclear effects. The effects of Fermi motion of the nucleons in steel and aluminum nuclei and in the deuteron have been calculated by Bodek and Ritchie⁷⁾ using an extension of the original calculations of Atwood and West²⁰⁾ for the deuteron. The expected contributions from Fermi motion effects to the ratios $\frac{\sigma_{Fe}}{\sigma_D}$ and $\frac{\sigma_{Al}}{\sigma_D}$ are shown in Figure 1. The cross sections for steel were expected to be larger than those for the deuteron for $x > 0.5$, because the momentum spread of the wave function for nucleons bound in steel is larger than the momentum spread of the deuteron wave function. The behavior of the data for $x < 0.80$ is opposite to that expected from Fermi motion. However, the data suggest that for $x > 0.8$ the effects of Fermi motion become dominant.

The variation of the data as shown in Figure 1 cannot in present models, be explained in terms of nuclear shadowing. Nuclear shadowing is expected to be important only at small values of x and Q^2 where deviations from the quark parton model are expected due to effects such as the coupling between the photon and vector mesons⁴⁾ (or "higher twist" effects in the language of QCD). Radiative corrections^{2,16)} are well understood and are not expected to result in the observed variation with x .

Within the quark-parton model, the x distributions of the structure func-

tions reflect the momentum distributions of the quarks in the nucleon. Thus the data indicate that the quark momentum distributions in the nucleon become distorted in the presence of other nucleons in the nucleus. In addition to our data we have included in Figure 1a the ratio σ_{Al}/σ_D for $\langle Q^2 \rangle \approx 1.2 (\text{GeV}/c)^2$ as measured by Stein et al.,²⁾ and the σ_{Al}/σ_D ratio as measured in photoproduction²¹⁾ ($Q^2 = 0$). The three experiments taken together indicate that at small x and small Q^2 the ratio exhibits a Q^2 dependence suggesting that nuclear shadowing¹⁵⁾ effects, which are presumably a higher twist effect in the language of QCD, may be important.

Figure 1b shows our measurements of σ_{Fe}/σ_D in a similar Q^2 range, and the EMC data^{5,6)} at much higher Q^2 . Also shown are values²⁾ for σ_{Cu}/σ_D for $\langle Q^2 \rangle = 1.2 (\text{GeV}/c)^2$ as well as σ_{Fe}/σ_D from photoproduction data.²¹⁾ These data taken together also indicate that at low Q^2 shadowing effects may cancel some of the nuclear enhancement at low x . These additional Q^2 dependent nuclear higher twist effects like higher twist effects in the nucleon are expected to be smaller at large values of Q^2 . Therefore, the extraction of Λ_{QCD} from structure function data taken with nuclear targets at high Q^2 are not affected by these terms.

We have performed a linear fit the σ_{Al}/σ_D ratios for our data in the range $0.2 \leq x \leq 0.6$ ($2 \leq Q^2 \leq 20 (\text{GeV}/c)^2$) and obtain an intercept at $x=0$ of 1.10 ± 0.02 and a slope of -0.30 ± 0.06 . A similar fit to our σ_{Fe}/σ_D results (see figure 1b) over the range $0.2 < x < 0.6$ ($4 \leq Q^2 \leq 20$) yields an intercept at $x=0$ of 1.15 ± 0.04 and a slope of -0.45 ± 0.08 . Our slope for steel is consistent with the slope of $-0.52 \pm 0.04 \pm 0.21$ reported by the EMC collaboration.^{5,6)} The fitted slopes, which are not affected by overall normalization uncertainties, indicate that the nuclear distortion in aluminum and steel exhibit a similar trend.

The understanding of the mechanisms responsible for the distortion of the structure functions of nucleons bound in a large nucleus has been the subject of several recent theoretical papers. These include ideas such as six quark bags,⁸⁾ pions and quasipions in nuclei,²²⁾ delta resonances in nuclei,²³⁾ diquark states²⁴⁾ and percolation of quarks from nucleon to nucleon in a large nucleus.²⁵⁾ The theoretical understanding of the effect is still in a very qualitative state and new experiments are being proposed²⁶⁾ to further investigate the structure functions of various nuclei.

References

- 1) A. Bodek et al., Phys. Lett. 30, 1087 (1973); J. S. Poucher et al., Phys. Rev. Lett. 32, 118 (1974); A. Bodek et al., Phys. Lett. 51B, 417 (1974); W. B. Atwood et al., Phys. Lett. 64B, 479 (1976); A. Bodek et al., Phys. Rev. D20, 1471 (1979).
- 2) S. Stein et al., Phys. Rev. D12, 1884 (1975).
- 3) W. R. Ditzler et al., Phys. Lett. 57B 201 (1975); J. Eickmeyer et al., Phys.

Rev. Lett. 36, 289 (1976); J. Bailey et al., Nucl. Phys. B151, 367 (1979); G. Huber et al., Z. Phys. C2, 279 (1979); J. Franz et al., Z. Phys. C10, 105 (1979); M. May et al., Phys. Rev. Lett. 35, 407 (1975); M. Miller et al., Phys. Rev. D24, 1 (1981).

- 4) G. Grammer and J. D. Sullivan, "Nuclear Shadowing of Electromagnetic Processes", in "Electromagnetic Interactions of Hadrons", Vol. 2, p.195; Ed. A. Donnachie and G. Shaw, Plenum Press, 1978. Submitted to Phys. Lett. B.
- 5) J. J. Aubert et al., CERN-EP/83-14 (submitted to Phys. Lett. B).
- 6) K. Rith, these proceedings.
- 7) A. Bodek and J. L. Ritchie, Phys. Rev. D23, 1070 (1981); D24, 1400 (1981).
- 8) R. L. Jaffe, Phys. Rev. Lett. 50, 228 (1983).
- 9) A. Bodek et al., Phys. Lett. 51B, 417 (1974). SLAC experiment E87 referred to as experiment B in A. Bodek et al., Phys. Rev. D20, 1471 (1979), see also A. Bodek et al., UR841 (to be published in Phys. Rev. Lett. May 9, '83) for σ_{Fe}/σ_D results.
- 10) A. Bodek et al., Phys. Rev. Lett. 30, 1087 (1973); SLAC experiment E49B (A/\bar{D}) referred to as experiment A in A. Bodek et al., Phys. Rev. D20, 1971 (1979), see also A. Bodek et al., UR846 (1983) for σ_{Al}/σ_D results.
- 11) Type 347 stainless steel nominal density 8.0 g/cm³, radiation length = 1.74 cm, mean A = 55.13, mean Z = 25.69, average composition mainly 66.8% Fe(A=55.8), 18.7% Cr(A=52), 11.3% Ni(A=58.7), 1.7% Mn(A=54.9). Note that the number of nucleons/cm² was directly measured (see ref. 9).
- 12) A. Bodek, Nucl. Inst. and Meth. 109, 603 (1973).
- 13) In experiment E87, the value used for the average amount of radiator before scattering was in (units of 10^{-2} radiation lengths) 1.122 and 1.065 for deuterium and steel, respectively. The average amounts after the scattering at angles of 15°, 19°, 26° and 34° were 1.558, 1.552, 1.537 and 1.513 for deuterium and 1.584, 1.607, 1.662 and 1.755 for steel, respectively. In experiment E49B, the value used for the average amount of radiator before scattering (in units of 10^{-2} radiation lengths) was 0.588 and 0.518 for deuterium and aluminum respectively. The average amounts after the scattering at angles of 18°, 26° and 34° were 1.117, 1.114, and 1.109 for deuterium and 1.035, 1.065, and 1.111 for aluminum, respectively.
- 14) Type 5052-0 aluminum, nominal density 2.68 g/cm³, radiation length = 9.0 cm, mean A = 27.02, mean Z = 13.02. Average composition 2.5% Mg (A=24.32), 0.25% Cr(A=52), 0.75% Max(Si, Fe, Cu, Mn, Zn), remainder Al(A=26.98). Note that the number of nucleons/cm² was directly measured (see ref. 10).
- 15) In experiment E49B (σ_{Al}/σ_D) the 7 cm target is almost a point source for the 8 GeV spectrometer. The acceptance for the empty target was smaller than the acceptance for the full target by 0.07%, 0.13% and 0.15% for data taken at 18°, 26° and 34° respectively. In experiment E87 (σ_{Fe}/σ_D , and 14 cm targets), the acceptance for the steel empty target was smaller than the acceptance for the full target by 0.4%, 0.5%, 0.7% and 1.1% for data taken at 15°, 19°, 26° and 34°, respectively.
- 16) L. W. Mo and Y. S. Tsai, Rev. Mod. Phys. 41, 205 (1969), L. C. Maximon, Rev. Mod. Phys. 41, 193 (1969).
- 17) A. Bodek, Nucl. Inst. and Meth. 117, 613 (1974); errata 150, 367 (1978); A. Bodek SLAC-TN-74-2, 1974 (unpublished).
- 18) The mean Q^2 of the data shown in Fig. 1a is 5.0, 6.4, 7.1, 7.2, 7.6, 7.6, 6.0, 7.8, 9.7, 11.4, 12.8, 17.0, 19.3 (GeV/c)² for the x bins starting at 0.25 and ending at 0.90, respectively.

19) The mean Q^2 of the data shown in fig. 1b is 1.9, 2.2, 2.4, 2.7, 2.4, 3.1, 3.8, 4.2, 5.2, 5.2, 7.0, 6.8, 7.5, 8.7, 8.3, 11.8, 11.4, 13.8 and 20.1 (GeV/c^2) for x bins starting at 0.075 and ending at 0.863 respectively.

20) A. Bodek and J. L. Ritchie, Phys. Rev. D23, 1070 (1981); D24 1400 (1981).

21) D. O. Caldwell et al., Phys. Rev. Lett. 42, 553 (1979); Phys. Rev. D7, 1362 (1973); A. M. Eisner, "Proceedings of the 1979 International Symposium on Lepton and Photon Interactions, Fermilab, Aug. 1979, p.448, ed. T. B. W. Kirk and H. D. I. Abarbanel.

22) C. H. Llewellyn Smith, Oxford Preprint 18/83; M. Ericson and A. W. Thomas, CERN TH3553 (1983).

23) J. Szwed, Jugelonian Univ., preprint TPJU-1/83.

24) J. D. Bjorken, private communication.

25) G. Baym, Physica 96A, 131 (1979).

26) SLAC proposal E-139 (American University, Maryland, Rochester, Saclay, SLAC collaboration); CERN muon proposal NA4 BCDMS collaboration.

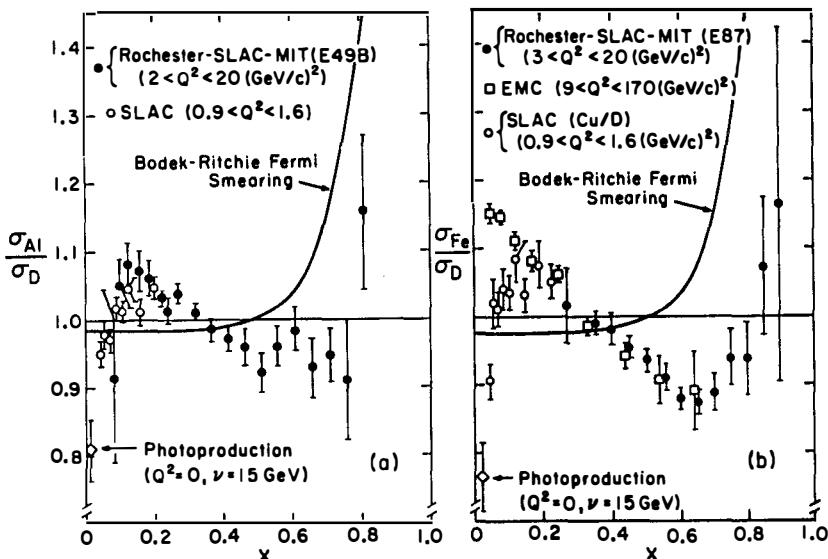


Figure 1: $\sigma_{\text{Al}}/\sigma_{\text{D}}$ (a) and $\sigma_{\text{Fe}}/\sigma_{\text{D}}$ (b) versus x . Only random errors are shown. The systematic errors is $\pm 3\%$ and $\pm 1.1\%$ for $\sigma_{\text{Al}}/\sigma_{\text{D}}$ (E49B) and $\sigma_{\text{Fe}}/\sigma_{\text{D}}$ (E87) respectively. All data for $W \geq 1.8 \text{ GeV}$ are included. The data have been corrected for the small neutron excess and have not been corrected for Fermi motion effects. The curve indicates the expected ratio if Fermi motion effects were the only effects present (Ref. 7). High Q^2 data from EMC (Ref. 5), low Q^2 data from Ref. 9, and $\sigma_{\text{Al}}/\sigma_{\text{D}}$ and $\sigma_{\text{Fe}}/\sigma_{\text{D}}$ from photoproduction data (Ref. 21) are shown for comparison. The systematic error in the EMC data is $\pm 1.5\%$ at $x=0.35$ and increases to $\pm 6\%$ for the points at $x=0.05$ and $x=0.65$.

PROMPT NEUTRINO RESULTS FROM FERMILAB

R.C. Ball, C.T. Coffin, H.R. Gustafson, L.W. Jones, M.J. Longo,
 T.J. Roberts, B.P. Roe and E. Wang
 University of Michigan, Ann Arbor, MI 48109

M.E. Duffy, G.K. Fanourakis, R.J. Loveless, D.D. Reeder,
 D.L. Schumann and E.S. Smith
 University of Wisconsin, Madison, WI 53706

M.B. Crisler, J.S. Hoftun, T.Y. Ling, T.A. Romanowski, and J.T. Volk
 Ohio State University, Columbus, OH 43210

C. Castoldi and G. Conforto
 I.N.F.N., Firenze, Italy

S. Childress
 Fermi National Laboratory, Batavia, IL 60510

Presented by: Michael J. Longo

ABSTRACT

Results from a Fermilab experiment to study prompt neutrino production by 400 GeV protons on a tungsten target are presented. Assuming the prompt neutrinos come from the decay of charmed mesons and an $A^{1.0}$ dependence we find a total $D\bar{D}$ production cross section $\sim 30 \mu b/\text{nucleon}$, in good agreement with previous CERN results. The best-fit charm production model is $\sigma(D\bar{D}) = c(1 - |x|)^5 e^{-2m_T}$ which gives a total charm production cross section of $36 \pm 5 \text{ (stat.)} \pm 7 \text{ (sys.) } \mu b/\text{nucleon}$. We find a prompt $\bar{\nu}_\mu/\nu_\mu$ ratio of 1.09 ± 0.25 overall, with no significant dependence on neutrino energy. The prompt ν_e/ν_μ ratio is 1.19 ± 0.22 overall, consistent with no energy dependence. Limits on the production of supersymmetric particles are also presented. A limit on the gluino mass of $\geq 4 \text{ GeV}$ is inferred from the absence of anomalous neutral-current events.



INTRODUCTION

The first prompt neutrino experiments were carried out at CERN in 1977.¹⁻³ These showed that there was an unexpected source of neutrinos which apparently came from the decay of shortlived particles. It gradually became clear that the most likely source was the semileptonic decay of charmed particles. From the neutrino rates the total charm production cross section was inferred to be $\sim 100 \mu b$ if an $A^{2/3}$ dependence on nucleon number was assumed.

The interest in the results from the first runs led to a second run at CERN in 1979. The results for the charm production cross section⁴⁻⁶ generally agreed with the first run's. However there were still some important unanswered questions.

If the prompt neutrinos come from central production of charmed meson pairs which then decay semileptonically, the flux of neutrinos $\phi(\nu)$ should be equal to that for antineutrinos. The results for $\phi(\bar{\nu})/\phi(\nu)$ were

$$\begin{aligned}
 \text{CDHS}^6] : \quad \phi(\bar{\nu}_\mu)/\phi(\nu_\mu) &= 0.46 & +0.21 \\
 \text{BEB}^4] : \quad \phi(\bar{\nu}_\mu)/\phi(\nu_\mu) &= 0.79 & \pm 0.62 \\
 & \phi(\bar{\nu}_e)/\phi(\nu_e) & = 0.65 \pm 0.33 \\
 \text{CHARM}^5] : \quad \phi(\bar{\nu}_\mu)/\phi(\nu_\mu) &= 1.3 & +0.6 \\
 & & \pm 0.5
 \end{aligned} \tag{1}$$

Now this ratio is really not very fundamental. The D and \bar{D} momentum spectra need not be the same, so $\phi(\nu) = \phi(\bar{\nu})$ only if integrated over energy and angle. We also have to assume $D^+ = D^-$ and $D^0 = \bar{D}^0$, which need not be the case. However this ratio is an important one in testing charm production models, and it would be nice to know what it is.

If the prompt neutrinos come from the semileptonic decays of massive particles we expect $\phi(\nu_e) \approx \phi(\nu_\mu)$. In this case the three experiments agree quite well,

$$\begin{aligned}
 \text{CDHS}^6] : \quad \phi(\nu_e)/\phi(\nu_\mu) &= 0.64 & +0.22 \\
 & & -0.15 \\
 \text{BEB}^4] : \quad \phi(\nu_e)/\phi(\nu_\mu) &= 0.59 & +0.35 \\
 & & -0.21 \\
 \text{CHARM}^5] : \quad \phi(\nu_e)/\phi(\nu_\mu) &= 0.48 & \pm 0.16
 \end{aligned} \tag{2}$$

If this ratio were significantly different from one, it would be a very important result. Possible explanations range from the mundane: e.g. - a contamination from nonprompt neutrinos (mostly ν_μ) from proton beam interactions upstream of the beam dump; to the exotic: e.g. - neutrino oscillations which transform ν_e to ν_τ or another species of neutrino.

In addition, the CHARM group^{5]} reported a 2.4 std. deviation excess of muonless events with visible energy < 20 GeV. The CDHS group saw no effect but their energy threshold was somewhat higher.^{6]}

Immediately following the first CERN prompt neutrino experiment our group proposed that a new beam specifically designed for prompt neutrinos be installed at Fermilab. The CERN neutrino beam was designed originally for neutrinos from pion and kaon decays which are produced at quite small angles to the proton beam. The detectors therefore can be quite far away. Prompt neutrinos (presumably) are from the decays of much more massive particles like D mesons and are produced with a much larger angular spread, so that the CERN detectors are not well matched to the prompt neutrino beam. Ideally one should use a detector with much larger transverse dimensions for prompt neutrinos or move the detector much closer to the production target. The only realistic solution for us was the latter. This was made possible through the use of a magnetized iron beam dump described below.

PROMPT NEUTRINO BEAM AND DETECTOR

The prompt neutrino beam and detector are shown schematically in Figure 1. A beam of 400 GeV protons with intensity about 2×10^{12} per beam pulse is incident from the left. The proton beam passes through a vertical pitching

magnet and strikes one of several targets: tungsten, copper, or beryllium with either normal density or about one-third normal density. Only the tungsten data have been analyzed so far. The target is followed immediately by 11 m of magnetized iron with the magnetic field horizontal. Thus muons are deflected vertically. Hadrons are absorbed in the dump, and most of the muons are ranged out or deflected away from the detector which is only 60 m from the target.

The detector is preceded by a triple wall of veto counters which are used to prevent triggers from charged particles entering the detector. The detector

E613 EXPERIMENT - OVERALL PLAN VIEW

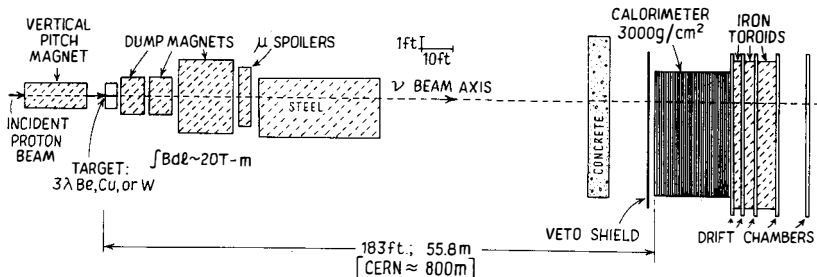


Figure 1. Fermilab prompt neutrino experiment

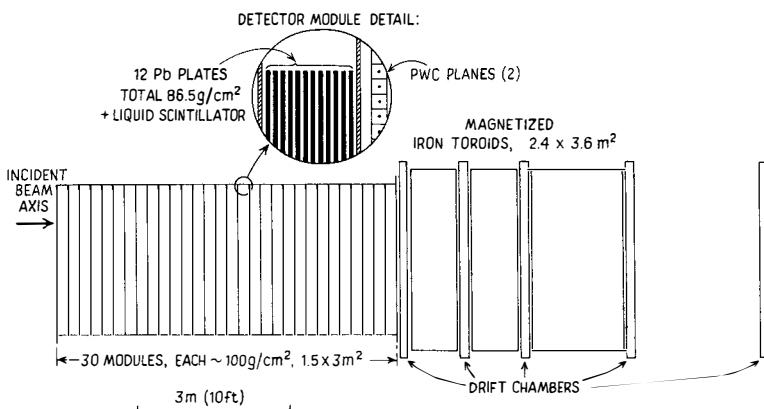


Figure 2. Fermilab prompt neutrino detector

is shown in somewhat more detail in Figure 2. The sensitive volume consists of a calorimeter with lead plates. The total mass is about 175 metric tons and the fiducial mass is about 65 tons. The lead is divided into 30 modules, each with 12 lead plates. (See inset of Fig. 2.) The modules are segmented vertically into 5 cells. The lead plates are covered with teflon and immersed

in liquid scintillator. Scintillation light travels by total reflection at the liquid-teflon interface and is brought to photomultiplier tubes at either end of each cell. There are a total of 300 phototubes on the calorimeter, each with its own analog-to-digital readout. Each of the 30 calorimeter modules is followed by two PWC planes, one with wires horizontal, the other with wires vertical. The wires are on 2.54 cm centers and have individual analog readouts^{7]} with a total of 6000 wires.

The calorimeter is followed by a muon spectrometer with solid iron magnets and drift chambers to track the muons from ν_μ charged-current events and measure their momenta.

The decision to trigger the event readout was based on the pulse-height information from the calorimeter phototubes. Minimum pulse-height requirements were imposed on overlapping groups of phototubes. Typically about 24 triggers were recorded per one-second long beam spill. Of these ≈ 6 were due to cosmic rays, and most of the rest came from muon interactions in the floor or roof blocks. In addition, approx. 6 cosmic ray triggers were recorded during a one-second "beam off" period; this provided a sample of cosmic ray triggers which allowed corrections for any cosmic ray events which faked real neutrino events. About one in 500 triggers yielded a neutrino event within the fiducial volume.

The triggering efficiency was mapped out as a function of energy deposited and position within the calorimeter by making use of the interactions of muons traversing the calorimeter. The ratio of muons which satisfy the energy trigger requirement to all muons in a given range of visible energy is the triggering efficiency for that E_{vis} . The trigger efficiency averaged over the entire detector was $> 50\%$ above about 6.5 GeV.

For our first data run in 1981 only the energy trigger was used. For our 1982 run a muon trigger was added. This required only a charged particle leaving the calorimeter and traversing the muon spectrometer with no front veto pulse. This trigger greatly improved our triggering efficiency for charged-current muon events with low hadronic energy. Results from the 1982 run are just now becoming available.

CHECKS AND CORRECTIONS

As a direct check on possible contamination of nonprompt neutrinos from upstream sources, we had a pitching magnet just upstream of the production target (Fig. 1). Because of this, the prompt events should be centered vertically in the detector, while neutrinos from sources upstream of the pitching magnet would be centered about 25 cm lower. We saw no sign of any excess of events in the lower half of the detector.

As further evidence that we are looking at neutrinos we can look at the

Bjorken x and y distributions of the events. Figure 3 compares the observed $x_{BJ} = Q^2 / [2m_p(E_\nu - E_\mu)]$ distributions for ν_μ with those expected. The y distributions observed are also consistent with those expected (Figure 4). Thus we conclude we are looking at "garden-variety" neutrinos.

The data contain a significant fraction of nonprompt ν 's from pion and kaon decays. We expect our nonprompt background to be generally lower than those observed in the CERN experiments because our detector subtends a much larger fraction of the prompt neutrinos.

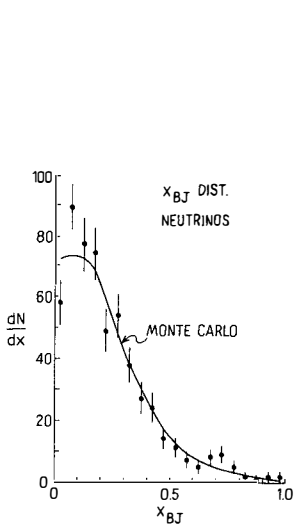


Figure 3. Bjorken x distribution

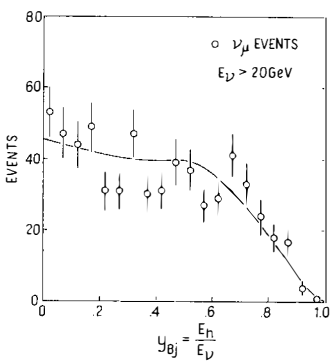


Figure 4. Bjorken y distribution (1982 data)

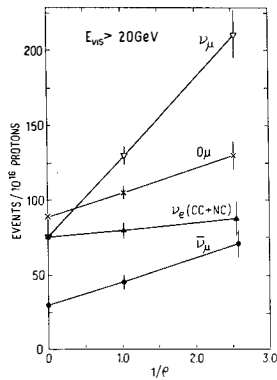


Figure 5. Extrapolation to infinite target density

The conventional way of subtracting the nonprompts is to extrapolate the rate to infinite target density. It is easy to show that the nonprompts go linearly to zero as $1/p \rightarrow 0$. Figure 5 shows the extrapolation for various subsets of our data. The "0 μ " events contain the $\nu_e + \bar{\nu}_e$ events plus the ν_μ and $\bar{\nu}_\mu$ neutral current events. If the $\nu_\mu + \bar{\nu}_\mu$ neutral current events are subtracted we can isolate the ν_e contribution. As expected, the nonprompt background in the ν_e sample is quite small; the main source of nonprompt ν_e is the semileptonic decays of K's and hyperons, which are suppressed by long lifetimes or small branching ratios.

We took great precautions with our proton beam line to minimize and understand any beam scraping which could be a source of what appear to be prompt neutrinos. Over 30 loss monitors were situated all along the beam line. These monitors were calibrated directly in counts/(interacting proton) by introducing foils of known thickness at various places in the beam and by improving or worsening the beam vacuum. The upstream background can be calculated readily in terms of the nonprompt background from the target. Both come from essentially the same mix of pion and kaon decays. The result is

$$\frac{\text{Upstream Background}}{\text{Nonprompts from Tungsten}} = 0.5\% \pm 0.25\%$$

or typically <1% of the prompt signal.

In addition there is a calculable background from vacuum windows, air, etc. just upstream of the target. This was approx. 16% of the prompts from tungsten.

RESULTS AND DISCUSSION

Once we have the prompt neutrino signal isolated, the next step is to calculate the neutrino flux. This is straightforward and noncontroversial. The ν and $\bar{\nu}$ interaction cross sections are well known. The rest involves triggering and geometric efficiencies. Corrections have been applied for scanning losses, etc. The total number of interacting protons comes from a secondary emission monitor calibrated frequently by standard foil activation techniques.

To go from neutrino fluxes to charm production cross sections does involve a number of assumptions. These are worth spelling out in detail:

- (1) Source is $p+N \rightarrow D+\bar{D}+x$ (not $\Lambda_c \bar{D}$, etc.).
- (2) Because the target is thick, we can get significant contributions from secondary hadrons. To account for this we assume the $D\bar{D}$ cross section varies as $s^{1.3}$ and the proton elasticity is 0.3.
- (3) To get the cross sections for nucleons from that for tungsten, the A dependence of charm production must be known. Conventional wisdom suggests that for central production of $D\bar{D}$ pairs, an $A^{1.0}$ dependence is to be expected. This is roughly what is observed for ψ/J production off nuclei. We therefore assume an $A^{1.0}$ dependence independent of x and P_T .
- (4) The dependence of the cross section on Feynman x and P_T is assumed to be

$$E \frac{d^3\sigma}{dp^3} = C (1-|x|)^n e^{-bP_T} \quad (3)$$

This factorized form is found to be only a fair approximation for other processes.

(5) The branching ratio of $D^+\mu^+\nu_\mu + X$ is taken to be .082. This is the average of D^+ and D^0 as compiled by the Particle Data Group.

Given these assumptions we can compute a total charm production cross section and compare it with the CERN results. This comparison is made in Table I with the same assumptions used in all cases. It is evident from Table I that the charm production cross sections are in good agreement if the same assumptions are used.

We find somewhat better fits to the data if e^{-bP_T} in Eq. 3 is replaced by $e^{-b\bar{m}_T}$ where $\bar{m}_T \equiv (m_D^2 + P_T^2)^{1/2}$. If n and b are varied to give the best fit to the data we find for the 1981 $1-\mu$ data

$$n = 5.0 \pm 1.0$$

$$b = 2.0 \pm 0.5$$

with a total $\bar{D}\bar{D}$ production cross section of 36 ± 5 (stat) ± 7 (sys) μb .

Historically it has been very difficult to reconcile the charm production cross sections observed at 400 GeV with the much larger cross sections observed at the CERN ISR. However, F. Halzen at the Paris Conference^{8]} pointed out that if an $A^{2/3}$ dependence for charm production is assumed, the heavy target results rise significantly, and much better agreement is obtained. It is worth noting that the difference between $A^{1.0}$ and $A^{2/3}$ is a factor of 5.7 for tungsten and 4.0 for copper. The uncertainty in the A dependence is thus the largest uncertainty in extracting the nucleon-nucleon cross section from the beam dump experiments. We expect to answer this important question soon when our copper and beryllium data are analyzed.

TABLE I

$$\sigma(\bar{D}\bar{D}) \text{ From Beam Dump Experiments}$$

$$[\text{Assuming } E \frac{d^3\sigma}{dp} = C s^{1.3} A^{1.0} (1-|x|)^3 e^{-2P_T}]$$

Group	Angle Covered	Particle Detected	$\sigma(\bar{D}\bar{D})$ ($\mu\text{b}/\text{nucleon}$)
This exp't	0-37 mr	ν_μ	20 ± 3
CHARM	0-2	ν_e, ν_μ	14 ± 5
BEBC	0-2	ν_μ ν_e	45 ± 15 26 ± 15
CCFRS	0-40 (350 GeV)	μ	15 ± 5 (18 at 400 GeV if $s^{1.3}$)

Another important question in testing the charm production models is the ratio of $\bar{\nu}$ and ν fluxes. We find $\bar{\nu}_\mu/\nu_\mu = 1.09 \pm 0.25$. Thus our result is consistent with unity, which is as expected in models with central $\bar{D}\bar{D}$ production.

Another important test of the production models is to determine whether

the energy and P_T spectra of the prompt neutrinos agree with those predicted. Figure 6 compares the observed P_T spectrum for prompt ν_μ with those predicted

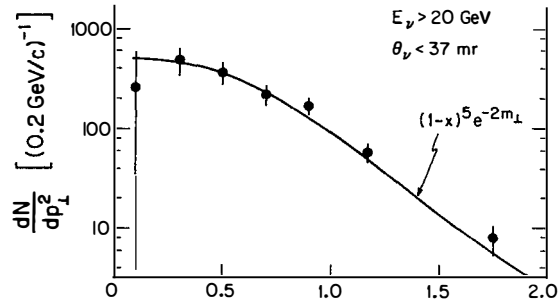


Figure 6.
Observed p_T spectrum of ν_μ compared to prediction of models.

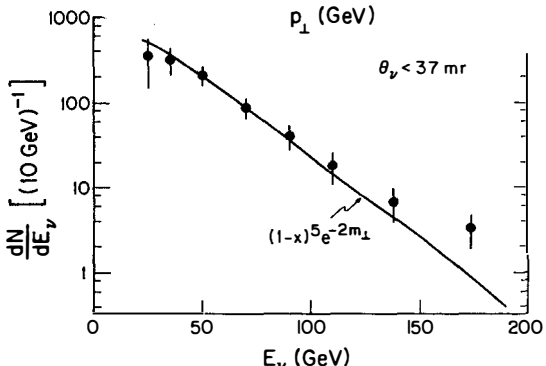


Figure 7.
Observed E_ν spectrum of prompt ν_μ compared with prediction of model.

for the best-fit production model. In Fig. 7 we compare the prompt ν_μ energy spectrum with the prediction of the model. The energy spectrum is consistent with $n = 5 \pm 1$. A substantial contribution of diffractive production with a flat spectrum in x or one which is peaked at $|x| > 0.5$ would not be consistent with the data.

A very important question is the ratio of prompt ν_e to ν_μ which seems low in the CERN results. (See introduction.) Figure 8 compares the ν_e and ν_μ yields as a function of neutrino energy for the 1982 data. The data are consistent with equal ν_e and ν_μ fluxes at all energies. Overall for these data

$$\frac{\nu_e}{\nu_\mu} = 1.19 \pm 0.22$$

In addition to prompt neutrinos per se, beam dumps are a favorite hunting ground for new, relatively weakly interacting particles which can penetrate lots of shielding. One example would be the supersymmetric counterpart of the photon, the photino $\tilde{\gamma}$. These might be produced from the decay of gluinos. The photinos can interact in our detector to produce muonless events with unusually large P_T . The absence of such anomalous events allows us to set rather stringent limits on the existence of gluinos of mass $< 4 \text{ GeV}/c^2$ which decay

into photinos or Goldstinos. Unfortunately the limits are different for every gluino production/lifetime/decay scenario, and it is hard to give a concise summary. Figure 9 gives one example, that of gluinos which decay quickly to $\tilde{\chi}q\bar{q}$ with the $\tilde{\chi}$ long-lived. As is typical, the limits depend on some unknown parameter in the theory. In this case it is m_ϕ , the mass of the lightest scalar quark, which is supposed to be less than the mass of the Z^0 . For further details, see Reference 9.

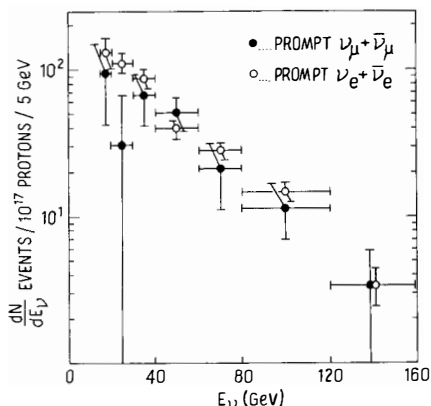


Figure 8. Comparison of prompt ν_μ and ν_e yields (1982 data).

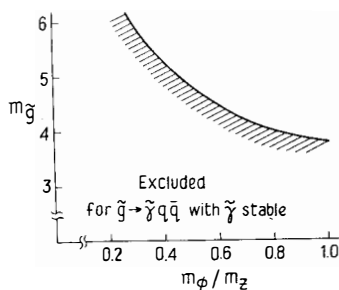


Figure 9. Example of limit on supersymmetric particles.

SUMMARY AND PROGNOSTICATION OF THINGS TO COME

In summary, we find

- (1) A charm production cross section of approx. $36 \mu\text{b}/\text{nucleon}$ (assuming an $A^{1.0}$ dependence), in good agreement with the CERN prompt neutrino experiments.
- (2) $\nu/\nu \approx 1.0$ as expected for $D\bar{D}$ production.
- (3) $\nu_e/\nu_\mu = 1.29 \pm 0.21$ which implies no exotic sources (or sinks!) of either neutrino species.
- (4) P_T and E_ν distributions consistent with reasonable charm production models.
- (5) No sign of gluinos, etc. ($m_{\tilde{g}} > 4 \text{ GeV}/c^2$).
- (6) Charm production models with a large component with a flat x dependence [or harder] are not consistent with the neutrino energy spectrum.

Data yet to be analyzed for beryllium and copper targets should answer the question of the A dependence. The analysis of events with $E_\nu < 20 \text{ GeV}$ is difficult because backgrounds are higher and efficiencies are lower. When this is complete, we hope to be able to shed some light on the excess of events seen by the CHARM group for $E_\nu \leq 20 \text{ GeV}$.

REFERENCES AND FOOTNOTES

1. P. Alibran et al., Phys. Lett. 74B, 134 (1978).
2. T. Hansl et al., Phys. Lett. 74B, 139 (1978).
3. P.C. Bosetti et al., Phys. Lett. 74B, 143 (1978).
4. P. Fritze et al., Phys. Lett. 96B, 427 (1980).
5. M. Jonker et al., Phys. Lett. 96B, 435 (1980).
6. H. Abramowicz et al., Z. Phys. C13, 179 (1982).
7. R. Ball et al., Nucl. Instr. and Meth. 197, 371 (1982).
8. Francis Halzen, Rapporteur's talk, XXI International Conference on High Energy Physics, Paris 1982.
9. R.C. Ball et al., Supersymmetry Mass and Lifetime Limits from a Proton Beam Dump Experiment, Univ. of Michigan Preprint UM HE 82-21.

ELASTIC NEUTRINO ELECTRON SCATTERING

A PROGRESS REPORT ON EXPERIMENT 734 AT BROOKHAVEN

BNL-Brown-KEK-Osaka-Penn-Stony Brook-Toykyo (INS) Collaboration[†]

presented by

David Cutts*

Brown University

Providence, RI 02906 USA

**ABSTRACT**

I will report preliminary results on elastic neutrino-electron scattering from data taken with the 200 ton segmented liquid scintillator - proportional drift tube neutrino detector at Brookhaven. Features of the detector (such as the active target and long radiation length) permit a uniquely clean signal. Prospects of results from the completed analysis and further data taking are discussed.

(†) K. Abe, L.A. Ahrens, K. Amako, S. H. Aronson, E. Beier, J. Callas, P.L. Connolly, D. Cutts, D.C. Doughty, R.S. Dulude, S. Durkin, T.E. Erickson, R.S. Galik, B.G. Gibbard, S.M. Heagy, D. Hedin, B. Hughlock, M. Hurley, S. Kabe, R.E. Lanou, Jr., Y. Maeda, A.K. Mann, M.D. Marx, J.T. Massimo, T. Miyachi, M.J. Murtagh, S.J. Murtagh, Y. Nagashima, F.M. Newcomer, T. Shinkawa, E. Stern, Y. Suzuki, S. Tatsumi, S. Terada, R. Van Berg, D.H. White, H.H. Williams, T. York.

(*) Supported in part through the Japan-USA Cooperative Research Project on High Energy Physics under the Japan Ministry of Education, Science, and Culture and the U.S. Department of Energy.

1. Introduction

The elastic scattering of muon neutrinos and antineutrinos on electrons,

$$(\bar{\nu}_\mu) e + (\bar{\nu}_\mu) e \quad (1)$$

is a purely leptonic process that allows a direct observation of the weak neutral current. With data from this process one can make a direct determination of the neutral current coupling constants g_V , g_A . These numbers can be interpreted within a given model to provide clean measurements of parameters such as $\sin^2 \theta_W$ or ρ .

To study elastic neutrino-electron scattering we have built a new neutrino detector¹ at Brookhaven National Lab. Operation of the detector at the Brookhaven AGS has a number of advantages relative to FNAL or the SPS despite the lower cross section. Indeed, with 10^{13} protons/pulse and 1.4 pulses/second the event rate at the AGS is comparable to that at other labs. The real difference in experiments at Brookhaven has to do with background: neutrino interactions at 1 GeV rather than 20 GeV have low multiplicities and have been well studied. Correspondingly, the backgrounds are simpler and easier to calculate and recognize. A recent development has been the recognition of the importance of coherent π^0 production:

$$\nu N \rightarrow \nu N \pi^0 \quad (2)$$

Calculations⁽²⁾ and experiments^(3,4) suggest that this process could be a serious background in the elastic neutrino-electron signal. With increasing energy the cross section for this process grows rapidly and becomes more sharply peaked in the forward direction, so low energy experiments have a decided advantage.

2. The Detector

The anticipated signal for elastic neutrino electron scattering is that of an isolated electromagnetic shower, constrained to be in the forward direction by the kinematic relation:

$$E\theta^2 \leq 2m_e \quad (3)$$

Typically at Brookhaven energies the electron energy E is around 400 MeV, with the electron angle θ then less than 50 milliradians. The total cross section

for the elastic scattering is roughly

$$\sigma_{\nu_\mu e \rightarrow \nu_\mu e} \sim 1.5 E_\nu \times 10^{-42} \text{ cm}^2 \quad (4)$$

Reactions which can also give forward showers, like

$$\nu_\mu n \rightarrow \nu_\mu n \pi^0 \quad (5)$$

or

$$\nu_e n \rightarrow e^- p \quad (6)$$

and which have cross sections three orders of magnitude larger, can be serious sources of background.

With these considerations in mind we have designed and built a new detector at Brookhaven. Its basic design is to combine an active target with multiple measurements of position and energy loss on a distance scale short compared to a radiation length. The target is liquid scintillator, contained within 4m long acrylic extrusions and packaged into planes 4m x 4m in area and 8.9 cm thick. As shown in the insert on Figure 1, each scintillator plane (16 cells each with a phototube at both ends) is followed by 2 planes of thin-walled proportional drift tubes (54 wires/plane), with alternating horizontal and vertical wires. Over 80% of the mass of the detector is liquid scintillator, permitting observation of energy deposits at the vertex as well as allowing approximately 75% of the total energy to be visible. The radiation length is 5 modules (one module = 1 scintillator plus 2 PDT planes), so multiple measurements of dE/dx in both the scintillator calorimeter and the PDTs are possible at an early stage in the growth of an electron shower. This aspect of the detector enables good separation of electron tracks from photon showers. Together with energy loss measurements, the PDTs (with spatial resolution of 1.5mm) provide a determination of the electron angle [important because of eqn. (3)] with an accuracy approximately

$$\Delta\theta \sim \frac{12 \text{ mrad}}{\sqrt{E}} \quad (7)$$

This number is derived from early prototype tests; measurements are in progress in a test beam to study fully this and other aspects of the detector.

The complete detector is shown in Figure 1. The total of 112 modules as described above (calorimeter and 2 PDT planes), 172 metric tons, is followed by

10 modules or 30 metric tons of alternating scintillator planes and 1 radiation length Pb sheets. This "gamma catcher" provides an energy measurement for showers which begin late in the detector, allowing a fiducial region for shower vertex position that extends through module 102. A spectrometer, using PDT planes, permits a determination of the momentum spectrum of a sample of quasi-elastic events to check the neutrino (anti neutrino) spectrum and (ν , $\bar{\nu}$) composition of the beam. The total detector occupies a volume of $4\text{m} \times 4\text{m} \times 24\text{m}$ and is instrumented by approximately 4000 phototubes and 14,000 PDT wires.

The detector data collection is designed to be deadtimeless. A $10\text{ }\mu\text{sec}$. electronic gate enables all elements shortly before the arrival of the $2.5\text{ }\mu\text{sec}$ neutrino burst. Both time and charge are recorded for every element with a signal above threshold. In data analysis, then, one can "time cluster" the hits and cleanly separate interactions (or delayed μ decays) within this gate. Additionally, all elements have multihit capability. Data readout proceeds in parallel through four microprocessors⁵; these also handle elaborate calibration and monitoring tasks between bursts.

3. Status of the Experiment

We have had two data taking periods, with the flux as summarized in Table 1. The early data, taken with 1/2 the number of modules installed and without the "gamma catcher" or spectrometer, was summarized at Balaton⁶. I will discuss the analysis of the neutrino electron elastic scattering data from our major run, with the full detector.

TABLE 1. EXP 734 Running Periods

<u>protons on target:</u>			
<u>period</u>	<u>detector</u>	<u>(ν beam)</u>	<u>($\bar{\nu}$ beam)</u>
June-July 1981	1/2	6.3×10^{18}	5.0×10^{17}
Dec.-Feb. 1982	full	8.8×10^{18}	9.1×10^{18}

The raw data from the ν running with the full detector consisted of recorded (time, charge) for all hit elements for each of 1.25×10^6 bursts. This data was first passed through a conservative software filter designed to eliminate beam muons and neutrino interactions without electromagnetic shower characteristics. The sample surviving, 4×10^4 "time clusters", was then scanned by physicists to select single showers within a 15° cone of the forward direction and eliminating events with extra tracks at the vertex, with multiple

showers, or with associated side or front entering particles. The remaining 1575 events were subjected to a fiducial cut (vertex within modules 6 to 102 and PDT wire numbers 7-50) and an energy cut (visible energy > 150 MeV).

The above selection process eliminated all but 1048 events. Of these events, 257 were found to have an energy deposit of at least 5 MeV correlated in time but upstream of the vertex. As discussed below this feature is suggestive of a π^0 decay; subtracting this data left 791 events, predominantly single electromagnetic showers. Using the PDT positions in the first 3 to 5 modules of the shower (within 1 radiation length) we calculated the angle of the candidate electron; requiring this angle to be less than 180 milliradians reduced the sample to 392 events. Finally, to tag "electrons" and "protons" we made a separation based on the energy deposited in the PDT and calorimeter cells within the first three modules after the vertex. At this stage the signal was already relatively clean, so we were able to apply this cut loosely, retaining 95% of the electron signal while eliminating 50% of the photon-like background. This separation left 265 "electron" events and 127 "photon" events.

We handle the π^0 and e^-p backgrounds (Eqns 5 and 6) remaining in our sample by making a cut based on the measured shower energy. Studies indicate that the electron from e^-p events has much higher energy than from elastic neutrino electron scattering; we require then that the visible shower energy be less than 1500 MeV. Forward photon showers from π^0 production, on the other hand, have energies that peak around 100 MeV. To reduce this contamination, we require that the visible shower energy E_{vis} be at least 150 MeV, and we study separately the regions $150 < E_{vis} < 300$ and $300 < E_{vis} < 1500$.

Using the energy selections mentioned above, the data tagged by dE/dx measurements as "electron" or "photon" events has a dependence on θ^2 as shown in Figures 2 and 3. Note that the kinematic constraint, Eqn. 3, puts a restriction on θ^2 that varies with E such that electrons at $E_{vis} = 1500$ MeV should fall within the first .001 bin of Figure 2, while at $E_{vis} = 150$ MeV the signal extends out to $\theta^2 = .005$ (radians) 2 . On the other hand, photons from reaction (5) should be isotropic in the forward direction or flat in θ^2 . Clearly in both energy regions there is a strong signal in the "electron" sample with an essentially flat background having the same shape as the "photon" events. Shown also in Figs. 2 and 3 are the same distributions for events with associated upstream energy deposit. The θ^2 distribution of these showers is consistent with their being photons from π^0 decay, as mentioned earlier. In figure 4, a plot of $E\theta^2$, we see for the full region $150 < E_{vis} < 1500$ MeV the pronounced signal in the "electron" sample. Note that although

the background is also peaked near zero (due to the predominantly low energy of forward π^0 photons) the signal to noise is better than 2/1.

Using Figures 2 and 3 we can estimate the number of elastic neutrino-electron events in our sample; these numbers are given in Table 2. Together with the early data reported previously⁶, our signal for neutrino-electron scattering totals 69 events. This sample should be compared with the 46 neutrino-electron and 77 antineutrino-electron events reported by the CHARM group⁷.

TABLE 2. Preliminary $\nu_\mu e \rightarrow \nu_\mu e$ data

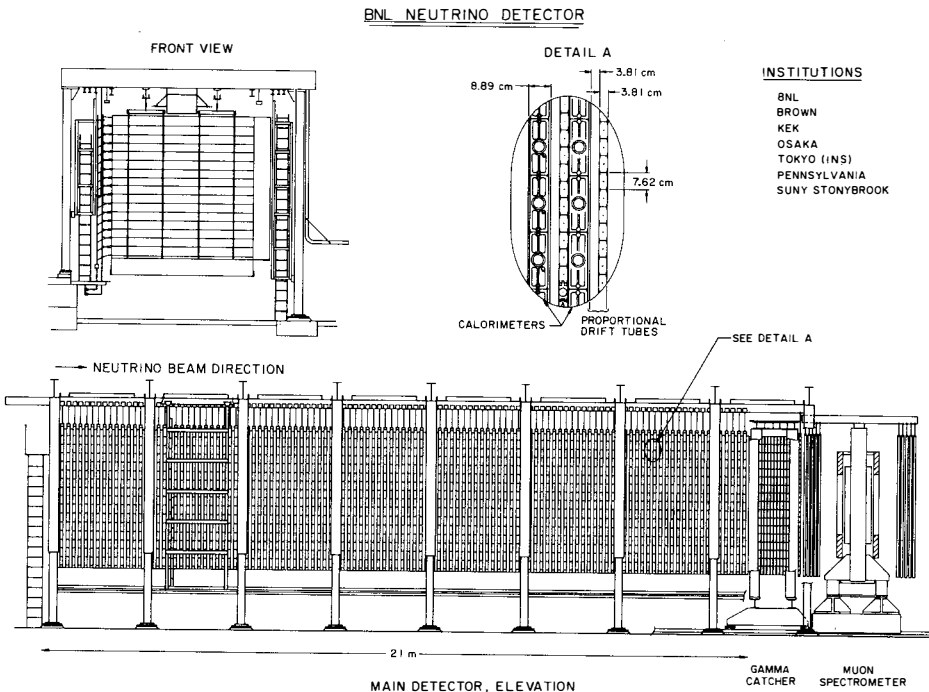
<u>Run</u>	<u>Signal + Background</u>	<u>Est. Background</u>	<u>Signal</u>
June-July '81	23	10	13
Dec-Feb '82			
$150 < E_{vis} < 300$	26	9	17
$300 < E_{vis} < 1500$	55	16	39
$150 < E_{vis} < 1500$	81	25	56
			total 69

Studies are now in progress of the detector performance with test beam electrons. Our signal/background ratio for elastic neutrino electron events, already outstanding, should improve as we understand and optimize our angular and energy resolutions. Analysis of the anti-neutrino data is now underway as is the normalization of the events to a measured quasi-elastic rate. With new data from running later this year we expect to have approximately 120 events of the process $\nu_\mu e \rightarrow \nu_\mu e$ and an equal number of the anti-neutrino electron scattering $\bar{\nu}_\mu e \rightarrow \bar{\nu}_\mu e$. Analysis of this data should provide a direct measurement of $\sin^2 \theta_W$ to better than .02.

REFERENCES

1. R.E. Lanou, Proceedings of the Fifteenth Rencontre de Moriond, Vol. 2, p401.
2. D. Rein and L. Sehgal, Aachen preprint, November 1982.
3. H. Faissner et al, Aachen preprint, 1983.
4. J.G. Morfin, Proceedings of the Europhysics Conference on Electroweak Effects at High Energies, Erice, 1983.
5. P.L. Connolly and D. Cutts, Proceedings of the Topical Conference on the Application of Microprocessors to High-Energy Physics Experiments, CERN 81-07, 1981, p290.
6. R.E. Lanou, Proceedings of the International Conference Neutrino '82 (Balaton), Vol. 2, p9.
7. J. Panman, report to this conference.

Figure 1. Diagram of the Brookhaven Neutrino Detector.



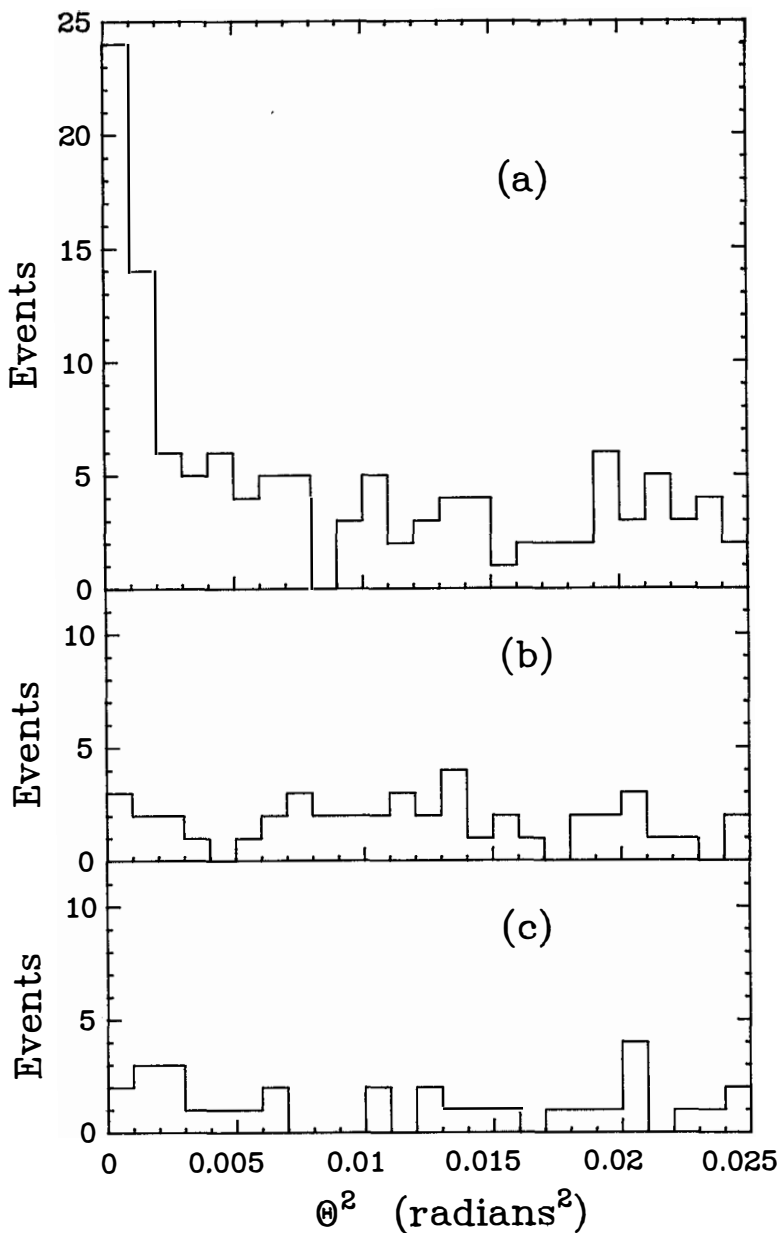


Figure 2. Distribution in Θ^2 for events with $300 < E_{\text{vis}} < 1500$ MeV, and (a) tagged as "electrons", (b) tagged as "photons", and (c) with associated upstream energy deposit.

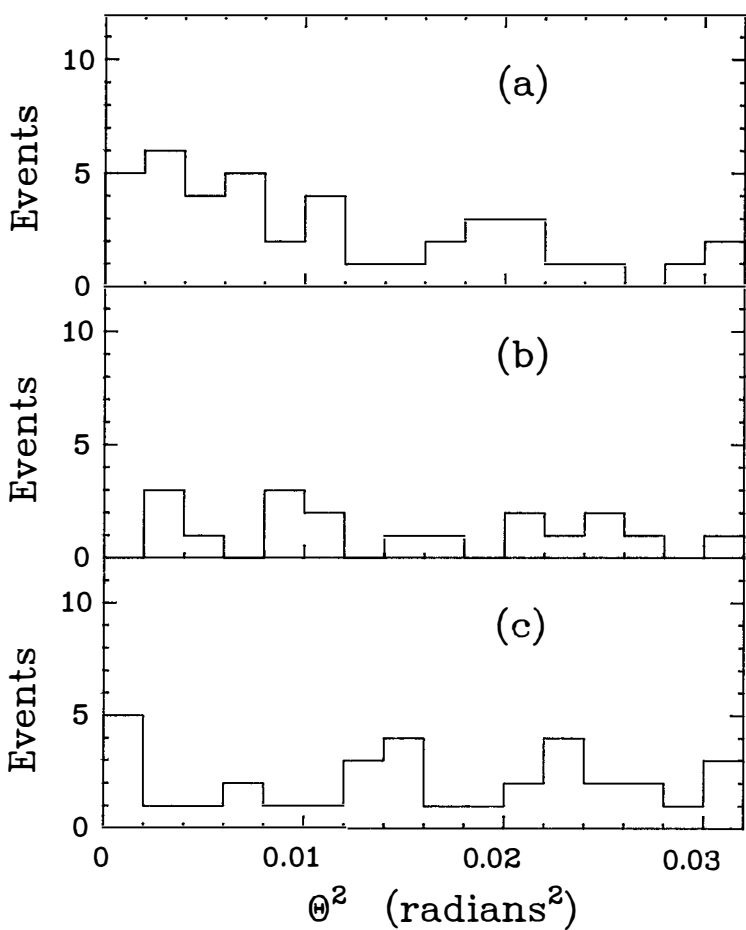


Figure 3. Distribution in θ^2 for events with $150 < E_{\text{vis}} < 300$ MeV, and (a) tagged as "electrons", (b) tagged as "photons", and (c) with associated upstream energy deposit.

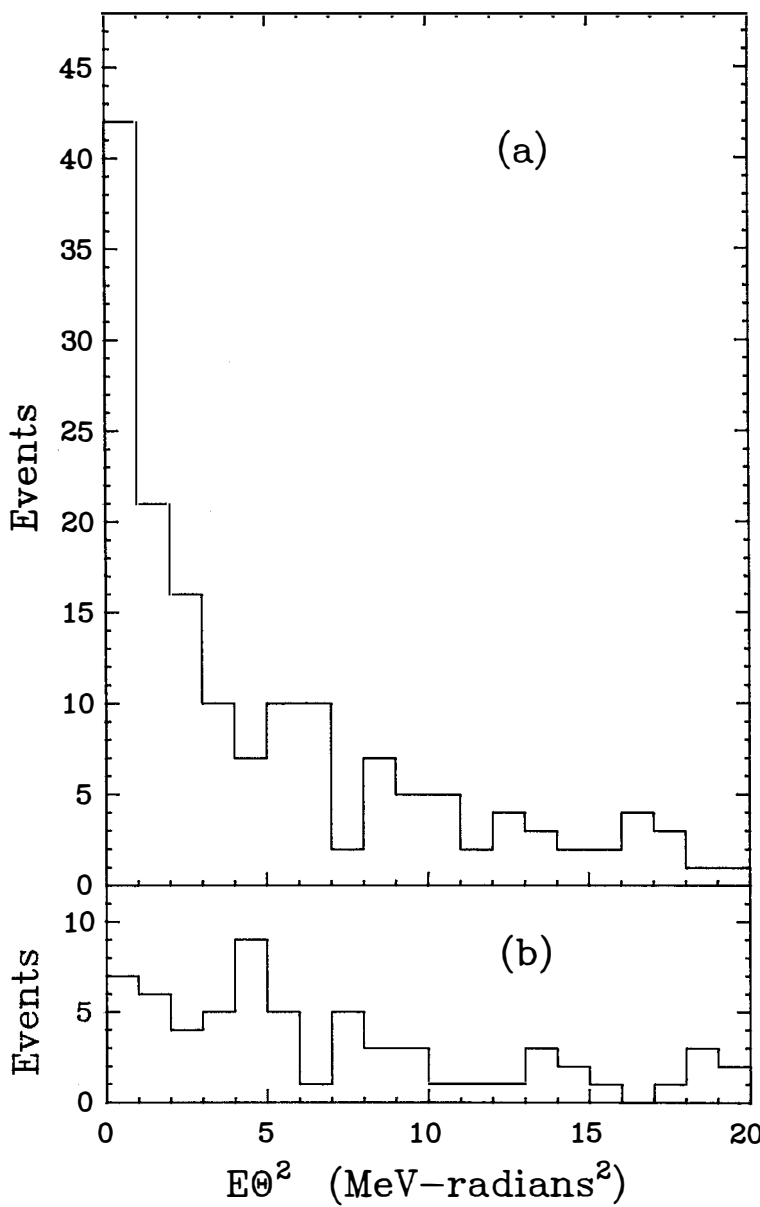


Figure 4. Distribution in E_θ^2 for events with $150 < E_{\text{vis}} < 1500$ MeV, and (a) tagged as "electrons" or (b) tagged as "photons".

STUDY OF A NEW DETECTOR FOR NEUTRINO-ELECTRON SCATTERING

CHARM Collaboration
(presented by J. Panman)
CERN, Geneva, Switzerland



ABSTRACT

A tentative design of a calorimeter dedicated to the study of neutrino-electron scattering is presented. The study is based on the experience of the CHARM Collaboration with such techniques.

Neutrino-electron scattering was discovered ten years ago by the Gargamelle Collaboration¹⁾. Several measurements of the cross sections for neutrino and antineutrino scattering on electrons have been performed in the meantime. Taking all experiments together, about 100 events have been observed in each channel. These results have been important for our understanding of the structure of the weak neutral current. The vector and axial vector coupling constants of the weak neutral current of the electron are determined with a four-fold ambiguity, two sign ambiguities and an ambiguity under the exchange of g_V and g_A . Combining these results with those from $\bar{\nu}_e e \rightarrow \bar{\nu}_e e$ scattering²⁾ and from $e^+ e^- \rightarrow \mu^+ \mu^-$ at PETRA³⁾ a unique solution emerges, the one predicted by the standard model of electroweak interactions, with $g_A^e = -0.523 \pm 0.035$ and⁴⁾ $\sin^2 \theta = 0.215 \pm 0.043$.

The most precise determination of the value of $\sin^2 \theta$ in the leptonic sector has been obtained by the CHARM Collaboration⁴⁾, making use of the direct relation between the ratio of $\sigma(\nu_e e)$ and $\sin^2 \theta$,

$$R = \frac{\sigma(v_\mu e)}{\sigma(\bar{v}_\mu e)} = 3 \frac{1-4\sin^2\theta + (16/3)\sin^4\theta}{1-4\sin^2\theta + 16\sin^4\theta}.$$

In the vicinity of $\sin^2\theta = 0.22$ this relation gives $\Delta\sin^2\theta \sim 0.1 \Delta R$ and, hence, a very precise determination of the mixing angle. The detection efficiency cancels in the ratio and many systematic uncertainties are reduced. Using their upgraded detector, incorporating now measurements of the shower barycentre in two orthogonal projections behind each target plate, the CHARM Collaboration will further improve the accuracy of this result, and expects to reach a statistical precision of $\Delta\sin^2\theta \sim \pm 0.02$ after the wide-band beam run of 1983.

The required precision to be obtained by future experiments can be defined by considering the higher order corrections to $\sin^2\theta$. The electroweak theory predicts the Born term ($Q^2 \sim 0$) of the mass of the Z^0 as a function of $\sin^2\theta$

$$M_{Z^0} = \frac{37.4 \text{ GeV}}{\sin\theta\cos\theta}$$

First order electroweak radiative corrections shift M_{Z^0} by $\sim 5 \text{ GeV}^5$), e.g. for $\sin^2\theta = 0.220 \pm 0.015$, as determined by the CHARM Collaboration from semileptonic neutral current interactions⁶⁾, Wheater and Llewellyn-Smith⁵⁾ predict

$$M_{Z^0} (\text{Born}) = 90 \pm 2.3 \text{ GeV}$$

$$M_{Z^0} (\text{physical}) = 94.6 \pm 2.3 \text{ GeV}$$

and hence a shift of $\sim 5 \text{ GeV}$. A precise experimental determination of this shift would constitute a decisive test of the underlying gauge theory. A significant test could be claimed if the present error on ΔM would be reduced to 0.7 GeV corresponding to an error on $\sin^2\theta$ of $\pm 0.005^7)$.

In order to achieve this sensitivity with this purely leptonic process, the following experimental problems have to be solved

1. EVENT RATE requiring a large fiducial mass and high selection efficiency over a wide window of electron energies;
2. BACKGROUND, dominantly due to quasi-elastic electron-neutrino scattering and to coherent π^0 production⁴⁾ has to be reduced by efficient e/π discrimination and precise measurements of the shower direction;
3. MONITORING of the relative flux of the different beam components v_μ , \bar{v}_μ , v_e and \bar{v}_e is required to determine the ratio of $\sigma(v_\mu e)/\sigma(\bar{v}_\mu e)$.

A tentative design of a new dedicated ($\nu_\mu e$) detector has been discussed by the CHARM Collaboration. It is based on the principle of a fine-grain target-calorimeter and on the accumulated experience of the CHARM Collaboration with instrumentation of this type. The main concern of this study was the question: can the present technique used for $\nu_\mu e$ studies be sufficiently improved to match the aim of $\Delta \sin^2 \theta = 0.005$ or is a new technique required?

The accuracy of shower direction measurements depends mainly on three contributions:

1. On the sampling frequency and on the method used to count the number of shower particles N ;
2. On the plate thickness and grain size of the calorimeter near the vertex;
3. On the lateral shower sampling used to determine of barycentre of the shower.

The limiting accuracy is given by the Z number of the target material

$$\sigma(\theta) \sim Z/\sqrt{E} \text{ const.}$$

The mean Z of the present marble target is 13, with glass a value of ~ 11 could be achieved. In these light targets with a nucleon absorption length of $\Lambda_{\text{abs}} \sim 4$ radiation lengths, electromagnetic and hadronic showers have very similar longitudinal profiles⁸⁾. The CHARM Collaboration has developed a new method to discriminate between electromagnetic and hadronic showers in low Z materials based on the characteristic difference of their lateral profiles (see figure 1). A discrimination by a factor of ~ 100 has been achieved⁸⁾. Figure 2 shows the resolution in shower direction measurements achieved with the present CHARM detector.

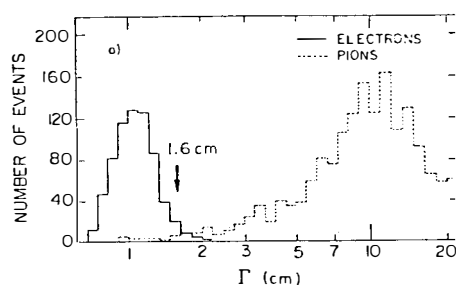


Fig. 1 Distribution of the width Γ of electron and pion induced showers as measured by the lateral energy deposition profile in the scintillator planes of the CHARM I detector

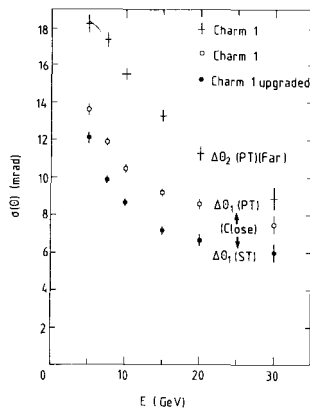


Fig. 2 Measured angular resolution for electron showers in the CHARM I and the upgraded CHARM I detector

The structure of the new, dedicated detector is sketched in figure 3. It consists of 330 modules of $3.5 \times 3.5 \text{ m}^2$ surface area, each composed of a 4 cm thick target plate (marble) and of a plane of streamer tubes with 1 cm wire spacing, read out by crossed cathode strips of 2 cm spacing in two orthogonal projections. Using analog electronics the centroid position of a track or a shower can be reconstructed with $\pm 2 \text{ mm}$ accuracy. Simulating this structure using Monte Carlo methods (EGS) we find an angular resolution of $\sigma(\theta) \sim 16 \text{ mrad}/\sqrt{E}/\text{GeV}$ and an energy resolution of $\sigma(E)/E \sim 20\%/\sqrt{E}/\text{GeV}$. Hence, we expect a reduction of background proportional to $\sigma^2(\theta)$ by a factor of ~ 9 .

The choice made of analog versus digital readout of strips is illustrated in figure 4. This configuration has a fiducial target weight of ~ 320 tons, whereas the CHARM I detector has 70 tons.

Monitoring of the beam composition has been studied in detail for the CHARM I experiments using quasi-elastic $\nu_\mu(\bar{\nu}_\mu)$ events. This method can be extended to lower neutrino energies by restricting the value of Q^2 to a small value to

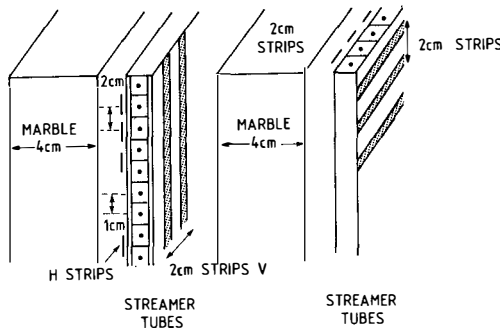


Fig. 3 Schematic sketch of a new dedicated CHARM II detector

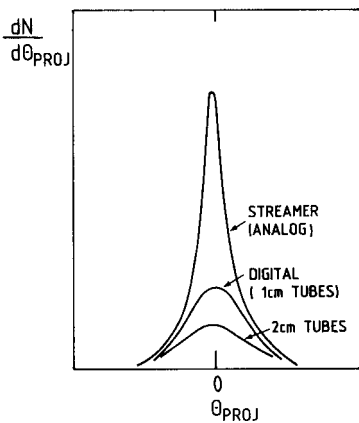


Fig. 4 Shower profile sampling by detectors with analog and with digital measurements

equalize the cross sections for the neutrino and the antineutrino induced reactions. The CHARM II detector, combined with a muon spectrometer, will therefore directly monitor the flux ratio $\phi(\nu_\mu)/\phi(\bar{\nu}_\mu)$ to $\pm 2\%$, required to evaluate the ratio R and the neutrino spectra.

Electron neutrino-electron scattering has a ten times higher cross section than $\nu_\mu e$ scattering. The beam contains approximately 2% electron neutrinos and antineutrinos. Aiming at a 5% measurement of R requires a knowledge of the $(\nu_e + \bar{\nu}_e)$ flux to better than $\pm 10\%$. We think that this can be achieved by making dE/dx measurements in the plane following the vertex, at angles outside the forward peak. We have also been able to recognize inclusive $\nu_e N \rightarrow e X$ events with $y < 0.6^8$) in the CHARM I calorimeter.

We summarize this study in Table 1 which gives the selection criteria, the angular resolution, the rate and background for $\bar{\nu}_\mu e$ scattering which would be obtained for 10^{19} protons on target.

The same statistics for $\nu_\mu e$ would be obtained with $5 \cdot 10^{18}$ protons. Hence, we expect to measure

$$R = \frac{N(\nu_\mu e)}{N(\bar{\nu}_\mu e)} \times F = \frac{1364 \pm 40}{1364 \pm 40} (F \pm 2\%) = \bar{R} \pm 5\% ,$$

corresponding to $\Delta \sin^2 \theta = \pm 0.005$.

Table 1

Rates and background of $\bar{\nu}_e$ scattering in CHARM I and in CHARM II for 10^{19} protons

Selection	CHARM I	CHARM II
Rate for $7.5 < E_e < 30$ GeV	154 ± 27	909 ± 33
Σ_e (1 hit)	61%	90%
$\sigma(\theta)$ at $E_e = 15$ GeV	12 mrad	4 mrad
Signal/background	1/2	1/0.22
Rate for $2.5 < E_e < 30$ GeV		1364 ± 40

An additional physics result may be obtained on the value of ρ , derived from a measurement of the ratio of cross sections for $\nu_\mu e \rightarrow \nu_\mu e$ and for $\nu_\mu e \rightarrow \mu^- \nu_e$. The flux monitoring is now internal and, apart from systematic uncertainties due to background subtraction, electron detection efficiency and spectrum determination, the statistical error of ρ would be $\pm 2\%$.

The main conclusion that we draw from this study is that the experiment seems to be feasible using the presently developed fine-grain calorimeter technique. Of course, many details have to be investigated further, mainly to optimize the performance to cost ratio. In particular, the combination of digital and analog readout and the use of a different plate thickness are considered.

REFERENCES

1. F.J. Hasert et al., Phys. Letters 46B (1973) 121.
J. Blietschau et al., Nucl. Phys. B114 (1976) 189.
2. F. Reines et al., Phys. Rev. Letters 37 (1976) 315.
3. See e.g. A. Böhm, DESY 82-084, December 1982, and
M. Davier, LAL 82/93, Oct. 1982.
4. F. Bergsma et al. (CHARM Collaboration) Phys. Letters 117B (1982) 272.
5. J. Wheater, C.H. Llewellyn-Smith, Phys. Letters 105B (1981) 265.
6. K. Winter, in Workshop on Weak Interactions, Javea (Spain), September 1982.
7. A.N. Diddens et al. (CHARM Collaboration) Nucl. Instr. Meth. 178 (1980) 27
M. Jonker et al. (CHARM Collaboration) Nucl. Instr. Meth. 200 (1982) 183.
8. F. Bergsma et al. (CHARM Collaboration) CERN-EP/82-206 and Phys. Letters 122B (1983) 465.

MEASUREMENT OF THE NEUTRAL CURRENT COUPLING CONSTANTS
IN (ANTI-)NEUTRINO INTERACTIONS WITH DEUTERIUM

Amsterdam - Bergen - Bologna - Padova - Pisa - Saclay - Torino WA25 Collaboration

P.H.A. van Dam

NIKHEF, P.O. Box 41882, 1009 DB Amsterdam, The Netherlands



Abstract: The neutral to charged current cross section ratios for ν_μ - and $\bar{\nu}_\mu$ -interactions with proton and neutron separately have been measured in BEBC, filled with deuterium and exposed to the CERN SPS wideband beams. From these ratios the neutral current chiral coupling constants are determined. From the observed neutral current cross section ratio for ν_μ -interactions on proton and neutron the ratio between the left-handed coupling constants is obtained.

In the framework of the quark parton model the neutral to charged current cross section ratios can be written as [1]:

$$R^k = f_1^k u_L^2 + f_2^k d_L^2 + f_3^k u_R^2 + f_4^k d_R^2 \quad (1)$$

where $k = (\nu_\mu p), (\nu_\mu n), (\bar{\nu}_\mu p), (\bar{\nu}_\mu n)$.

The coefficients f^k can be derived from the integrals of quark density distributions. The neutral current chiral coupling constants u_L^2 , d_L^2 , u_R^2 and d_R^2 were introduced by Bjorken and Sehgal [2,3]. We have measured for the first time the four ratios R^k simultaneously in one experiment. This uniquely determines the values of the four coupling constants.

In this experiment the bubble chamber BEBC filled with deuterium was exposed to the CERN SPS wideband neutrino and antineutrino beams, obtained from 400 GeV protons. This analysis is based on a sample of 38000 and 125000 pictures taken in the ν_μ - and $\bar{\nu}_\mu$ -beam, respectively. An event is classified as a charged current interaction (CC) if it contains at least one particle with momentum larger than 4 GeV/c, identified as a muon by hits in both planes of the external muon identifier (EMI) [4]. Otherwise it is classified as a neutral current candidate (NC). For further analysis only events with total visible hadronic energy E_h larger than 5 GeV are used. An event is classified initially as occurring on neutron (proton) if its charged multiplicity, excluding backward spectator protons, is even (odd). To correct for forward spectators and deuteron rescattering effects event weights are used as in [5]. The rescattering probability is taken to be 0.12 ± 0.03 [6].

Important corrections have to be applied to the raw number of events. They come primarily from two different sources:

- the limited geometrical acceptance of the EMI and its electronic inefficiency lead to a loss of CC events and a contamination of the NC sample.
- neutrino interactions in the material in front of the bubble chamber produce neutral hadrons (neutrons and K_L^0) which may interact inside the chamber and contaminate the NC sample.

The geometrical acceptance of the EMI as a function of the momentum of the muon, its angle with the beam direction and its charge, is determined with a simulation program which uses the spatial distribution of the neutrino interactions as input. The electronic efficiency of the EMI is determined from a sample of throughgoing muons and turns out to be $97 \pm 1\%$. Using the geometrical acceptance table and the electronic efficiency the loss of CC-events and the contamination in the NC-sample are calculated starting from the observed CC events. Since the EMI-acceptance drops sharply for muons with momentum smaller than 4 GeV/c, a different method of correction is needed there. This

correction is calculated using a Monte Carlo program which properly reproduces the observed features of the CC events with muon momentum larger than 4 GeV/c.

The correction of the NC sample for hadron induced events is performed using the B/AS method [9]. This method starts by attempting to associate NC candidates to upstream interactions visible in the bubble chamber. The number of events associated to an invisible origin (in front of the bubble chamber) is obtained by multiplying the number of associated events with a factor B/AS. This factor is calculated with a Monte Carlo program. Its value depends primarily on the density of matter in front of the bubble chamber (including its wall) and the density of the bubble chamber liquid. It also depends on the energy spectrum and the angular distribution of the neutral hadrons produced in the neutrino interactions. These quantities can be determined from the observed events and are used as input to the Monte Carlo program.

The corrections for unidentified muons and hadron induced events are large with respect to the number of observed events and produce considerable systematic uncertainties. As pointed out earlier [10] their effect can be strongly reduced by taking advantage of the following facts, observed in CC events:

- a) in a neutrino interaction the total transverse momentum with respect to the beam direction is smaller than the transverse momentum of the hadronic system alone.
- b) the transverse momentum of an individual hadron is smaller than the transverse momentum of the total hadronic system (P_h^t).

Consequently, by considering only events with P_h^t larger than some cutoff value the influence of the background can be drastically reduced. From the observed NC to CC ratio as a function of the cutoff value it was decided to use only events with P_h^t larger than 1.5 GeV/c.

Further corrections have to be applied for: hadrons being incorrectly identified as muon due to background hits in the EMI or decay in flight, interactions caused by the electron (anti)neutrino background in the beam and scanning losses.

After these corrections the CC sample is pure and complete. The corrected NC sample however still contains a mixture of ν_μ - and $\bar{\nu}_\mu$ -induced NC events. In the neutrino beam the $\bar{\nu}_\mu$ -background in the NC sample is small as indicated by the number of observed $\bar{\nu}_\mu$ -induced CC events (2% of the ν_μ -induced CC). The correction to the NC sample is calculated from the corrected number of $\bar{\nu}_\mu$ -induced CC events, using values of 0.25 and 0.50 for $R^{\nu p}$ and $R^{\bar{\nu} n}$ respectively. Since these corrections are relatively small the final values of $R^{\nu p}$ and $R^{\bar{\nu} n}$ are not sensitive to this correction. In the antineutrino beam the background in the NC sample is large and enhanced by the cuts in E_h and P_h^t : the

observed number of ν_μ -induced CC events is $\sim 40\%$ of the number of $\bar{\nu}_\mu$ -induced CC events. The correction to the NC sample is calculated from the corrected number of ν_μ -induced CC events using the values for $R^{\nu n}$ and $R^{\nu p}$ found in the neutrino beam.

The completely corrected numbers of events with $E_h > 5$ GeV and $P_h^t > 1.5$ GeV/c are :

	CC on proton	CC on neutron	NC on proton	NC on neutron
ν_μ -induced	814 ± 41	1801 ± 50	400 ± 32	461 ± 35
$\bar{\nu}_\mu$ -induced	817 ± 33	355 ± 22	211 ± 29	201 ± 31

The resulting values for the neutral to charged current cross section ratios are :

$$R^{\nu p} = 0.49 \pm .05$$

$$R^{\bar{\nu} p} = 0.26 \pm .04$$

with $E_h > 5$ GeV

$$R^{\nu n} = 0.26 \pm .02$$

$$R^{\bar{\nu} n} = 0.57 \pm .09$$

and $P_h^t > 1.5$ GeV/c

$$R^{\nu N} = 0.33 \pm .02$$

$$R^{\bar{\nu} N} = 0.35 \pm .04$$

The given errors are statistical only. The main contributions to the systematic errors come from :

- the uncertainty in the value of B/AS, used to calculate the hadron induced background. This introduces an uncertainty of $\sim 5\%$ in all the ratios, but with complete positive correlation.
- the uncertainty in the EMI-efficiency. This introduces an uncertainty of $\sim 3\%$ in all the ratios, again with complete positive correlation.
- the uncertainty in the rescattering probability. This introduces an uncertainty of $\sim 3\%$ only in $R^{\nu p}$ and $R^{\bar{\nu} p}$, with complete positive correlation.

The ratios on deuterium agree with results obtained on neon [11] ($R^{\nu N} = 0.345 \pm .015$ and $R^{\bar{\nu} N} = 0.364 \pm .029$) and with results obtained on other isoscalar targets [12,13]. The value for $R^{\nu p}$ agrees with results obtained in hydrogen [10,14] ($0.51 \pm .04$).

To obtain the values of the chiral coupling constants from the four ratios on proton and neutron equation (1) has to be solved. The coefficients f^k are calculated using the values of the integrals of the quark density distributions U , $\bar{U} + S$, $\bar{D} + S$ and U/D measured previously in this experiment [6,15]. The contribution of the strange quarks is taken into account using the value of S/D given in [16]. The effect of the cuts in E_h and P_h^t on the coefficients f^k is determined with the previously measured Monte Carlo program [7,8] which

properly reproduces the features of the observed CC events. This program uses the parametrization of Buras and Gaemers [7] for the dependence of the quark density distributions on the Bjorken variable x .

The resulting values for the coupling constants are :

$$\begin{aligned}
 u_L^2 &= 0.15 \pm .04 & u_L^2 + d_L^2 &= 0.33 \pm .03 \\
 d_L^2 &= 0.18 \pm .04 & u_R^2 + d_R^2 &= 0.02 \pm .02 \\
 u_R^2 &= 0.03 \pm .02 & u_L^2 - d_L^2 &= -.03 \pm .07 \\
 d_R^2 &= -0.01 \pm .02 & u_R^2 - d_R^2 &= .04 \pm .04
 \end{aligned}$$

The error includes the effect of the statistical uncertainties in the ratios and in the values of the quark densities used to calculate the coefficients f^k . It also includes the effect of the previously mentioned systematic uncertainties. The values of the sums of the couplings agree with results obtained on other isoscalar targets [11,12,13]. The values found for u_L^2 and d_L^2 are in good agreement with the ones obtained by combining R^{vp} measured in hydrogen with R^{vN} and $R^{v\bar{N}}$ measured in neon [11] ($u_L^2 = 0.15 \pm .04$ and $d_L^2 = 0.19 \pm .05$).

In the Glashow-Weinberg-Salam model [17] the coupling constants depend on one common parameter : $\sin^2 \theta_w$. From a fit of the coupling constants we obtain $\sin^2 \theta_w = 0.19 \pm .03$ with $\chi^2 = 1.2$ for 3 degrees of freedom.

The systematic uncertainty in $\sin^2 \theta_w$ is of the order of .02.

Since the righthanded coupling constants are relatively small, the ratio between the lefthanded coupling constants can be obtained directly from the observed neutral current cross section ratio between ν_μ -induced interactions on proton and neutron. Following a procedure similar to the one used to obtain the individual coupling constants we find

$$\frac{u_L^2}{d_L^2} = 0.66 \pm .21 \pm .13$$

This result is not sensitive to the uncertainties in the integrals of the quark density distributions. The systematic error comes only from the uncertainty in the rescattering probability.

References

- [1] P.Q. Hung and J.J. Sakurai, Ann.Rev.Nucl.Sci. 31 (1981) 375.
- [2] J.D. Bjorken, Proc. Summer Institute on Particle Physics, SLAC-198, page 1. Stanford, California.
- [3] L.M. Sehgal, Phys.Lett. 71B (1977) 99.
- [4] R. Beuselinck et al., Nucl.Instr. and Meth. 154 (1978) 445.
- [5] J. Hanlon et al., Phys.Rev.Lett. 45 (1980) 1817.
- [6] D. Allasia et al., Phys.Lett. 107B (1981) 148.
- [7] A.J. Buras and K.J.F. Gaemers, Nucl.Phys. B132 (1978) 249
Phys.Lett. 71B (1977) 106.
- [8] A. Grant, Nucl.Instr. and Meth. 131 (1975) 167.
- [9] W.F. Fry and D. Haidt, CERN yellow report 75-1, CERN, Geneva.
- [10] J. Blietschau et al., Phys.Lett. 88B (1979) 381.
- [11] P. Bosetti et al., "Measurement of the ratios of neutral current to charged current cross sections of neutrino and antineutrino interactions in Ne". Submitted to Nucl.Phys. B.
- [12] M. Jonker et al., Phys.Lett. 99B (1981) 265.
- [13] M. Holder et al., Phys.Lett. 72B (1977) 254.
- [14] N. Armenise et al., Phys.Lett. 122B (1983) 448.
- [15] D. Allasia et al., Phys.Lett. 117B (1982) 262.
D. Allasia et al., "Measurement of the ν_u - and $\bar{\nu}_u$ -nucleon charged current total cross sections". Paper submitted to the 21st Int. Conf. on High Energy Physics, Paris 1982.
- [16] M. Jonker et al., Phys.Lett. 107B (1982) 241.
- [17] S. Weinberg, Phys.Rev.Lett. 19 (1967) 1264.
A. Salam, Proc. 8th Nobel Symp., Ed. N. Svartholm (Stockholm, 1968).

APPLICATION OF A MULTIVARIATE DISCRIMINANT ANALYSIS
TO HIGH ENERGY PHYSICS IN BUBBLE CHAMBERS

W. Van Doninck
Inter-University Institute for High Energies,
ULB-VUB, Brussels, Belgium



ABSTRACT

Two examples are given of the application of a multivariate discriminant analysis to high energy physics. The first one concerns the measurement of the neutral to charged current cross section ratio for ν_{μ} interactions on free protons. The second application is related to the detection of tau-neutrinos in bubble chambers.

The multivariate discriminant analysis is a standard mathematical method for dealing with problems of pattern recognition^{1,2)}. The basic ideas behind its application to the analysis of bubble chamber events as presented here, are the following : Every event can be characterised by a "pattern" vector $V(x_1, \dots, x_n)$ in a n dimensional space where x_1, \dots, x_n are measured kinematical variables. Different event types, like for instance charged and neutral current ν_μ interactions, are then expected to have on average a different "pattern" and hence to cluster in different domains of the multidimensional space. If the spread of the clusters is small compared to the separation between them, individual event assignment becomes possible. These basic ideas are illustrated schematically in a simplified 2 dimensional example in figure 1 where two sets of "events" (dots and crosses) are shown in a scatter plot spanned by the variables x and y . It is clearly impossible to isolate any "event" type in a clean way by a cut in either x or y , whereas this is trivially achieved by a cut along the "discriminant axis" spanned by a single "canonical variable" $CNVR = ax + by$. In a multidimensional space and using real events, the situation will of course be less trivial but the problem essentially boils down to :

- The choice of the kinematical variables used to span the multidimensional space. Clearly, the separation of the clusters will improve, the better the individual "discrimination power" of these variables. Discrimination power which depends upon the mean value and the variance of the considered variable for the different event categories.
- The optimal choice of the "discriminant axis".
- The optimal choice of the "separation hyperplane".

The major ingredients required to achieve this with the help of "initial sets" are given in the next section. The initial sets consist of events whose assignment to one of the event categories is unambiguously known.

1. MATHEMATICAL FRAMEWORK

Only a brief survey will be given here, details can be found in the literature on the multivariate discriminant analy-

sis^{1,2}).

Consider a P dimensional space S^P and N events i.e. N vectors in S^P.

A metric in S^P can be defined in the following way :

$$d^2(a, b) = \sum_{i,j}^P q_{ij} (a_i - b_i)(a_j - b_j) = (a - b)' Q (a - b)$$

where Q is a symmetric and definite positive matrix.

The "compactness" of a group or cluster is defined as :

$$D^2 = \frac{1}{N(N-1)} \sum_{i,j}^N d^2(x_i, x_j) = \frac{1}{N(N-1)} \sum_{i,j}^N (x_i - x_j)' Q (x_i - x_j)$$

It can be shown²⁾ that this quantity is minimal if matrix Q is defined as follows :

$$Q = (\det \Sigma)^{1/P} \Sigma^{-1}$$

where Σ is the variance, covariance matrix. In the case where Q is diagonal, which can always be accomplished by a rotation, the "compactness" becomes :

$$D^2 = \frac{1}{N(N-1)} \sum_{p=1}^P \sum_{i,j}^N w_p^2 (x_{ip} - x_{jp})^2$$

with the "weight" w_p equal to :

$$w_p = \frac{1}{\sigma_p} \left(\frac{\sigma_i}{\sigma_p} \right)^{1/P}$$

from which follows that a variable x_p with large variance σ_p will carry little weight.

Consider now K substructures (groups or clusters) in S^P with N_k events per cluster ($k = 1 \dots K$). Define matrix T (proportional to Q) as follows :

$$T^P \rightarrow t_{\alpha\beta} = \frac{1}{N} \sum_i^N (x_{i\alpha} - \bar{x}_\alpha)(x_{i\beta} - \bar{x}_\beta)$$

called the total variance-covariance. According to a theorem due to Huygens one can write $T = W + B$ with :

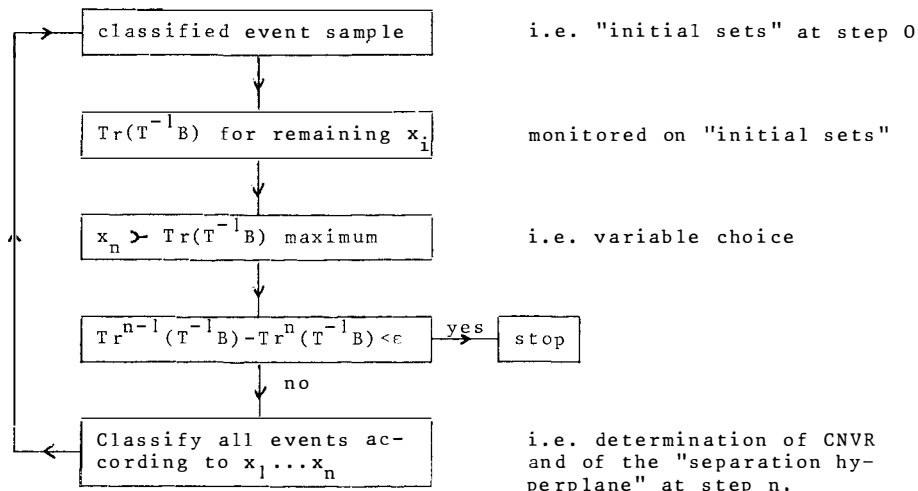
$$W^P \succ w_{\alpha\beta} = \frac{1}{N} \sum_k^K \sum_{i_k}^{N_k} (x_{i_k\alpha} - \bar{x}_{\alpha}^k) (x_{i_k\beta} - \bar{x}_{\beta}^k)$$

$$B^P \succ b_{\alpha\beta} = \sum_k^K \frac{N_k}{N} (\bar{x}_{\alpha}^k - \bar{x}_{\alpha}) (\bar{x}_{\beta}^k - \bar{x}_{\beta})$$

called the variance-covariance "within" and "between" groups, respectively.

The best discrimination of the groups will then occur if $(uBu')/(uWu')$ or equivalently $(uBu')/(uTu')$ is maximal, where u defines a direction in S^P . In this way the "discriminant axis" u is obtained by diagonalisation of $T^{-1}B$ or equivalently $W^{-1}B$. Hence $T^{-1}Bu' = \lambda u'$ where the eigenvectors u are the "discriminant axes" or "canonical variables"; the best one corresponding to the largest eigenvalue λ . The number of "discriminant axes" is given by $\min(K-1, P)$ but a good application of the method requires $P \gg K$.

An approximate flow chart of the discriminant analysis program BMDP³⁾ used here is given below.



2. MEASUREMENT OF R_{μ}^{ν} 4)

As a first example, the multivariate discriminant analysis was used to separate neutral current (NC) from charged current (CC) ν_{μ} interactions and from the background due to interactions of incident neutral hadrons (N^*), in order to measure the ratio (NC/CC) = R_{μ}^{ν} on free protons. The data are from experiment WA24⁵⁾ performed by a collaboration of groups from Bari, Birmingham, Brussels, Ecole Polytechnique, Rutherford Laboratory, Saclay and University College London.

BEBC equipped with a H_2 filled track sensitive target (TST) was exposed to the ν_{μ} wide band beam at the CERN SPS. About 2000 neutral induced interactions have been observed inside the H_2 . The advantage of the TST set up consists in the ability to detect a major part of the final state γ rays ($\sim 60\%$) in the surrounding H_2 -Ne mixture. Kinematical variables depending upon the hadron system will therefore be better measured than in a bare bubble chamber filled with H_2 resulting in a better "discrimination power" of such variables.

Among the variables used to build the multidimensional space, only a few with the best individual "discrimination power" will be defined here. The total longitudinal (p_L^i) and transverse (p_T^i) momenta of the events with respect to the incident ν direction are known to be on average quite different for charged, neutral current and neutral hadron interactions. The variable F has been defined in the following way. For each negatively charged particle i in an event, F_i is calculated as

$$F_i = p_T^i p_L^i p_L^i \left(\sum_{j \neq i} p_T^j {}^2 \right)^{-1/2}$$

where p_T^i and p_L^i are the transverse and longitudinal momenta of particle i with respect to the incident ν direction and p_T^i is the transverse momentum of all the other particles in the event, including detected neutral hadrons and γ rays. F is then defined as the maximum of the F_i and particle i giving this maximal value is called "muon". Similar variables have been used successfully in other experiments⁶⁾ to select charged current interactions in the absence of, or in addition to the information provided by the ex-

ternal muon identifier (EMI). Finally variable ϕ is defined as the supplement of the angle between the projections onto the plane perpendicular to the v direction of the momentum vectors of the selected "muon" and of the remaining "hadron" system. Several other kinematical variables have been determined for each event; with decreasing weight in the discriminant functions they include the transverse momentum out of the plane defined by the "muon" and the incident v direction, the ratio of the transverse momentum of the "muon" and the "hadron" system and so on.

The initial sets have been varied in order to check the stability of the event classification. As an example, the following initial sets have been used; where two alternatives for the initial N_i^* sample are explicitly given.

- CC_i Events with a μ^- identified in the EMI
- NC_i Obtained by removing the μ^- from the previous CC_i set (i.e. dummy event sample)
- N_i^*
 - a) Events yielding a unique 3C fit to :
 $np \rightarrow pp\pi^-$ or $K_L^0 p \rightarrow K^+ p\pi^-$ or $K_L^0 p \rightarrow K^- p\pi^+$
 - b) Neutral induced interactions observed in an exposure of BEBC + TST to a π^- beam ($p_{\pi^-} = 70$ GeV/c).

The event classification refers to 1908 neutral induced interactions occurring inside a 1.8 m^3 fiducial volume of H_2 . Of these, 586 were identified as initial CC events and 147 were attributed to the N_i^* category a). Thus 1175 events remained to be classified. The result of the discriminant analyses using in turn the two different initial samples of neutral hadron interactions as initial set together with CC_i and NC_i is given in table I.

Table I : Event classification via the multivariate discriminant analysis.

↓ Initial set	Event assignment					
	Charged current		Neutral current		Neutral hadron	
N_i^* sample	a)	b)	a)	b)	a)	b)
Unidentified	347	333	421	420	407	422
CC_i	565	565	20	20	1	1
N_i^* a)	6	5	15	23	126	119
NC_i	21	20	358	360	34	33
N_i^* b)	2	1	12	9	57	61

Only the first three rows correspond to events observed in the ν exposure. Within the statistical uncertainties, the event classifications agree no matter which initial N^* sample is used. Also when varying the initial CC and NC sets the event classification remains stable.

To illustrate that the different event types do cluster in different regions of the multidimensional space, figure 2 shows the distribution of the 1908 observed events in the 2 dimensional subspace spanned by the two canonical variables. A threefold structure is clearly exhibited by the data.

Some consistency checks given here indicate the quality of the event samples after discrimination (918 CC; 456 NC; 534 N^*). The y distribution for the 918 events classified as charged currents is shown in figure 3a. It is flat up to $y \approx 0.9$ in contrast to that of the initial CC_i sample shown in figure 3b. The solid curve in figure 3a corresponds to the y distribution of Monte Carlo generated charged currents in which the "muon" was chosen in the same way by maximizing the F variable. The decrease above $y \approx 0.9$ is essentially due to incorrect muon selection in very high y events. This check shows that using a biased initial sample does not necessarily result in a similar bias after classification. To check whether the 456 obtained neutral current events exhibit genuine

neutral current characteristics, the neutral to charged current ratio has been determined as a function of different cuts on the resultant transverse momentum of the hadron system. The presence of an important N^* or unidentified CC contamination would result in a substantial increase of this ratio at low values of the p_{T_H} cut, as demonstrated in ref.⁷⁾. Figure 4 shows that this ratio determined with the event samples after classification is found to be about constant down to the lowest values of the cut-off in p_{T_H} .

When determining R_p^V one has to account for some overlap between the different clusters; and hence for the loss of genuine events from a given category and the migration of events from another group into this given category.

The true numbers of events of the different types are related to the event numbers after classification by the following matrix equation :

$$\begin{pmatrix} CC \\ NC \\ N^* \end{pmatrix} = \begin{pmatrix} CC \rightarrow CC & NC \rightarrow CC & N^* \rightarrow CC \\ CC \rightarrow NC & NC \rightarrow NC & N^* \rightarrow NC \\ CC \rightarrow N^* & NC \rightarrow N^* & N^* \rightarrow N^* \end{pmatrix} \cdot \begin{pmatrix} CC_t \\ NC_t \\ N^*_t \end{pmatrix}$$

The off-diagonal elements in the 3×3 matrix correspond to the forbidden transitions which have been obtained from the initial sets.

Other corrections are due to one prong topologies, $\bar{\nu}_\mu$ contamination, scanning efficiencies etc. The results are summarised in table II.

Table II : Event numbers after the different corrections

	CC	NC
After classification	905	460
After correction for overlaps	896 ± 32	414 ± 30
After all corrections	891 ± 33	419 ± 31

The value for the neutral to charged current cross section ratio for ν_μ interactions on protons is found to be :

$$R_p^\nu = 0.47 \pm 0.04$$

Systematic uncertainties have been investigated and were found to be negligible with respect to the statistical error. The use of the multivariate discriminant analysis made it possible to avoid the severe cuts on the data inherent in previous experiments^{7,8,9)} and hence to reach similar precision to results from experiments disposing of more than three times the statistics of WA24.

Within the framework of the GWS model, the measured cross section ratio R_p^ν is related to $\sin^2 \theta_W$ via the quark-parton model. Following ref. 10) and using $\alpha = \sum \bar{q}_i / \sum q_i = 0.10$ the mixing angle is found to be : $\sin^2 \theta_W = 0.18 \pm 0.04$.

2. ν_τ DETECTION

The aim of this preliminary analysis is to separate the reaction :



from the generally much more abundant process :

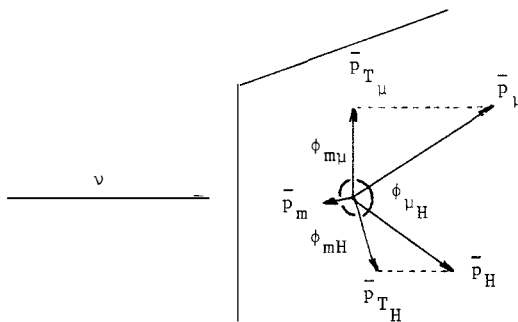


on a purely kinematical basis. In this application, the multivariate discriminant analysis is only used to determine the canonical variable which by construction has the best individual discrimination power.

Charged current ν_μ and ν_τ interactions were generated in BEBC filled with a heavy H₂-Ne mixture, using the LUND Monte Carlo. Fermi motion, measurement errors and the loss of final state neutral hadrons (π^0 , K_L^0 , n) were also simulated. The ν_μ energy spectrum was taken according to the wide band beam at the CERN SPS. The ν_τ were assumed to arise from $\nu_\mu \leftrightarrow \nu_\tau$ oscillations with $\Delta m^2 = 40$ eV². The $\tau \rightarrow \mu \nu \bar{\nu}$ decay was also simulated.

The kinematical variables introduced into the discriminant

nant analysis are defined in the drawing below :



The canonical variable* obtained from the analysis is plotted in figure 5 for 4000 generated ν_μ CC events and 2000 ν_τ CC interactions where the τ has a subsequent decay into $\mu\nu\nu$. The dashed histograms correspond to events where the momentum of the final state muon is below 5 GeV/c. The area of the histogram corresponding to the ν_μ CC events is shown dotted.

The results of the analysis are shown in figure 6 where the efficiency for detecting reaction (1) is given versus the percentage of ν_μ CC events contaminating the ν_τ sample. The curves correspond to a single cut on the canonical variable and can be compared to the combinations of cuts proposed in the literature^{11, 12, 13} which have also been applied to the same Monte Carlo samples:

A¹¹⁾ : $E_\mu > 4$ GeV; $E_H > 5$ GeV; $p_T > 1$ GeV/c; $\phi_{\mu H} > 90^\circ$; $\phi_{mH} > 120^\circ$

B¹²⁾ : $p_T > 2$ GeV/c; $\phi_{mH} > 135^\circ$; $x_{vis} \leq 0.2$

C¹³⁾ : $p_T > 1.6$ GeV/c; $\phi_{mH} > 115^\circ$.

In all cases it is found that a single cut on CNVR is substantially more efficient. The same results obviously also apply to the separation of $\nu_e N \rightarrow e^- H$ and $\nu_\tau N \rightarrow \tau H (\tau \rightarrow e\nu\nu)$ since the kinematics are the same.

$$\begin{aligned}
 * \text{ CNVR} = & 1.46 p_{T_\mu} + 0.08 |p_{T_H}/p_{T_\mu}| - 1.02 (p_{T_H} - p_m) + 0.14 \ln \phi_{m\mu} \\
 & - 0.18 \ln(p_T^2/p_L^2) - 0.12 \ln(p_m^2/p_L^2) - 3.54
 \end{aligned}$$

ACKNOWLEDGEMENTS

The author wishes to acknowledge his colleagues from the WA24 experiment⁵⁾ for a fruitful collaboration. He expresses his special thanks to J. Moreels and C. Vander Velde-Wilquet for their important contribution to the analysis of respectively, the NC/CC ratio and the ν_τ detection. Prof. Tran Thanh Van and the organising committee are kindly acknowledged for the hospitality at La Plagne.

REFERENCES

- 1) M.G. Kendall and A. Stuart
The advanced theory of statistics (Hafner, New York).
- 2) J.M. Romeder
Méthodes et programmes d'analyse discriminante (Dunod, Paris).
- 3) BMDP UCLA (University of California Press, 1979)*.
- 4) N. Armenise et al., Phys. Letters 122B (1983) 448.
- 5) N. Armenise, M. Calicchio, O. Erriquez, M.T. Fogli-Muciaccia, S. Natali, S. Nuzzo, F. Ruggieri (Bari); R. Belusevic, D.C. Colley, G.T. Jones, S. O'Neale, S. Sewell, M.F. Votruba (Birmingham); D. Bertrand, J. Moreels, J. Sacton, C. Vander Velde-Wilquet, W. Van Doninck (Brussels); V. Brisson, T. François, P. Petiau (Ecole Polytechnique Palaiseau); A. Cooper, J.G. Guy, A.G. Michette, M. Tyndell, W. Venus (Rutherford); J.P. Baton, G. Gerbier, C. Kochowski, M. Neveu (Saclay); H. Alamatsaz, T. Azemoon, J.H. Bartley, A. Parker (University College London)
- 6) J.W. Chapman et al., Phys. rev. D14 (1976) 5.
- 7) J. Blietschau et al., Phys. Letters 88B (1979) 381.
- 8) F.A. Harris et al., Phys. Rev. Lett. 39 (1977) 437.
- 9) T. Kafka et al., Phys. Rev. Lett. 48 (1982) 910.
- 10) J.E. Kim et al., Rev. Mod. Phys. 53 (1981) 211.
- 11) C.H. Albright et al., Phys. Rev. D 20 (1979) 2177.
- 12) D. Bogert et al., FNAL proposal P 656.
- 13) U. Camerini et al., FNAL proposal ν_e beam.

* Program developed at the Health Sciences Computing Facility, UCLA. Sponsored by NIH Special Research Resources Grant RR-3.

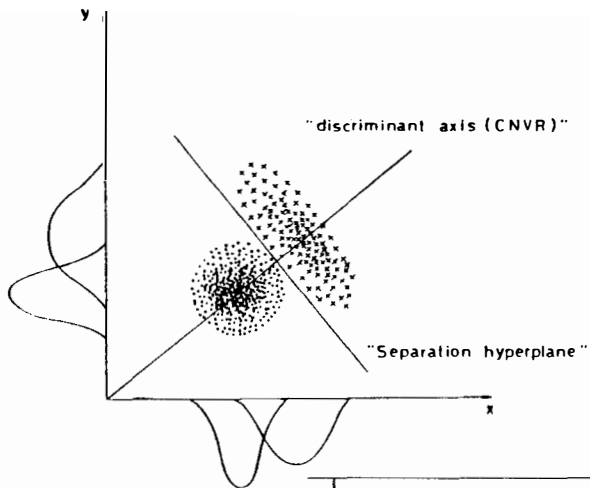
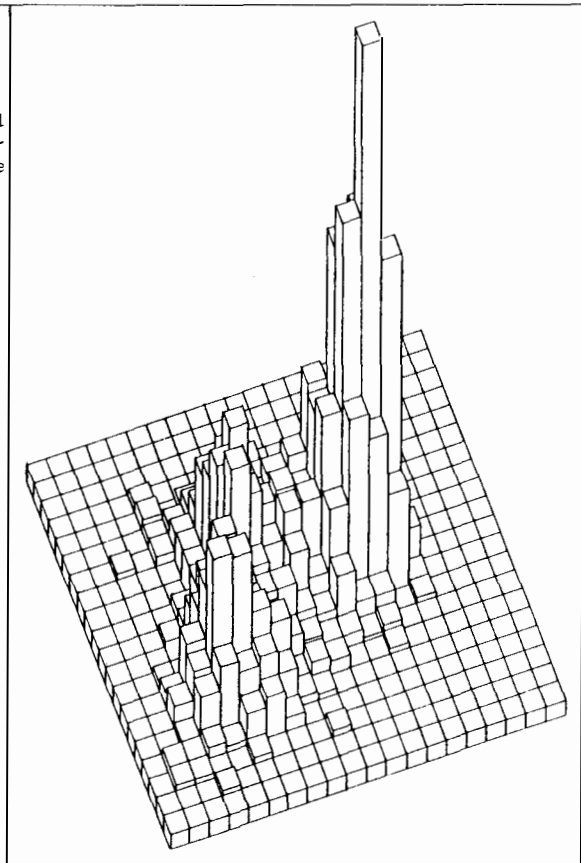


Fig. 1 : schematical 2 dimensional illustration of the discriminant analysis

Fig. 2 : Display of all the events observed inside the TST versus the two orthogonal canonical variables



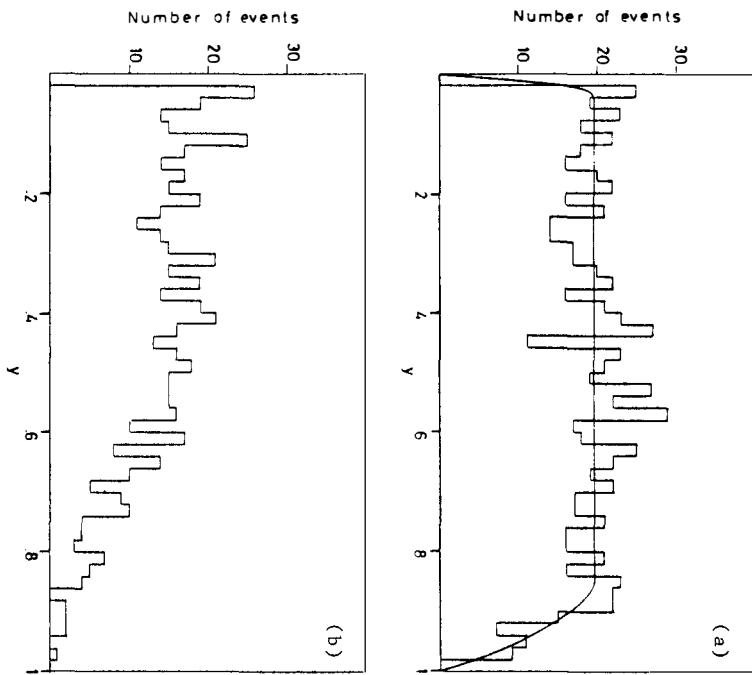
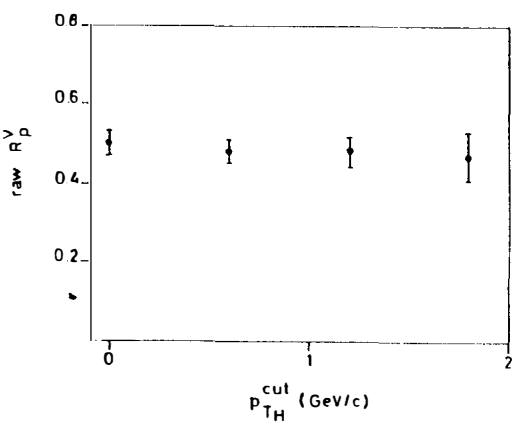


Fig. 3 : The y distribution of (a) CC events after classification. The solid line corresponds to the Monte Carlo events; (b) the initial CC sample

Fig. 4 : The ratio NC/CC as a function of different cut-offs in $p_{T_H}^{\text{cut}}$



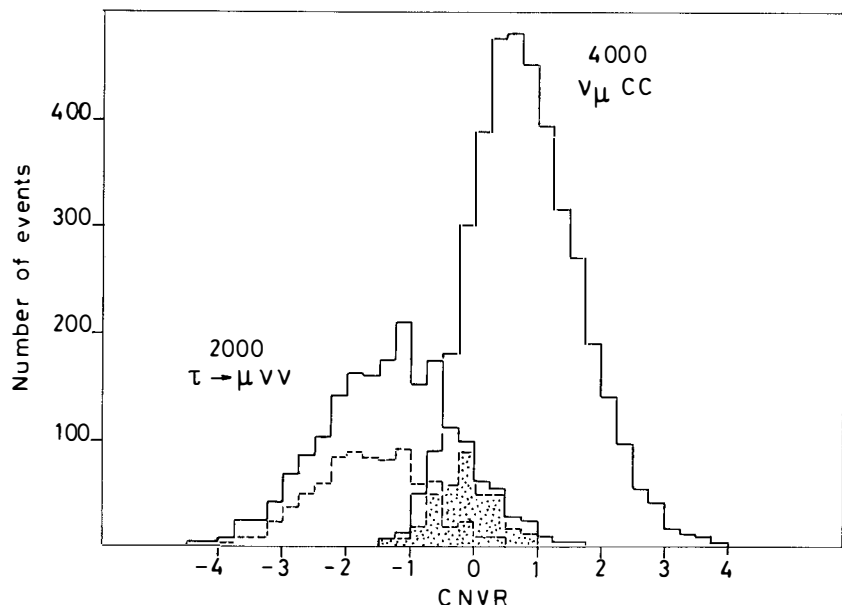


Fig. 5 : Distribution of the canonical variable for charged current ν_τ and ν_μ interactions (solid). The dashed histograms correspond to events with $p_\mu < 5$ GeV/c.

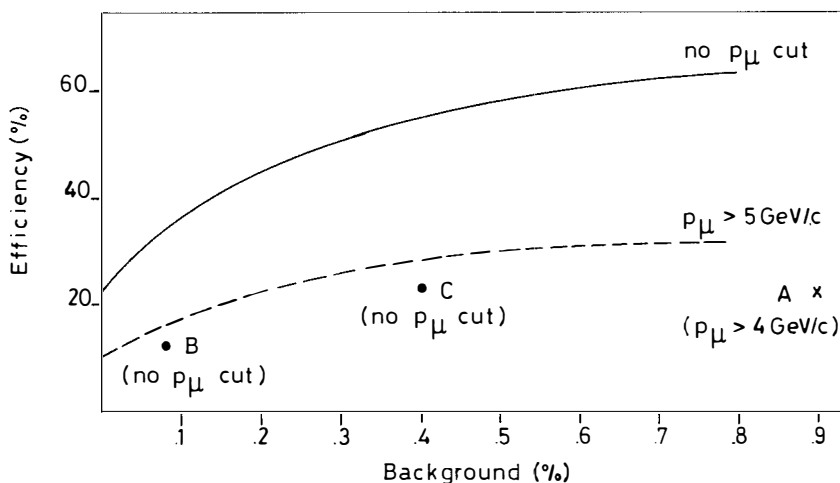


Fig. 6 : Efficiency for ν_τ detection versus the fraction of CC ν_μ events contaminating the sample.

SEARCH FOR RIGHT-HANDED CURRENTS IN MUON DECAY*

Bruno Gobbi

Department of Physics and Astronomy, Northwestern University
Evanston IL 60201, USA

Abstract

We report preliminary results of an experiment designed to measure the mass of the right-handed intermediate vector boson. The presence of such a particle in electroweak interactions is predicted by left-right symmetric gauge theories. The experiment measures the momentum spectrum of the positrons from the decay at rest of 1) longitudinally polarized muons produced in the decay at rest of $\pi^+ + \mu^+ \nu$ (polarization P_μ) and 2) unpolarized muons. The endpoints of these two spectra are used to determine the quantity ξP_μ where ξ is a Michel parameter. This product is related to the ratio of the mass of left and right handed W and to the phase between the two helicity states. We measure, at the 90% CL, $1 - \xi P_\mu \frac{\delta}{\beta} < 0.0041$ and infer the mass $M(W_R) > 380 \text{ GeV}/c^2$.

The present standard model of weak and electromagnetic interactions is based on the gauge group

$$SU(2)_L \times U(1).$$

The V-A character of β and μ decay is imposed on the theory by allowing only left handed components of fermions to couple to intermediate vector bosons (W_L^\pm). The possibility that both left-handed and right-handed fermions participate in β decay has been suggested 1)2)3) and models have been proposed for which the weak interaction is left-right symmetric at the lagrangian level. These models are

*) J. Carr, G. Gidal, A. Jodidio, K.A. Shinsky, H.M. Steiner
D. Stoker, M. Strovink, and R.D. Tripp, U. of Calif. Berkeley
and B. Gobbi, Northwestern U. and C.J. Oram, TRIUMF.

based on the gauge group

$$SU(2)_L \times SU(2)_R \times U(1)$$

which is completely left-right symmetric, except for the masses of the Higgs scalars. Due to spontaneous symmetry breaking the mass of the right-handed charged meson W_R is much heavier than the W_L and its effects are then manifest slow below the energy scale of the W_R mass. The V-A character of the interaction is the result of a natural suppression of right-handed gauge current. The mass eigenstates W_1 and W_2 are linear combinations of the helicity eigenstates W_L and W_R :

$$W_1 = W_L \cos\varsigma - W_R \sin\varsigma ,$$

$$W_2 = W_L \sin\varsigma + W_R \cos\varsigma .$$

It is this mixing and mass splitting that induces the observed parity violation. At an energy scale much larger than the W_R mass all interactions are supposed to be parity conserving.

The experiment described here is an attempt to measure the mass of the right handed gauge boson (W_R). The present experiment searches for the W_R by examining its effects on the decay $\mu^+ + e^+ \bar{\nu}_\mu \nu_e$. With this approach the sensitivity achievable with a very high energy experiment is obtained at low energy with a very precise measurement.

The mixing angle ς between left and right handed currents and α , the square of the ratio of the W 's masses,

$$\varsigma \equiv (W_L - W_R) \text{ mixing angle}$$

$$\alpha \equiv M^2(W_L)/M^2(W_R) \quad (1)$$

are the phenomenological parameters which provide a convenient physical description of right-handed charged-current.²⁾ These two quantities which parametrize the amount of V+A are related to correlations measured in weak decays. [See M. Strovin⁴⁾ for a summary of experiments sensitive to V+A.]

The experiment we describe here is a measurement of the e^+ momentum spectrum from the decay of longitudinally polarized μ^+ . Such a spectrum, after summing over positron spins, assuming zero mass neutrinos and neglecting radiative corrections is described by the following expression:

$$\frac{d^2\Gamma}{x^2 dx d\cos\theta} \sim (3-2x) + \left(\frac{4}{3}\rho-1\right)(4x-3) + 12\left(\frac{m_e}{m_\mu}x\right)(1-x)\eta - \left[(2x-1) + \left(\frac{4}{3}\delta-1\right)(4x-3)\right]\xi P_\mu \cos\theta . \quad (2)$$

The variable x is the reduced positron momentum ($x \equiv p(e^+)/p(e^+)_{\text{max}}$), θ is the angle between μ^+ spin and the e^+ momentum and P_μ is the polarization of the μ^+

from π^+ decay at rest.

The quantities ρ , δ , n , and ξ are the Michel parameters and they are tabulated below along with the expected values from the V-A theory and their experimental values.⁵⁾ The quantity measured in the present experiment is the

Parameter	(V - A) Value	World Average	Ref.
"Symmetric Shape"	ρ	3/4	.7517 \pm .0026
"Asymmetric Shape"	δ	0.0	-.12 \pm .21
"Low Energy parameter"	n	1.0	.972 \pm .014
"Polarization Parameter"	ξP_μ	3/4	.7551 \pm .0085

Table I. The Michel parameters.

product $\xi P_\mu \frac{\delta}{\rho}$ which in the limit $x \rightarrow 1$ and $\cos\theta \rightarrow -1$, is related¹⁰⁾ to α and ζ by the approximate relation:

$$\xi P_\mu \frac{\delta}{\rho} \sim 4(\alpha^2 + \alpha\zeta + \frac{1}{2}\zeta^2). \quad (3)$$

Experiments measuring ξ always determine the product ξP_μ . A V+A contribution to the $\pi^+ + \mu^+ \nu_\mu$ decay does effect P_μ by $|P_\mu| = 1 - 2(\alpha + \zeta)^2$; the sensitivity to α

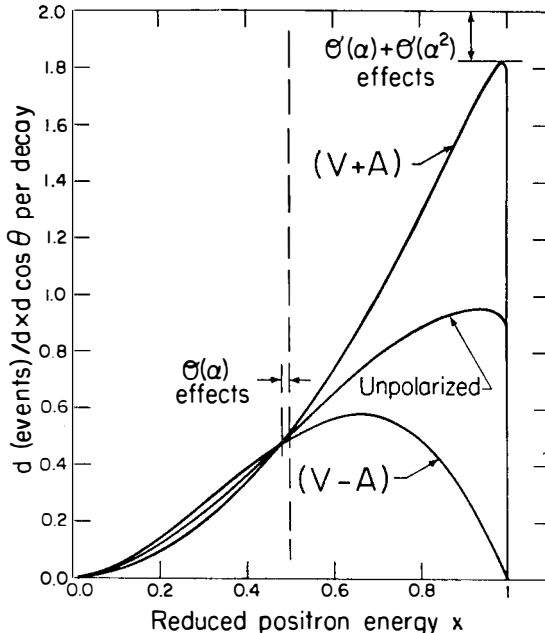


Figure 1: Positron momentum spectrum expected from decay at rest of polarized μ^+ decay via V-A (e^+ detected opposite to muon spin direction) and V+A currents. Also the expected spectrum from unpolarized μ^+ decays.

and ζ , over the entire range of x , is nearly doubled. For $x=1$ and $|\cos\theta|=1$, the sensitivity to α and ζ is very similar. The Michel parameters δ and n have the same value independently of the helicity of the coupling and ρ , for a V+A interaction is: $\rho=1-2\zeta^2$.

Equation (2) when rewritten with the theoretical values for ρ , δ , and n , and evaluated at $x \rightarrow 1$ and $\cos\theta \rightarrow -1$ give

$$\frac{d^2r}{dxd\cos\theta} \rightarrow 4(1-x)+(1+\cos\theta)+(1-P_\mu)+(1-\xi).$$

A measurement of the positron spectrum at the endpoint determines directly the quantity ξ .

Figure 1 shows the expected momentum spectrum of positrons produced from the decay at rest of longitudinally polarized muons when the e^+ are emitted opposite to S_μ ; both for the case where the decay is mediated by a left-handed current V-A and by a right-handed current V+A. Also shown is the momentum spectrum for the decay of unpolarized muons. These three spectra display two important features of this experiment. First, at $x=1$ the spectrum associated with a W_L vanishes, while the one associated with a W_R peaks. Second, the spectrum from unpolarized muon decay at $x=1$ is similar to the one expected from pure V+A contribution. To determine the product $\xi P_\mu \frac{\delta}{\rho}$ we measure two quantities: the spectrum of both unpolarized and polarized muons. The first measurement determines the shape and the second measurement the magnitude of the effect expected.

The Surface Muon Beam

This beam line is described in details by C. Oram¹¹). The 100 μ A, 500 MeV/c beam of the TRIUMF cyclotron (beamspot $\Delta x \sim 2\text{mm}$, $\Delta y \sim 4\text{mm}$) hits a 2mm thick carbon target. The beam has a 43 ns RF structure. Pions produced inside the target when decaying ($\pi^+ \rightarrow \mu^+\nu$) at rest will produce muons with 4.1 KeV kinetic energy and momentum 29.5 Mev/c ($\beta = .271$), they have helicity -1 in the case of V-A decays and equal to $|P_\mu| \approx 1-2(\alpha+\zeta)^2$ for left-right symmetry cases. The beam line makes an angle of 135° with respect to the proton beam. It is 9.6m long, includes two 60° bends and has an acceptance $\Delta x \approx 35$, $\Delta y \approx 70$ mrad. The flux of beam particles is plotted in figure 2 as a function of the beam momentum. The broad distribution of muons at about 25 MeV/c comes from the decay of pions that stop inside the target. Muons with less than 29.5 MeV/c are partially depolarized because they have undergone multiple scattering (coulomb scattering is relativistically helicity conserving and non relativistically spin conserving). The beam line, when used for a polarized beam, is tuned for particles with 29.5 MeV/c and has a $\Delta p/p = .5\%$ to ensure the acceptance of only μ^+ coming from the decay of π^+ that stop in a thin layer (6.2 mg/cm²) at the surface of the target which faces the transport system (hence the name "surface"

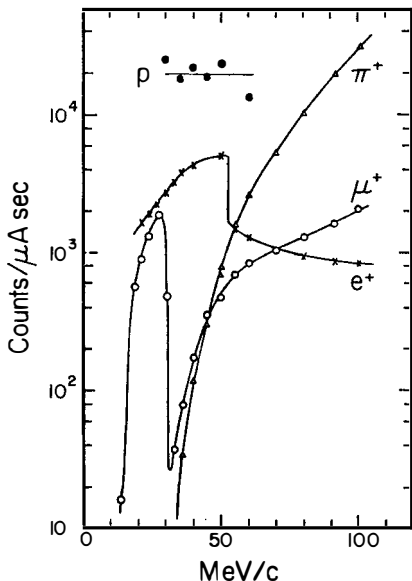


Figure 2: Flux of particles in the M₁₃ beam line at TRIUMF¹¹⁾ as a function of the beam line momentum. Primary proton beam has 500 MeV, production target is 2 mm thick carbon.

muon beam). Muons from π^+ decay in flight, that are accepted by the beam line are less polarized and are correlated in time with the RF of the cyclotron beam. Such muons (called "cloud" muons) are rejected by looking at their time correlation with respect to the accelerator RF structure. Figure 3 shows the time structure of surface muons.

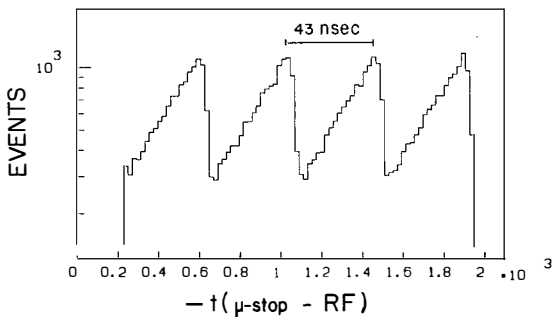


Figure 3: Timing of μ^+ with respect to cyclotron RF (time scale running from right to left) for "surface" muons with beam line at 29.5 MeV/c. The data reproduces the π^+ life time.

The Spectrometer.

The apparatus is sketched in figure 4. It consists of a target where the μ^+ are stopped followed by a cylindrical solenoid to increase the acceptance, and a 98° bend spectrometer where the positrons are momentum analyzed. Two sets of data are collected: the spectrum of e^+ from the decay of polarized and unpolarized muons. For each cases the spectrometer accepts e^+ with reduced momentum in the range $.8 < x < 1.2$. The target in which the μ^+ are stopped is a thin metallic foil (Al, Cu, Ag, or Au). When the spectrum of polarized muons is recorded, a 11k Gauss longitudinal magnetic field is applied to the target region to prevent the muon from depolarizing (Paschen-Bach effect). Unpolarized muons are produced by precessing the μ^+ in a 70 gauss transverse field applied to the area of the stopping target. The magnetic field in the target region is the only parameter of the spectrometer which is changed when the two sets of data (polarized and unpolarized μ^+ decay) are collected.

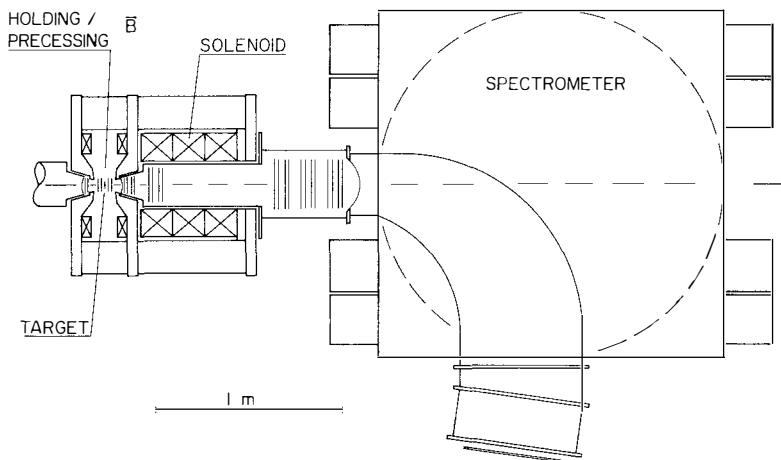


Figure 4: Top view of the spectrometer used to measure ξP_μ .

The direction of the incident μ^+ is measured by two sets of proportional chambers, with x, y read out, and the μ^+ are timed with the signal from a 120 μm thick scintillator counter. The proportional chambers also measure the dE/dx of the beam particles (~60% e^+ and 40% μ^+). The direction of the positron emerging from the target is recorded by an $x-y$ proportional chamber and by two sets of drift chambers placed at the beginning of a solenoid magnet. A scintillation counter (250 μm thick) downstream of the target, times the decay of the μ^+ .

The solenoidal magnet has a field of 10 Kgauss and accepts positrons emitted up to 200 mrad from the beam axis; it acts as a field lens which makes the e^+ parallel to the beam at the entering vacuum window of the analyzing magnet. Another set of drift chambers is located at the entrance and in the focal plane of the spectrometer magnet, this last set is followed by scintillation counters. The e^+ trajectory is measured by 24 drift chamber planes in addition to the PWC downstream of the target. The spectrometer has 576 drift chamber wires. All chambers are operated with a mixture of 92% methane and 8% methylal. The distribution of the electron drift distance versus time relation, in the gas of the chambers, is constantly updated as the computer program reconstructs the particles trajectories. With this technique we achieve a spatial resolution of $\sigma = 200 \mu\text{m}$ and the momentum resolution $\Delta p/p = .2\%$ RMS.

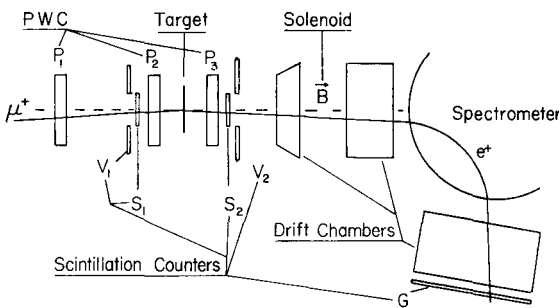


Figure 5: Schematic arrangement of the detector components. The " μ -stop" signal is defined by $P_1.P_2.S_1.V_1.P_3.S_2$ and is generated at a time t_1 . The " μ^+ -decay" trigger signal is defined by $(\mu\text{-stop}).P_3.S_2.G.V_2.P_1.S_1.V_1.P_2$ and takes place at a time t_2 ($.2 < t_2 < 10 \mu\text{sec}$) after t_1 . Beam rates are $\sim 15 \text{ KHz}$ and trigger rates $\sim 20 \text{ Hz}$.

The momentum resolution is determined from the shape of the endpoint spectrum for unpolarized muons; it is based on data collected over a period of 3 weeks. Figure 5 shows how the trigger is formed. Data are collected by cycling the four targets. For each, a spectrum with $\sim 100 \text{ k}$ events is recorded for both polarized and unpolarized muons. Each spectrum takes about 1 hour to acquire.

Data

The spectrometer was operated twice in 1982, in the spring and in the fall. The data collected in the spring have been analyzed and the results are presented here; they are based on 3.5×10^6 stopped muons. In the fall run another 10^7 events were logged. 99% of the recorded events have a μ^+ track entering the target, followed after 200 ns or later by an e^+ going

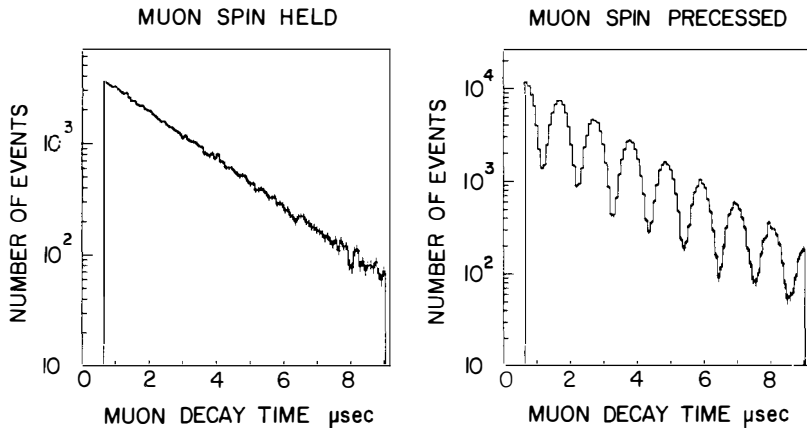


Figure 6: Muon decay time for polarized muon beam (left). Decay time when muons are precessed in a 70 Gauss transverse field (right).

through the spectrometer. Only events satisfying the following track reconstruction criteria are retained: no hits in the chambers in addition to the one used to reconstruct track segments, track segments must join in a continuous sequence, and the particle trajectory must be well within the sensitive volume of the spectrometer.

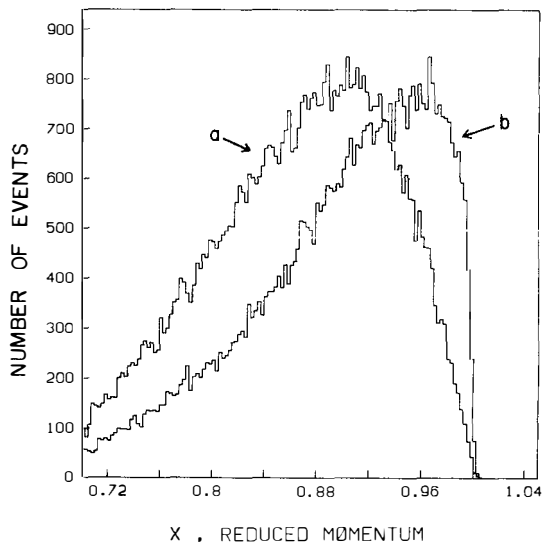


Figure 7: Reduced momentum spectrum for positrons from decay at rest a) of longitudinally polarized μ^+ and b) of unpolarized muons.

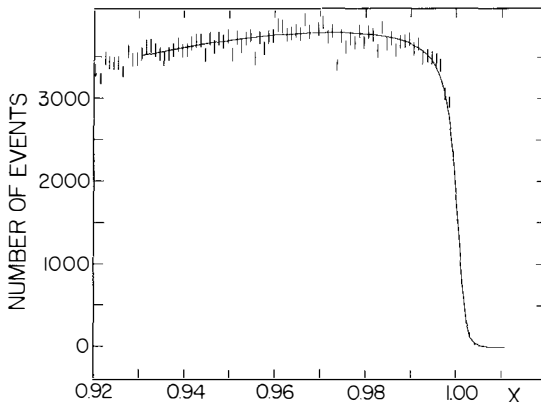


Figure 8: Reduced momentum spectrum for unpolarized muons. The curve is the prediction of the V-A theory. The shape of this curve at its endpoint is the same as expected in the case of a pure V+A interaction. In the text this function is called $f_+(x)$. This plot includes 175K events, collected with four stopping targets.

The time distribution of the μ^+ decay for both polarized and unpolarized muons are shown in figure 6. Both plots confirm that we are observing background free μ^+ decays. The momentum spectra for the e^+ are shown in figure 7. The quantity $\xi P_\mu \frac{\delta}{p}$ is obtained by considering these two spectra in the region $x > .92$ and $\cos\theta > .975$, obtained with only "surface" μ^+ (timing not correlated with RF).

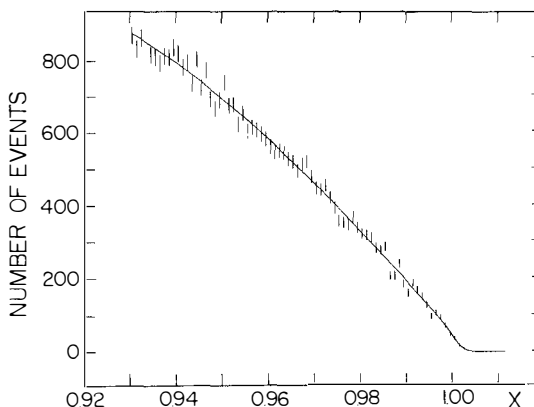


Figure 9: Reduced momentum spectrum of positrons from the decay at rest of longitudinally polarized μ^+ . See text for an explanation of the curve fitted through the data. There are 89K events in the plot.

The analyzed spectrum, from unpolarized μ^+ decays, is shown in fig. 8. The curve is a fit to the data with the spectrum shape predicted by the V-A theory including radiative corrections 12) and Bhabha's production in material. From the fit we can determine the spectrometer acceptance and its resolution at $x=1$, and the shape of the momentum distribution as expected by the V+A interaction. We denote this function as $f_+(x)$. The fit to this set of data is now used to calculate the shape of the endpoint positron spectrum as expected from a pure V+A interaction for the decay of polarized muons. We denote this function as $f_-(x)$. The spectrum of e^+ from polarized muons (fig. 9) is divided by the one for unpolarized μ^+ in order to eliminate to first order the spectrometer acceptance. This ratio is then fitted, for different intervals of $\cos \theta$, to the sum of the V-A contribution to the interaction ($f_-(x)$) plus some contribution due to the V+A interaction which shape is given by $f_+(x)$:

$$\text{ratio (polarized/unpol.)} \sim f_-(x) + \xi P_\mu \cos \theta \frac{\delta}{p} f_+(x) .$$

The quantity $\xi P_\mu \frac{\delta}{p}$ obtained from fitting the data at different intervals of $\cos \theta$ is plotted in figure 10. The limit of the variable at $|\cos \theta| = 1$ gives us the quantity we desire. The result obtained from the data for each of the four targets is plotted in figure 11. The four values are consistent. Before using our value for $\xi P_\mu \frac{\delta}{p}$ in equation 3 to determine the mass of the W_R the measured quantity must be corrected for μ^+ depolarization due to multiple

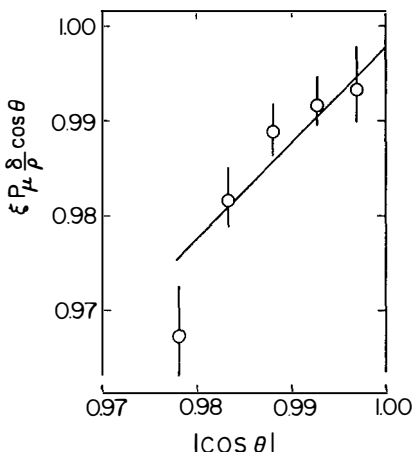


Figure 10: The quantity $\xi P_\mu \cos \theta \frac{\delta}{p}$ is plotted as function of $\cos \theta$. The slope of the linear fit to the data is taken from the theory. The intercept of this line at $|\cos \theta| = 1$ determines the quantity $\xi P_\mu \frac{\delta}{p}$ at $x = 1$ and $|\cos \theta| = 1$.

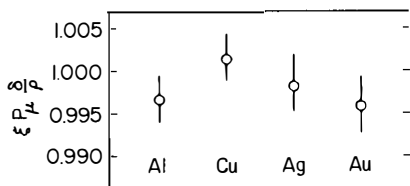


Figure 11: The quantity $\xi P_\mu \delta / \rho$ determined from data taken with different stopping targets is shown. The four results are in agreement showing that if muons depolarize in the target, depolarization takes place at an equal and extremely small level in all four targets.

scattering. The amount of material in the production target and upstream of the stopping target is 24.6 mg/cm^2 with a radiation length of $.654 \times 10^{-3} \text{ } \chi_0$; the calculated correction factor is $1.0012 \pm .005$. Possible depolarization of the beam in the stopping target foil has not been included, but can only strengthen the limit that we present.

Results

The preliminary results from the first set of data are presented as a 90% C.L. limit

$$1 - \xi P_\mu \frac{\delta}{\rho} < 0.0041 \text{ (90% CL)} .$$

When used in conjunction with Eq. 3 the following limits (90% CL) were obtained for $M(W_R)$ assuming $M(W_L) \sim 80 \text{ GeV}/c^2$, and zero mass neutrinos

$$\zeta \text{ free} : \alpha < 0.045 \quad M_R > 380 \text{ GeV}/c^2$$

$$\zeta \text{ fixed to 0} : \alpha < 0.032 \quad M_R > 450 \text{ GeV}/c^2 .$$

The limits on the phase ζ between left-and right-handed currents are:

$$\alpha \text{ free} : -0.064 < \zeta < 0.045$$

$$\alpha \text{ fixed to 0} : -0.045 < \zeta < 0.045 .$$

These results are displayed graphically in figure 12 together with the currents limits on right handed currents¹⁷⁾. Theoretical predictions varies between $1.6 \text{ TeV}/c^2$ ¹³⁾ and as low as $220 \text{ GeV}/c^2$ ¹⁴⁾.

I would like to extend my appreciation to the organizers of the XIIIfth Rencontre de Moriond for giving me the opportunity to spend an exciting week at this interesting meeting. Many thanks to my colleagues on this experiment for their help in preparing this material and to R. Oakes for many helpful discussions on the subject.

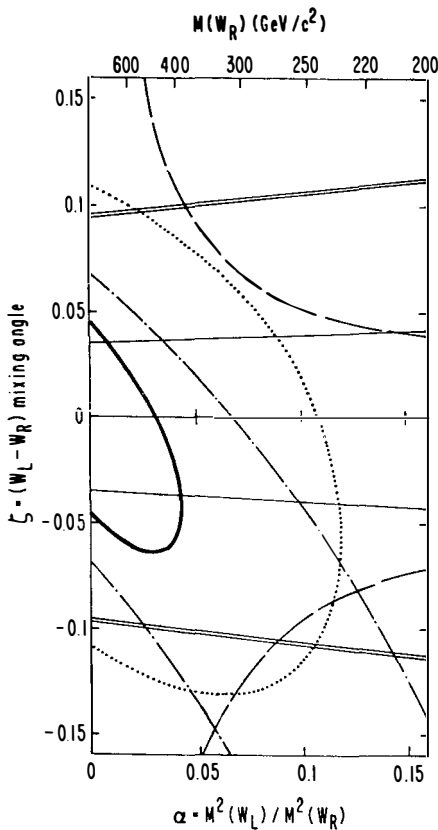


Figure 12: Plots of existing 90% CL limits on the phenomenological quantities α and ξ describing right-handed currents. Contours are derived from measurements of the polarization parameter ξP_μ (bold, this experiment, dotted, Ref. 9); the polarization of the β decay in Gamow-Teller transitions (dot-dashed, Ref. 15). Limits from the y distributions in νN and $\bar{\nu} N$ scattering (double line, Ref. 16) are valid irrespective of the ν_R mass.

This work was supported in part by the U.S. Department of Energy, Division of Basic Energy Sciences, Office of Energy Research under contracts W-7405ENG-48 and AC02-ER02289.

References

- 1) J.C. Pati and Salam, Phys.Rev. D10, 275 (1974).
- 2) R.N. Mohapatra and J.C. Pati, Phys.Rev. D11, 566, 2558 (1975).
- 3) M.A. Beg, R.V. Budny, R. Mohapatra and A. Sirlin, Phys. Rev. Lett. 38, 1252 (1977).
- 4) M. Strovink, in Weak Interactions as Probe of Unification, Virginia Polytechnic Institute, 1980, G.B. Collins, L.N. Change and J.R. Ficenec, eds (AIP Conference Proceedings No. 72).
- 5) Review of Particle Properties, LBL - 100 Revised, April 1982.
- 6) M. Bardon et.al., Phys.Rev.Lett. 14, 449 (1965).
- 7) D. Freyberger, Phys.Rev. 166, 1379 (1968).
- 8) S. Derenzo, Phys.Rev. 181, 1854 (1969).
- 9) V.V. Akhamonov et.al. Sov.J.Nucl.Phys. 6, 230 (1968).
- 10) M. Strovink, Proceedings of Summer Institute on Particle Physics, SLAC August 16-17, 1982.
- 11) C. Oram J.B. Warren, G.M. Marshall, and J. Doornbos, Nucl.Instr. Meth. 179 95 (1981).
- 12) F. Scheck, Phys. Rep. 49, No. 4, 201, 211 (1978).
- 13) G. Beall, M. Bander, and A. Soni, Phys. Rev. Lett. 48, 848 (1982).
- 14) M. Hwang and R.J. Oakes Fermilab-Pub. - 83/38-THY, Sub. Phys. Rev. D.
- 15) J. Van Klinken, Nucl.Phys. 75, 145 (1966).
- 16) H. Abramovicz et.al., Z.Phys.C 12, 225 (1982).
- 17) J. Carr et al. to be published in Phys. Rev. Lett.

BOUNDS ON SUPERSYMMETRIC PARTICLES FROM A PROTON BEAM-DUMP EXPERIMENT

CHARM Collaboration

F.Bergsma, J.Dorenbosch, M.Jonker and C.Nieuwenhuis
NIKHEF, Amsterdam, The Netherlands

J.V.Allaby, U.Amaldi, G.Barbiellini, L.Barone, A.Capone, W. Flegel, M. Metcalf,
J. Panman and K. Winter
CERN, Geneva, Switzerland

J.Aspiazu, F.W.Büsser, H. Daumann, P.D.Gall, E.Metz, F.Niebergall, K.H.Ranitzsch
and P.Stähelin
II. Institut für Experimentalphysik, Universität Hamburg, Hamburg, Fed. Rep.
Germany

P.Gorbunov, E.Grigoriev, V.Kaftanov, V.Khovansky, A.Rosanov, M.B.Voloshin
and M.I.Vysotsky
Institute for Theoretical and Experimental Physics, Moscow, USSR

A.Baroncelli, B.Borgia, C.Bosio, F.Ferroni, E. Longo, P. Monacelli,
F. de Notaristefani, P. Pistilli, C. Santoni, L. Tortora and V. Valente
Istituto Nazionale di Fisica Nucleare, Rome, Italy

Presented by C. Santoni



ABSTRACT

Limits on the gluino and scalar quark masses were obtained in a proton beam-dump experiment. The results do not favour the existence of low mass gluinos (< 2 GeV) and scalar quarks (< 100 GeV).

Supersymmetric theories predict the existence of partners of ordinary quarks, leptons, and bosons, at a mass scale of 100 GeV which will become accessible with future generations of accelerators. However some of these models also predict particles with small mass. These are the supersymmetric partners of gluons and photons: gluinos and photinos¹⁾. Limits on the gluino mass derived from existing data have been discussed elsewhere²⁾.

A search for events induced by reactions involving gluinos and photinos was performed by the CHARM Collaboration in a proton beam-dump experiment³⁾. As shown in Fig. 1, the gluinos could be produced by the proton-nucleus collisions in the copper dump ($pN \rightarrow \tilde{g}\tilde{g}X$). If the gluino is heavier than the photino, it decays into a photino and hadrons according to the reaction $\tilde{g} \rightarrow \tilde{\gamma}q\bar{q}$. The photino reaches the CHARM detector, where it interacts producing a gluino ($\tilde{\gamma}q \rightarrow \tilde{g}q$). Since a photino interaction resembles a neutral-current neutrino interaction, the number of events induced by the described chain was established from the muonless events in excess of those expected from neutrino interactions.

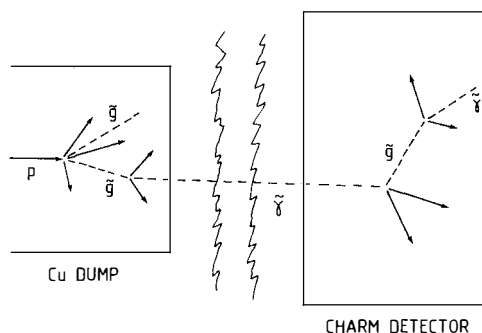


Fig. 1 Chain of the processes that leads to a supersymmetric signal in a proton beam-dump experiment.

The experiment was performed at the CERN SPS in 1979. In the exposure of 6.96×10^{17} protons on the full density target (a 2 m long copper block) 80.5 ± 14 (stat.) ± 6.3 (syst.) muonless events of prompt origin with shower energy (E_{shower}) > 20 GeV, have been observed in the fiducial volume of the CHARM detector⁴⁾ (100 t) covering a solid angle of 6.8×10^{-6} sr. The events include charged-current (CC) and neutral-current (NC) interactions of ν_e and $\bar{\nu}_e$ as well as interactions of neutrino-like particles without a muon in the final state. The number of prompt CC events induced by electron neutrinos has been estimated by direct identification³⁾. The procedure is based on the characteristic features of electromagnetic showers in the CHARM calorimeter⁵⁾: their small width, their regular longitudinal profile, and the strong correlation between

the total shower energy and the energy detected at the shower maximum. The energy detected in a row of scintillation counters of 15 cm width, starting at the vertex and crossing the shower maximum, has been calibrated using isolated electron showers obtained in a test beam. Ninety per cent of the total electron energy is detected in such a row with a resolution of $\sigma(E)/E = 0.25/\sqrt{E(\text{GeV})}$ ⁵⁾. These features allow the identification of showers with a large electromagnetic component ($y = E_{\text{em}}/E_{\text{shower}} > 0.4$). For $\nu_e N \rightarrow e X$ events a correction for hadron-shower energy overlapping the row was applied. Neutral-current events with π^0 's of large energy may simulate $\nu_e \rightarrow e \pi^0$ CC events. This contribution was determined using muonless events obtained in the wide-band beam. The number of prompt CC events induced by ν_e and $\bar{\nu}_e$ has been estimated fitting the y distributions of CC $\nu_e \rightarrow e \pi^0$ events and of NC π^0 background to the experimental data. A total of 60.7 ± 13 (stat.) ± 5.3 (syst.) events have been attributed to CC $\nu_e \rightarrow e \pi^0$ interactions. From this total the corresponding number of NC events with $E_{\text{shower}} > 20$ GeV was computed to be 15.8 ± 3.4 (stat.) ± 1.5 (syst.). Subtracting the electron neutrino events from the observed number of muonless events, 4 \pm 21 events with $E_{\text{shower}} > 20$ GeV could be attributed to the interaction of other neutrinos or neutrino-like particles.

From this result a limit on the gluino mass as a function of the scalar quark mass was derived. The expected number of photino events was computed by a Monte Carlo simulation. The gluino production cross-section was computed assuming the gluon fusion mechanism⁶⁾ shown in Fig. 2. Gluino hadroproduction via the gluon fusion mechanism is enhanced with respect to that of heavy quarks of comparable mass by the colour factor of $81/7$, because gluinos belong to the adjoint representation of the colour SU(3) group. Gluino decay into a photino and a $q\bar{q}$ pair is described by the diagram of Fig. 3. The interaction is mediated by a scalar quark whose mass is of the order of the supersymmetry-breaking mass scale $\{0(100)$ GeV $\}$. The dominant mechanism for the photino-nucleon interaction

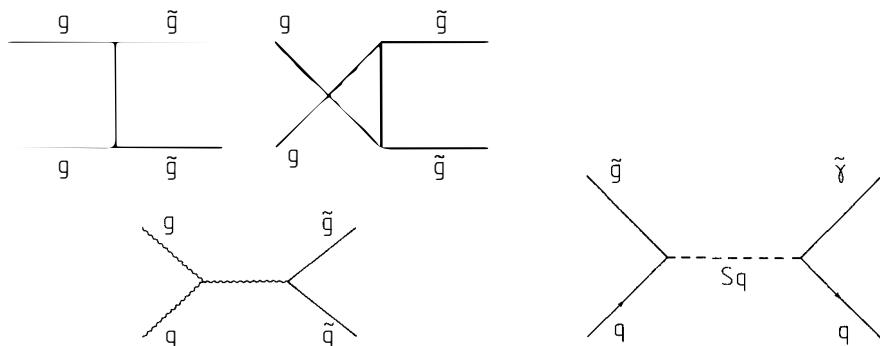


Fig. 2 Diagram for gluon fusion into a gluino pair.

Fig. 3 Diagram for the interaction of a gluino and a photino with quarks.

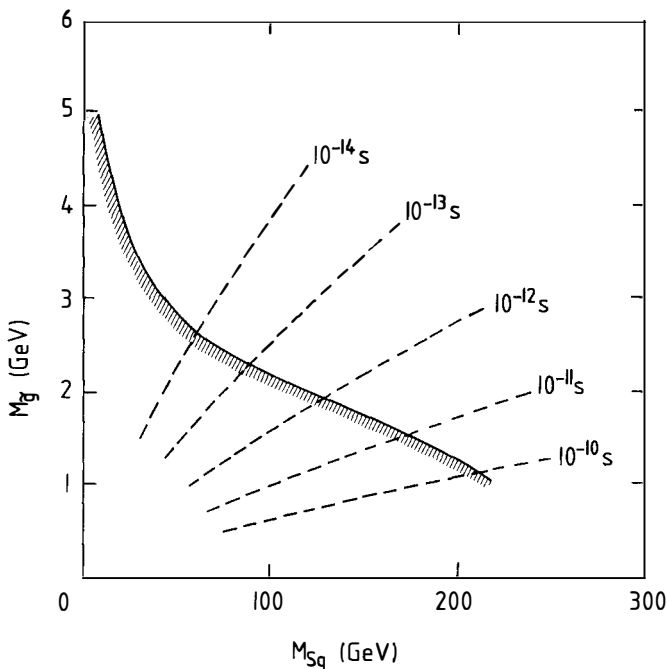


Fig. 4 The 90% CL lower bounds on the gluino mass as a function of the mass of the scalar quark. The broken lines show the gluino lifetime constraints.

is the inverse of gluino decay⁷⁾. For a scalar quark mass equal to the W-boson mass the photino cross-section is expected to be of the same order as the CC neutrino nucleon cross-section. The results are plotted in Fig. 4. The solid curve is a lower bound at the 90% CL on the gluino mass as a function of the scalar quark mass. The broken lines indicate the gluino lifetime constraints.

In conclusion, the results of this search for supersymmetric particles do not favour the existence of low-mass gluinos (< 2 GeV) and scalar quarks (< 100 GeV).

REFERENCES

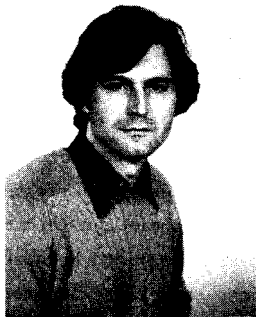
1. G.R.Farrar and P.Fayet, Phys. Lett. 76B, 575 (1978); P.Fayet, Phys. Lett. 78B, 417 (1978) 417; G.R.Farrar and P.Fayet 79B, 442 (1978).
2. B.A.Campbell, J.Ellis and S.Rudaz, Preprint CERN TH-3184 (1981); G.L.Kane and J.P.Leveille, Phys. Lett. 126B, 227 (1982).
3. M.Jonker et al. (CHARM Collaboration), Phys. Lett. 96B, 435 (1980).
4. A.N.Diddens et al. (CHARM Collaboration), Nucl. Instrum. Methods 178, 27 (1980).
5. M.Jonker et al. (CHARM Collaboration), Nucl. Instrum. Methods 200, 183 (1982).
6. H.M.Georgi, S.L.Glashow, M.E.Machacek and D.V.Nanopoulos, Ann. Phys. (NY) 114, 273 (1978).
7. M.I.Vysotsky, Preprint ITEP-43 (1982), submitted to Nucl. Phys. B.

SUPERSYMMETRIC PARTICLE PHYSICS : A PANORAMA^(*)

by

C.A. SAVOY

*Service de Physique Théorique
C.E.N. Saclay,
91191 Gif-sur-Yvette Cedex, France*



Supersymmetry is reviewed from a particle theorist viewpoint. The main underlying properties are described and confronted to the requirements of model building. The low-energy approximation to broken supergravity gauge theories is analysed, with some emphasis on the problem of the spontaneous breaking of $SU(2) \times U(1)$ invariance.

^(*) Invited talks at the XVIII Rencontres de Moriond, La Plagne, March 1983.

INTRODUCTION

Supersymmetry^(1,2) a major field of activity in nowadays particle physics, is becoming so familiar to have a nickname, Susy. It is generated by fermionic charges that transform bosons into fermions, and vice-versa, in contrast with the usual symmetries relating particles of the same spin.

Particle physics is formalized as a gauge field theory. The fundamental gauge interactions are mediated by vector bosons associated to local symmetries connecting matter species. Matter constituents (quarks and leptons) are described by fermionic degrees of freedom. Finally, Goldstone-Higgs scalars are introduced to break some of the gauge symmetries and to provide the additional degrees of freedom that make the corresponding vector bosons massive and their interactions short-ranged. They also give masses to the fermions through Yukawa interactions. Since Susy connects bosons and fermions it could in principle reduce the arbitrariness in the theory through the relations among interactions and between bosonic and fermionic masses. In practice this appealing idea has not yet been realized because gauge and Goldstone bosons have different quantum-numbers than those of matter fermions. Instead, in the existing realistic models one has to introduce a new degree of freedom, a supersymmetric partner with the opposite statistics, for each particle in a normal gauge model. This is a rather disappointing way to insert Susy in particle physics but it looks unavoidable if Susy has some relevance at low energies, which in this context are defined to be in the TeV region of the weak or Fermi scale. Indeed, there is no evidence for these new Susy particles in the present experimental ranges of energies, which means that Susy is broken at higher energies.

However, Susy has another fundamental property. In general, symmetries may reduce the quantum divergences. Actually, because of the boson-fermion degeneracy, there are cancellations between quantum loop corrections in supersymmetric theories. This has led to the construction of supersymmetric quantum gravities, or supergravities⁽³⁾, in order to palliate the non-renormalizability of the gravitational interactions. The next logical step is to couple supergravity to the gauge theory. In the appropriate flat limit at low energies, where gravitational interactions are neglected, one ends with a supersymmetric effective theory (eventually with some residual Susy breaking due to gravitational effects). An extremely ambitious design would be to relate gravity and gauge interactions through Susy, in a complete unification of the fundamental interactions. That would be hopefully realized in N=8 supergravity, in a way that is not clear yet, in spite of the recent

impressive progress in the field.

But Susy has a simpler, somewhat technical, application in gauge models of particle physics, which is more accessible at the present level of understanding of quantum field theory. Indeed, the introduction of Higgs scalars and their interactions in gauge models brings also quadratic divergences in the quantum theory. Even if these divergences may be controlled through the renormalization procedure, in grand-unified models their compensation becomes very unnatural due to the presence of very different scales in these models. This is the so-called hierarchy problem : how to incorporate in a gauge model both the grandunification scale ($M_x \gtrsim 10^{15}$ GeV) and the weak interaction or Fermi scale ($M_w \sim 10^2$ GeV). In supersymmetric theories there are no quadratic divergences. Small parameters can be kept small, and as such they are controlled by the scale of supersymmetry breaking, M_s . The technical hierarchy problem is solved and, even more, M_w may be related to M_s . This more pragmatic motivation⁽⁴⁾ has developed in several models of supersymmetric grandunification.

Supergravity (Sugra)⁽³⁾ or local Susy is the supersymmetric extension of quantum gravity. Model building started with global Susy by assuming that all gravitational effects may be neglected from the very beginning. The main problem in these early attempts was how to introduce Susy spontaneous breaking in such a way that all the bosonic Susy partners of the usual leptons and quarks are systematically lifted to a mass scale consistent with the fact that they have escaped observation. Instead, through the construction and the inspection of locally supersymmetric gauge theories⁽⁵⁾ it was recognized at once that : the spontaneous breaking of local Susy (Sugra) tends to make the scalar bosons massive. In spite of this, it has been shown that spontaneously broken supergravity is consistent with the existence of the massless Goldstone bosons needed for the breaking of gauge symmetries^(6,7). Because of these promising circumstances the supergravity fever has spread among theorists. Experimenters should now the contaminated also.

I shall try to describe, at an introductory level, the main properties of supersymmetric field theory that seem relevant to particle physics and could motivate the incorporation of this novelty in our understanding of Nature. Both the mathematics of a complete formulation and the technology of model building will be diminished in this otherwise theoretical review^(*).

(*) The references are strictly limited to a selection of some representative work related to supersymmetry. I apologize to authors whose contributions are omitted here and I urge the interested reader to inspect the review papers quoted here for a complete bibliography.

The crucial subject of experimental tests of Susy⁽⁸⁾ (theorist proposes, Experimenter disposes) will be essentially passed over since it is nicely covered in other contributions to this meeting⁽⁹⁾.

It goes without saying that several important topics have been skipped here. Fortunately, the important subject of cosmological implications of Susy models is discussed in other contributions to this meeting as well as to its twin meeting on astrophysics.

SUSY : A NEW KIND OF LOCAL SYMMETRY

Supersymmetry is the only non-trivial extension of the Poincaré invariance consistent with general principles of field theory. The usual symmetries, like the gauge invariances associated to the strong and electroweak forces, are generated by scalar charges, closing a Lie algebra. Susy generators are spin 1/2 charges, that will be denoted in two-component notation by Q_α ($\alpha=1,2$) and $\bar{Q}_\alpha = (Q_\alpha)^*$ (corresponding to the four real components of a Majorana spinor). Besides the obvious algebraic relations defined by the behaviour of the spinorial charges under Lorentz transformation, the Susy or SuperPoincaré algebra is characterized by the non-trivial anticommutator

$$\{Q_\alpha, \bar{Q}_\beta\} = 2(\sigma_\mu)_{\alpha\beta} P^\mu \quad (1)$$

where P^μ is the 4-momentum operator, generating translations. As a fermionic charge, Q_α transforms a fermion into a boson with the same quantum numbers (colour, flavour), and vice-versa.

Supersymmetry should be a local invariance. Indeed, quantum gravity is believed to be the dynamical theory of local Poincaré invariance, the graviton acting as the gauge boson. As a non-trivial extension, the SuperPoincaré invariance has to be also local, its quantum theory being supergravity. Global Susy could be at most a good approximation if all gravitational effects may be neglected. The gauge particle associated to the spinorial charge is a spin 3/2 fermion, the gravitino.

This leads to the aesthetical situation where all fundamental symmetries in Nature are local, and, as such, related to fundamental gauge interactions. Clearly, Yukawa and scalar interactions are also needed that in principle are not completely fixed by the local invariances. However they turn out to be severely restricted by Susy. This fact will result in less divergences and more predictions in the models, with the possibility of increasing the number of calculable parameters.

Supersymmetry may be extended by the introduction of a number $N \leq 8$ of spinorial charges, Q_α^i ($i=1,2,\dots,N$). This would introduce more restrictions

in the theory. In particular, there are less divergences as N increases : for $N=2$ masses are not renormalized⁽¹⁰⁾ and for $N=4$ the gauge coupling constants are not renormalized⁽¹¹⁾. However there is also a major difficulty for the construction of realistic models. For $N > 1$, left-handed and right-handed fermions are related by supersymmetry, so that they must behave in the same way under the gauge group, G , as far as the Susy charges commute with G . Then, there is no known mechanism to introduce parity violation in the gauge interactions since this is currently done by putting left-handed and right-handed fermions in different, complex representations of the gauge group.

Therefore we shall restrict ourselves to the case of gauge theories with local $N=1$ Susy, namely, to Yang-Mills theory coupled to supergravity.

THE PARTICLE SPECTRUM OF SUSY

In order to study supersymmetric theories, one has first to consider the sets of fields and particles that transform as irreducible representations of the Susy algebra, usually called supermultiplets. They consist of an equal number of bosonic and fermionic components.

A massless vector supermultiplet (W, λ) has a vector boson, W (helicities ± 1), and a Majorana fermion, λ (helicities $\pm 1/2$). These are the fields of the gauge sector, required in a supersymmetric pure Yang-Mills theory. One introduces one multiplet (W^A, λ^A) in correspondence with each charge T^A of the gauge group G ($A=1, 2, \dots, \text{dim } G$). The fermionic partners λ^A of the gauge bosons W^A are usually called gauginos. In the $SU(3) \times SU(2) \times U(1)$ gauge theory of strong and electroweak interactions, the vector multiplets are then :

$$\left(\begin{array}{c} g \\ \tilde{g} \end{array} \right) \left(\begin{array}{c} \lambda \\ \tilde{\lambda} \end{array} \right) \left(\begin{array}{c} W^+ \\ \tilde{W}^\pm \end{array} \right) \left(\begin{array}{c} Z^0 \\ \tilde{Z}^0 \end{array} \right) \quad (2)$$

where we denote by \sim the Susy partners of the usual particles. Here, the new fermions are named gluinos, photino, winos and zino, respectively. In the extension to a grandunified $SU(5)$ one has to add the gauge bosons X, Y , with lepto-quark quantum numbers and their gauginos \tilde{X}, \tilde{Y} .

The appropriate supermultiplet of particles to describe matter is the chiral multiplet (ψ, Z) . It consists of a Majorana fermion, ψ , and a complex scalar (i.e., two real scalars), Z . The Higgs scalars also belong to chiral multiplets together with new fermions. In practice one then needs the following types of chiral multiplets :

$$\begin{array}{lll} \left(\begin{array}{c} q \\ \tilde{q} \end{array} \right) & \text{quark} & \left(\begin{array}{c} l \\ \tilde{l} \end{array} \right) & \text{lepton} & \left(\begin{array}{c} \tilde{H} \\ H \end{array} \right) & \begin{array}{l} \text{Higgsino} \\ \text{Higgs boson} \end{array} \end{array} \quad (3)$$

Notice also the names and notations for the new states.

These are the supermultiplets that are needed in a phenomenological globally supersymmetric gauge model. For local Susy, the gauge supermultiplet of supergravity has obviously to be introduced. The graviton multiplet consists of the graviton (helicities ± 2) and the gravitino (helicities $\pm 3/2$). It couples to the vector and chiral multiplets of the gauge theory through the gravitational coupling constant, $\kappa = 1/M_p$, where M_p is the Planck mass of 10^{19} GeV.

The most general Lagrangian for supergravity coupled to a gauge theory has been recently produced⁽⁵⁾. The theory is not renormalizable, which is an embarrassing problem in the context of particle physics. The pragmatic attitude has been to take it as an effective Lagrangian and to consider its flat limit, $M_p \rightarrow \infty$, where the gravitational interactions are decoupled.

SUPERSYMMETRIC INTERACTIONS

A detailed discussion of the supergravity Lagrangian is far from the scope of this report. Furthermore, the matters will be simplified by assuming canonical kinetic terms⁽⁵⁾ for both gauge and matter fields (this assumption will be briefly revised later). We introduce the appropriate set of vector multiplets (w^A, λ^A) for the gauge group G and matter species ($i=1, 2, \dots, n$) through chiral multiplets (ψ^i, z^i) , transforming according to some representation of G :

$$\delta \left(\begin{array}{c} \psi^i \\ z^i \end{array} \right) = \epsilon_A T^A_j \left(\begin{array}{c} \psi^j \\ z^j \end{array} \right) \quad (4)$$

The complete theory is then determined by the choice of the "superpotential", an analytic G -invariant polynomial in Z , of dimension 3,

$$f(Z) = A + \eta_i z^i + \frac{1}{2} m_{ij} z^i z^j + \frac{1}{6} \lambda_{ijk} z^i z^j z^k + \frac{1}{M_p} (\dots) \quad (5)$$

where powers of M_p^{-1} are introduced in the terms with more than three scalar fields for dimensional reasons.

Then, besides the usual kinetic terms and the associated minimal couplings to the gauge bosons of all the gauge and matter fields, the theory has the following interactions ($f_i(Z) = \partial f / \partial Z^i$) :

(i) Yukawa interactions,

$$Lyukawa = -\frac{1}{2} f_{ij}(z) \psi^i \psi^j + g_A \sqrt{2} z_i^* T^A_j \psi^i \lambda^A + \text{h.c.} + \frac{1}{M_P} (\dots) \quad (6)$$

(ii) Scalar interactions,

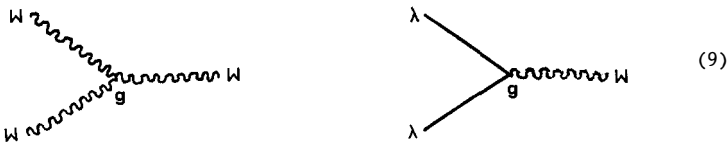
$$V = e^{|z_i|^2/M_P^2} \left\{ \left| f_i(z) + \frac{z_i^* f(z)}{M_P^2} \right|^2 - \frac{3|f(z)|^2}{M_P^2} \right\} + \frac{1}{2} g_A^2 |z_i^* T^A_j z^j|^2 \quad (7)$$

There are also other gravitational terms that are irrelevant for the discussion here. At energies $\ll M_P$, one can neglect the gravitational interactions. If there is no parameter of $O(M_P)$ in the superpotential $f(z)$ that defines the theory (in particular if no field acquires VEVs of $O(M_P)$) then all gravitational terms disappear, there remain no traces of local supersymmetry, and one ends with an effective low energy theory with global supersymmetry. The opposite case where residual supergravity interactions play some role at low energies will be discussed later. By neglecting all terms with inverse powers of M_P , the scalar potential becomes that of global Susy :

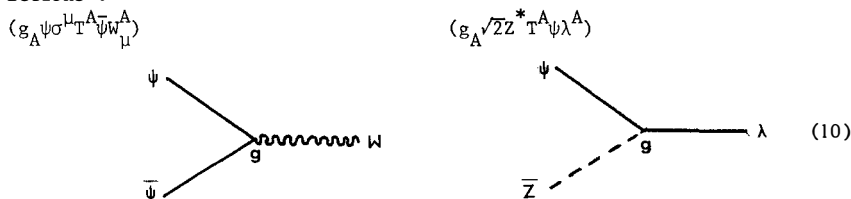
$$V(z) = |f_i(z)|^2 + \frac{1}{2} g_A^2 (z_i^* T^A_j z^j)^2 \quad (8)$$

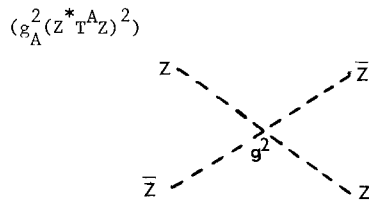
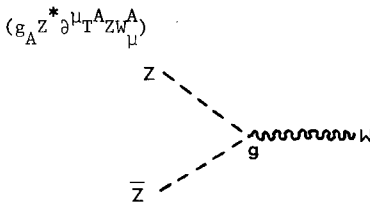
$$f_i = \eta_i + \frac{1}{2} m_{ij} z^j + \frac{1}{6} \lambda_{ijk} z^j z^k \quad .$$

Let us display the resulting interactions characteristic of global supersymmetry theories. For each one of the usual interactions in a normal theory there are new ones required by Susy transformations. Pure gauge interactions are related to those of gauginos :

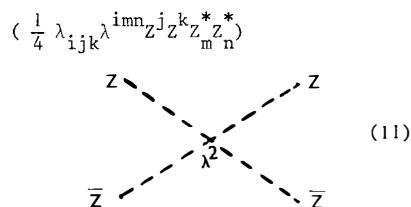
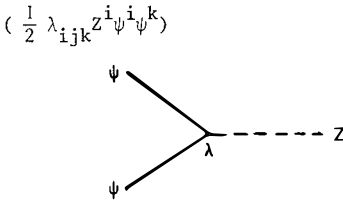


The gauge couplings of fermions and scalars to gauge bosons are completed by Yukawa interactions involving the gauginos and by special 4-scalar interactions :





Finally, for matter-matter interactions, the Yukawa couplings are related to scalar couplings :



This pattern of interactions has both theoretical and phenomenological implications to be discussed below. An obvious remark is that the interactions have the same strength for the new "Susy particles" as for the "usual" ones. Also, Susy particles should be produced by pairs. If they have not been observed, their production thresholds must be high enough (up to signature problems).

SUSY AND THE HIERARCHY PROBLEM

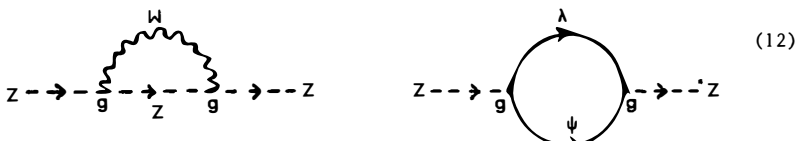
The set of constraints that Susy imposes on renormalization are often referred to as "non-renormalization theorems"⁽¹²⁾. Let us recall some of these important results without any proof.

(i) Susy may be spontaneously broken only at the tree (0th) level in perturbation theory, i.e., there is no Coleman-Weinberg mechanism⁽⁴⁶⁾ (breaking through quantum loops) for Susy. This means that spontaneous Susy breaking can be studied at the classical level (in the absence of non-perturbative effects)^(*), which is a comfortable simplification.

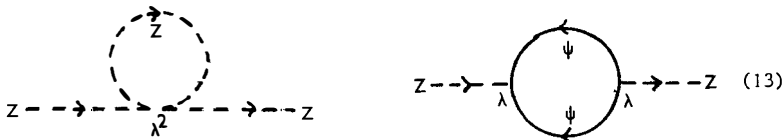
(ii) There is no quadratic divergences in Susy theories. In general, the scalar boson masses are quadratically divergent. However, Susy implies the degeneracy between scalar and fermion masses. Since the latter are only logarithmically divergent, scalar masses have also to share this property at any order of perturbation (also because of the theorem (i) above). It is instructive to see how the cancellation of quadratic divergences occur at

^(*)-----
Non-perturbative breaking of Susy has been first discussed by E. Witten, Ref. 4.

the one-loop level ; as a consequence of the Susy interactions. The diagrams contributing to scalar mass terms from the gauge interactions in Susy theories (*) are



and one easily checks that the quadratic divergences of these diagrams cancel each other. The same cancellation between bosonic and fermionic loops occur for diagrams arising from matter-matter interactions :



This property is a fundamental motivation for physical applications in connection with the hierarchy problem, as we will discuss later.

(iii) The logarithmic divergences also present remarkable properties. There is only one independent renormalization constant per supermultiplet. In the language of the renormalization group approach this means that :
 (a) the anomalous dimensions of the fermionic and bosonic fields are the same ;
 (b) the β -functions governing the scale dependence of the coupling constants are algebraically related to the anomalous dimensions. Indeed, in a particular gauge, the so-called Wess-Zumino-Landau gauge, one finds at the one-loop level, the following relations for the dependence on the renormalization scale $\mu^{(12)}$:

$$\begin{aligned} \frac{dm_{ij}}{d(\ln \mu)} &= \beta_i^k m_{kj} + \beta_j^k m_{ik} \\ \frac{d\lambda_{ijk}}{d(\ln \mu)} &= \beta_i^\lambda \lambda_{jk} + \beta_j^\lambda \lambda_{ik} + \beta_k^\lambda \lambda_{ij} \\ \beta_i^k &= \frac{1}{32\pi^2} \left\{ \lambda_{imn} \lambda^{kmn} - 4g_A^2 (T^A T^A)^k_{ij} \right\} \end{aligned} \quad (14)$$

while the anomalous dimensions are

(*) As a matter of fact, one has also to require that the generators T^A of the gauge group G are traceless, $\text{Tr} T_A = 0$.

$$\gamma_i^k = -\beta_i^k - \frac{1}{16\pi^2} g_A^2 (T^A T^A)_i^k \quad (15)$$

The β -function for the gauge coupling constant is

$$\beta = \frac{g^2}{16\pi^2} \{3C_2(G) - \text{Tr}(T^A T^A)\} \quad (16)$$

where $C_2(G)$ is the Casimir operator of the adjoint representation of the group G and the trace is taken over all chiral supermultiplets (the generalization to semi-simple groups and $U(1)$ -factors is straightforward).

Eqs. (14) have a very interesting consequence. Usually, if a particular coupling constant λ_{ijk} is arbitrarily assumed to vanish at some renormalization point μ_0 , it will be non-zero at different scales : the corresponding interactions are regenerated by radiative corrections. This situation can be avoided in Susy theories. Indeed, suppose one requires some $\lambda_{ijk} = 0$ at μ_0 . Then, according to Eq.(14), $\lambda_{ijk} = 0$ at any scale, unless it is connected to some $\lambda_{ljk} \neq 0$ through $\beta_i^l \neq 0$, which requires the existence of pairs of states coupled to both i and l . Unfortunately, this very special situation may occur in physical applications (e.g. in the so-called "decoupling property" and "singlet problem") and introduce unwanted couplings through radiative corrections even in Susy theories⁽¹³⁾.

An important property of the previous theorems is that in Susy theories the VEV's of fields (fixing the scales or order parameters of symmetry breaking) are essentially unaffected by radiative corrections. This has suggested^(4,14) to use Susy to solve the "hierarchy problem" which we now turn to discuss.

In $SU(5)$ grand unified theories^(*), one has to introduce two scales : (i) the $SU(5)$ breaking or GUT scale of $0(10^{15} \text{ GeV})$ associated to the VEV of some scalar, $\langle \Sigma \rangle$; (ii) the $SU(2) \times U(1)$ breaking or Fermi scale of $0(10^2 \text{ GeV})$ associated to the VEV of some Higgs doublet, $\langle H \rangle$. We will refer to these scales by the masses of the corresponding gauge bosons : $M_x \sim g \langle \Sigma \rangle$ and $M_w \sim g \langle H \rangle$, respectively. They have to satisfy the phenomenological requirement:

$$\frac{M_w}{M_x} \approx \frac{\langle H \rangle}{\langle \Sigma \rangle} \lesssim 10^{-13} \quad (17)$$

In normal GUTS one has to impose this relation at each order of perturbation

(*) For definiteness we assume the $SU(5)$ gauge group. The problem appears in any GUT.

theory. Indeed quantum loops introduce corrections of $O(g^n M_x^2)$ to M_w^2 , for instance from diagrams like (13) with H as external legs and Σ as internal fields (assuming that the quadratic subtractions are performed at the scale M_x , for instance). In order to have the relation in Eq.(17) one needs a fine-tuning of parameters within $\gtrsim 12$ digits at any perturbative level. This is the technical hierarchy problem.

Instead, in Susy GUTS, the non-renormalization theorems ensure a relation like Eq.(17) to be maintained at any order of perturbation, if it is assumed at the tree-level. In a sense, $\langle H \rangle$ is protected by Susy against radiative corrections proportional to $\langle \Sigma \rangle$. This solves the "hierarchy problem", giving a deep motivation for introducing supersymmetry in particle physics. Notice that solving this somewhat technical problem is needed as a first step towards models where M_w/M_x is understood, i.e., predicted, and the "physical" hierarchy problem can be settled.

SPONTANEOUS SUSY BREAKING

There is no experimental evidence for the Susy partners of the usual elementary particles. Therefore, if they exist, one has to assume that they are massive enough to escape observation. The mass splitting between Susy partners give a lower bound on the Susy breaking scale M_s . Since charged scalars have not been observed in e^+e^- colliding rings, there is an experimental bound on their masses of 16 GeV. The existence of very light quarks and leptons then imply that $M_s \gtrsim 16$ GeV. The present limit on the gluino masses, a few GeV, is more model dependent. Therefore, a crucial point is how to break Susy in order to produce the mass splittings in the particle spectrum, and, then, how to estimate the scale M_s .

In this context, it is interesting to notice that gauginos and scalars are precisely the particles whose masses are not protected by any symmetry but Susy itself. Indeed, gaugino masses of the Majorana type are not prevented by gauge symmetries. From this point of view, M_s is not restricted by gauge symmetries.

It is possible to construct Susy gauge models⁽¹⁵⁾ with explicit breaking of supersymmetry through mass terms in the Lagrangian which are specially chosen to provide the required mass splitting. These terms belong to the class of "soft" Susy breaking terms⁽¹⁶⁾, i.e., those that do not introduce quadratic divergences in the theory. Hence, these models solve the technical hierarchy problem. However, they have many free mass parameters and there is no

indication on how to restrict them^(*).

The idea of spontaneous Susy breaking is much more attractive. By remembering that Susy is intrinsically a local symmetry, we will proceed to discuss its spontaneous breaking through a parallel with the well-known properties of gauge symmetry breaking.

In gauge theories, the vacuum non-invariance is characterized by the matrix elements $\langle H^A | T^A | 0 \rangle = V^A = T^A V$, the order parameters. The scalars H^A are then massless Goldstone bosons that, through the Higgs mechanism, provide the gauge bosons W^A with a longitudinal mode. Then, the gauge bosons acquire masses $M_W^2 = g_A V^A$, proportional to the gauge coupling constants. Matter fields get masses $\sim \lambda V$ through their coupling, λ , to the Higgs boson multiplet.

Spontaneous Susy breaking is characterized by the non-invariance of the vacuum $Q^\alpha | 0 \rangle \neq 0$, implying the existence of a fermion, such that

$$\langle \psi_{G\alpha} | Q^\alpha | 0 \rangle = M_S^2 = \frac{1}{2} \langle 0 | \{ Q^\alpha, \psi_{G\alpha} \} | 0 \rangle \quad (18)$$

This Goldstone fermion is the goldstino (it would be massless if Susy could be a global symmetry). The order parameter, M_S^2 , gives the (square of the) Susy breaking scale. Through the super Higgs effect⁽¹⁸⁾, the gauge fermion (gravitino) with helicities $\pm 3/2$, together with the Goldstone fermion (goldstino) with helicities $\pm 1/2$, give rise to a massive spin 3/2 particle. The resulting mass of the gravitino is

$$m_{3/2} = \frac{M_S^2}{\sqrt{3}} = \frac{1}{M_p} \frac{M_S^2}{\sqrt{3}} \quad (19)$$

and is proportional to both the supergravity coupling constant and the order parameter, as expected from the analogy with the gauge boson masses.

From its very structure one sees that $m_{3/2}$ gives the scale of residual gravitational effects due to Susy breaking, in the flat limit (i.e., when gravitational interactions are neglected). By neglecting $m_{3/2}$ with respect to the lowest scale in the theory, usually M_W , one loses any trace of the gauge aspect of Susy. Therefore, global Susy is a good approximation as far as $M_W \gg m_{3/2}$, i.e., if

^(*) In particular, flavour conservation in neutral current interaction requires (15, 17) scalars corresponding to different fermion families to be almost degenerate in mass. In these models, this has to be put by hand.

$$M_s^2 = \sqrt{3} m_{3/2} M_P \ll M_W M_P \sim 0(10^{21} \text{ GeV}^2) \quad (20)$$

In this approximation, the gravitino couples to matter essentially through its ($\pm 1/2$) goldstino component, i.e., proportionally to the coupling constant between the goldstino supermultiplet and matter supermultiplets.

The relation between M_s^2 and mass differences inside the multiplets is analogous to the mass generation in spontaneously broken gauge theories. This relation is then,

$$m_{\text{boson}}^2 - m_{\text{fermion}}^2 = \lambda M_s^2$$

where λ is the coupling of the goldstino to the corresponding matter fields.

If the goldstino belongs to a matter or chiral multiplet, one notices that, from Susy, the term $\lambda \psi_G Z \psi$ in the lagrangian requires also a term $\lambda \{Q_\alpha, \psi_G^\alpha\} ZZ$. From Eq.(18) one then gets a mass term $\lambda M_s^2 ReZ^2$ that gives a mass splitting between the real and the imaginary parts of Z , symmetrically with respect to the corresponding fermion. If the goldstino is a gaugino, λ^A , the interaction $g_A \psi_G^* Z_i^T A^i j \psi$ is related by Susy to $g_A \{Q_\alpha, \psi_G^\alpha\} Z_i^* A^i j$, giving rise to a mass term $g_A^2 M_s^2 Z_i^* A^i j$. The two scalars described by are degenerate and shifted by $g_A^2 M_s^2$ with respect to the corresponding fermion. These shifts may have both signs as far as T^A is required to be traceless⁽¹⁹⁾.

It is now easy to understand the mass sum rule⁽²⁰⁾ :

$$\sum_{\text{bosons}} m^2 - \sum_{\text{fermions}} m^2 = 0 \quad (21)$$

valid for spontaneously broken Susy, at the tree level.

For gaugino masses the analysis is more complex. Let us just notice that, at the tree level, gaugino masses are only generated by a non-singlet goldstino. Hence the gluinos and photino may get a mass only through radiative corrections, the goldstino being colourless and neutral since $SU(3)_c \times U(1)_{e.m.}$ is an exact symmetry.

Indeed, if some fields are not coupled to the goldstino, implying mass degeneracy, the coupling may be generated by radiative corrections, under some circumstances that have been discussed before. In this case, the mass splittings will be typically of the form $\lambda^n M_s^2$, i.e., depressed by some powers of the coupling constant (plus logarithmic factors). But we have seen that in Susy theories it is possible to avoid such radiative couplings. Then, we may construct "decoupling" models^(13,21). In these models, the radiative mass splittings will appear only at order M_s^4 , so they will be of the form $\lambda^n M_s^4 / M_x^2$,

where M_x is the GUT scale, arising from loop integrations for dimensional reasons. These quantum contributions introduce corrections⁽²²⁾ to Eq.(21). For instance, in the decoupling situation, scalar bosons associated to light fermions tend to become massive, which goes in the direction required by experiments. The price is Susy breaking at a high scale, $\lambda^n M_s^4/M_x^2 \gtrsim (16 \text{ GeV})^2$, i.e., $M_s^2 \gtrsim M_w M_x$, not very far from the scale where supergravity effects become important.

Once gluinos become massive (through radiative corrections) they may, in turn, generate scalar quark masses through quantum loops. Indeed, the diagrams (12) do not cancel anymore, since the negative gluino contribution is depressed by its mass, and one ends with a positive (mass)² for scalar quarks.

Susy breaking in connection with diagrams (13) has a very interesting application to gauge symmetry breaking. Indeed, the scalars being heavier than the fermions, the positive contribution from the bosonic loops are dominated by the negative fermion loop contribution. This results in a negative mass term for the external scalars⁽²³⁾. If these are taken to be the Higgs bosons, the internal lines being quarks and squarks, the coupling constant λ is then related to the quark mass, m_q , through $\lambda \sim g m_q / M_w$. In order to obtain $SU(2) \times U(1)$ breaking at the Fermi scale, G_F , one needs (taking into account logarithmic factors) a large λ , such that $m_q > 60 \text{ GeV}$. The corresponding quark could be the t-quark or other heavy quark of a new fermion family. This idea has some elegance, since the $SU(2) \times U(1)$ breaking is induced by Susy breaking effects. It is clear that the t-quark (or other heavy fermion) mass also plays a role. Then there is a relation among M_s (through the scalar masses), M_w and m_t . At this stage of the experimental situation, the adoption of this scenario remains a question of personal taste.

The intention of this rather long discussion is to give an impression of the many aspects of Susy breaking that appear in global Susy GUT model building. We now turn to a very short summary of these models, their issues and problems. Then, we will discuss supergravity models and show their advantages.

GLOBAL SUSY GUT MODELS

We will give a simplified classification of global Susy GUTS in F-type^(*) and D-type^(**) models, based on the primordial Susy breaking mechanism^(24,25).

(*) Or Fayet-O'Raifeartaigh, see Ref. 24).

(**) Or Fayet-Iliopoulos, see Ref. 25).

In practice they often appear more or less mixed.

In F-type Susy GUT models^(21,26), the goldstino is in one of the chiral (matter) multiplets. Matter fields feel the Susy breaking through their Yukawa couplings to this goldstino, or, eventually through radiative corrections. Susy breaking is introduced by a rather special choice of the superpotential in Eq.(8)⁽²⁴⁾. In particular, one needs a non-vanishing η_i which is always associated to a gauge-singlet chiral multiplet. This superpotential has also to provide the breaking of $SU(5)$ into $SU(3) \times SU(2) \times U(1)$ at the scale M_x .

As far as the mass differences between squarks and quarks, sleptons and leptons, are concerned, the sum rule in Eq. (21) is not very promising as compared to the experimental requirements, and, in practice, it turns out to be inconsistent with realistic model building⁽¹⁵⁾. Therefore one has to exploit the radiative corrections to introduce mass splittings. The scalar quarks turn out to have masses of $O(g^4 \lambda^n M_s)$ ⁽²⁶⁾, or of $O(\lambda^2 M_s^2 / M_x)$ in models with decoupling⁽²¹⁾. Gluino and photino masses⁽²⁷⁾ are also radiative and of $O(g \lambda^n M_s)$ or of $O(g^2 M_s^2 / M_x)$, respectively. These masses are assumed to be around the TeV region.

The spectrum of these F-type Susy GUTS consists then of : a) a heavy world, with masses of $O(M_x)$ and $(mass)^2$ splittings of $O(M_s^2)$, consisting of states that couple more or less directly to the goldstino and also break $SU(5) \rightarrow SU(3) \times SU(2) \times U(1)$; b) a light world, consisting of quarks, squarks, leptons, sleptons and some Higgs bosons and their Higgsinos, that are not coupled directly to the goldstino and feel Susy breaking only through radiative corrections.

The $SU(2) \times U(1)$ breaking is achieved through radiative corrections and the non-degeneracy of states in the light world (that are those coupled to Higgs doublets). In decoupling models, one then obtains $\lambda^2 M_s^2 / M_x \sim M_w$ which gives

$$m_{3/2}^2 = \frac{M_s^2}{\sqrt{3} M_p} \simeq \frac{M_w M_x}{\lambda^2 M_p} \sim O(M_w) \quad (22)$$

Hence, one should worry about supergravity effects. For the other class of models M_s^2 is related to M_w through a large number of coupling constants and one could neglect supergravity effects if $M_s \sim 10^{-8} - 10^{-9}$. These models are consistent with approximate global Susy, but have a very cumbersome field content and ad hoc interactions^(21,26).

In D-type Susy GUT models^(27,28) the goldstino is a gaugino. It couples to matter through $g_A T^A$, i.e., with the same strength as the corresponding gauge boson. Supersymmetry may be broken only if one replaces⁽²⁵⁾

$$Z_i^* T_{\bar{j}}^{Ai} Z^j \rightarrow Z_i^* T_{\bar{j}}^{Ai} Z^j + \xi^A \quad (23)$$

The constants ξ^A may be added only to abelian charges T^A , because of the gauge invariance. This implies that the goldstino-gaugino has to be associated to a $U(1)$ factor in the gauge group. As discussed before, the difference in (mass)² between bosons and fermions will be proportional to T^A . Hence, this abelian symmetry cannot be the weak hypercharge, Y , which has both positive and negative eigenvalues. One needs some abelian charge that has the same sign for all quarks and leptons in order to give positive (mass)² to all squarks and sleptons. Then, some heavy matter fields are introduced with the opposite sign of the abelian charge that has to be traceless in a renormalizable model. A $SU(3) \times SU(2) \times U(1) \times U(1)$ model⁽²⁷⁾ has been constructed along this lines, but it has been noticed that triangle anomalies cannot be avoided. The proposed solution was to break this additional $U(1)$ at M_p , where renormalization is no more under control, through some $VEV \sim M_p$. But then one has to take care of supergravity effects⁽²⁹⁾. On the other hand, it is not clear how to build a grand-unified extension of this model.

As a general remark, the hierarchy problem is solved by Susy in all these models, at the expense of introducing a very complex structure. Susy breaking requires very special interactions, while reasonable scalar masses, through radiative corrections, ask for a very large scale of Susy breaking.^(*) All that points to local supersymmetry, which we now turn to discuss^(*).

EFFECTIVE THEORY FROM BROKEN LOCAL SUPERSYMMETRY

Supergravity interactions may induce the superHiggs phenomenon (spontaneous breaking of local supersymmetry) through scalar fields taking VEV's of $O(M_p)$, its natural scale⁽¹⁸⁾. In this case one has to reanalyse the flat limit, $M_p \rightarrow \infty$, in order to obtain an effective theory at energies $\ll M_p$ ⁽⁶⁾.

We start with a single chiral multiplet (ψ_G, Z_G) . The superpotential in Eq.(5) may be chosen in such a way that the supergravity potential, Eq.(7) has its minimum value for $\langle Z_G \rangle \sim O(M_p)$. This minimum of the potential is proportional to the square of the cosmological constant which has to vanish in a realistic theory. Interestingly enough, this situation,

$$\frac{\partial V}{\partial Z_G} = 0 \quad V = 0 \quad (24)$$

(*)-----
We refer to Ref.(30) for a complete, more technical review of the matters presented in the next two sections.

is very easily obtained with a simple choice of the superpotential, Eq.(5), such that supersymmetry is broken at the scale $M_s^2 = \sqrt{3} M_p m_{3/2}$, the gravitino mass $m_{3/2}$ being an arbitrary parameter. The ψ_G fermion is the would-be goldstino, incorporated with the gravitino through the superHiggs phenomenon.

The next steps in order to obtain an effective theory from spontaneously broken supergravity is then⁽⁶⁾ :

(i) The goldstino multiplet is coupled to matter multiplets describing the gauge theory through gravitational interactions. This may be realized through several choices of the superpotential (z^i refers to the whole set of complex scalars in matter multiplets), e.g. (6,30,31,32)

$$f_p(z_G) + f(z^i) \quad (25)$$

$$f_p(z_G) f(z^i) / M_p^3 \quad (26)$$

$$f_p(z_G) + f(z^i) + \frac{z_G}{M_p} g(z^i) \quad (27)$$

where $f_p(z_G)$ is the superpotential that induces the superHiggs effect, with $\langle z_G \rangle \sim 0(M_p)$, and defines the gravitino mass, $m_{3/2}$. The matter superpotentials, $f(z)$ and $g(z)$, will be defined accordingly to the gauge theory under consideration. The gravitational interactions between z_G and the matter scalars, z^i , are defined by the potential in Eq.(7).

(ii) The flat limit, $M_p \rightarrow \infty$ is taken, after the shift of z_G , with the gravitino mass fixed. This defines an effective gauge theory for energies $\ll M_p$. The resulting scalar potential consists of the global Susy potential, Eq.(8), plus terms that explicitly break supersymmetry. These are "soft" in the sense that the resulting theory is renormalizable without quadratic divergences⁽¹⁶⁾. They are proportional to $m_{3/2}$, that gives the strength of supergravity residual interactions. More precisely, one obtains the effective potential (6,30)

$$V_{\text{eff}} = |f_i + m_{3/2} z_i^*|^2 + \frac{1}{2} g_A^2 (z_i^* z_j^*)^2 + m_{3/2} (h(z) + h^*(z^*)) \quad (28)$$

where $h(z)$ is a cubic analytic polynomial that is defined by the particular choice of the superpotential, like, e.g., those in Eqs.(25,26,27). Supersymmetry is broken by two kind of terms :

$$m_{3/2}^2 z_i^* z_i \quad (29)$$

$$m_{3/2} (f_i z_i^* + h(z) + h.c.) \quad (30)$$

The mass terms (29) give a contribution $m_{3/2}^2$ to the masses of all scalars

in the model. This gives a very natural explanation why scalars should be heavier than the corresponding fermions, as required by experiments, and solves one of the major phenomenological problems in Susy theories^(5,33). The universality of this mass term is a result of the assumption of canonical kinetic terms. Including a field dependent metrics for the kinetic part of the supergravity lagrangian would just replace $m_{3/2}^2$ in (29) by an arbitrary matrix with matrix element of $O(m_{3/2})$ ^(30,32).

The cubic analytic polynomials⁽⁶⁾ in (30), proportional to $m_{3/2}$, has also an important role in the breaking of gauge symmetries. Indeed, the mass terms (29) would remove the minima with $Z \neq 0$, were it not for the terms in (30), that may give negative contributions to $V_{\text{eff}}^*(Z, Z)$. This point will be discussed in more detail later.

Notice that even if local Susy is broken at a scale of $\sqrt{m_{3/2} M_p}$, matter fields that are relevant at low energies only feel this breaking at an effective scale $m_{3/2}$, because of their gravitational coupling, $1/M_p$, to the goldstino. The arbitrary parameter $m_{3/2}$ is constrained by physical requirements. The fact that scalars get masses around $m_{3/2}$ from broken supergravity implies $m_{3/2} > 16$ GeV. But $m_{3/2}$ should not be much larger than M_W ^(5,6,33,34). Otherwise, $SU(2) \times U(1)$ symmetry breaking would be produced by some compensation between the terms (29) and (30) so that scalars would have vacuum expectation values of $O(m_{3/2})$. Then, M_W would be related to $m_{3/2}$ by some algebraic function of the coupling constants. An educated guess (confirmed by more detailed analyses) would then be $m_{3/2} < 1$ TeV. This puts broken supergravity effects just in the energy region that is now beginning to be explored in particle experiments.

Most of the models in the literature correspond to simple choices for the goldstino-matter coupling, such that, in these models

$$h(Z) = (A-3)f(Z) \quad (31)$$

An interesting class of models⁽³¹⁾ assumes Eq.(26) and has $A=3$, i.e., $h(Z) = 0$. They have the nice property that $V_{\text{eff}} \geq 0$. Their minima at $V_{\text{eff}} = 0$ are defined by the set of equations :

$$f_i + m_{3/2} z_i^* = 0 \quad (32)$$

Eq.(32) is also a sufficient condition for the vanishing of the $z_i^* t^{A_{ij}} z_j$ terms in the effective potential⁽³⁵⁾. In general, there are several degenerate minima, giving rise to different patterns of gauge symmetry breaking, in close

analogy with supersymmetric potentials.

The term $m_{3/2} Z^*$ in Eq.(32) may drive VEV's of $O(m_{3/2})$ in certain directions. Then, the gauge symmetry breaking may be induced by residual supergravity interactions, the characteristic scale being $O(m_{3/2})$. For more general expressions (e.g. $A \neq 3$) of the potential the minimization is more involved but the possibility of supergravity induced gauge symmetry breaking persists under some circumstances to be discussed later.

In the physical situation, the low energy broken gauge symmetry is the $SU(2) \times U(1)$ invariance of electroweak interactions, and the problem we will discuss is how to induce its spontaneous breaking through the residual supergravity interactions. The relevant low energy effective potential is defined after both supergravity and grandunified gauge symmetries are spontaneously broken. In particular, the heavy fields, with masses of $O(M_x)$ have decoupled^(*). All mass parameters in the effective theory have to be residues of the super-Higgs mechanism. They are of $O(m_{3/2}) \sim O(M_w) \ll M_x$. Any (technically "natural") fine-tuning of grandunified mass parameters has to be avoided. It is possible to construct GUT models where this situation is realized⁽³⁸⁾. The effective superpotential, $f(Z)$, in Eq.(28), as well as the analytic function $h(Z)$, can have only trilinear couplings :

$$f(Z) = \frac{1}{6} \lambda_{abc} Z^a Z^b Z^c \quad (33)$$

i.e., only dimensionless Yukawa coupling constants, to $O(m_{3/2}^2/M_x)$. Models that satisfy the relation in Eq.(31) with an homogeneous trilinear superpotential, Eq.(33) have the interesting property⁽³⁹⁾ that the existence of non-trivial ($Z_i \neq 0$) minima is controlled by the value of the parameter A . It is easily checked that for $A < 3$ the absolute minimum is the trivial one, $Z_i = 0$, $v = 0$. The first models^(6,7) had $A = 3 - \sqrt{3}$ and needed a (fine-tuned) mass parameter of $O(M_w)$ to break $SU(2) \times U(1)$. The case $A = 3$ has already been discussed : there are, in general, several degenerate minima.

The interesting case, at least at the tree-level, is $A > 3$, where the absolute minimum is obtained for $Z_i \neq 0$. This is just because the negative contributions from the trilinear terms become large enough. Therefore, gauge invariances may be spontaneous broken at the tree-level by supergravity

^(*)The decoupling of heavy fields in the presence of broken Susy has some peculiarities^(36,37). In particular, gaugino masses are generated, as discussed in the next section.

interactions at scales of $O(m_{3/2})$ for $A > 3$.

At the quantum level, however, the parameters in Eq.(28) will have a logarithmic dependence in the energy scale. Since $g^2 \ln(m_{3/2}/M_x) \sim O(1)$, the form of the effective potential at scales like $m_{3/2}$ or M_w , which is relevant for low-energy physics, may be rather different from the effective potential at scales of $O(M_x)$ or $O(M_p)$ where the contact is made with the supergravity lagrangian. In particular, the minima of this potential are no more constrained by non-renormalization theorems because of the explicit soft supersymmetry breaking interactions. Their pattern has to be analysed by taking radiative corrections into account. It looks attractive to require a simple form of the effective theory at very high energies (say, M_x , to take into account the grandunified symmetry breaking). Hence, we will assume canonical kinetic terms in the Sugra lagrangian and the effective potential in Eq.(28), together with the restrictions in Eqs.(31) and (33), as boundary conditions at scales of $O(M_x)$. Then we will introduce the energy dependence of these parameters at the one-loop level in order to discuss the $SU(2) \times U(1)$ breaking in the presence of supergravity. But, first, we have to study the question of gaugino masses which, besides their physical relevance, play also some role in the rescaling of the scalar potential parameters.

GAUGINO MASSES

Gaugino masses may arise in several ways. A (non-canonical) field dependent metrics for the kinetic terms of the gauge supermultiplets may give rise to a Majorana mass to gauginos⁽⁵⁾. This would introduce another soft supersymmetry breaking term in the effective Lagrangian. Such tree-level gaugino masses are free parameters of $O(m_{3/2})$ (one for each simple or abelian factor in the gauge group).

Spontaneous breaking of some gauge symmetries also give masses to the corresponding gauginos through their mixing with the fermionic partners of the would-be Goldstone bosons. This happens to gauginos with lepto-quark quantum members in the context of grandunification, which get masses of $O(M_x)$, as well as, to the fermionic partners of the intermediate weak bosons, which acquire masses of $O(M_w)$.

Gauginos associated to unbroken symmetries at the grand-unifying scale, M_x , get mass contributions from one-loop quantum corrections due to the Susy breaking splittings in the masses of the ultraheavy particles (those acquiring masses of $O(M_x)$). These radiative masses are given by the simple expression⁽⁴⁰⁾

$$\mu_A = \frac{\alpha_A(\mu_A)}{2\pi} \eta m_{3/2} T(R), \quad T(R) = \text{Tr}(T_A^2) \quad (34)$$

where the trace is taken over the gauge representation R of the heavy chiral supermultiplets. The contributions from usual representations of SU(5) are

$$T(5) = \frac{1}{2}, \quad T(24) = 5, \quad T(50) = \frac{35}{2}, \quad T(75) = 25 \quad (35)$$

For instance, in a recently proposed model (without fine-tuning)⁽³⁸⁾, one has $T(R) = 97$. The factor $\eta \sim 0(1)$ depends on the goldstino coupling to the heavy matter and, in particular, on the value of A . For the popular $A = 3$ case, $\eta = 1$. The logarithmic renormalization of μ_A is taken into account by the scale dependence in the gauge coupling α_A . In particular, the photino and gluino masses are related by

$$\frac{\mu_g}{\mu_g} = \frac{8}{3} \frac{\alpha_{e.m.}}{\alpha_s(m_{3/2})} \simeq \frac{1}{6} \quad (36)$$

Eq.(34) suggests rather large masses for gluinos in Sugra GUTS. Since $T(R) \geq 6$ (much larger in models without fine-tunings),

$$\mu_g \gtrsim \alpha_s(\mu_g) m_{3/2} \gtrsim 4 \text{ GeV} \quad (37)$$

as $m_{3/2} > 16$ GeV. This is consistent with the present experimental bounds⁽⁴¹⁾. From this point of view, non-canonical kinetic terms are not needed.

One-loop contributions to gaugino masses from light multiplets are very small⁽⁴²⁾. The trilinear soft interactions in Eq.(28) induce logarithmically divergent gaugino masses at the two-loop level^(16,42,43). This is consistent with the fact that gluino masses are free parameters in the effective theory. By imposing boundary conditions such to make the contact with minimal (i.e., canonical kinetic terms) supergravity at scales of $0(M_p)$, the two-loop corrections become negligible (as compared to one-loop contributions). Roughly speaking the gluino mass should not differ from $m_{3/2}$ by more than one order of magnitude, in either direction, whatever the mass generating mechanism may be.

RENORMALIZATION PROPERTIES

Let us consider the one-loop renormalization of the following scalar potential⁽⁴⁰⁾

$$V_{\text{eff}} = |\lambda_{ijk} Z^j Z^k|^2 + \frac{1}{2} g_A^2 (Z^* T^A Z)^2 + m_i^2 |Z^i|^2 + \frac{1}{6} m_{3/2} A_{ijk} \lambda_{ijk} Z^i Z^j Z^k \quad (38)$$

which is the most general form consistent with renormalization effects under the following assumptions for the boundary conditions at energies of $0(M_x, M_p)$:

a) Eq.(33), to avoid fine-tuned parameters.

b) $\lambda_{ijk} = \lambda_{\ell jk} \delta_i^\ell$, such that, e.g., $\beta_i^k = \beta_i \delta_i^k$ in Eq.(14), in order to avoid representation mixing, that could spoil decoupling properties and also flavour conserving in neutral current interactions. This allows for the definition of the parameters A_{ijk} .

c) We assume the boundary conditions $m_i^2(M_p) = m_{3/2}^2$ and $A_{ijk}(M_p) = A$, i.e., universality of the goldstino (gravitational) coupling to the matter fields. (The parameter $m_{3/2}$ so defined could differ from the actual gravitino mass by a factor of 0(1) if non-canonical terms are allowed consistently with our assumptions).

The scale (μ) dependence of the parameters in Eq.(38) at the one-loop level is given by the following renormalization group equations :

$$\begin{aligned} \frac{d}{d \ln \mu} A_{ijk} &= \frac{1}{16\pi^2} \left\{ |f_{imn}|^2 A_{imn} - 4 \left[\frac{\mu_A}{m_{3/2}} g_A^2 (T^A)^2 \right]_i^{(i+j)+(i+k)} \right\} \\ \frac{d}{d \ln \mu} m_i^2 &= \frac{1}{16\pi^2} \left\{ |f_{imn}|^2 [m_i^2 + m_m^2 + m_n^2 + m_{3/2}^2] - 8 [\mu_A^2 g_A^2 (T^A)^2]_i \right\} \end{aligned} \quad (39)$$

together with Eq.(14) for λ_{ijk} . These evolution equations are particular cases, appropriate to the assumptions b) and c) above, of more general results .

In order to illustrate the renormalization effects on the minima of the Sugra effective potential, let us consider a very simple case, with just one chiral multiplet, and

$$\begin{aligned} f(z) &= \frac{\lambda}{3} z^3 \\ v &= |\lambda z^2|^2 + m_z^2 |z|^2 + \frac{\lambda}{3} A m_{3/2} (z^3 + z^{*3}) \end{aligned} \quad (40)$$

which has a local minimum at $z = 0$ and another one at

$$\begin{aligned} |z| &= \frac{A m_{3/2}}{2\lambda} \sigma & \sigma &= \frac{1+\sqrt{1-8\rho}}{2} \\ v_{\min} &= - \frac{A^4 m_{3/2}^4}{8\lambda^2} \sigma^2 \left(\frac{\sigma}{6} - \rho \right) & \rho &= \frac{m_z^2}{A^2 m_{3/2}^2} \end{aligned} \quad (41)$$

for $\rho < 1/8$. The $z \neq 0$ solution is the absolute minimum for $\rho < 1/9$. From the renormalization group equations, Eqs.(14) and (39), one obtains (for $\rho < 1/3$)

$$\rho(\mu) = \rho(\mu_o) + \frac{\lambda^2(\mu_o)}{4\pi^2} [1 - 3\rho(\mu_o)] \ln \frac{\mu}{\mu_o} \quad (42)$$

Therefore, for μ of the order of $|z|$ in Eq.(5), the absolute minimum is

obtained at this non-trivial value of z , if $\rho(\mu) < 1/9$, i.e.,

$$\ln \frac{\mu_0}{\mu} > \frac{4\pi^2}{\lambda^2(\mu_0)} \frac{\rho(\mu_0)-1/9}{1-3\rho(\mu_0)} \quad (43)$$

Therefore, if $1/3 > \rho(\mu_0 = M_p) > 1/9$, for small enough values of μ/M_p the non-trivial minimum may be driven by radiative corrections^(*). In realistic models, which we now turn to discuss, the situation is more involved due to the coexistence of many fields.

SUPERGRAVITY WEINBERG-SALAM MODEL

Let us consider now an explicit $SU(3) \times SU(2) \times U(1)$ model with spontaneously broken local supersymmetry. Matter supermultiplets whose fermionic components are the usual (left-handed) quarks, antiquarks, leptons and antileptons have to be introduced in the following representations of the gauge group :

$$Q_i \sim (3, 2, 1/6), \quad U_i \sim (\bar{3}, 1, -2/3), \quad D_i \sim (\bar{3}, 1, 1/3), \\ L_i \sim (1, 2, -1/2) \quad E_i \sim (1, 1, 1) \quad (44)$$

where $i=1,2,3$ is a family index. $SU(3)$ and $SU(2)$ indices will be omitted. One has also to introduce two Higgs supermultiplets containing two doublets of Higgs scalars with opposite weak hypercharges :

$$H \sim (1, 2, 1/2) \quad H' \sim (1, 2, -1/2) \quad (45)$$

such that the contributions of their fermionic components to the anomalies will cancel each other. The most general trilinear $SU(3) \times SU(2) \times U(1)$ invariant superpotential constructed out of the complex scalars in the multiplets (44) and (45) is

$$f_M = h_{U_i} H Q_i U_i + h_{D_i} H' Q_i D_i + h_{E_i} H' L_i E_i \quad (46)$$

(the same notation is used for supermultiplets and for their scalar components). The Yukawa coupling constants are related to the lepton and quark masses through

$$m_{u_i} = h_{U_i} \langle H \rangle \quad m_{d_i} = h_{D_i} \langle H' \rangle \quad m_{e_i} = h_{E_i} \langle H' \rangle \quad (47)$$

and are required to be rather small as compared to the gauge coupling constants,

^(*) Notice, for further use, that the potential minimum in Eq.(41) is proportional to λ^{-2} .

with the possible exception of $m_t = m_{u_3}$.

As discussed before we want to induce VEV's for H and H' , that break $SU(2) \times U(1)$, from Sugra residual interactions. In a first step we neglect radiative corrections and consider the effective potential in Eq.(28) together with Eq.(31), defining the parameter A . For $A \geq 3$, the potential associated to f_M would have a minimum for $\langle H' \rangle = \langle L \rangle = \langle E \rangle$, which is unacceptable since it would break the electromagnetic gauge invariance. One has to introduce new terms in the superpotential involving only H and H' . This requires a new gauge singlet supermultiplet Y , and

$$f_B = \lambda Y H H' + \lambda' Y^3 \quad (48)$$

so that the whole superpotential is $f_M + f_B$ (the Y^3 term is needed to avoid a Goldstone boson associated to a broken global $U(1)$ symmetry for $\lambda' = 0$, when the scalars take non vanishing VEV's) We will discuss the role of f_M later on, and will first consider only the f_B superpotential. From the previous discussion, the corresponding potential has a non-trivial minimum $\langle H \rangle = \langle H' \rangle \neq 0$ for $A > 3$ (an inequality is also required between λ and λ' to avoid solutions with only $\langle Y \rangle \neq 0$). The $SU(2) \times U(1)$ breaking is induced by Sugra : this will be called the singlet mechanism⁽³⁹⁾. The weak boson mass will be related to $m_{3/2}$. For simplicity, we consider the "magic" case : $A = 3$. Solving the set of equations resulting from Eq.(32) we get a solution with⁽³⁸⁾

$$\langle H \rangle = \langle H' \rangle = \frac{m_{3/2}}{\lambda} \left(1 \pm \left| \frac{\lambda'}{3\lambda} \right| \right)^{1/2}, \quad \langle Y \rangle = \frac{m_{3/2}}{\lambda} \quad (49)$$

which breaks $SU(2) \times U(1)$. The resulting weak boson masses are related to $m_{3/2}$ by

$$M_w = \frac{g_w}{\lambda} m_{3/2} \left(1 \pm \left| \frac{\lambda'}{3\lambda} \right| \right)^{1/2} \quad (50)$$

The mass spectrum of the particles in the model is as follows⁽³⁸⁾. Their are two charged fermions, with masses

$$\left(M_w^2 + \frac{m_{3/2}^2}{4} \right)^{1/2} \pm \frac{m_{3/2}}{2} \quad (51)$$

and two neutral fermions with masses related to (51) by $M_w \rightarrow M_z = M_w / \cos \theta_w$, as well as two more neutral fermions with masses of $O(m_{3/2})$. Charged Higgs scalars acquire a mass

$$\left(M_w^2 + 4m_{3/2}^2 \right)^{1/2} \quad (52)$$

while a neutral scalar has a corresponding mass with $M_w \rightarrow M_z$. The remaining four neutral scalars have masses of $0(m_{3/2})^{(*)}$.

The scalar leptons have masses $m_{3/2}$, up to corrections of $0(m_\ell)$ and small renormalization effects. The scalar quarks get masses⁽⁴⁰⁾

$$\tilde{m}_q^2 = m_{3/2}^2 + \frac{8}{9} \tilde{\mu}_g^2 \left(1 - \frac{\alpha_s(M_x)}{\alpha_s(m_{3/2})} \right) \quad (53)$$

neglecting the quark masses (which could be a bad approximation for the t-quark scalar). The term proportional to the gluino (mass)² is introduced by the renormalization due to strong interactions.

Now, one has also to take into account the remaining part of the superpotential, f_M , given by Eq.(46), in addition to f_B . For $A=3$, this introduces a further series of degenerate solutions which break colour and/or e.m. invariance. One cannot assume $A > 3$ to lift this degeneracy, since this would always favour the wrong solution that breaks the e.m. gauge invariance⁽⁴³⁾. The origin of this problem is due to the fact that the Yukawa coupling associated to the electron is the smallest coupling constant in the whole superpotential (see Eq.(47)). Indeed, as suggested by the simple example in Eq.(41), the preferred solution will be that corresponding to the smallest coupling constant.

A possible way out of this puzzling situation is provided by the quantum corrections.

SU(2)×U(1) BREAKING IN SUPERGRAVITY

We have already emphasized the role of radiative corrections in the problem of supergravity induced gauge symmetry breaking. Now, we will discuss two approaches to this question in the physical situation of the extended Weinberg-Salam theory.

One possibility⁽⁴⁰⁾ is to consider the singlet method described above and to see under which conditions the acceptable solution $\langle H \rangle$, $\langle H' \rangle \neq 0$ may be favoured by radiative corrections. We start with the potential in Eq.(30), with the couplings defined by the superpotential $f_M + f_B$, Eqs.(46) and (48). Let us first note that the parameter λ cannot be very small because of Eq.(50),

^(*) See Ref.(47) for a more detailed discussion of the mass spectrum, including the gaugino masses neglected here.

where M_w and g_w are known and $m_{3/2} > 16\text{GeV}$. The other coupling constants that may be relatively large are the gauge couplings of $SU(3) \times SU(2) \times U(1)$ (g_S, g_w, g') and possibly the h_T coupling, governing the t -quark mass. These are the parameters that have to be taken into account in the adequate renormalization group equations, Eqs.(14) and (40). We assume $A_{ijk} = 3$ and $m_i^2 = m_{3/2}^2$ at M_p and study the behaviour and the minima of the scalar potential for reasonable choices of λ, λ', h_T . The $SU(3) \times SU(2) \times U(1)$ solution ($Y \neq 0, H = H' = 0$) is avoided if one chooses $\lambda' \sim \lambda$ at M_p . For instance, by taking at the scale M_x :

$$\frac{\lambda^2}{4\pi} = \frac{\lambda'^2}{4\pi} = 0.1 \quad \frac{h_T^2}{4\pi} = 0.0004$$

$$A_{YHH'} = A_{YYY} = A_{HTQ} = 3 \quad m_i^2 = m_{3/2}^2$$

We find after rescaling the parameters down to energies $\sim 0(M_w)$, the values (in $m_{3/2}$ units)

$$\frac{\lambda^2}{4\pi} = 0.03 \quad \frac{\lambda'^2}{4\pi} = 0.017 \quad \frac{h_T^2}{4\pi} = 0.0045$$

$$m_Y^2 = -0.62 \quad m_H^2 = 0.10 \quad m_{H'}^2 = 0.31$$

$$m_{Q_3}^2 = 0.95 \quad m_T^2 = 0.87$$

$$A_{YHH'} = 1.03 \quad A_{YYY} = -0.79 \quad A_{HTQ} = 2.74$$

The absolute minimum of the potential is the $SU(2) \times U(1)$ breaking, $U(1)_{e.m.}$ conserving one :

$$\langle H \rangle = 1.32 \quad \langle H' \rangle = 1.28 \quad \langle Y \rangle = 1.94$$

in units of $m_{3/2}$. From Eq.(50), this gives $m_{3/2} = 96\text{ GeV}$ and $m_t = 37.5$. The above figures have been obtained with a gluino mass of 12 GeV but varying this parameter by an order of magnitude does not change the pattern of the solution. The t -quark mass may be increased as well up to $\sim 100\text{ GeV}$, with a corresponding decreasing of $m_{3/2}$ to 75 GeV.

With lower initial values $\lambda^2/4\pi = \lambda'^2/4\pi = 0.01$ at M_x one still gets an analogous solution with $m_{3/2}$ around 30 GeV, an appealing value.

We conclude from this numerical analysis that the $SU(2) \times U(1)$ breaking may be correctly induced by supergravity effects, once radiative corrections are taken into account. The above results are consistent with $m_t \lesssim 100\text{ GeV}$,

this parameter playing a secondary role in the process.

Instead, in the alternative approach^(44,45) to $SU(2) \times U(1)$ breaking, the crucial parameter is a large h_T constant, giving rise to a very heavy t -quark. No singlet supermultiplet Y is needed since the auxiliary superpotential f_B is not introduced (this is a very appealing feature). The h_T parameter (hence m_t) tends to increase when strong interactions (controlled by Λ_{QCD}) become strong. Then, by a mechanism we have discussed before, the parameter m_H^2 becomes negative and $\langle H \rangle \neq 0$ is induced and $SU(2) \times U(1)$ is spontaneously broken. There is some complicated relation between $m_{3/2}$, M_w and m_t , which has to be as large as $m_t \gtrsim 100$ GeV (a lower limit, ~ 70 GeV, is obtained by assuming heavy gluinos). However, the model falls short in explaining some of the fermion masses, since $\langle H' \rangle = 0$, unless some modification is introduced.

An amusing variant⁽⁴⁵⁾ of this approach assumes a small value of $m_{3/2}$, 16 GeV $< m_{3/2} << m_t$. It follows rather closely the original Coleman-Weinberg mechanism⁽⁴⁶⁾ and its supersymmetric version⁽²³⁾. These assumptions are designed to animate experimenters, since the authors predict a relatively low-lying mass spectrum.

In summary, broken supergravity, at tree-level, without fine-tuned mass parameters, is not adequate to induce $SU(2) \times U(1)$ breaking, contrarily to our expectations. Interestingly enough, radiative corrections provide the required ingredients to reverse the situation. *Audaces fortuna juvat !*

CONCLUDING REMARK

There is no compelling reason for introducing supergravity in particle physics but there are good theoretical motivations to do so. It supplies a bridge-head in the field of gravitational interactions for further unification. It provides an elegant suppression of quadratic divergences and solves the hierarchy problem of grandunification. Finally, it should leave some tracks in the effective low-energy gauge theory that would allow for experimental tests of its reality.

The deviations from approximate supersymmetry are controlled by the fundamental parameter $m_{3/2}$, which is its natural scale for the partners of light particles. Moreover, the weak interaction scale M_w should not differ very much from $m_{3/2}$, at least in the simple approach that has been presented here. Therefore, the effects of supersymmetry, and of the underlying supergravity, are not expected to show up below those energies that are just beginning to be explored. Scalars and gauginos were never found where they were not expected to be ! But it is rather frustrating to realize that we probably have to wait until the next generation of accelerators to be or not

to be supersymmetric. DURA LEX, SED LEP.

ACKNOWLEDGEMENTS

I would like to thank J.-P. Derendinger and S. Ferrara for valuable discussions during the last few years. I also thank J. Tran Thanh Van and the organizers for their invitation as well as for the enjoyable atmosphere of this meeting.

REFERENCES

- 1) J.Wess and B.Zumino, Nucl.Phys. B70, 39 (1974)
- 2) See, e.g., P.Fayet and S.Ferrara, Phys.Rep. 32, 251 (1977)
- 3) D.Z.Freedman, P.van Nieuwenhuizen and S.Ferrara, Phys.Rev. D13, 3214 (1976)
S.Deser and B.Zumino, Phys.Lett. B62, 335 (1976)
For a review see, e.g. : P.van Nieuwenhuizen, Phys.Rep. C68, 189 (1981)
- 4) E.Witten, Nucl.Phys. B185, 153 (1981)
- 5) E.Cremmer, S.Ferrara, L.Girardello and A.van Proyen, Phys.Lett. 116B, 231 (1982) and Nucl.Phys. B212, 413 (1983)
- 6) R.Barbieri, S.Ferrara and C.A.Savoy, Phys.Lett. 119B, 343 (1982)
- 7) A.H.Chamseddine, R.Arnowitt and P.Nath, Phys.Rev.Lett. 49, 970 (1982)
- 8) See, e.g., proceedings of the CERN Workshop on Supersymmetry vs. Experiment, CERN preprint, TH 3311/EP82/63 (1982).
Also : P.Fayet, Plenary Talk at XXI Int.Conf.on High Energy Physics, Paris (1982) ; proceedings of the XVII Rencontres de Moriond, ed. by Tran Thahn Van (1982) A.Savoy-Navarro, to appear in Phys.Rep.C. ; C.Llewellyn-Smith, to appear in Phys.Rep.C. ; Talks at this meeting by G.Altarelli and L.Baulieu, J.M.Frere and G.Kane, University of Michigan preprint UMHE 83 (1983).
- 9) G.Kane, Introductory talk at this meeting.
- 10) R.Barbieri, L.Maiani, S.Ferrara, F.Palumbo and C.A.Savoy, Phys.Lett. 115B, 212 (1982)
- 11) M.Sohnius and P.West, Phys.Lett. 100B, 245 (1981)
S.Ferrara and B.Zumino, unpublished
- 12) J.Wess and B.Zumino, Phys.Lett. 49B, 52 (1974)
J.Iliopoulos and B.Zumino, Nucl.Phys. B76, 310 (1974)
S.Ferrara, J.Iliopoulos and B.Zumino, Nucl.Phys. B77, 413 (1974)
R.Barbieri et al., Ref.10)
M.Einhorn and D.R.T.Jones, Nucl.Phys. B196, 475 (1982)
- 13) J.Polshinski and L.Susskind, Phys.Rev. D26, 3661 (1982)
- 14) L.Maiani, in proc. Summer School of Gif-sur-Yvette (IN2P3, Paris, 1980)

15) S.Dimopoulos and H.Georgi, Nucl.Phys. B193, 150 (1981)
 N.Sakai, Zeit.für Phys. C11, 153 (1982)

16) L.Girardello and M.T.Grisaru, Nucl.Phys. B194, 65 (1982)

17) J.Ellis and D.V.Nanopoulos, Phys.Lett. 110B, 44 (1982)
 R.Barbieri and R.Gatto, Phys.Lett. 110B, 211 (1982)

18) S.Deser and B.Zumino, Phys.Rev.Lett. 38, 1433 (1977)

19) W.Fischler, H.P.Nilles, J.Polshinski, S.Raby and L.Susskind, Phys.Rev. Lett. 47, 557 (1981)

20) S.Ferrara, L.Girardello and F.Palumbo, Phys.Rev. D20, 403 (1979)

21) S.Dimopoulos and S.Raby, Los Alamos preprint LA-UR-82-1282 (1982)

22) L.Girardello and J.Iliopoulos, Phys.Lett. 88B, 85 (1979)

23) L.Ibanez and G.G.Ross, Phys.Lett. 110B, 215 (1982)

24) L.O'Raifeartaigh, Nucl.Phys. B96, 331 (1975)
 P.Fayet, Phys.Lett. 58B, 67 (1975)

25) P.Fayet and J.Iliopoulos, Phys.Lett. 51B, 461 (1974)

26) J.Ellis, L.Ibanez and G.G.Ross, Phys.Lett. 113B, 283 (1982)

27) M.Barbieri, S.Ferrara and D.V.Nanopoulos, Zeit.für Phys. C13, 267 (1982)

28) S.Weinberg, Phys.Rev. D26, 287 (1982)

29) M.Barbieri, S.Ferrara, D.V.Nanopoulos and K.S.Stelle, Phys.Lett. 113B, 219 (1982)

30) For a review see : R.Barbieri and S.Ferrara, CERN preprint, to appear in (1983)

31) E.Cremmer, P.Fayet and L.Girardello, Phys.Lett. 122B, 346 (1983)

32) S.K.Soni and H.A.Weldon, Univ. of Pennsylvania preprint (1983)

33) J.Ellis and D.V.Nanopoulos, Phys.Lett. 116B, 133 (1982)

34) M.K.Gaillard, L.J.Hall, B.Zumino, J.del Aguila, J.Polshinski and G.G.Ross, Phys.Lett. 122B, 355 (1983)

35) F.Buccella, J.P.Derendinger, S.Ferrara and C.A.Savoy, Phys.Lett. 115B, 375 (1982)

36) J.P.Derendinger and C.A.Savoy, Phys.Lett. 118B, 347 (1982)

37) N.Sakai, Phys.Lett. 121B, 130 (1982)

38) S.Ferrara, D.V.Nanopoulos and C.A.Savoy, Phys.Lett. 123B, 214 (1983)

39) H.P.Nilles, M.Srednicki and D.Wyler, Phys.Lett. 120B, 346 (1983)

40) J.P.Derendinger and C.A.Savoy, to be published

41) See talks by C.Santoni and M.Longo at this meeting

42) R.Barbieri, L.Girardello and A.Masiero, Padua preprint IFPD6/83 (1983)

43) J.M.Frère, D.R.T.Jones and S.Raby, Michigan preprint UMHE 82-58 (1982)

- 44) L.Alvarez-Gaumé, J.Polshinski and M.B.Wise, Harvard preprint HUTP-82/A063 (1983)
L.Ibanez, Madrid preprint FTUAM/83-1 (1983)
- 45) J.Ellis, J.S.Hagelin, D.V.Nanopoulos and K.Tamvakis, SLAC preprint SLAC-PUB-3029 (1983)
- 46) S.Coleman and E.Weinberg, Phys.Rev. D7, 1888 (1973)
- 47) P.Fayet, Ecole Normale Supérieure preprint, LPTENS 83/16 (1983).

VIRTUAL EFFECTS OF SUSY PARTICLES

G. Altarelli

Dipartimento di Fisica, Università "La Sapienza", Roma
INFN - Sezione di Roma, Roma, Italy.

Abstract

We briefly report on some recent work on virtual effects of SUSY particles on the muon $g-2$, on the electroweak parameter δ and on the e^+e^- hadronic cross section.

1. - Introduction

Broken supersymmetry theories^{/1/} imply the existence of many new heavy particles and perhaps also of a few very light ones. Limits on masses have been mostly derived from the fact that none have been directly observed in production experiments till now. On the other hand the presence of these new particles could modify measurable quantities through their virtual contributions. After recalling the example of the limits derived^{/2,3/} from the experimental value of the muon g-2, we report here on two recent calculations of virtual effects of SUSY particles. The first one^{/4/} is on the influence on the electroweak β parameter, $\beta = M_W^2/M_Z^2 \cos^2 \theta_W$ measured from the ratio of charged to neutral current cross sections. The second one^{/5/} refers to the leading order QCD corrections to the ratio $R_{e^+e^-}$ of the total hadronic and the pointlike e^+e^- cross sections. In both cases we shall see that the effects of SUSY particles are small and difficult to unveil in practical experiments.

2. - The muon anomalous magnetic moment

As well known the presently measured value of the muon anomalous magnetic moment a_μ agrees very well with the QED prediction^{/6/}, so that $|\delta a_\mu| \leq 2 \cdot 10^{-8}$. The effect on a_μ of virtual photino ($\tilde{\chi}$) and s-muon exchange was considered by Fayet some time ago^{/2/}. Assuming a massless $\tilde{\chi}$ and barring possible cancellations with other corrective terms, Fayet obtained the bound on the masses of the two scalars associated with the muon given by $m_{s,t} > 15$ GeV. More recently Barbieri and Maiani^{/3/} included in their analysis also the contribution to δa_μ of $\tilde{w}, \tilde{z}, \tilde{h}$ (where \tilde{h} is the Higgs-ino and so on). They did not consider the problem in its full generality, but rather restricted the freedom on the mass spectrum to the purely indicative situation where $m_{\tilde{z}} = m_z$, $m_s = m_t = m_{\tilde{\chi}}$, $m_{\tilde{w}} = 0$ with s, t being the two s-muons and $\tilde{\nu}$ is the s-neutrino. The contributions of $\tilde{\chi}, \tilde{z}, \tilde{w}$ are all proportional to the muon mass squared. Strong cancellations are present which reflect the vanishing of a_μ in the exact SUSY limit^{/7/}. In the $m_{s,t} - m_w$ plane the allowed region is shown in fig. 1.

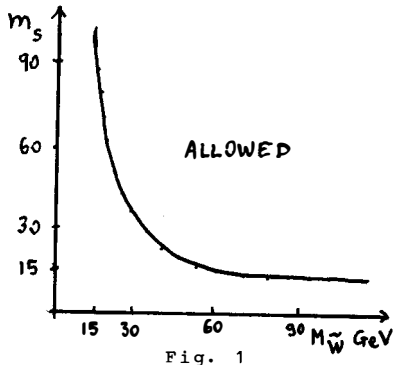


Fig. 1

3. - The ρ parameter

The ρ parameter equals unity at the tree level in the standard model with only Higgs doublets. Higher order effects modify the value of ρ . Defining $\delta\rho = 1 + \delta\rho$ one has^{8/}

$$\delta\rho = \frac{A_+(0) - A_3(0)}{M_W^2} \quad (1)$$

where $A_+, 3$ are defined as

$$W_{\mu\nu} = -ig_{\mu\nu} A_{+,3}(q^2) + \dots \quad (2)$$

from the self energy diagrams of fig. 2. A crucial observation is

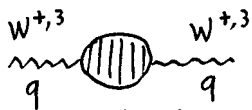


Fig. 2

that $\delta\rho$ vanishes in the limit of exact SU(2) symmetry (with w_i transforming as a triplet). For a fermion doublet (either quarks or leptons) of masses $m_{1,2}$ one obtains^{8/}:

$$\delta\rho = N_c \frac{G_F}{8\sqrt{2}\pi^2} \left[m_1^2 + m_2^2 - \frac{2 \frac{m_1^2}{m_1^2} \frac{m_2^2}{m_2^2}}{\frac{m_2^2}{m_1^2} - \frac{m_1^2}{m_2^2}} \ln \frac{\frac{m_2^2}{m_1^2}}{\frac{m_1^2}{m_2^2}} \right] \quad (3)$$

where N_c is the number of colour replicas ($N_c=3$ or 1 for quarks and leptons respectively) which in fact vanishes for $m_1=m_2$. In particular for $m_t \gg m_b \approx 0$ the top quark contribution is given by

$$(\delta\rho)_{\text{top}} \approx \frac{3G_F}{8\sqrt{2}\pi^2} m_t^2 \approx 1.25 \cdot 10^{-2} \left(\frac{m_t}{200 \text{ GeV}} \right)^2 \quad (4)$$

Conventional radiative corrections shift $^9/\rho$ downward by $\delta\rho_{\text{rad}} \approx -10^{-2}$. The experimental value of $\delta\rho$ is given ^[10] by

$$(\delta\rho)_{\text{exp}} = (2 \pm 15) \cdot 10^{-3} \quad (5)$$

From $(\delta\rho)_{\text{top}} \lesssim 2.5 \cdot 10^{-2}$ one obtains $m_t \lesssim 300 \text{ GeV}$.

In SUSY models one has contributions to $\delta\rho$ from s-quark and s-lepton doublets, weak gauginos, Higgs-inos and the additional charged and neutral Higgs scalars that are required in these models. For s-quark and s-lepton doublets the contribution to $\delta\rho$ does not depend on the absolute values of the masses but only on the mass splittings, again because of the vanishing of $\delta\rho$ in the $SU(2)$ limit. Mass splittings are severely constrained by existing limits on flavour changing neutral currents ^[11]. In minimal models with soft SUSY breaking induced by gravity ^[12] one has for the scalar masses:

$$m_s^2 = m_{3/2}^2 + m_f^2 \pm 2a m_{3/2} m_f \quad (6)$$

where $m_{3/2}$ is the gravitino mass, the \pm refer to the two scalars associated to each fermion f and a is of order unity and model dependent. For scalars associated to the $t-b$ doublet one finds, neglecting the b quark mass:

$$\delta\rho = \frac{3G_F}{8\sqrt{2}\pi^2} m_t^2 \quad \text{for } m_{3/2} \ll m_t \quad (7)$$

$$\delta\rho = \frac{2}{3} a^2 \frac{3G_F}{8\sqrt{2}\pi^2} m_t^2 \quad \text{from } m_{3/2} \gg m_t$$

Thus for $a \sim 1$ the contribution of the t - b scalars is almost the same as for the corresponding quarks and its only effect is to bring the limit on the t quark mass down to $m_t \lesssim 200$ GeV.

In the gaugino, Higgsino, Higgs sector there are strong cancellations because all dangerous quadratic or logarithmic terms in $\delta\rho$ cancel out exactly in the limit $m_{3/2} \rightarrow 0$ where the relevant couplings approach $SU(2)$ symmetry. What is left is a contribution of order

$$\delta\rho_{G-H} \simeq \frac{\alpha_W}{4\pi} \simeq 3 \cdot 10^{-3} \quad (8)$$

Where $\alpha_W = \alpha/s \sin^2 \theta_W$. Even more suppression is present if no Fayet-Iliopoulos term is associated to $U(1)$. In this case $\delta\rho_{G-H}$ vanishes for $\sin^2 \theta_W = 0$ and

$$\delta\rho_{G-H} \simeq \frac{\alpha}{4\pi} \simeq 6 \cdot 10^{-4} \quad (9)$$

In conclusion little can be learnt on SUSY particle spectroscopy from a precise measurement of ρ .

4. - The hadronic e^+e^- cross-section

It is well known that pair production of s -quarks and s -leptons is the most obvious signature for SUSY particles in e^+e^- annihilation. Negative results from searches of pairs of SUSY scalars at PETRA and PEP have led so far to lower limits^{/13/} on the masses given by $m_{s-1}, m_{s-q} \gtrsim 15-16$ GeV.

In view of these results we were led ^{/5/} to consider possible effects in the hadronic cross-sections below the threshold for s-quark pair production, i.e. at $Q \lesssim 2M$, where $Q = 2E_{beam}$ and M is the s-quark mass (for simplicity we neglect mass differences for (light) s-quarks which are expected to be small anyway ^{/11/}). Assuming that gluinos are lighter than s-quarks (present limits ^{/14/} give $m \gtrsim 2-3$ GeV, where m is the \tilde{g} mass) one possibility is to look for production of the final states $q\bar{s}_q\tilde{g} + q\bar{s}_q\tilde{g}$ (fig. 3a) or $\tilde{g}\tilde{g}$, $q\bar{q}\tilde{g}\tilde{g}$. The production of two \tilde{g} was studied in refs. ^{/15,16/} and is small being of order α_s^2 with the channel $\tilde{g}\tilde{g}$ vanishing in the limit of P and/or C conservation. A different interesting question is the effect of s-quarks and gluinos on the ratio $R_{e^+e^-}$ of the hadronic and pointlike e^+e^- cross-sections. At order α_s , in presence of SUSY particles one has for $Q \lesssim 2M$:

$$R_{e^+e^-} = R_0 \left[1 + \frac{\alpha_s(Q^2)}{\pi} + \delta(\gamma, r) \frac{\tilde{\alpha}_s(Q^2)}{\pi} \right] \quad (10)$$

where $R_0 = 3 \sum_i Q_i^2$, $\frac{\alpha_s}{\pi}$ is the ordinary QCD leading correction ^{/17/}, δ is the additional contribution from SUSY particles, with

$$\gamma = \frac{Q^2}{M^2}, \quad r = \frac{m^2}{M^2} \quad (11)$$

$\tilde{\alpha}_s = \tilde{g}_s^2 / 4\pi$ where \tilde{g}_s is the $q\tilde{g}$ coupling constants. One expects $\tilde{\alpha}_s \approx \alpha_s$, although the two are not exactly equal in presence of SUSY breaking.

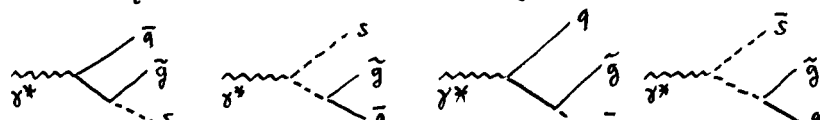
For massless quarks, in the interval $Q \lesssim M+m$ the only contribution to δ arises from virtual s_q and \tilde{g} corrections to the $q\bar{q}$ channel (fig. 3b). For $M+m \lesssim Q \lesssim 2M$ the contribution to δ from the real production diagrams of fig. 3a is also present. Note that for Q of order M , δ is expected to be of order 1, so that the QCD leading correction could be quite significantly altered producing a detectable effect somewhat below the threshold for open SUSY scalar pair production. On the other hand the accuracy of the data on the total hadronic e^+e^- cross-section is by now sufficient to

extract a significant, although not very precise, determination of the first order QCD correction, which at present leads to¹⁸ $\alpha_s(Q \approx 30 \text{ GeV}) \approx (0.20 + 0.06)$ and is about to be further improved in the near future. It is thus interesting to study δ as a function of M^2, m^2 and Q^2 .

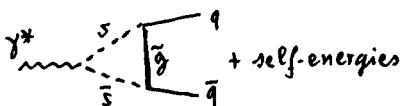
Our results can be summarized as follows:

a) The virtual contribution to δ below the threshold for pair production ($\eta < 4$) is given by:

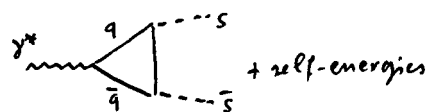
$$\delta_{\text{virtual}} = \frac{4}{3} \left\{ \frac{3}{4} + \frac{1}{2(1-r)} + \frac{r^2 \ln r}{2(1-r)^2} - \sqrt{\frac{4-r}{\eta}} \operatorname{erfc} \sqrt{\frac{\eta}{4-r}} + \right. \\ \left. + \int_0^1 dy \frac{r + (1-r)y}{y + r-1} \ln \frac{1 - \eta y(1-y)}{r + (1-r)y} \right\} \quad (12)$$



(a)



(b)



(c)

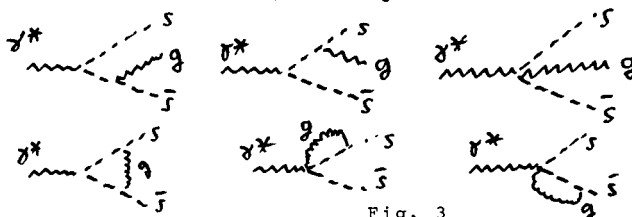


Fig. 3

Note that $\delta_{\text{virtual}} = 0$ for $Q = 0$ as a consequence of the Ward identities of QED. For $m=0$ and small values of Q^2 , an expansion of eq. 12 in η leads to

$$\delta_{\text{virtual}} \approx \frac{2}{27} \eta + 0(\eta^2) \quad (13)$$

This small value for the slope in Q^2 is responsible for the very slow increase of δ_{virtual} with Q^2 , as can be seen from fig.4 so that even at $Q=2M$ $\delta_{\text{virtual}} \lesssim 0.5$. Thus in the interval $Q \lesssim M+m$, where $\delta = \delta_{\text{virtual}}$, the effects of SUSY particles on $R_{e^+e^-}$ turn out to be particularly small and practically invisible.

b) In the interval $M+m \lesssim Q \lesssim 2M$ the real contribution from the final states $q \bar{s}_a \tilde{g} + \bar{q} s_q \tilde{g}$ also comes into play. The corresponding contribution to δ is a complicated expression, given in ref.5. It also turns out to be quite small. This is readily seen by the double differential cross section for $q \bar{s}_q \tilde{g}$ in the massless limit ($M = m = 0$):

$$\frac{1}{\sigma_0} \frac{d^2\sigma}{dx_s dx_g} = \frac{\tilde{\alpha}_s}{6\pi} \frac{(1-x_s)(1-x_g) + x_s x_g}{(1-x_s)(x_s + x_g - 1)} \quad (14)$$

While it is clear that the massless distribution is a drastic overestimate of the realistic effect expected from massive s_q and \tilde{g} at available energies, it is however useful for a direct comparison with the analogous three jet distribution^{17/} in ordinary QCD.

One immediately notices that the shape is different and the normalization $\frac{\tilde{\alpha}_s}{6\pi}$ is smaller by a factor of 4, which indicates that this effect is also very small, thus explaining the result plotted in fig. 4.

In ref. 5 one can also find a complete study of δ above threshold for pair production and in the limit of $Q \rightarrow \infty$, were the massless SUSY limit is approached.

In conclusion we have found that the effects of SUSY particles at low energies are remarkably suppressed and that supersymmetry is very effective in concealing its possible influence on measurable quantities.

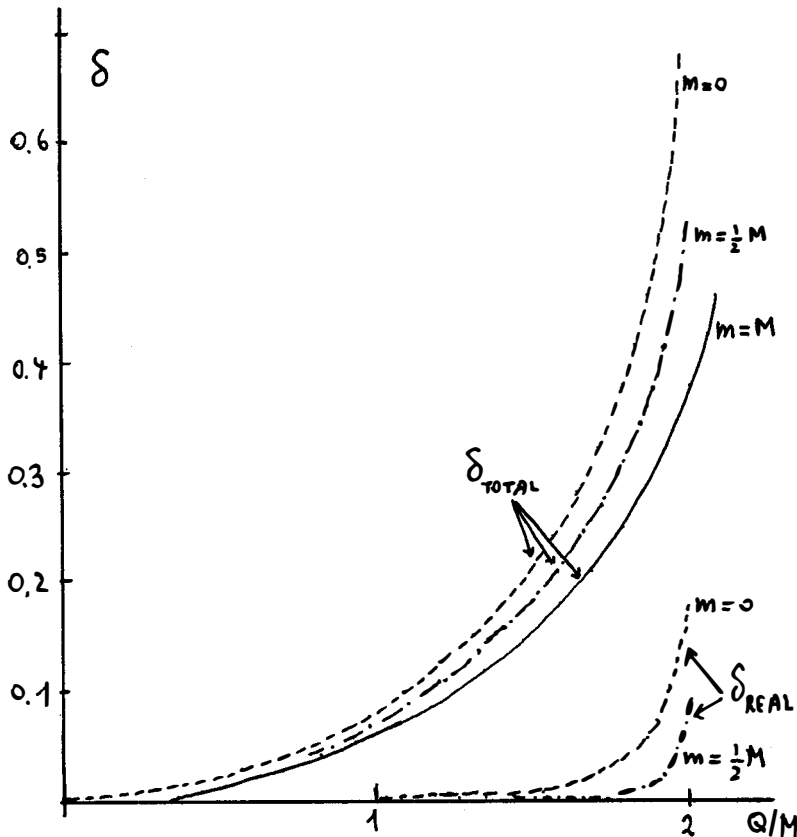


Fig. 4

References

- 1) For recent reviews see, for example: C.Savoy, these Proceedings and P.Fayet in Proc. of the XXI Int. Conf. on High En. Phys., Paris 1982, p. c-3, 673.
- 2) P.Fayet, in Unification of the Fundamental Particle Interactions, ed by S.Ferrara et al., Plenum, N.Y., 1980, P.587.
- 3) R.Barbieri, L.Maiani, Phys.Lett. 117B (1982) 203.

- 4) R.Barbieri, L.Maiani, Univ. of Rome Preprint.
- 5) G.Altarelli, B.Mele, R.Petronzio, CERN-TH (1983) to appear in Phys. Lett.
- 6) See e.g., J.Calmet, S.Narison, M.Perrottet, E. de Rafael, Rev. Mod. Phys. 49 (1977) 21;
J.Bailey et al., Nucl. Phys. B150 (1979) 1.
- 7) S.Ferrara, E.Remiddi, Phys. Lett. 53B (1974) 347.
- 8) M.Veltman, Nucl. Phys. B123 (1977) 89.
- 9) J.Kim, P.Langacker, M.Levine, H.H.Williams, Rev.Mod. Phys. 53 (1981) 211.
- 10) See e.g. M.Davier, Proc. of the XXI Int. Conf. on High En. Phys., Paris, 1982.
- 11) M.Suzuki, Phys. Lett. 115B (1982) 40 and UCB - PTH 8219 (1982);
J.Ellis, D.V.Nanopoulos, Phys. Lett. 110B (1982) 49.
- 12) R.Barbieri, J.Ferrara, C.Savoy, Phys. Lett. 119B (1982) 343;
H.P.Nilles, M.Fredricki, D.Wyler CERN - TH 3432 (1982);
E.Cremmer, P.Fayet, L.Girardello ENS - preprint LPTENS 82-83 (1982).
- 13) See e.g. S.Komaniya, Proc. of the Workshop on Supersymmetry vs.Experiment, CERN-TH 3311/EP.82/63 (1982).
- 14) F.Bergsma et al. (CHARM coll.) Phys. Lett. 110B (1983) 429;
R.C. Ball et al. (FNAL) these proceedings.
- 15) P.Nelson, P.Osland, Phys. Lett. 115B (1982) 407.
- 16) B.A.Campbell, J.Ellis, S.Rudaz, Nucl. Phys. B198 (1982) 1.
- 17) See e.g. G.Altarelli, Phys. Rep. 81 (1982) 1.
- 18) JADE Collaboration, these Proceedings.

LEFT-RIGHT SYMMETRY AND CP VIOLATION[†]

G. Beall

University of Oregon, Eugene, Oregon 97403

A. Soni

University of California, Los Angeles, CA 90024



ABSTRACT. Left-right symmetric electroweak theory is reviewed. Experimental consequences and constraints on its parameters are discussed. From $K_L - K_S$ mass difference one finds that $M_R \gtrsim 1.6$ TeV and the mixing angle $\zeta \lesssim .06$. Implications for CP violation especially for the electric dipole moment of the neutron, ϵ'/ϵ parameter for kaon decays and heavy quark decays are discussed.

[†]Presented by A. Soni.

Following is the outline of this talk:

1. A brief introduction to Left-Right Symmetric electroweak models.
2. Experimental consequences of and constraints on LR Symmetry.
3. CP violation in LRS models and comparison with other models. Herein we will deal with (a) the electric dipole moment of the neutron, (b) the ϵ' parameter from $K \rightarrow 2\pi$ decay, and (c) CP asymmetry in heavy quark (especially b quark) decays.
4. Summary.

Introduction.¹

Left-Right Symmetric electroweak models explain parity violation as the low energy behavior of a spontaneously broken theory, and as such provide an aesthetically appealing alternative to the standard model. They also provide a possible alleviation of the experimental desert by Grand Unified extensions of the standard model. The gauge group for LRS models is taken to be $G = SU_L(2) \times SU_R(2) \times U(1)_{B-L}$ where we take $g_R = g_L$. Fermions transform as doublets under the gauge group: $(\bar{v}_e \bar{e})_{L,R} \dots; (\bar{u} \bar{d})_{L,R} \dots$. The minimal Higgs sector consists of:

$$\begin{pmatrix} \chi^+ \\ \chi^0 \\ \chi^- \end{pmatrix}_{L,R}, \quad \Phi = \begin{pmatrix} \phi_1^0 & \phi_2^+ \\ \phi_1^- & \phi_4^0 \end{pmatrix}, \quad \tilde{\Phi} = \tau_2 \Phi^* \tau_2 \quad (1)$$

where Φ transforms under G as $\Phi \rightarrow U_L \Phi U_R^{-1}$. On symmetry breaking the scalars develop vacuum expectation value,

$$\langle \chi_L \rangle = \begin{pmatrix} 0 \\ v_L \end{pmatrix}; \quad \langle \chi_R \rangle = \begin{pmatrix} 0 \\ v_R \end{pmatrix}; \quad \langle \Phi \rangle = \begin{pmatrix} \kappa & 0 \\ 0 & \kappa' \end{pmatrix}. \quad (2)$$

The gauge fields $W_{L,R}$ that couple to the L,R charged currents are not, in principle, mass eigenstates. Rather one has:

$$\begin{aligned} W_L &= W_1 \cos\zeta + W_2 \sin\zeta \\ W_R &= -W_1 \sin\zeta + W_2 \cos\zeta \end{aligned} \quad (3)$$

where W_1, W_2 are mass eigenstates with masses M_1, M_2 given by ($v_L \rightarrow 0$ Limit):

$$M_1^2 = \frac{g^2}{4} \left\{ |\kappa|^2 + |\kappa'|^2 + \frac{1}{2} |v_R|^2 - \left[\frac{1}{4} |v_R|^4 + 4|\kappa^* \kappa'|^2 \right]^{1/2} \right\} \quad (4)$$

$$M_2^2 = \frac{g^2}{4} \left\{ |\kappa|^2 + |\kappa'|^2 + \frac{1}{2} |v_R|^2 + \left[\frac{1}{4} |v_R|^4 + 4|\kappa^* \kappa'|^2 \right]^{1/2} \right\} \quad (5)$$

and $\zeta = \tan^{-1}[4|\kappa^* \kappa'|/|v_R|^2]/2$. The observed parity violation at "low" energy is then a consequence of having $M_L^2 \ll M_R^2$, $\tan\zeta \ll 1$ or equivalently

$v_R^2 \gg |\kappa \kappa'|, v_L^2$. Note that for this minimal Higgs sector one gets a useful theoretical constraint:

$$\frac{1}{2} \tan 2\zeta \leq \beta/(1-\beta) \implies \zeta \leq \beta, \quad \beta, \zeta > 0 \quad (6)$$

where $\beta \equiv M_L^2/M_R^2$. The theory thus has two characteristic parameters: ζ and β . However, in making contact with experiment there is the additional complication of quark mixing angles. In general, the right-handed quark mixing matrix is independent of the left-handed mixing matrix. For three generations of quarks one then has altogether six angles and six phases rather than three angles and one phase as in the standard model. Béga² et al. proposed that the theory should be "manifest" left-right symmetric (MLRS) i.e. that the charged currents be invariant under $\gamma_5 \leftrightarrow -\gamma_5$ reflection. This results in the angles and phases in the right-hand sector being identically equal to those in the left-hand sector, making the theory considerably more manageable. One can show that manifest LRS emerges as a natural consequence if one requires Φ to have the LR Symmetry transformation

$$L \leftrightarrow R \quad \Phi \leftrightarrow \Phi^\dagger. \quad (7)$$

The resulting theory is not only simple and elegant but can also be extended to resolve the strong CP problem without the need for axions.

Experimental Consequences and Constraints.

Béga² et al. were the first to consider the constraints on a MLRS theory coming from existing data on e^- polarization and the Michel parameter in mu decay, beta decay of ^{16}O etc. They concluded that

$$\beta \lesssim .13 \implies M_R \gtrsim 2.8 M_L \quad (8)$$

and

$$\zeta \lesssim .06. \quad (9)$$

An important shortcoming of Béga et al.'s analysis is that it assumes light right-handed neutrinos (specifically $\nu_{\mu R}$ and $\nu_{e R}$). If the ν_R have large Majorana masses (as would be the case in several theoretical scenarios) then Béga et al.'s bounds become invalid. Gobbi³ et al. have analyzed new data which leads to the bound $M_R > 450$ GeV, $|\zeta| < .046$, however their analysis suffers from the same dependence on neutrino masses.

Recently⁴ the $K_L - K_S$ mass difference has been used to constrain the parameters of MLRS models. In the calculation of the diquark transition ($d\bar{s} \rightarrow \bar{d}s$) to construct the effective $\Delta s = 2$ Hamiltonian, one has to evaluate eight scattering graphs (shown in Figure 1) plus the corresponding eight annihilation graphs.

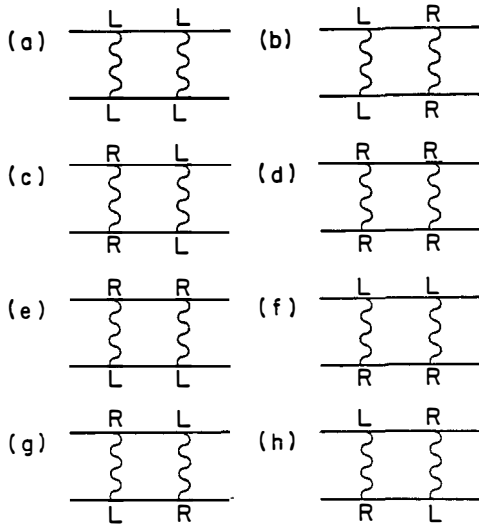


Figure 1. W_L , W_R exchange graphs that contribute to ΔM_K .

If the external momenta are taken to be negligible, the scattering and the annihilation graphs are found to make equal contributions. In our published calculation⁴ we assumed $\zeta = 0$. If we now include the contribution for finite ζ as well, again using vacuum saturation to evaluate $\langle K_0 | H_{\text{eff}} | \bar{K}^0 \rangle$, we find:¹

$$\begin{aligned}
 \Delta M_K &\approx \frac{G_F^2}{6\pi^2} f_K^2 M_K^2 \left\{ \lambda_c^2 m_c^2 \left[1 + (6y+1) \left(1 + \ln \frac{m_c^2}{M_L^2} \right) \beta + \beta^2 \right. \right. \\
 &\quad + \left. \left. \left(4y - 4 + (4y+1) \ln \frac{m_c^2}{M_L^2} \right) t^2 \right] \right. \\
 &\quad + \lambda_t^2 m_t^2 \left[1 + (6y+1) \left(1 + \ln \frac{m_t^2}{M_L^2} \right) \beta + \beta^2 \right. \\
 &\quad + \left. \left. \left(4y - 4 + (4y+1) \ln \frac{m_t^2}{M_L^2} \right) t^2 \right] + 2\lambda_c \lambda_t m_c m_t \left[\omega + (6y+1) \ln \frac{m_t^2}{M_L^2} \beta + \omega_\beta^2 \right. \\
 &\quad + \left. \left. \left((4y+1) \ln \frac{m_t^2}{M_L^2} - (4y+6) \omega \right) t^2 \right] \right\}, \tag{10}
 \end{aligned}$$

where $y \equiv M_K^2 / (m_s + m_d)^2$, $\omega \equiv (m_c/m_t) \ln m_t^2/m_c^2$, $t = \tan\zeta$ and $\beta, \zeta \ll 1$.

A firm numerical value for ΔM_K cannot be deduced from this calculation at present due to our lack of knowledge of m_t and of some of the mixing angles. Let us instead examine the four-quark contribution

$$\Delta M_K^{4q} \approx 3.4 \times 10^{-12} \text{ MeV} [1 - 420\beta - 290\zeta^2] \quad (11)$$

which we compare to the experimental value

$$\Delta M_K (\text{expt.}) = (3.521 \pm .014) \times 10^{-12} \text{ MeV} . \quad (12)$$

Thus, in the standard model, the four-quark contribution (given by the first term in (11)) essentially equals ΔM_K (expt.). This can be understood in two ways:

(1) Terms proportional to β , ζ or those containing the top quark (in Eq. (10)) or other contributions arising from the exchange of Higgs scalars but not shown in (10) are all very small in comparison to ΔM_K^{4q} . (2) Some of the individual contributions, which are functions of several unknown parameters (namely two K-M angles, the t-quark mass, and the mass of the Higgs) are actually large but the values of the unknown parameters are such that these contributions cancel. Since the second possibility would require seemingly contrived cancellations among unrelated factors, we regard it as implausible and do not consider it further. Even under the first set of assumptions, however, there remain considerable uncertainties due to the effects of strong interactions. To be conservative, we assume only that the LR contributions are not dominant which would give the wrong sign for ΔM_K . We thus obtain the bound:

$$420\beta + 290\zeta^2 < 1 \quad (13)$$

which yields a contour in β , ζ plane representing the asymptotic constraint:

$$\beta \lesssim 1/420 \implies M_R \gtrsim 1.6 \text{ TeV} \quad (14)$$

and

$$\zeta \lesssim .06 . \quad (15)$$

Figure 2 exhibits the constraints on MLRS models coming from various existing experiments and compares them with those resulting from the $K_L - K_S$ mass difference. Figure 3 compares the $K_L - K_S$ constraint with those anticipated from forthcoming high precision experiments. Note that if we accept the theoretical constraint $\zeta \leq \beta$ (Eq. (6)), we get a much tighter constraint on ζ

$$\zeta \lesssim 1/420 . \quad (16)$$

Recently there have been several related works,⁵⁻⁹ all of which have assumed $\zeta = 0$ so that they involve the calculation of graphs 1(a-d) only. In that limit all of these works reproduce the result given in Eq. (10). Some of these

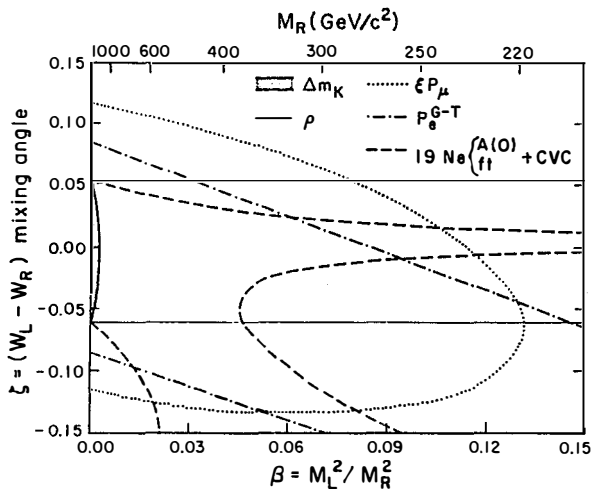


Figure 2. Comparison of the bounds set on β and ζ from ΔM_K to those deduced from leptonic and semileptonic decays.

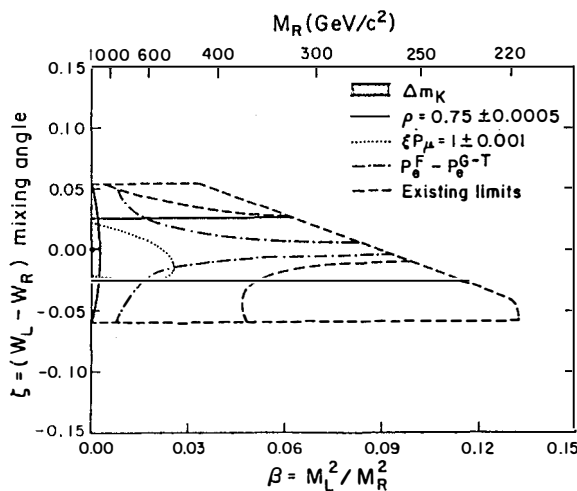


Figure 3. Comparison of the bounds set on β and ζ from ΔM_K to those anticipated from upcoming experiments.

authors⁷ have interpreted the bounds from the K_L - K_S mass difference to be bounds on the mixing angles in the right-handed quark sector (that is, they do not assume MLRS) in order to acquire a light W_R . This possibility cannot be discounted, but it requires a more complicated model while substantially reducing predictive ability. The possible resolution of the strong CP problem (without axions) previously noted is also lost.¹⁰ Evaluation of hadronic matrix elements has been studied by Trampetic⁵ in the context of ΔM_K and non-leptonic weak decays using various harmonic oscillator quark models. His results are in agreement with our bound (14) deduced using vacuum saturation. Senjanovic, Mohapatra and Tran⁸ have done a detailed (once again in the $\zeta = 0$ limit only) calculation in the six-quark model including the contribution from Higgs exchange. They also find that, in a MLRS model, to have values of M_R lower than (14) there have to be delicate cancellations between various contributions not explicitly written down in Eq. (10).

Another constraint on ζ has been deduced by Bigi and Frere⁹ who study weak non-leptonic decays of hyperons in a LR Symmetric model. They include QCD corrections to LL and LR currents and show that compatibility with experiment demands $\zeta \lesssim$ a few percent. We emphasize that their bounds on β as well as our bounds on β and ζ (Eqs. (14), (15)) are independent of V_R mass.

Implications for GUT's.

The bound (14) on M_R has additional implications if one embeds the LR Symmetric group in a grand unifying group such as SO(10). Neglecting the small Higgs contribution, one finds¹¹

$$\sin^2 \theta_W(M_L) = \frac{3}{8} - \frac{11\alpha(M_L)}{3\pi} \left[\frac{5}{8} \ln \frac{M_u}{M_L} - \frac{3}{8} \ln \frac{M_u}{M_R} \right] \quad (17)$$

where M_u is the unification mass. The second term in the parenthesis is seen to increase the value of $\sin^2 \theta_W$ above the SU(5) prediction. If, however, $M(Z_R^0) \gtrsim M_R \gtrsim 300$ GeV, as is indicated by (14), then the contribution of Z_R^0 to the neutral current is negligible and one finds from the neutral current data $\sin^2 \theta_W \approx .22-.23$ as in the standard model. Taken with (17), this requires $M_R > 10^9$ GeV. This result can be weakened somewhat if one allows the LR Symmetric group to break through the steps $SU(2)_L \times SU(2)_R \times U(1) \xrightarrow{2M_R} SU(2)_L \times U(1)_R \times U(1) \xrightarrow{2M_L} SU(2)_L \times U(1)$ with $M(Z_R^0) \approx M_L$. A careful analysis including the contribution from scalars gives¹² $M_R \gtrsim 10^6$ GeV.

CP Violation.

There are potentially six relative phases entering the quark mixing matrices in an LRS model.¹ For simplicity we will consider two natural but somewhat restricted models: (a) Manifest Left-Right Symmetry (MLRS). This case, which

arises when one takes complex Yukawa couplings and real scalar VEV's, has equal left and right quark mixing matrices, i.e. $U_R = U_L$, and hence only one phase. It is generally difficult to distinguish from the standard model. (b) Pseudo-Manifest Left-Right Symmetry (PLRS).¹ If one breaks CP spontaneously by having real Yukawa couplings and complex scalar VEV's one gets PLRS with $U_R = U_L^*$. This model has four relative phases which, on one hand, make it easy to distinguish from the standard model while, on the other hand, make it difficult to make definite predictions. Both of these models assume that the 2×2 scalar multiplet has the LR transformation $L \leftrightarrow R$, $\phi \leftrightarrow \phi^\dagger$.

In addition to phases in the quark mass matrix one can also have a phase in the W mixing matrix:¹³

$$W_L = W_1 \cos\zeta + W_2 \sin\zeta e^{i\lambda}, \quad W_R = -W_1 \sin\zeta e^{-i\lambda} + W_2 \cos\zeta. \quad (18)$$

This phase is equivalent to an overall phase in the quark mixing matrices for hadronic and semi-leptonic interactions. However, it can also cause CP violating effects in purely leptonic processes independent of the value of M_V . There is, of course, the possibility of additional phases from scalar mixing given an enlarged scalar sector. We do not consider this possibility.

Let us now consider the implications of LRS models of CP violation for (a) the electric dipole moment of the neutron (μ_n^e), (b) the ϵ' parameter of kaon decay and (c) heavy quark decays.

The Electric Dipole Moment of the Neutron (μ_n^e).¹³

We parameterize the quark charge-current gauge interaction in the form:

$$L_{cc} = \sum_{i,j} \sum_{k=1,2} \bar{\psi}_i \gamma_\mu (a_{ij}^k + b_{ij}^k \gamma_5) \psi_j W_k^\mu + \text{h.c.} \quad (19)$$

The one-loop contribution to the electric dipole moment (edm) of a quark is then seen to be:

$$\mu_q^e \propto \text{Im}(a_{ij}^k b_{ij}^{k*}) \quad (20)$$

which vanishes in the standard model where $a = b$. Shabalin¹⁴ has shown, furthermore, that the quark edm in the standard model vanishes even to two loops. It has been pointed out,^{15,16} however, that CP-violating diquark transitions lead to a neutron edm at one loop. When including the contribution of penguin-like diagrams, calculations of the neutron edm yield:¹⁷

$$\mu_n^e \sim 10^{-32} \text{ ecm}.$$

We recall that the current experimental bound is given by:¹⁸

$$\mu_n^e \leq 6 \times 10^{-25} \text{ ecm} \quad (\text{expt}) \quad (21)$$

and one anticipates an improvement of about two orders of magnitude in the next few years. The prediction of the standard model is thus some seven orders of magnitude smaller than the present experimental bound and beyond any anticipated improvements.

In models of CP violation other than the standard model one does not in general expect the one-loop contribution to the edm to vanish and one therefore expects $\mu_n^e >> 10^{-30}$ ecm. Specifically, for an LRS model the quark edm receives a contribution from Figure 4 and one has:¹

$$\begin{aligned} \mu_n^e = & \frac{eg^2}{72\pi^2} \sin 2\zeta \left(\frac{1}{M_R^2} - \frac{1}{M_L^2} \right) \{ (5m_u - m_d) c_{1L} c_{1R} s_\lambda, + (5m_c c_{2L} c_{2R} s_{(\delta_2 + \lambda')}) \right. \\ & \left. - m_s c_{3R} c_{3L} s_{(\delta_1 + \lambda')} + (5m_t s_{2L} s_{2R} s_{(\delta_4 + \lambda')} - m_b s_{3L} s_{3R} s_{(\delta_3 + \lambda')}) s_{1L} s_{1R} \} \end{aligned} \quad (22)$$

where

$$\begin{aligned} c_{iL,R} & \equiv \cos \theta_{iL,R}, \quad s_{iL,R} \equiv \sin \theta_{iL,R}, \quad s_\lambda \equiv \sin(\lambda + \delta_{oL} - \delta_{oR}), \\ s_{(\delta_i + \lambda')} & \equiv \sin(\delta_{iL} - \delta_{iR} + \lambda + \delta_{oL} - \delta_{oR}). \end{aligned} \quad (23)$$

For the case of MLRS, there is, as in the standard model, only one phase and one finds that

$$\mu_n^e \text{ (to 1 loop)} = 0. \quad (\text{MLRS}) \quad (24)$$

For PLRS the edm, given by (22), is non-vanishing to one loop but its numerical value is uncertain as so many of the parameters are unknown. In principle the edm can certainly be large. In particular, if one assumes t quark effects to be small, one can obtain a four-quark result:

$$|\mu_n^e| \approx (10^{-21} \text{ ecm}) \tan \zeta (4.2 \sin(\lambda + 2\delta_o) + 1.3 \sin(\lambda + 2\delta_o + 2\delta_1)), \quad (25)$$

where we have assumed $M_1^2 \ll M_2^2$ and used constituent quark masses. Using $\zeta < \beta < 1/420$ one finds

$$\mu_n^e (4q) < 10^{-23} \text{ ecm}. \quad (\text{PLRS}) \quad (26)$$

Thus, to be consistent with experiment, we find that either the CP violating phases are very small (i.e. $< 1/25$) or $\tan \zeta$ is even smaller than deduced in (6).

The Weinberg model of CP violation also gives a one-loop contribution to a quark edm. Beall and Deshpande¹⁹ have calculated the neutron's edm and find:

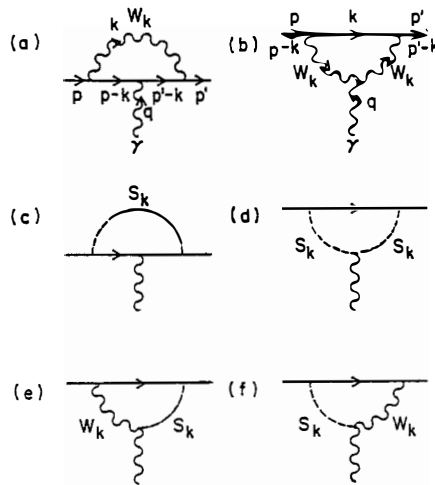


Figure 4. Vertex corrections contributing to the neutron's electric dipole moment in the 't Hooft-Feynman gauge. W here denotes the gauge fields and S the unphysical scalars.

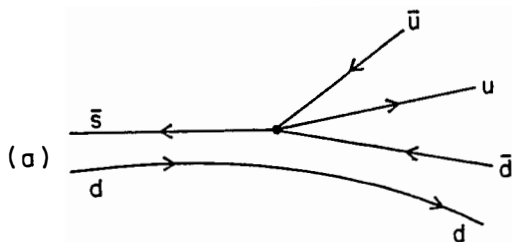


Figure 5. Diagram contributing to $K^0 \rightarrow 2\pi$ decay.

$$\mu_n^e \sim (2 \text{ to } 4) \times 10^{-26} \text{ ecm} . \quad (\text{Higgs model}) \quad (27)$$

Thus we see that (1) two orders of magnitude improvement in the experimental result could rule out the Weinberg model, and (2) any observation of a positive result, in the next few years, would clearly demonstrate that the Kobayashi-Maskawa phase is not the sole source of CP violation

$$\underline{\epsilon' / \epsilon}.$$

The primary parameter characterizing CP violation, and the only one thus far to have a measured non-zero value, is ϵ , defined by

$$K_{L,S}^0 = \frac{1}{\sqrt{2(1+\epsilon^2)}} ((1+\epsilon) K^0 \pm (1-\epsilon) \bar{K}^0) .$$

Corrections in the LRS model to the standard model calculation of ϵ are small and depend sensitively on the mass and couplings of the t-quark.

We recall that

$$\epsilon' \equiv \frac{i}{\sqrt{2}} \exp[i(\phi_2 - \phi_0)] \text{ Im}(A_2/A_0) \quad (28)$$

where

$$A_I e^{i\phi_I} \equiv \langle 2\pi, I | T | K^0 \rangle , \quad (29)$$

T is the $\Delta S = 1$ effective weak Hamiltonian, and $I = 0, 2$ is the isospin of the $\pi^+ \pi^-$ or $\pi^0 \pi^0$ system. In the standard model, estimates²⁰ range:

$$\epsilon'/\epsilon = 10^{-3} \text{ to } 10^{-2} . \quad (\text{standard model}) \quad (30)$$

For the LRS model, corrections to the standard model will be dominated by the graph shown in Figure 5. We find¹

$$\begin{aligned} \epsilon' |_{LR} &= \frac{i}{\sqrt{2}} e^{i(\phi_2 - \phi_0)} \\ &\times \text{Im} \left\{ \frac{(c_{LL} - c_{RR}) \left(1 + \frac{\sqrt{2}}{6} \right) + (c_{RL} - c_{LR}) \left(1 - \frac{z\sqrt{2}}{6} \right)}{(c_{LL} - c_{RR}) \left(1 - \frac{1}{6\sqrt{2}} \right) + (c_{RL} - c_{LR}) \left(1 + \frac{z}{6\sqrt{2}} \right)} \right\} \end{aligned} \quad (31)$$

where

$$c_{LL} = \bar{u}_{us}^{L*} u_{ud}^L \left(\frac{c^2}{M_1^2} + \frac{s^2}{M_2^2} \right) , \quad (32a)$$

$$c_{LR} = U_{us}^{L*} U_{ud}^R s_\zeta c_\zeta e^{-i\lambda} \left(\frac{1}{M_2^2} - \frac{1}{M_1^2} \right), \quad (32b)$$

$$c_{RL} = U_{us}^{R*} U_{ud}^L s_\zeta c_\zeta e^{+i\lambda} \left(\frac{1}{M_2^2} - \frac{1}{M_1^2} \right), \quad (32c)$$

$$c_{RR} = U_{us}^{R*} U_{ud}^R \left(\frac{c_\zeta^2}{M_2^2} + \frac{s_\zeta^2}{M_1^2} \right), \quad (32d)$$

$c_\zeta \equiv \cos\zeta$, $s_\zeta \equiv \sin\zeta$, M_1 and M_2 are the W mass eigenstates, and U^L and U^R are the left- and right-handed quark mixing matrices and

$$z \equiv \frac{m_\pi^2}{(m_s - m_d)m_u} \simeq 30.5. \quad (33)$$

As we expect, if we impose manifest LRS, this contribution is seen to vanish. If instead we assume PLRS ($U_R = U_L^*$), we find

$$\epsilon' |_{LR} \simeq - \frac{(1+z)}{2\sqrt{2}\gamma} \frac{\zeta \cos\delta_1 \sin(2\delta_0 + \delta_1 + \lambda)}{[1 - (1/6\sqrt{2})]^2} \quad (34)$$

where γ is a strong interaction enhancement factor anticipated to be of order 10. There are still too many unknown parameters in (34) to make a definite prediction for ϵ' . However, we see that even for $\zeta \leq \beta \leq 1/420$ this process could easily provide the dominant contribution to $|\epsilon'/\epsilon|$. In fact, as in the case of the neutron's edn, the experimental bound

$$|\epsilon'/\epsilon| \lesssim 0.02 \quad (\text{expt}) \quad (35)$$

requires either that the CP violating phases are $\ll 1$ or that ζ is much smaller even than the bound in (6).

Two experiments (FNAL #617 (Chicago-Stanford) and BNL #749 (BNL-Yale))^{21,22} are underway for an improved measurement. These experiments are expected to improve (35) by about an order of magnitude in the near future.

Chang²³ has demonstrated recently that much of the uncertainty generated by the numerous phases in LR models can be eliminated if, in addition to assuming PLRS, one assumes the minimal Higgs sector. In that case there is only one independent CP-violating phase coming from the Higgs sector and all of the phases in the quark mixing matrices can be expressed in terms of it. In a four-quark model Chang finds

$$|\epsilon'/\epsilon| \simeq |\omega| \frac{8}{430} \frac{m_s}{m_c} \chi \simeq 10^{-4} \chi \quad (36)$$

where $|\omega| \approx .05$ and χ is an enhanced matrix element estimated to be ~ 10 . Calculation of ϵ'/ϵ in the Weinberg model²⁴ of CP violation through Higgs exchange gives²⁵

$$\epsilon'/\epsilon = -\frac{1}{20} \left(\frac{2\xi}{2\xi + \epsilon_m} \right) \frac{1}{(1+z)} \quad (37)$$

where $\xi \ll \epsilon_m^{26}$ and z parameterizes long distance contributions and is presumed to be $|z| \lesssim 2$. In comparison with (35) we see that this model is again on the verge of being ruled out unless the experiments now in progress find a non-vanishing result for ϵ'/ϵ .

CP Violation in Decays of Heavy Quarks.

In gauge theories of CP violation there is no reason to expect CP non-conservation to be confined to the neutral kaon complex. Indeed it has been pointed out that in the standard model decays of charged or neutral mesons containing the b quark could exhibit appreciable CP asymmetries.^{27,29} Since the CP violation really occurs at the quark level (i.e. in comparing CP conjugate decays such as $b \rightarrow d(s) + q + \bar{q}$ versus $\bar{b} \rightarrow \bar{d}(\bar{s}) + q + \bar{q}$, where $q = u, d, s$ or c one expects nonvanishing asymmetry), it not only affects both charged and neutral B mesons but also inclusive and exclusive decay channels. The effects are supposed to be the most pronounced for Cabibbo suppressed decays. The precise magnitude of the asymmetries, being a function of the two unknown KM angles and the CP phase δ , is unknown but for many channels (such as $B \rightarrow \pi + X$, $3K + X$, $K\phi$, $D\bar{D}$, $K_S K_S X \dots$) can be as large as a few percent to a few tens of percents. Theoretical studies also show that the b quark in the standard model is rather unique in this regard. For the t quark such asymmetries tend to vanish; that is, they have extra suppression factors $\sim (\text{quark mass})^2/m_t^2$. For the charm quark the asymmetry is expected to be $\sim 4\alpha_s \epsilon/27$ (where $\epsilon \sim 10^{-3}$ is the amplitude for CP violation in kaon decays) $< 10^{-4}$.²⁷ An observation of CP asymmetry significantly larger than this estimate (in charm quark decay) may signal breakdown of the standard model.

In other models of CP violation similar studies of asymmetries in heavy quark decays have not been done. For MLRS there is only one phase and the theory is expected to be very similar to the standard model in so far as decays of quarks are concerned (so long as $m_{\text{quark}}^2 \ll m_L^2$).

Summary.

1. LRS provides an interesting and viable extension of the standard model. Current experiments indicate (under stated assumptions) $M_R \gtrsim 1.6$ TeV, $\xi \lesssim .06$.
2. The information regarding CP violating parameters μ_n^e , t'/t and asymmetries in b (c) quark decays is summarized in the Table.

Table^{a)}

Quantity	Experiment	Standard Model	LRS ^{b)}		Higgs	Superweak (Ref. 31)
			M	P		
μ_n^e (ecm)	$\leq 6 \times 10^{-25}$	$\simeq 10^{-30}$	10^{-30}	$(\leq 10^{-24})$	$(2-6) \times 10^{-26}$	10^{-29}
$ \epsilon'/\epsilon $	< .02	$10^{-3} - 10^{-2}$	$10^{-3} - 10^{-2}$	$0(10^{-3})$.02-.05	0
a_b^c	?	$\sim 10^{-2} - 10^{-1}$	$10^{-2} - 10^{-1}$	(?)	?	$\simeq 0$
a_c^c	?	$\lesssim 10^{-4}$	$\lesssim 10^{-4}$	(?)	?	$\simeq 0$

a) ? indicates that the experimental or theoretical value for the parameter is not known at this time.

b) M stands for manifest left-right symmetry; P stands for pseudo manifest left-right symmetry.

c) a_b^c, a_c^c are CP asymmetries in b and c quark decays respectively.

Remarks.

(a) Theoretical calculations of ϵ' are rather messy involving many uncertainties. An order of magnitude improvement in the experimental bound (i.e. a null result) would convincingly rule out the Higgs model and may mean the failure of the standard model.

(b) The fact that the theoretical prediction for μ_n^e in the KM model is $0(10^{-32}$ ecm) means that an observation of a non-vanishing result in the next several years would unambiguously³⁰ signal the breakdown of the standard model. An order of magnitude improvement in the current bound ($< 6 \times 10^{-25}$ ecm) would rule out the Higgs model.

(c) There is every reason to expect a non-vanishing manifestation of CP violation outside the neutral kaon system involving $B^{\pm,0}$ meson decays. These as well as D decays need to be pursued experimentally. Asymmetries much larger than $\sim 10^{-4}$ in D decays again signal the breakdown of the KM model.

References.

1. For details and earlier references see G. Beall, Ph.D. Thesis, University of California, Irvine.
2. M. Bég, R. Budny, R. Mohapatra and A. Sirlin, Phys. Rev. Lett. 38, 1252 (1977).
3. B. Gobbi, presentation of the Berkeley/LBL, Northwestern, Triumf experiment to this Conference.
4. G. Beall, M. Bander and A. Soni, Phys. Rev. Lett. 48, 848 (1982).
5. J. Trampetic, Max-Planck-Institut Report #MPI-PAE/pTh 43/82 (to be published).
6. P. de Forcrand, Ph.D. Thesis, University of California, Berkeley, 1982.

7. A. Datta and A. Raychaudri, Calcutta University Report #CUPP/82-7, 8 (1982); F. J. Olness and M. E. Ebel, University of Wisconsin preprint MAD/TH/88.
8. G. Senjanovic, R. N. Mohapatra and M. D. Tran, BNL preprint, 1983.
9. I. Bigi and J. Frere, Phys. Lett. 110B, 255 (1982).
10. M. A. Bég and H. S. Tsao, Phys. Rev. Lett. 41, 278 (1978); R. N. Mohapatra and G. Senjanovic, Phys. Lett. 79B, 283 (1978).
11. T. Rizzo and G. Senjanovic, Phys. Rev. D25, 235 (1982).
12. V. Barger, E. Ma, K. Whisnant, N. Deshpande and R. Johnson, Phys. Lett. 118B, 68 (1982).
13. G. Beall and A. Soni, Phys. Rev. Lett. 47, 552 (1981).
14. E. Shabalin, Sov. J. Nucl. Phys. 27, 253 (1978).
15. N. Deshpande, G. Eilam and W. Spence, Phys. Lett. 108B, 42 (1982).
16. N. D. Gavella, A. Le. Yaouanc, L. Oliver, O. Pene, J.-C. Raynal, and T. N. Pham, Phys. Lett. 109B, 83 (1982).
17. N. D. Gavella et al., Phys. Lett. 109B, 215 (1982); I. B. Kriplovich and A. R. Zhitnitsky, Phys. Lett. 109B, 490 (1982); E. B. Shabalin, ITEP (Moscow) preprint 65 (1982).
18. I. Altarev et al., Phys. Lett. 102B, 13 (1981) and as reported by Lobosov at Neutrino '82, Balatonfured, Hungary.
19. G. Beall and N. Deshpande (to be published).
20. F. Gilman and M. Wise, Phys. Lett. 83B, 83 (1979); B. Guberina and R. D. Peccei, Nucl. Phys. B163, 289 (1980).
21. See Proceedings of the Theoretical Symposium on Intense Medium Energy Sources of Strangeness, U.C., Santa Cruz, March 1983.
22. For another theoretical calculation see: G. C. Branco, J.-M. Frere and J.-M. Gerard, CERN-TH-3406 (1982).
23. D. Chang, Carnegie-Mellon Preprint CMU-HEG 82-8.
24. S. Weinberg, Phys. Rev. Lett. 37, 657 (1976); G. C. Branco, Phys. Rev. D22, 2901 (1980).
25. F. J. Gilman and M. B. Wise, Phys. Rev. D20, 2392 (1979).
26. A. Sanda, Phys. Rev. D23, 2647 (1981); N. G. Deshpande, Phys. Rev. D23, 2654 (1981); J. F. Donoghue, J. S. Hagelin and B. R. Holstein, Phys. Rev. D25, 195 (1982); D. Chang, Phys. Rev. D25, 1381 (1982); J. S. Hagelin, CERN-TH-3326 (1982); Y. DuPont and T. N. Pham, CNRS preprint 82-0408.
27. M. Bander, D. Silverman and A. Soni, Phys. Rev. Lett. 43, 242 (1979).
28. A. B. Carter and A. I. Sanda, Phys. Rev. Lett. 45, 952 (1980).
29. J. Bernabeu and C. Jarlskog, Zeit. Phys. C8, 233 (1981).
30. We are assuming that the strong CP problem would have a solution and not lead to effects in the electric dipole moment of the neutron.
31. L. Wolfenstein, Phys. Rev. Lett. 13, 562 (1966).

CP AND U(1) PROBLEMS, AND THEIR RELATIONSHIP IN QCD

G. Veneziano
CERN, Geneva, Switzerland

A B S T R A C T

We discuss why the so-called strong CP and U(1) problems are intimately related in QCD. Their resolution implies contrasting conditions, apparently forcing QCD into a squeeze. Bringing electroweak interactions into the picture allows a simultaneous resolution of both problems, but a new light, weakly coupled and so far elusive particle, the axion, is needed.

1. INTRODUCTION

In this talk I shall try to explain in simple terms two, apparently distinct, problems in QCD : the strong CP and U(1) problem. I will then argue that a tight, if somewhat concealed, relationship exists between the two problems, to the effect that the resolution of either one seems unavoidably related to the non-resolution of the other.

Next, I will show how, by extending QCD to include the electroweak interactions à la Glashow-Weinberg-Salam but with a somewhat modified Higgs sector, one is able to solve both problems simultaneously. The resulting picture implies a phantomatic gluonic object (the so-called ghost), as well as a true, light, and so far elusive particle, the axion.

Finally, I shall discuss how the new low energy antiproton ring (LEAR), which is due to operate soon at CERN, can help improving present laboratory bounds on the axion parameters.

2. THE U(1) PROBLEM

In Nature, the lightest hadron is, by far, the pion. Of the other pseudoscalar mesons, also the K and the η are somewhat light, while the η' is a lot heavier. Can QCD explain this phenomenological pattern (including mixing angles, decay rates, etc.) ?

The claim today is that it can, though in a subtle and, I would say, very deep way. In order to see that, let us start from the QCD Lagrangian, which, omitting heavy quarks, reads as follows

$$\mathcal{L}_{\text{QCD}} = \frac{1}{4} F_{\mu\nu}^a F_{\mu\nu}^a + \sum_{i=u,d,s} \bar{q}_i^\alpha \gamma_\mu (i\partial_\mu \delta_{\alpha\beta} + g A_\mu^\alpha T_{\alpha\beta}^a) q_i^\beta - m_i \bar{q}_i^\alpha q_i^\alpha \quad (1)$$

Here $F_{\mu\nu}^a$ are the gluon field strength tensors ($a=1, \dots, 8$), A_μ^a the corresponding vector potentials. Furthermore, q_i^α ($\alpha=1, 2, 3$; $i=u, d, s$) are the quark fields, m_i their masses and g is the gauge coupling.

Thus, apparently, \mathcal{L}_{QCD} depends upon $N_f + 1$ parameters *) for N_f quark flavours (here $N_f = 3$). In terms of so few adjustable numbers, QCD is supposed to explain all the rich world of strong interactions, from the proton mass and magnetic moment to $\pi\pi$ phase shifts, from the iron nucleus to the rate of W^\pm production at the CERN collider (within a given electro-weak theory). Needless to say, we are very far from that goal.

*) As we shall see below, this naïve counting is wrong by one unit.

It turns out, however, that the properties of the light pseudoscalar mesons mentioned above can be discussed without really solving completely the theory; the claim being that they come out correct if we choose our four parameters such that :

$$m_u, m_d \ll m_s < \Lambda \approx 200 \div 500 \text{ MeV} \quad (2)$$

where Λ is a scale which, through the quantum properties of the theory, gets to replace the dimensionless constant g as the true free parameter.

In order to see why (2) is phenomenologically needed, take the limiting case $m_i = 0$ ($i = u, d, s$). In this case \mathcal{L}_{QCD} possesses a $U(3)$ axial symmetry, i.e., is invariant under the transformations :

$$q_i \rightarrow (e^{i\gamma_5 \Omega q})_i \quad ; \quad \bar{q}_j \rightarrow (\bar{q} e^{i\gamma_5 \Omega})_j \quad ; \quad \Omega = 3 \times 3 \text{ matrix} \\ \Omega = \Omega^+ \quad (3)$$

Indeed, the kinetic term in (1) is invariant under (3) since

$$\bar{q} \gamma_\mu q \rightarrow \bar{q} e^{i\gamma_5 \Omega} \gamma_\mu e^{i\gamma_5 \Omega} q = \bar{q} \gamma_\mu q \quad (4)$$

while the mass term which would break such symmetry was put to zero.

If the ground state of QCD (the vacuum) would be invariant under this symmetry, the same would be true for the hadronic spectrum and we would expect to see in Nature parity doublets as well as massless nucleons. Since this is not the case, we have to conclude that the QCD vacuum cannot be $U(3)$ axial invariant. Theoretical indications in the same direction do also exist.

Accepting that, a general theorem, due to Nambu and Goldstone, predicts the existence of massless (Goldstone) bosons. In order to see that, consider the case of Fig. 1 corresponding to a $U(1)$ symmetry representing rotations in an internal space spanned by two fields ϕ_1 and ϕ_2 . If the potential has the shape shown in the Figure, the invariant point ($\phi_1 = \phi_2 = 0$) is not the true ground state. The minimum of V is reached on a perfectly flat valley having a certain non-zero value at $\phi_1^2 + \phi_2^2$. Different points of the valley go into each other under the $U(1)$ transformation and it costs no energy to move in such a valley : this means a zero energy mode, hence a massless particle.

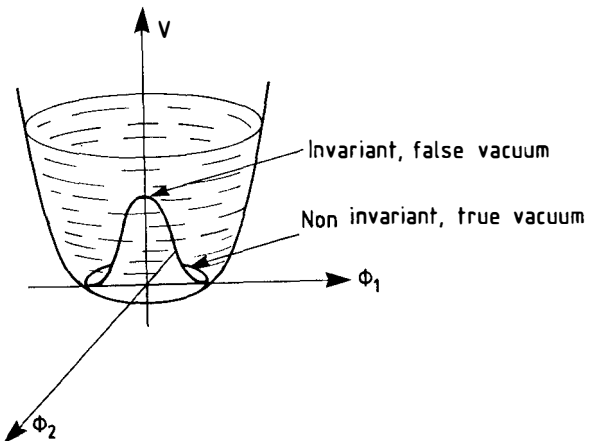


Fig. 1 - The Nambu-Goldstone phenomenon for a $U(1)$ symmetry.

The argument can be easily extended to the case of a larger symmetry in which case the valley has the same dimensionality as the number of symmetry generators that do not leave the ground state invariant ("spontaneously broken" generators). This is the expected number of Goldstone bosons; hence from our broken $U(3)_{\text{axial}}$ symmetry, we expect nine Goldstone bosons.

For $m_{u,d,s}$ small but non-zero, the valley is not perfectly flat and the Goldstone bosons have a small, non-zero mass. Here lies the source of the $U(1)$ problem.

- i) For $m_u, m_d \ll m_s$ we expect four roughly degenerate states, $\pi^+ = \bar{u}d$, $\pi^- = \bar{u}d$, $\pi^0, \eta^0 = \bar{u}\bar{u} \pm \bar{d}\bar{d}$, which is experimentally wrong.
- ii) For $m_{u,d,s} \ll \Lambda$ we expect nine light pseudoscalars π, K, η , and η' , which is again wrong experimentally.

The name "U(1) problem" came¹⁾ after realizing that all the difficulty lies in the apparent invariance of \mathcal{L}_{QCD} (at $m_i=0$) under both $SU(3)_{\text{axial}}$ and $U(1)_{\text{axial}}$ [Ω traceless, or $\Omega=1$ in Eq. (3)]. If this last symmetry could be disposed of, things could work out fine, but QCD seems to have automatically the $U(1)$ symmetry whenever it has the $SU(3)$ symmetry !

Amazingly, it turns out that the unwanted $U(1)_A$ symmetry, though valid at the classical level, is broken by quantum corrections : the effect is known as the Adler-Bell-Jackiw (ABJ) anomaly ²⁾. It says that under the $U(1)$ transformation

$$q_i \rightarrow e^{i\gamma_5 \beta} q_i ; \quad i = 1, 2 \dots f \quad (5)$$

$$\mathcal{L} \rightarrow \mathcal{L} + \text{usual mass term} + 2\beta f Q(x)$$

$$Q(x) = g^2/64\pi^2 \epsilon_{\mu\nu\rho\sigma} F_{\mu\nu}^a F_{\rho\sigma}^a$$

The extra piece has very interesting features :

- i) it is made entirely of the gluon field $F_{\mu\nu}^a$ and, as such, it carries no flavour quantum number. This is why it only affects the $U(1)$ current. Physically, it corresponds to the possibility of $q\bar{q}$ annihilation into gluons, a process that can only occur for the flavour singlet combination $q_i \bar{q}_i$.
- ii) $\epsilon_{\mu\nu\rho\sigma} F_{\mu\nu}^a F_{\rho\sigma}^a$ has negative parity ($P = -1$) and positive charge conjugation ($C = -1$), thus $CP = -1$. Such a term, if present in \mathcal{L} apparently breaks CP invariance, unlike the terms that we had written down in Eq. (1). We start to see the relation to the strong CP problem.
- iii) as it turns out, one can write $\epsilon_{\mu\nu\rho\sigma} F_{\mu\nu}^a F_{\rho\sigma}^a = \delta_\mu^\mu K_\mu$, with a suitable current K_μ . This is why the additional term in the transformation of \mathcal{L} , Eq. (5), was considered harmless and neglected for a long time (it vanishes naively upon space-time integration).

How can the ABJ anomaly save us from the $U(1)$ problem ? The way is sketched in Fig. 2. The non-annihilation diagrams (2a) do not feel the ABJ anomaly and lead to a pseudoscalar mass square matrix of the form

$$\langle \Pi_{ij} | M^2 | \Pi_{kl} \rangle |_{\substack{\text{no annihilation}}} \sim (m_i + m_j) \delta_{ik} \delta_{jl} \Lambda ; \quad i,j,k,l = u,d,s \quad (6)$$

which is exactly of the type that leads to the $U(1)$ problem. However, the annihilation diagrams of Fig. 2b provide the extra term

$$\langle \Pi_{ij} | M^2 | \Pi_{kl} \rangle |_{\substack{\text{annihilation}}} = \delta_{ij} \delta_{kl} \sqrt{a} q_\mu \frac{1}{q^2} q_\mu \sqrt{a} = \delta_{ij} \delta_{kl} a \quad (7)$$

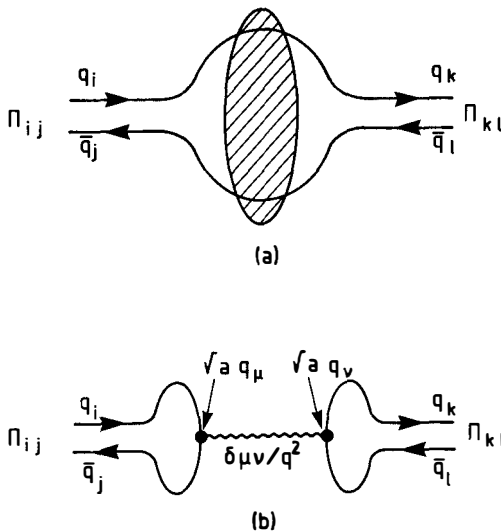


Fig. 2 - Contributions to the pseudoscalar squared matrix :
 (a) Non-annihilation diagrams
 (b) Ghost (wiggly line) dominated annihilation diagrams.

where $\sqrt{a} q_\mu$ is the coupling of the K_μ to the flavourless pseudoscalars, and the factor $1/q^2$ comes from the crucial assumption that there is a massless gluonic "bound state" coupled to K_μ . Because of the property iii) described above, in the absence of this "bound state" the ABJ anomaly is ineffective and the $U(1)$ problem remains with us. Several theoretical arguments ³⁾ and calculations ⁴⁾ suggest that such an object originates from the self-coupling of gluons.

Should we then observe a massless flavourless glueball in Nature ? The answer is no. The pole at $q^2=0$ appears only in the matrix elements of unphysical (technically non-gauge invariant) operators such as K_μ . Physical (i.e., measurable) matrix elements [like those of Eq. (7)] never exhibit the pole : the ghost prevents them from vanishing without going to the extreme of making them infinite [see again Eq. (7)]. For this reason, after Kogut and Susskind ¹⁾, this "bound state" has been named the "ghost".

The presence of the ghost can be shown ⁵⁾ to make QCD predictions compatible with the known pseudoscalar meson physics provided that $\sqrt{a} \approx 500$ MeV. In that case, as already explained, π^\pm , K , \bar{K} are not affected

by the ghost, while π^0 , η^0 and η' get additional contributions and mix. The parameters m_u , m_d , m_s can be fixed from π^\pm , K , \bar{K} properties while, with $\sqrt{a} = 500$ MeV the remaining mass eigenstates turn out to be

$$\pi^0 \approx \frac{1}{\sqrt{2}} (u\bar{u} - d\bar{d}) \quad (\text{no ghost or } m_s \text{ contribution} \Rightarrow m_{\pi^0} \sim m_\pi^\pm)$$

$$\eta \approx \cos \theta_p \eta_8 + \sin \theta_p \eta_1 \quad (\text{small ghost, large } m_s \text{ contr.} \Rightarrow m_\eta \gg m_\pi) \quad (8)$$

$$\eta' \approx -\sin \theta_p \eta_8 + \cos \theta_p \eta_1 \quad (\text{large ghost and } m_s \text{ contr.} \Rightarrow m_{\eta'} \gg m_\eta)$$

where θ_p , predicted to be close to the experimental value of 10° , is the pseudoscalar mixing angle. Pseudoscalar couplings and widths do also turn out to be satisfactory 5).

3. STRONG CP PROBLEM

Unfortunately, the above resolution of the $U(1)$ problem brings back the possibility that strong interactions do not conserve CP. It brings it back because there exists an old [i.e., pre- $U(1)$ problem solution] argument due to S. Weinberg according to which CP is automatically conserved in QCD. The argument goes as follows : the only possible renormalizable terms that can appear in a quark gluon interaction (up to total divergences) are a slight extension of those of Eq. (1) :

$$\mathcal{L}_{\text{QCD}} = \frac{1}{4} F_{\mu\nu}^2 + \sum_i \bar{q}_i \not{D} q_i - \sum_i (\bar{q}_{iR} m_i q_{iL} + \bar{q}_{iL} m_i^* q_{iR}) \quad (9)$$

$$q_{iL} \equiv 1/2 (1 + \gamma_5) q_i ; q_{iR} \equiv 1/2 (1 - \gamma_5) q_i$$

where the first two terms are a shorthand for those written out in Eq. (1) and the last two terms reduce to the last term of Eq. (1) if $m_i = m_i^*$. For $m_i \neq m_i^*$ Eq. (9) differs from Eq. (1) by the apparently CP violating term $\sum_i (m_i - m_i^*) \bar{q}_{iL} \gamma_5 q_{iR}$. It can be observed though that, defining new quark fields by :

$$q'_{iL} = e^{i\phi_i/2} q_{iL} ; q'_{iR} = e^{-i\phi_i/2} q_{iR} ; \phi_i = \arg m_i \quad (10)$$

the mass term can be rewritten as :

$$-\sum_i |m_i| \bar{q}'_{iR} q'_{iL} + \text{h.c.} = -\sum_i |m_i| \bar{q}'_i q'_i \quad (11)$$

which is CP conserving. The change of variable (10) is nothing but an axial $U(3)$ transformation. Unfortunately, as we have learned in the $U(1)$ problem, the $U(1)$ part of that transformation is anomalous in the sense that, under (10), \mathcal{L}_{QCD} acquires the extra term :

$$\delta \mathcal{L}_{ABJ} = \theta Q(x) ; \quad Q(x) = \frac{g^2}{64\pi^2} F_{\mu\nu}^a F_{\rho\sigma}^a \epsilon_{\mu\nu\rho\sigma}, \quad \theta = \sum_i \phi_i \quad (12)$$

We thus see that we could rotate away almost all the phases ϕ_i , the sum of them reappearing as a new parameter of QCD, the so-called vacuum angle θ ⁶⁾. In the old days, terms like (12) were neglected because they are total divergences. However, that was precisely what we had to argue to be incorrect in order to solve the $U(1)$ problem.

Thus, the introduction of the ghost implies that a $\theta Q(x)$ term added to \mathcal{L}_{QCD} does have observable consequences (as we shall see in a moment) and that QCD itself has indeed $N_f + 2$ free parameters⁶⁾. It also looks as if we got ourselves in a squeeze, in the sense that apparently :

$$U(1) \text{ O.K.} \Rightarrow \text{CP not O.K.} ; \quad \text{CP O.K.} \Rightarrow U(1) \text{ not O.K.}$$

How bad is it quantitatively ? The strongest experimental problem comes from the present upper bound on the CP violating electric dipole moment of the neutron⁷⁾ :

$$D_n < 6 \cdot 10^{-25} \text{ e.cm.} \quad \text{exp.} \quad (13)$$

Naïvely, we would expect that, at $\theta \neq 0$

$$D_n \approx 10^{-13} \text{ e.cm.} \theta \quad (14)$$

This is too simplistic. The effects of θ can be reduced by the presence of a symmetry. For instance, if we could take one of the quarks (say, the up quark) to be massless, $\theta \neq 0$ would give no effect⁸⁾. Roughly speaking, $\theta \sim \sum_i \phi_i$, but if $m_u = 0$, we can take $\theta = \phi_u$, $\phi_i = 0$ ($i \neq u$) and $\phi_u \neq 0$ is unobservable since $m_u = 0$. Using the standard values of m_u , m_d , m_s , D_n is reduced with respect to (14), but is still large⁸⁾ :

*) Unfortunately, $m_u = 0$ conflicts with K^+, K^0 mass difference $\eta \rightarrow 3\pi$, etc.; all current algebra calculations indicate $m_u \gtrsim 0.5 m_d \approx \text{a few MeV}$.

$$D_n \sim 3.6 \cdot 10^{-16} \text{ e.cm.} \theta \Rightarrow \theta < 2 \cdot 10^{-9} \text{ exp} \quad (15)$$

We are therefore faced with explaining an unnaturally small number. Rather than attempting that one can follow the possibility of adding an extra symmetry (as it was the case for $m_u = 0$) to QCD. This approach needs the bringing in of electroweak interactions and leads automatically to the axion.

4. THE AXION

In the Peccei-Quinn (PQ) scheme ⁹⁾, the extra symmetry needed to make Θ unobservable is achieved by enlarging the Higgs sector of the conventional Glashow-Weinberg-Salam model. The Higgs doublet ϕ is replaced by two such doublets ϕ_u and ϕ_d which, through the standard Yukawa coupling mechanism, give mass to charge $\frac{2}{3}$ and charge $-\frac{1}{3}$ quarks, respectively.

Both ϕ_u and ϕ_d break $SU(2)_L \times U(1)_Y$ to $U(1)_{\text{el.}}$, so that the standard relation $\langle \phi \rangle = (G_F \sqrt{2})^{-\frac{1}{2}} \simeq 250 \text{ GeV}$ becomes

$$\langle \phi_u \rangle = (G_F \sqrt{2})^{-1/2} \sin \alpha, \quad \langle \phi_d \rangle = (G_F \sqrt{2})^{-1/2} \cos \alpha \quad (16)$$

Unfortunately, several axion properties will depend upon the unknown parameter

$$x \equiv \cot \alpha \quad (17)$$

Parallel to the PQ scheme, we shall discuss an interesting alternative due to Dine, Fischler and Srednicki ¹⁰⁾ (DFS) in which a third Higgs field ϕ_o is added to the picture. ϕ_o is an $SU(2)_L \times U(1)_Y$ singlet so that $\langle \phi_o \rangle \equiv F$ is not related to the 100 GeV scale of $SU(2)_L \times U(1)_Y$ breaking. It can be taken to be a free parameter and is chosen in the DFS scheme to satisfy :

$$F \gg G_F^{-1/2} \quad (18)$$

It was Weinberg and Wilczek who realized ¹¹⁾ that the breaking of the PQ symmetry through $\langle \phi_{u,d} \rangle$ (or F) implies a Goldstone boson, which was termed the axion.

The ghost mechanism discussed above is readily applicable to the axion, which has no mass except for the ghost dominated annihilation diagram. In fact, the axion-axion and axion-pseudoscalar mass matrix elements are exactly like those of Fig. 2b, provided we rescale the ghost pseudoscalar coupling \sqrt{a} as

$$g_{\text{ghost-axion}} = a \cdot \rho ; \rho = \frac{\sqrt{2} F_\pi}{F} N \quad (\text{DFS})$$

$$(x + \frac{1}{x}) N F_\pi \left(\frac{G_F}{\sqrt{2}} \right)^{1/2} = 2.73 \cdot 10^{-4} (x + \frac{1}{x}) N \quad (\text{PQ})$$
(19)

where N is the number of families ($N = 3?$) and $F_\pi \approx 95$ MeV. It is straightforward to diagonalize the full mass matrix and find the axion mass and its mixing to ordinary pseudoscalar. One obtains, for instance,

$$m_a = \rho \left(\frac{1}{a} + \sum_j \frac{1}{\mu_j^2} \right)^{-1/2} = \frac{50N(x + \frac{1}{x}) R^{1/2} \text{ KeV}}{100 N R^{1/2} \left(\frac{250 \text{ GeV}}{F} \right) \text{ KeV}} \quad (\text{PQ})$$
(20)

where μ_j^2 , the pseudoscalar masses in absence of the ghost, are related to physical masses by :

$$m_\pi^2 = \frac{1}{2} (\mu_u^2 + \mu_d^2) ; m_{K^+}^2 = \frac{1}{2} (\mu_u^2 + \mu_s^2), \text{ etc.} \quad (21)$$

and $R \equiv m_u m_d (m_u + m_d)^{-2} \approx 0.23$. We see explicitly from (20) that the axion is massless (and actually decoupled and unnecessary) if either a quark is massless or if $a = 0$ [no ghost coupling, in which case we have no CP, but a $U(1)$ problem].

For reasonable values of x and F , the axion main decay is into 2γ 's with a very long lifetime :

$$\tau_a \approx 7 \left(\frac{100 \text{ KeV}}{m_a} \right)^5 \text{ s} \quad (22)$$

More generally, all axion couplings, including their mixing to ordinary pseudoscalars, go like the ρ parameter of Eq. (19) hence scale like F^{-1} . This is why for F extremely large, we get an "invisible axion".

How invisible, depends on the value of F and on the effect we are looking at. In laboratory experiments one can only get a lower bound on F and it seems that the PQ axion is already ruled out. Astrophysical arguments,

however, can also exclude very large values of F since in that case the axion becomes extremely light and affects stellar evolution or standard cosmology. Such arguments seem to leave out ¹²⁾ only a window for the F parameter ($10^{8\pm 1}$ GeV $< F < 10^{12}$ GeV) which is inaccessible to laboratory experiments.

On the other hand, it might be wiser to see how far one can push the lower limit on F by purely laboratory experiments that do not have to rely on (even very plausible) astrophysical and cosmological models.

5. AXIONS AT LEAR

It is not my aim here to review the present situation on axion search. I would just like to conclude by mentioning that the LEAR machine, which is soon due to start operating at CERN, can be a good place for testing the various ideas discussed in this talk and, in particular, for axion search (more generally for searching the light, weakly coupled particles predicted in several unified theories).

A rather favourable channel turns out to be ¹³⁾ :

$$\bar{p}p \mid_{\text{rest}} \rightarrow \pi^+ \pi^- + X_0 ; \quad X_0 = \pi^0, \eta, \eta', \text{axion, ?} \quad (23)$$

where the relative rates of neutral pseudoscalar meson production offer a test of the theoretical framework in which we have discussed the $U(1)$ problem (in particular η' production is sensitive to ghost couplings), while axion production is predicted to be as follows :

$$R > 1.2 \cdot 10^{-6} \quad (\text{PQ}) \quad (24)$$

$$6 \cdot 10^{-7} \left(\frac{250 \text{ GeV}}{F} \right)^2 < R < 2.4 \cdot 10^{-6} \left(\frac{250 \text{ GeV}}{F} \right)^2 \quad (\text{DFS})$$

where $R \equiv \sigma(\bar{p}p \rightarrow \pi^+ \pi^- \text{ axion}) / \sigma(\bar{p}p \rightarrow \pi^+ \pi^- \pi^0)$. Using a \bar{p} flux at LEAR of $10^6 / \text{s}$ and the known $\pi^+ \pi^- \pi^0$ yield of about 7%, we get rates of $10^4 / \text{day}$ for the PQ axion. The axion signal would consist of events in which the measured π^+ , π^- momenta reveal a large missing energy and a small missing mass (γ 's would have to be detected with good efficiency since they would constitute the main background). The experiment can rule out easily the PQ axion and explore scales for F of $0(10 \text{ TeV})$ for the DFS axion.

Even if one believes that astrophysical arguments have already ruled out DFS axions in that range, this type of experiments can be worth pursuing as a way to look at light, weakly coupled bosons which are predicted to exist whenever a global symmetry is spontaneously broken at a very large scale ^{*)}. This is how precise, low energy experiments can tell us a lot about particle physics at very high energy : it was after all β decay that taught us first about the existence of interesting physics in the 100 GeV region !

It is a pleasure to thank the organizers of this Rencontre de Moriond for giving me the opportunity to attend such a pleasant and lively meeting.

^{*)} For another use of LEAR, in connection with CP violation in the K^0 , \bar{K}^0 system, see Ref. 14).

REFErencEs

- 1) S. Weinberg, Phys.Rev. D11 (1975) 3583;
J. Kogut and L. Susskind, Phys.Rev. D11 (1975) 3594.
- 2) S.L. Adler, Phys.Rev. 177 (1969) 2426;
J.S. Bell and R. Jackiw, Nuovo Cimento 60A (1969) 47.
- 3) Here is an incomplete list of relevant papers :
G. 't Hooft, Phys.Rev.Letters 37 (1976) 8; Phys.Rev. D14 (1976) 3432;
E. Witten, Nuclear Phys. B156 (1979) 269;
G. Veneziano, Nuclear Phys. B159 (1979) 213.
- 4) P. Di Vecchia, K. Fabricius, G.C. Rossi and G. Veneziano, Nuclear Phys. B192 (1981) 392; Phys.Letters 108B (1982) 323.
- 5) G. Veneziano, Ref. 3);
C. Rosenzweig, J. Schechter and G. Trahern, Phys.Rev. D21 (1980) 3388;
P. Di Vecchia and G. Veneziano, Nuclear Phys. B171 (1980) 253;
E. Witten, Ann.Phys. 128 (1980) 363;
P. Nath and A. Arnowitt, Phys.Rev. D23 (1981) 473.
- 6) R. Jackiw and C. Rebbi, Phys.Rev.Letters 37 (1976) 172;
C. Callan, R. Dashen and D. Gross, Phys.Letters 63B (1976) 334.
- 7) W.B. Dress, P.D. Miller, J.M. Pendlebury, P. Perrin and N.F. Ramsey,
Phys.Rev. D15 (1977) 9.
- 8) V. Baluni, Phys.Rev. D19 (1979) 2227;
R.J. Crewther, P. Di Vecchia, G. Veneziano and E. Witten, Phys.Letters 88B (1979) 123; 91B (1980) 487(E).
- 9) R.D. Peccei and H.R. Quinn, Phys.Rev.Letters 38 (1977) 1440; Phys.Rev. D16 (1977) 1791.
- 10) M. Dine, W. Fischler and M. Srednicki, Phys.Letters 104B (1981) 199.
- 11) S. Weinberg, Phys.Rev.Letters 40 (1978) 223;
F. Wilczek, Phys.Rev.Letters 40 (1978) 279.
- 12) D. Dicus et al., Phys.Rev. D18 (1978) 1829;
P. Sikivie, Phys.Rev.Letters 48 (1982) 1156;
J. Preskill, M.B. Wise and F. Wilczek, Phys.Letters 120B (1983) 127;
L.F. Abbott and P. Sikivie, Phys.Letters 120B (1983) 133;
M. Dine and W. Fischler, Phys.Letters 120B (1983) 137.
- 13) E. Gabathuler, G. Veneziano and P. Pavlopoulos, Phys.Letters 114B (1982) 58.
- 14) E. Gabathuler and P. Pavlopoulos, CERN EP/82-118 (1982).

NEW TESTS FOR QUARK AND LEPTON SUBSTRUCTURE

Estia J. Eichten

Fermi National Accelerator Laboratory, Batavia, IL 60510
andEnrico Fermi Institute, University of Chicago
Chicago, IL 60637

† Kenneth D. Lane

Ohio State University, Columbus, OH 43210

Michael E. Peskin *

Stanford Linear Accelerator Center, Stanford, CA 94305

(Presented by Kenneth Lane)

ABSTRACT

If quarks and leptons are composite at the energy scale Λ , the strong forces binding their constituents induce flavor-diagonal contact interactions. Through their interference with standard color \otimes electro-weak model amplitudes, these contact interactions can have significant effects at reaction energies well below Λ . Consideration of their effect on Bhabha scattering produces a new stronger bound on the scale of electron compositeness: $\Lambda > 750$ GeV. Collider experiments now being planned will be sensitive to $\Lambda \sim 1 - 5$ TeV for both electrons and light quarks. The super-colliders of the next decade will be able to probe up to $\Lambda \sim 10 - 50$ TeV.

The proliferation of quarks and leptons has naturally led to the speculation that they are composite structures, bound states of more fundamental constituents which are often called "preons".^{1]} Many authors have proposed models of such composite structure, but no obviously correct or compelling model has yet emerged. There is not even consensus on the most fundamental aspect of quark and lepton substructure — the value of the mass scale Λ which characterizes the strength of preon-binding interactions and the physical size of composite states. It is therefore important to devise experiments which probe this potential substructure as deeply as possible and which, at the same time, test the widest possible variety of models. Here, we shall identify new observable consequences of quark and lepton substructure which do just that.^{2]} An immediate result of these is that existing Bhabha scattering measurements imply that $\Lambda > 750$ GeV for the electron, a factor of 5 larger than previous lower bounds.

Before spelling out our tests, let us review briefly what is known about Λ . At present, high-energy cross sections are well explained by the standard $SU(3) \otimes SU(2) \otimes U(1)$ gauge theory with elementary quarks and leptons. If these fermions are composite, then Λ is much larger than their masses, completely unlike the situation in nuclear and hadron physics. However, 't Hooft has argued that gauge theories of preon-binding quite naturally produce composite fermions much less massive than the binding scale provided certain chiral symmetry constraints are satisfied.^{3]} Since the energy $\Lambda_{EW} = 0(1$ TeV) at which electroweak symmetry is broken is the lowest new dynamical scale we foresee, we expect $\Lambda \geq \Lambda_{EW}$.

Modifications of gauge-field (γ, Z^0 , etc.) propagators and vertices with fermions occur in any preon model, though their precise form is model-dependent. In a favored parametrization,^{4]} one simply multiplies the gauge propagator by a form factor $F(q^2) \equiv 1 + q^2/\Lambda^2$. Measurements of $e^+e^- \rightarrow \bar{\psi}\psi$ ($\psi = e, \mu, \tau, q$) up to $\sqrt{s} = 35$ GeV at PETRA have excluded photon form factors for $\Lambda \leq 100 - 200$ GeV.^{5]} Composite fermions also possess new contact interactions generated by constituent exchange. These four-fermion interactions have strength $\pm g^2/\Lambda^2$, where g is an effective strong coupling constant analogous to the ρ -coupling $g_\rho^2/4\pi \equiv 2.1$. If contact interactions mediate flavor-changing processes such as $K_L^0 \rightarrow \mu e$, $D^0 \bar{D}^0$ and $K^0 \bar{K}^0$ mixing, the lower limits on Λ range from ~ 100 TeV to ~ 2800 TeV.^{6]} While these bounds are impressive, it is possible to construct composite models in which some^{6]} or all^{7]} of the dangerous flavor-changing interactions are absent. In summary, the only

relatively model-independent constraints are the much lower ones deduced
from the PETRA measurements. ^{8]}

Our new tests for substructure are based on two observations: First, in any model in which one or both chiral components of the fermion ψ is composite, there must occur flavor-diagonal, helicity-conserving contact interactions of the form ^{9]}

$$\mathcal{L}_{\psi\psi} = (g^2/2\Lambda^2) [\eta_{LL} \bar{\psi}_L \gamma_\mu \psi_L \bar{\psi}_L \gamma^\mu \psi_L + \eta_{RR} \bar{\psi}_R \gamma_\mu \psi_R \bar{\psi}_R \gamma^\mu \psi_R + 2\eta_{RL} \bar{\psi}_R \gamma_\mu \psi_R \bar{\psi}_L \gamma^\mu \psi_L] . \quad (1)$$

In our construction of Eq.(1), we assume that the standard $SU(3) \otimes SU(2) \otimes U(1)$ gauge theory is correct and that $\Lambda \geq \Lambda_{EW}$. ^{10]} Then ψ_L and ψ_R are distinct species and there is no reason by $\mathcal{L}_{\psi\psi}$ should conserve parity. We define Λ in Eq.(1) such that the strong coupling $g^2/4\pi = 1$ and the largest $|\eta_{ij}| = 1$. Color indices, if any, are suppressed in Eq.(1). Second, if some kinematic region of $\psi\psi$ elastic scattering is, in the standard theory, controlled by a gauge coupling $\alpha_\psi \ll 1$, then the helicity-conserving interaction $\mathcal{L}_{\psi\psi}$ produces interference terms in the cross section of order $(4\pi\alpha_\psi/q^2)^{-1} (g^2/\Lambda^2) = q^2/\alpha_\psi \Lambda^2$ relative to the standard-model contribution. ^{11]} This model-independent effect overwhelms the $0(q^2/\Lambda^2)$ contribution of form factors.

We apply our tests below to high-energy Bhabha scattering ($\alpha_\psi \cong \alpha$) and to jet production at high transverse momentum (p_T) in hadron-hadron colliders [$\alpha_\psi = \alpha_{QCD}(q^2)$]. It is also important to consider the model-dependent possibility that distinct fermions ψ_1 and ψ_2 have some constituents in common. Then an interaction such as (1) exists, with roughly the same strength, and will modify cross sections for $\psi_1 \bar{\psi}_1 - \psi_2 \bar{\psi}_2$, $\psi_1 \psi_2 - \psi_1 \psi_2$ and their $SU(2)_W$ transforms. Such flavor and helicity-conserving interactions certainly are generated by pre-color gluon exchange even if $\psi_{1L,R}$ and $\psi_{2L,R}$ have no fermionic constituents in common. We do not know if the usual argument for Zweig's rule suppression applies to this situation in which all momentum transfers are much less than Λ . (We thank Sid Drell for emphasizing to us the potential importance of pre-color gluon exchange.) As an example, we shall consider $e^+ e^- \rightarrow \mu^+ \mu^-$.

Bhabha Scattering. The unpolarized beam cross section, including γ and Z^0 exchanges and $\mathcal{L}_{\psi\psi}$ with $\psi = e$, is given by

$$\frac{d\sigma(e^+e^- \rightarrow e^+e^-)}{d(\cos \theta)} = (\pi \alpha^2 / 4s) [4A_0 + A_-(1 - \cos \theta)^2 + A_+(1 + \cos \theta)^2] ;$$

$$A_0 = \left(\frac{s}{t} \right)^2 \left| 1 + \frac{g_R g_L}{e^2} \frac{t}{t_z} + \frac{\eta_{RL} t}{\alpha \Lambda^2} \right|^2 ,$$

$$A_- = \left| 1 + \frac{g_R g_L}{e^2} \frac{s}{s_z} + \frac{\eta_{RL} s}{\alpha \Lambda^2} \right|^2 , \quad (2)$$

$$A_+ = \frac{1}{2} \left| 1 + \frac{s}{t} + \frac{g_R^2}{e^2} \left(\frac{s}{s_z} + \frac{s}{t_z} \right) + \frac{2\eta_{RR} s}{\alpha \Lambda^2} \right|^2$$

$$+ \frac{1}{2} \left| 1 + \frac{s}{t} + \frac{g_L^2}{e^2} \left(\frac{s}{s_z} + \frac{s}{t_z} \right) + \frac{2\eta_{LL} s}{\alpha \Lambda^2} \right|^2$$

In Eq.(2), $t = -s(1 - \cos \theta)/2$, $s_z = s - \mu_z^2 + i\mu_z \Gamma_z$ and $t_z = t - \mu_z^2 + i\mu_z \Gamma_z$; $g_R/e = \tan \theta_W$ and $g_L/e = -\cot 2\theta_W$.^[12]

A useful way to search experimentally for electron substructure is to plot the fractional deviation

$$\Delta_{ee}(\cos \theta) = \frac{d\sigma/d(\cos \theta)|_{\text{meas.}}}{d\sigma/d(\cos \theta)|_{\text{EW}}} - 1 , \quad (3)$$

where $d\sigma/d(\cos \theta)|_{\text{EW}}$ is given by Eq.(2) with $\Lambda = \infty$. Since Δ_{ee} must vanish in the forward direction, the measured cross section can be normalized there to the electroweak value.

We have used Eqs.(2) to calculate Δ_{ee} at $\sqrt{s} = 35$ GeV for the cases in which \mathcal{L}_{ee} reduces to the coupling of two left-handed (LL), right-handed (RR), vector (VV) and axial-vector (AA) currents. In the LL model, e.g., $\eta_{LL} = \pm 1$, $\eta_{RR} = \eta_{RL} = 0$. The results are shown in Fig. 1 for values of Λ such that $|\Delta_{ee}| = 3 - 5\%$ over a wide angular range, consistent with the PETRA measurements.^[5] Several comments are in order: (1) For $s \ll \mu_z^2$, the RR model is indistinguishable from LL, because the parity-violating z^0 -terms are negligible there. (2) Greater sensitivity to Λ occurs when both left- and right-handed electron components are composite and have common constituents ($|\eta_{RL}| \simeq 1$). (3) Even greater sensitivity to the space-time structure of \mathcal{L}_{ee} can be obtained

by using polarized e^+, e^- beams.^{13]} (4) The PETRA measurements imply the bounds

$$\Lambda(LL,RR) > 750 \text{ GeV}; \quad \Lambda(VV,AA) > 1500 \text{ GeV} . \quad (4)$$

Most other physically reasonable models will give bounds lying between these two.

Experiments at higher energy e^+e^- colliders will probe even deeper into the electron. Figure 2 shows Δ_{ee} at $\sqrt{s} = 100 \text{ GeV}$ for the same four models. We chose Λ in each case so that $|\Delta_{ee}| = 5 - 8\%$ over a large angular range. Note the distinctive effects of parity-violating Z^0 -terms. We expect that high-luminosity Z^0 -factories will be able to set the limits $\Lambda(LL,RR) > 2 \text{ TeV}$ and $\Lambda(VV,AA) > 5 \text{ TeV}$.^{2,13]}

$\bar{q}q$ and qq Hard Scattering. The most general $SU(3) \otimes SU(2) \otimes U(1)$ -invariant contact interaction involving only light quarks $q_{L,R} = (u,d)_{L,R}$ contains 10 independent helicity-conserving terms.^{13]} Here, we consider only the simple case of the product of two left-handed color- and isospin-singlet currents:

$$\mathcal{L}_{qq} = \pm (g^2/2\Lambda^2) \bar{q}_L \gamma_\mu q_L \bar{q}_L \gamma^\mu q_L . \quad (5)$$

We have calculated the cross section for high- p_T jet production using lowest-order QCD and the interaction (5). The contributions of light quark and gluon jets were included. The results are shown in Fig. 3 for $\bar{p}p$ and $p\bar{p}$ collisions at $\sqrt{s} = 2 \text{ TeV}$. We assume an effect is detectable if it gives a deviation from the expected QCD shape that is at least a factor of two and amounts to at least 100 events/yr. Then, for a $\bar{p}p$ collider with annual integrated luminosity of 10^{37} cm^{-2} , the limit $\Lambda > 1.0 \text{ TeV}$ can be set for the interaction (5). The corresponding limit for a $p\bar{p}$ collider with 10^{40} cm^{-2} is $\Lambda > 1.5 - 2.0 \text{ TeV}$. More immediately, the CERN $\bar{p}p$ collider, with integrated luminosity 10^{36} cm^{-2} , can limit $\Lambda > 200 \text{ GeV}$ for this interaction.

$e^+e^- \rightarrow \mu^+\mu^-$. If the electron and the muon have one or more constituents in common or pre-color gluon exchange between e and μ constituents is not Zweig-suppressed, the helicity-conserving terms in their contact interaction are

$$\mathcal{L}_{e\mu} = \frac{g^2}{\Lambda^2} \sum_{i,j=L,R} \eta'_{ij} \bar{e}_i \gamma_\lambda e_i \bar{\mu}_j \gamma^\lambda \mu_j + \text{SU(2)_W-transforms} , \quad (6)$$

where Λ, g^2 and η'_{ij} are normalized as in Eq.(1). For unpolarized e^+, e^- beams, the differential cross section is

$$\frac{d\sigma(e^+ e^- \rightarrow \mu^+ \mu^-)}{d(\cos \theta)} = (\pi \alpha^2 / 4s) [B_+ (1 + \cos \theta)^2 + B_- (1 - \cos \theta)^2] ;$$

$$B_+ = \frac{1}{2} \left| 1 + \frac{g_L^2}{e^2} \frac{s}{s_z} + \frac{\eta'_{LL} s}{\alpha \Lambda^2} \right|^2 + \frac{1}{2} \left| 1 + \frac{g_R^2}{e^2} \frac{s}{s_z} + \frac{\eta'_{RR} s}{\alpha \Lambda^2} \right|^2 , \quad (7)$$

$$B_- = \frac{1}{2} \left| 1 + \frac{g_R g_L}{e^2} \frac{s}{s_z} + \frac{\eta'_{RL} s}{\alpha \Lambda^2} \right|^2 + \frac{1}{2} \left| 1 + \frac{g_L g_R}{e^2} \frac{s}{s_z} + \frac{\eta'_{LR} s}{\alpha \Lambda^2} \right|^2 .$$

The fractional deviation $\Delta_{e\mu}$ from the electroweak cross section for $e^+ e^- \rightarrow \mu^+ \mu^-$ has the following properties: (1) Existing measurements at $\sqrt{s} = 35$ GeV are consistent with $|\Delta_{e\mu}| \leq 6 - 8\%$ over a wide angular range.^{5]} This corresponds to $\Lambda > 1.4$ TeV for LL and RR models and to $\Lambda > 2.2$ TeV for VV and AA. These bounds on lepton substructure are stronger, but more model-dependent, than those in Eq.(4). Muon decay and $\nu_\mu - e$ elastic scattering give $\Lambda \geq 6$ TeV for a LL isovector interaction and $\Lambda \geq 2$ TeV for a LL scalar interaction. (2) For $\sqrt{s} \ll \mu_z$, $\Delta_{e\mu}(\text{LL}) \cong \Delta_{e\mu}(\text{RR}) \propto (1 + \cos \theta)^2$. Also, $\Delta_{e\mu}(\text{VV}) \cong \text{constant}$, while $\Delta_{e\mu}(\text{AA}) \propto \cos \theta$; these effects could be hidden by a normalization error and by the Z^0 -induced asymmetry, respectively. (3) Because γ and z^0 appear only in the s-channel, the beam energy can be tuned to enhance the effect of particular space-time structures in $\Delta_{e\mu}$. When $\text{Re}(1 + g_i g_j s / e^2 s_z) = 0$, the η'_{ij} -contribution is negligible, $\sim s/\Lambda^4$, while the fractional deviations due to other couplings is greater than at nearby energies. This occurs at $\sqrt{s}_{LL} = 77.4$ GeV, $\sqrt{s}_{RR} = 82.2$ GeV and $\sqrt{s}_{RL} = 115.9$ GeV.

Finally, comparable limits on other flavor-nondiagonal interactions can be obtained from existing data on deep-inelastic $\nu_\mu - \text{nucleon}$ scattering, $\bar{p}p \rightarrow \mu^+ \mu^- X$ at $\sqrt{s} = 2$ TeV and $e - p$ collisions at $Q^2 = (100 \text{ GeV})^2$.

We have shown that flavor-diagonal contact interactions induced by preon-binding forces significantly alter hard-scattering cross sections at energies well below Λ . Searches for these effects are the most sensitive

model-independent tests of quark and lepton substructure. If $\Lambda = 1-5$ TeV, deviations from the standard model will soon be observable. The coming generation of multi-TeV colliders should be able to detect substructure up to $\Lambda = 10 - 50$ TeV. But, if Λ is only a few TeV, the implications for experiments at these colliders will be more profound. For example, if $\Lambda = 2$ TeV, the Bhabha cross section at a $1 \text{ TeV} \times 1 \text{ TeV}$ linear e^+e^- collider^{2]} would be $\sim 1/\Lambda^2 \simeq 0.1 \text{ nb}$, or about 5000 units of R .

This work was begun at the 1982 Summer Study in Snowmass. We thank several participants for stimulating discussions, particularly I. Hinchliffe, H. Kagan, J. Leveille, D. Pellett, M. Perl and H. Wiedemann. K.L. thanks the CERN and Fermilab theory groups for their hospitality during the course of this research. Finally, E.E. and K.L. thank the organizers of the XVIIIth Rencontre de Moriond for their splendid efforts.

[†]Work supported in part by the U.S. Department of Energy under Contract No. DOE/ER/01545-326.

^{*}Work supported in part by the U.S. Department of Energy under Contract No. DE-ACOB-76SF00515.

REFERENCES

1. Two recent reviews are: M. E. Peskin, in Proceedings of the 1981 International Symposium on Lepton and Photon Interactions at High Energy, W. Pfeil, ed., p. 880 (Bonn, 1981); L. Lyons, Oxford University Publication 52/82 (June 1982).
2. E. J. Eichten, K. D. Lane and M. E. Peskin, Phys. Rev. Lett. 50, 811 (1983). Preliminary accounts of our work appear in the following subgroup reports of the Division of Particles and Fields Summer Study on Elementary Particle Physics and Future Facilities, R. Donaldson, ed. (Fermilab, 1982): M. Abolins, et al.; H. Kagan; F. Bulos, et al.
3. G. 't Hooft, in Recent Developments in Gauge Theories, G. 't Hooft, et al., eds. (Plenum Press, New York, 1980).
4. M. S. Chanowitz and S. D. Drell, Phys. Rev. Lett. 30, 807 (1973).
5. J. G. Branson, in Proceedings of the 1981 International Symposium on Lepton and Photon Interactions at High Energy, W. Pfeil, ed., p. 279 (Bonn, 1981); R. Brandelik, et al., (Tasso Collaboration), Phys. Lett. 117B, 365 (1982).
6. I. Bars, in Proceedings of the XVII^{me} Rencontre de Moriond, J. Tran Thanh Van, ed. (1982). Similar contact interactions and bounds on Λ occur in theories of extended technicolor; see E. Eichten and K. Lane, Phys. Lett. 90B, 125 (1980).
7. See, for example: H. Terazawa, Y. Chikashige, and K. Akama, Phys. Rev. D15, 480 (1977); L. Abbott and E. Farhi, Phys. Lett. 101B, 69

(1981); H. Fritzsch and G. Mandelbaum, Phys. Lett. 102B, 319 (1981).

8. The only stronger bound comes from the agreement between theory and experiment for $(g-2)$ of the muon; this gives $\Lambda \geq 870$ GeV. See R. Barbieri, L. Maiani and R. Petronzio, Phys. Lett. 96B, 63 (1980); S. J. Brodsky and S. D. Drell, Phys. Rev. D22, 2236 (1980).
9. Only if ψ is a Goldstone fermion of spontaneously broken global supersymmetry will its associated dimension-six interactions vanish. See W. Bardeen and V. Visnjic, Nucl. Phys. B194, 422 (1982).
10. By implication, we assume that G_F and $\sin^2 \theta_W$ take the values determined from ν_μ -nucleon scattering by ignoring contact interactions. While this assumption is difficult to justify satisfactorily and models exist which violate it (see the last two papers in Ref. 7), it can be confirmed by the observation of Z^0 and W^\pm , at the predicted masses, in pp collisions.
11. The existence of such relatively large interference terms in Bhabha scattering has been noted by John Preskill, Invited Talk presented at the Vanderbilt Conference on "Novel Results in Particle Physics," May, 1982 (unpublished).
12. We use $\mu_z = 93.0$ GeV, $\Gamma_z = 2.92$ GeV and $\sin^2 \theta_W = 0.222$. See W. Marciano and Z. Parsa, in Proceedings of the Cornell Z⁰ Theory Workshop, M. E. Peskin and S.-H. H. Tye, eds., p. 127.
13. This will be discussed in more detail by E. Eichten, H. Kagan and K. Lane, in preparation.

FIGURE CAPTIONS

Fig. 1 $\Delta_{ee}(\cos \theta)$, in per cent, at $\sqrt{s} = 35$ GeV. (a) The LL and RR models with $\Lambda = 750$ GeV. (b) The VV model (solid lines) with $\Lambda = 1700$ GeV and the AA model (dashed lines) with $\Lambda = 1400$ GeV. The \pm signs refer to the overall sign of the contact interaction in each case.

Fig. 2 $\Delta_{ee}(\cos \theta)$, in per cent, at $\sqrt{s} = 100$ GeV. (a) The LL model (solid lines) and RR model (dashed lines) for $\Lambda = 2$ TeV. (b) The VV model (solid) and AA model (dashed) for $\Lambda = 5$ TeV. The \pm signs have the same meaning as in Fig. 1.

Fig. 3 The jet production cross section (in picobarns/GeV) at rapidity $y = 0$ vs. transverse momentum at $\sqrt{s} = 2$ TeV in (a) pp collisions for various Λ (in TeV). The solid and dashed lines in (b) refer, respectively, to the $+$ and $-$ signs in Eq.(5). Due to a cancellation near $y = 0$, the interference is negligible in (a).

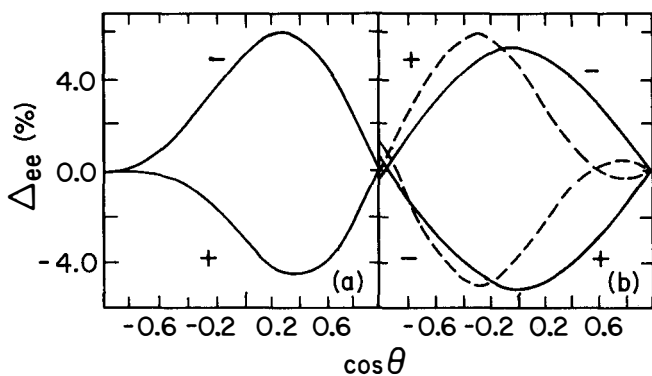


Figure 1

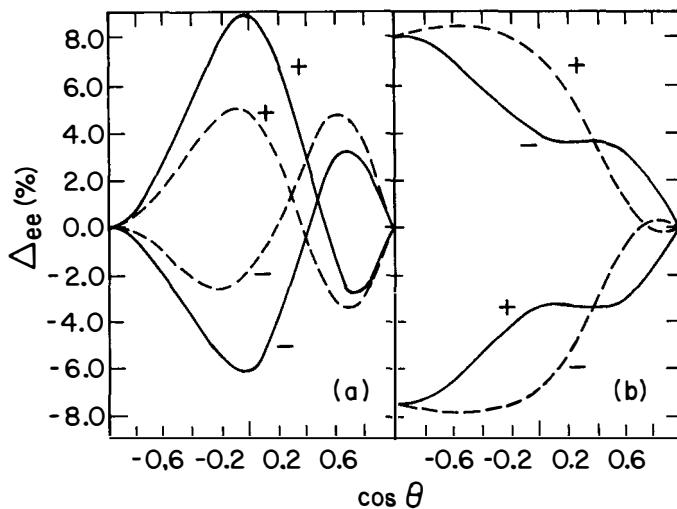


Figure 2

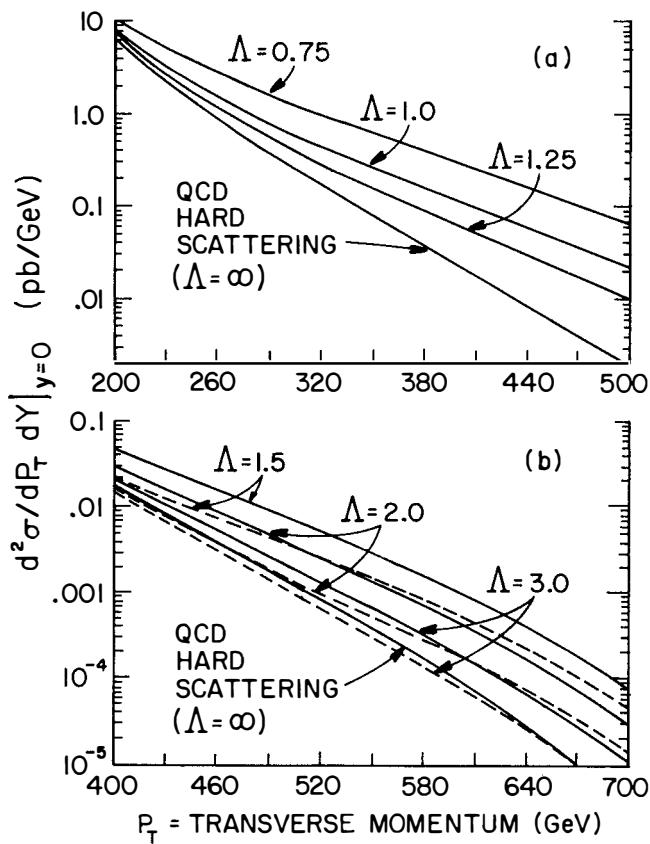


Figure 3

ELECTROMAGNETISM AS THE ORIGIN OF THE LEPTON AND QUARK MASSES *

Harald Fritzsch
Sektion Physik der Universität München
and
Max-Planck-Institut für Physik und Astrophysik
- Werner Heisenberg Institut für Physik -
München, Germany

During the progress of physics within the past hundred years it has happened twice that observed short range forces were recognized as indirect consequences of an underlying substructure of the objects considered. Thus the short-range molecular and van-der-Waals forces turned out to be indirect consequences of the substructure of atoms; they are remnants of the long range electromagnetic forces. Since 1970 something similar has happened to the short-range nuclear force, which has turned out to be a relict of the quark substructure of hadrons and the strong long range color forces between the quarks.

The only short range interaction left in physics which has not been traced back to a substructure and to a fundamental long range force between constituents is the weak interaction. Recently a number of authors has become interested in interpreting the weak force as some kind of "Van der Waals" remnant of an underlying lepton-quark substructure.¹⁾ The lepton- quark constituents for which I will use the name "haplons"²⁾ are supposed to be bound together by very strong so-called hypercolor forces which are supposed to be confining forces, presumably described by a non-Abelian gauge theory (although other types of forces are not excluded). The short range character of the weak interaction arises since the leptons and quarks are hypercolor singlets, but have a finite size. The energy scale provided by the Fermi constant is of the order of 300 GeV; the inverse size of the leptons, quarks and weak bosons is expected to be of the same order, i.e. their radii are of the order of 10^{-17} cm.

The observed weak interactions, including the neutral current interaction, can be described rather well by the standard $SU(2) \times U(1)$ gauge theory. In that theory the weak bosons and the photon are closely related to each other. The masses of the weak bosons are generated by the spontaneous breaking of the $SU(2) \times U(1)$ gauge symmetry. One of the four $SU(2) \times U(1)$ -charges remains unbroken. This charge is identified with the electric charge; the corresponding gauge boson (photon) remains massless.

If the weak interaction turns out to be a remnant of the hypercolor forces, a new interpretation of the relationship between the electromagnetic and weak interaction is required. The W- and Z- bosons cease to be fundamental gauge bosons, but acquire the less prestigious status of bound states of haplons, much like the ρ -mesons in QCD. However the photon remains an elementary object (at least at the scale of the order of 10^{-17} cm, discussed here). As a whole, the $SU(2) \times U(1)$ theory cannot be regarded anymore as a fundamental microscopic theory of the electroweak interactions, but at best can be interpreted as an effective theory, which is useful only at distances larger than the hypercolor confinement scale.

It acquires a status comparable to the one of the σ -model in QCD, which correctly describes the chiral dynamics of π -mesons and nucleons at relatively low energies, but fails to be a reasonable description of the strong interaction at high energies.

However I would like to emphasize that at the present time no indication whatsoever comes from the experimental side that leptons, quarks and weak bosons may be bound states of yet smaller constituents. It may well be that the weak force will turn out in the future as a fundamental gauge force, as fundamental as the electromagnetic one and the color force. In fact, interpreting the weak forces as effective forces poses a number of problems which have not been solved in a satisfactory manner. First of all, the weak interactions violate parity, and they do that not in an uncontrolled way, but in a very simple one: only the lefthanded leptons and quarks take part in the charged current interactions. If we interpret the weak interactions as Van der Waals type interactions, the parity violation is a point of worry. How should one interpret the observed parity violation? Does it mean that the lefthanded fermions have a different internal structure than the righthanded ones? Or are we dealing with two or several different hypercolor confinement scales, for example one for the lefthanded fermions, and one for the righthanded fermions, such that the resulting effective theory is similar to the left - right symmetric gauge theory, based on the group $SU(2)_L \times SU(2)_R$?

Another point of concern is the fact that the weak interactions show a number of regularities, e.g. the universality of the weak couplings, which one would not a priori expect if the weak interaction is merely a hypercolor remnant. On the other hand it is well - known that the interaction of pions or ρ -mesons with hadrons shows a number of regularities which can be traced back to current algebra, combined with chiral symmetry or vector meson dominance. Despite the fact that both the ρ -mesons and the pions are quark - antiquark bound states for which one would not a priori expect that their interaction with other hadrons exhibits remarkable simple properties (e.g. the universality of the vector meson couplings), the latter arise as a consequence of the underlying current algebra, which is saturated rather well at low energies by the lowest lying pole (either the pion pole in the case of the divergence of the axial vector current, or the ρ - or A_1 -pole in the case of the vector or axial vector current). The quality of these regularities is related to the quality of the pole dominance, which in the case of the pion pole is very good (the chiral $SU(2) \times SU(2)$ -symmetry is valid within a few %), while in the case of vector meson dominance it is good within about 10 %.

The observed weak interaction exhibits the global symmetry $SU(2)_L$ (L : left-handed). In the hypercolor schemes this symmetry is interpreted as a flavor symmetry of the hypercolor forces. For example, in the simple scheme discussed in refs. (2,3,4), the underlying haplons have either spin 1/2 or spin 0:

	spin	charge	color	hypercolor
α	1/2	1/2	1	n
β	1/2	-1/2	1	n
x	0	1/6	3	\bar{n}
y	0	-1/2	1	\bar{n}

The simplest hypercolor singlets are (for the hypercolor group we assume $SU(n)$ - the haplons are supposed to transform according to the n or \bar{n} representation of $SU(n)$):

$$\begin{pmatrix} \alpha & x \\ \beta & x \end{pmatrix} \quad \begin{pmatrix} \alpha & y \\ \beta & y \end{pmatrix}$$

These bound states having the charges 2/3, -1/3 or 0, -1 are supposed to represent the leptons and quarks in the various families. The W -bosons are bound states of the fermions α and β : $W^+ = (\bar{\beta}\alpha)$, $W^- = (\bar{\alpha}\beta)$ etc.

The weak currents j_μ^W , which in this model are bilinear in the haplon fields α and β , obey a local algebra of charge densities, e.g.

$$[j_0^+(x), j_0^-(y)]_{x_0=y_0} = 2 j_0^3(x) \delta^3(\vec{x} - \vec{y}).$$

The local current algebra is trivially fulfilled in a model in which leptons and quarks are pointlike objects and the weak currents are simply bilinear in the lepton and quark fields. However, if leptons and quarks are extended objects, the situation changes entirely. Currents, which are bilinear in the (composite) lepton and quark fields would not obey the local algebra, just like the currents, which are bilinear in nucleon fields, do not obey the local current algebra of QCD. Thus the local algebra becomes a highly non-trivial constraint. It is fulfilled in the haplon model discussed above, in which the currents are bilinear in α and β , and in any other model, in which the currents are bilinear in local fields. It is not known how the spectral functions of the weak isospin currents look. We shall suppose that the weak spectral functions at low frequencies are dominated by the lowest-lying pole (W dominance). Of course, at higher energies, higher excited states as well as the continuum will become relevant (see also ref. 2,5).

In the limit where the W -dominance is considered to be exact (i.e. in the limit where the continuum effects are neglected), one finds:

a) The local current algebra is saturated by the W -poles. As a consequence the W -fermion couplings are universal. The observed universality of the weak couplings is supposed to be due to the local weak current algebra and the W -dominance. The universality of the weak couplings is observed to be valid to at least 1 %. Thus the W -dominance hypothesis is presumably valid to a similar degree of accuracy. Taking into account that the W -mass is expected to be about 80 GeV (see below), we conclude that sizable contributions to the weak spectral functions are not expected to be present within the energy region starting at $E = M_W$ and about 1 TeV. The W poles can be compared to the π -meson pole in QCD, which dominates the divergence of the axial vector current at low energies to a high degree of accuracy (see also ref. 2,5).

b) The neutral W -boson W^3 , i.e. the neutral $SU(2)_L$ -partner of the charged intermediate W^\pm -bosons, is supposed to consist of two electrically charged constituents. Those can annihilate into a virtual photon and thus generate a dynamical mixing between the photon and the W^3 -boson, which is similar to the phenomenon of ρ -meson/photon mixing in QCD (for a general discussion of W - γ -mixing see refs. 2, 5, 6). Several effects follow:

The photon remains, of course, massless as a consequence of the electromagnetic gauge invariance. The neutral W -boson mass is lifted upward:

$$M_Z^2 = M_W^2 / (1 - \lambda^2)$$

(λ : W - γ -mixing parameter).

The neutral current interaction acquires a form which is identical to the one obtained in the standard $SU(2) \times U(1)$ -model. The $SU(2) \times U(1)$ -mixing angle is related to the W - γ -mixing parameter as follows:

$$\sin^2 \theta_W = \frac{e}{g} \cdot \lambda$$

(e : electric charge, g : W -fermion coupling constant).

Provided the lowest lying W -pole dominates the weak amplitudes at energies much below 1 TeV, one finds:

$$\lambda = \frac{e}{F_W/M_W}$$

(F_W : W -decay constant) and:

$$g = F_W/M_W \approx 0.65, \quad \sin\theta_W = e/g$$

(the numerical value for g is obtained for $\sin^2\theta_W = 0.22$.) Thus in all phenomenological consequences for the weak interactions at low energies the results are identical to the ones obtained in the standard $SU(2) \times U(1)$ -model. In addition, the spectrum of the W -bosons is identical to the one obtained in the $SU(2) \times U(1)$ -gauge theory. However small deviations caused by electromagnetic distortions of the W -wave functions are expected (see ref. (7)).

The remaining part of this talk is concerned with the fermion masses. The lepton and quark masses are given below (in MeV):

$$\begin{pmatrix} v_e & v_\mu & v_\tau \\ e^-(0.5) & \mu^-(106) & \tau^-(1784) \end{pmatrix}$$

$$\begin{pmatrix} u(5) & c(1,200) & t(>18,000) \\ d(8) & s(150) & b(4,600) \end{pmatrix}$$

For the "light" quarks u and d we have used typical mass values which are obtained in analyzing the chiral symmetry breaking (see e.g. ref. (8)). No masses are given for the neutrinos; the neutrino masses are assumed to be either zero or less than 100 eV, fulfilling the various experimental or astrophysical constraints. In any case the neutrino masses are at least four orders of magnitude smaller than the mass of the lightest charged fermion, the electron, which we take as a hint that the mechanism responsible for the generation of the neutrino masses (in case those masses differ from zero at all) must be qualitatively different from the one responsible for the masses of the charged fermions.

By considering the fermion mass spectrum one may observe the following facts:

- a) There exists a well-obeyed hierarchical structure. All charged fermions of the first family (e, u, d) are lighter than the ones of the second family (μ, c, s), and those in turn are lighter than the charged fermions of the third family (τ, t, b).
- b) The neutrinos are, of course, much lighter than the corresponding charged leptons. The quarks of electric charge $2/3$ of the second and third family are heavier than the corresponding quarks of charge $-1/3$:

$$\frac{m_c}{m_s} \approx 7 \quad \frac{m_t}{m_b} \gtrsim 4.$$

This pattern is broken by the u and d quarks: $m_u < m_d$.

c) There exists weak interaction mixing; the mass eigenstates are not identical to the eigenstates of the weak interactions. However the corresponding mixing angles (Cabibbo angles...) are observed to be relatively small, such that the classification of leptons and quarks in three different families makes sense, Nevertheless the fact of weak interaction mixing implies that there are no conserved quantum numbers associated to the various lepton- quark families.

Within the standard $SU(2) \times U(1)$ gauge theory it is easy to incorporate all the observed complexities of the fermion mass spectrum (masses, mixing angles) by adjusting the different Yukawa coupling constants describing the interactions of the fermions with the scalar fields. Since those coupling constants are arbitrary, the most general fermion mass matrix can be reproduced. No doubt, this is the most serious deficiency of the model.

If we take the point of view that the weak forces are effective forces due to the lepton-quark substructure, no scalar fields are needed to generate the masses of the composite W -bosons. The latter are manifestations of the hypercolor confinement scale, which is supposed to be of the order of 1 TeV. In that case the question arises, how the lepton- and quark masses are generated. After all, those masses are much smaller than 1 TeV. Below I shall describe a possible way to understand the lepton- quark mass spectrum which is still rather preliminary, but may eventually lead to a complete understanding of the fermion masses.

One surprising aspect of the lepton- quark mass spectrum is the absence of any approximate symmetry. (In comparison, the mass spectrum of hadrons shows the approximate isospin symmetry.) Furthermore the masses fluctuate wildly. Nevertheless it seems that there exists a definite relationship between the masses and the electric charges, as suggested by the properties listed above under b). Whenever wide fluctuations of energy levels were observed in physics, it has often turned out that those fluctuations were departures from zero energy levels by small perturbations. As an example we consider the mass spectrum of the π -mesons in the chiral limit of QCD ($m_u = m_d = 0$). In that limit all three π -mesons have zero mass. However the chiral symmetry is broken dynamically, if the electromagnetic interaction is introduced. The neutral π -meson remains at zero mass, however the charged pions acquire a mass of about 36 MeV (see e.g. ref. (9)). This mass is of order $e \cdot \Lambda [QCD]$ and is due to the finite electromagnetic charge radius of the pion. Thus a perturbation of the QCD Hamiltonian by the small electromagnetic interaction causes a relatively large mass splitting in the pion sector, due to the fact that the QCD Hamiltonian did not contribute to the pion mass before the perturbation was introduced. However for all states which acquired a mass of order of $\Lambda [QCD]$ by the QCD interaction (ρ -meson, nucleon, hyperons etc.), the electro-

magnetic perturbation causes only small mass splittings of the order of 1 % ... 1 %.

The exercise made above can be extended to a hypothetical situation where a new massless quark l of charge $-4/3$ is added to the massless quarks u and d . In that case there exists a chiral symmetry $SU(3) \times SU(3)$. The π -meson triplet is extended to an octet, including a doubly charged meson π^{++} (quark structure $\bar{u}u$). The latter acquires an electromagnetic mass of 72 MeV, and the following relations hold:

$$\frac{M(\pi^0)}{M(\pi^+)} = \frac{0}{1} \quad \frac{M(\pi^+)}{M(\pi^{++})} = \frac{1}{2} .$$

Below I shall describe a possibility to understand the fermion mass spectrum. This will be done without taking reference to a specific model. Only rather general assumptions are made.

A: If the weak forces are effective forces, the underlying theory will be based on a product of three different commuting gauge groups:

$$G = G_h \times SU(3)^c \times U_1^e$$

(G_h : hypercolor gauge group).

B: On the scale of the hypercolor interaction, both color and electromagnetism are small perturbations. Therefore it seems justified to consider the limit where those interactions are switched off. We suppose that all lepton and quark masses are zero in that limit. Of course, many other massive fermion states exist in addition, but those are expected to have masses of the order of 1 TeV. Taking into account the three lepton-quark families, we are dealing with 24 massless states. Those states are supposed to be massless due to an underlying chiral symmetry (either a continuous or a discrete chiral symmetry). The number of massless states (24 here) must be related to a specific property of the hypercolor dynamics; presumably it is directly related to the rank of G_h .

C: After the color and electromagnetic interactions are introduced, the fermions acquire a mass, for example, via a self energy diagram where a lepton or quark emits a virtual photon and turns into a massive fermion (mass ~ 1 TeV), which afterwards absorbs the virtual photon and turns back to a lepton or quark (see Figure). In general, the mass is due to the finite electromagnetic and color size of the fermion.

D: How much of a fermion mass is due to the color interaction, and how much is due to electromagnetism, depends on the specific model. In some models (e.g. in the one mentioned above) the color size is zero (only one of the haplons

carries color), while the electromagnetic one can never be zero, since otherwise the observed pattern of charges cannot be reproduced.

The QCD interaction will contribute to the mass of a fermion independent of the charge, i.e. the QCD mass is $SU(2)^W$ invariant. By looking at the quark masses given above it is apparent that not much room is left for a chromodynamic mass term; on the other hand a strong charge dependence of the mass is apparent. Therefore we shall assume that all lepton- and quark masses are electromagnetic in origin. We realize that this assumption puts very strong constraints on models for the lepton- quark substructure.

In principle there are infinitely many massive fermion states ($m \geq 1$ TeV), which contribute as intermediate states to the electromagnetic self energy diagram, mentioned above. The transition matrix element $\langle \text{lepton, quark} | j_\mu | \text{massive fermion} \rangle$ (j_μ : electromagnetic current) will depend on formfactors, depending on the internal structure of the fermions. One expects that the fermion mass self energy diagram (Fig.) is dominated by the lowest state which can contribute. (Something similar is true in hadron physics: the electromagnetic self energy of the proton is dominated by the lowest intermediate state). The resulting mass matrix for the fermions has the form:

$$m(\text{fermion}) = \frac{3\alpha}{4\pi} \cdot Q^2 \cdot \Lambda_h \begin{pmatrix} g_1^2 & g_1 & g_2 & g_1 & g_3 \\ g_2 & g_1 & g_2^2 & g_2 & g_3 \\ g_3 & g_1 & g_3 & g_2 & g_3^2 \end{pmatrix} + O(\alpha^2)$$

where Q^2 is the electric charge of the fermion and Λ_h the hypercolor confinement scale. The parameters g_i describe the relative strengths of the transitions $\langle i | j_\mu | \text{int. state} \rangle$ ($|i\rangle$: lepton or quark state); they are in general of order 1.

The mass matrix given above is of rank 1. Its diagonalization gives:

$$m(\text{fermion}) = \frac{3\alpha}{4\pi} \cdot Q^2 \cdot \Lambda_h \cdot \text{const.} \begin{pmatrix} 0 & 0 & 0 \\ 0 & 0 & 0 \\ 0 & 0 & 1 \end{pmatrix} + O(\alpha^2)$$

Thus in the approximation made above (only one intermediate state taken into account; terms of order α^2 are neglected) only one fermion of each electric charge acquires a mass. Those are identified with τ , b , and t ; the hierarchy pattern of the fermion masses starts to emerge. No weak interaction mixing exist in this approximation. The following relations are valid:

$$\frac{m(v_\tau)}{m(\tau)} = \frac{0}{1}$$

$$\frac{m(t)}{m(b)} = \frac{(2/3)^2}{(-1/3)^2} = 4$$

Before we return to these relations, we shall comment on the mass generation for the other fermions and on the weak interaction mixing.

As soon as we give up the assumption of the dominance of the fermion self energy by one intermediate state, the mass matrix ceases to be of rank 1, but acquires rank 2 (in case of two intermediate states) or rank 3 (more than 2 intermediate states). The hierarchy pattern of fermion masses is therefore related to the quality of the dominance of the fermion self energies by one or several massive fermion states ($m \sim 1$ TeV) (see ref. (7)).

The wave functions of the quarks of charge 2/3 and -1/3 are distorted by electromagnetic effects. The mass matrix of the charge 2/3 quarks deviates slightly from the mass matrix of charge -1/3 quarks (this effect is of order α^2). The net result is a flavor mixing; the weak mixing angles arise as functions of the quark masses (see ref. (7)). Within the mechanism of mass generation outlined here, the third family of leptons and quarks is singled out; their masses serve as driving terms for the generation of mass of all other fermions. Since the masses of the members of the third family are much larger than the other fermion masses, one expects not much weak interaction mixing between the third and the other families. Specifically the t-quark is expected to decay almost exclusively into the b-quark (plus a virtual W-boson). The b-quark, which would be stable in the absence of flavor mixing, is expected to have a relatively long life time, which may be close to the present experimental limit of the order of 10^{-12} s.

The mass relations given above imply:

- 1) The neutrinos being electrically neutral do not acquire a mass of order α , in accordance with observation. Nevertheless one expects the neutrinos to be massive, due to higher order effects.
- 2) The relation $m_t / m_b = 4$ is valid, if effects of order α^2 , including all flavor mixing effects, are neglected. It seems that the latter cannot change that relation by more than about 10 %, i.e.

$$\frac{m_t}{m_b} = 3.6 \dots 4.4$$

implying that the ($\bar{t}t$)-ground state should have a mass lower than 43 GeV. It could well be that the relation $m_t / m_b = 4$ is fulfilled rather accurately,

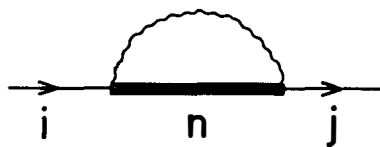
and the $t\bar{t}$ -ground state has a mass in the range between 36.8 and 38 GeV, i.e. it is just above the present lower limit for the $t\bar{t}$ -mass given by the PETRA-experiments.

Finally I would like to stress the importance of the QED interaction. If the weak forces are effective forces, one cannot escape the conclusion that the lepton and quark masses are either entirely or at least mostly of electromagnetic origin, reflecting the existence of a new fundamental mass scale of the order of 1 TeV. Some of the details of the new physics arising at 1 TeV can already be probed with a high energy electron-quark collider like the proposed HERA machine.

Finally I would like to thank Dr. Tran Thanh Van and his staff for organizing this Meeting in this wounderful part of the Haute Savoie and giving most of us the opportunity to do not only high energy physics, but also doing experiments in classical mechanics, using the gravitational interaction.

R E F E R E N C E S

1. L. Abbott and E. Farhi, Phys. Lett. 101 B (1981) 69,
H. Fritzsch and G. Mandelbaum, Phys. Lett. 102 B (1981) 319,
H. Harari and N. Seiberg, Phys. Lett. 98 B (1981) 269
R. Barbieri, A. Masiero and R.N. Mohapatra, Phys. Lett. 105 B (1981).
2. H. Fritzsch and G. Mandelbaum, Phys. Lett. 109 B (1982) 224;
H. Fritzsch, D. Schildknecht, and R. Kögerler, Phys. Lett. 114 B (1982) 157
3. O.W. Greenberg and J. Sucher, Phys. Lett. 99 B (1981) 339;
R. Casalbuoni and R. Gatto, Phys. Lett. 103 B (1981) 113
4. R. Barbieri et al., ref. (1).
5. P. Q. Hung and J.J. Sakurai,
Ann. Rev. Nucl. Sci. 31 (1981) 375;
E. de Groot and D. Schildknecht, Z.f. Phys. C 10 (1981) 55
P. Chen and J.J. Sakurai, Phys. Lett. 110 B (1982) 481
M. Kuroda and D. Schildknecht, Phys. Lett. 121 B (1983) 173.
6. J. D. Bjorken, Phys. Rev. D 19 (1979) 335.
7. U. Baur and H. Fritzsch, in preparation.
8. J. Gasser and H. Leutwyler, Physics Reports C 87 (1982) 77
9. H. Fritzsch, Proceedings of the Arctic School of Physics, Äkäslompolo, Finland (1982); MPI-PAE/PTh 75/82 (1982).



The self energy diagram which is supposed to be responsible for the generation of lepton and quark masses (i,j: lepton or quark state, n: intermediate state with mass of order 1 TeV).

SQUARKS CONTRIBUTIONS TO $p\text{-}\bar{p}$ COLLISIONS

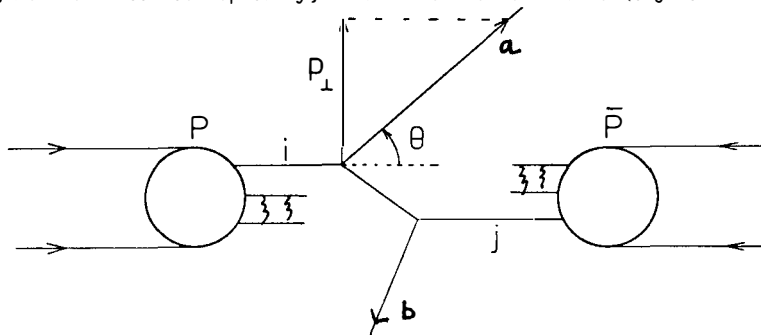
Laurent BAULIEU

Université Paris VI - LPTHE T.16 - 4, place Jussieu 75230 PARIS CEDEX 05

ABSTRACT

By extending the strong interaction theory from QCD to its simplest supersymmetric extension SQCD, the prediction for the cross section of two jets events in $p\text{-}\bar{p}$ collisions gets substantially larger. If the scalar partners of quarks have a mass of the order of magnitude of their experimental limit (~ 17 GeV) the cross section of 2-jet events with a transverse momentum of order 80-100 GeV gets multiplied by a factor 2.

$p-p$ high energy collisions are beautiful experiments for probing the parton model hypothesis. According to this model, in the center of mass frame, the proton and antiproton see each other as made of partons identified with elementary fields of the underlying asymptotically free strong interaction theory carrying all quantum numbers and propagating freely in the longitudinal direction. Two jet events with a large transverse momentum are predicted by this model in the lowest order approximation [1]. The scenario for their production is as follows. Two partons of proton and antiproton interact via a hard Born type process, yielding two other partons which may have a large scattering angle with respect to the beam axis while they carry out a substantial fraction of the total reaction energy \sqrt{s} . Then soft hadronizations dress both outgoing partons into hadronic jets with energy and angular dependences given by those of both partons. Obviously soft interactions also occur among all longitudinal spectator partons, and many hadrons with a small transverse momentum are expected to be produced, more or less isotropically, in addition to both hadronic jets.



Typically in the SPS $p-p$ collider where $\sqrt{s} = 540$ GeV, one observes two hadronic jets events with a transverse momentum $10 \lesssim p_{\perp} \lesssim 100$ GeV accompanied by a cloud of hadrons with a low p_{\perp} (few GeVs).

The parton model prediction for the cross section of the above process is as follows

$$\frac{d\sigma}{dp_{\perp} d\cos\theta} = \frac{2\pi}{s^{3/2}} \frac{1}{\sin^2\theta \tan\theta} \alpha_s^2 (p_{\perp}^2) \int_{x_{\min}}^1 \frac{dx_1}{x_1^2} \frac{dx_2}{x_2^2} x$$

$$x \sum_{i,j} \sum_{a,b} q_i^p \left(x_1, \bar{\alpha} (p_{\perp}^2) \right) |A_{ij}^{ab} (x_1, x_2)|^2 q_j^{\bar{p}} \left(x_2, \bar{\alpha} (p_{\perp}^2) \right) \quad (1)$$

with

$$x_2 = \frac{x_1 p_1 / \sqrt{s} \operatorname{tg} \frac{\theta}{2}}{x_1 - p_1 / \sqrt{s} \operatorname{cotg} \frac{\theta}{2}}$$

$$x_{\min} = \frac{p_1 / \sqrt{s} \operatorname{cotg} \frac{\theta}{2}}{1 - p_1 / \sqrt{s} \operatorname{tg} \frac{\theta}{2}} \quad \leq x_1 \leq 1 \quad (2)$$

i, j, a, b denote all possible parton types in the proton. $q_i(x_1, \bar{\alpha})$ and $q_j(x_2, \bar{\alpha})$ are the probabilities of finding the parton i and j respectively with longitudinal momentum $x_1 \frac{p_1}{\sqrt{s}}$ and $-x_2 \frac{p_1}{\sqrt{s}}$ in the proton and antiproton. These parton densities are to be extracted from an analysis of lepton hadron scattering deep inelastic structure functions and of their scaling violations. The A_{ij}^{ab} are the amplitudes for the parton processes $i + j \rightarrow a + b$ and are functions of p_1 , \sqrt{s} , x_1 , x_2 . In the lowest order approximation they can be computed from tree diagrams of the underlying asymptotically free strong interaction theory, the running coupling constant of which is $\bar{\alpha}(Q^2)$.

The phase space constraints in the integral (1) are model independent and reflect only the kinematics of a two bodies \rightarrow two bodies reaction. They are strongly dependent on the value of p_1 / \sqrt{s} , due to the presence of the factor x_1^{-2} in the integrand, and their consequence on the shape of the cross section has been beautifully verified when going from the p-p P.S. collider ($\sqrt{s} \sim 50$ GeV) to the p- \bar{p} SPS collider ($\sqrt{s} \sim 540$ GeV).

On the other hand, when going from QCD to a supersymmetric extension (SQCD), all factors in formula 1 (the parton densities, the A_{ij}^{ab} and $\bar{\alpha}$) are modified, and our purpose has been to compute the changes in the two jet cross section due to these modifications as a possible indication for the existence of supersymmetric particles.

The change due to parton densities is not expected to be quantitatively significant because the normalization of these quantities is kept fixed in any theory by sum rules expressing the fact that the partons carry all quantum numbers of the proton. Numerical analysis have indeed shown that one can fit as well deep inelastic data either with QCD or SQCD. Essentially, one gets redefinitions of parton densities according to the approximated formula

$$\begin{aligned} \left[q_{\text{Gluon}}(x, \bar{\alpha}) + q_{\text{Gluino}}(x, \bar{\alpha}) \right]_{\text{sQCD}} &\simeq A(\bar{\alpha}) \left[q_{\text{Gluon}}(x, \bar{\alpha}) \right]_{\text{QCD}} \\ \left[q_{\text{Quark}}(x, \bar{\alpha}) + q_{\text{Squark}}(x, \bar{\alpha}) \right]_{\text{sQCD}} &\simeq A'(\bar{\alpha}) \left[q_{\text{Quark}}(x, \bar{\alpha}) \right]_{\text{QCD}} \end{aligned} \quad (3-a)$$

where the normalization factors A, A' insure the conservation of energy momentum sum rules both in QCD and sQCD

$$A(\bar{\alpha}_s) = \frac{\left[q_{\text{Gluon}}^{(2)} + q_{\text{Gluino}}^{(2)} \right]_{\text{sQCD}}}{\left[q_{\text{Gluon}}^{(2)} \right]_{\text{QCD}}} \quad A'(\bar{\alpha}_s) = \frac{\left[q_{\text{Quark}}^{(2)} + q_{\text{Squark}}^{(2)} \right]_{\text{sQCD}}}{\left[q_{\text{Quark}}^{(2)} \right]_{\text{QCD}}} \quad (3-b)$$

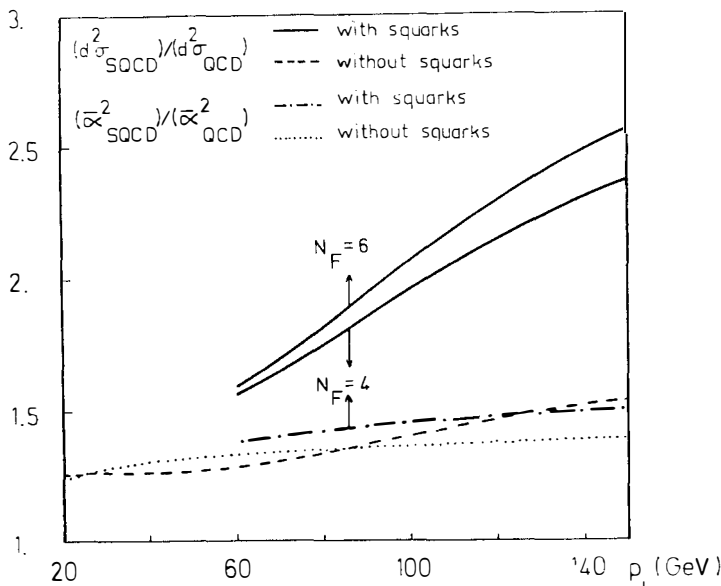
The change of the running coupling constant $\bar{\alpha}$ increases the cross section (1). Indeed, when going from QCD to SQCD, the theory becomes "less" asymptotically free, since new fermions (the gluinos) and scalars (the squarks) contribute positively to the β function, and the SQCD running coupling constant decreases slower than that of QCD.

The change of the A_{ij}^{ab} is also expected to increase the cross sections since new final states appear, for instance gluon + gluon \longrightarrow gluino + gluino, gluon + gluon \longrightarrow squark + anti-squark etc... Furthermore the p_\perp dependence of the cross section is expected to be different because of new Born diagrams. However the latter argument should be handled with care because if, effectively new squared amplitudes occur, new interference term also occur, sometimes with a negative sign, and the effect of the emergence of new thresholds can be small when going from QCD to SQCD. Then a full calculation is necessary.

In a previous communication [2], Delduc had shown that when squarks are neglected, supposing that they are too heavy, the effect of light gluinos is to increase the QCD cross section by a factor roughly independent of θ , and equal to $\alpha_{\text{sQCD}}^2 (p_1^2) / \alpha_{\text{QCD}}^2 (p_1^2)$. This factor is not very different from 1.

Here I present the result of our computation, done with Antoniadis and Delduc, when squarks are taken into account. We suppose that the squarks mass is the PETRA limit (~ 17 GeV) and, to be consistent, we only consider jets with

$p_T \gtrsim 34$ GeV. We have used parton densities satisfying eq.(3) and computed all necessary amplitudes A_{ij}^{ab} [3]. Putting everything together, we have obtained a significant enhancement factor when going from QCD to SQCD which is an increasing function of p_T , of order 2 when $p_T \approx 90$ GeV. This factor is still roughly independent of θ (except for small θ at the boundary of phase space), and the following figure displays its variation as a function of p_T . On this plot we also show the factor $\tilde{\alpha}_s^2 \text{SQCD}(p_T^2) / \tilde{\alpha}_s^2 \text{QCD}(p_T^2)$



One of us, Antoniadis in collaboration with Contogouris has done an analogous analysis for the production of a direct polarized photon (in $p\bar{p}$ collision) which is zero in massless QCD. If heavy quark masses are taken into consideration, a small polarization effect is present. It is however very small, because heavy quarks are all in the sea which is very much peaked at $x \sim 0$. If light gluinos are included in the analysis, the photon can have a polarization, but the effect is still small, of order 1 %. If squarks of 17 GeV are included in the analysis, then the polarization effect becomes much larger or order 10 %. This polarization effect comes from the presence of squarks among valence partons (then the squark density is not peaked towards $x \sim 0$) and from their large mass.

In conclusion, when going from QCD to SQCD the parton model predictions change in a significant way only when squarks are present. The effect of

introducing only light gluinos yield only minor modifications despite the naïve argument of color factors. The same conclusion has been also reached by Altarelli in his talk about the modification of virtual effects due to SUSY particles.

REFERENCES

- 1) D.I. Sivers, R. Blankenbecler and S.J. Brodsky, Phys. Rep. 23C (1976) 1.
S.D. Ellis and R. Stroynovski, Rev. Mod. Phys. 49 (1977) 753.
M. Jacob and P.V. Landshoff, Phys. Rep. 48 (1978) 285.
R. Stroynovski, QCD phenomenology of the Targe p_t processes, SLAC-PUB-2433
(1979).
- 2) F. Delduc, Annecy Meeting on SUSY at LAPP, LAPP TH-73 (preprint).
- 3) I. Antoniadis, L. Baulieu, F. Delduc, PAR LPTHE 83-10 preprint.
- 4) I. Antoniadis, A.P. Contogouris, in preparation.

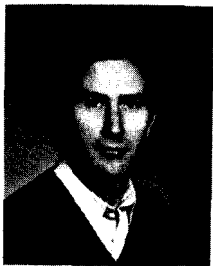
WEAK CORRECTIONS TO THE $e^+e^- \rightarrow \gamma\gamma, \gamma Z$ REACTIONS
by

M. CÀPDEQUI PEYRANERE

Y. LOUBATIERES

M. TALON

Laboratoire de Physique Mathématique
U.S.T.L. - Place E. Bataillon
34060 Montpellier Cedex
France



Abstract

The exact calculation of the fourth order weak corrections to these two reactions is performed in the Glashow-Weinberg-Salam pattern, using dimensional regularisation and Feynman parameters methods. It requires the electric charge "e" and the Weinberg angle θ_w renormalisation. We found corrections of 1% order in both cases.⁽¹⁾

I - INTRODUCTION

In a previous paper⁽²⁾, we concluded that the $e^+ e^- \rightarrow \gamma\gamma$ reaction is a good and clean place for testing the electro-weak standard model. In this calculation we used unitary gauge, followed by a dispersive evaluation of Feynman integrals. Here we use the 't Hooft gauge and the normalisation conventions introduced in Passarino-Veltman⁽³⁾ to perform the fourth order weak corrections of $e^+ e^- \rightarrow \gamma\gamma$ and $e^+ e^- \rightarrow \gamma Z$ reactions.

We find that the result is very sensitive to the electron beam polarizations = maximal for left polarized electrons and minimal for right polarized electrons. More important terms are diagrams with charged gauge boson w^\pm and coupling $W - e - \nu$ is left.

This provides us with a good characterization of weak corrections since strong and electromagnetic ones do not make the difference between left and right electrons.

$e^+ e^- \rightarrow \gamma\gamma$ process has been performed for polarized beams. But $e^+ e^- \gamma Z$ reaction, because of more technical difficulties, has been performed with mean on electron helicities. That explains the difference between $e^+ e^- \rightarrow \gamma\gamma$ and $e^+ e^- \rightarrow \gamma Z$ results.

II - DIAGRAMS

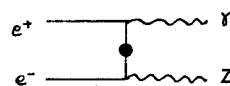
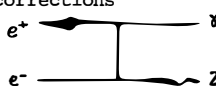
All particles are on-shell and we neglect electron mass. We list diagrams for $e^+ e^- \rightarrow \gamma Z$ process and indicate when there is not a corresponding diagram for $e^+ e^- \rightarrow \gamma\gamma$ process.

1) Born term:

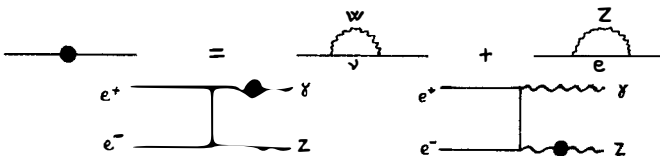


+ Bose symmetric

2) Weak corrections

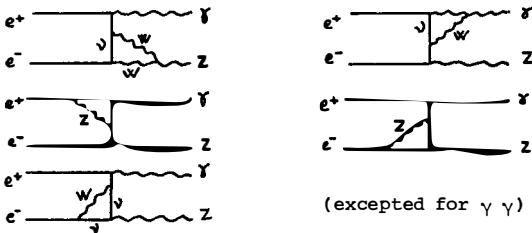


with

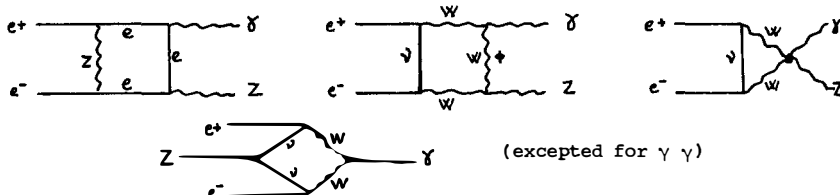


(excepted for $\gamma\gamma$)

where the bubble on photon line is photon self-energy and $Z - \gamma$ transition. The photon self-energy contains 7 loops and $Z - \gamma$ transition contains the same diagrams (with other couplings). The same things hold for the bubble on the Z line but the Z boson self-energy contains 12 loops, three of them depending on the physical Higgs (unknown mass).



All diagrams mentioned above are divergent.



These four diagrams are very difficult to compute but they converge.

III - RENORMALIZATION

Absorption of divergences needs electrical charge "e" and Weinberg angle " θ_w " renormalization.⁽⁴⁾

$e^+ e^- \gamma$ corrections lead to a shift δe of electrical charge with

$$\frac{\delta e^2}{e^2} = \frac{e^2}{16\pi^2} \left\{ 7 (\Delta - \log M_w^2) - \frac{4}{3} (\Delta - \log m_e^2) \right\}$$

where $\Delta = -\frac{2}{n-4} + \gamma - \log \pi$ (γ = Euler constant)

Absorption of divergences induced by $e^+ e^- Z$ corrections is more difficult because it needs a shift $\delta (\sin^2 \theta_w)$ and of precedent δe . We obtain ($s^2 = \sin^2 \theta_w$)

$$\frac{\delta s^2}{s^2} = \left(\frac{\delta s^2}{s^2} \right)_\infty + \left(\frac{\delta s^2}{s^2} \right)_{\text{finite}}$$

with $\left(\frac{\delta s^2}{s^2} \right)_\infty = \frac{-e^2}{16\pi^2 s^2} \left\{ (\Delta - \log M_w^2) \left(\frac{1}{6} + 7c^2 \right) - \left(\frac{1 - 4s^2}{3} \right) (\Delta - \log m_e^2) \right\}$

and $\left(\frac{\delta s^2}{s^2} \right)_{\text{finite}} = -0.012$ in agreement with Marciano and Sirlin⁽⁵⁾ result

and with SU (5) theory which predicates a decrease of $\sin^2 \theta_w$ when energy increases.

IV - RESULTS AND CONCLUSION

Correction percentages of cross section are 1,2 at $\sqrt{s} = 160$ GeV for $e^+e^- \rightarrow \gamma\gamma$ process (for left polarized beams) and 0,6% at $\sqrt{s} = 100$ GeV for $e^+e^- \rightarrow \gamma Z$ process. So $e^+e^- \rightarrow \gamma\gamma$ is the better process to test weak radiative corrections to the Weinberg-Salam model. Nevertheless a such experiment needs polarized beams.

REFERENCES

1. M. Capdequi Peyranère, Y. Loubatières, M. Talon, to be published.
2. M. Capdequi Peyranère et al., Nuclear Phys. B149, 243 (1979)
3. G. Passarino, M. Veltman, Nucl. Phys. B160, 151 (1979)
4. F. Antonelli et al., Nucl. Phys. B183, 195 (1981)
5. W. Marciano, A. Sirlin, Nucl. Phys. B189, 442 (1981)

MONOPOLES FOR ASTROPHYSICISTS

Curtis G. Callan, Jr.
Joseph Henry Laboratories
Princeton University
Princeton, New Jersey 08544

Magnetic Monopoles in Particle Physics

Almost exactly fifty years ago, Dirac discovered that point magnetic charges were consistent with the requirements of quantum mechanics provided that the quantum, g , of magnetic charge and the quantum, e , of electric charge satisfied the condition $eg=(n+1/2)$. Although Dirac's argument showed that monopoles were permitted, it in no way showed that they were required to exist and gave no hint as to how heavy a monopole should be.

About ten years ago, developments in quantum field theory made it possible to understand the strong interactions and the weak/electromagnetic interactions as non-abelian quantum gauge field theories. It also became reasonable to speculate that these separate gauge theories actually melted into one unifying gauge theory at very high energies or very short distances. The expected "unification scale" was not tied down precisely, but all arguments suggested that it should be somewhere in the vicinity of 10^{14} time the mass of the proton.

Physics at the unification scale is very different from the physics we are familiar with. As nearly everybody has heard, baryon number is not expected to be conserved at this level, so that the free nucleon should have a very small, but very finite, decay rate. Another strange feature is that the theory has solitons (stable finite-energy solutions of the classical field equations) whose existence, size and mass are determined by unification-scale physics and whose external properties are those of the Dirac magnetic monopole. The mass turns out to be $1/\alpha$ times the unification scale or 10^{16} times the proton mass!

In other words, unified gauge field theories complete Dirac's argument by giving us a physical framework in which monopoles are required and in which their properties can be computed. Astrophysical concerns enter immediately because, since the monopoles are so incredibly massive, they could have been produced only in the very earliest moments of the Big Bang. The observation of superheavy magnetic monopoles would simultaneously give evidence for grand unification and the Big Bang and would be of the greatest interest to both particle physicists and astrophysicists.

A new element has recently entered the picture with the theoretical discovery that a baryon has a strong cross-section (in the neighborhood of 10^{-26} square centimeters) to undergo baryon decay in the course of a collision with a monopole. This is about thirty orders of magnitude larger than naive estimates would have suggested! This remarkable synergism of the two characteristic features of unified gauge theories (monopoles and proton decay) has important consequences for monopole astrophysics which are just beginning to be worked out.

My aim in this talk is to give an audience of astrophysicists a general introduction to this set of topics. I will try to explain the theoretical background of the magnetic monopole, first at the level of Dirac's original argument and then at the level of modern unified gauge theories. This means that I will have to give an explanation, necessarily oversimplified, of how spontaneously broken gauge theories work and why they support magnetic monopoles. I aim to give enough detail so that the phenomenon of monopole catalysis of baryon decay can be given an intelligible, if qualitative, explanation. I will give a brief introduction to the astrophysical consequences of this new aspect of monopole physics, but will not discuss "conventional" monopole astrophysics in any detail, since that topic should be well-known to this audience.

This talk is too general for me to give an adequate set of references to all the topics discussed here. The reader looking for more details on general aspects of monopole physics could not do better than to consult ref. 1. The original papers on monopole catalysis, refs. 2 and 3, are probably too cryptic to be helpful to any reader of this article. The conference talk cited in ref. 4 might be more accessible.

Monopole Kinematics

Dirac's argument for the consistency of monopoles with quantum mechanics is very simple but very profound. A point monopole of magnetic charge, g , located at the origin of polar coordinates has field strength

$$\vec{B} = \hat{g}\hat{r}/r^2$$

In a particularly convenient gauge, the vector potential associated with this field strength is

$$\vec{A} = g(1+\cos\theta) \hat{r}/r\sin\theta$$

Although the magnetic field is singular only at $r=0$, the location of the point monopole, the vector potential is singular along the entire line $\theta=0$. This "string" singularity is a gauge artifact: it can be moved around by making gauge transformations, although it always starts at the monopole and

runs to infinity. It would be of no concern if physics could be formulated entirely in terms of the magnetic field. Unfortunately, the quantum mechanics of charged particles is formulated directly in terms of the vector potential and disaster will strike unless some way is found to make the string singularity invisible.

Consider the effect on the wave function of a particle of charge, e , of making a slow circuit around a very small path surrounding the string. In general the effect of carrying the particle around a closed path in the presence of a vector potential is

$$\psi \rightarrow \psi \exp(ieg\bar{dx} \cdot \bar{A})$$

Evaluating the line integral for a path around the string singularity of the monopole, we find that

$$\psi \rightarrow \psi \exp(i4\pi eg)$$

The condition for an invisible string is that the wave function should be unchanged after this circuit, or that

$$eg=n/2 \quad n=\dots, -1, 0, 1, 2, \dots$$

A careful investigation shows that, as long as this quantization condition on the magnetic charge is met, the quantum mechanics of charged particles moving in the fields of such monopoles is fully consistent.

If an experimentalist is to search for a monopole, he would like to know not only its charge, but also its mass. Here there is a small difficulty. One of Maxwell's equations asserts that the divergence of the magnetic field vanishes,

$$\vec{\nabla} \cdot \vec{B} = 0,$$

so that, with the possible exception of isolated points, there is no magnetic charge. In other words, according to Maxwell, the charge of a magnetic monopole must truly be located at a point and its electromagnetic mass must be divergent.

Now the electron is thought to be a point particle also and we have learned from renormalization theory that the divergence of its electromagnetic mass means, not that there is anything wrong with the physics of the point electron, but simply that its physical mass is a free parameter. If Maxwell's equations are valid down to arbitrarily short distances, we cannot predict the mass of the monopole. If the monopole mass is to be predictable, there has to be a short distance scale below which standard electromagnetism is modified and the question "what's inside the monopole?" must have a meaningful answer.

One significant extension is required to bring Dirac's argument up to date. We now know that electromagnetism is not the only unbroken gauge theory. There is also the SU3 "color" gauge theory responsible for the strong interactions and we must consider the possibility of color magnetic charge for the monopole. It turns out that, although the most plausible monopoles will have both ordinary and color magnetic charges, the allowed values of ordinary magnetic charge will still be the same as those identified by Dirac's original argument.

As has frequently been explained in the context of hadron physics, quantum phenomena are responsible for very peculiar long-range behavior of color fields. In particular, it is expected that color magnetic fields are screened by vacuum fluctuations at distance scales of order one fermi (the typical strong interaction scale). This means that at truly long distances, the monopole will show only ordinary electromagnetic effects and will be indistinguishable from Dirac's monopole, whereas, if it is examined at scales of a fermi or smaller it will have a more complicated structure with two types of magnetic charge. This more elaborate structure makes the interactions of the monopole with ordinary matter at ordinary energies a much richer subject than Dirac would have anticipated.

Interaction With Matter

The question of how the monopole interacts with matter is at the heart of the interesting recent developments in monopole physics. In the first instance, of course, the monopole possesses a very strong long-range magnetic field which can be detected either by its ionization of nearby matter or by its induction of currents in superconducting loops. More subtle monopole-matter interaction effects can be seen by solving the Dirac equation for the motion of a fundamental spin one-half particle (lepton or quark) in the background field of a monopole. Let us therefore study the Dirac equation for an electron (for simplicity temporarily taken to be massless) moving in the field of a standard Dirac monopole.

The conserved angular momentum of this system is

$$\vec{J} = \vec{L} + \vec{S} + e\vec{gr}$$

where \vec{L} and \vec{S} have their usual meaning, e and g are the charges of the electron and monopole respectively, and r is the unit vector pointing from the monopole to the electron. The $e\vec{gr}$ term is a special feature of the monopole system and can be thought of as arising from the need to rotate the string along with everything else. For most monopoles of physical interest, g takes on the value of $1/2$ and the total angular momentum takes on integer

values starting at 0. We will do a partial-wave decomposition with respect to total angular momentum and will concentrate on the s-wave ($J=0$) state, since it leads to the strongest interaction between the electron and the monopole center.

Along with angular momentum, helicity or γ_5 is also conserved since we are neglecting electron mass. The solutions to the s-wave Dirac equation for positive energy E and for the two values of helicity are easily written out explicitly:

$$\psi_E^{\pm} = \frac{e^{\pm iEr}}{r} \begin{pmatrix} n \\ \pm \eta \end{pmatrix}$$

where $n(\theta, \phi)$ is a special two-component spinor ensuring that the Dirac spinor has $J=0$. If we try to construct time-dependent wave packet solutions out of these energy eigenstates, we quickly see that the helicity + states can only make ingoing waves while the helicity - states can only make outgoing waves! The ingoing waves can only be swallowed with 100% efficiency by the monopole center -- there is no way, consistent with the conservation laws built into the Dirac equation, for the ingoing positive helicity s-waves to be reflected back out!

The situation looks like, and is, a problem for conservation of probability. What's happening is that the interaction between the inverse-square-law magnetic field of the monopole and the magnetic moment of the electron leads to such a singular attractive potential that the flux of electron probability into the point center of the monopole is finite, no matter what the electron's energy. The Dirac picture of the monopole treats the center as an undifferentiated singular point about which it is not necessary to ask questions. This is apparently not good enough: low-energy fermions apparently do "get inside" the monopole, and we cannot obtain a complete picture of the monopole-electron interaction without a detailed picture of "what's inside".

Broken Gauge Theories

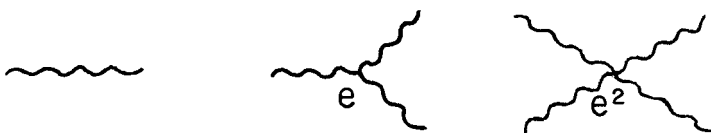
The key to understanding the internal structure of magnetic monopoles is provided by spontaneously broken non-abelian gauge theory. This class of field theory is the foundation of the current understanding of the strong, weak and electromagnetic interactions, individually as well as in their relations to one another. In the limited time available to me I cannot hope to explain their workings in any detail, but there are some essential facts that I must get across if I am to proceed with an explanation of magnetic monopole physics. I will assume that the audience has a limited degree of

familiarity with conventional quantum electrodynamics and of Feynman diagrams, at least as a pictorial rendition of the qualitative content of perturbation theory. What follows might convey some useful information even to those readers who do not feel themselves up to this specification.

Non-abelian gauge theories are a generalization of ordinary electromagnetism in which the gauge invariance is based on a general Lie group. Remember that is based on the abelian gauge group, $U1$, having one generator. There are as many gauge bosons (spin-one particles, generalizations of the photon) as G has generators. These particles not only transmit the forces between charges, but in general are themselves charged so that gauge bosons can exert forces on gauge bosons. The Lagrangian which describes all this for a theory in which there are N gauge bosons is

$$L = \frac{1}{4} \sum_{a=1}^N \sum_{\mu, \nu} (\partial_\mu A_\nu^a - \partial_\nu A_\mu^a + e f_{abc} A_\mu^b A_\nu^c)^2$$

where A_μ^a are the vector potentials for the N gauge bosons, f_{abc} are the structure constants of the Lie group and e is the gauge coupling constant. The quadratic terms describe the free propagation of the gauge bosons (identical to ordinary electromagnetism), while the cubic and quartic terms describe the point interaction of three and four gauge bosons. The Feynman diagrams corresponding to these three possibilities are shown in the accompanying diagram. Because of the gauge boson self-interactions, the pure gauge theory is already very non-trivial (indeed, if $G=SU(3)$, it describes the strong interactions.)



In any interesting theory, there are charged spin 1/2 particles which interact with each other through the gauge bosons. In electromagnetism these would be the electrons, but in general they would be some set of quarks and leptons. In a gauge theory based on a group G , the spin 1/2 particles must fill out representations of G . Their interactions with the gauge bosons is governed by a typical Dirac Lagrangian

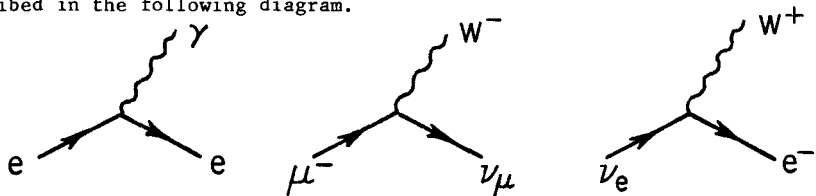
$$L = \sum_f \bar{\psi}_f (i \gamma^\mu \partial_\mu - m + ie \gamma^\mu A_\mu^a t_a) \psi_f$$

in which the index f runs over all the independent group representations which occur and the t_a are the corresponding matrix representations of the group generators: it is as if the charges of the spin 1/2 particles were

specified by matrices rather than simple numbers. This Lagrangian contains terms describing free propagation of the spin-1/2 particles as well as the emission of absorption of gauge bosons by them. The Feynman diagrams for these two possibilities are shown in the accompanying diagram

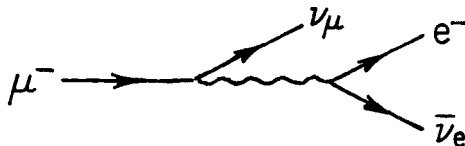


The minimal set of gauge bosons we need to describe something resembling the electroweak interactions is the triplet W^0 (same as photon) and W^\pm . Let us discuss the interaction of the leptons (electron, muon and their associated neutrinos) with these gauge bosons. The charged lepton interacts with the photon just as in quantum electrodynamics, while the interaction of a lepton with W^\pm clearly introduces something new in such an event the lepton's charge and particle type must change. The various possibilities are described in the following diagram.



The vertex in which the electron emits a photon contains a factor of e , the usual electromagnetic coupling constant. Since the W^\pm are symmetry partners of the photon, the vertex in which, say, the μ turns into a neutrino while emitting a W is governed by the same coupling strength.

The archetypical weak interaction is the decay of the muon. By putting together interaction vertices of the type just displayed we can easily produce a graph (shown in the following diagram)



for the muon to decay into an electron and two neutrinos (its standard decay mode). The key question is whether this diagram reproduces the actual (very slow) decay rate of the muon despite the fact that all the vertices have

coupling strengths typical of the electromagnetic interactions! Here the question of the mass of the gauge bosons arises in an essential way.

The photon, as everybody knows, is massless and we might be tempted, because of the symmetry between the photon and the W , to assign zero mass to the W bosons. A little experience with Feynman diagrams shows that the decay rate associated with the diagram just displayed is inversely proportional to the fourth power of the W mass. Zero mass for the W would give zero lifetime for the W ! It turns out that the correct answer for the muon lifetime (and all other questions we might pose about its decay) is given if we take the mass of the W to be about 100 times the mass of the proton. This choice of different masses for the gauge bosons clearly "breaks" the underlying gauge symmetry, but seems to be essential for a correct understanding of the phenomenology of the weak and electromagnetic interactions.

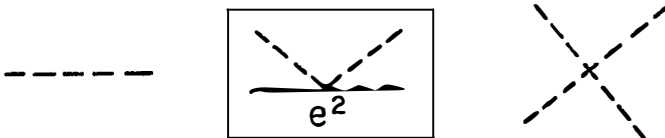
Broken Gauge Symmetry

I shall now try to explain in some detail how "broken gauge symmetry" works since it turns out to be the key to understanding not only how weak and electromagnetic interactions fit together, but also how the strong interactions fit in with them as well and how magnetic monopoles naturally arise. This is a difficult subject and you will have to allow me more than the usual amount of poetic license.

Our aim now is to "hide" the underlying gauge symmetry by giving the gauge bosons different masses. In all concrete realizations of such a scheme this is done by letting the gauge bosons interact with a new type of charged spin-0 matter called the Higgs boson. The most general Lagrangian describing the Higgs' interaction with themselves and the gauge bosons can be written as follows:

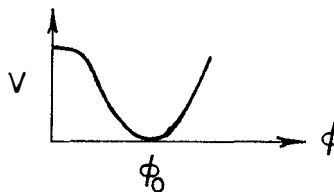
$$L = \sum_{\mu} |(\partial_{\mu}\phi - ie A_{\mu}^a t_a \phi)|^2 - V(\phi)$$

In this expression, the matrix t_a is the group generator in the representation filled out by the Higgs bosons, $V(\phi)$ is a function describing the Higgs boson self-interaction and A_{μ}^a is the gauge boson field. The special way in which the gauge boson field enters the kinetic energy term is dictated by gauge invariance. This Lagrangian describes free propagation of the Higgs boson, its interaction with the gauge boson and its self-interaction. Typical diagrams for all of these processes are displayed in the following figure



The graph in which the Higgs boson interacts with two gauge bosons is boxed to indicate that it will shortly play a special role.

The potential function $V(\phi)$ plays a crucial role in determining the physics of this theory. The field ϕ fills out some representation of the gauge group and therefore cannot be thought of as a single field: it is more like a multi-component vector. Although one cannot talk in a representation-independent (or gauge-invariant) way about the components of a vector, the length of the vector is a perfectly good invariant concept. Suppose, for instance that, as a function of the length of the ϕ vector, the potential function has the form shown in the following figure:



The lowest energy state (or vacuum) of this system will correspond to the point where the length of the Higgs vector takes on the value ϕ_0 , not 0. This "non-zero vacuum expectation value" of the Higgs field is responsible for a number of interesting effects known in the literature as "spontaneous breaking" of the gauge symmetry.

If we go back to the Lagrangian describing the Higgs gauge-boson interaction we see that, if the Higgs field takes on a uniform background value ϕ_0 , the Lagrangian reduces to something which is quadratic in the gauge field and equivalent to a mass term for the gauge field. Alternatively, the boxed interaction diagram shows the gauge field propagating in a constant background field, a circumstance which is equivalent to giving the gauge boson a mass. A careful study of the nature of this effective mass term shows that it is quite easy to arrange things so that the neutral gauge boson (the photon) is unaffected by this phenomenon and continues to have zero mass while the charged boson W^\pm acquire a mass $e\phi_0$. If we adjust the "vacuum expectation value" of ϕ to be about 250 times the mass of the proton, we reproduce the mass of the W which is needed to match the phenomenology of electro-weak physics. Note that much of the physics is built into the choice of $V(\phi)$. We could perfectly well have chosen it such that the minimum energy came at $\phi=0$, in which case all of the gauge bosons would have had zero mass and the symmetry would have been unbroken. Although this does not correspond to the real world, it is perfectly internally consistent.

It is important to note that once we have adopted this sort of scheme, the physics we see is dependent on the distance scale we probe. If we probe distances large compared to the Compton wavelength of the W (energies small compared to 100 proton masses), the W is invisible, we see only the photon and the underlying non-Abelian gauge symmetry is hidden. If we probe distances small compared to this scale, then the W bosons come into play on essentially the same footing as the photon and the underlying gauge symmetry becomes visible. This notion of hidden symmetry which can be revealed by looking at sufficiently short distances is crucial to many developments in particle physics. The recent experimental discovery of the W-meson at precisely the expected mass is strong confirmation that this symmetry breaking mechanism really plays a role in physics.

It is even possible to include the strong interactions in this framework in a scheme known as "grand unification". The strong interactions are described by an unbroken non-abelian gauge theory based on the gauge group SU(3). This means among other things that the strong forces are due to the exchanges of eight massless, self-interacting gauge bosons. The basic idea of grand unification is that the world is really described by a large non-abelian gauge group with more gauge bosons than those we can directly see in the strong and electroweak forces but that this larger symmetry is spontaneously broken at extremely short distances by the same sort of mechanism as breaks the electroweak gauge symmetry. This means that all of the "extra" gauge bosons (those not directly involved in strong and electroweak forces) acquire a very large mass (the Compton wavelength of the heavy bosons is essentially the same thing as the distance scale of the spontaneous symmetry breaking).

Several independent arguments suggest that the energy scale of this new level of spontaneous symmetry breaking must be about 10^{14} times the mass of the proton! Furthermore, it is extremely plausible that processes mediated by the exchange of the new gauge bosons conserve neither baryon number nor lepton number so that processes which involve the heavy gauge bosons in any way would most likely manifest baryon-number non-conservation. A typical such effect would be the spontaneous decay of the free proton. The other side of the coin is that since the typical energy scale for the dynamics of the proton is so small compared to the mass of the heavy gauge bosons, baryon number violating effects are heavily suppressed (the expected lifetime of the proton due to this sort of phenomenon is longer than 10^{30} years).

Gauge Theory Monopoles

Now that the general picture of the physics of spontaneously broken gauge theories has been laid out, it is possible to explain, at a very qualitative level, how these theories naturally support magnetic monopoles and to give an account of their mass, size and other properties.

As we explained in an earlier section, the magnetic monopole discussed by Dirac is necessarily a singular object because one of the Maxwell equations asserts that the magnetic field is everywhere divergenceless.

$$\vec{\nabla} \cdot \vec{B}^Y = 0$$

This forces the monopole magnetic field to grow like r^{-2} at arbitrarily small distances from the monopole center and leads to a divergent monopole mass. In non-abelian theories, the magnetic field obeys a subtly different divergence equation which permits an escape from this trap.

For simplicity, consider the electroweak gauge theory containing as gauge fields the massless photon and the heavy W^\pm . This time, it is not the ordinary divergence, but the gauge-covariant divergence of the magnetic field which must vanish. The explicit equation to be satisfied by the photon magnetic field is

$$\vec{D} \cdot \vec{B}^Y = \vec{\nabla} \cdot \vec{B}^Y + ie \vec{A}^+ \cdot \vec{B}^- - ie \vec{A}^- \cdot \vec{B}^+$$

This can be rearranged in the form

$$\vec{\nabla} \cdot \vec{B}^Y = \rho$$

where ρ is a source term built entirely out of the heavy, charged gauge fields:

$$\rho = ie (\vec{A}^+ \cdot \vec{B}^- - \vec{A}^- \cdot \vec{B}^+)$$

It is physically perfectly possible for this source term to have a static, non-zero value in a region of size equal to the Compton wavelength of the heavy gauge fields out of which it is built. This means that we can construct a non-Abelian gauge field configuration which has the long range ordinary fields of a Dirac monopole but has the source of these fields spread out over a region of size equal to the Compton wavelength of the heavy gauge fields. Once the source region is of finite size rather than a point, the mass and other physical properties of the monopole are perfectly well-defined and finite. On top of that, the question "what's inside the monopole" which arose in our discussion of the scattering of spin one-half particles from the monopole now has a precise and definite answer.

For technical reasons, the possibility just described does not actually work within the context of the purely electroweak gauge theory. It does,

however, work within the context of the grand unified gauge theories which unite the strong and electroweak interactions. The heavy gauge bosons which set the size of the monopole source region (or core) are therefore the objects mentioned in the last section which are 10^{14} times more massive than the proton. The size of the monopole core is therefore some 10^{-14} times smaller than the proton and, as far as interactions with other particles at typical accelerator energies are concerned, the monopole would behave like a point particle. The core turns out to have both ordinary and color magnetic charge and exerts strong and electromagnetic forces on particles at a distance from it. The tiny core region is constructed out of the superheavy gauge bosons whose interactions are likely to violate conservation of baryon number.

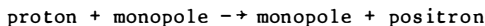
Since the mass of a monopole constructed in this way is largely electromagnetic, it is a simple "Coulomb energy" exercise to calculate the mass of a unit of magnetic charge confined to a region of this size. The answer turns out to be of order 10^{16} times the mass of the photon! Although this is finite, it is far too large for monopoles to be produced in any event which can occur in the current universe. They could only have been produced in the earliest instants of the Big-Bang and could only be seen today as a relic radiation in the cosmic ray flux. It is beyond our power to make reliable estimates of what the current monopole flux should be since the correct answer depends on physics and cosmology in energy domains about which we know almost nothing. Indeed, the mere knowledge that superheavy monopoles existed would be a valuable window into an otherwise inaccessible domain of physics. Hence the current interest in magnetic monopoles on the part of particle physicists.

Proton Decay Catalysis

The previous discussion implies that the mere existence of superheavy monopoles is evidence for the occurrence of new physics in the domain of supershort distances. In fact, it turns out that if we had a monopole to play with, we could learn a great deal about the details of the supershort distance physics by studying the interactions of the monopole with ordinary matter. That this is so is quite surprising. Because the core is so incredibly small, one is inclined to think that the rate of interaction of ordinary matter with the core itself would be negligibly small and that we could only hope to see the conventional interaction of matter with the long range color and electromagnetic fields of the monopole.

However, as was explained earlier in this talk, there is something special about the interaction of spin one-half particles with the monopoles in their lowest angular momentum partial wave state, they are "sucked into" the monopole center with unit probability, no matter what their energy. This means that they interact directly with the heavy gauge bosons of the core before they are "spit out" again. If the interactions of these bosons are, as expected, baryon number violating, then the overall interaction of even low-energy spin one-half particles with the monopole will not conserve baryon number!

A detailed discussion of this class of phenomena is rather complicated: one has to start with the fundamental spin one-half particles (quarks and leptons), straighten out their direct interaction with the monopole core and then deal with the hard problem of binding the quarks into the observed hadrons. Although this cannot yet be done in anything like complete quantitative detail, the outline of the answer is clear. Reactions like



etc. have cross-sections at low energies typical of the strong interactions (i.e. of order a few millibarns). This general class of process might be called "monopole catalysis of baryon decay" since the net effect is to destroy a proton while leaving the monopole unscathed and ready to do the same thing again. Since the catalysis cross-section is large and the reaction very exothermic, one might expect the occurrence of such reactions to have interesting experimental and astrophysical consequences.

I will give a brief outline of those consequences as they are now understood. As you all know, the direct test of the notion that baryon number is violated at extremely short distances consists of a search for spontaneous decay of the free proton. Since the expected lifetime is very long, it is necessary to observe a large volume of material under conditions of extremely low and well-understood background. The typical apparatus is a many-cubic-meter volume of scintillator buried deep underground and surrounded by detection devices capable of seeing the decay of a single proton inside it. If the proton decay catalysis cross-section is of strong interaction magnitude then this sort of device will also see, with unit probability, the induced proton decay produced by the passage of a single monopole. In this way, proton decay experiments are providing us with information on the monopole flux at the same time as the proton lifetime.

Another fascinating point is that because the monopole catalysis reaction is exothermic, the presence of monopoles in the dense core of stars would increase their energy output. In the case of neutron stars the effect is so strong that the non-observation of x-ray neutron stars puts a very stringent upper limit on the galactic flux of monopoles (several orders of magnitude stronger than the Parker bound, which is based on the persistence of the galactic magnetic field).⁵

Taken together these two types of argument put us in a very uncomfortable bind. The occurrence of proton decay at the rates suggested by grand unification and the presence of monopoles in the galaxy in large enough numbers to be detectable seem to be mutually exclusive possibilities! How this will all turn out is not at all clear -- our understanding of all the questions discussed in this talk is still developing and there might be further surprises in store for us.

For the particle physicist, the remarkable thing about the monopole is that, without yet having deigned to put in an appearance in the real world, it has been implicated in an important way in most of the successive improvements in our understanding of the particle world and continues to entertain us with theoretical surprises. Perhaps some of these surprises will suggest astrophysical ways and means of finally tracking down this elusive particle or of finallling ruling it out of our universe altogether.

References

1. S. Coleman, "The Magnetic Monopole Fifty Years Later," Proceedings of the 1981 International School of Subnuclear Physics, "Ettore Majorana".
2. V. Rubakov, ZhETF Pis'ma 33, 658 (1981), Nucl. Phys. B203, 311 (1982).
3. C. Callan, Phys. Rev. D25, 2141 (1982), Phys. Rev. D26, 2058 (1982), Nucl. Phys. B204, 391 (1982).
4. C. Callan, "The Proton Decay Magnetic-Monopole Connection," in "Particles and Fields - 1982," W. Caswell and G. Snow eds., American Institute of Physics, New York, 1983.
5. E. Kolb, S. Colgate and J. Harvey, Phys. Rev. Lett. 49, 1373 (1982); S. Dimopoulos, J. Preskill and F. Wilczek, Phys. Lett. B (1982).

THE SEARCH FOR MAGNETIC MONOPOLES *

Barry C. Barish
California Institute of Technology
Pasadena, California 91125



Abstract: In this review, I discuss the status and prospects for experimental studies aimed at the detection of Grand Unified Monopoles. The only positive evidence, at this time, remains the one observed candidate of Cabrera.¹⁾ The relations of this observation to the expected abundance in cosmic rays and to limits from other detection techniques are discussed. Lastly, prospects for future studies with sensitivity to much smaller fluxes are also presented.

I. INTRODUCTION:

Physicists have long been interested in the existence (or non-existence) of magnetic monopoles. The early historical interest in monopoles was due to the symmetry between Electric and Magnetic fields in Maxwell's equations. However, due to the lack of abundance of free magnetic charges compared to electric charges they were not included in the final formulation of those equations.

In 1931, Dirac showed that the existence of free magnetic charges (Dirac monopole) could provide reason for quantization of electric charge ($n\hbar/e$).^{2,3} This work motivated renewed interest in searching for monopoles.

Although there was no guidance as to the mass, size, etc. of these monopoles, several experimental consequences were apparent. First, these monopoles, which were quantized to $137/2$ electric charge would produce a great deal of ionization passing through matter. It was assumed that the monopole mass would not be very different from other elementary particles (e.g. protons) and would be highly relativistic. A second possibility, that could result from such high ionization is that these monopoles could come to rest in matter and might be abundant in certain forms (e.g. sediment, moon rocks, etc.). Finally, if monopoles were this light they might be directly produced in accelerators.

All these effects were extensively looked for, with the final results being that there was no evidence for Dirac Monopoles. Earlier indications of possible evidence⁴⁾ proved incorrect.

More recently, 't Hooft and Polyakov^{5,6)} showed that monopoles exist as solutions in many non-Abelian Gauge Theories. The possibility of these GUT monopoles provided stimulus for much recent theoretical and experimental interest in the subject. The fact that Grand Unified Monopoles are extremely heavy ($M \sim 10^{16}$ GeV) makes most previous searches irrelevant. The fluxes in cosmic rays are expected to be extremely small, and experimental techniques required for detection are different.

These GUT monopoles are so massive that they will necessarily be slow ($\beta \approx 10^{-3}$) if they are galactic in origin. At this low β a monopole has great penetrating power and easily passes through the earth. This means that both previous searches using ionization losses for direct detection or searched for monopoles trapped in matter would be insensitive.

II. INDUCTION EXPERIMENTS:

The most straightforward technique to search for GUT monopoles is by the electromagnetic induction from passage of a magnetic monopole through a closed conducting loop. This technique was first used to search for the presence of

magnetic monopoles in various materials.^{7,8)} This idea has been extended to the case of free GUT magnetic monopoles by Cabrera,⁹⁾ who applied the combination of a SQUID (Superconducting Quantum Interferometer Device), and a very well magnetically shielded loop to reach the needed sensitivity to detect the passage of a single magnetic monopole.

This technique is ideal, since it is based solely on long range electromagnetic interaction between the magnetic charge and the macroscopic quantum state in a superconducting ring. The method is independent of the monopole mass, velocity, electric charge, etc.

A schematic view of this detection method is shown in Fig. 1. From Maxwell's equation,

$$\nabla \times \vec{E} + \frac{1}{c} \frac{\partial \vec{B}}{\partial t} = - \left(\frac{4\pi}{c} \right) \vec{j}_m ,$$

integrate over the plane of the ring, obtaining

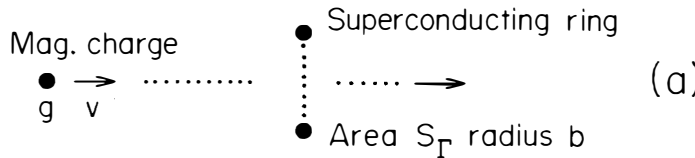
$$\oint_{\Gamma} \vec{E} \cdot d\vec{l} + \frac{1}{c} \frac{\partial \phi}{\partial t} = - \frac{4\pi g}{c} \delta(t) .$$

E vanishes along the path Γ , therefore,

$$\phi(t) = -4\pi g \theta(t)$$

$$= \phi_g + \phi_s .$$

Technique



Detection

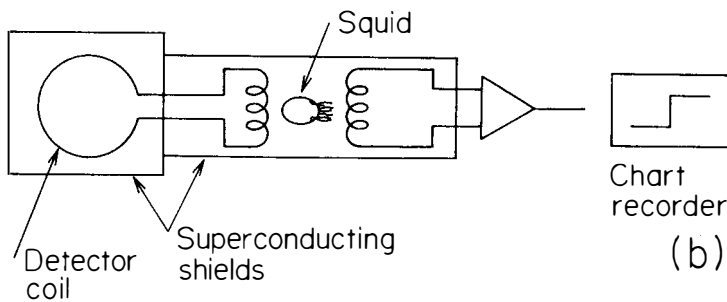


Figure 1

The induction technique used in the Cabrera experiment is shown. The flux change from passage of a monopole is $2\phi_0$ (the flux quantum in a superconductor).

where ϕ_g is from the monopole, ϕ_s is the induced supercurrent, and $\phi_s = -I(t) L$ (the self inductance of the ring). Note that ϕ changes by $2\phi_0$, where $\phi_0 = hc/2e$ is the flux quantum in a superconductor and $4\pi g = hc/e$.

To get an idea of the sensitivity, $\Delta I = \frac{2\phi_0}{L} \sim 10^{-9} A$; $\Delta E = \frac{8 \cdot 10^{-30}}{L}$ joules. So consider the example of a loop of 5 mil wire with $D \sim 1$ meter.

$$L \sim 2 \mu H$$

$$\Delta E = 4 \cdot 10^{-24} \text{ joules (2 fluxons)}$$

For comparison a commercial squid has a sensitivity of $\Delta E \sim 10^{-27}$ joules or $\sim 10^{-3}$ fluxons! Therefore the combination of a SQUID and a superconducting loop are ideal.

The limitation of this technique comes from the problem of shielding the loop magnetically. The change in flux due to a monopole ($2\phi_0$) is $4 \cdot 10^{-7}$ Gauss -cm^2 , while the earth's magnetic field is approximately .01 -1 Gauss, so the earth's field is 10^6 fluxons/ cm^2 .

Cabrera's experiment uses a superconducting lead shield of $\sim 10^{-8}$ Gauss. Therefore, it has the needed sensitivity. However, if the technique were extrapolated to a 1m^2 detector, it becomes extremely difficult, since the field would need to be shielded to $\sim 10^{-12}$ Gauss.

The results of the Cabrera experiment remain at one observed event, but with increased sensitivity from continuing to run the original detector, plus running with a 3 coil detector with a much larger "effective" area.

Including the new data, the results are now

#Coils	$\bar{\sigma}(\text{cm}^2)$	Days
1	10	370
3	70	61

The one candidate corresponds to a limit of

$$F \lesssim 1.6 \cdot 10^{-10} \text{cm}^{-2} \text{ sr}^{-1} \text{ s}^{-1}$$

and based on one event a rate

$$F \sim 6 \cdot 10^{-4} \text{cm}^{-2} \text{ sr}^{-1} \text{ s}^{-1}$$

III. CONSTRAINTS ON THE FLUX OF GUT MONOPOLES FROM ASTROPHYSICS:

Estimates of the fluxes of GUT monopoles in cosmic rays requires understanding of the production mechanisms, acceleration ($W = g_0 B L = 2 \text{ MeV/Gauss}$), gravitational dynamics, annihilations, trapping, etc. These have not been worked out in any detail due to the various uncertainties in the calculations. The best that can be done with our present knowledge is to place some constraints on the presence of GUT monopoles in cosmic rays.

The constraints come from two sources: (1) limits on the total mass of the Universe; and (2) the existence of Galactic magnetic fields. Below I briefly outline these constraints.

(1) Mass of the Universe

The most straightforward astrophysical limit comes from assuming that magnetic monopoles account for most of the mass of the Universe.¹⁰⁾

The mass density contained in galaxies ρ_G accounts for about $0.02\rho_c$, the critical density to close the Universe. This implies that the number of monopoles,

$$\frac{n}{m} \leq \frac{10 \times [(Galactic\ Mass/Monopole\ Mass)]}{(Dist.\ between\ Galaxies)^3}$$

$$n_M \sim 4 \times 10^{-20} \text{ cm}^{-3}$$

For comparison, the number of nucleons is

$$n_n \sim 4 \times 10^{-6} \text{ cm}^{-3}$$

and,

$$\frac{n_M}{m_N} \sim 10^{-14} \frac{\text{monopoles}}{\text{nucleon}}$$

From this, one obtains a flux limit

$$F \leq 5.4 \times 10^{-18} \text{ cm}^{-2} \text{ sr}^{-1} \text{ sec}^{-1} m_{19}^{-1} \left[\frac{v}{10^{-3}c} \right]$$

A more optimistic flux limit is obtained using the fact that monopoles could cluster like mass in our galaxy (10^{12} \odot within 30 kpc). This implies a flux limit of

$$F_c \leq 3 \times 10^{-13} \text{ cm}^{-2} \text{ sr}^{-1} \text{ sec}^{-1} m_{19}^{-1} \left[\frac{v}{10^{-3}c} \right]$$

(2) Survival of Galactic Field

If galactic fields are due to persistent currents, ($\nabla \times B_{gal} \neq 0$), monopoles move along field lines and gain kinetic energy at the expense of the field. In order for the fields to survive, the field energy cannot be dissipated more rapidly than currents can be regenerated by dynamo action ($t_{regeneration} \approx 10^8$ yr).¹¹⁾ This requirement places a limit on the fluxes, usually called the Parker Bound.

$$F \leq 10^{-16} \text{ cm}^{-2} \text{ sr}^{-1} \text{ sec}^{-1} \quad (\text{Parker Bound})$$

This bound has been reexamined by Turner, Parker, and Bogdan using the monopole mass, velocity distributions, etc. They obtain a less restrictive bound for $M_M > 10^{16}$ GeV. Combined with the flux bounds from the mass-density of the Universe

$$F_{max} \leq 10^{-12} \text{ cm}^{-2} \text{ sr}^{-1} \text{ sec}^{-1}$$

for $M_M \sim 10^{19}$ GeV, $\beta \sim 3 \times 10^{-3}$, and clustering.

IV. CONFRONTING THE ASTROPHYSICS BOUNDS WITH EXPERIMENT

The Astrophysics bounds I have just discussed are orders of magnitude below the level indicated by the Calbrera event even with the most favorable choice of parameters. These combined bounds are shown in Fig. 2. This emphasizes the need for confirmation of that event.

If that event is correct and the level is much higher than the bounds, what are the implications for Astrophysics? Two suggestions have been discussed:

(1) Monopoles are the source of the intergalactic B-field and there is an plasma oscillation (e.g. $B^2/8\pi \rightarrow KE_M \rightarrow B^2/8\pi$) back and forth between the field and the monopoles;^{12,13} and (2) that the source of monopoles is actually "local" rather than intergalactic. That is, monopoles have been captured in a cloud and orbit around the sun and pass by the earth. Freeze and Turner¹⁴⁾ have shown that this gives a maximum enhancement of 0(50).

Another possibility is that the Cabrera event is misleading and the rate indicated from Astrophysics should be regarded seriously. If so, NO PRESENT SEARCH is yet below these bounds. The induction technique cannot be extrapolated to such large areas and alternate (less direct) techniques are needed. Ionization techniques appear the most promising, although other alternatives are also being considered. The rest of this report reviews the status and prospects using Ionization and other techniques.

V. LARGE AREA DETECTION TECHNIQUES

(1) Ionization Techniques

A monopole passing through matter will lose energy by ionization loss. The amount of energy loss for charged particles (or monopoles) is well understood for relativistic particles. However, the ionization loss for very slow particles is much less understood. Discrepancies in the various calculations for slow monopoles ($\beta \sim 10^{-3}$) have plagued the interpretation of the present generation of scintillator experiments and evaluation of scintillator for a large array. Much work is presently being done to clarify this situation.

In general, ionization loss varies as a function of β ($\beta < 10^{-3}$) differ by several orders of magnitude. These calculations of the atomic collisions and excitation are quite complicated. At relativistic energies the impulse approximation can be used and the problem is simplified. However, at low β , a detailed model of the atom must be used in order to understand the dynamics and this requires various approximations. Ahlen and Kinoshita¹⁵⁾ have done a detailed calculation of this energy loss in analogy to calculations of Lindhard¹⁶⁾ for protons. The results of this calculation vs. β are shown in Fig. 3.

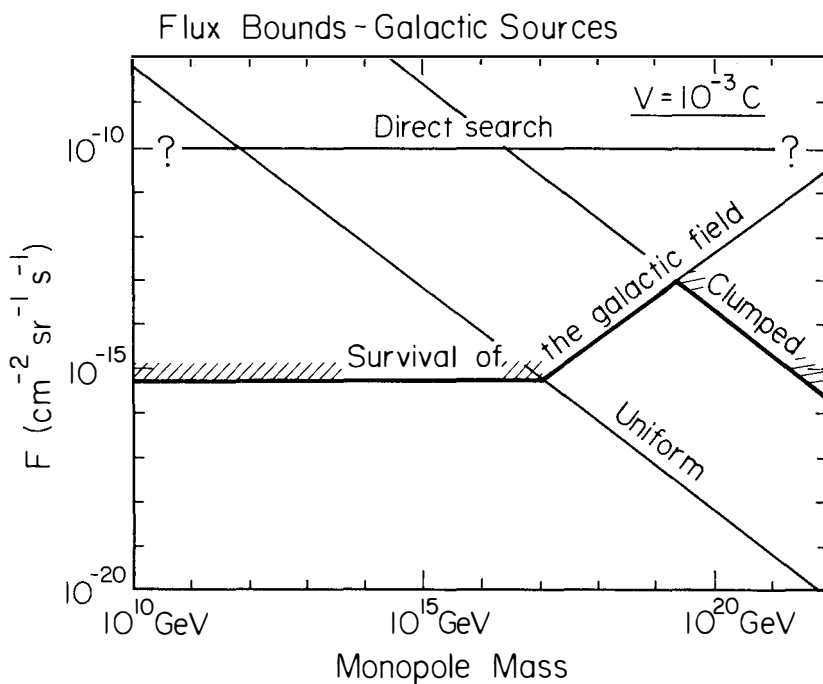


Figure 2

Bounds on the flux of monopoles from Astrophysics considerations. These bounds are orders of magnitude below the Cabrera level.

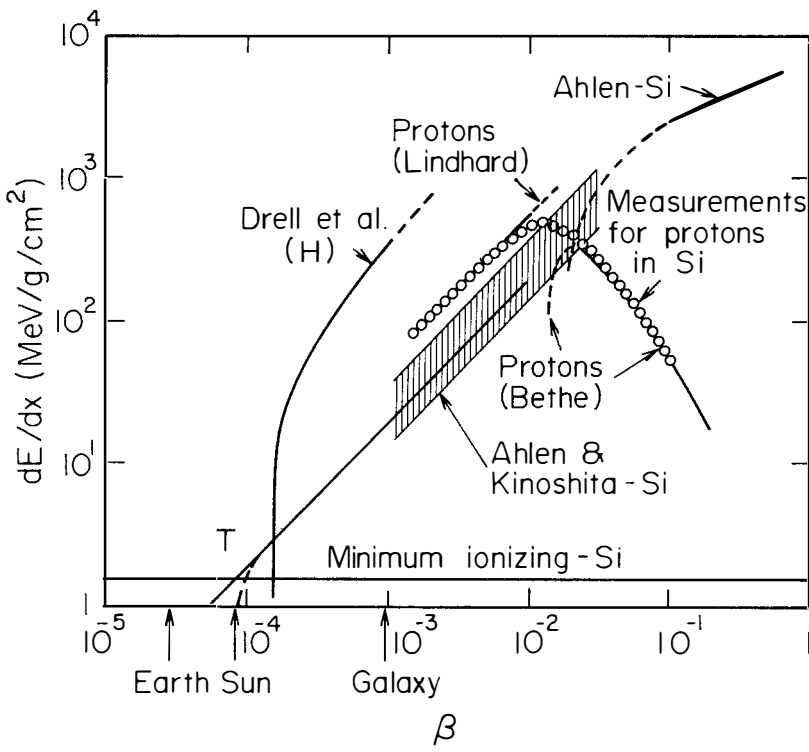


Figure 3

Ionization loss for slow magnetic monopoles. The calculations for Ahlen and Kinoshita at low β has been used to analyze scintillator experiments. Also shown is the energy loss in hydrogen due to Zeeman splitting which might be exploited in future detectors.

It has been shown recently¹⁷⁾ that energy losses due to Zeeman splitting at low velocity are quite large in hydrogen and enhance the signal for low β . What this means for a complex material like plastic scintillator is unclear, but it could indicate the desirability to use a different material in a future monopole detector.

Considerable work has been done experimentally on searching for heavy slow monopoles by ionization loss. Typically, the detectors consist of multiple layers of ionization detectors (e.g. scintillator) set to respond to low light levels. This threshold level, combined with the energy loss calculations discussed above determine the lowest detectable β for each experiment. The actual "signal" of a monopole is from recording the time-of-flight between layers and searching for a very slow moving penetrating particle.

All results from these searches are negative,¹⁸⁻²⁴⁾ but each measurement has different limitations in terms of solid angle acceptance, ionization material, electronics and minimum β accepted. Fig. 4 summarizes these results. Note that none of the results yet approach the astrophysics bounds and a large array, approximately the size of a football field, is needed to reach such sensitivities. Also, note that two of the experiments^{20,21)} have taken special measures to be sensitive at low β . This requires electronics that will respond to the low level, stretched pulse coming from the passage of a very slow particle. (At $\beta \sim 10^{-4}$, it takes the monopole hundreds of nanoseconds just to pass through the individual layers).

These final results, sensitive to low β , are particularly important since they are significantly below Cabrera and are sensitive to the lower β ($\beta \sim 10^{-4}$) expected from local sources of monopoles. These experiments appear to be in direct contradiction to that result.

(2) Other Techniques for Direct Detection

A second mechanism for energy loss exists for monopoles passing through conductors. The energy loss by this mechanism has been calculated by Martem'yanov and Khakimov²⁵⁾ and more recently by Ahlen and Kinoshita²⁶⁾. Ahlen obtains

$$\frac{dE}{dx} = \frac{4\pi^2 N_s e^2 g^2}{m_s c^2} \frac{\beta c}{v_F} \approx 1 \text{ GeV/cm}$$

for aluminum and $\beta \sim 3 \times 10^{-3}$. This is considerably larger than ionization loss, but also varies as β making detection more difficult for very slow monopoles.

At Caltech,²⁷⁾ we have built a prototype detector to study empirically the problems of detecting monopoles by acoustic techniques. The present detector is meant to be a test device to study sensitivity and not a design for a "real" monopole detector. This prototype monopole detector consists of two aluminum

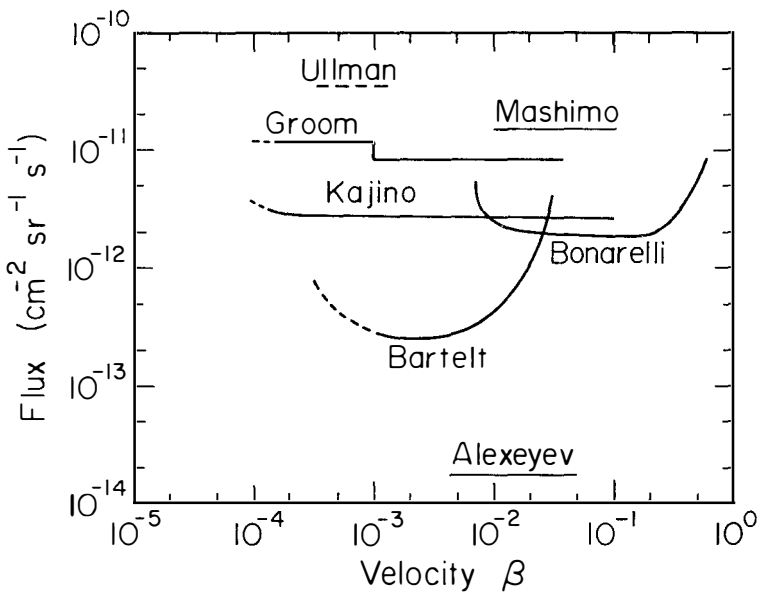


Figure 4

Summary of limits versus β for various scintillation experiments. The limits are well below the Cabrera level but do not approach the astrophysics bounds.

disks which are 144cm in diameter and 10cm thick. Six transducers are coupled to each disk to detect ultrasonic pulses. These transducers are sensitive from 8 to 12 MHz and were developed specifically for this project. Two scintillator arrays are mounted on the disks, one between the disks and one above them, to provide triggering information and a cosmic ray veto.

Considering the very small signal, to evaluate this technique, it is important to understand where the technique will be fundamentally limited due to acoustic noise. In order to minimize this problem we have chosen to work at high frequency (~ 10 MHz). This is about the highest frequency where the acoustic pulse will pass through the aluminum with small absorption.

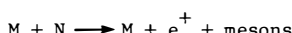
The primary frequency of the acoustic pulse generated when a monopole passes through the medium is much higher (>100 MHz), however that frequency is absorbed with some of the energy becoming thermal and some re-emitted at lower frequency. Below ~ 15 MHz the acoustic pulse will pass through the medium. This inefficiency of turning the energy loss into an acoustic pulse is the fundamental limitation in this method. We have estimated that the final signal is comparable or greater than the acoustic noise from the aluminum medium itself. This has encouraged us to pursue the technique to determine where it will ultimately be limited.

At present, the real limit should come from the noise in the transducer itself. In our present detector, transducers, and electronics we expect this noise to be about 50 times greater than the monopole signal. We are empirically determining this level and studying various methods such as focusing the acoustic pulse for improving this S/N ratio.

A theoretical study of the intrinsic limit due to acoustic noise has been made by Akerlof²⁸⁾ with the conclusion that this technique is practically unfeasible. Although our approach is somewhat more empirical, we agree that present techniques appear to be about a factor of 10^2 away from the required sensitivity. Although some improvements can be envisioned, whether the necessary sensitivity can be obtained remains unclear.

VI. PROTON CATALYSIS

There has been a great deal of interest recently in the possibility that monopoles can catalyze proton decay. The work of Dokos and Tomaras,²⁹⁾ Rubakov,³⁰⁾ and Callan³¹⁾ has lead to the possibility of detecting the passage of monopoles through a proton decay detector by the detection of proton decay by the process



where N = proton or neutron. If these catalyzed decays occur with cross sections typical of the strong interaction ($\sigma \sim 10^{-26} \text{ cm}^2$) several decays will

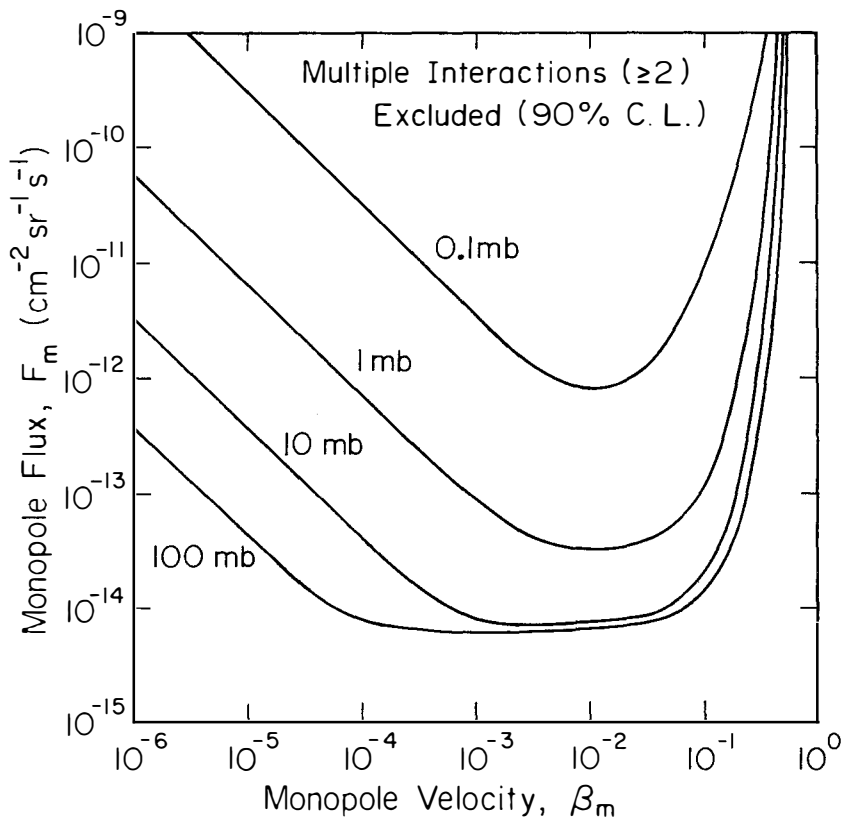


Figure 5

Limits on monopole flux from proton catalysis search for multiple decays along the monopole track. This result is for 100 days of running on the IMB detector.

occur along the trail of the monopole path through the detector. These will be separated by time characteristics of the β of the monopole.

The IMB proton decay detector has been used for such a search.³²⁾ The effective cross sectional area of the detector is 550m^2 for an isotropic flux of monopoles, with area times solid angle of $6900\text{m}^2\text{-sr}$. The mean path length through the detector is 12.8m for an isotropic flux.

The most sensitive search involves looking for multiple interactions, since a single interaction gives events that are kinematically difficult to distinguish from the ~ 1 event/day of cosmic ray neutrino interactions depositing ~ 940 MeV. The back to back kinematical constraint applied to the "natural" $p \rightarrow \pi^0 e^+$ decay mode is not applicable here.

For multiple interactions, 100 days of data have been analyzed looking for two proton decay candidates within 8 μsec . No events of this type have been observed and therefore a 90% C.L. upper limit on the product of the monopole flux times the cross section has been determined. For $\sigma_c > 10$ mb, this corresponds to $F_m(\text{min}) = 7.2 \times 10^{-15} \text{cm}^{-2} \text{sr}^{-1} \text{s}^{-1}$ within a velocity window $10^{-4} < \beta_m < 10^{-1}$. The 90% C.L. upper limit on the product $F_m \times \sigma_c$ has a min value $(F_m \times \sigma_c)_{\text{min}} = 3.6 \times 10^{-41} \text{sr}^{-1} \text{s}^{-1}$ at $\sigma_c = 1\text{mb}$ and monopole velocity. These results are summarized in Fig. 5. The significance of this result clearly depends heavily on the catalysis cross section. This is very uncertain and active theoretical work is in progress to better determine this cross section.

V. CONCLUSIONS:

At present the only positive experimental evidence for the existence of GUT magnetic monopoles is the original Cabrera event. That event has not been confirmed by Cabrera or others. The level seems in conflict with recent scintillator results optimized for low β . In addition, the level is in conflict with bounds from Astrophysical considerations.

No detectors are as yet large enough to be sensitive below these astrophysics bounds. Work is proceeding on various techniques to develop a detector array large enough to be capable of detecting fluxes below that level.

REFERENCES

- 1) B. Cabrera, Phys. Rev. Letters 48, 1378 (1982).
- 2) P. A. M. Dirac, "Quantized Singularities in the Electromagnetic Field", Proc. Royal Soc. London, A233, p.60, (1931).
- 3) P. A. M. Dirac "Theory of Magnetic Poles", Physical Review 74, p.817, (1948).
- 4) P. B. Price, E. K. Shirk, W. Z. Osborne, and L. S. Pinsky, Phys. Rev. Lett. 35, 487, (1975).
- 5) G. 't Hooft, "Magnetic Monopoles in Gauge Theories", Nucl. Phys. B79, p.276, (1974).
- 6) A. Polyakov, "Particle Spectrum in the Quantum Field Theory", Pis'ma Zh. Eksp. Teor. Fiz. [JETP Lett.] 20 [20] p.430 [194] (1974).
- 7) L. W. Alvarez, Lawrence Radiation Laboratory Physics Note 470, (1963).
- 8) L. W. Alvarez, P. H. Eberhard, R. R. Ross, and R. D. Watt, Science 167, 701, (1970); Phys. Rev. D4, 3260, (1971), Phys. Rev. D8, 698, (1973), and P. H. Eberhard, R. R. Ross, J. D. Taylor, L. W. Alvarez, and H. Oberlack, Phys. Rev. D11, 3099, (1975).
- 9) Cabrera reported on more running with a single coil and initial running with 3 coils at the Monopole Workshop, Wingspread, Wisconsin, Oct. 1982.
- 10) M. J. Longo, "Massive Magnetic Monopoles: Indirect and Direct Limits on Their Number Density and Flux", Phys. Rev. D25, p.2399, (1982).
- 11) M. S. Turner, E. N. Parker, and T. J. Bogdan, "Magnetic Monopoles and the Survival of Galactic Magnetic Fields", Phys. Rev. D26, p.1296, (1982).
- 12) E. E. Salpeter, S. L. Shapiro, and I. Wasserman, Phys. Rev. Lett. 49, 1114, (1982).
- 13) J. Arons and R. D. Blanford, Phys. Rev. Lett. 50, 544, (1983).
- 14) K. Freeze and M. Turner, Enrico Fermi Institute Preprint 82-56, submitted to Phys. Lett. B.
- 15) S. P. Ahlen and K. Kinoshita, Phys. Rev. D. 26, 2347, (1982).
- 16) J. Lindhard, Mat. Phys. Medd. Dan. Vid. Selsk. 28, #8, (1954).
- 17) S. D. Drell, N. M. Kroll, M. T. Mueller, S. J. Parke, and M. A. Ruderman, Phys. Rev. Lett. 50, 644, (1983).
- 18) J. D. Ullman, Phys. Rev. Lett. 47, 289, (1981).
- 19) T. Mashima, K. Kawagoe, and M. Koshiba, J. Phys. Soc. Jpn 51, 3067, (1982).
- 20) D. E. Groom, E. C. Loh, H. N. Nelson, and D. M. Ritson, Phys. Rev. Lett. 50, 573, (1983).
- 21) F. Kajino, S. Matsuno, Y. K. Yuan, T. Aoki, T. Kitamura, K. Mitsui, Y. Ohashi, and A. Okada, Inst. Cosmic Ray Research, Univ. of Tokyo Preprint (1983).

- 22) R. Bonarelli, P. Capiluppi, I. D'antone, G. Giacomelli, G. Mandrioli, C. Merli, and A. M. Rossi, Phys. Lett. 112B, 100, (1982).
- 23) J. Bartelt, H. Courant, K. Heller, T. Joyce, M. Marshak, E. Peterson, D. S. Ayres, J. W. Dawson, T. H. Fields, E. N. May, and L. E. Price, Phys. Rev. Lett. 50, 655, (1983).
- 24) E. N. Alexevert, M. M. Boliev, A. E. Chudakov, B. A. Makoev, S. P. Mikheyev, and Y. V. Sten'kin, Lett. Nuova Cimento 35, 413, (1982).
- 25) V. P. Martem'yanov and S. Kh. Khakimov, "Slowing-Down of a Dirac Monopole in Metals and Ferromagnetic Substances", Zh. Eksp. Teor. Fiz. [Sov. Phys. JETP] 62 [35] p.35 [20] (1972).
- 26) S. P. Ahlen and K. Kinoshita, Phys. Rev. 26D, 2347, (1982).
- 27) B. C. Barish, R. G. Cooper, C. E. Lane, and G. Liu, Caltech Preprint CALT 68-988, (1983).
- 28) C. W. Akerloff, Phys. Rev. D26, 1116, (1982); and Phys. Rev. D, (1983), to be published.
- 29) C. R. Dokos, T. N. Tomaras, Phys. Rev. D21, 2940, (1980).
- 30) V. A. Rubakov, Nucl. Phys. B203, 311, (1982); JETP 33, 644, (1981).
- 31) C. Callan, Jr., Phys. Rev. D26, 2058, (1982); and Phys. Rev. D25, 2141, (1982).
- 32) S. Errede, et al., IMB Preprint (April 29, 1983) submitted to Phys. Rev. Letters.

A SEARCH FOR MAGNETIC MONPOLE CATALYSIS OF NUCLEON DECA

S. Errede², J. L. Stone², J. C. van der Velde², R. M. Bionta²,
G. Blewitt⁴, C. B. Bratton⁵, B. G. Cortez^{2, a}, G. W. Foster^{2, a},
W. Gajewski¹, M. Goldhaber³, T. J. Haines¹, T. W. Jones^{2, 7},
D. Kielczewska^{1, b}, W. R. Kropp¹, J. G. Learned⁶, E. Lehmann⁴,
J. M. LoSecco⁴, H. S. Park², F. Reines¹, J. Schultz¹, E. Shumard²,
D. Sinclair², H. W. Sobell¹, L. R. Sulak², R. Svboda⁶, and C. Wuest¹.

- (1) The University of California at Irvine
Irvine, California 92717
- (2) The University of Michigan
Ann Arbor, Michigan 48109
- (3) Brookhaven National Laboratory
Upton, Long Island, New York 11973
- (4) California Institute of Technology
Pasadena, California 91125
- (5) Cleveland State University
Cleveland, Ohio 44115
- (6) The University of Hawaii
Honolulu, Hawaii 96822
- (7) University College
London, United Kingdom

ABSTRACT

A search for superheavy magnetic monopoles "catalyzing" nucleon decay in an underground water Cherenkov detector has been carried out. No positive evidence for such a process has been found during 100 days of detector live time. Cross section and velocity dependent limits on the monopole flux are presented, which have a minimum of $7.2 \times 10^{-15} \text{ cm}^{-2} \text{ sr}^{-1} \text{ s}^{-1}$ for catalysis cross sections $> 10 \text{ mb}$ and monopole velocities $10^{-4} < \beta_m < 10^{-1}$. For low cross sections, we obtain velocity independent limits on the monopole flux. Limits on the monopole interaction rate are presented.

*Presented by S. Errede

Theoretical and experimental interest in magnetic monopoles has not ceased since Dirac's pioneering work¹ in 1931. Recently, a resurgence of interest has resulted from the work of 't Hooft and Polyakov² in 1974 which showed that superheavy magnetic monopoles are a natural consequence of grand unified theories (GUTs) which spontaneously break and eventually yield a U(1) gauge group. The monopole mass in GUTs is expected to be of the order of the unification scale, $M_m \sim 10^{16}$ GeV.^{3,4} Such superheavy monopoles could have been produced in large numbers in the early moments of the universe.^{3,5} In the present epoch the flux of a superheavy magnetically charged particles is constrained by the mass density of the universe.^{6,9} The most stringent astrophysical limit on the monopole flux can be estimated from the maximum flux within our galaxy that can be tolerated without destroying the observed galactic magnetic field ($\sim 3 \mu G$). This upper limit, known as the Parker Bound⁷, is $F_m < 6 \times 10^{-16} \text{ cm}^{-2} \text{ sr}^{-1} \text{ s}^{-1}$. Furthermore, various considerations suggest their present velocities are of order $10^{-4} < \beta_m < 10^{-2}$ in our galaxy and solar system.^{8,9} Monopoles within this velocity range and mass are unlikely to be stopped in their passage through the earth.

In 1980, Dokos and Tomaras suggested that the presence of a grand unified monopole in proximity to hadronic matter may act as a catalyst, strongly enhancing baryon number violating processes¹⁰. Subsequently, Rubakov¹¹ and Callan¹² in studying the interaction mechanism of fermions with monopoles showed that processes such as



are essentially independent of the unification mass. Catalysis cross sections typical of strong interactions $\sigma_C \sim 10^{-26} \text{ cm}^2$ are predicted, but with a large uncertainty.

Kolb, Colgate, and Harvey¹³ have obtained an indirect, model dependent limit on the flux of monopoles incident on neutron stars from consideration of the increase in luminosity due to catalysis of nuclear matter within the star. From the use of experimental limits on the interstellar x-ray luminosity, they obtain a limit on the monopole flux times catalysis cross section, $F_m \times \sigma_C < 5 \times 10^{-49} \text{ sr}^{-1} \text{ s}^{-1}$. Other authors¹⁴ have suggested neutron star models which yield far less stringent limits, compatible even with the Parker bound for large catalysis cross sections.

Direct experimental evidence for monopole catalyzed nucleon decay would be of profound importance for grand unified theories since a single unambiguous observation could simultaneously prove the existence of magnetic monopole and proton decay. Large detectors designed to look for nucleon decay are well suited to search for the reaction of equation (1).

The Irvine-Michigan-Brookhaven (IMB) water Cherenkov detector¹⁵, located underground at a depth of 760 m in a salt mine near Cleveland, Ohio, was designed and built expressly to search for evidence of nucleon decay. The detector consists of a total of 2048 hemispherical (5" dia.) photomultiplier tubes (PMT's) placed on a regular surface lattice (~ 1 m spacing) of dimensions, $23 \times 17 \times 18$ m³ and is shown in Figure 1. The effective cross sectional area of the detector is 550 m² for an isotropic flux of monopoles, with area \times solid angle of 6900 m²-sr. The PMT's look inward at 7.0 metric kilotons ($\sim 4 \times 10^{33}$ nucleons) of chemically pure water. Relativistic charged particles from nucleon decays or entering cosmic rays are detected via their light impinging on the PMT's. The readout electronics independently records for each tube above threshold (0.25 p.e.) the time of arrival (T1) and the amount Cherenkov light at that tube. The resolution of the T1 time scale is 1 ns with a full scale of 512 ns. For triggering the detector the PMT's are divided into 32 groups of 8 \times 8 matrices. A trigger requires > 3 PMT's in a group to within 50 ns and > 2 groups firing within 150 ns. A second unbiased trigger simply requires > 12 PMTs to fire within 50 ns. Each photoelectron of recorded Cherenkov light corresponds to ~ 4 MeV of energy loss in water, hence, the above trigger energy thresholds are 24 MeV and 48 MeV, respectively. For nucleon decay the energy deposited in the detector may be as high as the nucleon rest mass. Hence, for $p \rightarrow e^+ \pi^0$ decay we expect 170 ± 25 PMT's to fire with an energy deposition of 940 ± 100 MeV.

Following a trigger on the T1 scale, the electronics activates for each tube a second time scale (T2) for an additional 7.5 μ s, with 15 ns resolution. The T2 time scale enables the detection of $\mu \rightarrow e \nu \bar{\nu}$ decays for muons which stop in the detector. For monopoles the T2 timing enables the detection of a sequence of multiple catalyzed nucleon decays occurring within 8 μ s. The monopole would not be directly observed unless its velocity were above Cherenkov threshold.

SEARCH FOR MULTIPLE INTERACTIONS

We have searched 100 days of livetime data for evidence of multiple catalyzed nucleon decays (> 2) occurring within the detector volume. Specifically, we require an event with > 30 PMT's in the T1 time scale and at least one additional event with > 50 PMT's firing within any 300 ns time window in the T2 time scale. Furthermore, to enable unambiguous rejection of entering cosmic ray backgrounds, we require at least one of the events to occur within the detector fiducial volume (inset 2 m from the PMT planes). We measure a rate of 4.6 ± 0.3 events/day for events occurring anywhere in the detector volume, consistent with the expected trigger rate from random two-fold coincidences due to 2.7 cosmic rays/second through the detector. No > 3 -fold coincidences have been observed.

The overall efficiency for detecting a monopole catalyzed nucleon decay has 3 components:

- (1) The trigger detection efficiency ϵ_d is somewhat dependent on the specific nucleon decay mode. The results of computer simulations for various modes of nucleon decay indicate an overall detection efficiency for multiple interactions in the detector of $\epsilon_d = 0.9 \pm 0.1$ for neutrinoless decay modes.¹⁶
- (2) The geometrical acceptance of the detector fiducial volume, ϵ_g , is also a function of the catalysis cross section σ_c . $\epsilon_g(\sigma_c)$ is defined as the ratio of events with single (multiple) interactions satisfying the fiducial volume requirement to all events with single (multiple) interactions in the total detector volume. We determine ϵ_g by computer simulations of monopoles traversing the detector, assuming an isotropic monopole flux. The mean path length through the detector is 12.8 m. Figure 2 shows $\epsilon_g(\sigma_c)$ versus σ_c for single and multiple interactions in the detector.
- (3) For multiple interactions (> 2) in the detector, the constraints imposed by the T1 and T2 time scales give an efficiency, or interaction probability $\epsilon(\sigma_c, \beta_m)$ which is dependent upon the catalysis cross section and monopole velocity. This efficiency was also determined by computer simulations and is reflected by the flux limit curves shown in Figure (discussed below). In the absence of any velocity dependence, $\epsilon(\sigma_c, \beta_m)$ reduces to the Poisson probability for > 2 interactions in the detector.

We have found no events passing the event selection criteria consistent with multiple interactions from magnetic monopole catalyzed nucleon decays. Hence, we obtain an upper limit on the monopole flux from

$$F_m < \frac{N_0}{A \cdot \Omega \cdot \Delta t \cdot \epsilon_d \cdot \epsilon_g(\sigma_c) \cdot \epsilon(\sigma_c, \beta_m)} \quad (2)$$

where for no observed events, $N_0 = 2.3$ for 90% confidence, A is the effective cross sectional area of the detector, Ω is the solid angle (4π), Δt is the detector livetime, the efficiencies ϵ_d , $\epsilon_g(\sigma_c)$ and $\epsilon(\sigma_c, \beta_m)$ are defined above. In Figure 2 we show the 90% C.L. upper limits on the monopole flux for multiple interactions in our detector as a function of monopole velocity, for several values of the catalysis cross section. For large cross sections, $\sigma_c > 100$ mb, the 90% C.L. upper limit on the monopole flux, F_m , has a minimum of $F_m(\min) = 7.2 \times 10^{-15} \text{ cm}^{-2} \text{ sr}^{-1} \text{ s}^{-1}$ within the velocity range $10^{-4} < \beta_m < 10^{-1}$. The 90% C.L. upper limit for the interaction rate, $F_m \times \sigma_c$, for multiple interaction has a minimum of $(F_m \times \sigma_c)_{\min} = 3.6 \times 10^{-41} \text{ sr}^{-1} \text{ s}^{-1}$ at $\sigma_c = 1$ mb and monopole velocity $\beta_m = 5 \times 10^{-3}$.

Throughout this work, we have tacitly assumed a linear A -dependence for the catalysis cross section. Hence, the interaction length $\lambda_c = (n \sigma_c)^{-1}$ where n is the nucleon number density. The A -dependence of the catalysis cross section is uncertain at the present time. The monopole flux limits we have obtained should be modified accordingly if an A -dependence other than A^1 is assumed.

SEARCH FOR SINGLE INTERACTIONS

For catalysis cross sections, $\sigma_c < 1$ mb the interaction length, λ_c , becomes larger than the mean path length, considerably reducing the probability for multiple interactions in the detector. Under these circumstances we can, nevertheless, set limits on the monopole flux and interaction rate from single interactions in the detector. In deriving these limits one must consider the background due to atmospheric neutrino interactions and possibly "spontaneous" nucleon decays and/or nn oscillations. Spontaneous 2-body nucleon decays will have a characteristic back-to-back signature with the opening angle of the decay products typically $> 150^\circ$. The signature for a monopole catalysis nucleon decay

can be quite different due to the kinematics of the reaction. In its own rest frame, the heavy monopole absorbs a negligible fraction of disintegrating nucleon rest energy. It can, however, acquire up to 1 GeV/c momentum which, by momentum conservation, is transferred to the decay products. Thus, catalyzed decays or $n\bar{n}$ transitions can have the same general appearance as atmospheric neutrino interactions of $E_\nu < 2$ GeV in the detector.

During our independent search for spontaneous nucleon decay in the detector, a total of 69 single interaction events in 80 days of detector time were found.¹⁷ The event rate and characteristics of these events are consistent with neutrino interactions in the detector. Of the 69 events, 66 have energies below twice the nucleon rest mass, M_N . We use these events to obtain conservative limits on the monopole flux and interaction rate with further event selection in order to incorporate the broadest range of possibilities for monopole catalysis of nucleon decay.

The absolute rate of neutrino interactions which pass our filtering is calculated to be $R_\nu = 0.9 \pm 0.4$ events per day¹⁷, based on estimated fluxes and cross sections appropriate to the energy range we observe. The estimated overall efficiency for the detection of atmospheric neutrinos $N_\nu = 48 \pm 7$ (stat.) ± 25 (syst.) events in 80 days of detector live time, to be compared with the 66 events below $2 M_N$. Thus, as many as 52 events (90% C.L.) could be due to monopole interactions.

We use equation (2) in determining flux limits for single interactions. The detection efficiency for single catalysis interactions in the fiducial volume is calculated to be $\epsilon_d = 0.9 \pm 0.1$ for neutrinoless decay modes.¹⁶ The geometrical acceptance ϵ_g for single interactions in the fiducial volume is shown in Figure 1. The efficiency $\epsilon(\sigma_c)$ is merely the Poisson probability for single interactions within the detector.

The upper limits on the monopole flux, F_m , and interaction rate, $F_m \times \sigma_c$, for single interactions are velocity independent, and are shown in Figure 4. The 90% C.L. upper limit on the monopole flux has a minimum of $F_m(\min) = 1.1 \times 10^{-12} \text{ cm}^{-2} \text{ sr}^{-1} \text{ s}^{-1}$ at a catalysis cross section $\sigma_c = 1 \text{ mb}$. For cross sections $\sigma_c < 0.1 \text{ mb}$, the upper limit on the monopole single interaction is $F_m \times \sigma_c < 3.6 \times 10^{-40} \text{ sr}^{-1} \text{ s}^{-1}$ (90% C.L.).

This experiment has searched for magnetic monopoles via the new and unique mechanism of magnetic monopole catalysis of nucleon decay. The cross section dependent limits on the monopole flux encompass a significantly wider velocity range and are considerably lower than, or comparable to those of previous experiments¹⁸, which are sensitive to the electromagnetic interaction of magnetic monopoles with matter. Figure 5 shows limits on the monopole flux as set these experiments.

ACKNOWLEDGEMENTS

We wish to thank the many people who made this detector a reality and especially the employees of Morton-Thiokol who operate the Fairport mine. This work is supported in part by the U.S. Department of Energy.

REFERENCES AND FOOTNOTES

- (a) Also at Harvard University.
- (b) Permanent address: Warsaw University, Poland.
- 1. P. A. M. Dirac, Proc. Roy. Soc. 133A, 60 (1931); Phys. Rev. 74, 817 (1948).
- 2. G. 't Hooft, Nucl. Phys. B79, 276 (1974);
A. M. Polyakov, JETP Lett. 20, 194 (1974).
- 3. J. P. Preskill, Phys. Rev. Lett. 43, 1365 (1979).
- 4. H. Georgi and S. L. Glashow, Phys. Rev. Lett. 32, 438 (1974);
H. Georgi, H. R. Quinn and S. Weinberg, Phys. Rev. Lett. 33, 451 (1974).
- 5. A. H. Guth and S.-H. H. Tye, Phys. Rev. Lett. 44, 631 (1980);
J. N. Fry and D. N. Schramm, Phys. Rev. Lett. 44, 1361 (1980);
P. Langacker and S. Y. Pi, Phys. Rev. Lett. 45, 1 (1980);
M. Einhorn, D. L. Stein and D. Toussaint, Phys. Rev. D21, 3295 (1980);
A. Bais and S. Rudaz, Nucl. Phys. B170, 507 (1980);
G. Lazarides and Q. Shafi, Phys. Lett. 91B, 72 (1980);
G. Lazarides and Q. Shafi, Phys. Lett. 94B, 149 (1980);
G. Lazarides, Q. Shafi and T. Walsh, Phys. Lett. 100B, 21 (1981);
M. S. Turner, Phys. Lett. B115, 95 (1982).
- 6. M. J. Longo, Phys. Rev. D25, 2399 (1982).
- 7. M. S. Turner, E. N. Parker and T. J. Bogdan, Phys. Rev. D26, 1296 (1982).

8. J. Ellis, D. V. Nanopoulos and K. A. Olive, CERN preprint TH-3323 CERN (June, 1982).
9. M. S. Turner, Proceedings of Magnetic Monopole Workshop, Wingspread, Racine, Wisconsin, Oct. 1982, ed. by R. A. Carrigan, W. P. Trower.
10. C. R. Dokos, T. N. Tomaras, Phys. Rev. D21, 2940 (1980).
11. V. A. Rubakov, Nucl. Phys. B203, 311 (1982); JETP 33, 644 (1981).
12. C. Callan, Jr., Phys. Rev. D26, 2058 (1982); Phys. Rev. D25, 2141 (1982); (LPTENS preprint 82/20 (1982). See also C. Callan, talk presented at conference.
13. E. W. Kolb, S. A. Colgate and J. A. Harvey, Phys. Rev. Lett. 49, 137 (1982).
14. V. A. Kuzmin and V. A. Rubakov, ICTP preprint IC/83/17, to be published.
S. Dimopoulos, J. Preskill and F. Wilczek, submitted to Phys. Lett. (UCSB preprint NSF-ITP-82-91); F. A. Bais, J. Ellis, D. N. Nanopoulos and K. A. Olive, CERN preprint 3383-CERN (August 1982).
15. J. C. van der Velde, in the "Proceedings of Neutrinos '81," Maui, Hawaii (July, 1981), ed. by R. J. Cence, E. Ma, A. Roberts, Vol. 1, p. 205.
16. The detection efficiency for single and multiple interactions with decay modes involving neutrinos is $\epsilon_d = 0.6 \pm 0.2$. The flux limits for multiple and single interactions for these modes should therefore be increased accordingly.
17. R. M. Bionta, et al., Phys. Rev. Lett. 50 (1983).
See also J. C. van der Velde, talk presented at this conference.
18. J. D. Ullman, Phys. Rev. Lett. 47, 289 (1981);
R. Bonarelli, et al., Phys. Lett. 112B, 100 (1982);
D. E. Groom, et al., Phys. Rev. Lett. 50, 573 (1983);
B. Cabrera, Phys. Rev. Lett. 48, 1378 (1982);
J. Bartelt, et al., Phys. Rev. Lett. 50, 655 (1983);
D. Ayres, et al., in the Snowmass DPF Proceedings, p. 603 (June/July 1982), ed. by R. Donaldson, H. R. Gustafson and F. Paige.
See also B. Barish, talk presented at this conference.

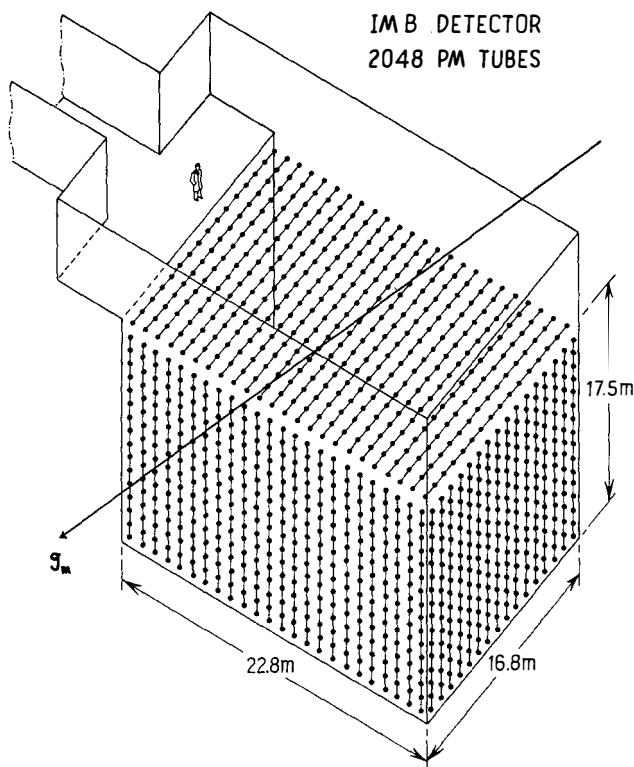


Figure 1. The Irvine-Michigan-Brookhaven 8000 ton water Cherenkov Detector.

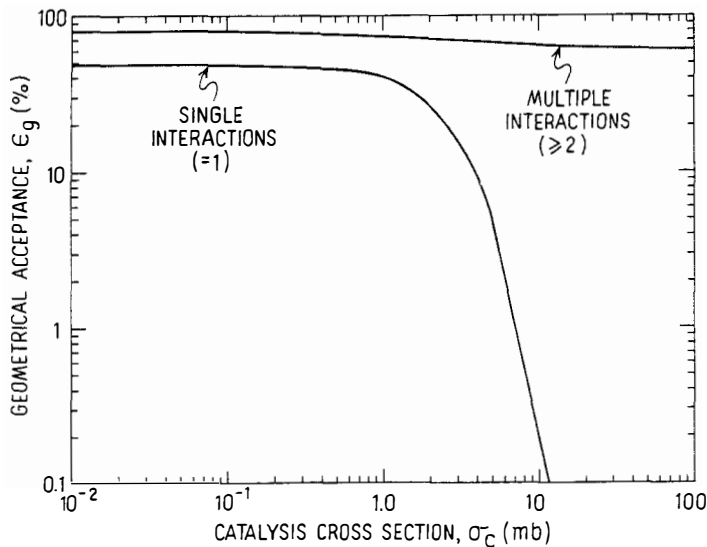


Figure 2. The geometrical detection efficiency, ϵ_g (σ_c), versus catalysis cross section, σ_c , for single and multiple interactions, for an isotropic flux of magnetic monopoles.

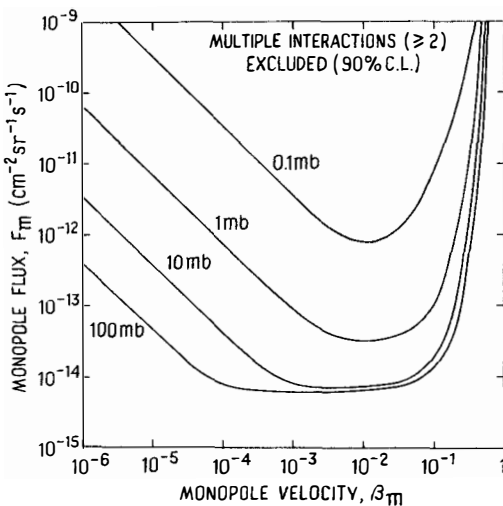


Figure 3. Upper limits (90% C.L.) on the monopole flux, F_m , versus monopole velocity, β_m , for multiple interactions in the detector, for several values of catalysis cross section, σ_c .

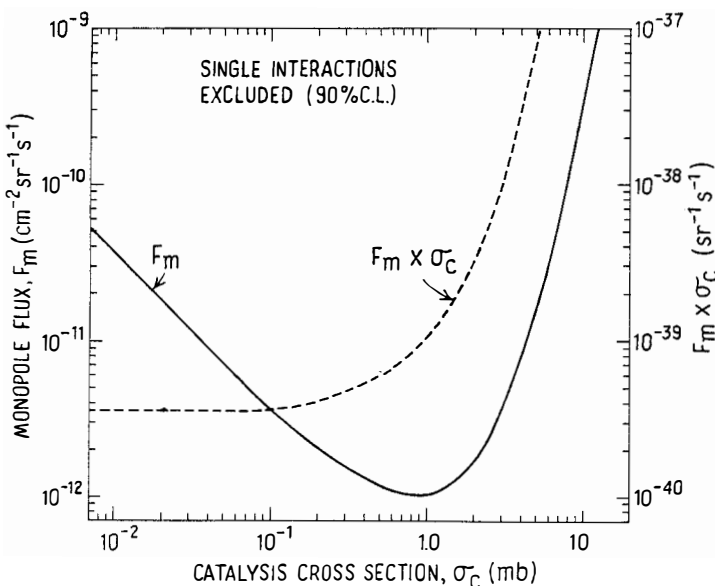


Figure 4. Upper limit (90% C.L.) on the monopole flux, F_m , (left axis, solid curve) and interaction rate, $F_m \times \sigma_c$, (right axis, dashed curve) versus the catalysis cross section, σ_c , for single interactions in the detector fiducial volume.

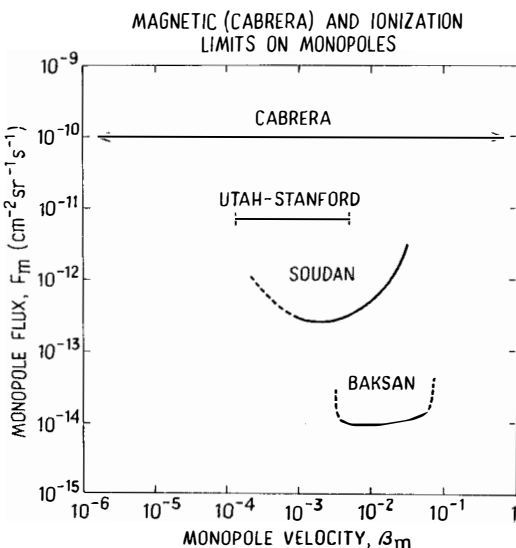


Figure 5. Monopole flux limits set by previous experiments which rely upon electromagnetic interactions of magnetic monopoles with matter.

WHAT IS THE DARK MATTER?
IMPLICATIONS FOR GALAXY FORMATION AND PARTICLE PHYSICS

Joel R. Primack* and George R. Blumenthal†

*Board of Studies in Physics and Santa Cruz Institute
for Particle Physics, †Lick Observatory, Board of Studies
in Astronomy and Astrophysics, University of California,
Santa Cruz, CA 95064, U.S.A.

ABSTRACT We discuss three arguments that the dark matter which dominates the present universe is not baryonic - based on excluding specific baryonic models, deuterium abundance, and the absence of small-angle fluctuations in the microwave background radiation. If the dark matter consists of elementary particles, it may be classified as hot (free streaming erases all but supercluster-scale fluctuations), warm (free streaming erases fluctuations smaller than galaxies), or cold (free streaming is unimportant). We consider scenarios for galaxy formation in all three cases. We discuss several potential problems with the hot (neutrino) case: making galaxies early enough, with enough baryons, and without too much increase in $M_{\text{tot}}/M_{\text{bary}}$ from galaxy to rich cluster scales. The reported existence of dwarf spheroidal galaxies with relatively heavy halos is a serious problem for both hot and warm scenarios. Zeldovich ($n=1$) adiabatic initial fluctuations in cold dark matter (axions, or a heavy stable "ino") appear to be lead to observed sizes and other properties of galaxies, and may also yield large scale structure such as voids and filaments.

I. INTRODUCTION

There is abundant observational evidence that dark matter (DM) is responsible for most of the mass in the universe (1). Dark matter is detected through its gravitational attraction in the massive extended halos of disk galaxies and in groups and clusters of galaxies of all sizes. It is appropriate to call this matter "dark" because it is detected in no other way; it is not observed to emit or absorb electromagnetic radiation of any wavelength. Matter observed in these latter ways we will call "luminous". Here we consider the nature of the dark matter.

II. THE DM IS PROBABLY NOT BARYONIC

There are three arguments that the DM is not "baryonic", that is, that it is not made of protons, neutrons, and electrons as all ordinary matter is. As Richard Feynman has said in other contexts, one argument would suffice if it were convincing. All three arguments have loopholes. The arguments that DM \neq baryons are as follows:

A. Excluding Baryonic Models (2)

The dark matter in galaxy halos cannot be gas (it would have to be hot to be pressure supported, and would radiate); nor frozen hydrogen "snowballs" (they would sublimate); nor dust grains (their "metals", elements of atomic number ≥ 3 , would have prevented formation of the observed low-metallicity Population II stars); nor "jupiters" (how to make so many hydrogen balls too small to initiate nuclear burning without making a few large enough to do so?); nor collapsed stars (where is the matter they must have ejected in collapsing?).

The weakest argument is probably that which attempts to exclude "jupiters": arguments of the form "how could it be that way?" are rarely entirely convincing.

B. Deuterium Abundance (3)

In the early universe, almost all the neutrons which "freeze out" are synthesized into ^4He . The fraction remaining in D and ^3He is a rapidly decreasing function of η , the ratio of baryon to photon number densities. The presently observed D abundance (compared, by number, to H) is $(1-4) \times 10^{-5}$. Since D is readily consumed but not produced in stars, 10^{-5} is also a lower limit on the primordial D abundance. This, in turn, implies an upper limit $\eta \leq 10^{-9}$, or

$$\Omega_b \leq 0.035 h^{-2} (T_o/2.7)^3, \quad (1)$$

where Ω_b is the ratio of the present average baryon density ρ_b to the critical density

$$\rho_c = 3H_o^2/8\pi G = 1.9 \times 10^{-29} h^2 \text{ g cm}^{-3} = 11 h^2 \text{ keV cm}^{-3}, \quad (2)$$

H_o is the Hubble parameter (the subscript o denotes the present

epoch), and observationally $h \equiv H_0 (100 \text{ km s}^{-1} \text{ Mpc}^{-1})^{-1}$ lies in the range $\frac{1}{2} \leq h \leq 1$. The total cosmological density $\Omega \equiv \rho_{\text{tot}}/\rho_c$ is very difficult to determine observationally, but it appears to lie in the range $0.1 \leq \Omega \leq 2$. Cosmological models in which the universe passes through an early de Sitter "inflationary" stage, predict Ω very close to unity.

In a baryon dominated universe ($\Omega \approx \Omega_b$), the deuterium bound, Eq. (1), is consistent only with the lower limit on Ω , and then only for the Hubble parameter at its lower limit. An Einstein-de Sitter or inflationary ($\Omega = 1$) or closed ($\Omega > 1$) universe cannot be baryonic.

C. Galaxy Formation

In the standard cosmological model, which we will adopt, large scale structure forms when perturbations $\delta \equiv \delta\rho/\rho$ grow to $\delta \gtrsim 1$, after which they cease to expand with the Hubble flow. Let us further assume that perturbations in matter and radiation density are correlated (these are called adiabatic perturbations, since the entropy per baryon is constant; these are the sort of perturbations predicted in grand unified models). Then photon diffusion ("Silk damping") erases perturbations of baryonic mass smaller than (4)

$$M_{\text{Silk},b} \approx 3 \times 10^{13} \Omega_b^{-1/2} \Omega^{-3/4} h^{-5/2} M_\theta. \quad (3)$$

Thus galaxies ($M_b \lesssim 10^{11-12} M_\theta$) can form only after the "pancake" collapse of larger-scale perturbations (5). Perturbations δ in a matter dominated universe grow linearly with the scale factor

$$\delta \propto a = (1+z)^{-1} = T_0/T \quad (4)$$

where $z = (\lambda_0 - \lambda)/\lambda$ is the redshift and T is the radiation temperature. In a baryonic universe, δ grows only between the epoch of hydrogen recombination, $z_r \approx 1300$, and $z \approx \Omega^{-1}$. It follows that at recombination $\delta T/T \approx \delta\rho/3\rho \gtrsim 3 \times 10^{-3}$ for $M \gtrsim M_{\text{Silk}}$, which corresponds to fluctuations on observable angular scales $\theta > 4'$ today. Such temperature fluctuations are an order of magnitude larger than present observational upper limits (6).

The main loophole in this argument is the assumption of adiabatic perturbations. It is true that the orthogonal mode, perturbations in baryonic density which are uncorrelated with radiation (called isothermal perturbations), do not arise naturally in currently fashionable particle physics theories where baryon number is generated in the decay of massive grand unified theory (GUT) bosons, since in such theories $\eta = n_b/n_\gamma$ is determined by the underlying particle physics and should not vary from point to point in space. But galaxies originating as isothermal perturbations do avoid both Silk damping and contradiction with present $\delta T/T$ limits.

A second loophole is the possibility that matter was reionized at some $z \gg$, by hypothetical very uv sources. Then the fluctuations in $\delta T/T$ at recombination associated with baryonic proto-pancakes could be washed out by rescattering.

Despite the loopholes in each argument, we find the three arguments together to be rather persuasive, even if not entirely compelling. If it is indeed true that the bulk of the mass in the universe is not baryonic, that is yet another blow to anthropocentricity: not only is man not the center of the universe physically (Copernicus) or biologically (Darwin), we and all that we see are not even made of the predominant variety of matter in the universe!

III. THREE TYPES OF DM PARTICLES: HOT, WARM & COLD

If the dark matter is not baryonic, what is it? We will consider here the physical and astrophysical implications of three classes of elementary particle DM candidates, which we will call hot, warm, and cold. (We are grateful to Dick Bond for proposing this apt terminology.)

Hot DM refers to particles, such as neutrinos, which were still in thermal equilibrium after the most recent phase transition in the hot early universe, the QCD deconfinement transition, which presumably took place at $T_{QCD} \sim 10^2$ MeV. Hot DM particles have a cosmological number density roughly comparable to that of the microwave background photons, which implies an upper bound to their mass of a few tens of eV. As we shall discuss shortly, free streaming destroys any perturbations smaller than supercluster size, $\sim 10^{15} M_\odot$.

Warm DM particles interact much more weakly than neutrinos. They decouple (i.e., their mean free path first exceeds the horizon size) at $T > T_{QCD}$, and consequently their number density is roughly an order of magnitude lower, and their mass an order of magnitude higher, than hot DM particles. Perturbations as small as large galaxy halos, $\sim 10^{12} M_\odot$, could then survive free streaming. It was initially suggested that, in theories of local supersymmetry broken at $\sim 10^6$ GeV, gravitinos could be DM of the warm variety (7). Other candidates are also possible, as we will discuss.

Cold DM consists of particles for which free streaming is of no cosmological importance. Two different sorts have been proposed, a cold Bose condensate such as axions, and heavy remnants of annihilation or decay such as heavy stable neutrinos. As we will see, a universe dominated by cold DM looks remarkably like the one astronomers actually observe.

It is of course also possible that the dark matter is NOTA -

none of the above! A perennial candidate, primordial black holes, is becoming increasingly implausible (8-10). Another possibility which, for simplicity, we will not discuss, is that the dark matter is a mixture, for example "jupiters" in galaxy halos plus neutrinos on large scales (3).

IV. GALAXY FORMATION WITH HOT DM

The standard hot DM candidate is massive neutrinos (3-5), although other, more exotic, theoretical possibilities have been suggested, such as a "majoron" of nonzero mass which is lighter than the lightest neutrino species, and into which all neutrinos decay (11). For definiteness, we will discuss neutrinos.

A. Mass Constraints

Left-handed neutrinos of mass $\leq 1 \text{ MeV}$ will remain in thermal equilibrium until the temperature drops to T_{vd} , at which point their mean free path first exceeds the horizon size and they essentially cease interacting thereafter, except gravitationally (12). Their mean free path is, in natural units ($\hbar = c = 1$), $\lambda_v \sim [\sigma_v n_{v\pm}]^{-1} \sim [(G_{wk}^2 T^2)(T^3)]^{-1}$, and the horizon size is $\lambda_h \sim (G_P)^{-1/2} \sim M_{Pl} T^{-2}$, where the Planck mass $M_{Pl} \equiv G^{-1/2} = 1.22 \times 10^{19} \text{ GeV} = 2.18 \times 10^{-3} \text{ g}$. Thus $\lambda_h/\lambda_v \sim (T/T_{vd})^3$, with the neutrino decoupling temperature

$$T_{vd} \sim M_{Pl}^{-1/3} G_{wk}^{-2/3} \sim 1 \text{ MeV}. \quad (5)$$

After T drops below 1 MeV, e^+e^- annihilation ceases to be balanced by pair creation, and the entropy of the e^+e^- pairs heats the photons. Above 1 MeV, the number density n_{vi} of each left-handed neutrino species (counting both ν_i and $\bar{\nu}_i$) is equal to that of the photons, n_γ , times the factor $3/4$ from Fermi vs. Bose statistics; but e^+e^- annihilation increases the photon number density relative to that of the neutrinos by a factor of $11/4$.¹ Thus today, for each species,

$$n_v^0 = \frac{3}{4} \cdot \frac{4}{11} n_\gamma^0 = 109 \left(\frac{T_\gamma}{2.7K} \right)^3 \text{ cm}^{-3}. \quad (6)$$

Since the cosmological density

$$\rho = \Omega \rho_c = 11 \Omega h^2 \text{ keV cm}^{-3}, \quad (7)$$

it follows that

$$\sum_i m_{vi} < \rho/n_v^0 \leq 100 \Omega h^2 \text{ eV}, \quad (8)$$

where the sum runs over all neutrino species with $m_{\nu_i} \leq 1 \text{ MeV}$.² Observational data imply that Ωh^2 is less than unity (3). Thus if one species of neutrino is substantially more massive than the others and dominates the cosmological mass density, as for definiteness we will assume for the rest of this section, then a reasonable estimate for its mass is $m_{\nu} \sim 30 \text{ eV}$.

At present there is apparently no reliable experimental evidence for nonzero neutrino mass. Although one group reported (15) that $14 \text{ eV} < m_{\nu_e} < 40 \text{ eV}$ from tritium β end point data, according to Boehm (16) their data are consistent with $m_{\nu_e} = 0$ with the resolution corrections pointed out by Simpson. The so far unsuccessful attempts to detect neutrino oscillations also give only upper limits on neutrino masses times mixing parameters (16).

B. Free Streaming

The most salient feature of hot DM is the erasure of small fluctuations by free streaming. It is easy to see that the minimum mass of a surviving fluctuation is of order M_{Pl}^3/m_{ν}^2 (17,4).

Let us suppose that some process in the very early universe - for example, thermal fluctuations subsequently vastly inflated, in the inflationary scenario (18) - gave rise to adiabatic fluctuations on all scales. Neutrinos of nonzero mass m_{ν} stream relativistically from decoupling until the temperature drops to m_{ν} , during which time they will traverse a distance $d_{\nu} \approx \lambda_h(T = m_{\nu}) \sim M_{Pl} m_{\nu}^{-2}$. In order to survive this free streaming, a neutrino fluctuation must be larger in linear dimension than d_{ν} . Correspondingly, the minimum mass in neutrinos of a surviving fluctuation is $M_{J,\nu} \sim d_{\nu}^3 m_{\nu} n_{\nu}(T = m_{\nu}) \sim d_{\nu}^3 m_{\nu}^4 \sim M_{Pl}^3 m_{\nu}^{-2}$. By analogy with Jeans' calculation of the minimum mass of an ordinary fluid perturbation for which gravity can overcome pressure, this is referred to as the (free-streaming) Jeans mass. A more careful calculation (4,19) gives

$$d_{\nu} = 41 (m_{\nu}/30 \text{ eV})^{-1} (1+z)^{-1} \text{ Mpc}, \quad (9)$$

and

$$M_{J,\nu} = 1.77 M_{Pl}^3 m_{\nu}^{-2} = 3.2 \times 10^{15} (m_{\nu}/30 \text{ eV})^{-2} M_{\odot}, \quad (10)$$

which is the mass scale of superclusters. Objects of this size are the first to form in a ν -dominated universe, and smaller scale structures such as galaxies can form only after the initial collapse of supercluster-size fluctuations.

C. Growth of Fluctuations

The absence of small angle $\delta T/T$ fluctuations is compatible with this picture. When a fluctuation of total mass $\sim 10^{15} M_\odot$ enters the horizon at $z \sim 10^4$, the density contrast of the radiation plus baryons δ_{RB} ceases growing and instead starts oscillating as an acoustic wave, while that of the neutrinos δ_ν continues to grow linearly with the scale factor $a = (1+z)^{-1}$. Thus by recombination, at $z_r \approx 1300$, $\delta_{RB}/\delta_\nu < 10^{-1}$, with possible additional suppression of δ_{RB} by Silk damping (depending on the parameters in Eq. (3)). This picture, as well as the warm and cold DM schemes, predicts small angle fluctuations in the microwave background radiation just slightly below current observational upper limits (6).

In numerical simulations of dissipationless gravitational clustering starting with a fluctuation spectrum appropriately peaked at $\lambda \approx d_\nu$, the regions of high density form a network of filaments, with the highest densities occurring at the intersections and with voids in between (5,20-22). The similarity of these features to those seen in observations (23,24) is certainly evidence in favor of this model.

D. Potential Problems with ν DM

A number of potential problems with the neutrino dominated universe have emerged in recent studies, however. (1) From studies both of nonlinear (22) clustering ($\lambda \lesssim 10$ Mpc) and of streaming velocities (25) in the linear regime ($\lambda > 10$ Mpc), it follows that supercluster collapse must have occurred recently: $z_{sc} \lesssim 0.5$ is indicated (25), and in any case $z_{sc} < 2$ (22). But then, if QSOs are associated with galaxies, their abundance at $z > 2$ is inconsistent with the "top-down" neutrino dominated scheme in which superclusters form first: $z_{sf} > z_{galaxies}$. (2) Numerical simulations of the nonlinear "pancake" collapse taking into account dissipation of the baryonic matter show that at least 85% of the baryons are so heated by the associated shock that they remain ionized and unable to condense, attract neutrino halos, and eventually form galaxies (25a). (3) The neutrino picture predicts (26) that there should be a factor of ~ 5 increase in M_{tot}/M_{lum} between large galaxies ($M_{tot} \sim 10^{12} M_\odot$) and large clusters ($M_{tot} \gtrsim 10^{14} M_\odot$), since the larger clusters, with their higher escape velocities, are able to trap a considerably larger fraction of the neutrinos. Although there is indeed evidence for a trend of increasing M_{tot}/L with M_{tot} (1,27), when one takes into account the large amount of x-ray emitting gas in rich clusters (28) one finds comparable $M_{tot}/M_{lum} \sim 14$ for galaxies with large halos and for rich clusters (29,30). (M_{lum} here includes matter luminous in x-ray as well as optical wavelengths, in contrast to luminosity L that includes only the latter.) (4) Both theoretical arguments (31) and data on Draco (32,33) imply that dark matter dominates the gravitational potential of dwarf spheroidal galaxies. The

phase-space constraint (34) then sets a lower limit (33) $m_\nu > 500$ eV, which is completely incompatible with the cosmological constraint Eq. (8). (Note that for neutrinos as the DM in spiral galaxies, the phase space constraint implies $m_\nu > 30$ eV.)

These problems, while serious, may not be fatal for the hypothesis that neutrinos are the dark matter. It is possible that galaxy density does not closely correlate with the density of dark matter, for example because the first generation of luminous objects heats nearby matter, thereby increasing the baryon Jeans mass and suppressing galaxy formation. This could complicate the comparison of nonlinear simulations (22) with the data. Also, if dark matter halos of large clusters are much larger in extent than those of individual galaxies and small groups, then virial estimates would underestimate M_{tot} on large scales and the data could be consistent with $M_{\text{tot}}/M_{\text{lum}}$ increasing with M_{lum} . But it is hard to avoid the constraint on z_{sc} from streaming velocities in the linear regime (25) except by assuming that the local group velocity is abnormally low. And the only explanation for the high M_{tot}/L of dwarf spheroidal galaxies in a neutrino-dominated universe is the rather ad hoc assumption that the dark matter in such objects is baryons rather than neutrinos. Of course, the evidence for massive halos around dwarf spheroidals is not yet solid.

V. GALAXY FORMATION WITH WARM DM

Suppose the dark matter consists of an elementary particle species X that interacts much more weakly than neutrinos. The X s decouple thermally at a temperature $T_{\text{Xd}} \gg T_{\text{vd}}$ and their number density is not thereafter increased by particle annihilation at temperatures below T_{Xd} . With the standard assumption of conservation of entropy per comoving volume, the X number density today n_X^0 and mass m_X can be calculated in terms of the effective number of helicity states of interacting bosons (B) and fermions (F), $g = g_B + (7/8)g_F$, evaluated at T_{Xd} (35). These are plotted in Fig. 1, assuming the "standard model" of particle physics. The simplest grand unified theories predict $g(T) = 100$ for T between 10^2 GeV and $T_{\text{GUT}} \sim 10^{14}$ GeV, with possibly a factor of two increase in g beginning near 10^2 GeV due to $N = 1$ supersymmetry partner particles. Then for T_{Xd} in the enormous range from ~ 1 GeV to $\sim T_{\text{GUT}}$, $n_X^0 \sim 5 g_X \text{cm}^{-3}$ and correspondingly $m_X \sim 2\Omega h^2 g_X^{-1} \text{keV}$ (36), where g_X is the number of X helicity states. Such "warm" DM particles of mass $m_X \sim 1$ keV will cluster on a scale $\sim M_p m_X^{-2} \sim 10^{12} M_\odot$, the scale of large galaxies such as our own (7,37,38).

What might be the identity of the warm DM particles X ? It was initially (7) suggested that they might be the $\pm\frac{1}{2}$ helicity states of the gravitino \tilde{G} , the spin 3/2 supersymmetric partner of the graviton G . The gravitino mass is related to the scale of

supersymmetry breaking by $m_{\tilde{G}} = (4\pi/3)^{1/2} m_{\text{SUSY}}^2 m_{\text{Pl}}^{-1}$, so $m_{\tilde{G}} \sim 1 \text{ keV}$ corresponds to $m_{\text{SUSY}} \sim 10^6 \text{ GeV}$. This now appears to be phenomenologically dubious, and supersymmetry models with $m_{\text{SUSY}} \sim 10^{11} \text{ GeV}$ and $m_{\tilde{G}} \sim 10^2 \text{ GeV}$ are currently popular (39). In such models, the photino $\tilde{\gamma}$, the spin $\frac{1}{2}$ supersymmetric partner of the photon, is probably the lightest R-odd particle, and hence stable. But in supersymmetric GUT models $m_{\tilde{\gamma}} \sim 10 m_{\tilde{g}}$, and there is a phenomenological lower bound on the mass of the gluino $m_{\tilde{g}} > 2 \text{ GeV}$ (40). The requirement that the photinos almost all annihilate, so that they do not contribute too much mass density, implies that $m_{\tilde{\gamma}} \gtrsim 2 \text{ GeV}$ (14,41), and they become a candidate for cold rather than warm dark matter.

A hypothetical right-handed neutrino ν_R could be the warm DM particle (42), since if right-handed weak interactions exist they must be much weaker than the ordinary left-handed weak interactions, so $T_{\nu_R d} \gg T_{\nu d}$ as required. But particle physics provides no good reason why any ν_R should be light.

Thus there is at present no obvious warm DM candidate elementary particle, in contrast to the hot and cold DM cases. But our ignorance about the physics above the ordinary weak interaction scale hardly allows us to preclude the existence of very weakly interacting light particles, so we will consider the warm DM case, mindful of Hamlet's prophetic admonition

There are more things in heaven and earth, Horatio,
Than are dreamt of in your philosophy.

A. Fluctuation Spectrum

The spectrum of fluctuations δ_ν at late times in the hot DM model is controlled mainly by free streaming; $\delta_\nu(M)$ is peaked at $\sim M_{J,\nu}$, Eq. (10), for any reasonable primordial fluctuation spectrum. This is not the case for warm or cold DM.

The primordial fluctuation spectrum can be characterized by the magnitude of fluctuations as they just enter the horizon. It is expected that no mass scale is singled out, so the spectrum is just a power law

$$\delta_{\text{DM},H} = \left(\frac{\delta \rho_{\text{DM}}}{\rho_{\text{DM}}} \right)_H = \kappa \left(\frac{M_{\text{DM}}}{M_0} \right)^{-\alpha} \quad (11)$$

Furthermore, to avoid too much power on large or small mass scales requires $\alpha \approx 0$ (43), and to form galaxies and large scale structure by the present epoch without violating the upper limits on both small (6) and large (44) scale (quadrupole) angular variations in the microwave background radiation requires $\kappa \sim 10^{-4}$. Eq. (11)

corresponds to $|\delta_k|^2 \propto k^n$ with $n = 6\alpha + 1$. The case $\alpha = 0$ ($n = 1$) is commonly referred to as the Zeldovich spectrum.

Inflationary models predict adiabatic fluctuations with the Zeldovich spectrum (18). In the simplest models κ is several orders of magnitude too large, but it is hoped that this will be remedied in more realistic - possible supersymmetric - models (45).

The important difference between the fluctuation spectra δ_{DM} at late times in the hot and warm DM cases is that $\delta_{DM, warm}$ has power over an increased range of masses, roughly from 10^{11} to $10^{15} M_\Theta$. As for the hot case, the lower limit, $M_X \sim M_{Pl}^3 m_X^{-2}$, arises from the damping of smaller-scale fluctuations by free streaming. In the hot case, the DM particles become nonrelativistic at essentially the same time as they become gravitationally dominant, because their number density is nearly the same as that of the photons. But in the warm case, the X particles become nonrelativistic and thus essentially stop free streaming at $T \sim m_X$, well before they begin to dominate gravitationally at $T_{eq} \sim 6\Omega h^2$ eV. The subscript "eq" refers to the epoch when the energy density of massless particles equals that of massive ones:

$$z_{eq} = \frac{\Omega \rho_c c}{4\sigma T_0^4 (1+\gamma)} = 2.47 \times 10^4 \Omega h^2 \left(\frac{1.681}{1+\gamma} \right) \theta^{-4}. \quad (12)$$

We assume here that there are n_ν species of very light or massless neutrinos, and $\gamma \equiv \rho_\nu^0 / \rho_Y^0 = (7/8)(4/11)^{1/3} n_\nu$ ($= 0.681$ for $n_\nu = 3$), $\theta \equiv T_0 / 2.7$ K, and σ is the Stefan-Boltzmann constant. During the interval between $T \sim m_X$ and $T \sim T_{eq}$, growth of δ_{DM} is inhibited by the "stagnation" phenomenon (also known as the Meszaros (46) effect), which we will discuss in detail in the section on cold DM. Thus the spectrum δ_{DM} is relatively flat between M_X and

$$M_{eq} = \frac{4\pi}{3} \left(\frac{c t_{eq}}{1+z_{eq}} \right)^3 \rho_c \Omega = 2.2 \times 10^{15} (\Omega h^2)^{-2} M_\Theta. \quad (13)$$

Fluctuations with masses larger than M_{eq} enter the horizon at $z < z_{eq}$, and thereafter δ_{DM} grows linearly with $a = (1+z)^{-1}$ until nonlinear gravitational effects become important when $\delta_{DM} \sim 1$. Since for $\alpha = 0$ all fluctuations enter the horizon with the same magnitude, and those with larger M enter the horizon later in the matter-dominated era and subsequently have less time to grow, the fluctuation spectrum falls with M for $M > M_{eq}$: $\delta_{DM} \propto M^{-2/3}$. For a power-law primordial spectrum of arbitrary index,

$$\delta_{DM} \propto M^{-\alpha - 2/3} = M^{-(n+3)/6}, \quad M > M_{eq}. \quad (14)$$

This is true for hot, warm, or cold DM. In each case, after recombination at $z_r \approx 1300$ the baryons "fall in" to the dominating DM fluctuations on all scales larger than the baryon Jeans mass, and by $z \approx 100$, $\delta_b \approx \delta_{DM}$ (47).

In the simplest approximation, neglecting all growth during the "stagspansion" era, the fluctuation spectrum for $M_X < M < M_{eq}$ is just $\delta_{DM} \propto M^{-\alpha} = M^{-(n-1)/6} = M^{-(n_{eff}+3)/6}$, where $n_{eff} = n - 4$; i.e., the spectrum is flattened by a factor of $M^{2/3}$ compared to the primordial spectrum. The small amount of growth that does occur during the "stagspansion" era slightly increases the fluctuation strength on smaller mass scales: $n_{eff} \approx n - 3$. Detailed calculations of these spectra are now available (19,37).

B. Which Formed First, Galaxies or Superclusters?

For $\alpha \geq 0$, $\delta_X(M)$ has a fairly broad peak at $M \sim M_X$. Consequently, objects of this mass - galaxies and small groups - are the first to form, and larger-scale structures - clusters and superclusters - form later as $\delta_X(M)$ grows toward unity on successively larger mass scales. For a particular primordial spectral index α , one can follow Peebles (48,49) and use the fact that the galaxy autocovariance function $\xi(R) \approx 1$ for $R = 5h^{-1}$, together with the (uncertain) assumption that the DM is distributed on such scales roughly like the galaxies, to estimate when galaxies form in this scenario. For $\alpha = 0$, $z_{galaxies} \approx 4$, which is consistent with the observed existence of quasars at such redshifts. But superclusters do not begin to collapse until $z < 2$, so one would not expect to find similar Lyman α absorption line redshifts for quasars separated by $\sim 1h^{-1}$ Mpc perpendicular to the line of sight (50). Indeed, Sargent et al. (51) found no such correlations. This is additional evidence against hot DM.

C. Potential Problems with Warm DM

The warm DM hypothesis is probably consistent with the observed features of typical large galaxies, whose formation would probably follow roughly the "core condensation in heavy halos" scenario (52,29,53). The potentially serious problems with warm DM are on scales both larger and smaller than M_X . On large scales, the question is whether the model can account for the observed network of filamentary superclusters enclosing large voids (23,24). A productive approach to this question may require sophisticated N-body simulations with $N \sim 10^6$ in order to model the large mass range that is relevant (54). We will discuss this further in the next section in connection with cold DM, for which the same question arises.

On small scales, the preliminary indications that dwarf spheroidal galaxies have large DM halos (31-33) pose problems nearly as serious for warm as for hot DM. Unlike hot DM, warm DM is (barely) consistent with the phase space constraint (32-34). But since free streaming of warm DM washes out fluctuations δ_X for $M \lesssim M_X \sim 10^{11} M_\odot$, dwarf galaxies with $M \sim 10^7 M_\odot$ can form in this picture only via fragmentation following the collapse of structures of mass $\sim M_X$, much as ordinary galaxies form from superclusters fragmentation in the hot DM picture. The problem here is that dwarf galaxies, with their small escape velocities $\sim 10 \text{ km s}^{-1}$, would not be expected to bind more than a small fraction of the X particles, whose typical velocity must be $\sim 10^2 \text{ km s}^{-1}$ (\sim rotation

velocity of spirals). Thus we expect $M_{\text{tot}}/M_{\text{lum}}$ for dwarf galaxies to be much smaller than for large galaxies - but the indications are that they are comparable (31-33). Understanding dwarf galaxies may well be crucial for unravelling the mystery of the identity of the DM. Fortunately, data on Carina, another dwarf spheroidal companion of the Milky Way, is presently being analyzed (55).

VI. GALAXY FORMATION WITH COLD DM

Damping of fluctuations by free streaming occurs only on scales too small to be cosmologically relevant for DM which either is not characterized by a thermal spectrum, or is much more massive than 1 keV. We refer to this as cold DM.

A. Cold DM Candidates

Quantum chromodynamics (QCD) with quarks of nonzero mass violates CP and T due to instantons. This leads to a neutron electric dipole moment that is many orders of magnitude larger than the experimental upper limit, unless an otherwise undetermined complex phase θ_{QCD} is arbitrarily chosen to be extremely small. Peccei and Quinn (56) have proposed the simplest and probably the most appealing way to avoid this problem, by postulating an otherwise unsuspected symmetry that is spontaneously broken when an associated pseudoscalar field - the axion (57) - gets a nonzero vacuum expectation value $\langle \phi_a \rangle \sim f_a e^{i\theta}$. This occurs when $T \sim f_a$. Later, when the QCD interactions become strong at $T \sim \Lambda_{\text{QCD}} \sim 10^3$ MeV, instanton effects generate a mass for the axion $m_a = m_\pi f_\pi / f_a \sim 10^{-5}$ eV (10^{12} GeV/ f_a). Thereafter, the axion contribution to the energy density is (58) $\rho_a = 3m_a T^3 f_a^2 (M_{\text{Pl}} \Lambda_{\text{QCD}})^{-1}$. The requirement $\rho_a^0 < \rho_c \Omega$ implies that $f_a \lesssim 10^{12}$ GeV, and $m_a \gtrsim 10^{-5}$ eV.⁴ The longevity of helium-burning stars implies (59) that $m_a < 10^{-2}$ eV, $f_a > 10^9$ GeV. Thus if the hypothetical axion exists, it is probably important cosmologically, and for $m_a \sim 10^{-5}$ eV gravitationally dominant. (The mass range 10^{9-12} GeV, in which f_a must lie, is also currently popular with particle theorists as the scale of supersymmetry (39) or family symmetry breaking, the later possibility connected with the axion (60).)

Two quite different sorts of cold DM particles are also possible. One is a heavy stable "ino", such as a photino (41) of mass $m_\gamma > 2$ GeV as discussed above. By a delicate adjustment of the theoretical parameters controlling the γ mass and interactions, the γ s can be made to almost all annihilate at high temperatures, leaving behind a small remnant that, because m_γ is large, can contribute a critical density today (14).

The second possibility may seem even more contrived: a particle, such as a v_R , that decouples while still relativistic but whose number density relative to the photons is subsequently diluted by entropy generated in a first-order phase transition such as the Weinberg-Salam symmetry breaking (36). (Recall that the m_X bound in Fig. 1 assumes no generation of entropy.) More than a factor $\lesssim 10^3$ entropy increase would over dilute $n = n_b/n_\gamma$, if we assume n was initially generated by GUT baryosynthesis; correspondingly, $m_X \lesssim 1$ MeV, and $M_X \gtrsim 10^6 M_\odot$.

Actually, it is not clear that we have a good basis to judge the plausibility of any of these DM candidates, since in no case is there a fundamental explanation - or, even better, a prediction - for the ratio $\omega \equiv \rho_{DM}^0/\rho_{plum}^0$, which is known to lie in the range $10 \leq \omega \leq 10^2$. Two fundamental questions about the universe which the fruitful marriage of particle physics and cosmology has yet to address are the value of ω and of the cosmological constant Λ . (We have here assumed $\Lambda = 0$, as usual.)

B. "Stagspanion"

Peebles (49) has calculated the fluctuation spectrum for cold DM, with results that are well approximated by the expression

$$|\delta_k|^2 = k^n (1 + \alpha k + \beta k^2)^{-2},$$

$$\alpha = 6 \theta^2 h^{-2} \text{ Mpc}, \beta = 2.65 \theta^4 h^{-4} \text{ Mpc}^2, \theta = T_0/2.7 \text{ K.} \quad (15)$$

This calculation neglects the massless neutrinos; we find qualitatively similar results with their inclusion (61). For an adiabatic Zeldovich ($n=1$) primordial fluctuation spectrum, the spectrum of rms fluctuations in the mass found within a randomly placed sphere, $\delta M/M$, is relatively flat for $M < 10^9 M_\odot$, $\propto M^{-1/6}$ ($n_{eff} \approx -2$) for $10^9 M_\odot \leq M \leq 10^{12} M_\odot$, $\propto M^{-1/3}$ ($n_{eff} \approx -1$) for $10^{12} M_\odot \leq M \leq M_{eq}$, and $\propto M^{-2/3}$ ($n=1$, reflecting the primordial spectrum) for $M \geq M_{eq}$.

The flattening of the spectrum for $M < M_{eq}$ is a consequence of "stagspanion",³ the inhibition of the growth of δ_{DM} for fluctuations which enter the horizon when $z > z_{eq}$, before the era of matter domination. In the conventional formalism (12,48,62) - synchronous gauge, time-orthogonal coordinates - the fastest growing adiabatic fluctuations grow $\propto a^2$ when they are larger than the horizon. When they enter the horizon, however, the radiation and charged particles begin to oscillate as an acoustic wave with constant amplitude (later damped by photon diffusion for $M < M_{Silk}$), and the neutrinos free stream away. As a result, the main source term for the growth of δ_{DM} disappears, and once the fluctuation is well inside the horizon δ_{DM} grows only as (46), (48, pp. 56-59)

$$\delta_{DM} \propto 1 + \frac{3a}{2a_{eq}} \quad (16)$$

until matter dominance ($a = a_{eq}$); thereafter, $\delta_{DM} \propto a$. Based on Eq. (16), it has sometimes been erroneously remarked [also by the present authors (38), alas] that there is only a factor of 2.5 growth in δ_{DM} during the entire stagspanion regime, from horizon crossing until matter dominance. There is actually a considerable amount of growth in δ_{DM} just after the fluctuation enters the horizon, since $d\delta_{DM}/da$ is initially large and the photon and neutrino source terms for the growth of dark matter fluctuations do not disappear instantaneously. (See reference 61 for details.) This explains how $(\delta M/M)_{DM}$ can grow by a factor ~30 between M_{eq} and $10^9 M_\odot$.

C. Galaxy Formation

When δ reaches unity, nonlinear gravitational effects become

important. The fluctuation separates from the Hubble expansion, reaches a maximum radius, and then contracts to about half that radius (for spherically symmetric fluctuations), at which point the rapidly changing gravitational field has converted enough energy from potential to kinetic for the virial relation $\langle PE \rangle = -2\langle KE \rangle$ to be satisfied. (For reviews see (63) and (48).)

Although small-mass fluctuations will be the first to go nonlinear in the cold DM picture, baryons will be inhibited by pressure from falling into them if $M < M_{J,b}$. What is more important is that even for $M > M_{J,b}$, the baryons will not be able to contract further unless they can lose kinetic energy by radiation. Without such mass segregation between baryons and DM, the resulting structures will be disrupted by virialization as fluctuations that contain them go nonlinear (52). Moreover, successively larger fluctuations will collapse relatively soon after one another if they have masses in the flattest part of the $\delta M/M$ spectrum, i.e., (total) mass $\lesssim 10^9 M_\odot$.

Gas of primordial composition (about 75% atomic hydrogen and 25% helium, by mass) cannot cool significantly unless it is first heated to $\sim 10^4 K$, when it begins to ionize (65). Assuming a primordial Zeldovich spectrum and normalizing (49) so that

$$\frac{\delta M}{M} (R = 8h^{-1}) = 1, \quad (17)$$

the smallest protogalaxies for which the gas is sufficiently heated by virialization to radiate rapidly and contract have $M_{\text{tot}} \sim 10^9 M_\odot$ (65). One can also deduce an upper bound on galaxy masses from the requirement that the cooling time be shorter than the dynamical time (64); with the same assumptions as before, this upper bound is $M_{\text{tot}} \lesssim 10^{12} M_\odot$ (65). It may be significant that this is indeed the range of masses of ordinary galaxies. The collapse of fluctuations of larger mass is expected in this picture to lead to clusters of galaxies. Only the outer parts of the member galaxy halos are stripped off; and the inner baryon cores continue to contract, presumably until star formation halts dissipation (29).⁶

D. Potential Problems with Cold DM

Dwarf galaxies with heavy DM halos are less of a problem in the cold than in the hot or warm DM pictures. There is certainly plenty of power in the cold DM fluctuation spectrum at small masses; the problem is to get sufficient baryon cooling and avoid disruption. Perhaps dwarf spheroidals are relatively rare because most suffered disruption.

The potentially serious difficulties for the cold and warm DM pictures arise on very large scales, where galaxies are observed to form filamentary superclusters with large voids between them (23,24). These features have seemed to some authors to favor the hot DM model, apparently for two main reasons: (1) it is thought that formation of caustics of supercluster size by gravitational collapse requires a fluctuation power spectrum sharply peaked at the corresponding wavelength, and (2) the relatively low peculiar velocities of galaxies in superclusters are seen as evidence for the sort of dissipation expected in the baryonic shock in the

"pancake" model. Recent work by Dekel (67) suggests, however, that nondissipative collapse fits the observed features of super-clusters. Results from N-body simulations with $N \sim 10^6$ (54) will soon show whether broad fluctuation spectra lead to filaments.

VII. SUMMARY AND REFLECTIONS

The hot, warm, and cold DM pictures are compared schematically in Fig. 2. Although only very tentative conclusions can be drawn on the basis of present information, it is our impression that the hot DM model is in fairly serious trouble. Maybe that is mainly because it has been the most intensively studied of the three possibilities considered here.

Probably the greatest theoretical uncertainty in all three DM pictures concerns the relative roles of heredity vs. environment. For example, are elliptical galaxies found primarily in regions of high galaxy density, and disk galaxies in lower density regions, because such galaxies form after the regions have undergone a large-scale dissipative collapse which provides the appropriate initial conditions, as in the hot DM picture? Or is it because disks form relatively late from infall of baryons in an extended DM halo, which is disrupted or stripped in regions of high galaxy density? An exciting aspect of the study of large scale structure and DM is the remarkable recent increase in the quality and quantity of relevant observational data, and the promise of much more to come.

Perhaps even more remarkable is the fact that this data may shed important light on the interactions of elementary particles on very small scales. Fig. 3 is redrawn from a sketch by Shelley Glashow which recently was reproduced in *The New York Times Magazine* (68). Glashow uses the snake eating its tail - the *uroboros*, an ancient symbol associated with creation myths (69) - to represent the idea that gravity may determine the structure of the universe on both the largest and smallest scales. But there is another fascinating aspect to this picture. There are left-right connections across it: medium-small-to-medium-large, very-small-to-very-large, etc. Not only does electromagnetism determine structure from atoms to mountains (70), and the strong and weak interactions control properties and compositions of stars and solar systems. The dark matter, which is gravitationally dominant on all scales larger than galaxy cores, may reflect fundamental physics on still smaller scales. And if cosmic inflation is to be believed, cosmological structure on scales even larger than the present horizon arose from interactions on the seemingly infinitesimal grand unification scale.

ACKNOWLEDGMENTS Our interest in the subject of dark matter grew out of collaboration with Heinz Pagels (7,38). In preparing this paper we benefited from conversations with N. Abrams, J.R. Bond, A. Dekel, M. Davis, G. Efstatiou, C. Frenk, D. Lin, J. Silk, A. Szalay, M. Turner, S. White, and especially from extensive discussions with S. Faber at Santa Cruz and M. Rees at the Moriond Conference and subsequently. We received partial support from NSF grants and from the Santa Cruz Institute for Particle Physics.

FOOTNOTES

1. This discussion is approximate. Since neutrino decoupling and e^+e^- annihilation so nearly coincide, there is actually a little heating of the neutrinos too (13).
2. It is also possible that the DM is heavy stable neutrinos with mass $\gtrsim 2$ GeV, almost all of which would have annihilated (14). This is a possible form of cold DM, discussed below.
3. In economic "stagflation", the economy stagnates but the economic yardstick inflates. The behavior of δ_{DM} during the "stagflation" era is analogous: $\delta_{DM} \approx$ constant but a expanding. We suggest here the term stagflation rather than stagflation for this phenomenon since it occurs during the ordinary expansion (Friedmann) era rather than during a possible very early "inflationary" (de Sitter) era.
4. One might worry that such a light particle could give rise to a force that at short distances $(10^{-5} \text{ eV})^{-1} \sim 2 \text{ cm}$ would be much stronger than gravity. But because the axion is pseudoscalar, its nonrelativistic couplings to fermions are $\sim \vec{\delta} \cdot \vec{p}$.
5. One calculates δ_k initially. In order to discuss mass fluctuations it is more convenient to use $\delta M/M$ than $\delta \rho/\rho$, the Fourier transform of δ_k (49). Note that there is a simple relationship between $|\delta \rho/\rho|^2$ and $|\delta_k|^2$ only for a power law fluctuation spectrum $|\delta_k|^2 \propto k^n$.
6. The model presented by Peebles at the Moriond conference differs from that sketched here mainly in Peebles' assumption that there is sufficient cooling from molecular hydrogen for baryon condensation to occur rapidly even on globular cluster mass scales.

REFERENCES

1. Faber,S.M. and Gallagher,J.S.1979 *Ann.Rev.Astron. and Astrophys.*17,pp 135-187.
2. Hegyi,D.J. and Olive,K.A.1982 *U.Mich.preprint*; Hegyi,D.J.1983 *Rencontre de Moriond, Astrophysics*.
3. Steigman,G.1981 in *v81* and in Heusch,C.ed.,*Particles and Fields 1981: Testing the Standard Model* (A.I.P.Conf.Proc.,No.81) pp 548-571; Schramm,D.N. and Steigman,G.1981 *Astrophys.J.*,241, pp 1-7.
4. Bond,J.R.,Efstathiou,G. and Silk,J.1980 *Phys.Rev.Lett.*45,pp 1980-1984.
5. Doroshkevich,A.G.,Khlopov,M.Yu.,Sunyaev,R.A.,Szalay,A.S. and Zeldovich,Ya.B.1981 *Proc. Xth Texas Symposium on Relativistic Astrophysics* *Ann.N.Y.Acad.Sci.*375,pp 32-42; Sato,H.,*ibid*,pp 43-53; and ref. therein.
6. Partridge,R.B.1980 *Astrophys.J.*,235,pp 681-687.
7. Pagels,H.R. and Primack,J.R.1982 *Phys.Rev.Lett.*48,pp 223-226.
8. Carr,B.1978 *Comments on Astrophys.*7,pp 161-173.
9. Canizares,R.1982 *Astrophys.J.*,263,pp 508-517.
10. Lacey,C.1983 *Rencontre de Moriond Astrophysics*.
11. Gelmini,G.B.,Nussinov,S. and Roncadelli,M.1982 *Nucl. Phys.*B209, pp 157.
12. Weinberg,S.,*Gravitation and Cosmology* (Wiley,1972),pp 534.

13. Dicus, D.A., Kolb, E.W., Gleeson, A.M., Sudarshan, E.C.G., Teplitz, V.L. and Turner, M.S. 1982 *Phys. Rev. D* 26, pp 2694-2706.
14. Lee, B.W. and Weinberg, S. 1977 *Phys. Rev. Lett.* 39, pp 165-168.
15. Lyubimov, V.A., et al. 1980 *Phys. Lett.* 94B, pp 266-268.
16. Boehm, F. 1983 *Proc. 4th Workshop on Grand Unification*, in press.
17. Bisnovatyi-Kogan, G.S. and Novikov, I.D. 1980 *Sov. Astron.* 24, pp 516-517.
18. Gibbons, G., Hawking, S., and Siklos, S., eds. 1983 *The Very Early Universe* (Cambridge Univ. Press) and ref. therein.
19. Bond, J.R. and Szalay, A.S. 1981 *Proc. v81*, 1, pp 59; *Astrophys. J.*, in press.
20. Melott, A. 1983 *Mon. Not. R. astr. Soc.* 202, pp 595-604, and ref. therein.
21. Klypin, A.A. and Shandarin, S.F. 1982 preprint.
22. Frenk, C., White, S.D.M. and Davis, M. 1983 *Astrophys. J.*, in press; White, S.D.M., Frenk, C. and Davis, M. 1983 *Rencontre de Moriond, Astrophysics*.
23. Zeldovich, Ya.B., Einasto, J. and Shandarin, S.F. 1982 *Nature*, 300, 407-413, and refs. therein.
24. Oort, J. 1983 *Ann. Rev. Astron. and Astrophys.* in press and refs. therein.
25. Kaiser, N. Berkeley preprint.
- 25a. Bond, J.R. 1983 *Rencontre de Moriond, Astrophysics*; Shapiro, P.R., Struck-Marcell, C. and Melott, A.L. 1983 preprint.
26. Bond, J.R., Szalay, A.S. and White, S.D.M. 1983 *Nature*, 301, pp 584-585.
27. Press, W.H. and Davis, M. 1982 *Astrophys. J.*, 259, pp 449-473.
28. Forman, W. and Jónes, C. 1982 *Ann. Rev. Astron. Astrophys.* 20, pp 547-585.
29. Faber, S.M. 1982 *Astrophysical Cosmology* (eds. Bruck, H., Coyne, G. and Longair, M.), pp 191-234.
30. Gunn, J.E. 1982 *ibid.*
31. Faber, S.M. and Lin, D.N.C. 1983 *Astrophys. J. (Lett.)* 266, pp L17-L20.
32. Aronson, M. 1983 *Astrophys. J. (Lett.)* 266, pp L11-L15.
33. Lin, D.N.C. and Faber, S.M. 1983 *Astrophys. J. (Lett.)* 266, pp L21-L25.
34. Tremaine, S.D. and Gunn, J.E. 1979 *Phys. Rev. Lett.* 42, pp 407-410.
35. Steigman, G. 1979 *Ann. Rev. Astron. Astrophys.* 17, pp 135-
36. Primack, J.R. 1981 *Proc. 1981 Banff Summer Institute on Particles and Fields*, in press.
37. Bond, J.R., Szalay, A.S. and Turner, M.S. 1982 *Phys. Rev. Lett.* 48, pp 1636-1639.
38. Blumenthal, G.R., Pagels, H. and Primack, J.R. 1982 *Nature*, 299, pp 37-38.
39. Savoy, C.A. 1983 *Rencontre de Moriond, Elementary Particles*.
40. Ellis, J. 1983 private communication.
41. Goldberg, H. 1983 *Phys. Rev. Lett.* 50, pp 1419-1422.
42. Olive, K.A. and Turner, M.S. 1982 *Phys. Rev. D* 25, pp 213-216.

43. Harrison, E.R. 1970 *Phys. Rev. D1*, pp 2726-2730; Peebles, P.J.E. and Yu, J.T. 1970 *Astrophys. J.*, 162, pp 815-836; Zeldovich, Ya.B. 1972 *Mon. Not. R. astr. Soc.* 160, pp 1P-3P.
44. Lubin, P.M., Epstein, G.L. and Smoot, G.F. 1983 *Phys. Rev. Lett.* 50, pp. 616-619; Fixin, D.J., Cheng, E.S. and Wilkinson, D.T. 1983 *Phys. Rev. Lett.* 50, pp 620-622.
45. Olive, K.A. 1983 *Rencontre de Moriond, Astrophysics*.
46. Guyot, M. and Zeldovich, Ya.B. 1970 *Astron. Astrophys.* 9, pp 227-231; Meszaros, P. 1974 *Astron. Astrophys.* 37, pp 225-228.
47. Doroshkevich, A.G., Zeldovich, Ya.B., Sunyaev, R.A. and Khlopov, M.Yu. 1980 *Sov. Astron. Lett.* 6, pp 252; Chernin, A.D. 1981 *Sov. Astron.* 25, pp 14-16.
48. Peebles, P.J.E. 1980 *The Large Scale Structure of the Universe*, Princeton Univ. Press.
49. Peebles, P.J.E. 1982 *Astrophys. J. (Lett.)* 263, pp L1-L5; *Astrophys. J.*, 258, pp 415-424.
50. Dekel, A. 1982 *Astrophys. J. (Lett.)* 261, pp. L13-L17.
51. Sargent, W.L.W., Young, P. and Schneider, D.P. 1981 *Astrophys. J.*, 256, pp 374-385.
52. White, S.D.M. and Rees, M. 1977 *Mon. Not. R. astr. Soc.*
53. Silk, J. 1983 *Nature*, 301, pp 574-578.
54. Davis, M., Efstathiou, G., Frenk, C. and White, S.D.M. 1983 *private communication*.
55. Schechter, P. 1983 *private communication*.
56. Peccei, R. and Quinn, H. 1977 *Phys. Rev. Lett.* 38, pp 140.
57. Weinberg, S. 1978 *Phys. Rev. Lett.* 40, pp 223; Wilczek, F. 1978 *Phys. Rev. Lett.* 40, pp 279.
58. Abbott, L. and Sikivie, P. 1983 *Phys. Lett.* 120B, pp 133; Dine, M. and Fischler, W. 1983 *Phys. Lett.* 120B, pp 137; Preskill, J., Wise, M. and Wilczek, F. 1983 *Phys. Lett.* 120B, pp. 127; Ipser, J. and Sikivie, P. 1983 *Phys. Rev. Lett.* 50, pp 925.
59. Dicus, D., Kolb, E., Teplitz, V. and Wagoner, R. 1978 *Phys. Rev. D18*, pp 1829; Fukugita, M., Watamura, S. and Yoshimura, M. 1982 *Phys. Rev. Lett.* 48, pp. 1522.
60. Wilczek, F. 1982 *preprint* NSF-ITP-82-100.
61. Blumenthal, G.R. and Primack, J.R., *in preparation*.
62. Press, W.H. and Vishniac, E.T. 1980 *Astrophys. J.*, 239, pp 1-11.
63. Gott, J.R. 1977 *Ann. Rev. Astron. Astrophys.* 15, pp 235-266.
64. Rees, M.J. and Ostriker, J.P. 1977 *Mon. Not. R. astr. Soc.* 179, pp 541-559.
65. Blumenthal, G.R., Faber, S.M., Primack, J.R. and Rees, M., *in preparation*.
66. Peebles, P.J.E. 1983 *Rencontre de Moriond, Astrophysics*.
67. Dekel, A. 1983 *Astrophys. J.*, 264, pp 373-391.
68. Ferris, T. 1982 *The New York Times Magazine*, Sept. 26, 1982, pp 38.
69. Neumann, E. 1954 *Origins and History of Consciousness*, Princeton Univ. Press.
70. Weisskopf, V.F. 1962 *Knowledge and Wonder*, Hinemann.

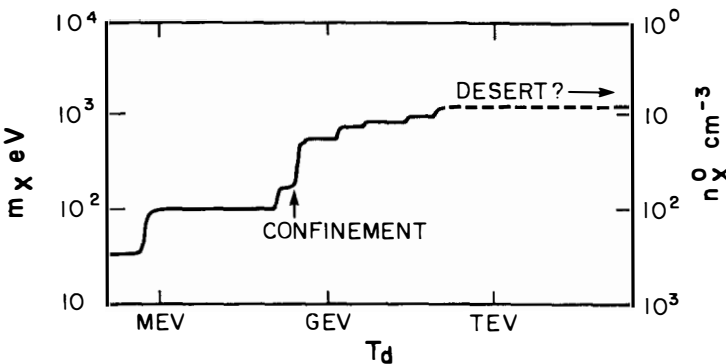


Figure 1. The mass m_X and present number density n_X^0 of warm dark matter particles X, calculated assuming the standard particle physics model and no entropy generation. The mass scale should be multiplied by the factor $h^2 \Omega$.

TYPE	δ vs M	M_t / M_b vs M	DWARF GALAXIES	$z_{\text{GAL}} > 2$	FILAMENTS & VOIDS
HOT	^	/	🚫	🚫	✓
WARM	~	~	🚫 ?	✓	?
COLD	—	---	✓	✓	?

$\log M / M_\odot$

Figure 2. Consumers' Guide to dark matter. The circle with a bar means trouble and the box with a check means consistency.

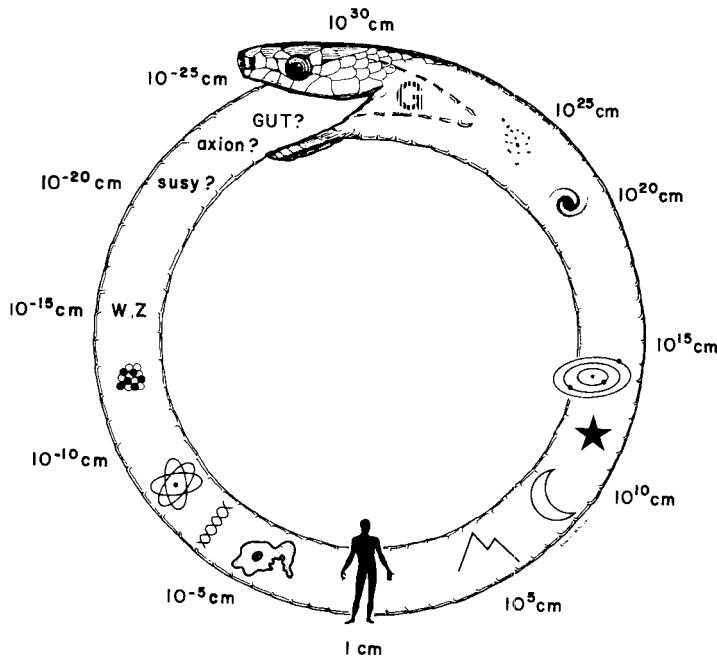


Figure 3. Physics Uroboros (after Glashow (68)).

COSMOLOGICAL NEUTRINOS AND THEIR DETECTION

Paul Langacker

Department of Physics, University of Pennsylvania
Philadelphia, Pennsylvania 19104, U.S.A.

The predictions of the standard cosmological model and its variations for the cosmological relic neutrinos are discussed. It is shown that the detection of the relic neutrinos could provide important information concerning (a) a possible anisotropic expansion in the early universe, (b) a possible large lepton asymmetry of the present and early universes (which could only occur if the universe did not undergo a major inflationary period), and (c) the magnitude, nature (Majorana or Dirac), and origin of the masses of the light neutrinos. In particular it is shown that if the lightest neutrino has a Majorana mass in the 10eV range then for a large class of models any large initial lepton asymmetry would have been reduced to a fixed point of order unity prior to nucleosynthesis. This is precisely the range that would substantially modify the usual nucleosynthesis scenario and therefore alter the standard limits on the number of neutrino flavors and other sources of energy density and the determination of the baryon density. Finally, the possibility of detecting the relic neutrinos is discussed. In particular, it is shown that recent proposals to detect the neutrinos by their coherent interaction with matter are incorrect. A general theorem is established that the momentum, energy, and angular momentum transferred from the neutrinos to a macroscopic or microscopic unpolarized detector vanishes to first order in the weak interactions.

The Standard Hot Big Bang Model

The major tests of the standard hot big bang cosmological model include the Hubble expansion of distant galaxies (which is sensitive to the relatively late period $T \lesssim 10^0$ K when the galaxies formed), the $T_0 = 2.7^0$ K microwave radiation (which probes back to the time of photon decoupling at $T_Y \sim 4000$ K, $t_Y \sim 4 \times 10^5$ yr), and the primordial nucleosynthesis of light elements (for which the relevant event is the freeze-out of the neutron/proton ratio at $T_{n/p} \sim 1$ MeV, $t_{n/p} \sim 1$ sec). In addition, the standard model and its variations predict the existence of a sea of cosmological relic neutrinos¹⁾ which, if they could be detected and studied, could give a wealth of complementary information from the same period as primordial nucleosynthesis.

In the standard model the neutrinos were kept in equilibrium in the early universe by ordinary charged and neutral current scattering processes such as $v\bar{v} \leftrightarrow v\bar{v}$, $e^-\bar{e}'$, $\nu\bar{\nu} \leftrightarrow \bar{\nu}\bar{\nu}$, etc. as long as the reaction rate

$$\Gamma_R = \langle \sigma v \rangle_T n_a(T) \sim (G_F^2 T^2) (g_*^! T^3) \sim g_*^! G_F^2 T^5 \quad (1)$$

exceeded the expansion rate

$$H = \frac{\dot{R}}{R} = \frac{1}{2t} = \sqrt{\frac{8\pi G\rho}{3}} \simeq 1.66 g_*^! T^2 / m_P \quad (2)$$

In (1) and (2), $\langle \rangle$ denotes a thermal average at temperatures T , $n_a \simeq 1.2 g_*^! T^3 / \pi^2$ is the density of target particles, R is the scale parameter, ρ is the energy density, $m_P = G^{-1/2} = 1.2 \times 10^{19}$ GeV is the Planck mass, $g_* = g_B + \frac{7}{8} g_F$ and $g_*^! = g_B + \frac{3}{4} g_F$, where $g_B(g_F)$ is the number of light boson (fermion) degrees of freedom at T . For $T \gtrsim 1$ MeV, $g_* \simeq g_*^! \simeq 10$. Comparing (1) and (2) we see that the neutrinos stayed in equilibrium until T dropped to a decoupling temperature

$$T_D \simeq (G_F^2 m_P)^{-1/3} \simeq 1 \text{ MeV}, \quad (3)$$

which occurred at a time $t_D \sim 1$ sec. after the big bang.

At the time of decoupling the phase space distribution functions $F_{\nu_i}(p)$ for the i^{th} neutrino species were therefore given by the equilibrium functions

$$F_{\nu_i}(p) = F_{\text{eq}}(p, m_i, \mu_{D_i}, T_D) \equiv \frac{1}{\exp \left\{ \frac{\sqrt{p^2 + m_i^2} - \mu_{D_i}}{T_D} \right\} + 1} \quad (4)$$

$$F_{\bar{\nu}_i}(p) = F_{\text{eq}}(p, m_i, -\mu_{D_i}, T_D)$$

where m_i is the mass of ν_i and μ_{D_i} is a possible chemical potential which distinguishes between ν_i and $\bar{\nu}_i$.

For $T \ll T_D$ ($t \gg t_D$) the interaction rate was negligible compared to H . Hence (in most models) these relic neutrinos should still exist in the present universe, essentially undisturbed since t_D except for a redshifting of their momenta by the

expansion of the universe.

If the universe expanded by a factor $\eta \equiv R(t_0)/R(t_D)$ between t_D and the present (t_0) then an individual neutrino with initial momentum \vec{p}' would be redshifted to a final momentum $\vec{p} = \vec{p}'/\eta$. (An intuitive way to see this is to consider a quantum mechanical particle with momentum $\vec{p} = \vec{p}/\hbar/2R$ in a box of linear dimension R , where the n_i are integers. Clearly $\vec{p}' \rightarrow \vec{p} = \vec{p}'/\eta$ as the box adiabatically expands to size ηR). The phase space volume element $d\tau = d^3x d^3p/h^3$ is left invariant by the expansion, so the phase space density $F_{\nu_i}(p)$ of the decoupled neutrinos in the present universe is the same as that at t_D , except the equilibrium form in (4) must be evaluated at the larger momentum $\vec{p}' = \eta \vec{p}$ which redshifted into \vec{p} . That is

$$F_{\nu_i}(p) = F_{eq}(p', m_i, \mu_{D_i}, T_D) = \frac{1}{\exp\left\{\frac{\sqrt{p'^2 + m_{eff,i}^2} - \mu_i}{T_V}\right\} + 1} \quad (5)$$

The last expression has been written in terms of rescaled effective variables

$$T_V \equiv \frac{T_D}{\eta} = \left(\frac{4}{11}\right)^{1/3} T_0 \approx 1.9^0 K \approx 1.7 \times 10^{-4} \text{ eV} \quad (6)$$

(T_V is smaller than the present photon temperature T_0 due to the reheating of the photons from $e^+ e^-$ annihilation at $T \sim 4 \times 10^9$ $^0 K$),

$$m_{eff,i} \equiv \frac{m_i}{\eta} = m_i \frac{T}{T_D} \quad (7)$$

and

$$\mu_i \equiv \frac{\mu_{D_i}}{\eta} = \mu_{D_i} \frac{T_V}{T_D} \quad . \quad (8)$$

Hence, the distributions maintain a thermal form with an effective "temperature" T_V long after decoupling. Note that it is the effective mass $m_{eff,i} = m_i/\eta$ which appears. Hence, if the neutrinos were relativistic at decoupling ($m_i \ll T_D$) then F_{ν_i} is of relativistic form even if $T_V \ll m_i$, because there were no interactions to reduce F_{ν_i} to a non-relativistic distribution. Also, the ratio $\xi_i = \mu_i/T_V$ of effective chemical potential to temperature is constant for an adiabatically expanding universe provided that lepton number L_i is conserved (this is true before decoupling as well).

In the standard model it is usually assumed that $|\xi_i| \ll 1$. Assuming $m_i \ll T_D$ as well we therefore have

$$n_{\nu_i} = \bar{n}_{\bar{\nu}_i} = \int \frac{d^3p}{h^3} \frac{1}{e^{p/T} + 1} \approx 50/\text{cm}^3 \quad . \quad (9)$$

For three flavors of neutrinos this implies a very large density $n_{tot} \sim 300/\text{cm}^3$ of ν 's and $\bar{\nu}$'s. The average momentum and energy are

$$\langle p \rangle \approx 3.2 T_V \approx 6.0^0 K \approx 5.2 \times 10^{-4} \text{ eV} \quad (10a)$$

$$\langle E \rangle = \begin{cases} \langle p \rangle, m_i \ll T_\nu \\ m_i, m_i \gg T_\nu, \end{cases} \quad (10b)$$

and the corresponding average velocity is

$$\frac{\langle v \rangle}{c} \sim \frac{\langle p \rangle}{\langle E \rangle} \sim \begin{cases} 1, & m_\nu \sim 0 \\ 2 \times 10^{-5}, & m_\nu \sim 30 \text{ eV} \end{cases} \quad (11)$$

If m_{ν_i} has a 30 eV mass the neutrinos are moving very slowly (even though $F_{\nu_i}(p)$ has a relativistic form). The flux of neutrinos is

$$j_\nu \sim j_{\bar{\nu}} \sim n \langle v \rangle \sim \begin{cases} 10^{13}/\text{cm}^2 \text{ s}, & m_\nu = 0 \\ 10^8/\text{cm}^2 \text{ s}, & m_\nu = 30 \text{ eV} \end{cases} \quad (12)$$

The predicted flux for massless neutrinos is very large: it is comparable to the flux of $\bar{\nu}$'s at reactors and much larger than the estimated flux²⁾ of solar neutrinos ($\approx 6 \times 10^{10}/\text{cm}^2\text{-s}$) or of high energy ${}^8\text{B}$ neutrinos ($\approx 3 \times 10^6 \text{ cm}^2\text{-s}$) presumably measured in the Davis experiment²⁾. As we shall see, however, the extremely low energy of the neutrinos renders their detection incredibly difficult.

Before proceeding to variations on the standard model it should be commented that if the neutrinos are massive then within the galaxy they would be speeded up to typical speeds of $v_{\text{gal}} \approx 300 \text{ Km/s}$, implying enhancement of $\langle p \rangle$ and j of ≈ 50 . Such massive neutrinos could possibly provide the dark matter in galactic clusters³⁾ and could dominate the dynamics of the universe.⁴⁾ Furthermore, if they cluster on the scale of galaxies then the local density in our galaxy could be enhanced by as much as 10^5 (Fermi statistics allow n_{ν_i} as large as $m_i^3 v_{\text{gal}}^3 / 6\pi^2 \hbar^3 \approx 6 \times 10^7 (m_i/30 \text{ eV})^3 \text{ cm}^{-3}$). These issues are currently under intense debate³⁾ and will not be discussed further here.

It should also be remarked that there is one sensible model⁵⁾ (in which the neutrinos have a Majorana mass generated by a Higgs triplet) in which the neutrinos annihilated⁶⁾ into Majorons (massless Goldstone bosons associated with the spontaneous violation of lepton number) at $T \lesssim m_\nu$, so that there would be no neutrinos in the present universe.

I now turn to two variations on the standard cosmological model.

Lepton Asymmetric Cosmologies

A possible asymmetry between neutrinos and antineutrinos enhances the number density and average neutrino momentum. From (5) the neutrino energy density for $m_{\nu_i} \ll T_\nu$ is⁷⁾

$$\rho_{\nu_i} + \rho_{\bar{\nu}_i} = \frac{\pi^2}{15} T_\nu^4 \left[\frac{7}{8} + \frac{15}{4\pi^2} \xi_i^2 + \frac{15}{8\pi^4} \xi_i^4 \right], \quad (13)$$

where $\xi_i \equiv \nu_i/T_\nu$ is constant for an adiabatically expanding universe if i-type lepton number is conserved. Similarly, the lepton asymmetry is

$$L_i \equiv \frac{n_{e_i^-} - n_{e_i^+} + n_{\nu_i} - n_{\bar{\nu}_i}}{n_\gamma} \approx \frac{n_{\nu_i} - n_{\bar{\nu}_i}}{n_\gamma} = \frac{2}{3} \left(\frac{T_\nu}{T_\gamma} \right)^3 (\xi_i + \frac{1}{\pi^2} \xi_i^3) \quad (14)$$

For large $|\xi_i|$, (13) and (14) reduce to the usual formulas for a degenerate Fermi gas. It is usually assumed⁸⁾ that the lepton asymmetry is negligibly small. This would be expected in most grand unified theories because the lepton number violating interactions would first reduce any initial asymmetry to zero and then create a new asymmetry comparable to the baryon asymmetry $n_B/n_\gamma \sim 10^{-10}$. However, Harvey and Kolb⁹⁾ have shown that it is possible to have large asymmetries subsequent to the GUT epoch if (a) there is a large initial asymmetry in L_i or some related quantity and (b) there is an approximately conserved quantum number. Realistic cosmologies^{10,11)} allow $|L_i| \gtrsim 0(1)$. Inflationary models¹²⁾ predict $|L_i| \ll 1$ because any large asymmetries will be diluted to negligible levels during the inflationary phase. Subsequent reheating should produce small L_i comparable to n_B/n_γ .

Linde¹³⁾ has pointed out a very interesting feature of lepton asymmetric cosmologies. In most field theories (excepting some with complicated Higgs structures) broken symmetries are restored at sufficiently high temperatures, i.e. the effective vacuum expectation value (VEV) $v(T) \equiv \langle \phi \rangle_T$ of a Higgs field ϕ goes to zero for $T \gg v(0)$ because of the positive interaction energy between ϕ and the plasma of gauge and Higgs fields at temperature T . However, Linde argued that a large lepton asymmetry L would prevent symmetry restoration. In fact, $v(L, T) \equiv \langle \phi \rangle_{L, T}$ actually grows linearly in T for $T \gg v(0)$ if $|L|$ is larger than a critical value L_c of order unity. This is due to a negative energy associated with the interaction of ϕ with the asymmetric neutrinos (mediated by Z 's). The behavior of $v(L, T)^2/T^2$ as a function of L^2 is shown in Figure 1.

Segrè, Soni, and I^{10,14)} have recently considered the role of a Majorana (lepton number violating) neutrino mass in reducing a possible large initial lepton asymmetry prior to nucleosynthesis (where a lepton asymmetry would play a significant role, as described below). The idea is that a Majorana mass term violates lepton number by two units. There is therefore an amplitude $\propto m_{\nu_i}/E_\nu$ for a neutrino to be changed into an antineutrino or positron in a neutral or charged current scattering process.

In the early universe an initial asymmetry would therefore be reduced at a rate

$$\frac{dL_i}{dt} = - 2n_a L_i \langle v\sigma \rangle \quad , \quad (15)$$

where n_a is the density of target particles and $\langle v\sigma \rangle \approx a g^4 m_{\nu_i}^2/T^4$, with $a \approx 10^{-2} - 10^{-3}$. m_{ν_i} is presumably produced by some sort of Higgs mechanism and is therefore itself a function of $L \equiv \sum_i L_i$ and T . We have studied two particular

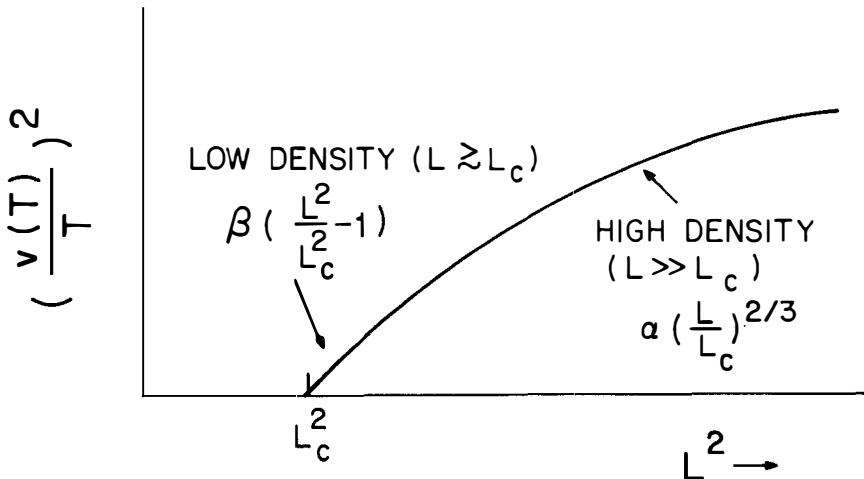


Figure 1. $v(L,T)^2/T^2$ as a function of L^2 for $T \gg v(0)$. It is seen that $v \neq 0$ for $|L| > L_c$. α , β , and L_c are model dependent, but typically of order unity. In the $SU_2 \times U_1$ model, $L_c \approx 2.3 (1 + \lambda/2.8e^2)^{1/2}$, where λ is the quartic Higgs coupling.

models in detail: (a) the triplet model¹⁵⁾ in which $m_{\nu_i}(L,T) = H_i v(L,T)$; $v(L,T) = \langle \chi^0 \rangle_{L,T}$ is the VEV of the neutral member of a Higgs triplet and H_i is the Yukawa coupling in the interaction $L = H_i \ell_i \ell_i^\dagger \chi^\dagger$ of χ to the lepton doublet $\ell_i = (\nu_i, e^-)_L$. If there is no explicit lepton number violation in the model (e.g. from a $\phi \phi \chi^\dagger$ coupling, where ϕ is the Higgs doublet) then L violation is spontaneous and the theory involves a Goldstone boson (Majoron) M which couples mainly to neutrinos. (b) The other model is the singlet model¹⁶⁾, in which one introduces an $SU_2 \times U_1$ singlet neutrino field N with a very large Majorana mass M_N . Then the ordinary doublet neutrino acquires a small Majorana mass $m_{\nu_i}(L,T) \approx h_i^2 v(L,T)^2/M_N$, where $v(L,T)$ is the VEV of the ordinary Higgs doublet ϕ^0 and h_i is the Yukawa coupling between ν_i and N_R .

We therefore have that the rate of erasure of L_i is proportional to $v(L,T)^2$ or $v(L,T)^4$, where $v(L,T)$ is the relevant VEV for the triplet or singlet model, respectively. One would normally expect $v(L,T)$ and hence $m_{\nu_i}(L,T)$ to be small or zero at high temperature so that dL_i/dT is unimportant. However, we have seen (Figure 1) that this is not the case for $L \equiv \sum L_i > L_c$.

We have shown¹⁰⁾ that for a wide class of large initial asymmetries in both models the asymmetries are reduced to a fixed point $L_1 \rightarrow L_c$ and $L_2, L_3, \dots \rightarrow 0$ for $T \gg M_W$, where the neutrino species are labeled by $m_{\nu_1}(0) < m_{\nu_2}(0) < m_{\nu_3}(0) \dots$. This is because the asymmetries in the more massive species are reduced most rapidly so that eventually only L_1 remains. L_1 is then reduced to L_c at which

point the mechanism turns itself off (i.e. $v \rightarrow 0$). The asymmetries then remain constant until $T \ll M_W$. Then L_1 is diluted to $\approx L_c/10$ due to the production of additional photons from $q\bar{q}$ and $\mu^+\mu^-$ annihilation. It is this value that is relevant to nucleosynthesis. In the singlet model, the final value of L_1 ranges from 0.23 to 1.0 as the quartic Higgs coupling λ (Higgs mass m_H) varies from $\lambda \ll e^2$ ($m_H \sim 10$ GeV) to $\lambda = 8\pi/3$ ($m_H \sim 1$ TeV). In the triplet model, L_1 depends on unknown Higgs parameters, but is typically of order unity.

The behavior of L_1 as a function of T^{-1} is shown for the two models in Figure 2. Two additional events occur after nucleosynthesis in the triplet model:

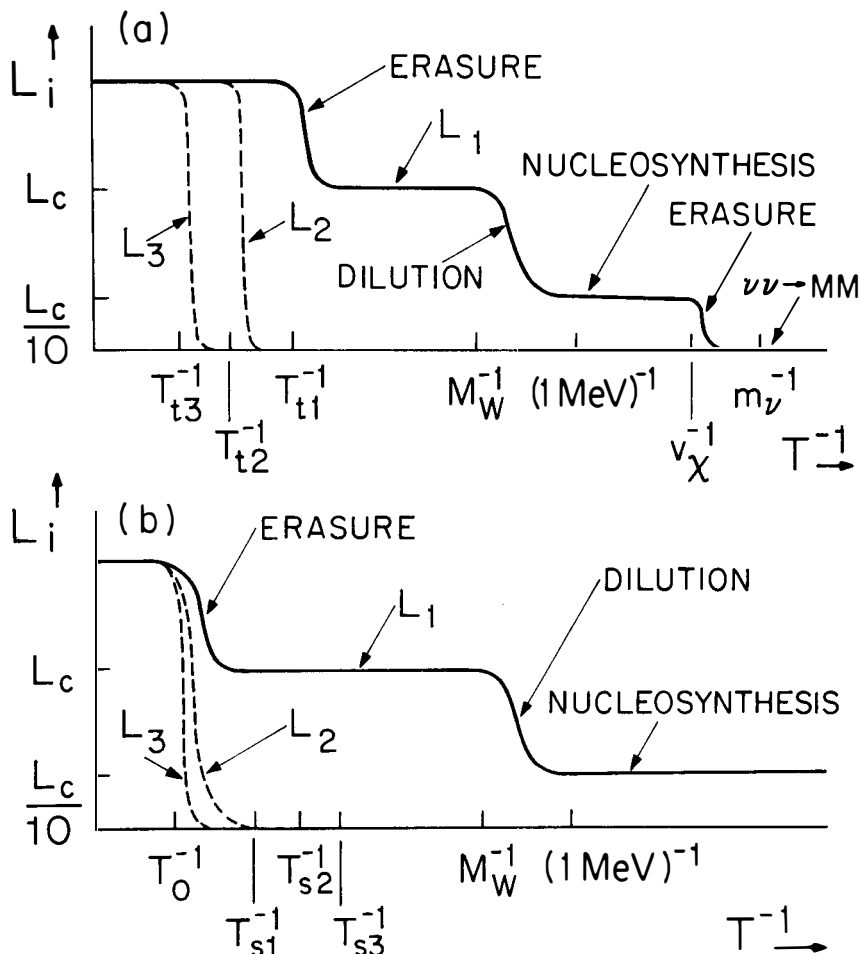


Figure 2. The lepton asymmetries as a function of T^{-1} in the triplet (top) and singlet (bottom) models.

(i) The asymmetry is driven to zero by $\nu\nu + M \rightarrow \bar{\nu}\bar{\nu}$, where M is the Majoron, for $T \lesssim v_\chi(0)$. (ii) Neutrinos disappear⁶⁾ entirely due to $\nu\nu \rightarrow MM$ for $T < m_\nu(0)$.

Anisotropic Cosmologies

The relic neutrinos can in principle be used to limit¹⁷⁾ the possible anisotropy in the expansion of the universe between neutrino decoupling at $T_D \sim 1$ MeV and photon decoupling at $T_\gamma \sim 4000^0$ K. (The approximate isotropy of the microwave radiation to one point in 10^3 rules out any significant anisotropy subsequent to T_γ). Prior to T_D the neutrino distribution F_{ν_i} would have been maintained in the isotropic equilibrium form (5) by collisions even if the universe were expanding anisotropically. If, for example, the universe expanded by a factor $\eta_i \equiv R_i(t_0)/R_i(t_D)$ in the i^{th} rectangular direction between decoupling and the present then the present distribution is easily computed to be (for $|\xi_i| \ll 1$,

$$m_i \ll T_D$$

$$F_{\nu_i}(\vec{p}) = \frac{1}{\exp[(\gamma_1^2 p_1^2 + \gamma_2^2 p_2^2 + \gamma_3^2 p_3^2)^{1/2}/T_\nu] + 1}, \quad (16)$$

where $T_\nu = T_D/(\eta_1 \eta_2 \eta_3)^{1/3}$ and where the parameters $\gamma_i \equiv \eta_i/(\eta_1 \eta_2 \eta_3)^{1/3}$ measure the anisotropy of the expansion. Since $\gamma_1 \gamma_2 \gamma_3 = 1$ one still has the number densities $n_{\nu_i} \approx n_{\nu_i} \approx 50/\text{cm}^3$ (these would be reduced if the decay of the anisotropic shear created extra photons¹⁸⁾). However, the neutrino momentum distribution would be anisotropic. More important, the average neutrino energy (for $m_\nu \approx 0$) would be increased from (10a) by a factor of order γ_{\min}^{-1} , where γ_{\min} is the smaller of γ_1 , γ_2 , and γ_3 .

Limits on γ_{\min} from the relic neutrinos will be discussed below. Other possible implications of anisotropy are the creation of entropy and particles by dissipation¹⁸⁾, galaxy formation¹⁹⁾, a modification of the baryosynthesis scenario in GUTs²⁰⁾, and a modification of nucleosynthesis (the anisotropic shear energy raises the helium abundance but the anisotropy in the neutrino distribution decreases it²¹⁾). Anisotropy may also lead to fine tuning problems²²⁾ to avoid modes in which the anisotropy grows. A substantial inflationary phase prior to decoupling would destroy a moderate preexisting anisotropy²³⁾ and therefore imply $\gamma_i = 1$, while large initial anisotropies present inflation²³⁾.

Limits and Detection Possibilities

We have seen that a direct study of the relic neutrinos could provide a great deal of information relevant to both particle physics and cosmology. We will now see, however, that the prospects for such a direct detection are extremely discouraging.

Astrophysical Limits

There are several types of indirect astrophysical limits on the properties of the relic neutrinos. Many authors²⁴⁾ have considered the scattering of high

energy cosmic rays of energy $E = \gamma m_p$ by the relic neutrinos, which in principle can distort the primary cosmic ray spectrum and also produce high energy scattered neutrinos. However, the cross section (for $E_{VL} < m_p$)

$$\sigma \sim G_F^2 E_{VL}^2 \approx 10^{-56} \text{ cm}^2 \left(\frac{E_{VL}}{1 \text{ eV}} \right)^2, \quad (17)$$

where

$$E_{VL} = \begin{cases} \gamma p_\nu (1 - \hat{p}_\nu \cdot \hat{p}_p), & m_\nu \ll p_\nu \\ \gamma m_\nu, & p_\nu \ll m_\nu \end{cases} \quad (18)$$

is the neutrino energy in the proton rest frame, is much too small to yield interesting results unless there are enormous deviations from the standard model. Using the order of magnitude criterion of Cowsik, et al²⁴⁾ that a 10^{18} eV proton could have suffered no more than 14 collisions in 50 million years one finds^{17, 24)} the weak limits

$$|\xi_i| < \begin{cases} 1.4 \times 10^4, & m_{\nu_i} = 0 \\ 160, & m_{\nu_i} = 30 \text{ eV} \end{cases} \quad (19)$$

for the lepton asymmetry, and

$$\gamma_{\min} > 5 \times 10^{-9}, \quad (\langle E \rangle < 100 \text{ KeV}) \quad (20)$$

for the anisotropic expansion between T_D and T_γ . Weiler²⁴⁾ has recently made the interesting suggestion that if the neutrinos have a mass in the 30 eV range then the resonant process $\nu\bar{\nu} \rightarrow Z$ could lead to a dip in the spectrum of very high energy ($E \sim 10^{11 \pm 1}$ GeV) primary neutrinos. However, such an effect would only be measurable if the (unknown) primary ν flux was enormous (several orders of magnitude larger than the proton flux at comparable energies).

Clarke, et al.²⁵⁾ have discussed the very tiny optical activity for radio waves in intergalactic space induced by the relic neutrinos.

More stringent limits can be obtained from the requirement that the neutrino energy density ρ_ν not exceed the upper limit²⁶⁾ $\rho_0 < 8 \times 10^{-29} \text{ gm/cm}^3$ of the present universe. For massless non-degenerate neutrinos this is easily satisfied. One has

$$\rho_\nu = \frac{7\pi^2}{15 \times 16} T_\nu^4 g = 4 \times 10^{-6} \rho_0 \quad (21)$$

where g is the number of neutrino helicity states. For massive non-degenerate neutrinos²⁷⁾, on the other hand,

$$\rho_\nu = 2 n_{\nu_i} \sum m_{\nu_i} = \frac{\rho_0}{400 \text{ eV}} \sum m_{\nu_i} \quad (22)$$

so that the sum of the masses of the light stable neutrinos cannot exceed 400 eV. (A comparable but independent estimate on $\sum m_{\nu_i}$ is obtained²⁸⁾ from the requirement that neutrino friction not damp peculiar galactic motions.) Similarly, for massless degenerate neutrinos one has^{29,30)}

$$\left[\sum_i \xi_i^4 \right]^{1/4} < 80 , \quad (23)$$

while for $m_{\nu_i} = (20-30)$ eV,

$$|\xi_i| < 6 \quad (24)$$

The latter limit can be strengthened³⁰⁾ to $|\xi_i| < 3-4$ by various considerations concerning galaxy formation. Finally, one has¹⁷⁾ the limit

$$\gamma_{\min} > 4 \times 10^{-6} \quad (\langle E \rangle < 400 \text{ eV})$$

on anisotropy from the present energy density. This limit can be considerably strengthened^{17,22)} by the observation that the universe has expanded isotropically since photon decoupling at $T_{\gamma} \sim 4000^{\circ}\text{K}$. Hence, the neutrinos, with their anisotropic momentum distribution, should not have dominated the universe at T_{γ} , implying

$$\rho_{\nu}(T_{\gamma}) = \rho_{\nu}(T_0) \left(\frac{T_{\gamma}}{T_0} \right)^4 < \rho_{\text{matter}}(T_{\gamma}) < \rho_0 \left(\frac{T_{\gamma}}{T_0} \right)^3 , \quad (25)$$

so that

$$\gamma_{\min} > 6 \times 10^{-3} \quad (\langle E \rangle < 0.085 \text{ eV} \sim 10^3 \text{ }^{\circ}\text{K}) \quad (26)$$

Finally, one has the constraint of primordial nucleosynthesis^{31,1)}. The neutron to proton ratio was kept in equilibrium by $v_e n \leftrightarrow e^- p$, $\bar{v}_e p \leftrightarrow e^+ n$ until they froze out at the value

$$\left(\frac{n_n}{n_p} \right)_{T_D} = \exp \left\{ - \frac{(m_n - m_p)}{T_D} + \xi_{\nu_e} \right\} \quad (27)$$

Most of the neutrons were eventually incorporated into He^4 . For $\xi_{\nu_e} = 0$ the He^4 abundance is correctly predicted and the D abundance (which depends more sensitively on the baryon abundance) leads to the precise determination $n_B/n_{\gamma} = (4 \pm 1) \times 10^{-10}$. This implies a low baryon density universe with $0.01 < \Omega_N < 0.1$, where Ω_N is the ratio of baryon density to critical density. Furthermore, extra sources of energy density would speed up the expansion leading to more He^4 (because of a higher T_D and less β decay). Hence, one obtains the limits $N_{\nu} \leq 4$ on the number of light neutrino flavors, on the monopole density, etc.

Many authors³²⁾ have considered the modifications due to lepton asymmetries. $\xi_{\nu_e} > 0$ decreases the n/p ratio and the abundance of He^4 while $|\xi_{\nu_{\mu}}|$, $|\xi_{\nu_{\tau}}| \neq 0$ can increase the amount of He^4 because of the speedup. David and Reeves³¹⁾ in particular have shown that these effects can be balanced: ξ_{ν_e} as large as $0(1)$

can be tolerated provided it is compensated by extra energy density, which can be provided by extra neutrino flavors, magnetic monopoles, anisotropic shear, or $|\xi_i|$ ($i = \mu, \tau$) in the range 0-100. The required Ω_N increases to 0(1) as ξ_{ν_e} increases. Hence, the usual successful predictions of nucleosynthesis and the constraints derived from it would be lost if ξ_{ν_e} were of order unity. Note that this is precisely the fixed point range that would be obtained from a large initial asymmetry if ν_e were the lightest (Majorana) neutrino.¹⁰⁾

Laboratory Limits

In order to test the various ideas described above, it would clearly be extremely useful to be able to directly detect and study the relic neutrinos. Unfortunately, this appears to be extremely difficult if not impossible.

Conventional Scattering

The cross section for elastic scattering of a relic neutrino is

$$\sigma_{\nu} \sim G_F^2 E_{\nu}^2 \sim \begin{cases} 10^{-62} \text{ cm}^2, & m_{\nu} = 0 \\ 10^{-53} \text{ cm}^2, & m_{\nu} \approx 30 \text{ eV} \end{cases} \quad (28)$$

which is hopelessly small because of the small value of E_{ν} . One can achieve enhanced cross sections for (exothermic) induced β transitions³³⁾ of order $G_F^2 \Delta^2$, where Δ is the energy release. However, one finds that the absolute transition rate $0(j_{\nu} G_F^2 \Delta^2)$ and/or the ratio of signal to background (from spontaneous decay with rate $\sim G_F^2 \Delta^5$) is always extremely tiny. As emphasized by Weinberg³³⁾, the most prominent effects are modifications of the electron spectrum near the endpoint on the Kurie plot. For example, one has³⁴⁾ the limit $|\mu_{\nu_e}| < 60$ eV from tritium β decay (for $\mu_{\nu_e} < 0$ the spectrum would be cut off $|\mu_{\nu_e}|$ below the endpoint because the $\bar{\nu}_e$ levels are filled; for $\mu_{\nu_e} > 0$ the inverse reaction $\nu_e H^3 \rightarrow e^- He^3$ will produce electrons with energies up to μ_{ν_e} above the endpoint, in apparent violation of energy conservation), which is far less stringent than the cosmological limits on μ_{ν} . Similarly, anisotropy produces no significant effect on the β spectrum¹⁷⁾. If the electron neutrino has a mass in the 30 eV range then the inverse reaction would produce a peak m_{ν_e} above the endpoint. This would be a very dramatic signature, but even assuming that the neutrinos are clustered with density 10^7 cm^{-3} in the galaxy, one would need an enormous source of around a mole (10^5 Ci) of tritium to obtain a significant event rate of several hundred/day.³³⁾ This is to be compared with sources $\approx 10^{-3} \text{ Ci}$ typical of existing experiments and would imply a background rate for spontaneous decay of $\approx 10^{20}/\text{day}$.

Another possibility is to look for the scattering of high energy protons from an accelerator from the neutrinos in an evacuated pipe of length ℓ . However, the probability of scattering per proton is only (for $\ell \approx 100 \text{ m}$, $E_p = 10 \text{ TeV}$)

$$P = \sigma n_{\nu} \lambda \sim G_F^2 \left(\frac{E_p}{m_p} \right)^2 E_{\nu}^2 n_{\nu} \lambda \sim \begin{cases} 10^{-48}, m_{\nu} = 0 \\ 10^{-34}, m_{\nu} = 30 \text{ eV} \end{cases} \quad (29)$$

where $n_{\nu} = 10^7 \text{ cm}^{-3}$ was taken for the massive case.

This is hopelessly small, even ignoring practical difficulties from residual gas and from the tiny deflection of the elastically scattered proton.

Coherent Scattering

There have been several suggestions³⁵⁻³⁸⁾ that the relic neutrinos could be detected by their coherent interaction with matter.

The basic idea is to think of a low energy neutrino passing through matter as a wave with wavelength $\lambda = h/p \sim 2.4 \text{ mm}$. Since λ is large compared to the interatomic spacing the effect of the medium can be described by introducing an index of refraction n in the free field equation for the propagation of the neutrino wave. If λ is also small compared to the size of the scatterer, so that diffraction can be ignored, one can describe the propagation of a neutrino "ray" through matter by geometrical optics.

The index of refraction for $\nu(\bar{\nu})$ is given (for small $n-1$) by

$$n_{\nu, \bar{\nu}} - 1 = \frac{2\pi}{p^2} \sum_a n_a f_{\nu, \bar{\nu}}^a (0) \quad (30)$$

where n_a is the number density of scatterers of type a and $f_{\nu}^a(0)$ ($f_{\bar{\nu}}^a(0)$) is the forward scattering amplitude for νa ($\bar{\nu} a$) elastic scattering. For the $SU_2 \times U_1$ model, for example, one has for an iron target³⁹⁾

$$n_{\nu_e, \bar{\nu}_e} - 1 = \begin{cases} \pm 2.3 \times 10^{-10}, m_{\nu_e} = 0 \\ \pm 6.6 \times 10^{-6}, m_{\nu_e} = 30 \text{ eV} \end{cases} \quad (31)$$

and

$$n_{\nu_i, \bar{\nu}_i} - 1 = \begin{cases} \pm 3.1 \times 10^{-10}, m_{\nu_i} = 0 \\ \pm 8.9 \times 10^{-6}, m_{\nu_i} = 30 \text{ eV} \end{cases} \quad (32)$$

where $i = \mu$ or τ .

Several experiments have been proposed to measure the energy, momentum, or angular momentum transferred from the neutrino sea to a macroscopic target due to the refractive bending of a neutrino ray as it passes through the target or the total external reflection that might be expected for neutrinos incident on a surface with angle (with respect to the plane) $\theta < \theta_c \equiv \sqrt{2(1-n)}$ (for $n < 1$). It was claimed that such effects exist to first order in $n-1$ (i.e. first order in G_F)

and that they could be detected by devices not too much more sensitive than gravity wave detectors. Unfortunately, however, all but one³⁵⁾ of these proposals is incorrect^{39,40)} and the one exception is probably immeasurably small^{39,41)}. Rather than discuss the details and problems with the individual proposals, I will simply quote a general no-go theorem proved by Cabibbo and Maiani⁴⁰⁾ for special cases of massive neutrinos and independently in the general case by Leveille, Sheiman, and myself.³⁹⁾ If the time average of the neutrino flux is spatially homogeneous over the extent of the detector (which is expected for cosmological neutrinos) then to first order in the weak coupling the energy and momentum transfer to any microscopic or macroscopic target is zero.⁴²⁾ No assumption is needed concerning the isotropy of the neutrino flux. This theorem invalidates the proposals in Ref. 36-38 (see 39 for a discussion of the specific problems in each proposal). These results hold to first order in G_F , which is a good approximation as long as the detector size a is small compared with the optical free path

$$a < \frac{\lambda}{n-1} = \begin{cases} 10^7 \text{ m} & , m_\nu = 0 \\ 300 \text{ m} & , m_\nu = 30 \text{ eV.} \end{cases} \quad (33)$$

This is the case for feasible laboratory detectors. (Effects of $0(G_F^2)$ are expected to be immeasurably small.)

Similarly, the theorem states that the angular momentum transfer is zero unless i) the target has a non-zero polarization or current density; ii) there is a neutrino-antineutrino asymmetry, and iii) the neutrino flux is anisotropic. For example, if conditions (ii) and (iii) are satisfied there can be a net torque on an electron or ferromagnet. This reproduces an old result obtained in a somewhat different way by Stodolsky.³⁵⁾ However, for neutrino parameters consistent with the astrophysical bounds the effect is incredibly tiny^{39,41)}. For example, if the anisotropy is due to a motion of the target with speed $v_e/c \sim 10^{-3}$ through the rest frame of the neutrino sea (this is consistent with the anisotropy in the microwave photons and the typical motions of galaxies) and if the lepton asymmetries are of order unity, then the energy difference between an electron polarized parallel or antiparallel to v_e is of order 10^{-38} eV, which is tiny compared to magnetic energy differences $\approx 10^{-8}$ eV B(Gauss). (For a ferromagnetic, both signal and background are enhanced by the total number of polarized electrons.)

Summary and Conclusions

The standard hot big bang model predicts a large density (300 cm^{-3}) of very low momentum ($\langle p \rangle \sim 5 \times 10^{-4} \text{ eV}$) relic neutrinos left from the first second of the big bang. These neutrinos, if massive, could well control the dynamics of galaxies, clusters, and the universe as a whole. Their detection and study could

provide a useful verification of these ideas and could yield useful constraints on anisotropy, the existence of inflationary phases in the early universe, a possible lepton asymmetry, and on the value, nature (Majorana or Dirac) and origin of possible neutrino masses. In particular, if the neutrino has a Majorana mass in the 10 eV range then for a large class of models large initial asymmetries would be reduced to a fixed point of order unity prior to nucleosynthesis. In this case the usual limits on the baryon density of the universe and on the number of light neutrino species and other sources of energy would be lost.

Unfortunately, direct detection of the relic neutrinos to test these ideas appears to be virtually impossible. Their low energy makes detection via conventional scattering extremely unlikely. A general no-go theorem establishes that the coherent interaction of the neutrinos with matter vanishes to order G_F in almost all cases, and the one exception appears to be hopelessly small.

Acknowledgement

It is a pleasure to thank M. Cherry, A. Dar, G. Karl, E. W. Kolb, J. Learned, G. Steigman, R. Steinberg, M. Turner, and my collaborators J. Cohen, J. Leveille, G. Segre, J. Sheiman, and S. Soni for many useful discussions.

REFERENCES

1. General references on relic neutrinos include S. Weinberg, Gravitation and Cosmology (Wiley, New York, 1972); M. Turner in Weak Interactions as Probes of Unification, ed. G. B. Collins et al., AIP 72, 335 (1981); R. Cowsik in Neutrino Mass Miniconference, ed. V. Barger and D. Cline (U. Wisconsin, 1980) p. 50; E. W. Kolb, *ibid.* p. 61.
2. J. N. Bahcall, et al., *Phys. Rev. Lett.* 45, 945 (1980) and references therein.
3. See, for example, J. Primack, these proceedings and M. Turner, ref. 1.
4. R. Cowsik and J. McClelland, *Phys. Rev. Lett.* 29, 669 (1972). For recent discussions see J. Bernstein and G. Feinberg, *Phys. Lett.* 101B, 39 (1981) and 103B, 470(E) (1981); D. Schramm and G. Steigman, *Astrophys. J.* 243, 1 (1980), and references therein.
5. G. B. Gelmini and M. Roncadelli, *Phys. Lett.* 99B 411 (1981).
6. H. M. Georgi, S. L. Glashow and S. Nussinov, *Nucl. Phys.* B193, 297 (1981).
7. G. Beaudet and P. Goret, *Astron. Astro.* 49, 415 (1976).
8. S. Dimopoulos and G. Feinberg, *Phys. Rev. D20*, 1283 (1979); D. Schramm and G. Steigman, *Phys. Lett.* 87B, 141 (1979); D. V. Nanopoulos, D. Sutherland and A. Yildiz, *Lett. Nuovo Cimento* 28, 205 (1980); M. S. Turner, *Phys. Lett.* 98B, 145 (1981).
9. J. Harvey and E. W. Kolb, *Phys. Rev. D24*, 2090 (1980).
10. P. Langacker, G. Segre, and S. Soni, *Phys. Rev. D26*, 3425 (1982).
11. J. Fry and C. Hogan, *Phys. Rev. Lett.* 49, 1873 (1982).

12. A. Guth, Phys. Rev. D23, 347 (1981).
13. A. D. Linde, Phys. Rev. D14, 3345 (1976) and Rep. Prog. Phys. 42, 25 (1979).
14. P. Langacker and G. Segré, Phys. Rev. Lett. 49, 1363 (1982).
15. See References 5 and 6. For additional references, see 10.
16. M. Gell-Mann, P. Ramond, and R. Slansky, in Supergravity, ed. P. van Nieuwenhuizen and D. Z. Freedman (North Holland, Amsterdam, 1979) p. 315.
17. J. Cohen and P. Langacker, unpublished.
18. The dissipation of anisotropy is discussed in N. Caderni and R. Fabbri, Phys. Rev. D20, 1251 (1979); J. D. Barrow and R. A. Matzner, MNRAS 181, 719 (1977) and references therein. Dissipation in the GUT epoch is considered by J. D. Barrow, MNRAS 199, 45 (1982). Particle creation is considered by L. Parker in Asymptotic Structure of Space Time, ed. F. P. Esposito and L. Witten (Plenum, N.Y., 1977).
19. J. R. Bond, E. W. Kolb, and J. Silk, Astrophys. J. 255, 341 (1982); J. D. Barrow and M. S. Turner, Nature 291, 469 (1981).
20. J. D. Barrow, MNRAS 189, 23p (1979).
21. T. Rothman and R. Matzner, Phys. Rev. Lett. 48, 1565 (1982) and references therein.
22. E. T. Vishniac, Astrophys. J. 257, 456 (1982).
23. J. D. Barrow and M. S. Turner, Nature 292, 35 (1981).
24. J. Bernstein, M. Ruderman and G. Feinberg, Phys. Rev. 132, 1227 (1963).
R. Cowsik, Y. Pal and S. N. Tandon, Phys. Lett. 13, 265 (1964);
B. P. Konstantinov and G. E. Kocharov, Soviet Physics J.E.T.P. 19, 992 (1964);
B. P. Konstantinov, G. E. Kocharov and Yu. N. Starbunov, Izvestia Akad. Nauk. U.S.S.R., Ser. Fiz. 32, 1841 (1968); K. Greisen, Phys. Rev. Lett. 16, 748 (1966); T. Hara and H. Sato, Progress Theor. Phys. 64, 1089 (1980); 65, 477 (1981); T. Weiler, Phys. Rev. Lett. 49, 234 (1982); J. Cohen and P. Langacker Ref. 17.
25. J. N. Clarke, G. Karl and P. J. S. Watson, Can. J. Phys. 60, 1561 (1982).
26. J. Kristian, A. Sandage and J. Westphal, Astrophys. Journal 221, 383 (1978).
27. R. Cowsik and J. McClelland, Phys. Rev. Lett. 29, 669 (1972).
For more recent analyses, see J. Bernstein and G. Feinberg, Phys. Lett. 101B, 39 (1981), 103B, 470(E) (1981) and D. Schramm and G. Steigman, Astrophys. J. 243, 1 (1981).
28. J. Fry, Neutrino Mass Miniconference, p. 81.
29. S. Weinberg, ref. 1, J. Cohen and P. Langacker, ref. 17, J. Harvey and E. W. Kolb, ref. 9.
30. K. Freese, E. W. Kolb, and M. S. Turner; Chicago preprint, G. Steigman, private communication.

31. For recent papers on the subject see K. A. Olive, D. N. Schramm, G. Steigman, M. S. Turner and J. Yang, *Astrophys. Journ.* 246, 557 (1981), and G. Steigman, Proc. of the Intl. Colloq. on Baryon Nonconservation, eds. V. S. Narasimham et al. (Indian Academy of Sciences, Bangalore, 1982) p. 237.
32. R. V. Wagoner, W. A. Fowler and F. Hoyle, *Astrophys. Journal* 14B, 3 (1967); A. Yahil and G. Beaudet, *Astrophys. Journal* 206, 261 (1976); G. Beaudet and P. Goret, Ref. 7; A. Linde, *Phys. Lett.* 83B, 311 (1979); Y. David and H. Reeves, *Phil. Trans. R. Soc. Lond.* A296, 415 (1980); N. C. Rana, *Phys. Rev. Lett.* 48, 209 (1982); J. Fry and C. Hogan, Ref. 11; A. Szalay, *Phys. Lett.* 101B, 453 (1981).
33. S. Weinberg, *Phys. Rev.* 128, 1457 (1967); Weak Interactions as Probes of Unification, p. 353; and ref. 1.
34. K. E. Bergkvist, *Nucl. Phys.* B39, 317, 371 (1972).
35. L. Stodolsky, *Phys. Rev. Lett.* 34, 110 (1975).
36. R. Opher, *Astron. and Astrophys.* 37, 135 (1974).
37. R. R. Lewis, *Phys. Rev.* D21, 663 (1980).
38. R. Opher, *Astron. and Astrophys.* 108, 1 (1982).
39. P. Langacker, J. P. Leveille, and J. Sheiman, *Phys. Rev.* D27, 1228 (1983).
40. N. Cabibbo, L. Maiani, *Phys. Lett.* 114B, 115 (1982).
41. B. A. Campbell and P. J. O'Donnell, *Phys. Rev.* D26, 1487 (1982).
42. The neutrinos may induce a pressure of order $G_F(n_\nu - n_\bar{\nu})n_T$ on a target with number density n_T . This merely leads to a relative change of $\lesssim 10^{-36}$ in the size of the body.

CONFERENCE SUMMARY

G.J. Feldman*
CERN, Geneva, Switzerland



* On sabbatical leave from the Stanford Linear Accelerator Center, Stanford University, Stanford, California, USA. Work supported in part by the US Department of Energy under contract DE-AC03-76SF00515.

1. INTRODUCTION

In the opening talk of this meeting¹⁾, G. Kane defined "the minimal standard model" to be:

- a) Three generations of quarks and leptons;
- b) Massless neutrinos;
- c) $SU(3)$ _{colour} $\times SU(2)$ _L gauge theory;
- d) One neutral Higgs boson; and
- e) CP violation solely in the mass matrix.

Reaching this point has been the tremendous achievement of the past decade. We have witnessed the discoveries of charm and the third generation, the discovery of neutral currents and the detailed confirmation of $SU(2)$ _L $\times U(1)$, and the discovery of asymptotic freedom and the development of QCD and its experimental tests. In spite of these achievements, the resulting standard model is not entirely esthetically pleasing. It lacks a coherence which would explain its varied form and parameters; as a result, I would wager that none of us here believes that it represents the end of physics.

Our experimental activities fall into three general categories. The first is searching for evidence of physics beyond the minimal standard model. At the moment, we have no solid evidence, in the sense of a confirmed experiment, of any such physics. The first such evidence, whenever we obtain it, will undoubtedly be an important clue to what lies ahead. Thus, it is appropriate that we spend an appreciable part of our time and resources searching for it, even though the chance of success for any single experiment may be small.

Our searches are often motivated by the theoretical ideas we have heard discussed at this meeting -- grand unified theories, supersymmetry, composite models, among others. Often, however, we are motivated only by a sense of "pourquoi pas?" -- it could exist; let us look for it. In this spirit, we search for extended gauge group structures, extended Higgs sectors, and extra quarks and leptons.

The second category of experimental activity is testing the standard model. In this regard, it is important to remember that there are four particles which are required by the standard model but which have not yet been fully confirmed. The W and the Z have masses which are specified by the model, and we now have some evidence for both. As we will discuss in

a few minutes, the evidence is rather direct for the W , but considerably less direct for the Z . The masses of the other two particles, the t quark and the Higgs boson, are not specified by the model, and for these two particles we have no evidence whatsoever. The existence of a single neutral Higgs boson is the weakest point of the standard model; thus its discovery would be of tremendous importance because it would put important constraints on the physics beyond the standard model.

Finally, the third category of experimental activity is making detailed measurements within this standard model. For want of a better name we can call this "spectroscopy". Some of these measurements are clearly fundamental, such as the measurement of the Kobayashi-Maskawa mixing angles. Others are apparently less so, involving detailed structure controlled by non-perturbative QCD. But taken in total these measurements provide the building blocks of our knowledge.

These three categories do not always have clear boundaries. It is clear that if one performs a test of the standard model and the test fails, one has found evidence for physics beyond the standard model. And many times in the history of physics a routine measurement has uncovered a surprise which has led to a new level of understanding. Nevertheless, I will use these three categories to organize the contributions to this meeting.

2. SEARCHES FOR PHYSICS BEYOND THE STANDARD MODEL

2.1 Monopole catalysis of proton decay

These are only two major windows to the energy scale of physics required by the theories of grand unification -- magnetic monopoles and proton decay. We have heard discussed at this meeting the marvelous suggestion²⁾ that perhaps both could be seen in the same experiment, and, furthermore, that perhaps this would be the best way to see both phenomena.

Perhaps the suggestion is too good to be true, for we have also seen the impressive result from the Irvine-Michigan-Brookhaven (IMB) proton decay experiment that, in 80 days of running with a detector of effective area 340 m^2 (about a tenth of a football field), no candidates for successive proton decays were seen³⁾. With the most optimistic cross section assumptions, this result sets an upper limit on the magnetic monopole flux of $6 \times 10^{-15} \text{ cm}^{-2} \text{ str}^{-1} \text{ s}^{-1}$, a limit which approaches the

Parker bound of about $10^{-15} \text{ cm}^{-2} \text{ str}^{-1} \text{ s}^{-1}$, an upper limit to magnetic monopole fluxes obtained from astrophysical considerations⁴⁾.

2.2 Other searches for monopoles

This subject has been beautifully reviewed by B. Barrish at this meeting⁵⁾, and there is nothing useful that I can add to his talk. Let me only underline his statement that there are no experiments which are sensitive at the level of the Parker bound. If we are going to search seriously for magnetic monopoles, then we may have to consider detectors the size of football fields.

2.3 Searches for proton decay

The major new development in these searches was the report to this meeting of the first results from the IMB experiment⁶⁾. The experimenters have analysed 80 days of running with a 3300 ton fiducial volume for the $e^+ \pi^0$ and $\mu^+ K^0$ modes. They find no candidates for the $e^+ \pi^0$ mode, yielding a lifetime divided by branching ratio of $\tau/B > 6.5 \times 10^{31} \text{ yr}$. There is one candidate for the $\mu^+ K^0$ mode. The significance of this is not that there is one candidate (for, indeed, no evidence was presented to indicate that this event was not due to backgrounds), but that there is only one candidate.

I have three comments to make at this stage:

- 1) The IMB experiment seems to work well.
- 2) From the first results, it is clear that protons do not decay as readily as some had hoped. It would seem imprudent to build any future detectors with fiducial masses less than 1000 tons, because no matter how powerful they might be, they simply would not have the rate to be effective.
- 3) It is too early to say anything more. Regardless of the results of the IMB experiment, we will need fine-grained detectors such as the one being planned for the Fréjus tunnel⁷⁾.

2.4 Searches for supersymmetric particles

Supersymmetry is an elegant theoretical idea⁸⁾, but one which is somewhat frustrating for experimenters for two reasons:

- 1) There are no solid predictions. The theory has a large number of branch points which allow the creation of an endless number of models. No experimental results can eliminate the theory; the most they can do (other than discover supersymmetric particles) is to limit the possible models.
- 2) The presently accessible energies are probably too low to detect these particles.

Nonetheless, there has been a large effort to search for these particles. Above threshold, scalar leptons would be copiously produced in e^+e^- annihilation and be easily recognized. Searches for these particles give lower limits for their masses just slightly lower than the available beam energies, around 16 to 17 GeV⁹⁾. We have also heard negative results on searches for massive, unstable photinos in e^+e^- annihilations⁹⁾, and for gluinos in neutrino beam dump experiments^{10,11)}.

2.5 Searches for fundamental scalars

Charged fundamental scalars, either charged Higgs bosons or technicoloured pseudo-Goldstone bosons, would be produced in a predictable way in e^+e^- annihilations. Despite the criticism we have heard at this meeting¹²⁾, there have been reasonable searches for these particles⁹⁾ which set lower limits on the mass at about 13 GeV.

2.6 Search for right-handed currents in muon decay

Many people commented to me that they felt the highlight of the meeting was the report of the beautiful experiment of the Berkeley-Northwestern-TRIUMF Collaboration¹³⁾. I have no argument with this assessment. By measuring the polarization of muon decay, this experiment has set an upper limit on $(1 - \xi_P \delta/\rho)_\mu$, which is zero in the absence of right-handed currents, of 0.0041. This increases the previous lower bound on the mass of a right-handed W from 220 GeV to 380 GeV.

2.7 Searches for neutrino oscillations

Progress reports were given on searches for neutrino oscillations which have been done or are underway at Fermilab¹⁴⁾ and CERN¹⁵⁾. These searches are looking primarily for " ν_μ disappearance", that is, an oscillation of ν_μ into any other form. There are presently no

limits on ν_μ disappearance. These experiments together will be sensitive to mass squared differences in the entire range between 0.3 eV^2 and 1000 eV^2 .

2.8 Neutrino beam dump experiments

The outstanding anomaly in the beam dump experiments is the ratio of prompt ν_e to prompt ν_μ . All known sources of prompt neutrinos would give a value of this ratio close to unity. The results of three CERN experiments (all in the same beam line) gave values of ν_e/ν_μ ranging from 0.49 to 0.64 with typical errors of $0.2^{16)}$. The latest results from the Fermilab beam dump experiment which were reported to this meeting give a ratio of $1.29 \pm 0.21^{11)}$. Thus, there is a discrepancy of three standard deviations in the combined errors between CERN and Fermilab. The only thing we can do is wait for the results of latest round of beam dump experiments from CERN, which should be ready this summer, to see if we still have an anomaly.

2.9 Other searches

There were a fair number of other searches for physics beyond the standard model which I do not have time to review here. The total extent of our efforts on all these searches is impressive, and, as I said at the outset, quite appropriate.

3. TESTS OF THE STANDARD MODEL

3.1 The W discovery

It appears unavoidable to me that there is some particle being produced in the CERN $p\bar{p}$ collision which has a mass of around 80 GeV or more and whose decay produces an electron and missing energy. I have taken the liberty of combining the UA1 ¹⁷⁾ and UA2 ¹⁸⁾ data for events with an isolated electron and missing transverse momentum as a function of the electron's transverse momentum. The data are shown in Fig. 1.

Both experiments have a similar analysis chain with a cut at 15 GeV/c, but no bias beyond that point. The data do not pile up against the cut, as would be expected for any reasonable background, but rather peak between 35 and 40 GeV/c.

Since these data show the expected signature of the W, it is logical to make this assignment. However, on the basis of the present meager data other explanations are probably not excluded.

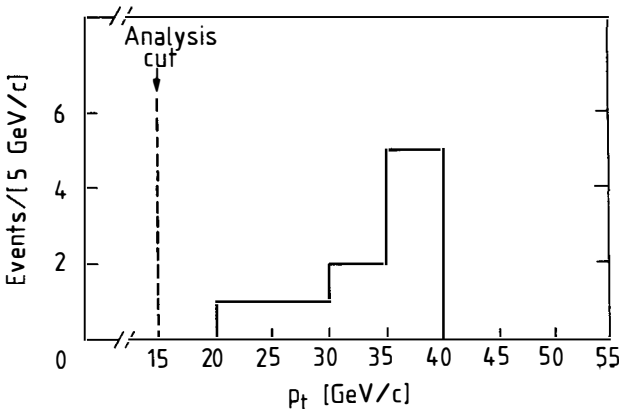


Fig. 1 Electron transverse momentum for events with an isolated electron and missing energy in the combined UA1 and UA2 data.

In particular there is one UA1 event which has the wrong asymmetry for a W decay. There are three possibilities:

- 1) It is a background event (10% confidence level, i.e. the number of background events in the sample is expected to be of the order of 0.1).
- 2) It is an unusual W decay (10% confidence level, i.e. it is ten times more likely to have the opposite asymmetry).
- 3) It is something interesting (there is no way to estimate a confidence level on the unknown).

In any case we look forward to the large increase in data expected by this summer.

If there has been a surprise in the $p\bar{p}$ running so far, it is that the data are very clean at high transverse momentum. Jets are unambiguous and one does not need complicated algorithms to count them. This bodes well for the future of high-energy $p\bar{p}$ physics.

3.2 Neutral currents in e^+e^- annihilation

The best way to see the effect of weak neutral currents in present energy e^+e^- annihilation data is in the backward-forward asymmetry in μ pair production. This asymmetry is proportional to $s/(1 - s/m_Z^2)$.

Thus, at sufficiently high s and sufficiently high precision one is sensitive to the Z mass. The combined results of five PETRA experiments measure this asymmetry to be $(-11.3 \pm 1.3)\%$ and set limits on the Z mass: $55 < m_Z < 110$ GeV⁹⁾. Thus, in some sense, one can claim to have seen evidence for the Z , albeit with rather poor mass resolution.

At this meeting we have heard reported the first measurement of the neutral current coupling to the c quark by a measurement of the asymmetry in the angular distribution of D^* production⁹⁾. The TASSO result gives $g_A^c = 0.89 \pm 0.44$.

3.3 Neutral currents in ν scattering

The only comment I have here is to underline arguments that were put forth at the recent CERN Workshop on SPS Fixed-Target Physics¹⁹⁾. At present the most precise measurements of $\sin^2 \theta_W$ come from neutral current ν interactions. In the future one will be able to measure the Z mass to about 100 MeV which will give $\sin^2 \theta_W$ to a precision of better than 0.001, subject, however, to weak radiative corrections of about 0.02. These weak radiative corrections will be our first look at weak interactions beyond the Born approximation. To measure the radiative correction we need an independent determination of $\sin^2 \theta_W$ to a precision of at least 0.005, a value which is factors of 8 and 3 below that now obtainable from ν_e scattering and from $\nu_\mu N$ scattering, respectively. In the former case there are no theoretical uncertainties and the present experiments are limited by statistics; in the latter case hadronic corrections have to be understood. The question is whether either or both measurements can be improved to the required accuracy.

3.4 τ lifetime

The Mark II measurement²⁰⁾ which sets bounds on the τ coupling to the charged weak current, $g_\tau/g_e = 0.92 \pm 0.12$, is the last of a long series of measurements on the τ lepton which appear to rule out the possibility that the τ is anything other than a sequential lepton with its associated neutrino coupling in a universal way to the weak current²¹⁾.

4. SPECTROSCOPY

4.1 The EMC effect

The biggest physics surprise in the past year has been the discovery by the European Muon Collaboration at CERN that structure functions

measured in iron differ significantly from those measured in deuterium²²⁾. At this meeting we have heard a delightful report from Bodek¹⁴⁾ which showed that decade-old SLAC empty-target data confirm this effect and even might clear up an old mystery as to why shadowing disappears so quickly with q^2 in electroproduction²³⁾.

The data from these two experiments seem clear and convincing. What are the consequences? There are two basic reasons for studying deep inelastic scattering. One is to study the q^2 development of QCD. This can be done just as well in iron as on free nucleons, so for this purpose the EMC effect is unimportant. The second reason, however, is to measure the parton distributions in protons and neutrons. It is now clear that for this purpose measurements in iron distort these distributions at the 15% level.

There has been a great deal of enthusiasm voiced at this meeting for systematic programs to measure parton distributions in nuclei. This should be recognized, however, as the study of a (probably quite interesting) nuclear physics question, rather than anything fundamental in elementary particle physics. If one is going to be serious about studying this effect, then it would be useful to have a detailed measurement of νd interactions, since it is only through neutrino interactions that one can separate valence and sea quark contributions.

4.2 Search for gluonium states

The radiative decays of heavy charmonium states such as the ψ or the Υ are presumably among the best places to search for gluonium states because the decay results in two gluons in a colour-singlet state of variable mass. Searches were made for ψ decays into a photon and a resonance. In addition to the expected resonances such as the η , η' , and f , two surprises were found, the $\psi(1440)$ ²⁴⁾ decaying into $K\bar{K}\pi$ and the $\Theta(1670)$ ²⁵⁾ decaying into $\eta\eta$. Since then there have been attempts to measure or set upper limits on other decay modes of these resonances^{26,27)}. At this meeting we have had a report from DCI setting an upper limit of $B(\psi \rightarrow \gamma\Theta) \cdot B(\Theta \rightarrow \rho\gamma) < 8 \times 10^{-5}$ at the 99% confidence level²⁸⁾.

A clear picture of the identity of these particles has not yet emerged. Part of the problem is that there is no quantum number which defines a gluonium state; in general it will mix with $q\bar{q}$ and $qq\bar{q}\bar{q}$

states. Furthermore, hadronic states in this mass region are wide, and in any given final state at any given mass it is likely that there will be several overlapping states.

What is needed is a more systematic and detailed study with considerably more data than we have now. With detectors such as the Mark III at SPEAR this can be done. The question is will it?

4.3 Heavy quark fragmentation

Progress has been made recently on measuring heavy quark fragmentation functions, that is, answering the question "How much of the energy of a heavy quark does the weakly decaying heavy meson carry?" The charmed quark fragmentation function has been measured directly by reconstructing exclusive D^{*+} decays^{9,20,29}. The data from the three high-energy experiments are plotted in Fig. 2.

The fractional cross section, $(1/\sigma) d\sigma/dz$, is used to eliminate differences in normalizations and branching fraction assumptions among the three experiments. The results show that the charm fragmentation function is fairly hard, with an average z of about 0.6.

The Mark II experiment has measured the bottom quark fragmentation by statistically separating electrons from b decay from those from c decay and backgrounds²⁰. The result is an even harder fragmentation function for b quarks with an average z of about 0.75.

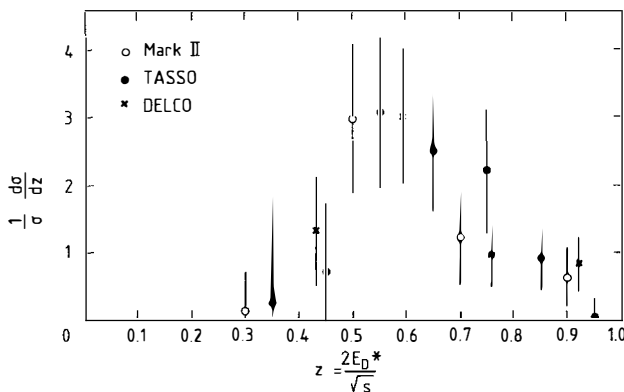


Fig. 2 The fractional cross section for D^{*+} production as a function of $z \equiv 2E_{D^*}/\sqrt{s}$.

4.4 Lifetime

The Mark II has measured the D^0 lifetime to be $(3.7^{+2.5}_{-1.5} \pm 1.0) \times 10^{-19}$ s, based on a sample of seven high-z reconstructed D^+ decays. The importance of this result is that it demonstrates that it is possible for e^+e^- storage rings to compete in this field. With the additional data which will be available soon we can expect higher statistics on the D^0 lifetime as well as measurements of the D^+ and B lifetimes.

4.5 $b\bar{b}$ spectroscopy

At this meeting we have seen very beautiful single photon spectra from $\Upsilon(2s)$ and $\Upsilon(3s)$ decays from the CUSB experiment³⁰⁾. Although the individual transitions have not been separated, the centre-of-gravity of the x_b masses has been determined. We look forward to upcoming Crystal Ball results from DORIS, which may have higher resolution.

4.6 Studies of B decay

In recent years we have accumulated an impressive amount of information on the decays of the B mesons. I will just briefly list here some of the measurements which have been reported to this meeting.

1) $b \rightarrow u/b \rightarrow c$

Both CUSB and CLEO have tried to determine the fundamental mixing angle of b decay by measuring the electron spectrum^{29,30)}. The shape of this spectrum is affected by the mass of the hadronic state produced in the semi-leptonic decay. The result is somewhat model-dependent, but assuming that the hadronic state produced from a u quark has a mass of not more than 1 GeV, the fraction of $b \rightarrow u$ decays is limited to 5% or less.

2) B semi-leptonic decay fractions

Four experiments have reported results with an average value of $B(B \rightarrow l\nu X) = (12.6 \pm 1.2)\%$ ^{20,29,30)}. This agrees well with the value expected from a simple spectator model, 1/9.

3) Observation of B exclusive states

The branching ratio for the B meson to go into any given exclusive state is quite small. Thus, CLEO has accomplished a formidable task in reconstructing enough B exclusive states to measure the B masses and mass difference²⁹⁾. This was only possible because of the mass constraint provided by the $\Upsilon(4s)$ state.

4) ψ production in B decays

CLEO has measured the branching fraction for $B \rightarrow \psi X$ to be $(6.4 \pm 2.3) \times 10^{-3}$, a value smaller than had been expected by some predictions²⁹). This has obvious practical consequences for anyone hoping to use the ψ to tag B's.

CONCLUSION

The conclusion to this talk was really given in the introduction: our field is quite healthy. We have made tremendous gains in the past decade and we are consolidating these gains while, at the same time, earnestly searching for the clues which will tell us what lies beyond the standard model.

Acknowledgements

I thank all of the speakers at this meeting for their cooperation which made the preparation of this talk sufficiently simple that I was able to ski at least a little each afternoon. I am particularly indebted to F. Dydak for several discussions which helped to clarify some of the points covered in this talk.

Enfin, comme j'étais le dernier à parler à cette semaine de la Rencontre de Moriond, j'ai l'honneur, de la part de tous les participants, de remercier Tran, le Secrétariat, et tous les organisateurs d'avoir fait une conférence très agréable, qui était pleine de physique et pleine de soleil.

REFERENCES

- 1) G. Kane, these proceedings.
- 2) C. Callen, these proceedings.
- 3) S. Erede, these proceedings.
- 4) E.N. Parker, *Astrophys. J.* 160, 383 (1970).
- 5) B. Barrish, these proceedings.
- 6) J.C. Vander Velde, these proceedings.
- 7) G. Chardin, these proceedings.
- 8) C. Savoy, these proceedings.
- 9) S. Yamada, these proceedings.
- 10) C. Santoni, these proceedings.
- 11) M.J. Longo, these proceedings.
- 12) K. Lane, these proceedings.
- 13) B. Gobbi, these proceedings.
- 14) A. Bodek, these proceedings.
- 15) Y. Eisenberg, these proceedings.
- 16) See, for example, F. Dydak in *Neutrino Physics and Astrophysics* (the Proc. of Neutrino 1980, Erice, Italy, 23-28 June 1980), edited by E. Fiorini, p. 341 (Plenum Press, New York, 1982).
- 17) A. Norton, these proceedings.
- 18) P. Bloch, these proceedings.
- 19) D. Haidt, in the Proc. of the Workshop on SPS Fixed Target Physics in the Years 1984-1989 (ed. I. Mannelli), p. 63, CERN preprint CERN-EP/83-02 (1983).
- 20) G. Goldhaber, these proceedings.
- 21) See, for example, G.J. Feldman in *Particles and Fields -- 1981: Testing the Standard Model*, Proc. of the Meeting of the Division of Particles and Fields of the American Physical Society, Santa Cruz, Calif., September 1981 (eds. C.A. Heusch and W.T. Kirk), (American Institute of Physics, New York, 1982).
- 22) K. Rith, these proceedings.
- 23) See, for example, R.E. Taylor in the Proc. of 1975 Int. Symp. on Lepton and Photon Interactions at High Energies, Stanford University, 21-27 August 1975 (ed. W.T. Kirk), p. 679 (SLAC, Stanford, Calif., 1975).
- 24) D.L. Scharre et al., *Phys. Lett.* 97B, 329 (1980).

- 25) C. Edwards et al., *Phys. Rev. Lett.* **48**, 458 (1982).
- 26) See, for example, E.D. Bloom in the Proc. of 21st Int. Conf. on High-Energy Physics, 26-31 July 1982, *J. de Physique* **43**, C3-407 (1982).
- 27) K. Wacker, these proceedings.
- 28) G. Cosme, these proceedings.
- 29) E. Thorndike, these proceedings.
- 30) P.M. Tuts, these proceedings.

LIST OF PARTICIPANTS

ALTARELLI Guido	Ist. di Fisica, Univ. di Roma Roma I, Place Aldo Moro 00185 ROMA ITALY
BARBIELLINI Guido	INFN Via E. Fermi 40, C.P. 13 00044 FRASCATI ITALY
BARISH Edmund	California Inst. of Technology HEP-256-48 PASADENA CA 91125 USA
BAULIEU Laurent	LPTHE, Univ. Paris VI 4 Place Jussieu, Tour 16 75230 PARIS Cedex 05 FRANCE
BECKER Lutz	DESY Notkestr. 85 2000 HAMBURG 52 GERMANY
BELLAMY Barry	Westfield College Kidderpore Av. LONDON NW3 7ST ENGLAND
BELLOTI Enrico	INFN, Università di Milano Via Celoria 16 20133 MILANO ITALY
BILLOIRE Alain	SPhT, C.E.N. Saclay Orme les Merisiers 91191 GIF/YVETTE Cedex FRANCE
BLANKENBECLER Richard	Stanford Linear Acc. Center SLAC, P.O. Box 4349 STANFORD CA 94305 USA
BLOCH Philippe	DPhPE/SEE C.E.N. Saclay 91191 GIF/YVETTE Cedex FRANCE
BLUMENFELD Barry	Johns Hopkins Univ. Dept. of Physics BALTIMORE MD 21218 USA
BODEK Arie	Physics & Astrophysics Dept. Univ. of Rochester ROCHESTER NY 14627 USA
BOUQUET Alain	LPTHE, Univ. Paris VII 4 Place Jussieu 75230 PARIS Cedex 05 FRANCE
BOWLER Michael	Nuclear Physics Lab. Keble Road OXFORD OX1 3RH ENGLAND

CALLAN Curtis	Physics Dept. Princeton Univ. PRINCETON NJ 08540 USA
CAPDEQUI-PEYRANERE Michel	Lab. de Phys. Maths. U.S.T.L. 34060 MONTPELLIER Cedex FRANCE
CHARDIN Gabriel	DPhPE C.E.N. Saclay 91191 GIF/YVETTE Cedex FRANCE
COQUEREAUX Robert	C.E.R.N. TH Division 1211 GENEVA 23 SWITZERLAND
COSME Gérard	Lab. Acc. Linéaire Université Paris Sud, Bat 200 91405 ORSAY Cedex FRANCE
CRIEGEE Lutz	DESY Notkestr 85 2000 HAMBURG 52 GERMANY
CRUZ Andres	Dept. de Fisica Teorica Facultad de Ciencias ZARAGOZA SPAIN
CUTTS David	Dept of Physics Brown University PROVIDENCE RI 02912 USA
DAR Arnon	Physics Dept. Technion - Israel Inst. Tech. TECHNION CITY Haifa 32000 ISRAEL
DE RAFAEL Eduardo	CPT, Section 2 CNRS Luminy, Case 907 13288 MARSEILLE Cedex 2 FRANCE
DEBU Pascal	DPHPE C.E.N. Saclay 91191 GIF/YVETTE Cedex FRANCE
DE FORCRAND Philippe	Centre de Physique Theorique Ecole Polytechnique 91128 PALAISEAU FRANCE
DELDUC Francois	LPTHE, Univ. Paris VII Tour 33, 4 place Jussieu 75230 PARIS Cedex 05 FRANCE
DELCIERRE Pierre	Lab. Phys. Theor., Col. de France 11 Place M. Berthelot 75231 PARIS Cedex 5 FRANCE
DONOHUE Jack	Lab. Phys.Theorique Univ. de Bordeaux 33170 GRADIGNAN FRANCE

DORFAN Jonathan	SLAC P.O. Box 4349 STANFORD CA 94305 USA
DUCROS Yves	DPHPE C.E.N. Saclay 91191 GIF/YVETTE Cedex FRANCE
DURKIN Stanley	Physics Dept. Univ. Pennsylvania PHILADELPHIA PA 19104 USA
DYDAK Friedrich	C.E.R.N. EP Division 1211 GENEVA 23 SWITZERLAND
EICHTEN Estia	FERMILAB P.O. Box 500 BATAVIA IL 60555 USA
EISELE Franz	Universitat Dortmund Abt Physik, Postfach 500500 4600 DORTMUND 50 GERMANY
EISENBERG Yehuda	C.E.R.N. EP Division 1211 GENEVA 23 SWITZERLAND
ERREDE Steven	Randall Lab. of Physics Univ. of Michigan ANN ARBOR MI 48109 USA
FAYET Pierre	Lab. Phys. Theor., E.N.S 24 rue Lhomond 75231 PARIS Cedex 05 FRANCE
FELDMAN Gary	C.E.R.N./SLAC P.O.Box 4349 STANFORD CA 94305 USA
FELTESSE Joel	DPHPE SECB C.E.N. Saclay 91191 GIF/YVETTE CEDEX FRANCE
FIEGEL Jan	II Inst. f. Exp.Phys. Hamburg Univ, Luruper-Chausse 149 2000 HAMBURG 50 GERMANY
FOA Lorenzo	Lab. di S. Piero INFN Via Livornese S. Piero a Grado 56010 PISA ITALY
FRANZINI Paolo	Columbia Univ. Dept.of Physics NEW YORK NY 10027 USA
FRITZSCH Harald	Univ. of Munich Theresienstr. 37 A 8000 MUNCHEN GERMANY

GIACOMELLI Giorgio	Ist. di Fisica Via Irnerio 46 40126 BOLOGNA ITALY
GOBBI Bruno	Dept. of Physics Northwestern Univ. EVANSTON IL 60201 USA
GOLDHABER Gerson	Lawrence Berkeley Lab. Dept of Physics BERKELEY CA 94720 USA
GRARD Fernand	Univ. de l'Etat Fac. de Sciences Avenue Maistriau 19 7000 MONS BELGIUM
GRIVAZ Jean-Francois	Lab. Acc. Linéaire Univ. Paris Sud, Bat. 200 91405 ORSAY FRANCE
GUY Jon	Rutherford Lab. Chilton, Didcot, OXON OX11 OQX ENGLAND
HALPRIN Arthur	Physics Dept Univ. of Delaware NEWARK DE 19711 USA
HAYOT Fernand	SPhT C.E.N. Saclay 91191 GIF/YVETTE Cedex FRANCE
JACQUET Francois	Centre de Physique Theorique Ecole Polytechnique 91128 PALAISEAU FRANCE
JARLSKOG Cecilia	Dept of Physics Univ. of Bergen, Allig.55 5000 BERGEN NORWAY
JOHNSON James	Univ. of Wisconsin Physics Dept. MADISON WI 53706 USA
KANE Gordon	Randall Lab. of Physics Univ. of Michigan ANN ARBOR MI 48109 USA
KIM Jae Kwan	K.A.I.S. Cheongryang P.O. Box 131 SEOUL Korea
KOLTICK David	Purdue University Physics Dept. WEST LAFAYETTE IN 47904 USA
LANE Kenneth	Dept of Physics Ohio State University COLOMBUS OH 43210 USA

LANGACKER Paul	University of Pennsylvania Dept of Physics PHILADELPHIA PA 19104 USA
LAPLANCHE Francis	Lab. Acc. Linéaire Université Paris-Sud, Bat 200 91405 ORSAY FRANCE
LAUNER Guy	Centre de Physique Theorique CNRS Luminy Case 907 13288 MARSEILLE Cedex 09 FRANCE
LEADER Elliot	Westfield College Kidderpore Av. LONDON NW3 7ST ENGLAND
LOCKYER Nigel	SLAC, Bin 95 P.O.Box 4349 STANFORD CA 94305 USA
LUTZ Pierre	Col. de France, Lab. Phys. Corp. 11 place M. Berthelot 75231 PARIS Cedex 05 FRANCE
MANDELBAUM Gerd	Lyman Lab. of Physics Harvard University CAMBRIDGE MA 02138 USA
MARTYN Hans-Ulrich	I.Phys. Inst. RWTH-Aachen Sommerfeldstr. 5100 AACHEN 1 GERMANY
MONTANET Lucien	C.E.R.N EP Division 1211 GENEVA 23 SWITZERLAND
MOREL André	SPhT C.E.N. Saclay 91191 GIF/YVETTE Cedex FRANCE
NASH Thomas	FERMILAB P.O. Box 500 BATAVIA IL 60510 USA
NIEBERGALL Friedrich	CERN/Univ. Hamburg II.Inst. f. Exper. 2000 HAMBURG 52 GERMANY
OLIVIER Louis	LPTPE Univ. Paris Sud, Bat 211 91405 ORSAY FRANCE
PACHECO Amalio	Dept. Fisica Nuclear Fac. Ciencias ZARAGOZA SPAIN
PANMAN Jaap	C.E.R.N. EP Division 1211 GENEVA 23 SWITZERLAND

PEYROU Charles	C.E.R.N. EF Division 1211 GENEVA 23 SWITZERLAND
PHAM Tri Nang	Ecole Polytechnique Centre de Physique Theorique 91128 PALAISEAU FRANCE
PLANO Richard	Rutgers University Physics Dept. NEW BRUNSWICK NJ 08903 USA
POHL MARTIN	DESY F-13 Notkestr. 85 2000 HAMBURG 52 GERMANY
PRIMACK Joel	Phys. Dept. Univ. of California SANTA CRUZ CA 95064 USA
RANDER John	DPHPE-SEE C.E.N. Saclay 91191 GIF/YVETTE FRANCE
RITH Klaus	Physik Fak., Freiburg Univ. Hermann-Herderstr. 3 7800 FREIBURG GERMANY
ROMANO Francesco	Dept. di Fisica Bari Univ. Via Amendola 70126 BARI ITALY
RUDAZ Serge	University of Minnesota Physics & Astromy School MINNEAPOLIS MI 55455 USA
RYKACZEWSKI Hans	NIKHEF P.O. Box 41882 1009 DB AMSTERDAM HOLLAND
SANTONI Claudio	INFN, Sez. Sanita Viale Regina Elena 29 00161 ROMA ITALY
SAVOY Carlos	SPhT C.E.N. Saclay 91191 GIF/YVETTE Cedex FRANCE
SCHMID Christoph	Inst f. Thoer. Physik ETH-Hoggerberg 8093 ZURICH SWITZERLAND
SCHMID Peter	C.E.R.N. EP Division 1211 GENEVA 23 SWITZERLAND
SCHMIDT Michael	Inst. f. Theor. Physik der Univ. Heidelberg 6900 HEIDELBERG GERMANY

SONI Amarjit	Dept. of Physics, UCLA Univ. of California LOS ANGELES CA 90024 USA
TALBY Mossadek	Centre Phys. des Part. U.E.R. Luminy, Case 907 13288 MARSEILLE Cedex 2 FRANCE
THORNDIKE Edward	Dept. Physics and Astronomy Univ. of Rochester ROCHESTER NY 14627 USA
TITTEL Klaus	Inst. f. Hochenergiephysik Schroederstr. 90 6900 HEIDELBERG 1 GERMANY
TRAN THANH VAN Jean	LPNHE Univ. Paris Sud, Bat 211 91405 ORSAY FRANCE
TURLAY Rene	DPhPE C.E.N. Saclay 91191 GIF/YVETTE Cedex FRANCE
TURLUER Maria Luisa	DPhPE C.E.N. Saclay 91191 GIF/YVETTE Cedex FRANCE
TUTS Philip	Stony Brook/Cornell Univ. Wilson Laboratory ITHACA NY 14853 USA
VALLE Jose	C.E.R.N./Theory Division Rutherford Appleton Lab. DIDCOT OXON OX11 0QX ENGLAND
VAN DAM Piet	NIKHEF-H P.O.Box 41882 1009 AMSTERDAM DB Holland
VAN DER VELDE Jack	Physics Dept. Univ. of Michigan ANN ARBOR MI 48109 USA
VAN DONINCK Walter	V R U E - Univ. Brussel Pleinlaan 2 1050 BRUSSELS BELGIUM
VENEZIANO Gabriele	C.E.R.N. TH Division 1211 GENEVA 23 SWITZERLAND
WACKER Klaus	SLAC, Bin 98 P.O. Box 4349 STANFORD CA 94305 USA
WAHL Hienrich	C.E.R.N. EP Division GENEVA 23 1211 SWITZERLAND

WEERTS Harry

FERMILAB
P.O. Box 500
BATAVIA IL 60510 USA

WHITE Marion

Lab. for Nuclear Science
M.I.T./DESY Collaboration
CAMBRIDGE MA 020139 USA

WISER David

SLAC
P.O. Box 4349
STANFORD CA 94305 USA

YAMADA Sakue

DESY/LICEPP, Science Fac.
Tokyo Univ., Bunkyo-ku
TOKYO JAPAN.